(Thio)Carbonyl Pseudohalogenide

–

Synthese, Spektroskopie und Reaktivität

Kumulative Dissertation

zur Erlangung des akademischen Grades eines

Doktor der Naturwissenschaften

(Dr. rer. nat.)

dem Fachbereich Chemie

der Philipps-Universität Marburg

vorgelegt von

Jonathan Pfeiffer, M. Sc.

aus Marburg / Wehrda

(Thio)Carbonyl Pseudohalogenide

–

Synthese, Spektroskopie und Reaktivität

Kumulative Dissertation

zur Erlangung des akademischen Grades eines

Doktor der Naturwissenschaften

(Dr. rer. nat.)

dem Fachbereich Chemie

der Philipps-Universität Marburg

vorgelegt von

Jonathan Pfeiffer, M. Sc.

aus Marburg / Wehrda

Erstgutachter: Dr. Frank Tambornino

Zweitgutachter: Prof. Dr. Crispin Lichtenberg

Marburg (Lahn) 2024

Hochschulkennziffer 1180

Die vorliegende Dissertation wurde von Mai 2020 bis April 2024 am Fachbereich Chemie der Philipps-Universität Marburg unter Leitung von Dr. Frank Tambornino angefertigt.

Erstgutachter: Dr. Frank Tambornino
Zweitgutachter: Prof. Dr. Crispin Lichtenberg

Annahme der Dissertation: _____

Tag der Disputation: _____

Erklärung

Ich erkläre, dass eine Promotion noch an keiner anderen Hochschule als der Philipps-Universität Marburg, Fachbereich Chemie, versucht wurde.

Hiermit versichere ich, dass ich die vorliegende Dissertation

„(Thio)Carbonyl Pseudohalogenide – Synthese, Spektroskopie und Reaktivität"

selbstständig, ohne unerlaubte Hilfe Dritter angefertigt und andere als die in der Dissertation angegebenen Hilfsmittel nicht benutzt habe. Alle Stellen, die wörtlich oder sinngemäß aus veröffentlichten oder unveröffentlichten Schriften entnommen sind, habe ich als solche kenntlich gemacht. Dritte waren an der inhaltlich-materiellen Erstellung der Dissertation nicht beteiligt; insbesondere habe ich hierfür nicht die Hilfe eines Promotionsberaters in Anspruch genommen. Kein Teil dieser Arbeit ist in einem anderen Promotions- oder Habilitationsverfahren verwendet worden. Mit dem Einsatz von Software zur Erkennung von Plagiaten bin ich einverstanden.

_____   _____

Ort/Datum   Jonathan Pfeiffer

„I've got an idea.
An idea so smart
that my head would explode,
if I even began to know
what I'm talking about."

Peter Griffin

Inhaltsverzeichnis

Abkürzungsverzeichnis

CD*PsH* Carbonyldipseudohalogenid

DFT Dichtefunktionaltheorie (*Density Functional Theory*)

Dipp 2,6-Diisopropylphenyl

DTCH *N*,*N*'-Bis(**d**iisopropylphenyl)-*N*,*N*'-di**t**rimethylsilyl**c**arbamoyl**h**arnstoff

ESI Elektrosprayionisation

GED Gasphasen-Elektronenbeugung (*Gas-phase Electron Diffraction*)

HC*PsH* Halogencarbonylpseudohalogenid

ICS **I**so**c**yanur**s**äure

IDCDA **I**mido**dic**arbonsäure**dia**mid

IR Infrarot

LIFDI *Liquid Injection Field Desorption Ionization*

MS Massenspektrometrie

NBO *Natural Bond Orbital*

NMR Kernspinresonanz (*Nuclear Magnetic Resonance*)

OxD*PsH* Oxalyldipseudohalogenid

PXRD Röntgenpulverdiffraktometrie (*Powder X-ray Diffraction*)

RT Raumtemperatur

SC-XRD Einkristallstrukturanalyse (*Single Crystal X-ray Diffraction*)

Sdp. Siedepunkt

SI *Supporting Information*

Smp. Schmelzpunkt

TCCA Trichlorisocyanursäure (*Trichloroisocyanuricacid*)

THF Tetrahydrofuran

TIDCDA **T**hio**i**mido**dic**arbonsäure**dia**mid

TMS Trimethylsilyl

UV Ultraviolett

Zsp. Zersetzungspunkt

1 Einleitung

1.1 Kohlensäure und ihre Derivate

Das wohl bekannteste carbonylhaltige Molekül ist die Kohlensäure mit der Summenformel $CO(OH)_2$. Im alltäglichen Sprachgebrauch wird diese oftmals mit in z.B. Mineralwasser gelöstem Kohlenstoffdioxid verwechselt und deshalb auch als „freie" Kohlensäure bezeichnet. Sie ist heutzutage noch Gegenstand aktueller Forschung, wie es die erst kürzliche Aufklärung ihrer Molekülstruktur im Festkörper zeigt.[1] Ausgehend von der Kohlensäure können Carbonyldihalogenide, wie Phosgen ($COCl_2$), und Carbonyldiamide, wie Harnstoff ($CO(NH_2)_2$), abgeleitet werden (Schema 1.1). Beide Moleküle sind heutzutage wichtige Bausteine als C1 Synthons in der chemischen Industrie. Harnstoff, welcher hauptsächlich für die Produktion von Dünger verwendet wird,[2] wurde 2021 weltweit mit einem jährlichen Volumen von 179.81 Mt[3] produziert. Phosgen wurde 2018 mit einem jährlichen Produktionsvolumen von 12 Mt hergestellt und findet Anwendung in der Synthese von Polymeren, wie Polyurethanen und Polycarbonaten.[4]
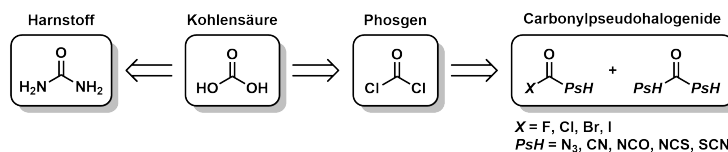
Schema 1.1: Kohlensäure und davon abgeleitete Derivate wie Harnstoff, Phosgen und Carbonylpseudohalogenide mit *X* = Halogen und *PsH* = Pseudohalogen.

1.1.1 Harnstoff

Harnstoff, das Diamid der Kohlensäure ($CO(NH_2)_2$), wurde erstmals 1727 von BOERHAAVE beschrieben, als er Urin untersuchte.[5,6] Rund 50 Jahre später wurde es von ROUELLE bei der Extraktion von Urin mit Alkohol erneut entdeckt[6,7] und in 1797 schließlich als Nitratsalz kristallisiert.[6,8,9] DAVY stellte Harnstoff 1812, ohne es zu wissen, aus Phosgen und Ammoniak her.[10] Berühmtheit erlangte Harnstoff als WÖHLER in 1828 bei dem Versuch Ammoniumcyanat (NH_4OCN) aus Silbercyanat (AgOCN) und Ammoniumchlorid (NH_4Cl) herzustellen, stattdessen aber Harnstoff erhielt.[11] Es gilt allgemein als die erste Synthese eines organischen Stoffes aus anorganischen Ausgangssubstanzen, obwohl ihm dies bereits vier Jahre zuvor bei der Hydrolyse von Dicyan ($(CN)_2$) zu Oxalsäure ($(COOH)_2$) gelang.[12] In 1922 wurde erstmals eine großtechnische Synthese von BOSCH und MEISER entwickelt und der BASF AG patentiert.[13] Diese beruht auf der Bildung von

Ammoniumcarbamat (NH_4OOCNH_2) aus Ammoniak (NH_3) und Kohlenstoffdioxid (CO_2) und dessen Spaltung in Harnstoff und Wasser (Schema 1.2), welche BASAROFF erstmals beschrieb.[14] Bis heute wird dieses Syntheseverfahren in optimierten Prozessen zur industriellen Harnstoffproduktion angewendet.[2,15]
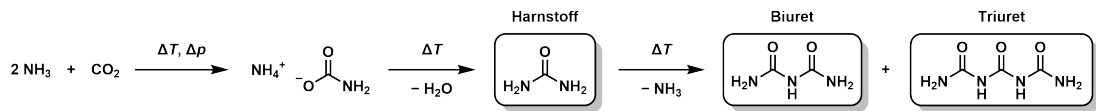
Schema 1.2: Industrielle Harnstoffproduktion aus Kohlenstoffdioxid und Ammoniak, sowie Thermolyse von Harnstoff zu Biuret und Triuret.

Neben Harnstoff sind noch unter ihren Trivialnamen Biuret, Carbamoylharnstoff (($CO(NH_2)_2)NH$), und Triuret, Carbonyldiharnstoff ($CO(NHCO(NH_2))_2$), bekannt. Biuret wurde beim Erhitzen von Harnstoff mit Salpetersäure (HNO_3) unter Abspaltung von Ammoniumnitrat (NH_4NO_3) in 1848 von WIEDEMANN entdeckt.[16–19] SCHMIDT entdeckte 1872 schließlich Triuret bei der Reaktion von Harnstoff mit Phosgen.[20] Beide Moleküle sind auch durch Thermolyse von Harnstoff unter formaler Abspaltung von Ammoniak darstellbar (Schema 1.2).[2,21]

1.1.2 Phosgen

Phosgen, das Dichlorid der Kohlensäure ($COCl_2$), wurde erstmals 1812 von DAVY erhalten, welcher Kohlenstoffmonoxid (CO) und Chlor (Cl_2) in einer Glasampulle Sonnenlicht aussetzte (Schema 1.3).[10] Phosgen ist ein farbloses Gas mit einem Siedepunkt von 7 °C. Sein süßlicher Geruch wird mit frisch geschnittenem Gras oder feuchtem Heu assoziiert. Aufgrund seiner Toxizität wurde es im 1. Weltkrieg als Giftgas eingesetzt und wird deshalb heutzutage direkt dort verbraucht, wo es großtechnisch hergestellt wird.[4] Ein erstes Patent zur Produktion von Phosgen wurde 1917 erteilt.[22] Bis heute wird es industriell aus Kohlenstoffmonoxid und Chlor mit einem Aktivkohle-Katalysator, welcher stetig weiterentwickelt wird,[23,24] hergestellt.[4]
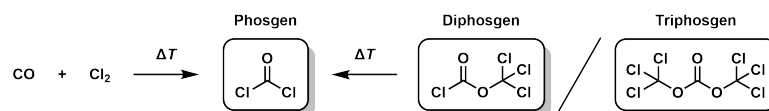
Schema 1.3: Industriellen Produktion von Phosgen aus Kohlenstoffmonoxid und Chlor, sowie thermische Spaltung von Diphosgen oder Triphosgen zu Phosgen.

Im Labormaßstab kann Phosgen aus Diphosgen oder Triphosgen mittels thermischer Spaltung erhalten werden.[4] Dabei sind die Moleküle kein Dimer bzw. Trimer von Phosgen, sondern spalten sich lediglich in zwei oder drei Moleküle Phosgen (Schema 1.3). Diphosgen, Trichlormethylchlorkohlensäureester (CO(OCCl$_3$)Cl), wurde erstmals 1887 von HENTSCHEL als farblose Flüssigkeit beschrieben, welche er beim Chlorieren von Methylchlorcarbonat (CO(OCH$_3$)Cl) erhielt.[25,26] Triphosgen, Bis(trichlormethyl)carbonat (CO(OCCl$_3$)$_2$), wurde von COUNCLER 1880 erstmals in Form von farblosen Kristallen bei der Reaktion von Chlor mit Dimethylcarbonat (CO(OCH$_3$)$_2$) erhalten.[27] Beide Moleküle gelten als sichere Substitute für Phosgen aufgrund ihrer Aggregatzustände, sind allerdings nicht weniger toxisch oder ungefährlicher als Phosgen selbst.[4,28] Eine Variante Phosgen herzustellen ist Triphosgen mit Kupferphthalocyanin als Katalysator thermisch zu spalten. Die Reaktion verläuft quantitativ und ist lösungsmittelfrei.[29] Eine neue Variante beruht auf Triethylmethylammoniumchlorid ([NEt$_3$Me]Cl). Dieses speichert zunächst Chlor in Form der ionischen Flüssigkeit ([NEt$_3$Me][Cl$_3$]), welche mit Kohlenstoffmonoxid bereits bei Raumtemperatur (RT) und Atmosphärendruck zu Phosgen reagiert.[30]

1.1.3 Carbonylpseudohalogenide

Etwas entferntere Derivate der Kohlensäure sind Carbonylpseudohalogenide. Diese können ausgehend von Carbonylhalogeniden durch Substitution des Halogens (*X*) durch ein Pseudohalogen (*PsH*) beschrieben werden (Schema 1.4). Hier ist zu unterscheiden zwischen einer einfachen oder zweifachen Substitution, welche entweder zu Halogencarbonylpseudohalogeniden (HC*PsH*) (CO(*PsH*)*X*) oder Carbonyldipseudohalogeniden (CD*PsH*) (CO(*PsH*)$_2$) führt. Die Pseudohalogene können hier Azid (−N$_3$), Cyanid (−CN), Isocyanat (−NCO), Isothiocyanat (−NCS) oder Thiocyanat (−SCN) sein.
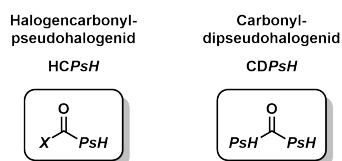
Schema 1.4: Allgemeine Strukturformel von Halogencarbonylpseudohalogeniden und Carbonyldipseudohalogeniden.

Die vorliegende Arbeit legt ihren Fokus auf die Synthese, Eigenschaften und Reaktivität von CD*PsH* und deren Reaktionsprodukte. In den folgenden Abschnitten werden die bisher in der Literatur veröffentlichen Ergebnisse zu den drei genannten Punkten vorgestellt. Der Vollständigkeit halber werden die Synthesen von HC*PsH* vorgestellt, aber Eigenschaften und Reaktivität nicht näher ausgeführt.

1.2 Synthese von Carbonylpseudohalogeniden

1.2.1 Halogencarbonylpseudohalogenide

HC*PsH* können mit der allgemeinen Summenformel C*Ch*(*PsH*)*X* angegeben werden, wobei *Ch* für die Chalkogene O, S, Se, *X* für die Halogene F, Cl, Br, I und *PsH* für die Pseudohalogene CN, NCO, NCS, SCN, N_3 stehen kann. Halogencarbonylisocyanate, (CO(NCO)*X*), sind die bekanntesten Verbindungen. So gibt es einige Synthesen und Reaktionen mit dem Chlorderivat (CO(NCO)Cl).[31–37] Dieses kann durch Photolyse von Chlorisocyanat ClNCO[31,32] (Schema 1.5), Salzmetathese von $COCl_2$ mit KOCN[33] oder partieller Verseifung von CO(NCCl$_2$)Cl mit Methansulfonsäure ($H_3CS(O)_2OH$)[34] erhalten werden. Für CO(NCO)F[33,37–40] und CO(NCO)Br[41] sind ebenfalls Synthesen bekannt, wobei beide beispielsweise ausgehend von CO(NCO)Cl über einen Halogenaustausch mittels Chlorfluorid (ClF)[40] oder Bortribromid (BBr$_3$)[41] darstellbar sind (Schema 1.5). Dahingegen ist CO(NCO)I[42] bisher nur in einer Argon Matrix bei 14 K beobachtet worden.
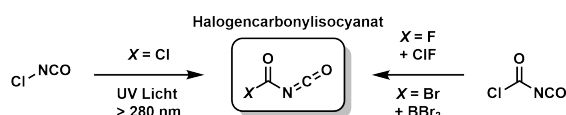
Schema 1.5: Ausgewählte Beispiele für die Synthesen von CO(NCO)*X* Verbindungen.

Von den denkbaren Isothiocyanaten, CO(NCS)*X*, sind Fluor,[33,39,43] Chlor[44,45] und Brom[44] bekannt. CO(NCS)F kann durch Einleiten von Fluorphosgen (COF$_2$) in eine Salzschmelze aus LiCl:KCl bei 400 °C mit gelöstem KSCN erhalten werden (Schema 1.6 oben).[33,39] Für das Chlor- und Bromderivat ist eine Synthese durch Decarbonylierung von *X*(CO)$_2$NCS (*X* = Cl, Br) mit Aktivkohle beschrieben.[44] Zusätzlich sind ausführliche spektroskopische, kristallographische und quantenchemische Untersuchungen sowohl für die Isothiocyanate CO(NCS)*X*, als auch die Thiocyanate CO(SCN)*X* mit jeweils *X* = F, Cl veröffentlicht.[43,45] Das Fluor- und Chlorcarbonylthiocyanat sind ausgehend von CO(SCl)*X* (*X* = F, Cl) durch Zugabe von Silbercyanid (AgCN) synthetisierbar (Schema 1.6 unten).[46,47]
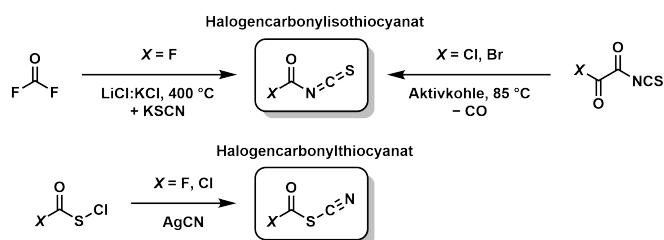
Schema 1.6: Synthesen für Verbindungen der Summenformel CO(NCS)*X* (oben) und CO(SCN)*X* (unten).

Zu HC*PsH* mit Selenocyanat- oder Isoselenocyanatgruppe gibt es ebenso wie zu Verbindungen, in denen *Ch* als Schwefel oder Selen vorliegt, bisher keine bekannten Veröffentlichungen. Allerdings sind Dichtefunktionaltheorie (*Density Functional Theory*, DFT) Rechnungen, die sich unter anderem mit der Umlagerung von $CS(NCO)X$ zu $CO(NCS)X$ ($X =$ Cl, Br) (Schema 1.7 links) beschäftigen, durchgeführt worden. In jedem Fall ist $CO(NCS)X$ das energetisch günstigere Konstitutionsisomer.[48] Mittels DFT und *Natural Bond Orbital* (NBO) Analysen wurde die Stabilität der Verbindungen $CCh(NCO)X$ ($Ch =$ O, S, Se, $X =$ F, Cl, Br) in zwei Konformeren (Schema 1.7 rechts) berechnet. Die Stabilität des *trans* Konformers nimmt von Fluor über Chlor zu Brom zu. Im Fall von Fluor ist *cis* das günstigere Konformer, wohingegen im Fall von Brom *trans* begünstigt ist. Die Energien der *cis* und *trans* Anordnung befinden sich für Chlor nahezu in Waage.[49]
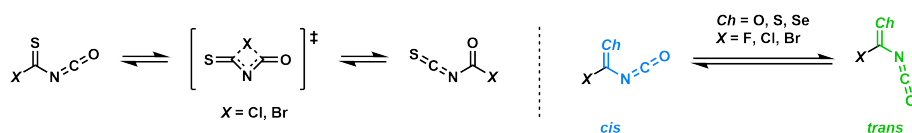
Schema 1.7: Umlagerung von $CS(NCO)X$ zu $CO(NCS)X$ (links) und Konformere von $CCh(NCO)X$ Verbindungen (rechts).

Synthesen der Cyanid Vertreter $CO(CN)X$ mit $X =$ F, Cl, Br sind über die Thermolyse von 2-Halogen-2-(halogenthioimino)acetylhalogenid $CO(CCl(NSCl))X$ (Fluor[50] und Chlor[50,51]) oder Dihalogenfuroxan (Chlor[51,52] und Brom[51,53]) möglich (Schema 1.8). $CO(CN)F$ wurde zudem aus Phosgen, Natriumfluorid (NaF) und Cyanwasserstoff (HCN)[54] oder aus Fluorphosgen und Trimethylsilylcyanid ($(CH_3)_3SiCN$)[39] erhalten. Von den Azid Derivaten ist lediglich $CO(N_3)F$ aus Natriumazid (NaN_3) und Carbonylchloridfluorid (COFCl) isoliert worden.[55,56] Aus DFT Rechnungen geht hervor, dass auch $CO(N_3)Cl$ und $CO(N_3)Br$ stabile Moleküle sein sollten.[57]
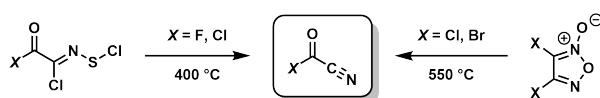
Schema 1.8: Mögliche Synthesewege zu $CO(CN)X$ Verbindungen.

1.2.2 Carbonyldipseudohalogenide

CD*PsH*, in der allgemeinen Schreibweise $CCh(PsH)_2$ mit $Ch =$ O, S, Se und $PsH =$ N_3, CN, NCO, NCS, SCN sind weitaus unbekannter. So sind bis heute ausschließlich sieben Moleküle dieser Art beschrieben. In historischer Reihenfolge angefangen beim Carbonyldiazid ($CO(N_3)_2$), welches erstmals 1894 von CURTIUS und HEIDENREICH aus Car-

bodihydraziniumchlorid (CO(NHNH$_2$)$_2$) und Natriumnitrit (NaNO$_2$) erhalten wurde (Schema 1.9 links).[58] In moderneren Synthesemethoden wird Carbonylchloridfluorid (COClF) und Natriumazid[59] oder Triphosgen und Tetra-*n*-butylammoniumazid (N^{n}Bu$_4$N$_3$) bzw. Natriumazid verwendet.[60]

1937 beschreibt MALACHOWSKI die Isolierung von Carbonyldicyanid (CO(CN)$_2$). Dies wurde aus der Thermolyse von 1,3-Bis(acetoxyimino)aceton (CO(CHNOOCCH$_3$)$_2$) bei 160 °C unter Abspaltung von Essigsäure (CH$_3$COOH) erhalten (Schema 1.9 rechts).[61,62] Zudem entsteht es bei der Reaktion von Tetracyanoethylenoxid ((C(CN)$_2$C(CN)$_2$)O) mit *n*-Butylsulfid (S^{n}Bu$_2$) neben (Dicyanomethylid)dimethylsulfonium ((^{n}Bu)$_2$SC(CN)$_2$)[63,64] oder durch das Einleiten von Fluorphosgen in eine Salzschmelze aus Lithium- und Kaliumchlorid (LiCl:KCl $\stackrel{\wedge}{=}$ 58:42 mol %) bei 400 °C, in der 10 wt% Kaliumcyanid (KCN) gelöst sind.[39]
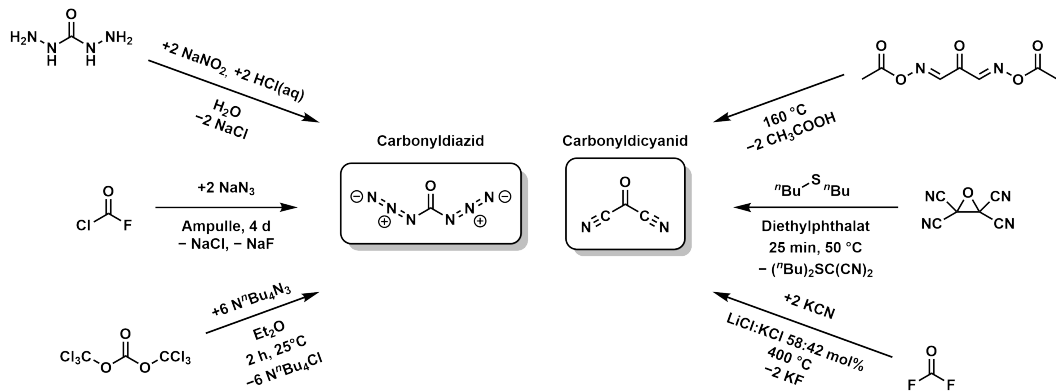
Schema 1.9: Synthesen für die Verbindungen CO(N$_3$)$_2$ (links) und CO(CN)$_2$ (rechts).

Das dritte beschriebene Carbonyldipseudohalogenid ist das Carbonyldiisothiocyanat (CO(NCS)$_2$). Dieses wurde bereits 1902 durch DIXON beschrieben, welcher Phosgen mit Bleithiocyanat (Pb(SCN)$_2$) umsetzte, es aber nicht isolieren konnte (Schema 1.10).[65] Erst in einem Patent aus 1966 geht die erfolgreiche Isolierung bei der Umsetzung von Phosgen mit Trimethylsilylisothiocyanat ((CH$_3$)$_3$SiNCS) hervor.[66] Eine Synthese aus der LiCl:KCl Salzschmelze, analog zum CO(CN)$_2$, mit gelöstem Kaliumthiocyanat (KSCN) (6.5 wt%) ist ebenso möglich.[33] Zuletzt wurde von JOCHIMS die Darstellung aus Phosgen und Ammoniumthiocyanat (NH$_4$SCN) in Tetrahydrofuran (THF) oder Schwefeldioxid (SO$_2$) etabliert.[67,68]
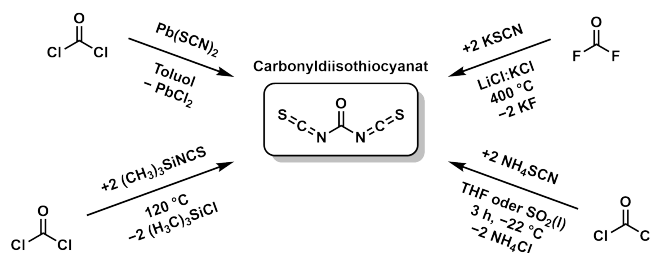
Schema 1.10: Syntheserouten zur Verbindung CO(NCS)$_2$.

Carbonyldiisocyanat (CO(NCO)$_2$) wurde erstmalig 1966 aus der thermischen Zersetzung von Trichlorisocyanursäure ((N(Cl)CO)$_3$) neben hochexplosivem Trichlorstickstof (NCl$_3$) von NACHBAUR erhalten (Schema 1.11).[69] Erneut ist eine Synthese aus der LiCl:KCl Salzschmelze, in der 10 wt% Kaliumcyanat (KOCN) gelöst ist, mit Phosgen oder Fluorphosgen möglich.[33,39] Patentiert wurden zwei Verfahren in denen Carbonyldiisocyanat in einem hochsiedendem Lösungsmittel aus Trichlorisocyanursäure und Chlorcarbonylisocyanat oder Phosgen hergestellt wird.[70,71] Das Verfahren wurde von JOCHIMS auf Labormaßstab angepasst und Trichlorisocyanaursäure durch Tri-*n*-butylzinnisocyanat ((*^{n}*Bu)$_3$SnNCO) ersetzt.[72] Aus Tris(trimethylsilyl)cyanurat ((NC(OSi(CH$_3$)$_3$))$_3$) unter Zugabe von Chlorcabonylisocyanat wurde das formale Trimer des Carbonyldiisocyanats im ersten Schritt erhalten, welches sich im zweiten Schritt thermisch zu diesem spalten lässt.[73] Die neueste Synthese von KLAPÖTKE aus 2016 beruht wiederum auf Trichlorisocyanursäure und dem leichter handhabbaren Diphosgen.[74]
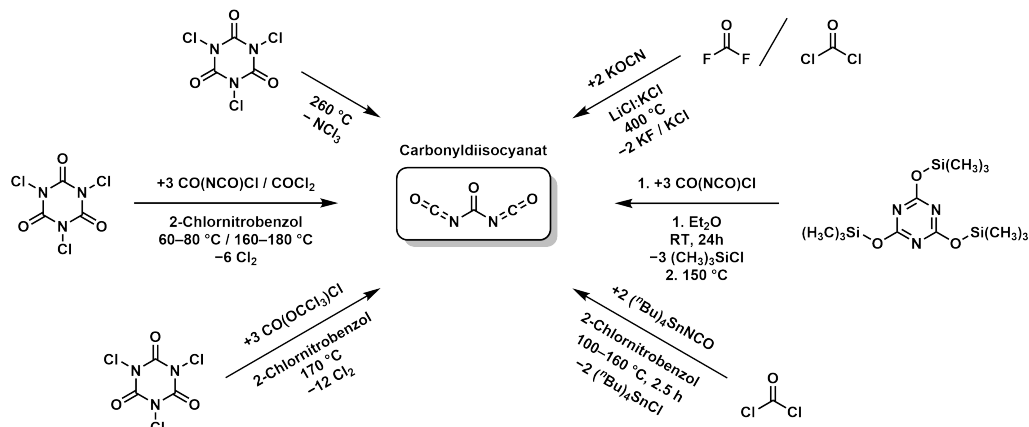
Schema 1.11: Synthesen Zur Darstellung von CO(NCO)$_2$.

Erwähnung finden zudem noch die zwei asymmetrischen CD*PsH* Carbonylazidisocyanat (CO(N$_3$)(NCO)) und Carbonylisocyanatisothiocyanat (CO(NCO)(NCS)). Ersteres entsteht bei der Zersetzung von Oxalyldiazid ((CON$_3$)$_2$) in Lösung[75,76] und Letzteres analog zum CO(NCS)$_2$ aus Chlorcabonylisocyanat und Ammoniumthiocyanat (NH$_4$SCN) in flüssigem Schwefeldioxid[77] (Schema 1.12).
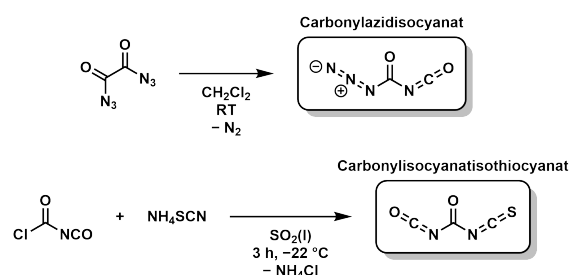
Schema 1.12: Synthesewege zu den asymmetrischen Carbonyldipseudohalogeniden CO(N$_3$)(NCO) und CO(NCO)(NCS).

Zuletzt wurde die Synthese des bisher einzigen Thiocarbonyls dem Thiocarbonyldithiocyanat (CS(SCN)$_2$) von JOCHIMS in 1981 beschrieben.[78] Dieses wird erneut analog zu CO(NCS)$_2$ aus Thiophosgen (CSCl$_2$) und Ammoniumthiocyanat in flüssigem Schwefeldioxid erhalten (Schema 1.13).
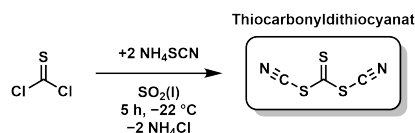
Schema 1.13: Synthese von CS(SCN)$_2$.

1.2.3 Oxalylpseudohalogenide

Neben den Carbonylpseudohalogeniden sind Verbindungen mit zwei Carbonylfunktionen, dem Oxalylgerüst entsprechend, bekannt. Oxalyldipseudohalogenide (OxD*PsH*) (CO*PsH*)$_2$ sind weitaus weniger untersucht. Oxalyldiazid ((CON$_3$)$_2$) ist eine explosive Verbindung, welche durch Umsetzung von Oxalyldihydrazid ((CO(NHNH$_2$))$_2$) in salzsaurer Lösung mit Natriumnitrit erhalten werden kann (Schema 1.14 oben).[75,76,79,80] Die Reaktion von Oxalylchlorid ((COCl)$_2$) mit Silberazid (AgN$_3$) konnte in der Gasphase verwirklicht werden.[81] Es wurde zudem versucht aus Oxalylbromid ((COBr)$_2$) und Natriumazid oder aus Oxalylchlorid und Tri-*n*-butylzinnazid (*n*Bu$_3$SnN$_3$) herzustellen.[76]

Oxalyldicyanid ((COCN)$_2$) wird aus Diiminosuccinonitril ((CNH(CN))$_2$) unter Zugabe von *para*-Toluolsulfonsäure (*p*-CH$_3$(C$_6$H$_4$)SO$_2$OH) gewonnen (Schema 1.14 unten links).[82,83] Zuletzt wurde Oxalyldiisothiocyanat ((CONCS)$_2$) aus Oxalylchlorid und Ammoniumthiocyanat erhalten (Schema 1.14 unten rechts).[44] Eine Synthese zum Diisocyanat ist nicht bekannt, allerdings wurde Chloroxalylisocyanat (Cl(CO)$_2$NCO) aus Oxalylchlorid und Silbercyanat (AgOCN) erhalten.[84]
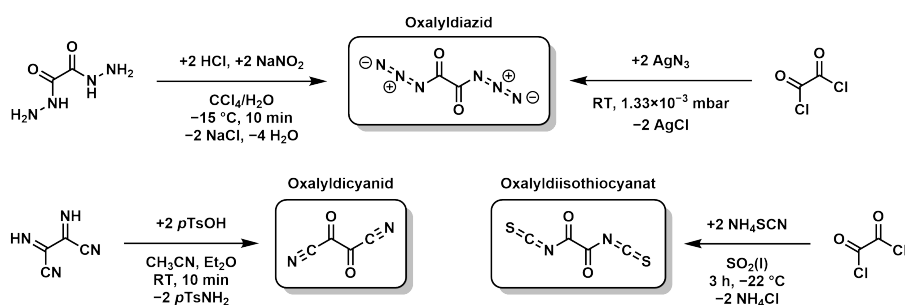
Schema 1.14: Syntheserouten zu den Oxalyldipseudohalogeniden $(CON_3)_2$ (oben), $(COCN)_2$ (unten links) und $(CONCS)_2$ (unten rechts).

1.3 Eigenschaften von Carbonyldipseudohalogeniden

Die physikalischen Eigenschaften von CD*PsH* sind abgesehen von $CO(CN)_2$[62] spärlich untersucht. Bei Raumtemperatur liegen sie alle bis auf $CS(SCN)_2$ als Feststoff in flüssiger Form vor. $CO(N_3)(NCO)$ ist ausschließlich als farblose Flüssigkeit beschrieben.[76] Ihre Schmelzpunkte (Smp.), Siedepunkte (Sdp.) und Zersetzungspunkte (Zsp.) sind in Tabelle 1.1 angegeben. $CO(N_3)_2$ hat im Vergleich zu den restlichen CD*PsH* ($< -25\,°C$) einen relativ hohen Schmelzpunkt mit $16\,°C$. Es hat keinen Siedepunkt, da es zuvor explosiv zerfällt. Die anderen Siedepunkte liegen zwischen $65\,°C$ und oberhalb von $100\,°C$. Die einzige Ausnahme ist $CS(SCN)_2$, welches weder einen Schmelzpunkt, noch Siedepunkt besitzt, da es sich oberhalb von $-20\,°C$ zu zersetzen beginnt.

Tabelle 1.1: Physikalische Eigenschaften von Carbonyldipseudohalogeniden.

Molekül	Farbe	Smp. [°C]	Sdp. [°C]	Zsp. [°C]
$CO(CN)_2$[62]	gelblich	-38	65	$-$
$CO(N_3)_2$[59]	farblos	16	$-$	explosiv
$CO(N_3)(NCO)$[76]	farblos	$-$	$-$	$-$
$CO(NCO)_2$[69,74]	farblos	-57	104	$-$
$CO(NCO)(NCS)$[77]	gelb	$-36 - -35$	$32 - 33^a$	> -18
$CO(NCS)_2$[67]	rosa	$-24 - -23$	$25 - 30^b$	> 22
$CS(SCN)_2$[78]	gelb	$-$	$-$	> -20

a: bei 17.33 mbar, b: bei 0.066 mbar

1.3.1 Kernspinresonanzspektroskopie

CD*PsH* lassen sich mittels ^{13}C-Kernspinresonanz (*Nuclear Magnetic Resonance*, NMR) spektroskopischer Analyse eindeutig identifizieren. So sind die chemischen Verschiebungen der Resonanzsignale molekülspezifisch (Tabelle 1.2). Das Kohlenstoffatom der Carbonylgruppe wird bei 162.6 ppm in $CO(N_3)_2$,[85] bei ungefähr 143 ppm in $CO(NCO)_2$,[74] $CO(NCO)(NCS)$[77] und $CO(NCS)_2$[67] und bei 189.8 ppm in $CS(SCN)_2$[78] detektiert. Die Verschiebungen verdeutlichen nicht nur den Einfluss des Chalkogenatoms, sondern auch des Pseudohalogens auf das Carbonylkohlenstoffatom. Im Vergleich dazu ist das Resonanzsignal von Phosgen bei 141.8 ppm und Thiophosgen bei 169.7 ppm.[86] Die Kohlenstoffatome der Isocyanat- und Isothiocyanatgruppe sind mit ca. 130 ppm und 152 ppm eindeutig unterscheidbar. Auch die chemische Verschiebung der Thiocyanatgruppe ist bei 106 ppm spezifisch. Nicht vollständig charakterisiert ist die ^{15}N-NMR spektroskopische Verschiebung, welche für $CO(NCO)(NCS)$, $CO(NCS)_2$ und $CO(SCN)_2$ noch ausstehend ist. Für $CO(CN)_2$ sind bisher keine ^{13}C-NMR spektroskopischen Daten bekannt.

Tabelle 1.2: ^{13}C- und ^{15}N-NMR spektroskopische Verschiebungen in [ppm] von Carbonyldipseudohalogeniden.

Molekül	C (Carbonyl)	C (Pseudohalogen)	N (Pseudohalogen)
$CO(N_3)_2$[85]	162.6[a]	–	–257.3, –145.5, –137.9[a,d]
$CO(NCO)_2$[74]	144.4[b]	130.2[b]	–302.0[b,d]
$CO(NCO)(NCS)$[77]	143.5[c]	151.9, 130.6[c]	–
$CO(NCS)_2$[67]	142.7[c]	152.4[c]	–
$CS(SCN)_2$[78]	189.8[c]	106.2[c]	–

a: CD_3CN, b: $CDCl_3$, c: CD_2Cl_2, d: CH_3NO_2 externer Standard

1.3.2 Schwingungsspektroskopie

Ausgiebige schwingungsspektroskopische Analysen, Infrarot (IR)- und Raman-Spektroskopie, sind für $CO(CN)_2$,[87,88] $CO(N_3)_2$[59,60] und $CO(NCO)_2$[89] beschrieben. Während für $CO(CN)_2$ nur ein Konformer mit C_{2v} Symmetrie beobachtet werden kann, werden für $CO(N_3)_2$ und $CO(NCO)_2$ je zwei Konformere detektiert. Alle drei Moleküle liegen planar vor. CD*PsH* mit dreiatomigem Pseudohalogenid können allgemein in drei Konformeren existieren: *syn-syn* (C_{2v}), *syn-anti* (C_s) und *anti-anti* (C_{2v}). Diese sind in Schema 1.15 am Beispiel von Carbonyldiisocyanat gegenüber von Carbonyldicyanid illustriert. Dabei wird unter *syn* die Anordnung von C=*Ch* und C−*PsH* auf der selben Seite verstanden, welche

auch als *cis* interpretiert werden kann. Dementsprechend ist unter *anti* eine *trans* Anordnung der C=*Ch* und C−*PsH* Gruppen zu verstehen.
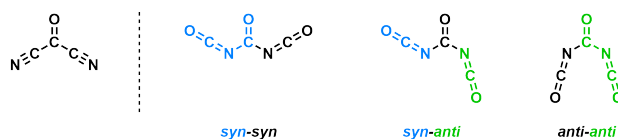
Schema 1.15: Gegenüberstellung der Konformere von Carbonyldipseudohalogeniden am Beispiel von Carbonyldicyanid und Carbonyldiisocyanat.

Anhand der spektroskopischen Daten konnte in Kombination mit Gasphasen-Elektronenbeugung (*Gas-phase Electron Diffraction*, GED) und DFT Rechnungen die Molekülstruktur von $CO(CN)_2$ in der Gasphase aufgeklärt werden.[90] Für $CO(N_3)_2$ wurde ein Gleichgewicht des *syn-syn* und *syn-anti* Konformers in der Gasphase mittels IR, Raman und *Millimeter-Wave* Spektroskopie beobachtet.[59,60,91] Das *syn-syn* Konformer liegt mit einem Anteil 88 % bevorzugt vor.[59] Unterstützt ist dies durch DFT Rechnungen, welche das *syn-syn* Konformer als energetisch günstigstes vorhersagen. Das *anti-anti* Konformer ist energetisch 11 kcal mol^{-1} ungünstiger als *syn-syn* oder *syn-anti* und wird nicht beobachtet.[60,91] Gleiche Ergebnisse sind für $CO(NCO)_2$ ermittelt worden. Es liegt ebenfalls ein Gleichgewicht aus *syn-syn* und *syn-anti* Konformer in der gasförmigen und flüssigen Phase vor.[89] Mittels IR-Spektroskopie wird ein *syn-syn* zu *syn-anti* Verhältnis von 62:38 %[92] und mittels GED eine Bevorzugung von *syn-syn* mit 66(3) %[74] angegeben. DFT Berechnungen ergeben erneut *syn-syn* als stabilstes Konformer,[74,92] wohingegen *anti-anti* kein echtes Minimum auf der Potentialhyperfläche ist.[74] Die Verbindungen $CO(NCO)(NCS)$, $CO(NCS)_2$ und $CS(SCN)_2$ lassen ausführliche schwingungsspektroskopische Analysen missen.

1.3.3 Molekülstrukturen im Festkörper

Die Molekülstrukturen im Festkörper sind bisher nur von $CO(N_3)_2$[59] und $CO(NCO)_2$[74] bestimmt worden. Beide Moleküle kristallisieren in ihrem *syn-syn* Konformer (Abbildung 1.1). Sie kristallisieren isotyp in der orthorhombischen Raumgruppe *Pnma* mit je einem Molekül in der asymmetrischen Einheit und vier Molekülen in der Elementarzelle. Die Gitterparameter sind a = 5.431(2) Å, b = 5.797(2) Å, c = 13.800(4) Å und V = 434.47(25) Å^3 für $CO(N_3)_2$ und a = 5.4789(2) Å, b = 5.5658(2) Å, c = 14.0998(5) Å und V = 429.73(3) Å^3 für $CO(NCO)_2$.
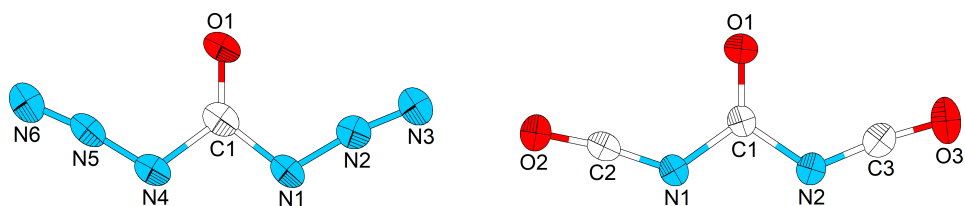
Abbildung 1.1: Molekülstruktur im Festkörper von Carbonyldiazid[59] (links) und Carbonyldiisocyanat[74] (rechts). Ellipsoide sind mit einer Aufenthaltswahrscheinlichkeit von 75 % dargestellt.

Die Bindungslängen der Molekülstrukturen unterstützen die Strukturformeln (Tabelle 1.3). Die Bindungslänge der Carbonylgruppe (C=O) entspricht mit 1.20 Å einer Doppelbindung, wohingegen die Kohlenstoff-Stickstoff-Bindungen (C−N) mit 1.40 Å Einfachbindungen sind. Innerhalb der Pseudohalogenidgruppen (N=N=N und N=C=O) spiegeln die Bindungslängen von 1.23 Å und 1.11 Å bzw. 1.15 Å ein kumuliertes Doppelbindungssystem wieder.

Tabelle 1.3: Bindungslängen der Molekülstrukturen im Festkörper von Carbonyldiazid, Carbonyldiisocyanat und Oxalyldiazid in [Å].

Molekül	C=O	C−N	N=E_1	E_1=E_2
$CO(N_3)_2$,[59]a	1.2005(65)	1.4064(69)	1.2747(68)	1.1112(70)
		1.4117(66)	1.2653(59)	1.1117(69)
$CO(NCO)_2$,[74]b	1.2016(12)	1.3919(12)	1.2268(13)	1.1496(12)
		1.3994(13)	1.2262(13)	1.1505(13)
$(CON_3)_2$,[80]a	1.1932(35)	1.3996(28)	1.2638(28)	1.1127(28)
	1.2056(28)	1.3960(33)	1.2645(29)	1.1157(30)

a: E_1=E_2=N, b: E_1=C, E_2=O

1.3.4 Oxalyldipseudohalogenide

$(CON_3)_2$ ist ein farbloser Feststoff, welcher bei Berührung explodiert.[75,80] Er schmilzt bei 45 °C und zersetzt sich bei 46 °C explosionsartig. Im ^{13}C-NMR-Spektrum wird ein Resonanzsignal bei 163.9 ppm und im ^{15}N-NMR-Spektrum drei Signale bei −130.9 ppm, −146.6 ppm und −252.4 ppm detektiert.[80] Es kristallisiert in der monoklinen Raumgruppe $P2_1/c$ mit zwei unabhängigen Molekülen in der asymmetrischen Einheit und vier pro Elementarzelle.[80] Dabei liegt es in seinem stabilsten Konformer mit den C=O Gruppen in *trans* Anordnung zueinander und den Azid-Gruppen in *cis* Position zu C=O vor (Abbildung 1.2).[81] Die Bindungslängen der Molekülstruktur (Tabelle 1.3) sind innerhalb der 3σ Standardabweichung identisch zu $CO(N_3)_2$.
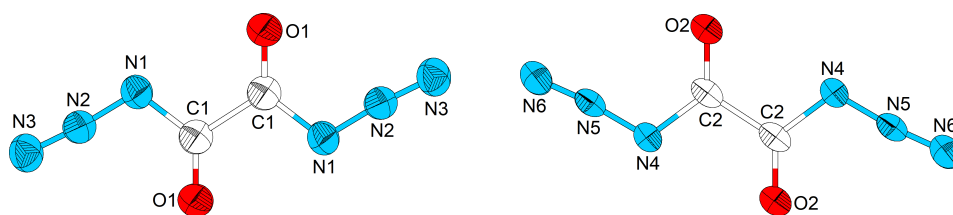
Abbildung 1.2: Molekülstruktur im Festkörper von Oxalyldiazid.[80] Ellipsoide sind mit einer Aufenthaltswahrscheinlichkeit von 75 % dargestellt.

$(COCN)_2$ ist ein orangener Feststoff mit einem Schmelzpunkt von 62 °C.[83] Es sind keine weiteren physikalischen, NMR spektroskopischen oder röntgendiffraktometrischen Daten bekannt.

$(CONCS)_2$ ist ein farbloser Feststoff mit einem Schmelzpunkt von 90 °C, welcher sich bei Raumtemperatur langsam zersetzt. Ein exothermer Zersetzungspunkt ist bei 95 °C zu beobachten. Im ^{13}C-NMR-Spektrum liegt die chemische Verschiebung von *C*O bei 156.6 ppm und von N*C*S bei 154.5 ppm.[44] Eine Molekülstruktur im Festkörper wurde bisher nicht bestimmt.

1.4 Reaktivität von Carbonyldipseudohalogeniden

1.4.1 Carbonyldiazid

Zur Reaktivität von Carbonyldiazid ist wenig bekannt. So wurde es zum erstmaligen, indirekten Nachweis mit Anilin zu Diphenylharnstoff umgesetzt (Schema 1.16).[58] In Autoklavenversuchen wurde es zusammen mit aromatischen Kohlenwasserstoffen unter der Einwirkung von Wasser zu Anilin-Derivaten umgesetzt. Die Reaktion verläuft unter Abspaltung von Stickstoff und intermediär entstehenden Harnstoffen, welche mit Wasser zu den Anilinen und Kohlenstoffdioxid abreagieren.[93] Mit einem Äquivalent nukleophilem Alkohol reagiert $CO(N_3)_2$ zu Azidoformiaten.[94]
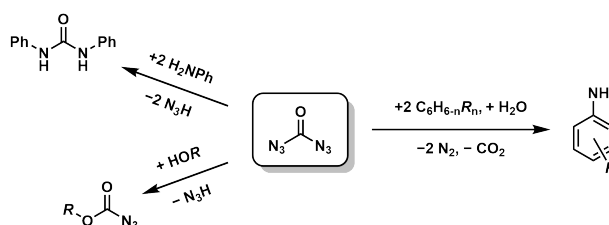
Schema 1.16: Reaktivitäten von $CO(N_3)_2$ gegenüber Nukleophilen.

Dahingegen ist der Zerfall von $CO(N_3)_2$ genauer untersucht (Schema 1.17). Es zersetzt sich explosiv bei Berührung oder ohne erkennbaren Grund zu Kohlenstoffmonoxid und Stickstoff.[58–60] In einer Argon-Matrix zersetzt es sich photolytisch unter Bestrahlung mit

Ultraviolett (UV)-Licht zu Azidocarbonylnitren (CO(N$_3$)N). Beim Bestrahlen mit sichtbarem Licht isomerisiert dieses zu Azidoisocyanat (N$_3$NCO), welches sich wiederum unter UV-Licht zu Kohlenstoffmonoxid und Stickstoff zersetzt.[95,96] CO(N$_3$)$_3$ lässt sich thermisch bei 400 °C unter vermindertem Druck in Diazirinon (CO(N$_2$)), welches ein vergleichsweise stabiles Gas (t$_{1/2}$ = 30 h[97]) ist, zersetzen. Bei Bestrahlung in einer Argon-Matrix zersetzt es sich entweder mit sichtbarem Licht zu Kohlenstoffmonoxid und Stickstoff, oder isomerisiert mit dem Licht eines ArF-Lasers zu Cyanoiminoxonium (NOCN), Nitrosylisocyanid (ONNC) und Nitrosylcyanid (ONCN).[96–99]
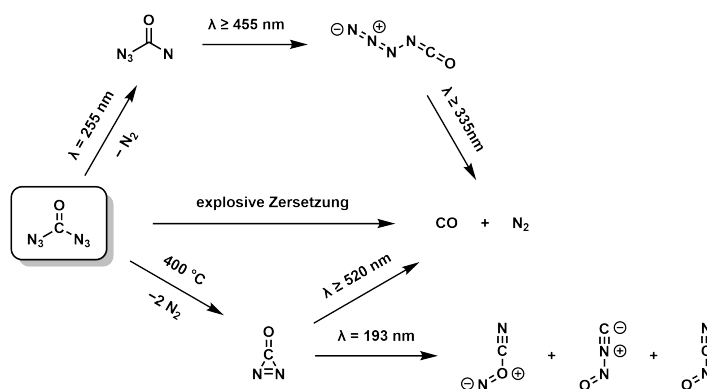
Schema 1.17: Photolytische und thermische Zersetzung von CO(N$_3$)$_2$.

1.4.2 Carbonyldicyanid

Carbonyldicyanid reagiert mit Wasser explosionsartig zu Cyanwasserstoff und Kohlensäure.[61] Mit je einem Äquivalent Alkohol,[61,100] Amin[101–104] oder Thiol[105] werden unter Abspaltung von Cyanwasserstoff Cyanformiate, Cyanformamide oder Cyanthiolester erhalten (Schema 1.18). Bei letzteren wurden zusätzlich die als Zwischenstufe entstehenden Dicyanohydrine beobachtet.[105] Aus substituierten Phenolen können säurekatalysiert unter Abspaltung von Wasser entsprechend substituierte Derivate des Malonitrils erzeugt werden.[106,107] Substituierte Dicyanohydrine entstehen ebenfalls bei der Reaktion mit C−H aciden 1,3-Dicarbonylen.[108] CO(CN)$_2$ reagiert mit Dienen in einer [4+2]-Cycloaddition zu substituierten Dicyandihydropyranen.[109,110] Mit Alkenen verläuft eine En-Reaktion erneut zu Dicyanohydrinen, welche mit einem zweiten Molekül Carbonyldicyanid unter Verlust von Cyanwasserstoff zu Malonitril-Derivaten reagieren.[109,111] Beide Cyanidgruppen setzen sich mit dem Dithionitronium-Kation ([SNS]$^+$) unter doppelter Cycloaddition zu einem Carbonylbis(dithiadiazol-1-ium)-Dikation mit [SbF$_6$]$^-$ als Gegenion um.[112]
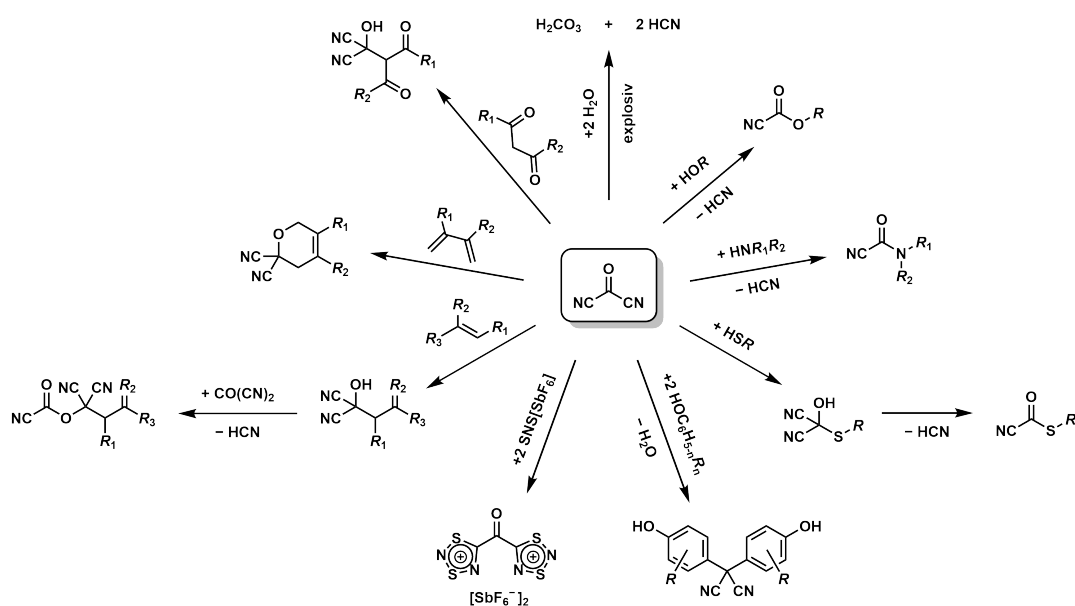
Schema 1.18: Reaktivitäten von CO(CN)$_2$ gegenüber Nukleophilen und Doppelbindungen.

CO(CN)$_2$ lässt sich photolytisch mit Licht eines ArF-Lasers spalten (Schema 1.19). In der Gasphase entstehen vorwiegend die Radikale CN$^\bullet$ und NCCO$^\bullet$, von welchem letzteres sich weiter zu CN$^\bullet$ und Kohlenstoffmonoxid zersetzt. In einem geringeren Anteil entstehen Dicyan ((CN)$_2$) und Kohlenstoffmonoxid.[113–117] Bei Bestrahlung in einer Argon-Matrix kann in geringem Maße eine Isomerisierung zum (CO(CN)(NC)) stattfinden. CO(CN)(NC) und CO(CN)$_2$ spalten sich bei weiteren Laserpulsen zu Isocyanogen (NCNC), Dicyan und Kohlenstoffmonoxid.[118]
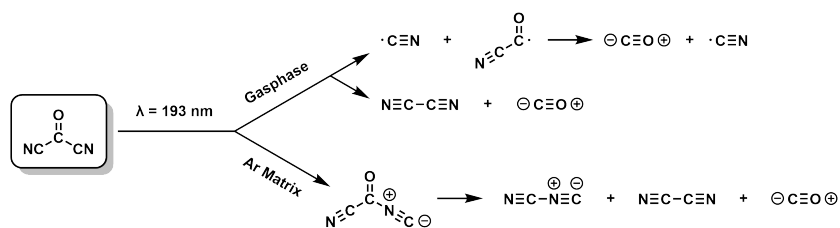
Schema 1.19: Photolytische Zersetzung von CO(CN)$_2$ in der Gasphase und Argon-Matrix.

Bisher ist nur eine einzige Komplexverbindung mit CD*PsH* als Ligand bekannt. Diese konnte ausgehend von Carbonyldicyanid erhalten werden. Aus flüssigem Schwefeldioxid wurde mit AgSbF$_6$ [Ag{NCC(O)CN}$_2$]$_n$[SbF$_6$]$_n$ isoliert. Das Kation bestehend aus einem Silberion, welches von vier CO(CN)$_2$ Molekülen über Stickstoff koordiniert (Abbildung 1.3 links) wird, bildet so verbrückt zu vier weiteren Kationen ein 2D polymeres Netzwerk. Es bilden sich rautenförmige Lücken in denen die [SbF$_6$]$^-$ Anionen eingelagert sind (Abbildung 1.3 rechts) und so über zwei Fluoratome die oktaedrische Koordinationssphäre des Silberions absättigen.
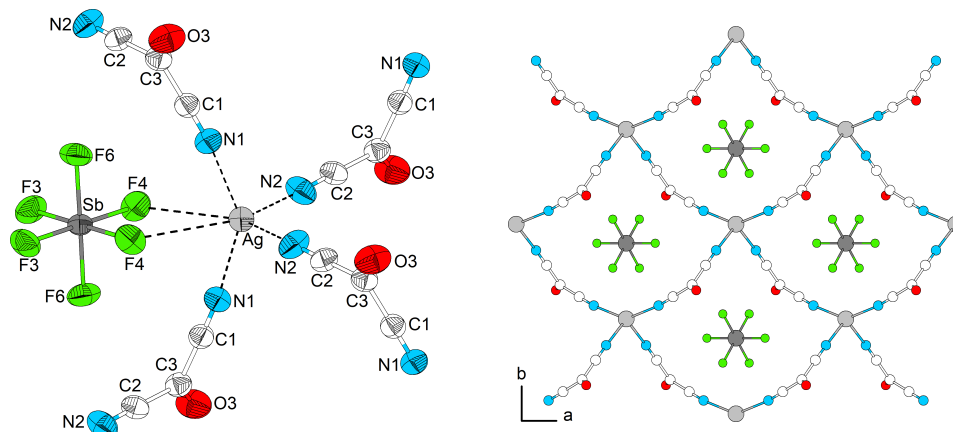
Abbildung 1.3: Molekülstruktur im Festkörper von [Ag{NCC(O)CN}$_2$]$_n$[SbF$_6$]$_n$. Koordinationsspähre von Silber (links) und polymeres 2D Netzwerk (rechts). Ellipsoide sind mit einer Aufenthaltswahrscheinlichkeit von 50 % dargestellt.

1.4.3 Carbonyldiisocyanat

Carbonyldiisocyanat trimerisiert bei Raumtemperatur über einen längeren Zeitraum zu einem Triazin-Derivat (Schema 1.20). Dieses ist ein farbloser Feststoff, welcher schlecht löslich in organischen Lösungsmitteln ist, aber dennoch mittels ^{13}C-NMR-Spektroskopie nachgewiesen werden konnte. Unter Hitzezufuhr kann das Trimer zurück in das Monomer, CO(NCO)$_2$, überführt werden. In Gegenwart von Wasser oder Methanol zersetzt sich das Trimer zur Isocyanursäure ((NHCO)$_3$).[72]
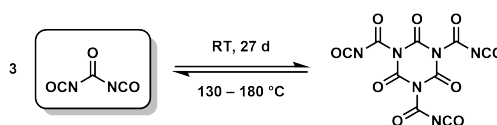
Schema 1.20: Reversible Trimerisierung von CO(NCO)$_2$ bei Raumtemperatur.

CO(NCO)$_2$ ist gegenüber Nukleophilen besonders reaktiv. Mit Wasser und Schwefelwasserstoff reagiert es jeweils unter Ringschluss zum Oxadiazin bzw. zum Thiadiazin (Schema 1.21).[69,72] Durch Reaktion mit Ammoniak bildet sich Triuret.[69] Nukleophile wie Alkohole, Thiole, Amine und Halogenwasserstoffe werden zweifach addiert zu *N,N'*-Carbonylbis(carbamaten), *N,N'*-Carbonylbis(*S*-thiocarbamaten), *N,N'*-Bis(carbamoyl)harnstoffen und Carbonylbis(carbamoylhalogeniden).[72,119,120] *N*-unsubstituierte Imine formen *N,N'*-Bis(alkyliden)harnstoffe. Durch die Addition von Carbonsäuren ist die Bildung von pentacarbonyl Verbindungen möglich.[72] Gleiches gilt für die Reaktion mit zwei Äquivalenten

eines Carboxamides, wohingegen mit einem Äquivalent ein Oxadiazin gebildet wird. Dieses unterliegt im Falle einer weiteren N−H Funktionalität einer Dimroth-Umlagerung zur einfach substituierten Isocyanursäure.[119]
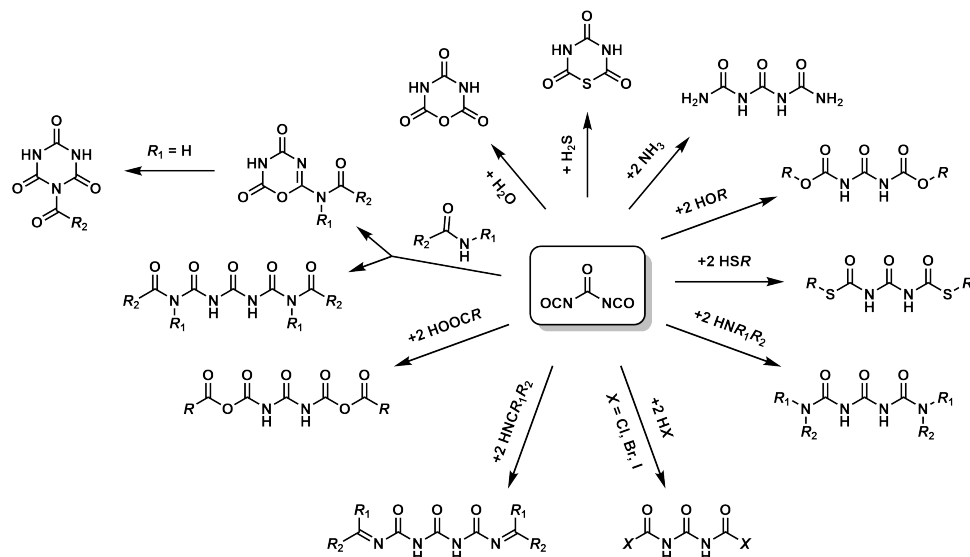
Schema 1.21: Reaktivität von CO(NCO)$_2$ gegenüber Nukleophilen.

Neben nukleophilen Additionen kann CO(NCO)$_2$ auch Cycloadditionen mit polarisierten Mehrfachbindungen (*A*=*E*) eingehen (Schema 1.22). Dies führt zu einer doppelten [2+4]-Cycloaddition und der Bildung von Heterodecalinen. Eine Cycloaddition mit einer O=C Doppelbindung ist nur mit Cyclohexanon beschrieben.[121,122] Aus Cyanamiden (N≡C−N) ist ausschließlich mit Dimethylcyanamid ein Heterocyclus erhalten worden. Andere Dialkylcyanamide führen zur Bildung von Produktmischungen. Mit Iminen (N=C), organischen Isocyanaten (N=C=O) und Carbodiimiden (N=C=N) kann ein Reihe an unterschiedlichen Heterocyclen synthetisiert werden. Bei Umsetzung mit Enaminen (N=C=C) kommt es zu heftigen, unkontrollierbaren Reaktionen.[122]
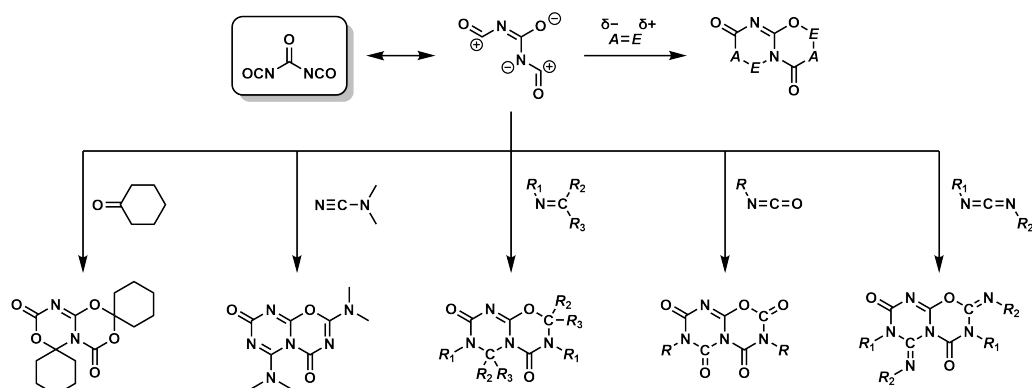
Schema 1.22: Reaktivität von CO(NCS)$_2$ gegenüber polarisierten Mehrfachbindungen.

Photolytisch zersetzt sich $CO(NCO)_2$ in einer Argon-Matrix durch das Licht eines ArF-Lasers unter Abspaltung von Kohlenstoffmonoxid zu Isocyanatcarbonylnitren $(CO(NCO)N)$ (Schema 1.23). Bei weiterer Bestrahlung mit sichtbarem Licht isomerisiert es mittels einer Curtius-Umlagerung zum Diisocyanat $((NCO)_2)$, welches wiederum mit Laserimpulsen unter erneuter Abspaltung von Kohlenstoffmonoxid zu NOCN umlagert.[92]
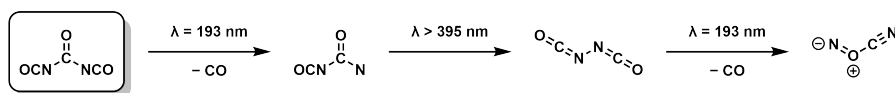
Schema 1.23: Photolytische Zersetzung von $CO(NCO)_2$.

1.4.4 Carbonylisocyanatisothiocyanat

$CO(NCO)(NCS)$ reagiert mit Wasser, Schwefelwasserstoff und Chlorwasserstof unter Ringschluss zu Thiadiazinen (Schema 1.24). Mit alkoholischen Nukleophilen reagiert es ähnlich zu $CO(NCO)_2$ unter Addition. Es addiert zwei Moleküle Alkohol und formt *N,N'*-Carbonylcarbamat-*O*-thiocarbamate. Mit *tert*-Butanol kommt es unter Abspaltung von Thiocyanursäure zur Bildung von Di-*tert*-butyliminocarbonat. Ebenfalls unter Abspaltung von Thiocyanursäure führt die Umsetzung mit Aminen zu Derivaten des Biurets. Eine Ausnahme bilden Reaktionen mit Anilin. Wird $CO(NCO)(NCO)$ zuerst mit einem Äquivalent Alkohol oder Amin und anschließend mit Anilin umgesetzt, bilden sich in beiden Fällen Monothiotriuret ähnliche Strukturen. In flüssigem Chlor reagiert es zu Carbonylisocyanatisocyaniddichlorid, $CO(NCO)(NCCl_2)$.[77]
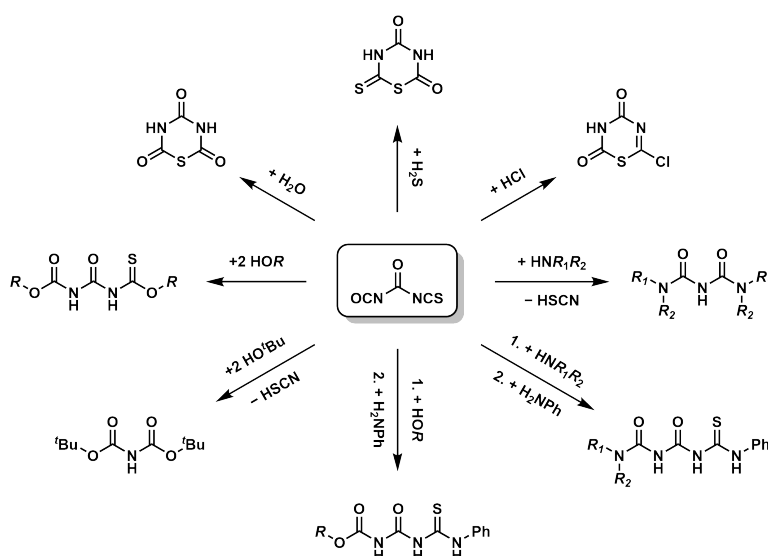
Schema 1.24: Reaktivität von $CO(NCO)(NCS)$ gegenüber Nukleophilen.

1.4.5 Carbonyldiisothiocyanat

Carbonyldiisothiocyanat reagiert mit Nukleophilen fast ausschließlich zu 1,3,5-Thiadiazin-Derivaten (Schema 1.25). Es verläuft immer eine einfache nukleophile Addition unter Ringschluss bei Umsetzung mit Wasser, Schwefelwasserstoff, Chlorwasserstoff, Alkoholen, Thiolen oder Aminen. Bei den Thiadiazin-Amino-Derivaten öffnet sich unter Zugabe von Anilin der Ring zur Bildung von *N,N'*-Bis(thiocarbamoyl)harnstoffen. Durch Reaktion mit Ammoniak wird Ammoniumthiocyanat abgespalten und Monothiobiuret gebildet. Die Reaktion mit flüssigem Chlor bewirkt die Bildung von Carbonyldiisocyaniddichlorid.[67,68]
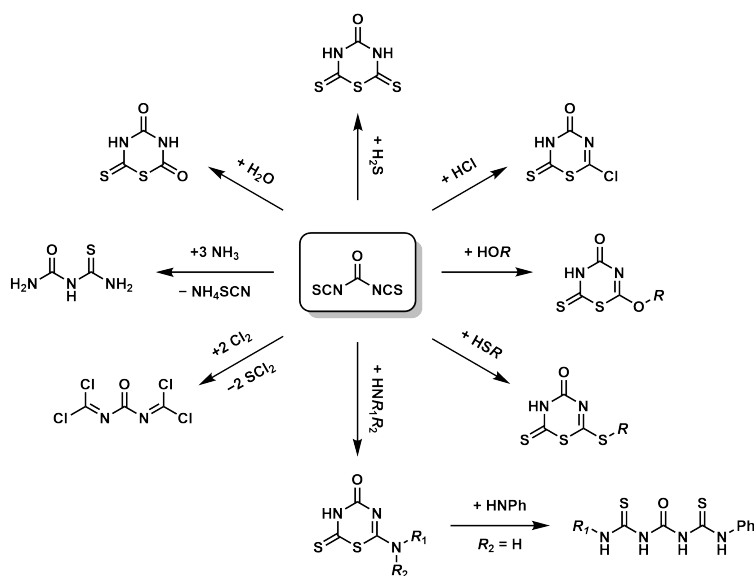
Schema 1.25: Reaktivität von $CO(NCS)_2$ gegenüber Nukleophilen.

1.4.6 Thiocarbonyldithiocyanat

Die Reaktivität von Thiocarbonyldithiocyanat ist am wenigsten untersucht. Es reagiert mit Alkoholen zu Thioimidodikohlensäure-*O,O*-estern, wobei Thiocyanursäure freigesetzt wird (Schema 1.26). Dabei findet eine Umlagerung statt, deren Mechanismus ungeklärt bleibt. Mit primären und sekundären Aminen zersetzt es sich zu undefinierten Produkten. Einzig mit *N*-Benzylanilin konnte ein Thiadiazin gewonnen werden. Mit Chlorgas wird die Thiocarbonylgruppe chloriert und ein Sulfenylchlorid ($CCl(SCl)(SCN)_2$) erzeugt, welches unter Abspaltung von Schwefeldichlorid weiter zu Dichlordithiocyanatmethan ($CCl_2(SCN)_2$) reagiert. Anhand von Thermoanalysen und IR-Spektroskopie in Lösung wird vermutet, dass $CS(SCN)_2$ zu den Isothiocyanaten $CS(SCN)(NCS)$ und $CS(NCS)_2$ isomerisiert.[78]
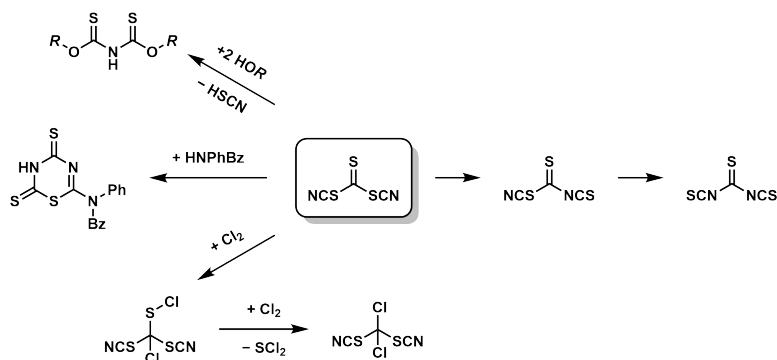
Schema 1.26: Reaktivität von CS(SCN)$_2$ gegenüber Nukleophilen.

1.4.7 Oxalyldipseudohalogenide

Die Reaktivität von OxD*PsH* ist spärlich untersucht. Oxalyldiazid zersetzt sich schnell in Wasser und protischen Lösungsmitteln.[80,123] Oxalyldiisothiocyanat reagiert mit Anilin zum *N*,*N*'-Diphenyloxamid unter Abspaltung von Thiocyanursäure (Schema 1.27).[44] Oxalyldicyanid reagiert mit Phenylhydrazin zum 1-*N*',2-*N*'-Diphenyloxalhydrazid.[83] Reaktionen, die einen Ringschluss zur Folge haben, sind zum einen mit 1,2-Diaminobenzol, welches zu 2,3-Dihydroxychinoxalin reagiert,[83] und zum anderen mit Diiminosuccinonitril, welches unselektiv zu drei Pyrazin-Derivaten führt,[124] möglich.
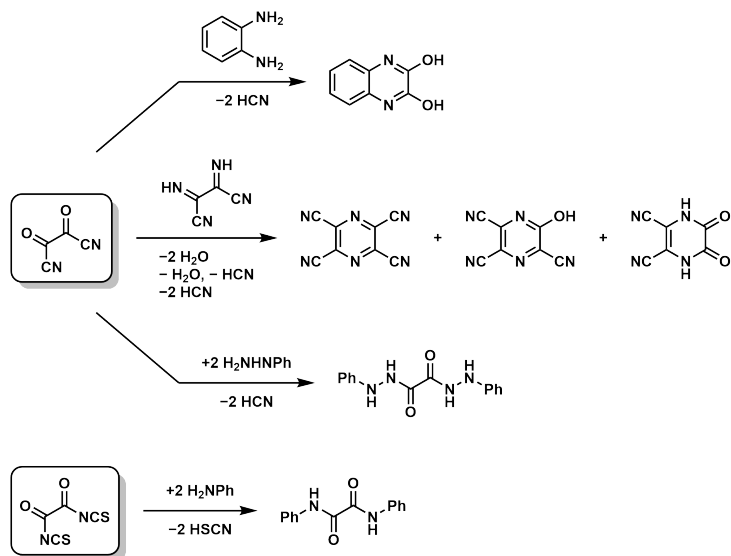
Schema 1.27: Reaktivitäten von (COCN)$_2$ und (CONCS)$_2$ gegenüber Nukleophilen.

2 Motivation und Zielsetzung

Das Ziel dieser Promotion soll die Synthese und Charakterisierung von neuen und bekannten Carbonyldipseudohalogeniden (CD*PsH*) sein. Hierbei soll das Augenmerk vorrangig auf den höheren Homologen des Carbonyldiisocyanats liegen. Die denkbaren Homologen sind in Schema 2.1 für die Sauerstoff, Schwefel und Selen Analoga gezeigt. Die Homologen mit Tellur sind ausgegraut dargestellt, da die Synthesen dieser sehr herausfordernd sein sollten. Einerseits ist die Kohlenstoff-Tellur Bindung schwach und andererseits sind selbst anorganische Tellurocyanate schwer handhabbar.[125,126] Aus diesen neun Homologen sind bereits Carbonyldiisocyanat und Carbonyldiisothiocyanat (Abschnitt 1.2.2) bekannt.
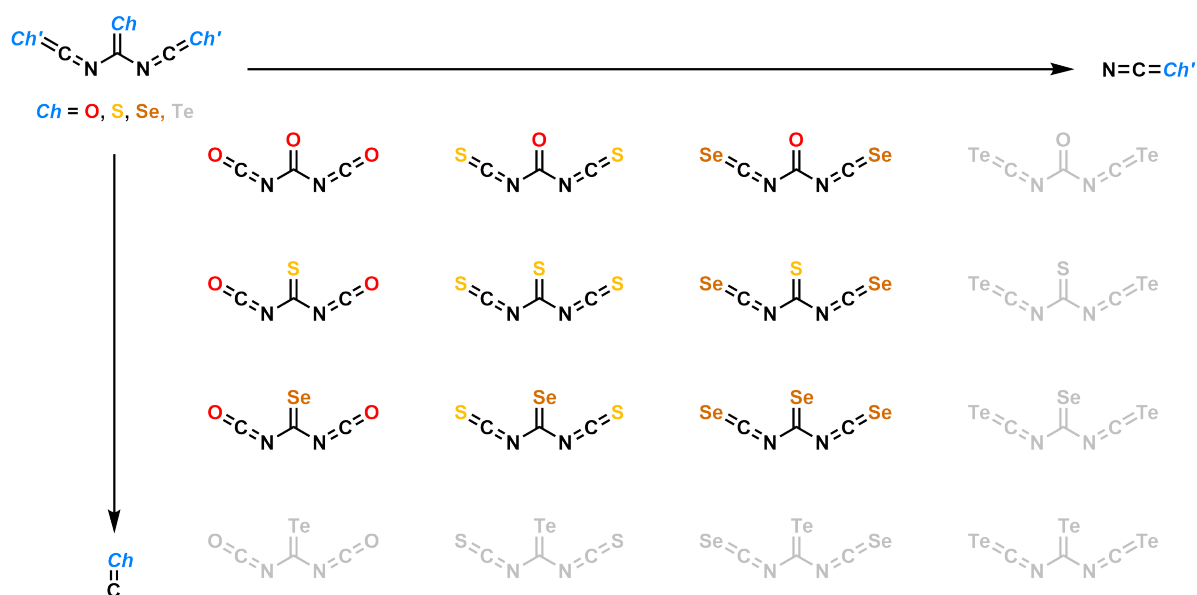
Schema 2.1: Theoretisch denkbare höhere Homologe von Carbonyldiisocyanat (oben rechts).

Die Synthesen von $CO(NCO)_2$ und $CO(NCS)_2$ (Abschnitt 1.2.2) sollen zunächst reproduziert und im Anschluss auf die Synthese neuer CD*PsH* übertragen werden. Hierbei sollen vorrangig die ersten beiden Reihen (Schema 2.1) bearbeitet werden, da für diese bereits mögliche Ausgangsverbindungen bekannt, kommerziell erhältlich und lagerstabil sind. Für das C=O und C=S Motiv sind z.B. Phosgen und Thiophosgen und für die Motive N=C=O, N=C=S und N=C=Se z.B. AgOCN, NH_4SCN oder KSeCN potentielle Chemikalien. Das C=Se Motiv kann etwa über Selenocarbonyldifluorid $CSeF_2$, welches zuvor frisch hergestellt werden muss,[127–129] eingeführt werden. Thiocarbonyldiisocyanat ($CS(NCO)_2$) könnte aus Thiophosgen und Trichlorisocyanursäure (*Trichloroisocyanuric-*

acid), TCCA) (Schema 2.2) analog zur Synthese von CO(NCO)$_2$ erhalten werden. Carbonyldiisoselenocyanat (CO(NCSe)$_2$) und Thiocarbonyldiisoselenocyanat (CS(NCSe)$_2$) wären potentiell durch eine Salzmetathese von Kaliumselenocyanat (KSeCN) aus Phosgen oder Thiophosgen darstellbar. Thiocarbonyldiisothiocyanat (CS(NCS)$_2$) könnte ebenfalls aus Thiophosgen und einem thiophilen Metallsalz wie Silberthiocyanat (AgSCN) oder mit Trimethylsilylisothiocyanat ((CH$_3$)$_3$SiNCS) analog der Synthesen von CO(NCS)$_2$ synthetisierbar sein.
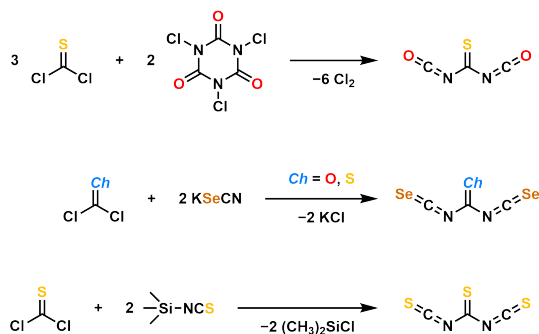
Schema 2.2: Mögliche Zugangswege zu den höheren Homologen von Carbonyldiisocyanat basierend auf den bereits bekannten Synthesen von CO(NCO)$_2$ und CO(NCS)$_2$.

Im Zuge der Reproduktion der Synthese von CO(NCS)$_2$ und auch (CONCS)$_2$ sollen die Molekülstrukturen im Festkörper, sowie IR und Raman spektroskopischen Daten genauer untersucht und Lücken in der Literatur geschlossen werden. Analytische Daten von neu synthetisierten CD*PsH* sollen stets vollständig ermittelt werden. Dies inkludiert NMR-, IR- und Raman-Spektroskopie, Massenspektrometrie (MS), Einkristallstrukturanalyse (*Single Crystal X-ray Diffraction*, SC-XRD) und ggf. Röntgenpulverdiffraktometrie (*Powder X-ray Diffraction*, PXRD), sowie Elementaranalyse. Quantenchemische Rechnungen nach der DFT Methodik sollen dabei die analytischen Daten unterstützen.

Obwohl die Reaktivität von CO(NCO)$_2$ (Abschnitt 1.4.3) und CO(NCS)$_2$ (Abschnitt 1.4.5) ausführlich untersucht ist, sind die analytischen Daten der Reaktionsprodukte oft unvollständig. Insbesondere sind über die Molekülstrukturen im Festkörper bis heute keine Berichte veröffentlicht. Sowohl die tricarbonyl-haltigen Moleküle, welche aus CO(NCO)$_2$ erhalten werden, als auch die Thiadiazin-Ringe, welche aus CO(NCS)$_2$ entstehen, sollen nach Literaturvorschriften synthetisiert und nach zuvor genannten Methoden analysiert werden. Insbesondere sollen sie zur Kristallstrukturbestimmung, um das Verständnis biologisch relevanter Moleküle im Festkörper zu erweitern und mögliche Trends aufzudecken, kristallisiert werden.

3 Kumulativer Teil

Die vorliegende Dissertation besteht aus zwei Teilen: kumulativ und monographisch. Der Hauptteil dieser Arbeit besteht aus einem kumulativem Kapitel, welches die Ergebnisse aus Veröffentlichungen zusammenfasst (Kapitel 3). Es beinhaltet insgesamt sechs Publikationen mit Erstautorenschaft. Es folgt ein monographisches Kapitel mit bisher unveröffentlichten Ergebnissen, welche die Ergebnisse der Arbeit komplettieren (Kapitel 4).

Die Gesamtheit der Dissertation umfasst vorrangig die Synthese von Carbonyldiisocyanat und dessen höheren Homologen, sowie darauffolgende Untersuchungen zur Reaktivität. In diesem Kapitel wird zunächst auf die Synthese und spektroskopische Untersuchung von Carbonyldiisothiocyanat und Oxalyldiisothiocyanat eingegangen (Abschnitt 3.1 und Abschnitte 3.2 bis 3.3). Darauffolgend wird die Reaktivität von Carbonyldiisocyanat und Carbonyldiisothiocyanat gegenüber Nukleophilen näher erläutert, sowie die Produkte dieser Reaktionen kristallographisch untersucht (Abschnitte 3.4 bis 3.6). Zuletzt wird die Synthese, Charakterisierung und Reaktivität von Thiocarbonyldithiocyanat vorgestellt (Abschnitt 3.7).

3.1 A Crystallographic, Spectroscopic, and Computational Investigation of Carbonyl and Oxalyl Diisothiocyanate

J. Pfeiffer, C. Trost, A. Pachkovska, F. Tambornino, *Inorg. Chem.* **2021**, *60*, 10722-10728.

3.2 Rotational Conformers and Nuclear Spin Isomers of Carbonyl Diisothiocyanate

E. Gougoula, J. Pfeiffer, F. Tambornino, M. Schnell, *submitted.*

3.3 Photolytic Decarbonylation of Oxalyl Diisothiocyanate in Solid Argon Matrices to *syn-anti* Carbonyl Diisothiocyanate and Its Isomerization

Inside Cover Feature: J. Pfeiffer, J. P. Wagner, F. Tambornino, *Eur. J. Inorg. Chem.* **2023**, *26*, e202300290.

3.4 Double Addition *vs.* Ring Closure: Systematic Reactivity Study of CO(NCO)$_2$ and CO(NCS)$_2$ towards Hydrogen Halides

Inside Cover Feature: J. Pfeiffer, H. Günther, L. Völlinger, D. Botros, B. Scheibe, M. Möbs, F. Kraus, F. Weigend, F. Tambornino, *Chem. Eur. J.* **2023**, *29*, e202203983.

3.5 Intra- and Intermolecular Hydrogen Bonding in *N,N'*-Carbonyl bis(carbamates), -(*S*-thiocarbamates) and *N,N'*-biscarbamoyl ureas

J. Pfeiffer, M. Möbs, S. Reith, M. Tallu, F. Tambornino, *J. Mol. Struct.* **2024**, *1309*, 138198.

3.6 Synthesis, Crystal Structure Study and Spectroscopic Analysis of Substituted 2,3-dihydro-2-thioxo-4*H*-1,3,5-thiadiazin-4-ones

J. Pfeiffer, C. Trost, F. Tambornino, *J. Mol. Struct.* **2024**, *1308*, 138079.

3.7 Thiocarbonyl pseudohalides – the curious case of thiocarbonyl dithiocyanate

J. Pfeiffer, H. Günther, P. Fuzon, F. Weigend, F. Tambornino, *submitted*.

3.1 A Crystallographic, Spectroscopic, and Computational Investigation of Carbonyl and Oxalyl Diisothiocyanate

Jonathan Pfeiffer, Clemens Trost, Anna Pachkovska, Frank Tambornino

Abstract: *Carbonyl diisothiocyanate (**1**) and oxalyl diisothiocyanate (**2**) were synthesized by reactions of phosgene and oxalyl chloride with ammonium thiocyanate, respectively. Their structures were elucidated by single-crystal X-ray diffraction. **1** exhibits weak intermolecular S–O contacts forming a loosely connected network of molecules, whereas **2** exhibits weak intermolecular $C_{carbonyl}$–O contacts resulting in the formation of layers. Both compounds were further characterized by nuclear magnetic resonance, infrared, and Raman spectroscopy. Quantum-chemical calculations reproduced the experimental structures and enabled the interpretation of the vibrational spectra.*

Zusammenfassung:

Carbonyldiisothiocyanat (**1**) und Oxalyldiisothiocyanat (**2**) wurden durch Reaktionen von Phosgen bzw. Oxalylchlorid mit Ammoniumthiocyanat synthetisiert. Ihre Strukturen wurden durch Röntgenbeugung am Einkistall aufgeklärt. **1** zeigt schwache intermolekulare S−O Wechselwirkungen, die ein lockeres Netzwerk bilden, während **2** schwache intermolekulare $C_{Carbonyl}$−O Kontakte aufweist, die in der Ausbildung von Schichten resultieren. Beide Verbindungen wurden des Weiteren mit Kernspinresonanz-, Infrarot- und Raman-Spektroskopie charakterisiert. Quantenchemische Rechnungen bestätigen die experimentellen Strukturen und erlauben die Interpretation der Schwingungsspektren.

Beiträge der Autoren:

Die Publikation beinhaltet Ergebnisse der Masterarbeit von CLEMENS TROST[130] und der Bachelorarbeit von ANNA PACHKOVSKA.[131] TROST hat Carbonyldiisothiocyanat synthetisiert und charakterisiert (^{13}C{^{1}H}-NMR- und IR-Spektroskopie, Elementaranalytik, SC-XRD, Hirshfeld Analyse). Die dazugehörige DFT Rechnung wurde von TAMBORNINO ausgeführt. Unter meiner Anleitung und Betreuung hat PACHKOVSKA Oxalyldiisothiocyanat synthetisiert und charakterisiert (^{13}C{^{1}H}-NMR, Elementaranalytik, SC-XRD). Für beide Moleküle wurde von mir Raman-Spektroskopie durchgeführt. Zusätzlich führte ich für $(CONCS)_2$ IR-Spektroskopie, Hirshfeld Analyse und DFT Rechnungen aus. SC-XRD Analytik wurde von TAMBORNINO durchgeführt. Die Strukturen wurden von TAMBORNINO $(CO(NCS)_2)$ und mir $((CONCS)_2)$ gelöst und verfeinert. Das Manuskript und die *Supporting Information* wurden von TAMBORNINO und mir in Zusammenarbeit erstellt.

A Crystallographic, Spectroscopic, and Computational Investigation of Carbonyl and Oxalyl Diisothiocyanate

Jonathan Pfeiffer, Clemens Trost, Anna Pachkovska, and Frank Tambornino*

Read Online

ACCESS | Metrics & More | Article Recommendations | Supporting Information

ABSTRACT: Carbonyl diisothiocyanate (**1**) and oxalyl diisothiocyanate (**2**) were synthesized by reactions of phosgene and oxalyl chloride with ammonium thiocyanate, respectively. Their structures were elucidated by single-crystal X-ray diffraction. **1** exhibits weak intermolecular S−O contacts forming a loosely connected network of molecules, whereas **2** exhibits weak intermolecular $C_{carbonyl}$−O contacts resulting in the formation of layers. Both compounds were further characterized by nuclear magnetic resonance, infrared, and Raman spectroscopy. Quantum-chemical calculations reproduced the experimental structures and enabled the interpretation of the vibrational spectra.

INTRODUCTION

Carbonyl diisothiocyanate (**1**) was first synthesized in 1902 by the reaction of carbonyl chloride (phosgene) with an excess of a thiocyanate salt [either NaSCN, KSCN, Ba(SCN)₂, Hg(SCN)₂, or Pb(SCN)₂] in toluene (see Scheme 1, III).[1]

Scheme 1. Previously Published Syntheses of Carbonyl and Oxalyl Diisothiocyanate [M = Na, K, Ba, Hg, or Pb; TMS = (CH₃)₃Si][a]
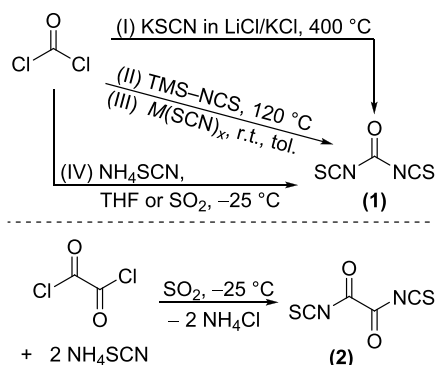
[a]For references, see the text.

The reaction proceeded slowly and not quantitatively, and a pure product could not be isolated. Some reactions with the impure product were performed, but the publication received scant attention. More than 60 years later, a patent regarding syntheses of various carbonyl thiocyanates, among which also is carbonyl diisothiocyanate, was published.[2] Those syntheses also use phosgene but trimethylsilyl isothiocyanate as the

thiocyanate source (see Scheme 1, II). However, both works lacked detailed experimental procedures. In 1973, another synthesis of carbonyl diisothiocyanate was published in which a phosgene stream passed through a LiCl/KCl eutectic melt in which KSCN was dissolved (see Scheme 1, I).[3] The product was described as an unstable, lachrymatory compound that rapidly decomposes at room temperature. The most thorough studies concerning carbonyl diisothiocyanate were published in quick succession in 1981[4] and 1982 (see Scheme 1, IV).[5] Here for the first time the synthesis was described in detail starting from phosgene and ammonium thiocyanate in tetrahydrofuran (THF) or liquid SO₂ at low temperatures. Subsequently, its chemistry as a strong electrophile was exploited and a number of substituted thiadiazines were synthesized. Since then, its chemistry lay dormant.

Reports on oxalyl diisothiocyanate (**2**) are even scarcer. Only one publication from 1981 describes its synthesis, which proceeds from oxalyl chloride and ammonium thiocyanate in liquid SO₂, claiming the reaction in THF to be unfeasible (see Scheme 1).[6] Characterized only by ¹³C nuclear magnetic resonance (NMR) and infrared (IR) spectroscopy, its further chemistry was not explored.

In contrast to the few reports on carbonyl diisothiocyanate, the chemistry of its lighter homologue, carbonyl diisocyanate, has been better explored.[7−9] In 2016, an improved synthetic
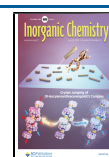
procedure was published in which phosgene was substituted with the easier to handle diphosgene.[10] To gain facile access to carbonyl diisothiocyanate, we aimed to modify its synthesis accordingly, also focusing on the related oxalyl diisothiocyanate.

In this work, we report our findings regarding the syntheses of carbonyl diisothiocyanate and oxalyl diisothiocyanate and their hitherto unknown crystal structures. Vibrational spectroscopy of both compounds is presented alongside quantum-mechanical investigations. These studies pave the way toward a thorough exploration of their chemistry, a hitherto largely vacant area in the chemical space.

■ EXPERIMENTAL SECTION

General Synthetic Methods. All reactions and manipulations were performed under an inert atmosphere of argon using a standard Schlenk-line or glovebox techniques (MBraun UNIlab glovebox, maintained at <0.1 ppm H_2O and <0.1 ppm O_2). Solvents were dried according to standard procedures. Phosgene was prepared from triphosgene (abcr, 98%, used as received) by a literature procedure.[11] Oxalyl chloride (Sigma-Aldrich, 98%) was degassed prior to use. Ammonium thiocyanate (Merck, 99%) was recrystallized from methanol and dried until no residual methanol signals were observed by ^{1}H NMR. $CDCl_3$ (Eurisotope, 99.8%) and THF-d_8 (Eurisotope, 99.5%) were degassed and stored over molecular sieves (4 Å) prior to use.

Syntheses. *Carbonyl Diisothiocyanate (1).* Phosgene (4.37 g, 0.047 mol, 1 equiv) was condensed into a round-bottom flask and cooled to −78 °C, and THF (10 mL, precooled to −23 °C) was added. In a separate flask, ammonium thiocyanate (4.37 g, 0.079 mol, 1.8 equiv) was dissolved in THF (60 mL). The ammonium thiocyanate solution was added to the phosgene solution via a dropping funnel under vigorous stirring at −78 °C, and immediately, an initially colorless precipitate of ammonium chloride formed. Gradually, the suspension assumed an orange hue and was yellow/orange after the addition had been completed. The reaction mixture was allowed to warm to room temperature and subsequently filtered through a G4 sintered glass-frit. The residue was washed with a small amount of cold THF, and the filtrate was carefully concentrated *in vacuo* to half volume. The slightly viscous, now red solution was subject to fractional vacuum distillation with the remaining THF as the first fraction and the product as the second fraction ($p \approx 1.0 \times 10^{-1}$ mbar; $T_{oil\ bath}$ = 50 °C). A red heavily viscous remnant remained in the flask. Carbonyl diisothiocyanate (3.06 g, 0.021 mol, 45%) was obtained in pure form after a second fractional distillation as a slightly yellowish clear and slightly viscous liquid. Crystals suitable for single-crystal diffraction were grown by slowly cooling the neat sample to −50 °C. ^{13}C NMR (75 MHz, $CDCl_3$): δ 151.0 (s, NCS), 140.2 (CO). ^{13}C NMR (125.79 MHz, neat sample): δ 150.3 (NCS), 139.0 (CO). ^{15}N NMR (50.69 MHz, neat sample): δ −245.2 (NCS). Elem. Anal. Calcd. for $C_3N_2O_1S_2$: C, 24.99; N, 19.43; S, 44.48. Found: C, 22.65; N, 19.43; S, 42.57.

Oxalyl Diisothiocyanate (2). To a stirred solution of oxalyl chloride (5 mL, 0.058 mol, 1 equiv) in THF (50 mL) was aded a solution of ammonium thiocyanate (8.37 g, 0.110 mol, 1.9 equiv) in THF (100 mL) at −78 °C. Immediately, a white precipitate of ammonium chloride formed, and upon further addition, the reaction mixture gradually turned orange/red. After the addition had been completed, the reaction mixture was stirred for 2 h at −78 °C and subsequently allowed to warm to room temperature. The suspension was filtered through a G4 sintered glass-frit, and the residue was washed with a small amount of cold THF. The resulting red solution was carefully concentrated to dryness *in vacuo* at 0 °C to avoid sublimation of the product. The red impure raw material was dissolved in ∼50 mL of boiling n-hexane and filtered hot, affording a slightly yellowish solution that upon cooling precipitated oxalyl diisothiocyanate in the form of colorless plates that exhibited an orange hue as the bulk material (7.42 g, 0.043 mol, 74%). Crystals suitable for single-crystal

diffraction were grown by sublimation in a dynamic vacuum ($p < 1.0 \times 10^{-3}$ mbar; $T_{oil\ bath}$ = 40 °C; $T_{cooling\ finger} \approx 10$ °C). ^{13}C NMR (75 MHz, $CDCl_3$): δ 156.7 (NCS), 154.5 (CO). ^{15}N NMR (50.69 MHz, THF-d_8): δ −254.5 (NCS). Elem. Anal. Calcd. for $C_4N_2O_2S_2$: C, 27.90; N, 16.43; S, 37.56. Found: C, 28.17; N, 16.43; S, 37.56.

Methods. *Nuclear Magnetic Resonance Spectroscopy.* NMR spectra were recorded on a Bruker AVANCE II 500 NMR spectrometer equipped with a 5 mm BBO (broadband observation) Cryo Probe Prodigy at 298 K if not stated otherwise. ^{1}H and ^{13}C NMR spectra were referenced to the most downfield solvent resonance. For ^{15}N measurement, a neat sample of **1** and a saturated solution of **2** in THF-d_8 sealed in a 5 mm NMR tube and a single pulse sequence with 30° pulses were used. The spectral width was 600 ppm, with 3300 scans and a relaxation delay of 20 s. The chemical shift of ^{15}N spectra was referenced to CH_3NO_2 (δ 0.0). By making use of the remaining trace of the reaction solvent THF, shimming on the sample was fulfilled by optimizing the line shape of the ^{1}H resonance signal. The spectra were evaluated with the MestReNova software suite.

Elemental Analysis. Elemental analyses were performed by the in-house service personnel. CHN(S) analyses were performed on a CHN(S)-Analysator vario MICRO CUBE (Elementar).

Single-Crystal X-ray Structure Determination. Single-crystal X-ray diffraction data were collected using a StadiVari (Stoe, Darmstadt, Germany) diffraction system equipped with mirror monochromated Cu K_α radiation (λ = 1.54186 Å; Xenocs Microfocus Source) and a Pilatus 300K detector. Crystals were selected under dry oil, mounted on micromount loops, and quench-cooled using an Oxford Cryosystems open flow N_2 cooling device. Data were collected at 100 K if not stated otherwise and processed using the X-Area program package, including unit cell parameter refinement and interframe scaling (which was carried out using LANA within X-Area).[12] Structures were subsequently determined using direct methods (SHELXT)[13] and refined on F^2 with SHELXL[14] using the Olex2[15] user interface. For further details regarding single-crystal refinements, see Table S1.

Powder X-ray Diffractometry. Powder diffraction patterns were recorded on a STADI MP (Stoe) powder diffraction system equipped with mirror monochromated Cu $K_{\alpha 1}$ radiation (λ = 1.54175 Å) and a Silicon strip MYTHEN 1K detector. Data were collected at room temperature in transmission mode (Debye−Scherrer geometry). The powder sample was ground in an agate mortar and measured between X-ray amorphous tape in transmission geometry. Rietveld refinement[16] of oxalyl diisothiocyanate was performed with the TOPAS 6.0 program package.[17] The structural model derived from single-crystal X-ray data was used as the starting point for the refinement. Due to the pronounced formation of plates, a preferred orientation along [010] was considered. Background functions were modeled using shifted Chebyshev polynomials, and profile functions were described with the modified Thompson−Cox−Hastings pseudo-Voigt "TCHZ" function as implemented in TOPAS. For further details regarding Rietveld refinements, see Table S2.

Hirschfeld Surface. Hirschfeld surface analyses were conducted with the Crystal Explorer (version 17.5) software suite.[18]

Quantum-Chemical Calculations. Periodic quantum-chemical calculations were carried out for carbonyl and oxalyl diisothiocyanate with the PBE0 hybrid density functional theory method (DFT-PBE0).[19,20] All calculations were performed with the CRYSTAL17 program package.[21] Triple-ζ-valence + polarization (TZVP) level basis sets were applied for C, N, O, and S. The basis sets have been previously derived from the Karlsruhe def2 basis sets.[22,23] Intermolecular van der Waals dispersion interactions were taken into account using Grimme's empirical D3 dispersion correction with zero damping.[24] Reciprocal space was sampled by Monkhorst−Pack type k-meshes (carbonyl diisothiocyanate, $3 \times 8 \times 4$; oxalyl diisothiocyanate, $6 \times 3 \times 6$).[25] For the evaluation of the Coulomb and exchange integrals (TOLINTEG), tolerance factors of 8, 8, 8, 8, and 16 were used for all calculations. Atomic positions and lattice parameters were fully optimized considering the space group type symmetry (details can be found in the Supporting Information). Default DFT

integration grids and optimization convergence thresholds were applied in all calculations. The harmonic vibrational frequencies and Raman and IR intensities were obtained using CRYSTAL.[26−29] Raman and IR intensities were calculated for a polycrystalline powder sample (total isotropic intensity in arbitrary units). The Raman spectra were obtained by using a pseudo-Voigt band profile (50:50 Lorentzian:Gaussian) and a full width at half-maximum (fwhm) of 8 cm^{-1} and simulated taking into account the experimental setup (T = 193.15 K for **1** and 293.15 K for **2**; λ = 532 nm). Bands for the Raman spectrum were assigned by visual inspection of the normal modes with the Jmol program package at http://crysplot.crystalsolutions.eu/.[30,31] Bands for the IR spectrum were not assigned due to the low quality of the experimental data.

Vibrational Spectroscopy. Raman spectra were recorded on a Monovista CRS+ confocal Raman microscope (Spectroscopy & Imaging GmbH) using a 532 or 633 nm solid-state laser and a 300 grooves/mm grating. Samples were sealed in borosilicate ampules and measured at −80 °C (**1**) or room temperature (**2**). IR spectra were recorded on a Bruker Alpha FT-IR spectrometer equipped with a diamond ATR unit mounted in a nitrogen-filled glovebox (MBraun UNIlab glovebox, maintained at <0.1 ppm H$_2$O and <0.1 ppm O$_2$).

■ RESULTS AND DISCUSSION

Syntheses. Both carbonyl diisothiocyanate and oxalyl diisothiocyanate were prepared by largely similar protocols, differing only in their purification procedures. In a typical experiment, a solution of 1.8 equiv of ammonium thiocyanate in THF was added to a chilled (−78 °C) solution of 1 equiv of phosgene or oxalyl chloride in THF (see Scheme 2).

Scheme 2. Syntheses of Carbonyl and Oxalyl Diisothiocyanate
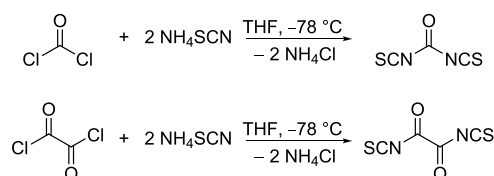
In both cases, the immediate precipitation of ammonium chloride was observed concurrent with formation of a yellow hue. Upon further addition, the suspensions developed an orange (in the case of carbonyl diisothiocyanate) or red (in the case of oxalyl diisothiocyanate) color. If an excess of thiocyanate is used, an instantaneous darkening of the suspensions is observed and yields decrease starkly. The suspensions were stirred for 2 h at −78 °C, allowed to warm to room temperature, and filtered. Carbonyl diisothiocyanate was isolated as a pale yellow liquid after fractional distillation in good yields. The compound can be stored for months at −75 °C without decomposition. Storage at room temperature leads to formation of an orange-red suspension over 24 h and gives an insoluble red precipitate after some days. Oxalyl diisothiocyanate was isolated by evaporation of the solution to dryness and subsequent recrystallization of the red tar-like residue from hexane yielding colorless crystals that showed an orange hue in bulk. If stored under argon, the substance is stable at room temperature. Attempts to replace phosgene with the easier to handle diphosgene or triphosgene in the synthesis of **1** were unsuccessful and yielded only trace amounts of the product.

The purities of carbonyl diisothiocyanate and oxalyl diisothiocyanate were checked by IR, Raman, and ^{13}C NMR spectroscopy, and elemental analysis. For carbonyl diisothio-

cyanate, ^{13}C NMR signals at 151.0 and 140.2 ppm were observed and assigned to the carbon atoms of the isothiocyanate (NCS) and the carbonyl (C=O) groups, respectively. Similarly, oxalyl diisothiocyanate shows two signals in its ^{13}C NMR spectrum. The signal at 156.7 ppm was assigned to the isothiocyanate, and the signal at 154.5 ppm to the carbonyl carbon atom. ^{15}N NMR spectra of **1** (neat sample) and **2** (in THF-d_8) showed signals at −245.2 and −254.5 ppm, respectively, which are in the usual range for heterocumulene type systems.

Molecular Structures in the Solid State. Colorless crystals of **1** suitable for X-ray structure determination were grown by slow cooling of a neat liquid sample in an isopropanol/dry ice bath. Suitable specimens were selected under dry oil and a cooled (−78 °C) stream of dry nitrogen. We found every specimen to be systematically twinned (twin law −1 0 −1 0 −1 0 0 0 1). **1** crystallizes in space group $P2_1/c$ [No. 14, a = 20.5118(13) Å, b = 3.84410(10) Å, c = 15.9661(11) Å, β = 112.464(5)°, V = 1163.39(12) Å^3] with eight formula units in the unit cell comprising two crystallographically independent carbonyl diisothiocyanate molecules (see Figure 1). All atoms of both molecules lie on individual crystallographic orbits.
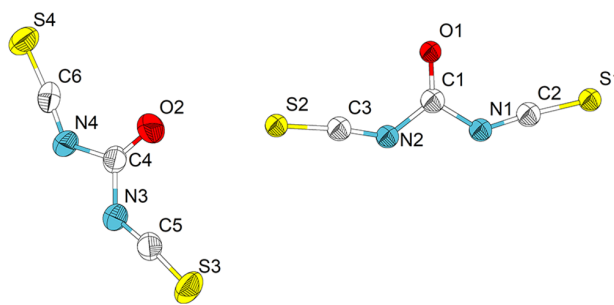
Figure 1. Molecular structures of the two crystallographically independent carbonyl diisothiocyanate molecules in the solid state measured at 200 K. Ellipsoids are drawn at the 75% probability level.

Both molecules approach planar geometries with torsion angles 3.58(2)° and 3.14(2)°, leading to nearly C_{2v} symmetry. All thiocyanate groups are oriented *syn* to the C=O bond with regard to their N=C bonds.

Colorless crystals of **2** suitable for X-ray structure determination were grown by sublimation in a dynamic vacuum ($\rho < 1 \times 10^{-3}$ mbar) over 1 h on a cooling finger maintained at 10 °C from a flask at 40 °C (oil bath temperature). Suitable specimens were selected under dry oil. **2** crystallizes in space group $Pbca$ [No. 61, a = 5.4245(2) Å, b = 20.2875(12) Å, c = 6.1642(4) Å, V = 678.37(6) Å^3] with four formula units in the unit cell (Z' = 0.5). Additionally, powder X-ray diffraction and subsequent Rietveld refinement (see Figure 2) indicated the absence of crystalline impurities and confirmed the accuracy of the structural model derived from single-crystal XRD.

The center of the planar molecule is located on an inversion center leading to strict C_{2h} molecular symmetry (see Figure 3). In contrast to **1**, the thiocyanate groups, and thus the carbonyl groups, are oriented *trans* to one another, which has also been observed for the related compounds oxalyl chloride and oxalyl bromide.[32]

The C=O carbonyl bond lengths of **1** and **2** are 1.181(6)/1.177(5) and 1.198(3) Å, respectively, and thus equal within
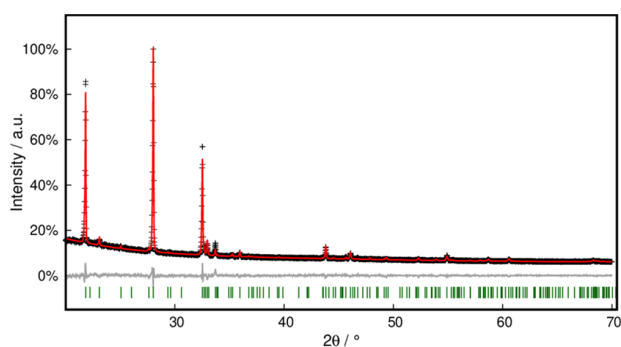
Figure 2. Rietveld refinement of oxalyl diisothiocyanate. Black crosses display measured data, and the red line shows the refined model. Green bars indicate Bragg positions, and the gray line displays the difference plot. Further data are compiled in Table S2.
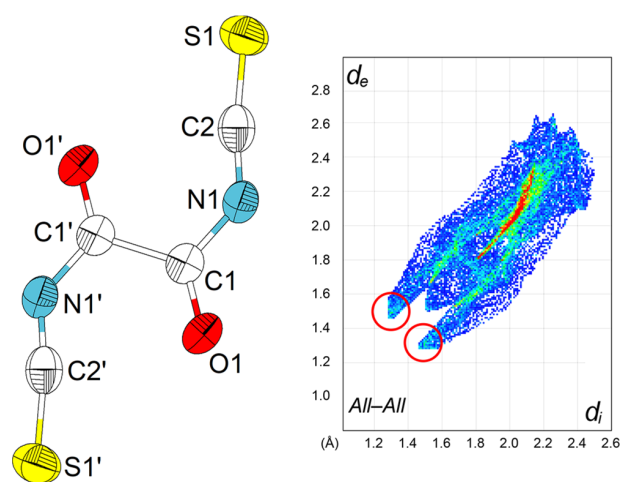
Figure 3. Molecular structure of oxalyl diisothiocyanate in the solid state measured at 100 K (left). Ellipsoids are drawn at the 75% probability level. Fingerprint plot of the Hirschfeld surface analysis for **2** (right). Red circles indicate short intermolecular C−O distances. d_e is the distance from the surface to the nearest nucleus outside the surface. d_i is the distance from the surface to the nearest nucleus inside the surface.

the packing in the solid state, and commonly observed for molecular thiocyanates.[34]

Packing of the Molecules in the Crystal and Hirschfeld Analysis. Both crystallographically independent molecules of **1** show weak intermolecular O−S contacts [3.106(3)−3.290(4) Å], shorter than their combined van der Waals radii [3.32 Å],[36] as visualized by Hirschfeld surface analysis and two-dimensional fingerprint plots (see Figure 4
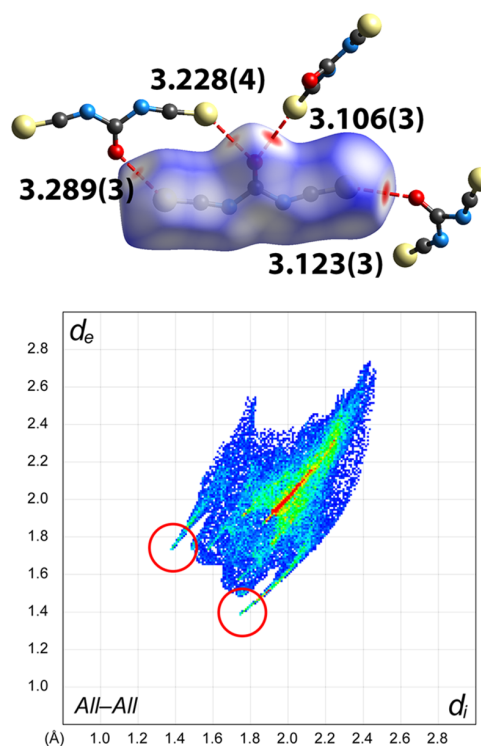
Figure 4. Hirschfeld surface of carbonyl diisothiocyanate with adjacent molecules (top). Red areas indicate distances shorter than the sum of van der Waals radii. Short contacts are shown as dashed lines with values given. Fingerprint plot of carbonyl diisothiocyanate (bottom). Red circles indicate short intermolecular O−S contacts. d_e is the distance from the surface to the nearest nucleus outside the surface. d_i is the distance from the surface to the nearest nucleus inside the surface.

the 3σ range. While similar to the C=O bond length in carbonyl diisocyanate [1.202(1) Å],[10] carbonyl diazide [1.200(6) Å],[33] and fluorocarbonyl isothiocyanate [1.176(3)/1.183(3) Å],[34] it is somewhat shorter than that in urea [1.258 Å].[35] The $C_{carbonyl}$−N bond lengths of **1** and **2** are in the range of 1.381(5)−1.393(6) Å, which are slightly shorter than in carbonyl diisocyanate [1.392−1.399 Å] and slightly longer than in urea [1.338 Å]. The central ∠(NCN) angles of **1** are 110.8(4)° and 111.0(4)° and thus similar within the 3σ range. In **2**, the corresponding angle is ∠(NCC) with a value of 114.1(2)°. The deviation is due to the different steric demand of the substituents. For both compounds, the N=$C_{thiocyanate}$ distances are relatively similar, ranging from 1.207(4) to 1.217(6) Å. In contrast, the $C_{thiocyanate}$=S bond lengths of **1** [1.526(4)−1.542(5) Å] are somewhat shorter than in **2** [1.553(2) Å] but again similar within the 3σ range. Angles ∠(NCS) values of the thiocyanate substituent are 173.7(4)−175.7(4)° for **1** and 172.2(2)° for **2**. The deviations from linearity are intrinsic features of the molecules, not a result of

and Figures S10−S15). Each oxygen atom is connected to S atoms of two neighboring carbonyl diisothiocyanate molecules. Similarly, the two terminal sulfur atoms are each connected to one O atom of one neighboring molecule, resulting in a three-dimensional network. Intermolecular contacts between the two individual molecules are 3.106(3) Å (O2−S2) and 3.123(3) Å (O1−S2), respectively, leading to puckered zigzag chains along [001] (see Figure S17). This is shorter than the contacts to their symmetry-generated crystallographic pair [3.228(4) Å for O2−S4 and 3.289(4) Å for O1−S1 (see Figure S16)]. All other intermolecular contacts are within the expected ranges of the sums of their van der Waals radii, and the respective fingerprint plots can be found in the Supporting Information.

Whereas the crystal packing of **1** can be rationalized by short S−O contacts, in **2** $C_{carbonyl}$−O contacts [2.769(2) Å] are shorter than the sum of their van der Waals radii [3.22 Å]. This can be visualized by the Hirschfeld surface (see Figure S18) and the corresponding fingerprint plot (red circles in Figure 3).

Those contacts result in the formation of layers as shown in Figure 5.
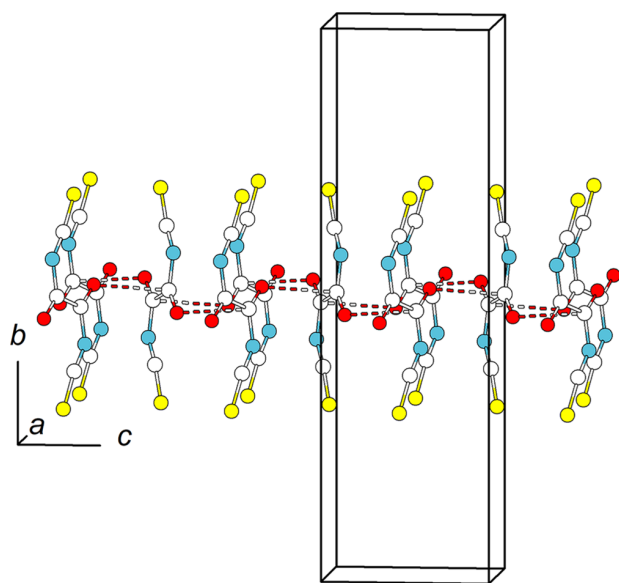
Figure 5. Extended unit cell of **2** viewed approximately along [100]. Intramolecular C$_{carbonyl}$−O contacts are highlighted as dashes. Color code: red for oxygen, white for carbon, blue for nitrogen, and yellow for sulfur. Atoms drawn with arbitrary radii.

The layers are held together by dispersion forces as the shortest S−S distances are 3.6486(9) and 3.9264(9) Å, which are in the expected range of the sum of their van der Waals radii and additionally visualized in Hirschfeld fingerprint plots (see Figures S19−S23). This also explains the formation of platelike single crystals.

Vibrational Spectroscopy. Experimental Raman spectra (baseline-corrected) of **1** and **2** are shown in Figure 6. Values and assignments are listed in Tables S4 and S6. The solid-state IR and Raman spectra of the compounds have also been calculated with the DFT-PBE0 method. Details and band assignments can be found in the Supporting Information.

The high-wavenumber region of the solid-state Raman spectrum of **1**, collected at −80 °C, is dominated by the v(C=O) stretching vibration recorded at 1670 cm^{-1}. Antisymmetric stretching vibrations computed at 2150 and 2050 cm^{-1} are too weak and not observed. At 1084 cm^{-1}, v(C=O) stretching coupled with v(C−N) stretching can be found, which also couples to the symmetric v_s(NCS) stretching vibration. δ(N−C−N) scissoring, δ(NCS) out of plane rocking, and δ(N−C−N) deformation coupled with minor amounts of v(NCS) stretching vibration are observed at 808, 484, and 331 cm^{-1}, respectively. At low wavenumbers of 96 and 50 cm^{-1}, out of plane wagging deformation and lattice vibration modes show strong bands. The calculated solid-state Raman spectra reproduced the energies within close margins.

In contrast, the IR spectrum of **1** shows three intense bands at 1839, 1692, and 1174 cm^{-1}, which are assigned to the asymmetric v_{as}(NCS) stretching, symmetric v(C=O) stretching, and in plane δ(N$_2$C=O) rocking vibrations, respectively. The IR spectrum shows additional bands that probably originate from decomposition products as the stability of **1** is limited at room temperature (Figure S6).
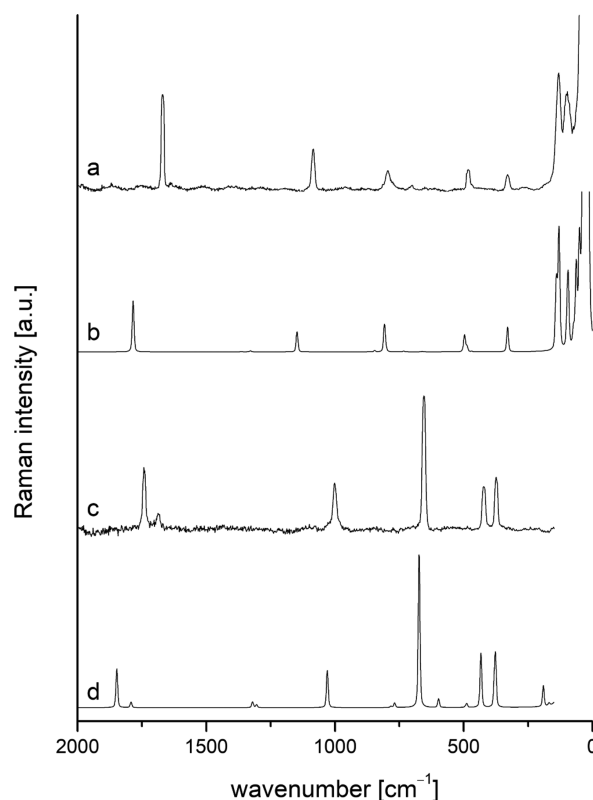
Figure 6. Measured and calculated Raman spectra for **1** (a and b) and **2** (c and d). The spectra of **1** were measured with a 532 nm laser at −80 °C, and the spectra of **2** with a 532 nm laser at room temperature.

Diagnostic Raman spectra for **2** were measured at room temperature by excitation with 532 or 633 nm lasers. The antisymmetric v_{as}(NCS) vibrations, computed at 2135 and 2045 cm^{-1}, are too weak to be observed. The v(C=O) carbonyl stretching vibrations of the two carbonyl groups are in phase, additionally coupled to the v(C−C) stretching vibration, and can be observed at 1742 cm^{-1}. Out of phase v(C=O) vibrations are coupled to v(C−C) stretching and v_{as}(NCS) and are shifted to slightly lower energies (1688 cm^{-1}). At 999 cm^{-1}, the stretching vibration between the two connected C1 atom positions, v(C−C) coupled with v_s(NCS) and δ(N−C−O) scissoring, can be observed. Symmetric stretching vibrations involving the central O=C−C=O unit coupled to δ(NCS) scissoring give the strongest signal of the spectrum at 655 cm^{-1}. δ(O=C−N) scissoring coupled with δ(NCS) scissoring vibrations gives rise to two signals at 422 and 373 cm^{-1}. If the 633 nm laser is used for excitation, the spectra can be recorded as low as 80 cm^{-1}, making possible the observation of lattice vibration modes at 121 and 92 cm^{-1}. Unfortunately, we were unable to obtain meaningful IR spectra of **2** that allowed for band assignment. The spectrum is shown in Figure S7.

■ CONCLUSION

Reaction of ammonium thiocyanate with phosgene or oxalyl chloride led to the synthesis of carbonyl diisothiocyanate **1** and oxalyl diisothiocyanate **2**. Crystallographic investigation and Hirschfeld analysis of **1** show a network structure dominated by O···S short contacts with thiocyanate substituents oriented

syn to the C=O bond. In contrast, the structure of **2** is layered with short intralayer C···O contacts. Interlayer S···S contacts do not exceed the sum of van der Waals radii. The thiocyanate substituents are oriented *trans* to one another. Vibrational spectra for **1** are dominated by the $\nu(C=O)$ stretching mode, whereas spectra for **2** are dominated by a coupled $\delta(O=C-C=O)$ deformation and $\delta(NCS)$ scissoring vibration. The further reactivity of both compounds is currently under investigation by our group.

■ ASSOCIATED CONTENT

Ⓢ Supporting Information

The Supporting Information is available free of charge at https://pubs.acs.org/doi/10.1021/acs.inorgchem.1c01421.

> Details of X-ray crystallography, computational data, full Raman and IR spectra, full nuclear magnetic resonance spectra, and additional Hirschfeld surfaces and finger-print plots (PDF)

Accession Codes

CCDC 2080495−2080497 contain the supplementary crystallographic data for this paper. These data can be obtained free of charge via www.ccdc.cam.ac.uk/data_request/cif, or by emailing data_request@ccdc.cam.ac.uk, or by contacting The Cambridge Crystallographic Data Centre, 12 Union Road, Cambridge CB2 1EZ, UK; fax: +44 1223 336033.

■ AUTHOR INFORMATION

Corresponding Author

Frank Tambornino − *Fachbereich Chemie, Wissenschaftliches Zentrum für Materialwissenschaften (WZMW), Philipps-Universität Marburg, D-35043 Marburg, Germany;* ⓘ orcid.org/0000-0003-3538-6049; Email: Frank.Tambornino@chemie.uni-marburg.de

Authors

Jonathan Pfeiffer − *Fachbereich Chemie, Wissenschaftliches Zentrum für Materialwissenschaften (WZMW), Philipps-Universität Marburg, D-35043 Marburg, Germany*

Clemens Trost − *Fachbereich Chemie, Wissenschaftliches Zentrum für Materialwissenschaften (WZMW), Philipps-Universität Marburg, D-35043 Marburg, Germany*

Anna Pachkovska − *Fachbereich Chemie, Wissenschaftliches Zentrum für Materialwissenschaften (WZMW), Philipps-Universität Marburg, D-35043 Marburg, Germany*

Complete contact information is available at:
https://pubs.acs.org/10.1021/acs.inorgchem.1c01421

Notes

The authors declare no competing financial interest.

■ ACKNOWLEDGMENTS

■ REFERENCES

(1) Dixon, A. E. *Proc. Chem. Soc., London* **1902**, *18* (257), 235.

(2) Anders, B.; Malz, H. Verfahren Zur Herstellung von Acylsenfoelen. DE1215144B, 1966.

(3) Jäckh, C.; Sundermeyer, W. Chemische Reaktionen in Salzschmelzen. XV. Darstellung und Reaktionen von Carbonylhalogeniden und -pseudohalogeniden. *Chem. Ber.* **1973**, *106* (6), 1752−1757.

(4) Bunnenberg, R.; Jochims, J. C. Carbonyldiisothiocyanat. *Chem. Ber.* **1981**, *114* (6), 2075−2086.

(5) Bunnenberg, R.; Jochims, J. C.; Härle, H. Zur Darstellung und Chlorierung von Carbonyl-diisothiocyanat. *Chem. Ber.* **1982**, *115* (11), 3587−3596.

(6) Bunnenberg, R.; Jochims, J. C. Oxalyl-isothiocyanate und Carbonyl-halogenid-isothiocyanate. *Chem. Ber.* **1981**, *114* (5), 1746−1751.

(7) Akteries, B.; Jochims, J. C. Reactions of Carbonyl Diisocyanate with Amides and Acids. *Chem. Ber.* **1986**, *119* (2), 669−682.

(8) Akteries, B.; Jochims, J. C. Carbonyl Diisocyanate: A New Preparation and Some Reactions. *Chem. Ber.* **1986**, *119* (1), 83−95.

(9) Nachbaur, E. Darstellung Und Eigenschaften von Carbonylisocyanat. *Monatsh. Chem.* **1966**, *97* (2), 361−367.

(10) Klapötke, T. M.; Krumm, B.; Rest, S.; Scharf, R.; Schwabedissen, J.; Stammler, H.-G.; Mitzel, N. W. Carbonyl Diisocyanate $CO(NCO)_2$: Synthesis and Structures in Solid State and Gas Phase. *J. Phys. Chem. A* **2016**, *120* (26), 4534−4541.

(11) Cotarca, L.; Geller, T.; Répási, J. Bis(Trichloromethyl)-Carbonate (BTC, Triphosgene): A Safer Alternative to Phosgene? *Org. Process Res. Dev.* **2017**, *21* (9), 1439−1446.

(12) *X-Area*, ver. 1.88; Stoe & Cie GmbH: Darmstadt, Germany, 2019.

(13) Sheldrick, G. M. SHELXT - Integrated Space-Group and Crystal-Structure Determination. *Acta Crystallogr., Sect. A: Found. Adv.* **2015**, *71* (1), 3−8.

(14) Sheldrick, G. M. A Short History of SHELX. *Acta Crystallogr., Sect. A: Found. Crystallogr.* **2008**, *64* (1), 112−122.

(15) Dolomanov, O. V.; Bourhis, L. J.; Gildea, R. J.; Howard, J. A. K.; Puschmann, H. OLEX2: A Complete Structure Solution, Refinement and Analysis Program. *J. Appl. Crystallogr.* **2009**, *42* (2), 339−341.

(16) Rietveld, H. M. A Profile Refinement Method for Nuclear and Magnetic Structures. *J. Appl. Crystallogr.* **1969**, *2* (2), 65−71.

(17) Coelho, A. A. TOPAS and TOPAS-Academic: An Optimization Program Integrating Computer Algebra and Crystallographic Objects Written in C++. *J. Appl. Crystallogr.* **2018**, *51* (1), 210−218.

(18) Turner, M. J.; McKinnon, J. J.; Wolff, S. K.; Grimwood, D. J.; Spackman, P. R.; Jayatilaka, D.; Spackman, M. A. *CrystalExplorer17*, University of Western Australia, 2017.

(19) Adamo, C.; Barone, V. Toward Reliable Density Functional Methods without Adjustable Parameters: The PBE0 Model. *J. Chem. Phys.* **1999**, *110* (13), 6158−6170.

(20) Perdew, J. P.; Burke, K.; Ernzerhof, M. Generalized Gradient Approximation Made Simple. *Phys. Rev. Lett.* **1996**, *77* (18), 3865−3868.

(21) Dovesi, R.; Erba, A.; Orlando, R.; Zicovich-Wilson, C. M.; Civalleri, B.; Maschio, L.; Rérat, M.; Casassa, S.; Baima, J.; Salustro, S.; Kirtman, B. Quantum-Mechanical Condensed Matter Simulations with CRYSTAL. *Wiley Interdiscip. Rev.: Comput. Mol. Sci.* **2018**, *8* (4), 1−36.

(22) Weigend, F.; Ahlrichs, R. Balanced Basis Sets of Split Valence, Triple Zeta Valence and Quadruple Zeta Valence Quality for H to Rn: Design and Assessment of Accuracy. *Phys. Chem. Chem. Phys.* **2005**, *7* (18), 3297−3305.

(23) Karttunen, A. J.; Tynell, T.; Karppinen, M. Atomic-Level Structural and Electronic Properties of Hybrid Inorganic-Organic ZnO:Hydroquinone Superlattices Fabricated by ALD/MLD. *J. Phys. Chem. C* **2015**, *119* (23), 13105−13114.

(24) Grimme, S.; Antony, J.; Ehrlich, S.; Krieg, H. A Consistent and Accurate Ab Initio Parametrization of Density Functional Dispersion

Correction (DFT-D) for the 94 Elements H-Pu. *J. Chem. Phys.* **2010**, *132* (15), 154104.

(25) Monkhorst, H. J.; Pack, J. D. Special Points for Brillouin-Zone Integrations. *Phys. Rev. B* **1976**, *13* (12), 5188−5192.

(26) Pascale, F.; Zicovich-Wilson, C. M.; López Gejo, F.; Civalleri, B.; Orlando, R.; Dovesi, R. The Calculation of the Vibrational Frequencies of Crystalline Compounds and Its Implementation in the CRYSTAL Code. *J. Comput. Chem.* **2004**, *25* (6), 888−897.

(27) Zicovich-Wilson, C. M.; Pascale, F.; Roetti, C.; Saunders, V. R.; Orlando, R.; Dovesi, R. Calculation of the Vibration Frequencies of α-Quartz: The Effect of Hamiltonian and Basis Set. *J. Comput. Chem.* **2004**, *25* (15), 1873−1881.

(28) Maschio, L.; Kirtman, B.; Orlando, R.; Rèrat, M. Ab Initio Analytical Infrared Intensities for Periodic Systems through a Coupled Perturbed Hartree-Fock/Kohn-Sham Method. *J. Chem. Phys.* **2012**, *137* (20), 204113.

(29) Maschio, L.; Kirtman, B.; Rérat, M.; Orlando, R.; Dovesi, R. Ab Initio Analytical Raman Intensities for Periodic Systems through a Coupled Perturbed Hartree-Fock/Kohn-Sham Method in an Atomic Orbital Basis. II. Validation and Comparison with Experiments. *J. Chem. Phys.* **2013**, *139* (16), 164102.

(30) Beata, G.; Perego, G.; Civalleri, B. CRYSPLOT: A New Tool to Visualize Physical and Chemical Properties of Molecules, Polymers, Surfaces, and Crystalline Solids. *J. Comput. Chem.* **2019**, *40* (26), 2329−2338.

(31) Jmol: an open-source Java viewer for chemical structures in 3D. http://www.jmol.org.

(32) Groth, P.; Hassel, O.; Römming, C.; Block-Bolten, A.; Toguri, J. M.; Flood, H. Crystal Structures of Oxalyl Bromide and Oxalyl Chloride. *Acta Chem. Scand.* **1962**, *16*, 2311−2317.

(33) Zeng, X.; Gerken, M.; Beckers, H.; Willner, H. Synthesis and Characterization of Carbonyl Diazide, $OC(N_3)_2$. *Inorg. Chem.* **2010**, *49* (20), 9694−9699.

(34) Ramos, L. A.; Ulic, S. E.; Romano, R. M.; Erben, M. F.; Lehmann, C. W.; Bernhardt, E.; Beckers, H.; Willner, H.; Della Védova, C. O. Vibrational Spectra, Crystal Structures, Constitutional and Rotational Isomerism of FC(O)SCN and FC(O)NCS. *Inorg. Chem.* **2010**, *49* (23), 11142−11157.

(35) Guth, H.; Heger, G.; Klein, S.; Treutmann, W.; Scheringer, C. Strukturverfeinerung von Harnstoff mit Neutronenbeugungsdaten Bei 60, 123 Und 293 K Und X−N- Und X−X(1s2)-Synthesen bei etwa 100 K. *Z. Kristallogr. - Cryst. Mater.* **1980**, *153* (3−4), 237−254.

(36) Mantina, M.; Chamberlin, A. C.; Valero, R.; Cramer, C. J.; Truhlar, D. G. Consistent van Der Waals Radii for the Whole Main Group. *J. Phys. Chem. A* **2009**, *113* (19), 5806−5812.

3.2 Rotational Conformers and Nuclear Spin Isomers of Carbonyl Diisothiocyanate

Eva Gougoula, Jonathan Pfeiffer, Frank Tambornino, and Melanie Schnell

submitted

Abstract: *Nuclear spin isomers of molecules play a pivotal role in our understanding of quantum mechanics and can have significant implications for various fields. In this work, we report the isolation and characterization of stable nuclear spin isomers, as well as conformational isomers of a reactive compound, namely carbonyl diisothiocyanate. It can exist as three rotational conformers, two of which, the syn-syn and syn-anti, were observed in a pulsed supersonic jet by chirped pulse Fourier transform microwave spectroscopy in the 2–12 GHz frequency region. The rotational spectra of two distinct nuclear spin isomers of syn-syn-carbonyl diisothiocyanate, ortho and para, were recorded and analyzed. Experimental molecular rotational parameters for the identified rotational and nuclear spin isomers were determined, including rotational constants, centrifugal distortion constants and nuclear quadrupole coupling constants. The two nuclear spin isomers are distinguished by unique nuclear quadrupole coupling signatures as an outcome of their different nuclear spin states. The relative abundances of the two observed conformers in the gasphase were estimated from the intensity of their rotational transitions. Following detection of singly substituted rare isotopologues of the syn-syn conformer, a partial substitution (r_s) structure was determined.*

Zusammenfassung:

Kernspinisomere von Molekülen spielen eine zentrale Rolle für unser Verständnis von Quantenmechanik und können bedeutende Auswirkungen für verschiedene Bereiche haben. In dieser Arbeit berichten wir von der Isolierung und Charakterisierung von stabilen Kernspinisomeren, sowie Konformationsisomeren einer reaktiven Verbindung, nämlich Carbonyldiisothiocyanat. Es kann in drei Rotationskonformeren existieren, wovon zwei, *syn-syn* und *syn-anti*, in einem gepulsten Überschallstrahl mittels *chirped-pulse* Fourier-Transformation Mikrowellen-Spektroskopie im 2–12 GHz Frequenzbereich beobachtet wurden. Die Rotationsspektren von zwei unterscheidbaren Kernspinisomeren von *syn-syn* Carbonyldiisothiocyanat, *ortho* und *para*, wurden detektiert und analysiert. Für die identifizierten Rotations- und Kernspinisomere wurden experimentelle molekulare Rotationsparameter einschließlich Rotationskonstanten, zentrifugale Verzerrungskonstanten und Kernquadrupolkopplungskonstanten bestimmt. Die zwei Kernspinisomere sind unter-

scheidbar durch einzigartige Signaturen der Kernquadrupolkopplung, die durch ihre unterschiedlichen Kernspinzustände entstehen. Die relative Häufigkeiten der beiden beobachteten Konformere in der Gasphase wurden aus der Intensität ihrer Rotationsübergänge abgeschätzt. Nach dem Nachweis von einfach besetzten Isotopologen des *syn-syn*-Konformers wurde eine partielle Substitutionsstruktur (r_s) bestimmt.

Beiträge der Autoren:

Synthese von Carbonyldiisothiocyanat und Bereitstellung des Materials für die Messungen wurden von mir durchgeführt. Die Messungen wurden von EVA GOUGOULA durchgeführt und ausgewertet (*chirped-pulse* Fourier-Transformation Mikrowellen-Spektroskopie, DFT Rechnungen). Das Manuskript wurde von allen Autoren gemeinsam verfasst, wobei GOUGOULA und SCHNELL die Ergebnisse und Diskussion gestalteten. TAMBORNINO und ich formulierten Entwürfe für die Einleitung, sowie Zusammenfassung und führten die Literaturrecherche zu den bekannten Konformeren vergleichbarer Moleküle durch.

Rotational Conformers and Nuclear Spin Isomers of Carbonyl Diisothiocyanate

Eva Gougoula[1,*], Jonathan Pfeiffer[2], Melanie Schnell[1, 3, *], and Frank Tambornino[2,*]

Affiliations:

[1] Deutsches-Elektronen Synchrotron DESY, Notkestr. 85, 22607 Hamburg, Germany

[2] Fachbereich Chemie, Philipps-Universität Marburg, Hans-Meerwein-Straße 4, 35043 Marburg, Germany

[3] Institut für Physikalische Chemie, Christian-Albrechts-Universität zu Kiel, D-24118 Kiel, Germany

* Corresponding authors: melanie.schnell@desy.de, eva.gougoula@desy.de, tamborni@chemie.uni-marburg.de

ORCIDs:

Eva Gougoula: https://orcid.org/0000-0002-2037-1314

Melanie Schnell: https://orcid.org/0000-0001-7801-7134

Frank Tambornino: https://orcid.org/0000-0003-3538-6049

Abstract

Nuclear spin isomers of molecules play a pivotal role in our understanding of quantum mechanics and can have significant implications for various fields. In this work, we report the isolation and characterization of stable nuclear spin isomers, as well as conformational isomers of a reactive compound, namely carbonyl diisothiocyanate. It can exist as three rotational conformers, two of which, the *syn-syn* and *syn-anti*, were observed in a pulsed supersonic jet by chirped pulse Fourier transform microwave spectroscopy in the 2-12 GHz frequency region. The rotational spectra of two distinct nuclear spin isomers of *syn-syn*-carbonyl diisothiocyanate, *ortho* and *para*, were recorded and analyzed. Experimental molecular rotational parameters for the identified rotational and nuclear spin isomers were determined, including rotational constants, centrifugal distortion constants and nuclear quadrupole coupling constants. The two nuclear spin isomers are distinguished by unique nuclear quadrupole coupling signatures as an outcome of their different nuclear spin states. The relative abundances of the two observed conformers in the gas-phase were estimated from the intensity of their rotational transitions. Following detection of singly substituted rare isotopologues of the *syn-syn* conformer, a partial substitution (r_s) structure was determined.

Introduction

Molecules with equivalent nuclei with non-zero spin can exist as nuclear spin isomers which are characterized by different sets of rotational quantum numbers that they are allowed to populate[1]. Nuclear spin isomers have a pivotal role in the manifestation of quantum mechanics and our understanding of fundamental science as well as across various disciplines. To name a few, the unique properties of nuclear spin isomers may find potential applications in quantum computing[2,3], medical imaging[4,5], and astrophysics where the measured ratios between different nuclear spin isomers can provide an insight into astrophysical processes and stellar environments[6–8]. The first observation of nuclear spin isomers is reported in 1929[9] with the separation and interconversion of *ortho-* and *para-*H_2, where the orientation of the spin of each hydrogen can be parallel or anti-parallel, respectively. Separation and conversion of nuclear spin isomers was later observed for a number of other molecules, *e.g.* water[10,11], methanol[12], ethylene[13–15], and fluoromethane[16,17], to name a few. However, in the gas phase, the probability of interconversion between isomers is generally considered improbable, and thus spectroscopic studies in the gas phase can be an ideal way to study isolated nuclear spin isomers.

Advances in modern synthetic chemistry play a key role in engineering molecules with unique symmetry properties that can serve as prototypes to study the properties of isolated nuclear spin isomers. Carbonyl diisothiocyanate (CDIT, C=O(NCS)$_2$), a reactive compound that consists of a carbonyl (C=O) and two isothiocyanate groups (–N=C=S), was first reported in 1902[18], and reliable synthetic routes to its formation were established in 1981[19,20] and reinvestigated in 2021[21]. In principle, the compound can exist as three different rotational conformers (Fig. 1), *syn-syn*, *syn-anti*, and *anti-anti* (with respect to the carbonyl bond relative to the heterocumulene). Additionally, it consists exclusively of non-
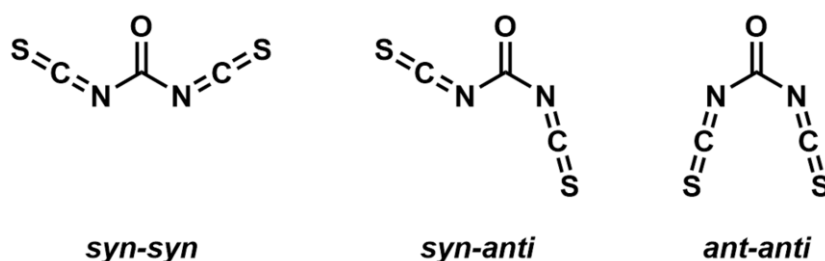
Figure 1. Possible conformers of carbonyl dipseudohalides (*syn-syn*, *syn-anti* and *anti-anti*) illustrated by the example of carbonyl diisothiocyanate. *Syn*: carbonyl group and isocyanate group on the same side, *anti*: carbonyl group and isocyanate group on different sides.

hydrogen atoms, all of which have a nuclear spin (I) of 0 or 1, and thus are bosons. In the *syn-syn* and *anti-anti* forms, due to the overall symmetry of the molecules, the atoms of the –NCS groups are equivalent upon exchange and Bose-Einstein statistics are expected to influence their rotational spectra.

Information on the structure and relative conformational abundances of carbonyl diisocyanate (C=O(NCO)$_2$)[22,23] and carbonyl diazide (C=O(N$_3$)$_2$)[24] is available through gas-phase electron diffraction (GED) and infrared (IR) spectroscopy. The two are closely related to CDIT, both in terms of the available conformations they can adopt, but also by possessing isoelectronic functional groups attached to the carbonyl, and displaying high reactivity. Both the *syn-syn* and *syn-anti* forms have been characterized for C=O(NCO)$_2$ and C=O(N$_3$)$_2$, with the *syn-syn* form being the dominant species in both cases, an observation that is also supported by quantum chemical calculations. Condensed phase studies on CDIT with X-ray diffraction (XRD) only identified the *syn-syn* conformer in the crystal, which is also the most stable form. An important step towards characterizing and rationalizing the properties of CDIT is to obtain spectroscopic insight into the *syn-anti* conformation, as well as to experimentally determine its conformational preferences.

In this work, we report the rotational spectrum of CDIT in the gas phase using chirped pulse Fourier transform microwave (CP-FTMW) spectroscopy. The *syn-syn* and *syn-anti* conformations are detected, providing access to the molecular properties of the elusive conformer. Their relative abundances fall within the broader expectations based on similar systems, and on their computed energies. Interesting effects are observed in the spectrum of the *syn-syn* conformer consistent with the presence of two distinct nuclear spin isomers that follow nuclear spin statistics for bosons. The structure of *syn-syn*-CDIT was partially determined through isotopic substitution of the atoms in the –NCS groups.

Results and Discussion

The three possible conformers of CDIT (Fig. 1), *syn-syn*, *syn-anti*, and *anti-anti*, arise through rotation of the isothiocyanate groups –N=C=S around the C2–N6 or C2–N3 bonds, respectively. The calculated molecular parameters of the conformers of CDIT (Table 1) show that the *syn-syn* and *syn-anti* conformers are near-prolate asymmetric tops. The potential energy surface connecting the three possible conformers is calculated at the PEBh-3c level of theory. The two conformers are separated by a high energy barrier (~16 kJ mol^{-1}), with *syn-anti*-CDIT lying approximately 4.5 kJ mol^{-1} higher than *syn-syn*-CDIT, the global minimum. *Anti-anti*-CDIT is a near-oblate asymmetric top, and it is calculated to be approximately 9.5 kJ mol^{-1} higher in energy than *syn-syn*-CDIT. All three conformers have a sizeable electric dipole moment component along the b-axis of inertia. In *syn-syn*- and *anti-anti*-CDIT, due to symmetry, the C_2 axis is aligned with the b-axis of inertia and the C=O bond, which results in three equivalent pairs of atoms between the two isothiocyanate –N=C=S groups (Fig. 2).

syn-syn-CDIT

0 (cm^{-1}, kJ mol^{-1})

syn-anti-CDIT

377.4, 4.5

anti-anti-CDIT

791.9, 9.5
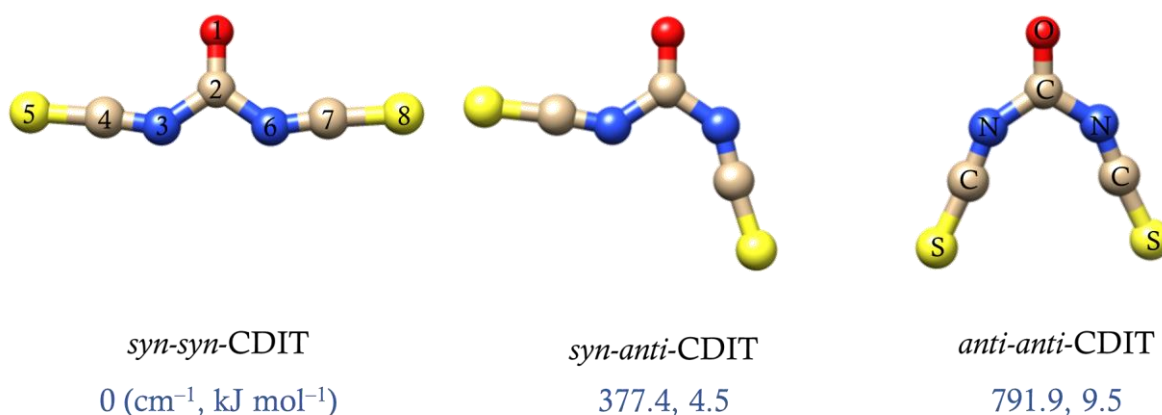
Figure 2. Optimized (r_e) geometries of the three possible conformers of CDIT at the B3LYP-D3(BJ)/aug-cc-pVTZ level.

Table 1. Calculated rotational parameters, including nuclear quadrupole coupling constants of the two ^{14}N nuclei and relative energies of the three possible conformers of CDIT obtained at the B3LYP-D3(BJ)/aug-cc-pVTZ level.

	syn-syn	*syn-anti*	*anti-anti*
A_e (MHz)	10335.6	2901.6	1425.6
B_e (MHz)	443.7	612.0	1165.6
C_e (MHz)	425.4	505.4	641.3
$\chi_{aa}(N_3)$ (MHz)	1.763	1.618	1.861
$\chi_{bb}(N_3) - \chi_{cc}(N_3)$ (MHz)	0.936	−1.030	0.823
$\chi_{aa}(N_6)$ (MHz)	1.763	0.245	1.861
$\chi_{bb}(N_6) - \chi_{cc}(N_6)$ (MHz)	0.936	0.742	0.823
$|\mu_a|, |\mu_b|, |\mu_c|$ (D)	0, 1.2, 0	0.4, 2.2, 0	0, 2.6, 0
κ [a]	−0.99	−0.91	0.34
ΔE_{rel} (cm^{-1}, kJ mol^{-1}) [b]	0	377.4, 4.5	791.9, 9.5
$\Delta E_{barrier}$ (cm^{-1}, kJ mol^{-1}) [c]	1305, 16	1190, 14	

[a] Ray's asymmetry parameter $\kappa = \frac{2B-A-C}{A-C}$

[b] Relative energies calculated with respect to *syn-syn*-CDIT at the B3LYP-D3(BJ)/aug-cc-pVTZ level.

[c] Energy barriers between *syn-syn*-CDIT and *syn-anti*-CDIT, and *syn-anti*-CDIT and *anti-anti*-CDIT obtained at the PEBh-3c level, and shown with respect to the relative energies of the conformers at the same level of theory.

Spectrum of *syn-syn*-CDIT

The jet-cooled rotational spectrum of CDIT was collected over the 2-12 GHz frequency range, in segments of 2-8 and 8-12 GHz. Upon initial inspection of the 8-12 GHz region, the most intense feature is a pattern consistent with a *b*-type, *Q*-branch transition. The lines exhibit hyperfine splitting as expected for a molecule with one or two N nuclei with nuclear spin $I = 1$. Watson's S-reduction[25], as implemented in Western's PGOPHER[26], was used to perform the initial assignment of the spectrum, without consideration of the hyperfine splitting. The $1_{1,0} \leftarrow 1_{0,1}$ transition was identified at approximately 10615 MHz which gave an excellent initial value of the A_0 rotational constant. A preliminary fit including *b*-type, *Q*-, *P*-, and *R*-branch transitions was performed and yielded the initial set of the A_0, B_0, and C_0 rotational constants which were assigned to *syn-syn*-CDIT, based on agreement (see Table S1, Supplementary Information) between the calculated and experimentally determined rotational constants.

Upon inclusion of the nuclear quadrupole coupling terms $\chi_{aa}(^{14}N)$ and $\chi_{bb}(^{14}N)-\chi_{cc}(^{14}N)$. in the fit, the experimental hyperfine splitting appears to vary. For some transitions it is consistent with one N nucleus ($I = 1$), while for others it is consistent with two N ($I_1 = 1$ and $I_2 = 1$) nuclei. As a result, two separate fits, Fit 1 and Fit 2, were performed with PGOPHER[26], and the experimentally determined spectroscopic parameters are summarized in Table 1. The types of transitions, *Q*-, *P*-, and *R*-branch, with odd or even $K_{sum}'' = K_a'' + K_c''$, that were included in each fit are indicated in the last rows of Table 1. The hyperfine splitting of some representative rotational transitions is showcased in the expanded part of Fig. 3. The two fits yield similar rotational constants which are within the standard deviation of each other, thus excluding the possibility that the individual fits are associated with a large amplitude motion within the molecule. This is further supported by the value of D_{JK}, which is in the range of just a couple of kHz. Regarding the nuclear quadrupole coupling constants of the two fits, these are of similar magnitude, however, their signs are reversed. These observations suggest that there are two nuclear spin isomers of *syn-syn*-CDIT, *ortho* and *para*.

Table 2. Experimentally determined spectroscopic parameters yielded by Fit 1 and Fit 2 of *syn-syn*-CDIT using Watson's S-reduction as implemented in PGOPHER.

	Fit 1 (*para*)	Fit 2 (*ortho*)
A_0 (MHz)	11046.3560(36)[a]	11046.3586(41)
B_0 (MHz)	449.80163(53)	449.80145(53)
C_0 (MHz)	432.27053(70)	432.27030(80)
D_{JK} (kHz)	1.222(39)	1.353(50)
$\chi_{aa}(N_3)$ (MHz)	−1.9176(99)	1.9240(65)[b]
$\chi_{bb}(N_3) - \chi_{cc}(N_3)$ (MHz)	0.772(21)	−0.756(14)[b]
$\chi_{aa}(N_6)$ (MHz)	–	1.9240(65)[b]
$\chi_{bb}(N_6) - \chi_{cc}(N_6)$ (MHz)	–	−0.756(14)[b]
N[c]	42	50
σ_{RMS}[d] (kHz)	13.0	13.2
Q-Branch, $\Delta J = 0$, $\Delta K_a = 1$	odd[e]	even
P-Branch, $\Delta J = -1$, $\Delta K_a = 1$	odd	even
R-Branch, $\Delta J = 1$, $\Delta K_a = 1$	odd	even

[a] Numbers in parentheses are one standard deviation in units of the last significant figures.

[b] The two nitrogen atoms are assumed as equivalent in Fit 2.

[c] Number of hyperfine transitions included in the fit.

[d] Root mean square deviation of the fit.

[e] Odd/even refers to the sum of $K_a'' + K_c'' = K_{sum}''$
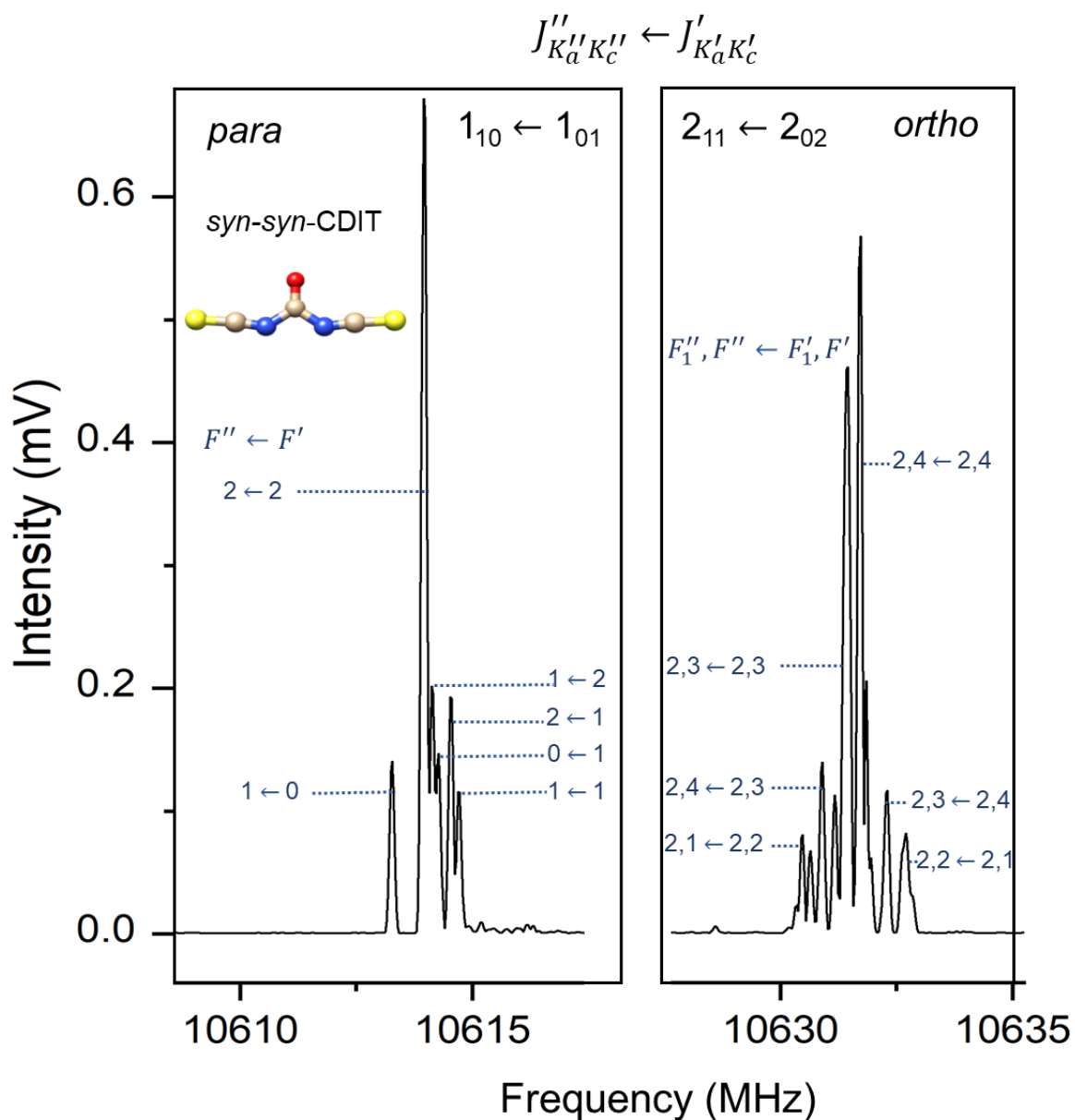
Figure 3. Representative rotational transitions $J''_{K''_a K''_c} \leftarrow J'_{K'_a K'_c}$ of *ortho-* and *para-syn-syn-* CDIT carrying hyperfine splitting due to ^{14}N nuclei. The splitting in the spectrum of the *para* isomer is consistent with one ^{14}N nucleus, while that for the *ortho* isomer is analogous to two ^{14}N nuclei. Some $F'' \leftarrow F'$ and $F''_1, F'' \leftarrow F'_1, F'$ hyperfine transitions are annotated, respectively.

Following the work of Grubbs *et al.*[27], it is possible to perform a global fit of both *ortho*- and *para-(syn-syn-CDIT)* using Pickett's SPFIT/SPCAT[28]. Watson's S-reduced Hamiltonian[25] as implemented in SPFIT was used in the form:

$$\hat{H}_{TOT} = \hat{H}_{ROT} + \hat{H}_{CD} + \hat{H}_Q(N) + \hat{H}_{SS}(N)$$

where $\widehat{H}_{ROT}$, $\widehat{H}_{CD}$, $\widehat{H}_Q$, and $\widehat{H}_{SS}$ are the rotational, centrifugal distortion, nuclear quadrupole coupling, and nuclear spin-nuclear spin coupling terms, respectively. The high degree of similarity between the rotational and centrifugal distortion constants of the two nuclear spin isomers (see Table 2) allows for simultaneous fitting of the $\widehat{H}_{ROT}$ and $\widehat{H}_{CD}$ terms to both isomers, yielding average values for these constants. The nuclear quadrupole coupling term was fitted individually for each N atom of both isomers, and these results are summarized in Table 3. The nuclear spin-nuclear spin coupling term is inseparable from the nuclear quadrupole coupling term, and therefore determination of $\widehat{H}_Q$ is a linear combination of the two[29]. The detailed operator codes that were used for this fit are given in the Supplementary Information.

The coupling scheme that was used for the *para* isomer is $J + I_{N_3} = F_1$. For the *ortho* isomer the nuclear spin can in principle be treated either as two individual N nuclei with $J + I_{N_3} = F_1$ and $F_1 + I_{N_6} = F$, or by combining the spin as $I_{N_3} + I_{N_6} = I_{tot}$ and $J + I_{tot} = F$, as demonstrated in reference 27. The fit parameters in Table 4 were generated through the former scheme. Treatment of the nuclear spin of the *ortho* isomer as a total spin of $I_{tot} = 2$ does not reproduce all experimental transitions and thus does not generate a satisfactory fit for *ortho*-(*syn-syn*-CDIT). This could potentially be explained by the 2.3 Å distance between the two N nuclei (at the B3LYP-D3(BJ)/aug-cc-pVTZ level) resulting in only weak coupling between the two nuclei.

Table 3. Final fits of the rotational spectra of *syn-syn* and *syn-anti*-CDIT performed with SPFIT/SPCAT using Watson's S-reduction.

		syn-syn-CDIT $I_{N_3} = 1, I_{N_6} = 1$	*syn-anti*-CDIT
$A_0{}^{[a]}$ (MHz)		11046.3541(23)[b]	2938.6797(15)
B_0 (MHz)		449.80106(48)	626.51962(71)
C_0 (MHz)		432.26941(86)	516.14194(50)
$D_J{}^{[c]}$ (kHz)		–	0.2008(52)
D_{JK} (kHz)		1.45(10)	–3.099(39)
D_K (kHz)		–	–20.74(16)
d_1 (kHz)		–	–0.0779(19)
$\chi_{aa}(N_3){}^{[d]}$ (MHz)	*para*	–1.927(17)	1.745(11)
$\chi_{bb}(N_3) - \chi_{cc}(N_3)$ (MHz)		0.740(28)	–0.634(14)
$\chi_{aa}(N_3)$ (MHz)	*ortho*	1.925(11)	–
$\chi_{bb}(N_3) - \chi_{cc}(N_3)$ (MHz)		–0.746(17)	–
$\chi_{aa}(N_6)$ (MHz)	*ortho*	1.925(11)	0
$\chi_{bb}(N_6) - \chi_{cc}(N_6)$ (MHz)		–0.746(17)	0.881(17)
$|\mu_a|, |\mu_b|, |\mu_c|{}^{[e]}$ (D)		0, 1.2, 0	0.4, 2.2, 0
a-/b-/c-type [f]		N/Y/N	N/Y/N
κ [g]		–0.99	–0.91
N [h]		188	161
$\sigma_{RMS}{}^{[i]}$ (kHz)		13.3	16.3

[a] A_0, B_0, C_0: experimentally determined effective rotational constants simultaneously determined for the *ortho* and *para* nuclear spin isomers.

[b] Numbers in parentheses are one standard deviation in units of the last significant figures.

[c] D_J, D_{JK}, D_K, d_1: quartic centrifugal distortion constants simultaneously determined for the *ortho* and *para* nuclear spin isomers.

[d] χ_{aa} and $\chi_{bb} - \chi_{cc}$: nuclear quadrupole coupling constants. The *ortho* and *para* labels refer to the nuclear spin isomers of *syn-syn*-CDIT.

[e] Magnitude of the calculated dipole moment components.

[f] a-/b-/c-type transitions. Y and N correspond to "yes" and "no", respectively, indicating whether the type of transition is detected.

[g] Ray's asymmetry parameter $\kappa = \frac{2B - A - C}{A - C}$

The assignment of the fits to the *ortho* and *para* nuclear spin isomers of *syn-syn*-CDIT was based on arguments around nuclear spin statistics for bosons. The C_{2v} symmetry of this conformer implies that rotation about the b-axis, which coincides with the C_2 axis, interchanges equivalent bosons. It holds that the total wavefunction:

$$\psi_{tot} = \psi_{elec} \times \psi_{vib} \times \psi_{rot} \times \psi_{ns} \qquad \text{Eq.1}$$

where ψ_{elec}, ψ_{vib}, ψ_{rot}, and ψ_{ns} are the electronic, vibrational, rotational, and nuclear spin wavefunctions, respectively, is symmetric and of positive parity. Thus, upon C_2 rotation, *i.e.*, exchange of identical bosons, we have:

$$\psi(2,1) = +\psi(1,2) \qquad \text{Eq.2}$$

Considering that our experiment probes the vibronic ground state, the electronic and vibrational wavefunctions for *syn-syn*-CDIT both have a positive parity. Therefore, the total parity of ψ_{tot} is determined by the product of $\psi_{rot} \times \psi_{ns}$ such that:

$$\psi_{tot} = \begin{cases} \psi_{rot}^{(+)} \times \psi_{ns}^{(+)} \\ \qquad \text{or} \qquad \qquad \text{Eq.3} \\ \psi_{rot}^{(-)} \times \psi_{ns}^{(-)} \end{cases}$$

where the symbols in parentheses indicate the parity. Upon a C_2 permutation, the rotational wavefunction is multiplied by a factor of -1. The parity of ψ_{rot} depends on the sum of $K_a'' + K_c'' = K_{sum}''$, specific to each $J'' \leftarrow J'$ rotational transition, such that:

$$\psi_{rot} = \begin{cases} \psi_{rot}^{(+)} \sim (-1)^{2n} \\ \qquad \text{or} \qquad \qquad \text{Eq.4} \\ \psi_{rot}^{(-)} \sim (-1)^{(2n+1)} \end{cases}$$

for even K_{sum}'' $(2n)$ the parity of ψ_{rot} is positive and for odd K_{sum}'' $(2n + 1)$ the parity of ψ_{rot} is negative. From Eq. 3 and 4 it follows that ψ_{ns} must be of positive parity (*ortho*-isomers) for even K_{sum}'' and of negative parity (*para*-isomers) for odd K_{sum}''. The ratio between symmetric and antisymmetric nuclear spin wavefunctions is given by:

$$\frac{N_+}{N_-} = \frac{(I+1)(2I+1)}{I(2I+1)} = \frac{I+1}{I} \qquad \text{Eq.5}$$

There are two symmetric and one antisymmetric spin wavefunctions, corresponding to two *ortho*-isomers ($I_{tot} = 0, 2$), associated with even K''_{sum}, and one *para*-isomer, associated with odd K''_{sum}.

Sufficient signal to noise ratio for several rotational transitions of the parent *syn-syn*-CDIT allowed for detection of the singly substituted [34]S, ^{13}C, and ^{15}N isotopologues in their natural isotopic abundances, 4.4%, 1.1%, and 0.4%, respectively. Detection of these isotopologues further confirms the assignment of the fitted rotational constants to *syn-syn*-CDIT. The C_2 axis of symmetry renders the atoms of the two isothiocyanate groups equivalent to each other which results in doubling of the signal intensity of the respective singly substituted isotopologue. It should be noted that it is possible to perform a global fit for each rare isotopologue, including all the available transitions. Single isotopic substitution reduces the C_{2v} symmetry to C_s, meaning that the N, C, and S atoms are no longer equivalent. This holds as further evidence that the observed spectral behavior of the parent *syn-syn*-CDIT isotopologue is an outcome of the presence of two distinct nuclear spin isomers.

The fitted spectroscopic parameters of the singly substituted [34]S, ^{13}C, and ^{15}N isotopologues of *syn-syn*-CDIT are collected in Table 4. To generate these parameters, a pseudo-C_{2v}[*] geometry is assumed. Attempts to treat the symmetry as C_s with non-equivalent N atoms prevents the fit from converging and generates unrealistically large nuclear quadrupole coupling constants in the fits for the [34]S and ^{13}C isotopologues. The high intensity of the spectrum of the [34]S isotopologue allowed for the assignment of 138 transitions, and for the determination of the quartic centrifugal distortion constant D_{JK}, and nuclear quadrupole coupling constants $\chi_{aa}(^{14}\text{N})$ and $\chi_{bb}(^{14}\text{N}) - \chi_{cc}(^{14}\text{N})$. The D_{JK} distortion constant in the ^{13}C isotopologue fit was kept fixed to the value that was determined for the [34]S isotopologue. Finally, due to the small number of available transitions of the ^{15}N isotopologue, the D_{JK} and $\chi_{aa}(^{14}\text{N})$ and $\chi_{bb}(^{14}\text{N}) - \chi_{cc}(^{14}\text{N})$ constants were both kept fixed to the values determined for the [34]S isotopologue. The experimentally determined A_0, B_0, and C_0

---

[*] Single isotopic substitution reduces the symmetry of *syn-syn*-CDIT from C_{2v} to C_s, making the atoms in the –N=C=S groups non-equivalent. Pseudo-C_{2v} refers to the treatment of the C_s as C_{2v} for the sake of obtaining a fit that can converge with reasonable values of nuclear quadrupole coupling constants.

rotational constants will be used in Section 4.5 to determine the atomic coordinates of the atoms in the isothiocyanate groups in *syn-syn*-CDIT.

Table 4. Experimentally determined spectroscopic parameters of the singly substituted ^{34}S, ^{13}C, and ^{15}N isotopologues of *syn-syn*-CDIT in their natural isotopic abundances.

	^{34}S	^{13}C	^{15}N
A_0 (MHz)	11042.9488(27)[a]	11029.0588(35)	11002.9140(90)
B_0 (MHz)	438.30798(69)	447.6461(18)	449.3334(98)
C_0 (MHz)	421.6377(14)	430.2687(18)	431.7588(90)
D_{JK} (kHz)	1.86(24)	[1.86]	[1.86]
χ_{aa}(N) (MHz)[b]	1.9870(80)	1.962(13)	[1.9870]
χ_{bb}(N) $-\chi_{cc}$(N) (MHz)	−0.751(12)	−0.692(18)	[−0.751]
N[c]	138	66	6
σ_{RMS} (kHz)[d]	14.4	14.9	10.8

[a] Numbers in parentheses are one standard deviation in units of the last significant figures.

[b] Two equivalent nitrogen atoms assumed in the fit.

[c] Number of rotational transitions included in the fit.

[d] Root mean square deviation of the fit.

Spectrum of *syn-anti*-CDIT

Following the assignment of *syn-syn*-CDIT and its singly substituted [34]S, ^{13}C, and ^{15}N isotopologues, a large number of lines with hyperfine splitting remained unassigned. A second pattern, with significantly lower intensity than the one identified for *syn-syn*-CDIT, consistent with *Q*-branch, *b*-type transitions exhibiting extensive hyperfine splitting was found. Using the calculated rotational constants for *syn-anti*-CDIT as a guide, the pattern was fitted to a set of rotational parameters and allowed for identification of more lines. The final spectroscopic parameters were generated with Pickett's SPFIT/SPCAT[28] and are summarized in Table 3. The N atoms in *syn-anti*-CDIT are not equivalent, and individual $\chi_{aa}(^{14}N)$ and $\chi_{bb}(^{14}N)-\chi_{cc}(^{14}N)$ constants can be determined. A representative example of fitted transitions of *syn-anti*-CDIT showcasing the hyperfine splitting is given in Fig. 4. The lower intensity of the rotational lines of *syn-anti*-CDIT did not allow for detection of singly substituted isotopologues to determine an experimental structure. However, the agreement between experimental and calculated rotational constants, the detected *b*-type transitions and the significantly lower intensity of this species supports the assignment to *syn-anti*-CDIT.
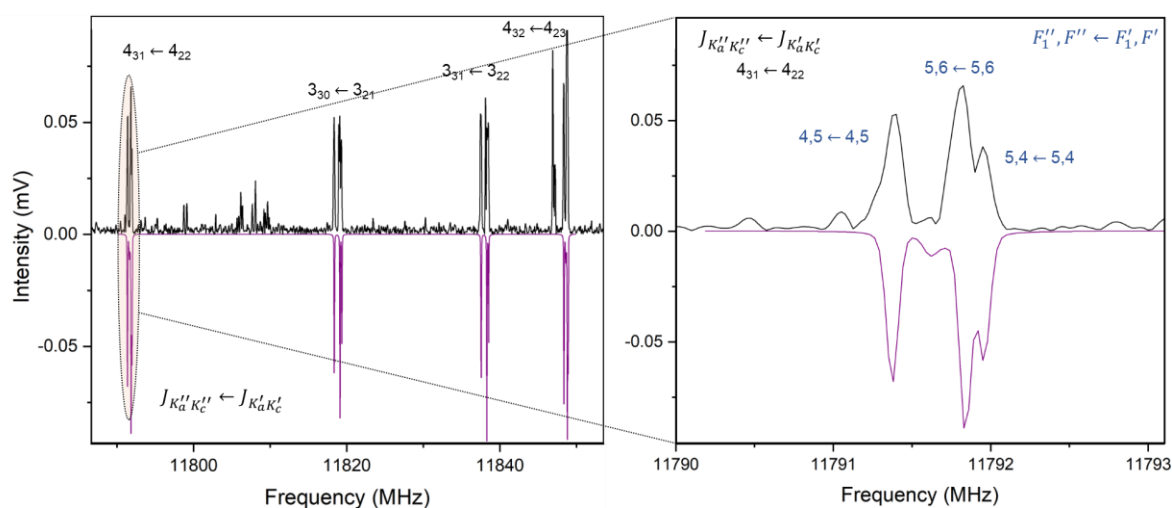
Figure 4. Portion of the experimental spectrum of *syn-anti*-CDIT (upper black trace) showcasing the resolution of the hyperfine structure. The simulation (lower purple trace) based on fitted rotational parameters reproduces the hyperfine splitting at a rotational temperature of 0.5 K.

Relative abundances

It is immediately apparent that *syn-syn*-CDIT is the most abundant species in this experiment. This observation is in line with previous condensed phase studies on CDIT[21] and other related compounds[24,30–33], and further supported by DFT calculations identifying this conformer as the global minimum, followed by *syn-anti*-CDIT approximately 4.5 kJ mol^{-1} higher in energy. The relative abundances of *syn-syn* and *syn-anti*-CDIT can be estimated from the relative intensities of their rotational transitions. According to the procedure described by Quesada-Moreno *et al.*[34], a set of three or four rotational transitions of the two species with the same $J''_{K''_a K''_c} \leftarrow J'_{K'_a K'_c}$ quantum numbers are selected, and their intensities are normalized by the square of the respective electric dipole moment. To get a reliable insight into the relative abundances, it is key that the selected transitions fall within a relatively narrow frequency range, *e.g.* up to 2 GHz. However, even though *syn-syn* and *syn-anti*-CDIT are conformers of the same compound, the experimentally determined A_0 rotational constants differ by an order of magnitude. In our rotational spectra there are no assigned transitions that fulfill these requirements and therefore this method would give an unreliable result.

An alternative procedure to estimate the relative abundances of the two species is to use the simulation function of PGOPHER[26]. The spectra of *syn-syn* and *syn-anti*-CDIT were simulated simultaneously at a rotational temperature of 0.5 K, using the calculated $|\mu_b|$ dipole moment of 1.2 and 2.2 D, respectively. The rotational temperature of 0.5 K was selected as it can reproduce the experimental intensities of rotational transitions of each species individually. It should be noted that the rotational partition function of each molecule at the given temperature is by default taken into account when the intensities are simulated with PGOPHER. Finally, the simulated abundance of *syn-syn*-CDIT was set to 1 while the abundance of *syn-anti*-CDIT was adjusted until the relative intensities of the two simulations could reproduce those of the experimental spectrum. Following this procedure, it is estimated that *syn-syn*-CDIT is approximately 8 to 10 times more abundant that *syn-anti*-CDIT under the given experimental conditions.

The estimated 8:1 to 10:1 abundance ratio between *syn-syn* and *syn-anti*-CDIT is supported by the computed relative energies of the two at the B3LYP-D3(BJ)/aug-cc-pVTZ level. The two conformers are separated by an energetic barrier of 16 kJ mol^{-1} with the local *syn-anti* minimum lying 4.5 kJ mol^{-1} higher than the global *syn-syn*-CDIT minimum. The *anti-*

anti conformation is not identified in the spectrum collected under our experimental conditions. Despite the fact that *anti-anti*-CDIT possesses the largest $|\mu_b|$ electric dipole moment out of the three conformers, this conformation is energetically disfavored by lying 14 kJ mol^{-1} above the global minimum. The relative populations of the three conformers of CDIT can be calculated according to their Boltzmann distributions at the temperature of the sample during the experiment (75 °C/348 K), prior to collisional cooling due to supersonic expansion, and by considering their computed energies, relative to the global minimum. Using the expression $N = \exp(-\frac{\Delta E}{kT})$, where N is the number of molecules in a certain conformation, ΔE is the computed relative energy, k is the Boltzmann constant, and T is the temperature of the sample, we calculate that 80% of CDIT is in the *syn-syn* conformer, while the *syn-anti* and *anti-anti* conformers take up approximately 17% and 3%, respectively. The calculated abundances are broadly consistent with the estimated abundances from the rotational spectrum.

Previous studies have explored the conformational equilibrium of compounds structurally related to CDIT, both in the condensed and gas-phase. A summary of their determined relative abundances, as well as their barriers to interconversion are summarized in Table 5. Compounds with the general formula $X(C=O)NCO$ (X = F, Cl, Br) consist of a central carbonyl group, which is substituted by a halogen atom and a pseudohalide group. In relation to CDIT, those can also exist as different rotational conformers: *syn* and *anti* (see Fig. 1). Both IR and Raman spectroscopy for fluoro-[31–33,35], chloro-[32,36], and bromocarbonyl[37] isocyanate show that their conformers are in an equilibrium state at room temperature. For X = F the *syn* conformer is with 75(12) %[33] preferred, according to gas phase electron diffraction (GED), while for X = Cl, and X = Br the *anti*-conformer is the dominant form. The *syn* to *anti* ratio for chlorocarbonyl isocyanate calculated from GED is 25(8):75(8)[36].

Fluoro- and chlorocarbonyl isothiocyanate (X(C=O)NCS (X = F, Cl))[38] as well as their isomers, fluoro- and chlorocarbonyl thiocyanate (X(C=O)SCN (X = F, Cl))[39], also show an equilibrium state in the gas and liquid phase. In the solid state, solely the thermodynamically more stable *syn* conformers of F(C=O)NCS, F(C=O)SCN, Cl(C=O)SCN are present, as it was deduced from single crystal XRD and solid-state Raman spectroscopy. The structure of Cl(C=O)NCS was determined by GED and the outcoming conformer *syn* to *anti* ratio is 84(6):16(6)[39], being the only determined ratio. As

already discussed, CDIT and its related dipseudohalides, carbonyl diisocyanate ($CO(NCO)_2$) and carbonyl diazide ($CO(N_3)_2$), can in principle exist as three different conformers: *syn-syn*, *syn-anti*, and *anti-anti* (see Fig. 1)[22]. Both $CO(NCO)_2$ and $CO(N_3)_2$ show an equilibrium in the gas phase between their *syn-syn* and *syn-anti* conformers with a ratio of 62:38[40] and 88:12[24] (values estimated from IR spectroscopy), respectively. For carbonyl diisocyanate the ratio was refined from GED and is 66(3):34(3)[23]. These values fit well with the computed energy difference of 4.3 kJ mol^{-1} and 6.9 kJ mol^{-1} (B3LYP/6−311+G(3d,f) level of theory) between the *syn-syn*- and *syn-anti*-conformers of $CO(NCO)_2$ and $CO(N_3)_2$, respectively[23,24,40]. For both compounds, the *anti-anti* conformer is not found spectroscopically, probably as it lies much higher in energy, as a result of steric repulsion between the pseudohalide groups both being *anti* oriented with respect to the carbonyl group. In the solid state, both crystallize with their thermodynamically stable rotamer, which is the *syn-syn* conformer[23,24]. Pfeiffer *et al.*[41] discussed a correlation between the *syn-syn* to *syn-anti* conformational ratio and the computed energy difference between conformers. The general trend suggests that a higher *syn-syn* to *syn-anti* ratio is consistent with a higher energy difference between the two conformers. From Table 5, we also observe that a higher ratio is associated with a lower energy barrier to interconversion, suggesting a lower conversion rate to *syn-anti*, and the findings for CDIT fit well with this observation.

Table 5. An overview of the (*syn-*)*syn* to (*syn-*)*anti* ratio of CDIT and other related compounds, determined through different methods, alongside computed energy barriers.

Compound	(*syn-*)*syn* : (*syn-*)*anti* ratio	ΔE (kJ mol^{-1})	Barrier (kJ mol^{-1})	Method
$CO(N_3)_2$ [a]	88:12 (~7:1)	5-6.7	40.6	Matrix IR
$CO(NCO)_2$ [b]	66:34 (~2:1)	3.8(8)	12.6	GED
CDIT $CO(NCS)_2$ [c]	10:1	2.9-4.5	8-16	CP-FTMW
F(C=O)NCO [d]	77:23	2.1-5.0	–	GED
Cl(C=O)NCO [e]	25(8): 75(8)	1.7-6.7	–	GED
Br(C=O)NCO [f]	mainly *anti*	–	–	IR and Raman
sCl(C=O)NCS [g]	84(6): 16(6)	1.3	5.9	GED
Cl(C=O)SCN [g]	mainly *syn*	7.1	38.9	IR

[a]. Ratio between *syn-syn-* to *syn-anti-*$CO(N_3)_2$ from reference 24, computed energy difference and barrier to interconversion from references 24 and 41

[b]. Ratio between *syn-syn-* to *syn-anti-*$CO(NCO)_2$ and experimentally determined energy difference from reference 40, computed barrier from reference 41

[c]. *Syn-syn-* to *syn-anti-*$CO(NCS)_2$ ratio determined in this work, computed energy difference and barrier to interconversion from this work and reference 41

[d]. From reference 31 and 42

[e]. From reference 42

[f]. From reference 37, the ratio is not explicitly determined, however, the *anti*-conformer is favoured. Decreased electronegativity of the halogen atom [$\chi(F) > \chi(Cl) > \chi(Br)$] favors the adoption of an *anti*-orientation of the –NCO group.

[g]. From reference 39

Nuclear quadrupole coupling constants

The nuclear quadrupole coupling constants determined for *syn-syn* and *syn-anti*-CDIT were diagonalized according to a common set of orthogonal x, y, z axes. These are positioned on each individual N nucleus, yielding the diagonalized χ_{xx}, χ_{yy}, *and* χ_{zz} constants summarized in Table 8. The diagonalization was performed with QDIAG[43], and a visualization of the orientation of the axes is shown in Fig. S1 in the SI. The off-diagonal $|\chi_{ab}|$ constants were obtained through DFT calculations at the B3LYP-D3(BJ)/aug-cc-pVTZ level and given a 10% uncertainty. The same procedure was performed for other related compounds with a N nucleus within a –NCS group, as well as for compounds with a –NH$_2$ group.

From the values in Table 8, we observe that the local electronic environment of a N nucleus in a –NCS group displays significant differences to that of a –NH$_2$ group, *e.g.*, in phenyl isothiocyanate (Ph-NCS)[44] and urea[45]. These differences can be attributed to electron withdrawing and donating properties of the two groups, with –NCS being a strongly electron withdrawing group. *Syn-syn* and *syn-anti*-CDIT exhibit similar electronic environments around the N nuclei, suggesting that the reactivity of the molecule is not exclusively associated with a certain conformer. However, following the earlier arguments around the relative abundances, the *syn-syn* form is expected to partake in most reactions. The closely related molecules, ethoxycarbonyl isothiocyanate[46] and Ph–NCS[44], display a similar electronic environment around the N nucleus suggesting that the component attached to the –NCS group has little effect on the local electronic environment of the N nucleus.

Table 6. Diagonalized nuclear quadrupole coupling constants χ_{xx}, χ_{yy}, and χ_{zz} for CDIT and other related compounds.

		χ_{xx} (MHz)	χ_{yy} (MHz)	χ_{zz} (MHz)
syn-syn-CDIT [a]	N_3/N_6	−1.789(82)	2.382(82)	−0.594(12)
syn-anti-CDIT [a]	N_3	−2.24(16)	2.79(16)	−0.554(12)
	N_6	−1.87(21)	2.31(21)	−0.441(13)
Ethoxycarbonyl isothiocyanate [b]	N	−1.685(86)	2.338(86)	−0.6532(25)
Ph–NCS [c]	N	−1.4635	1.94656	−0.483069
Aniline [d]	N	4.20(13)	0	−4.20(6)
Urea [e]	N	2.311(18)	1.778(18)	−4.0889(26)

a. This work.
b. From reference 46
   From reference 44
d. From reference 47
e. From reference 45

Structural Analysis

Experimental determination of the rotational constants of the parent *syn-syn*-CDIT (Table 4) and its singly substituted ^{34}S, ^{13}C, and ^{15}N isotopologues (Table 5) allows for Kraitchman[48,49] analysis to be performed to obtain the substitution (r_s) coordinates of the atoms in the –NCS groups. The analysis was performed with the program KRA from the PROSPE website[43]. The resulting r_s coordinates, alongside their fractional uncertainties[50] to partially account for rotation-vibration effects, are shown in Table 6. The r_s method can only provide the magnitude of each coordinate, so the signs were inferred from the calculated DFT geometry. The $|c|$ coordinates were calculated as zero, consistent with planarity of the molecule, which is also supported by the value of the inertia defect[51] $\Delta_0 = I_c - I_a - I_b = -0.182$ u Å^2, where I_x corresponds to the respective moment of inertia for each axis. The magnitude and the sign of Δ_0 is consistent with low-lying out-of-plane motions of the –NCS groups at the zero point. The r_s coordinates were evaluated with EVAL[43] to yield bond lengths and angles relevant to the –NCS groups and are summarized in Table 6.

The experimentally determined r_s coordinates are shown alongside the r_e calculated coordinates in Table 6 and Fig. 6. The high level of agreement between the two provides strong evidence in support of the geometry for *syn-syn*-CDIT. The values of the r_s bond lengths r(C=S) and r(N=C), and the angle ∠(SCN) are compared to those determined by single-crystal X-ray diffraction (XRD)[21]. A slight elongation of all determined bond lengths is observed for the gas phase structure while the ∠(SCN) angle shows an essentially linear arrangement in the atoms of the –NCS groups. The more compact structure as well as the slight distortion from linearity in the ∠(SCN) angle that is observed with XRD is likely due to packing effects in the crystal. It is worth noting that only the *syn-syn* conformer crystallizes and therefore there is no structural information for the *syn-anti* conformer[21].

Table 7. Atomic r_s coordinates of *syn-syn*-CDIT determined experimentally alongside the calculated r_e coordinates, and structural parameters determined with XRD and CP-FTMW.

syn-syn-CDIT		$|a|^{\ddagger}$ (Å)	b (Å)
N	r_e	1.1426	−0.4410
	r_s	1.087(12)	−0.4273(35)
C	r_e	2.3366	−0.2639
	r_s	2.3298(13)	−0.2690(56)
S	r_e	3.8920	−0.1624
	r_s	3.8686(13)	−0.086(17)
		XRD	r_s
C=O (Å)		1.181(16)	–
C$_{carbonyl}$-N (Å)		1.381(5)	–
N=C (Å)		1.207(4)	1.253(12)
C=S (Å)		1.526(4)	1.5497(28)
∠(SCN) (º)		173.7(4)-175.7(4)	179.5(8)

‡ Only the magnitude of the a-coordinates is provided here. Due to the C_{2v} symmetry, to describe the positions of the atoms in either one of the –NCS groups, the a-coordinates need to all carry a positive or negative sign, respectively.

Figure 5. The experimental r_s coordinates (solid spheres) of *syn-syn*-CDIT compared to the calculated B3LYP-D3(BJ)/aug-cc-pVTZ r_e coordinates (translucent underlying structure).

Conclusions

The rotational spectrum of two conformers of the reactive compound carbonyl diisothiocyanate, *syn-syn* and *syn-anti*, were recorded with CP-FTMW spectroscopy in the 2-12 GHz frequency region. We estimated that the *syn-syn* form is approximately ten times more abundant than the *syn-anti* form, which fits well with the observed relative abundances of conformers of other related compounds. The spectrum of *syn-syn*-carbonyl diisothiocyanate was manifested as two distinct nuclear spin isomers, *ortho* and *para*, that exhibit characteristics of nuclear spin statistics for bosons, and were identified by the varying hyperfine structure of their rotational transitions. Observation of singly substituted isotopologues allowed for partial structure determination of *syn-syn*-carbonyl diisothiocyanate and determination of the atomic coordinates of the atoms in the –NCS groups. The gas-phase structure of isolated *syn-syn*-carbonyl diisothiocyanate shows a slight elongation of the bond lengths between the atoms of the –NCS groups when compared to the structure determined with XRD using crystals.

Carbonyl diisothiocyanate is a unique example of a molecule composed exclusively of eight bosons ($I = 0$ and 1), six of which, in the *syn-syn* and *anti-anti* forms, appear as three equivalent pairs (–NCS groups). S*yn-syn*-carbonyl diisothiocyanate is present as two nuclear spin isomers, *ortho* and *para*, which are distinguished by their nuclear quadrupole coupling signatures, as an outcome of differing symmetries in their nuclear states. Their nuclear quadrupole coupling constants χ_{aa} and $\chi_{bb} - \chi_{cc}$ are of the same magnitude, but show opposite signs, as seen in Tables 3 and 4. Observation of *ortho* and *para* nuclear spin isomers in molecules that exhibit nuclear spin statistics for bosons have previously been reported for several systems, however, these mainly include small linear molecules[52,53] (e.g., D_2, N_2) and asymmetric tops such as non-covalently bound complexes[54–56] (e.g., CO…N_2, N_2…HCl, N_2…OCS) where the C_2 axis coincides with the a-axis of inertia. In terms of nuclear spin statistics, these complexes were shown to exhibit characteristics of their respective boson counterparts that exchange upon a C_2 permutation, and the linkage between their nuclear spin isomers lies within the J and K_a quantum numbers. In the case of *syn-syn*-carbonyl diisothiocyanate, the C_2 axis is aligned with the b-axis of inertia, meaning that inclusion of the K_c quantum number is necessary to link the two isomers. Considering the lack of examples of complex molecules in the literature with nuclear spin

isomers where the J, K_a, and K_c quantum numbers are required to properly describe them, *syn-syn*-carbonyl diisothiocyanate makes for a noteworthy case.

Data availability

The data reported in this manuscript are available upon reasonable request from the corresponding authors.

Conflicts of Interest

The authors declare no conflicts of interest.

Acknowledgements

References

1   L. D. Landau and E. M. Lifshitz, *Quantum mechanics: non-relativistic theory*, Elsevier, 2013, vol. 3.

2   E. Moreno-Pineda, M. Damjanović, O. Fuhr, W. Wernsdorfer and M. Ruben, Nuclear Spin Isomers: Engineering a $Et_4N[DyPc_2]$ Spin Qudit, *Angew. Chemie Int. Ed.*, 2017, **56**, 9915–9919.

3   A. Gaita-Ariño, F. Luis, S. Hill and E. Coronado, Molecular spins for quantum computation, *Nat. Chem.*, 2019, **11**, 301–309.

4   S. S. Kaushik, Z. I. Cleveland, G. P. Cofer, G. Metz, D. Beaver, J. Nouls, M. Kraft, W. Auffermann, J. Wolber, H. P. McAdams and B. Driehuys, Diffusion-weighted hyperpolarized 129 Xe MRI in healthy volunteers and subjects with chronic obstructive pulmonary disease, *Magn. Reson. Med.*, 2011, **65**, 1154–1165.

5   J. R. Birchall, M. R. H. Chowdhury, P. Nikolaou, Y. A. Chekmenev, A. Shcherbakov, M. J. Barlow, B. M. Goodson and E. Y. Chekmenev, Pilot Quality-Assurance Study of a Third-Generation Batch-Mode Clinical-Scale Automated Xenon-129 Hyperpolarizer, *Molecules*, 2022, **27**, 1327.

6   T. Hama, A. Kouchi and N. Watanabe, Statistical ortho-to-para ratio of water desorbed from ice at 10 kelvin, *Science*, 2016, **351**, 65–67.

7   H. Kawakita, J. Watanabe, H. Ando, W. Aoki, T. Fuse, S. Honda, H. Izumiura, T. Kajino, E. Kambe, S. Kawanomoto, K. Noguchi, K. Okita, K. Sadakane, B. Sato, M. Takada-Hidai, Y. Takeda, T. Usuda, E. Watanabe and M. Yoshida, The Spin Temperature of NH_3 in Comet C/1999S4 (LINEAR), *Science*, 2001, **294**, 1089–1091.

8   J. E. Dickens and W. M. Irvine, The Formaldehyde Ortho/Para Ratio as a Probe of Dark Cloud Chemistry and Evolution, *Astrophys. J.*, 1999, **518**, 733–739.

9   K. F. Bonhoeffer and P. Harteck, Experimente über Para- und Orthowasserstoff, *Naturwissenschaften*, 1929, **17**, 182.

10   D. A. Horke, Y.-P. Chang, K. Długołęcki and J. Küpper, Separating Para and Ortho Water, *Angew. Chemie Int. Ed.*, 2014, **53**, 11965–11968.

11   P. Cacciani, J. Cosléou and M. Khelkhal, Nuclear spin conversion in H₂O, *Phys. Rev. A*, 2012, **85**, 12521.

12   Z.-D. Sun, M. Ge and Y. Zheng, Separation and conversion dynamics of nuclear-spin isomers of gaseous methanol, *Nat. Commun.*, 2015, **6**, 6877.

13   P. L. Chapovsky, J. Cosléou, F. Herlemont, M. Khelkhal and J. Legrand, Separation and conversion of nuclear spin isomers of ethylene, *Chem. Phys. Lett.*, 2000, **322**, 424–428.

14   Z.-D. Sun, K. Takagi and F. Matsushima, Separation and Conversion Dynamics of Four Nuclear Spin Isomers of Ethylene, *Science*, 2005, **310**, 1938–1941.

15   P. L. Chapovsky, V. V Zhivonitko and I. V Koptyug, Conversion of Nuclear Spin Isomers of Ethylene, *J. Phys. Chem. A*, 2013, **117**, 9673–9683.

16   B. Nagels, M. Schuurman, P. L. Chapovsky and L. J. F. Hermans, Nuclear spin conversion in molecules: Experiments on ¹³CH₃F support a mixing-of-states model, *Phys. Rev. A*, 1996, **54**, 2050.

17   P. L. Chapovskii, Conversion of nuclear spin modifications of CH₃F molecules in the gaseous phase, *Sov. J. Exp. Theor. Phys.*, 1990, **70**, 895.

18   A. E. Dixon, The action of metallic thiocyanates upon carbonyl chloride, *Proc. R. Soc. London.*, 1902, **18**, 235.

19   R. Bunnenberg and J. C. Jochims, Carbonyldiisothiocyanat, *Chem. Ber.*, 1981, **114**, 2075–2086.

20   R. Bunnenberg, J. C. Jochims and H. Härle, Zur Darstellung und Chlorierung von Carbonyl-diisothiocyanat, *Chem. Ber.*, 1982, **115**, 3587–3596.

21   J. Pfeiffer, C. Trost, A. Pachkovska and F. Tambornino, A Crystallographic, Spectroscopic, and Computational Investigation of Carbonyl and Oxalyl Diisothiocyanate, *Inorg. Chem.*, 2021, **60**, 10722–10728.

22   W. J. Balfour, S. G. Fougere, D. Klapstein and W. M. Nau, The infrared and Raman spectra of carbonyl diisocyanate, *Spectrochim. Acta Part A Mol. Spectrosc.*, 1994, **50**, 1039–1046.

23   T. M. Klapötke, B. Krumm, S. Rest, R. Scharf, J. Schwabedissen, H.-G. Stammler and N. W. Mitzel, Carbonyl Diisocyanate $CO(NCO)_2$: Synthesis and Structures in Solid State and Gas Phase, *J. Phys. Chem. A*, 2016, **120**, 4534–4541.

24   X. Zeng, M. Gerken, H. Beckers and H. Willner, Synthesis and Characterization of Carbonyl Diazide, $OC(N_3)_2$, *Inorg. Chem.*, 2010, **49**, 9694–9699.

25   J. K. G. Watson, Determination of Centrifugal Distortion Coefficients of Asymmetric-Top Molecules. III. Sextic Coefficients, *J. Chem. Phys.*, 2003, **48**, 4517–4524.

26   C. M. Western, PGOPHER: A program for simulating rotational, vibrational and electronic spectra, *J. Quant. Spectrosc. Radiat. Transf.*, 2017, **186**, 221–242.

27   G. S. 2nd Grubbs, D. A. Obenchain, H. M. Pickett and S. E. Novick, H_2-AgCl: a spectroscopic study of a dihydrogen complex., *J. Chem. Phys.*, 2014, **141**, 114306.

28   H. M. Pickett, The fitting and prediction of vibration-rotation spectra with spin interactions, *J. Mol. Spectrosc.*, 1991, **148**, 371–377.

29   R. F. Code and N. F. Ramsey, Molecular-Beam Magnetic Resonance Studies of HD and D_2, *Phys. Rev. A*, 1971, **4**, 1945–1959.

30   D. W. Ball, Carbonyl diazide, $OC(N_3)_2$: Calculated thermodynamic properties, *Comput. Theor. Chem.*, 2011, **965**, 176–179.

31   D. Klapstein and W. M. Nau, Conformational properties of carbonyl isocyanates—stereoelectronic effects favouring the cisoid conformation, *J. Mol. Struct.*, 1993, **299**, 29–41.

32   D. Klapstein and W. M. Nau, Spectroscopy of acyl and carbonyl isocyanates, *Spectrochim. Acta Part A Mol. Spectrosc.*, 1994, **50**, 307–316.

33   H.-G. Mack, C. O. Della Védova and H. Willner, Structures and conformations of carbonyl isocyanates and carbonyl azides. An experimental and theoretical investigation, *J. Mol. Struct.*, 1993, **291**, 197–209.

34   M. M. Quesada-Moreno, A. Krin and M. Schnell, Analysis of thyme essential oils using gas-phase broadband rotational spectroscopy, *Phys. Chem. Chem. Phys.*, 2019, **21**, 26569–26579.

35 J. R. Durig, G. A. Guirgis, K. A. Krutules, H. Phan and H. D. Stidham, Raman and infrared spectra, conformational stability, barriers to internal rotation and ab initio calculations of fluorocarbonyl isocyanate, *J. Raman Spectrosc.*, 1994, **25**, 221–232.

36 H.-G. Mack, H. Oberhammer and C. O. Della Védova, How reliable are ab initio calculations? Experimental and theoretical investigation of the structure and conformation of chlorocarbonyl isocyanate, ClC(O)NCO, *J. Mol. Struct. THEOCHEM*, 1989, **200**, 277–288.

37 C. O. D. Védova, Preparation and properties of bromocarbonyl isocyanate, BrC(O)NCO, *Spectrochim. Acta Part A Mol. Spectrosc.*, 1992, **48**, 1179–1185.

38 L. A. Ramos, S. E. Ulic, R. M. Romano, M. F. Erben, C. W. Lehmann, E. Bernhardt, H. Beckers, H. Willner and C. O. Della Védova, Vibrational Spectra, Crystal Structures, Constitutional and Rotational Isomerism of FC(O)SCN and FC(O)NCS, *Inorg. Chem.*, 2010, **49**, 11142–11157.

39 L. A. Ramos, S. E. Ulic, R. M. Romano, M. F. Erben, Y. V. Vishnevskiy, C. G. Reuter, N. W. Mitzel, H. Beckers, H. Willner, X. Zeng, E. Bernhardt, M. Ge, S. Tong and C. O. Della Védova., Spectroscopic Characterization and Constitutional and Rotational Isomerism of ClC(O)SCN and ClC(O)NCS, *J. Phys. Chem. A*, 2013, **117**, 2383–2399.

40 Q. Liu, H. Li, Z. Wu, D. Li, H. Beckers, G. Rauhut and X. Zeng, Photolysis of Carbonyl Diisocyanate: Generation of Isocyanatocarbonyl Nitrene and Diazomethanone, *Chem. – An Asian J.*, 2016, **11**, 2953–2959.

41 J. Pfeiffer, J. P. Wagner and F. Tambornino, Photolytic Decarbonylation of Oxalyl Diisothiocyanate in Solid Argon Matrices to *syn-anti* Carbonyl Diisothiocyanate and its Isomerization, *Eur. J. Inorg. Chem.*, 2023, **26**, e202300290.

42 M. Tho Nguyen, M. R. Hajnal and L. G. Vanquickenborne, How reliable are ab initio calculations?, *J. Mol. Struct. THEOCHEM*, 1991, **231**, 185–193.

43 Z. Kisiel, PROSPE - Programs for ROtational SPEctroscopy, http://info.ifpan.edu.pl/~kisiel/prospe.htm, accessed March 2024

44 W. Sun, W. G. D. P. Silva and J. van Wijngaarden, Rotational Spectra and

Structures of Phenyl Isocyanate and Phenyl Isothiocyanate, *J. Phys. Chem. A*, 2019, **123**, 2351–2360.

45   U. Kretschmer, D. Consalvo, A. Knaack, W. Schade, W. Stahl and H. Dreizler, The 14N quadrupole hyperfine structure in the rotational spectrum of laser vaporized urea observed by molecular beam Fourier transform microwave spectroscopy, *Mol. Phys.*, 1996, **87**, 1159–1168.

46   Y. Xu, W. Li, J. Zhang and G. Feng, Conformations and structures of ethoxycarbonyl isothiocyanate revealed by rotational spectroscopy, *Chinese J. Chem. Phys.*, 2022, **35**, 875–882.

47   A. Hatta, M. Suzuki and K. Kozima, Nuclear Quadrupole Effects in the Microwave Spectrum and Dipole Moment of Aniline, *Bull. Chem. Soc. Jpn.*, 1973, **46**, 2321–2323.

48   J. Kraitchman, Determination of Molecular Structure from Microwave Spectroscopic Data, *Am. J. Phys.*, 1953, **21**, 17–24.

49   H. D. Rudolph, Extending Kraitchman's equations, *J. Mol. Spectrosc.*, 1981, **89**, 430–439.

50   C. Costain, Further comments on the accuracy of rs substitution structures, *Trans. Am. Crystallogr. Assoc*, 1966, **2**, 157–164.

51   R. K. Bohn, J. A. Montgomery, H. H. Michels and J. A. Fournier, Second moments and rotational spectroscopy, *J. Mol. Spectrosc.*, 2016, **325**, 42–49.

52   F. G. Brickwedde, R. B. Scott and H. S. Taylor, The Difference in Vapor Pressures of Ortho and Para Deuterium, *J. Chem. Phys.*, 1935, **3**, 653–660.

53   S. Fleischer, I. S. Averbukh and Y. Prior, Selective Alignment of Molecular Spin Isomers, *Phys. Rev. Lett.*, 2007, **99**, 93002.

54   C. Xia, A. R. W. McKellar and Y. Xu, Infrared spectrum of the CO–N_2 van der Waals complex: Assignments for CO-paraN_2 and observation of a bending state for CO-orthoN2, *J. Chem. Phys.*, 2000, **113**, 525–533.

55   R. S. Altman, M. D. Marshall and W. Klemperer, The microwave spectrum and molecular structure of N_2–HCl, *J. Chem. Phys.*, 1983, **79**, 57–64.

56   J. P. Connelly, S. P. Duxon, S. K. Kennedy, B. J. Howard and J. S. Muenter, Hyperfine and Tunneling Effects in the Microwave Spectrum of N_2–OCS, *J. Mol. Spectrosc.*, 1996, **175**, 85–98.

3.3 Photolytic Decarbonylation of Oxalyl Diisothiocyanate in Solid Argon Matrices to *syn-anti* Carbonyl Diisothiocyanate and Its Isomerization

Jonathan Pfeiffer, Dr. J. Philipp Wagner, Dr. Frank Tambornino
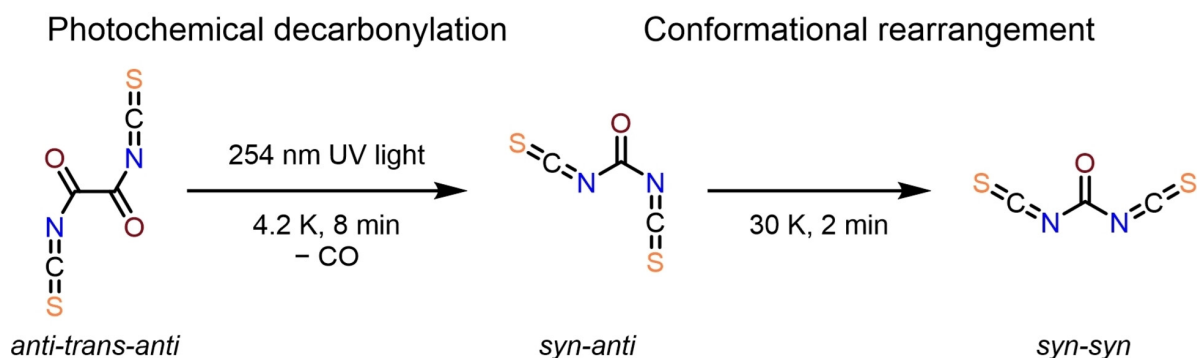
Abstract: *Oxalyl diisothiocyanate, ((CO)NCS)$_2$, has been studied in solid argon matrices at 4.2 K with the aid of infrared (IR) spectroscopy. The spectra show mainly signals attributed to the most stable anti-anti conformer, which is corroborated by comparison to computed anharmonic fundamental IR transitions. Upon irradiation with 254 nm UV light, oxalyl diisothiocyanate eliminates carbon monoxide under formation of carbonyl diisothiocyanate, CO(NCS)$_2$. This reaction is only slightly exothermic by 0.4 kcal mol^{-1} at the DLPNO-CCSD(T)/def2-QZVPP//B3LYP-D3/def2-TZVPP level of theory. Remarkably, photolysis produces mostly the less stable syn-anti conformer of carbonyl diisothiocyanate. Subsequent annealing at 30 K for two minutes results in a structural relaxation to the 0.7 kcal mol^{-1} more stable syn-syn conformer confirming a low torsional barrier height between the isomers.*

Zusammenfassung:

Oxalyldiisothiocyanat, ((CO)NCS)$_2$, wurde in einer festen Argon-Matrix bei 4.2 K mit der Hilfe von Infrarot (IR)-Spektroskopie untersucht. Die Spektren zeigen überwiegend Signale, die dem stabilsten *anti-anti* Konformer zugeordnet werden, was durch den Vergleich mit berechneten anharmonischen, fundamentalen IR Übergängen bestätigt wird. Unter Bestrahlung mit 254 nm UV-Licht eliminiert Oxalyldiisothiocyanat Kohlenstoffmonoxid und bildet Carbonyldiisothiocyanat, CO(NCS)$_2$. Diese Reaktion ist auf dem DLPNO-

CCSD(T)/def2-QZVPP//B3LYP-D3/def2-TZVPP Theorielevel mit 0.4 kcal mol^{-1} leicht exotherm. Bemerkenswert ist, dass die Photolyse hauptsächlich das weniger stabile *syn-anti* Konformer von Carbonyldiisothiocyanat erzeugt. Nachfolgendes Tempern bei 30 K für zwei Minuten resultiert in einer strukturellen Relaxation zu dem um 0.7 kcal mol^{-1} stabileren *syn-syn* Konformer, was eine geringe Torsionsbarriere zwischen den Isomeren bestätigt.

Beiträge der Autoren:

Oxalyldiisothiocyanat wurde von mir synthetisiert und für die Messungen bereitgestellt. Die darauffolgenden Messungen und DFT Rechnungen wurden von WAGNER durchgeführt und ausgewertet. Das Manuskript wurde von TAMBORNINO in Hauptarbeit und mir verfasst.

Cover Feature:

J. Pfeiffer, J. P. Wagner, and F. Tambornino
Photolytic Decarbonylation of Oxalyl Diisothiocyanate in Solid Argon Matrices
to *syn-anti* Carbonyl Diisothiocyanate and Its Isomerization
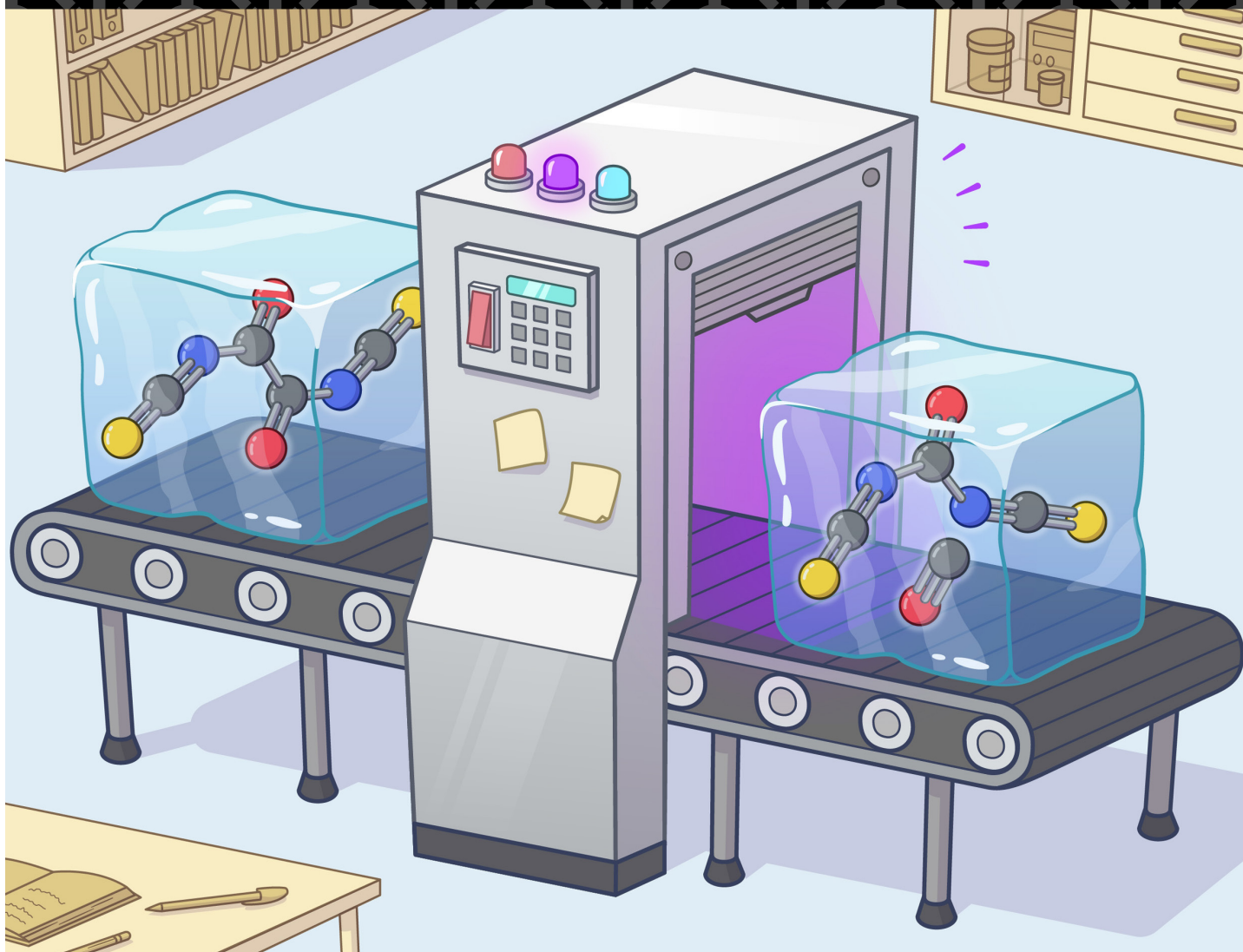
Photolytic Decarbonylation of Oxalyl Diisothiocyanate in Solid Argon Matrices to *syn-anti* Carbonyl Diisothiocyanate and Its Isomerization

Jonathan Pfeiffer,[a] J. Philipp Wagner,*[b] and Frank Tambornino*[a]

Oxalyl diisothiocyanate, $((CO)NCS)_2$, has been studied in solid argon matrices at 4.2 K with the aid of infrared (IR) spectroscopy. The spectra show mainly signals attributed to the most stable *anti-anti* conformer, which is corroborated by comparison to computed anharmonic fundamental IR transitions. Upon irradiation with 254 nm UV light, oxalyl diisothiocyanate eliminates carbon monoxide under formation of carbonyl diisothiocyanate, $CO(NCS)_2$. This reaction is only slightly exo-

thermic by 0.4 kcal mol^{-1} at the DLPNO-CCSD(T)/def2-QZVPP// B3LYP-D3/def2-TZVPP level of theory. Remarkably, photolysis produces mostly the less stable *syn-anti* conformer of carbonyl diisothiocyanate. Subsequent annealing at 30 K for two minutes results in a structural relaxation to the 0.7 kcal mol^{-1} more stable *syn-syn* conformer confirming a low torsional barrier height between the isomers.

Introduction

Oxalic acid is the simplest dicarboxylic acid and an abundant molecule in nature. It was first isolated as its potassium salt as early as 1769 from the eponymous *Oxalis* plant. While the first synthesis of oxalic acid from sugar and nitric acid can be attributed to Scheele and Bergman in 1776,[1–3] its first synthesis from inorganic starting materials was performed by Wöhler in 1824.[4,5] This procedure even precedes the famous urea synthesis of 1828 by four years.[6] Nowadays, industrial production does not rely on plant-based materials but rather uses thermal decomposition of sodium formate which itself is produced from CO and NaOH. The resulting sodium formate is then treated with calcium hydroxide and subsequently with sulfuric acid to obtain oxalic acid. Currently, its production volume is in the range of 100.000–200.000 tons annually.[7]

The corresponding acid halides (called oxalyl halides), of which oxalyl chloride is the most commonly known derivative, can be obtained from the parent acid. It is a key starting material for a wide range of chemicals, e.g. pharmaceuticals and agrochemicals.[8,9] Oxalyl bromide shows a similar reactivity but is a niche chemical in organic synthesis.[10] The lightest homologue, oxalyl fluoride, is not commonly available.[11] The pseudohalides of oxalic acid are even more exotic compounds. The only known congeners as of now are oxalyl diisothiocyanate and oxalyl dicyanide. While the former has recently been revisited, the latter is only scarcely characterized.[12,13]

Regarding the structure, oxalic acid,[14] oxalyl chloride and bromide,[15] as well as oxalyl diisothiocyanate[12] exhibit the carbonyl groups in a *trans* orientation in the solid state (see Scheme 1). If the substituents are not monoatomic, as in the case of oxalic acid and oxalyl diisothiocyanate (**1**), further conformational freedom is introduced into the molecule. While the OH groups are *syn* to the adjacent carbonyl groups in the solid-state structure of the parent acid, an *anti*-conformation is found for oxalyl diisothiocyanate (Scheme 1). Interestingly, oxalic acid's conformational preference changes in the gas phase and in noble gas matrices, where the *anti*-conformation gets stabilized by intramolecular hydrogen-bonding.[16–20]

[a] J. Pfeiffer, Dr. F. Tambornino
     Fachbereich Chemie
     Philipps-Universität Marburg
     Hans-Meerwein-Straße 4, 35043 Marburg, Germany
     E-mail: frank.tambornino@chemie.uni-marburg.de
[b] Dr. J. P. Wagner
     Institut für Organische Chemie
     Eberhard Karls Universität Tübingen
     Auf der Morgenstelle 18, 72076 Tübingen, Germany
     E-mail: philipp.wagner@orgchem.uni-tuebingen.de
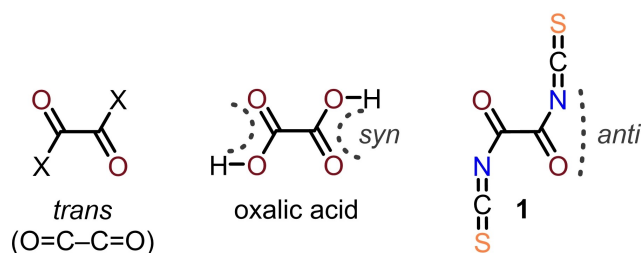
Scheme 1. Conformations of oxalic acid (middle), oxalyl chloride and bromide (left) and oxalyl diisothiocyanate (right). All molecules exhibit a *trans* conformation of the C=O moieties. In oxalic acid, the O–H groups are *syn* while in oxalyl diisothiocyanate the NCS groups are *anti* to the adjacent C=O groups.

EurJIC
European Journal of Inorganic Chemistry

Research Article
doi.org/10.1002/ejic.202300290

Chemistry Europe
European Chemical
Societies Publishing

In this contribution, we study oxalyl diisothiocyanate (**1**) isolated in a solid argon matrix with a combination of infrared (IR) spectroscopy and high-level DLPNO-CCSD(T) computations. We probe the photosensitivity of **1** and show the formation of carbonyl diisothiocyanate (CO(NCS)$_2$, **2**) which is obtained in an excited conformational state. Hence, our study provides fundamental insights into structure and photochemistry of a previously elusive class of compounds.

Results and Discussion

Conformation of Oxalyl Diisothiocyanate

In principle, oxalyl diisothiocyanate can exist in the form of six different conformational isomers. In order to explore their energetic viability, we deployed accurate computations at the DLPNO/CCSD(T)/def2-QZVPP//B3LPY-D3/def2-TZVPP level of theory and depict the resulting conformational energy landscape in Figure 1. We found that conformers are energetically preferred when the carbonyl groups are oriented *trans* (**T**) to one another which minimizes the local dipole moment of the O=C–C=O unit. Accordingly, the overall minimum energy structure corresponds to a *trans*-isomer in which both isothiocyanate groups assume an *anti*-orientation (**aTa**). Reorientation of one NCS moiety into a *syn*-position comes with an energetic penalty of 2.0 kcal mol^{-1} (**aTs**), while the *syn-syn* isomer **sTs** is even less favored by 3.4 kcal mol^{-1}. Higher in energy, the respective conformers with *cis* oriented carbonyl groups are found corresponding to the *syn-cis-syn* (**sCs**) and *syn-cis-anti* (**sCa**) structures. The respective *anti-anti* conformer with *cis* carbonyl groups is not a local minimum due to steric repulsion of the isothiocyanate substituents. Our quantum chemical computations predict a strong preference for the most stable **aTa** conformer which is also the sole species in the crystal structure. In principle, due to the low torsional barriers, all conformers could be accessible at room temperature, however, these states are not significantly populated at the measurement conditions.

In order to scrutinize the conformational preference experimentally, we evaporated a sample of oxalyl diisothiocyanate from a glass flask under ice cooling into a high vacuum (~10^{-6}
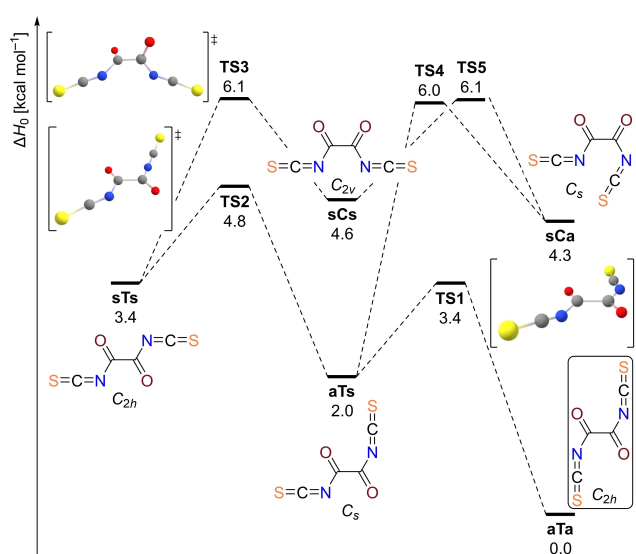
Figure 1. Conformer landscape of oxalyl diisothiocyanate at the DLPNO-CCSD(T)/def2-QZVPP//B3LYP-D3/def2-TZVPP level of theory.

mbar) and co-condensed the compound with an excess of argon onto a cold spectroscopic window (4.2 K). Subsequently, the deposited species were characterized by vibrational spectroscopy. The so obtained IR spectrum, which is depicted in the lower black trace of Figure 2, is characterized by its simplicity and a low number of observed features, hinting at the trapping of a conformer with C_{2h} symmetry, i.e. with equivalent NCS substituents. The features of this spectrum correspond well with the computed anharmonic fundamental vibrations of the most stable oxalyl diisothiocyanate conformer, which are plotted in the upper trace of Figure 2. It appears that mainly the **aTa** conformer is trapped in the cryogenic noble gas matrix. At 1922 cm^{-1}, the very strong band assigned to the out-of-phase antisymmetric stretching vibration of the NCS groups dominates the spectrum. A characteristic feature of the carbonyl C=O bonds is observed at 1738 cm^{-1}. The signal at 1171 cm^{-1} is attributed to an antisymmetric C–N stretching and the signal at 872 cm^{-1} to the antisymmetric δ_{as}(N–C=O) bending vibration. Smaller bands nearby the main absorption features could in principle stem from less stable isomers, however, we deem this

Philipp Wagner (born 1988) studied chemistry at the Justus-Liebig University Giessen (Germany), where he also received his doctorate in organic chemistry with Prof. Peter R. Schreiner. He was a postdoc in the lab of Prof. Mike Duncan at the University of Georgia, USA, studying mass-selected cations with photo-dissociation spectroscopy. In 2019, Philipp started his independent career at the University of Tübingen (Germany) supported by a Liebig fellowship. His research revolves around the chemistry of reactive intermediates utilizing a combination of organic synthesis, matrix isolation spectroscopy, and computational chemistry.

Frank Tambornino studied chemistry and biochemistry at the Ludwig Maximilian University of Munich, Germany, where he obtained his PhD in inorganic chemistry (2016) under the guidance of Dr. Constantin Hoch. He then joined the laboratory of Prof. Jose Goicoechea at the University of Oxford as a postdoc. In 2019 he moved to Marburg, starting his independent career first as a Liebig-grant recipient and currently as a Fellow of the Emmy-Noether-Programme of the German Research Council (DFG). In his research he focusses on the molecular and solid-state chemistry of pseudohalides.

EurJIC
European Journal of Inorganic Chemistry

Research Article
doi.org/10.1002/ejic.202300290

Chemistry Europe
European Chemical Societies Publishing

Figure 2. The bottom trace shows the IR spectrum of oxalyl diisothiocyanate as deposited in solid argon at 4.2 K. It is compared to the anharmonic fundamentals computed at the B3LYP-D3/def2-TZVPP level of theory within the VPT2 approximation (upper trace).

Figure 3. The lower trace corresponds to the difference IR spectrum of oxalyl diisothiocyanate in solid argon after 8 min of irradiation with 254 nm UV light. The experiment is compared to the fundamental IR spectrum of carbonyl diisothiocyanate computed at the B3LYP-D3/def2-TZVPP level within the VPT2 approximation (top trace). For the full spectrum including negative bands see Figure S1 in the Supporting Information.

Scheme 2. Different conformers for carbonyl diisothiocyanate.

option unlikely. The most intense carbonyl stretching vibration of the second-most stable **aTs** conformer is expected red-shifted from the corresponding infrared transition in **aTa**, while the experiment exhi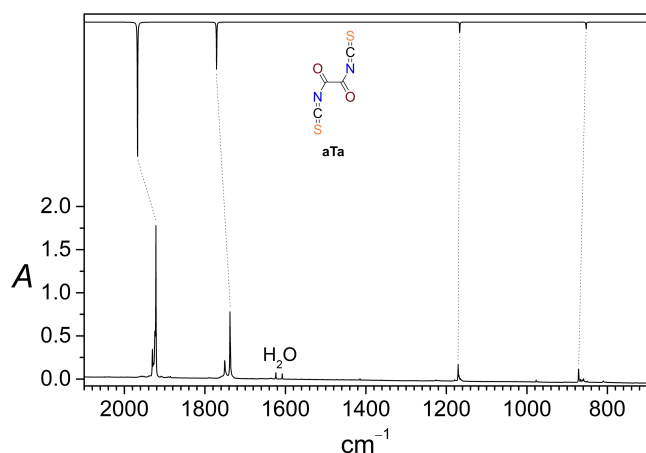bits a blue-shift ($1751\,\mathrm{cm}^{-1}$). Therefore, these bands are rather associated with overtones and combination bands of the most stable isomer. A more detailed summary of our vibrational assignments can be found in the Supporting Information (Table S1).

Photolysis of Oxalyl Diisothiocyanate

After trapping of oxalyl diisothiocyanate in an inert environment, we were interested in its photochemistry. The photolysis of oxalyl diisothiocyanate was performed in the solid argon matrix through irradiation with 254 nm UV light in increments of several minutes. The resulting difference IR spectrum after eight minutes of irradiation is shown in Figure 3, including a comparison to the computed IR spectrum of the *syn-anti* conformer of carbonyl diisothiocyanate **2** (top trace).

The intensities of all bands attributed to oxalyl diisothiocyanate drop sharply, indicating decomposition (Figure S1, Supporting Information) and, concurrently, the emergence of small signals near $2138\,\mathrm{cm}^{-1}$ can be observed suggesting the formation of carbon monoxide. For stoichiometric reasons, carbonyl diisothiocyanate appears to be a reasonable product of our photolysis experiment. Remarkably, the formation of two bands in the region expected for the NCS stretching vibrations at 1990 and $1905\,\mathrm{cm}^{-1}$ directly indicates the formation of a product with two symmetrically inequivalent isothiocyanate moieties. For carbonyl dipseudohalides, three different conformers can in principle be expected corresponding to the *syn-syn*, *syn-anti*, and *anti-anti* isomers depicted in Scheme 2.

A comparison with the computed IR spectrum of the low symmetry (C_s) *syn-anti* conformer shows that both bands can be assigned to the antisymmetric stretching modes of the NCS
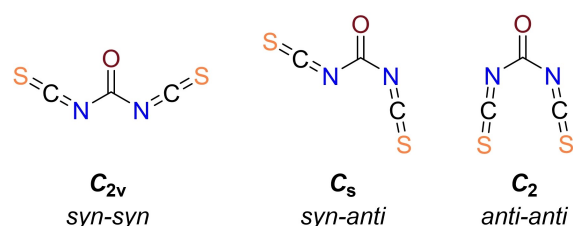
groups with the signal at $1990\,\mathrm{cm}^{-1}$ corresponding to the in-phase and the signal at $1905\,\mathrm{cm}^{-1}$ to the out-of-phase stretching vibrational motion, respectively. The carbonyl band appears nearby the analogous absorption in oxalyl diisothiocyanate and can be found at $1745\,\mathrm{cm}^{-1}$. At lower wavenumbers, the signal at $1213\,\mathrm{cm}^{-1}$ can be attributed to the antisymmetric C–N stretching vibration and the signal at $867\,\mathrm{cm}^{-1}$ to a $\delta(\mathrm{N-C=O})$ (*anti*-substituent) deformation vibration. While the fundamental vibrational modes for the *syn-syn* and *syn-anti* conformer of carbonyl diisothiocyanate are similar in energy, the occurrence of two different vibrational bands of non-negligible intensity for the isothiocyanate moieties allows for a unique identification of the *syn-anti* conformer in the matrix. In addition, the spectrum also exhibits minor contributions from the strongest bands of the *syn-syn* conformer, which could be corroborated in the subsequent annealing experiment (*vide infra*).

The exact mechanism of the decarbonylation remains unknown because it is unclear whether the reaction proceeds photochemically or in a hot ground state after deexcitation. However, the reaction is slightly favorable and concomitant with an energy gain of $0.4\,\mathrm{kcal\,mol}^{-1}$. The carbonyl diisothiocyanate photoproduct itself is unstable towards photodecomposition and its IR signals decrease in intensity upon further UV

EurJIC
European Journal of Inorganic Chemistry

Research Article
doi.org/10.1002/ejic.202300290

Chemistry Europe
European Chemical Societies Publishing

irradiation. The product of this consecutive photochemistry could not be discerned, unfortunately, due to the very low intensity of the emerging spectral features.

Syn-anti to syn-syn Rearrangement of Carbonyl Diisothiocyanate

As outlined above, carbonyl dipseudohalides can exist in the form of three distinct conformers which differ in relative energy depending on the nature of the substituent. In the case of carbonyl diisocyanate, gas-phase electron diffraction experiments showed a ratio of 66:34 in favor of the *syn-syn* conformer with a computed energy difference in the range of 0.7–1.0 kcal mol^{-1}.[21] Similarly, carbonyl diazide (CO(N$_3$)$_2$) exhibits a comparable equilibrium with an 88:12 ratio of the conformers also in favor of the *syn-syn* conformation. The higher ratio is associated with a higher energy difference of 1.2–1.6 kcal mol^{-1} between the conformers (depending on the computational method).[22] In all cases, the *anti-anti* conformer is not observed due to its higher potential energy that is associated with steric clashes, although an unfavorable alignment of local dipole moments might also play a role.

Here, the case of carbonyl diisothiocyanate is very much alike. Its molecular structure in the single crystal was recently reported, where the molecule adopts the *syn-syn* conformation.[12] While there are no gas-phase studies as of yet, our computations (see Figure 4) show that the *syn-anti* conformation is disfavored by 0.7 kcal mol^{-1} and the *anti-anti* conformation by 1.8 kcal mol^{-1}.

According to the low computed torsional barrier of only 1.2 kcal mol^{-1} it was reasonable to assume, that *syn-anti* carbonyl diisothiocyanate generated by photo-decarbonylation in the matrix would relax into its conformational ground state under mild thermal treatment. Thus, annealing was performed with the as-synthesized sample at 30 K for 2 min. Figure 5 shows the resulting difference IR spectrum (blue middle trace) and its comparison to the computed infrared fundamentals of
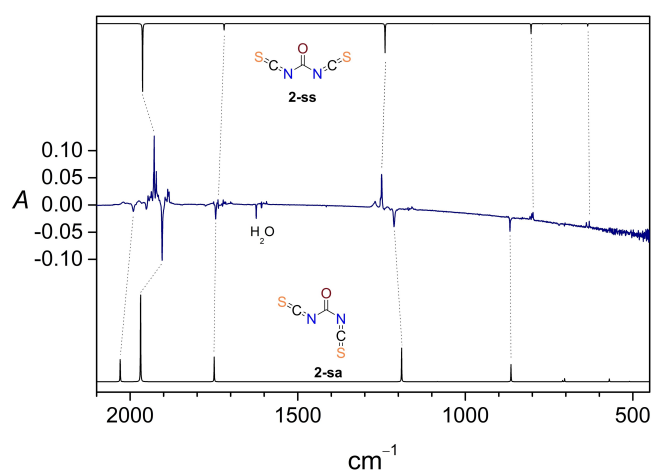
Figure 5. The blue trace in the middle shows the difference IR spectrum after annealing an argon matrix containing oxalyl diisothiocyanate for 2 min at 30 K, that was irradiated with UV light before (254 nm, 8 min). The experiment is compared to the infrared fundamentals of two carbonyl diisothiocyanate conformers computed at the B3LYP-D3/def2-TZVPP level within the VPT2 approximation.

carbonyl diisothiocyanate in the *syn-anti* (bottom) and *syn-syn* (top) conformation.

In the difference IR spectrum, the decreasing bands coincide with the features assigned to the *syn-anti* conformer of **2** which was formed in the photolysis of oxalyl diisothiocyanate. Simultaneously, new signals appear the strongest of which corresponds to a band at 1928 cm^{-1} which can be attributed to the antisymmetric stretching mode of the symmetrically equivalent NCS moieties in the *syn-syn* conformer. Further emerging IR bands also provide a good match for prominent computed IR transitions of the *syn-syn* conformer such as the carbonyl stretching at 1738 cm^{-1}, an antisymmetric C–N stretching vibration at 1250 cm^{-1} and an N–C≡O deformation at 801 cm^{-1}. Hence, we conclude that the mild thermal activation provided by annealing of the matrix to 30 K was sufficient to incite the conformational interconversion of carbonyl diisothiocyanate from its *syn-anti* to the more stable *syn-syn* conformer. This grants confidence to the computed barrier height of only 1.2 kcal mol^{-1}, which is similar in magnitude to, albeit smaller than that of carbonyl diisocyanate (3.0 kcal mol^{-1}) or carbonyl diazide (7.9 kcal mol^{-1}, Figure S2, Supporting Information).[21,22] The energetically most disfavored *anti-anti* conformer is 1.8 kcal mol^{-1} higher in energy in comparison to the *syn-syn* conformer and was thus not observed in our experiments. This also holds true for gas-phase studies of carbonyl diisocyanate and carbonyl diazide.[21,22]

Conclusion

All in all, we have demonstrated by a combination of cryogenic matrix isolation spectroscopy and high-level computational chemistry that oxalyl diisothiocyanate prefers to assume a conformation in which the NCS groups are *syn* to the carbonyl

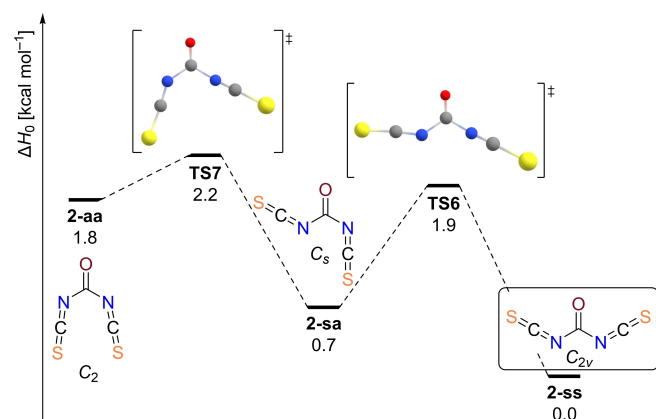**Figure 4.** Conformer landscape of carbonyl diisothiocyanate at the DLPNO-CCSD(T)/def2-QZVPP//B3LYP-D3/def2-TZVPP level of theory.

groups which themselves exhibit a *trans* orientation to each other. The matrix isolated oxalyl diisothiocyanate (**1**) releases carbon monoxide under UV irradiation leading to the formation of carbonyl diisothiocyanate (**2**) in its *syn-anti* conformation. Upon annealing, the latter isomerizes to the thermodynamically more stable *syn-syn* form even at the low experimental temperature of only 30 K. This seminal study opens the path towards the development of photolytic decarbonylation for this substance class on a preparative scale for both inorganic and organic chemists alike. Concurrently, in our laboratories efforts towards further photolytic reactions of **2** in noble gas matrices are under way, as well as the investigation of other related molecules.

Experimental Section

Matrix Isolation. Matrix isolation experiments were performed according to well-established experimental techniques.[23] Oxalyl diisothiocyanate, which was prepared according to a previously published procedure,[12] was evaporated from a glass flask maintained at a temperature of 0 °C for several hours. An argon flow of 2.0 sccm was provided by a PR400B MKS mass flow controller. Sample and inert gas were co-condensed onto a CsI spectroscopic window kept at a temperature of 15 K. After the deposition, the final experimental temperature of 4.2 K was approached. UV irradiation was performed with the 254 nm output of a PenRay low-pressure mercury lamp. The IR spectra were collected over 50 scans with a Bruker Vertex 70 IR spectrometer operating at a resolution of 0.5 cm^{-1}.

Computational Methods. All structures were optimized at the B3LYP-D3/def2-TZVPP level of theory with the Gaussian16 electronic structure code.[24–27] Vibrational frequencies were computed to characterize the nature of the localized stationary points as minima or transition states. For comparative purposes, the vibrational frequencies were further refined within the framework of second order vibrational perturbation theory (VPT2).[28] Final energies were obtained by computing DLPNO-CCSD(T)/def2-QZVPP single-point energies on top of the optimized structures with the ORCA 4 program package.[29]

Conflict of Interests

The authors declare no conflict of interest.

Data Availability Statement

The data that support the findings of this study are available in the supplementary material of this article.

[1] O. Zekert, *Carl Wilhelm Scheele, Gedenkschrift Zum 150. Todestage*, Springer-Verlag Wien GmbH, **1936**.
[2] T. Thomson, C. Hatchett, *Philos. Trans. R. Soc. London* **1808**, *98*, 63–95.
[3] T. Bergman, *Dissertatio de Chemica de Acido Sacchari*, **1776**.
[4] F. Wöhler, *K. Sven. vetensk. akad. handl.* **1824**, 328–333.
[5] F. Wöhler, *Ann. Phys. Chem.* **1825**, *79*, 177–182.
[6] F. Wöhler, *Ann. Phys. Chem.* **1828**, *12*, 253–256.
[7] W. Riemenschneider, M. Tanifuji in *Ullmann's Encyclopedia of Industrial Chemistry*, Wiley-VCH, Weinheim, Germany, **2011**, pp. 6–9.
[8] L. Mohammadkhani, M. M. Heravi, *ChemistrySelect* **2019**, *4*, 6309–6337.
[9] R. Salmon, I. V. Efremov, *Encycl. Reagents Org. Synth.* **2008**, 1–5.
[10] M. D. Ennis, W. S. Bechara, in *Encycl. Reagents Org. Synth.*, John Wiley & Sons, Ltd, Chichester, UK, **2012**, pp. 18–20.
[11] C. W. Tullock, D. D. Copfman, *J. Org. Chem.* **1960**, *25*, 2016–2019.
[12] J. Pfeiffer, C. Trost, A. Pachkovska, F. Tambornino, *Inorg. Chem.* **2021**, *60*, 10722–10728.
[13] R. W. Begland, D. R. Hartter, *J. Org. Chem.* **1972**, *37*, 4136–4145.
[14] J. L. Derissen, P. H. Smith, *Acta Crystallogr. Sect. B* **1974**, *30*, 2240–2242.
[15] P. Groth, O. Hassel, C. Römming, A. Block-Bolten, J. M. Toguri, H. Flood, *Acta Chem. Scand.* **1962**, *16*, 2311–2317.
[16] J. Nieminen, M. Räsänen, J. Murto, *J. Phys. Chem.* **1992**, *96*, 5303–5308.
[17] P. D. Godfrey, M. J. Mirabella, R. D. Brown, *J. Phys. Chem. A* **2000**, *104*, 258–264.
[18] B. C. Stace, C. Oralratmanee, *J. Mol. Struct.* **1973**, *18*, 339–342.
[19] P. R. Schreiner, J. P. Wagner, H. P. Reisenauer, D. Gerbig, D. Ley, J. Sarka, A. G. Császár, A. Vaughn, W. D. Allen, *J. Am. Chem. Soc.* **2015**, *137*, 7828–7834.
[20] R. L. Redington, T. E. Redington, *J. Mol. Struct.* **1978**, *48*, 165–176.
[21] T. M. Klapötke, B. Krumm, S. Rest, R. Scharf, J. Schwabedissen, H.-G. Stammler, N. W. Mitzel, *J. Phys. Chem. A* **2016**, *120*, 4534–4541.
[22] X. Zeng, M. Gerken, H. Beckers, H. Willner, *Inorg. Chem.* **2010**, *49*, 9694–9699.
[23] I. R. Dunkin, *Matrix Isolation Techniques - A Practical Approach*, Oxford University Press: University Of Strathclyde, **1998**.
[24] A. D. Becke, *J. Chem. Phys.* **1993**, *98*, 5648–5652.
[25] P. J. Stephens, F. J. Devlin, C. F. Chabalowski, M. J. Frisch, *J. Phys. Chem.* **1994**, *98*, 11623–11627.
[26] F. Weigend, R. Ahlrichs, *Phys. Chem. Chem. Phys.* **2005**, *7*, 3297–3305.
[27] Gaussian 16, Revision C.01, M. J. Frisch, G. W. Trucks, H. B. Schlegel, G. E. Scuseria, M. A. Robb, J. R. Cheeseman, G. Scalmani, V. Barone, G. A. Petersson, H. Nakatsuji, X. Li, M. Caricato, A. V Marenich, J. Bloino, B. G. Janesko, R. Gomperts, B. Mennucci, H. P. Hratchian, J. V Ortiz, A. F. Izmaylov, J. L. Sonnenberg, D. Williams-Young, F. Ding, F. Lipparini, F. Egidi, J. Goings, B. Peng, A. Petrone, T. Henderson, D. Ranasinghe, V. G. Zakrzewski, J. Gao, N. Rega, G. Zheng, W. Liang, M. Hada, M. Ehara, K. Toyota, R. Fukuda, J. Hasegawa, M. Ishida, T. Nakajima, Y. Honda, O. Kitao, H. Nakai, T. Vreven, K. Throssell, J. A. Montgomery Jr., J. E. Peralta, F. Ogliaro, M. J. Bearpark, J. J. Heyd, E. N. Brothers, K. N. Kudin, V. N. Staroverov, T. A. Keith, R. Kobayashi, J. Normand, K. Raghavachari, A. P. Rendell, J. C. Burant, S. S. Iyengar, J. Tomasi, M. Cossi, J. M. Millam, M. Klene, C. Adamo, R. Cammi, J. W. Ochterski, R. L. Martin, K. Morokuma, O. Farkas, J. B. Foresman, D. J. Fox, Gaussian, Inc., Wallingford CT, **2016**.
[28] M. Piccardo, J. Bloino, V. Barone, *Int. J. Quantum Chem.* **2015**, *115*, 948–982.
[29] F. Neese, *WIREs Comput. Mol. Sci.* **2018**, 8, e1327..

3.4 Double Addition *vs.* Ring Closure: Systematic Reactivity Study of CO(NCO)₂ and CO(NCS)₂ towards Hydrogen Halides

Jonathan Pfeiffer, Hennes Günther, Lena Völlinger, Demian Botros, Benjamin Scheibe, Martin Möbs, Florian Kraus, Florian Weigend, Frank Tambornino

Carbonyl bis(carbamoylhalide)

Halogenido-dihydro-thioxo-thiadiazine-4-one

Abstract: *The reactivity of carbonyl diisocyanate, CO(NCO)₂, and carbonyl diisothiocyanate, CO(NCS)₂ with nucleophiles shows different patterns: Whereas carbonyl diisocyanate adds two equivalents of nucleophile forming carbonyl bis(carbamoylhalides), carbonyl diisothiocyanate only adds one equivalent and undergoes intramolecular ring closure, resulting in the formation of substituted thiadiazines. In this study we have reacted both carbonyl diisocyanate and carbonyl diisothiocyanate with the full series of hydrogen halides HF to HI, isolating carbonyl bis(carbamoylfluoride) (**1**), -chloride (**2**), -bromide (**3**), and -iodide (**4**) as well as 6-chloro-2,3-dihydro-2-thioxo-4H-1,3,5-thiadiazin-4-one (**5**), and 6-bromo-2,3-dihydro-2-thioxo-4H-1,3,5-thiadiazin-4-one (**6**). The compounds were analysed by single-crystal X-ray diffraction, NMR spectroscopy, IR and Raman spectroscopy, and elemental analysis. Quantum mechanical calculations show thermodynamic reasons for the differences in reactivity.*

Zusammenfassung:

Die Reaktivität von Carbonyldiisocyanat, CO(NCO)₂, und Carbonyldiisothiocyanat, CO(NCS)₂, mit Nukleophilen zeigt zwei verschiedene Muster: Während Carbonyldiisocyanat zwei Äquivalente eines Nukleophils addiert und Carbonylbis(carbamoylhalogenide)

bildet, addiert Carbonyldiisothiocyanat nur ein Äquivalent und unterläuft einem intramolekularen Ringschluss, der in der Bildung von substituierten Thiadiazinen resultiert. In dieser Studie haben wir Carbonyldiisocyanat, sowie Carbonyldiisothiocyanat mit der kompletten Reihe an Halogenwasserstoffen, HF bis HI, umgesetzt und Carbonylbis(carbamoylfluorid) (**1**), -chlorid (**2**), -bromid (**3**) und -iodid (**4**), wie auch 6-Chloro-2,3-dihydro-2-thioxo-4*H*-1,3,5-thiadiazin-4-on (**5**) und 6-Bromo-2,3-dihydro-2-thioxo-4*H*-1,3,5-thiadiazin-4-on (**6**) isoliert. Die Verbindungen wurden mittels Röntgenbeugung am Einkristall, NMR-Spektroskopie, IR- und Raman-Spektroskopie und Elementaranalytik analysiert. Quantenchemische Rechnungen zeigen thermodynamische Gründe für die unterschiedlichen Reaktivitäten.

Beiträge der Autoren: Die Publikation beinhaltet Ergebnisse der Bachelorarbeit von HENNES GÜNTHER,[132] in welcher unter meiner Betreuung und Anleitung Verbindungen **2-6** synthetisiert und charakterisiert (^{1}H & ^{13}C{^{1}H}-NMR-Spektroskopie, Elementaranalytik, IR-Spektroskopie), sowie die Struktur von **6** ermittelt wurde. VÖLLINGER hat ein Forschungspraktikum, in welchem die Struktur von **5** bestimmt wurde, unter meiner Betreuung und Anleitung in unserer Arbeitsgruppe ausgeführt. SCHEIBE und MÖBS aus der Arbeitsgruppe KRAUS führten Umsetzungen mit Fluorwasserstoff durch und bestimmten die Strukturen von **1** und **8a** durch SC-XRD. **1** wurde NMR, IR und Raman spektroskopisch und mit Elementaranalytik von mir untersucht. Ich unternahm Syntheseversuche zu **7** und kristallisierte Verbindungen **2** und **3**. Ebenso wurden von mir die SC-XRD Messungen von **2-6** und **8b** durchgeführt, sowie anschließend die Strukturen gelöst und verfeinert. DFT Rechnungen mit *CRYSTAL17* der theoretischen IR- und Raman-Spektren wurden für alle Moleküle von mir durchgeführt. BOTROS hat unter Anleitung und Betreuung von WEIGEND DFT Rechnungen mit *TURBOMOLE* durchgeführt. Das Manuskript und die *Supporting Information* wurden von mir in Zusammenarbeit mit TAMBORNINO verfasst.

Double Addition *vs.* Ring Closure: Systematic Reactivity Study of CO(NCO)$_2$ and CO(NCS)$_2$ towards Hydrogen Halides

Jonathan Pfeiffer,[a] Hennes Günther,[a] Lena Völlinger,[a] Demian Botros,[a] Benjamin Scheibe,[a] Martin Möbs,[a] Florian Kraus,[a] Florian Weigend,[a] and Frank Tambornino*[a]

Abstract: The reactivity of carbonyl diisocyanate, CO(NCO)$_2$, and carbonyl diisothiocyanate, CO(NCS)$_2$ with nucleophiles shows different patterns: Whereas carbonyl diisocyanate adds two equivalents of nucleophile forming carbonyl bis(carbamoylhalides), carbonyl diisothiocyanate only adds one equivalent and undergoes intramolecular ring closure, resulting in the formation of substituted thiadiazines. In this study we have reacted both carbonyl diisocyanate and carbonyl diisothiocyanate with the full series of hydrogen halides HF to HI, isolating carbonyl bis(carbamoylfluoride) (**1**), -chloride (**2**), -bromide (**3**), and -iodide (**4**) as well as (6-chloro-2,3-dihydro-2-thioxo-4*H*-1,3,5-thiadiazin-4-one (**5**), and 6-bromo-2,3-dihydro-2-thioxo-4*H*-1,3,5-thiadiazin-4-one (**6**). The compounds were analysed by single-crystal X-ray diffraction, NMR spectroscopy, IR and Raman spectroscopy, and elemental analysis. Quantum mechanical calculations show thermodynamic reasons for the differences in reactivity.

Introduction

Phosgene, the dichloride of carbonic acid, is one of the most important C1 synthons in chemical industry and is being produced in more than 200 plants worldwide. In 2013 its estimated world production was 10^7 tons, in 2021 its global market size was valued at 39.2 billion USD and it is speculated that its share will increase to roughly 65 billion USD by 2031.[1] Phosgene is used as an intermediate chemical for the production of a wide range of substances ranging from agrochemicals, pharmaceuticals and polymers to dies and fine chemicals.[1]

Related to phosgene are the pseudohalides of carbonic acid. Of those simple compounds only a mere handful have been reported on, among which are carbonyl diisocyanate, CO(NCO)$_2$,[2,3] carbonyl diisothiocyanate, CO(NCS)$_2$,[4–6] carbonyl dicyanide, CO(CN)$_2$,[7,8] and carbonyl diazide, CO(N$_3$)$_2$.[9,10] All of these are toxic and sensitive compounds and their chemistry has been only scantly explored. Almost 60 years ago, reactions of carbonyl diisocyanate and carbonyl diisothiocyanate with nucleophiles were first reported on, but the studies relied mainly on NMR and elemental analysis data.[5,11–14] It was found that the former adds two equivalents of nucleophile, whereas the latter adds only one and cyclizes through an intramolecular reaction yielding differently substituted thiadiazine heterocycles, see Scheme 1. Additionally, it was speculated that the ring closure might be a kinetic effect proceeding faster than the addition of a second nucleophile.[5]

It is somewhat surprising that the crystal structures of the reaction products remained unknown for more than 40 years and thus complementary structural information in the solid state has remained unavailable.

[a] J. Pfeiffer, H. Günther, L. Völlinger, D. Botros, B. Scheibe, M. Möbs, Prof. Dr. F. Kraus, Prof. Dr. F. Weigend, Dr. F. Tambornino
Fachbereich Chemie
Philipps-Universität Marburg
Hans-Meerwein-Strasse 4, 35043 Marburg (Germany)
E-mail: frank.tambornino@chemie.uni-marburg.de
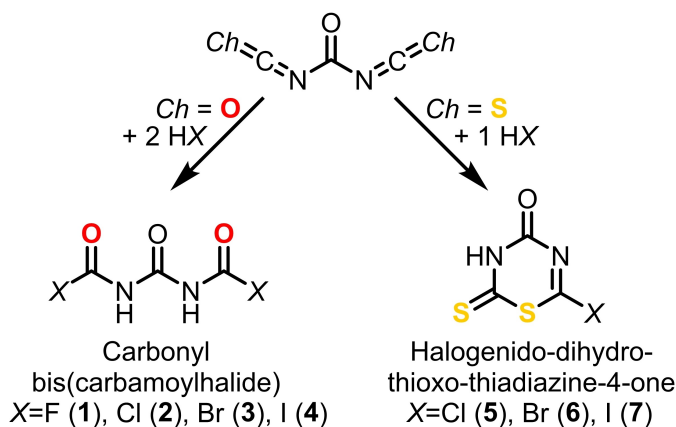
Scheme 1. Principle reaction patterns of carbonyl diisocyanate (*Ch*=O, left) and carbonyl diisothiocyanate (*Ch*=S, right) with hydrogen halides H*X* (*X*=F–I).

Chemistry–A European Journal

Research Article
doi.org/10.1002/chem.202203983

**Chemistry
Europe**
European Chemical
Societies Publishing

Here, we report a systematic reactivity study of carbonyl diisocyanate and carbonyl diisothiocyanate with the full series of hydrogen halides H*X* (*X* = F–I). Carbonyl diisocyanate adds two equivalents of hydrogen halide on the cyanate-carbon atom forming carbonyl bis(carbamoylhalides) (see Scheme 1, carbonyl bis(carbamoylfluoride) (**1**), carbonyl bis(carbamoylchloride) (**2**), carbonyl bis(carbamoylbromide) (**3**), carbonyl bis(carbamoyliodide) (**4**)), whereas carbonyl diisothiocyanate adds only one equivalent hydrogen halide. The latter reaction proceeds *via* intramolecular ring-closure and forms the uncommon thiadiazine motif (6-chloro-2,3-dihydro-2-thioxo-4*H*-1,3,5-thiadiazin-4-one, (**5**), 6-bromo-2,3-dihydro-2-thioxo-4*H*-1,3,5-thiadiazin-4-one (**6**) 6-iodo-2,3-dihydro-2-thioxo-4*H*-1,3,5-thiadiazin-4-one (**7**)). We present an in-depth analysis of their syntheses, crystal structures, NMR signatures and vibrational spectra. Additionally, we use quantum chemical methods to rationalize the differing reaction patterns of carbonyl diisocyanate and diisothiocyanate and give insight into the stability of the compounds.

Results and Discussion

Reactivity of carbonyl diisocyanate towards H–*X* (*X* = F–I)

A sample of carbonyl diisocyanate in a perfluoroalkoxy alkane (PFA) tube was cooled to $-78\,°C$ and anhydrous HF was condensed onto it. The mixture was allowed to warm to room temperature upon which the formation of colorless crystals in liquid hydrogen fluoride was observed through the translucent walls of the PFA tube. After removal of surplus hydrogen fluoride under reduced pressure a colorless powder of the pure compound was obtained in 90 % yield which already contained crystals suitable for X-ray diffraction. The ^{1}H NMR spectrum showed a signal at 9.40 ppm which is in accordance with an N–*H* moiety. The ^{13}C NMR spectrum contains a doublet at 143.0 ppm with $^1J_{C-F} = 297.5$ Hz and a triplet at 146.7 ppm with $^3J_{C-F} = 10.7$ Hz (see Figure 1). Those values corroborate the

molecular structure of **1**, and the connectivity was further proven by single-crystal X-ray diffraction (see below).

Compounds **2**, **3**, and **4** were synthesized according to a modified literature procedure.[14] The respective H*X* gas was dried by passing over P_4O_{10} and subsequently led through a solution of carbonyl diisocyanate in dichloromethane at $-78\,°C$. For *X* = Br and I, the gases were freshly prepared (HBr 10 equiv., HI 40 equiv.) and Ar was used as carrier gas. Solvent removal at $-20\,°C$ yielded colorless powders. For compounds **2**, **3** and **4**, ^{1}H NMR spectra showed a singlet around 9.7 ppm each, again in accordance with a N–*H* moiety. The respective ^{13}C NMR spectra showed two singlets (see Figure 1). For the carbamoyl halide moiety, resonances at 145.1 ppm (**2**), 136.4 ppm (**3**) and 114.0 ppm (**4**) were observed, showing a trend towards high field shifts with decreasing electronegativity of the halogen atom. The signal for the central *C*=O moiety shows a similar trend towards high field shift with decreasing electronegativity of the halogen atom *X* starting from 146.7 ppm (**1**), 146.4 ppm (**2**), 143.9 ppm (**3**) to 142.2 ppm (**4**). Compound **4** decomposed quickly as can be seen by further signals in the ^{13}C NMR spectrum.

Single crystals of compounds **2** and **3** suitable for X-ray diffraction were grown by slow concentration of saturated solutions in diethyl ether at $-78\,°C$ (for details see Supporting Information). Compound **4** proved to be too unstable to grow single crystals from solution.

Reactivity of carbonyl diisothiocyanate

For the reaction of carbonyl diisothiocyanate with anhydrous HF a sample of the starting material in a PFA tube was cooled to $-78\,°C$ and anhydrous HF was condensed onto it. Subsequently, the vessel was allowed to warm to room temperature upon which the formation of a yellow crystalline solid was observed. All volatiles were removed under reduced pressure and a red product was obtained which no longer was crystalline. A signal at 12.7 ppm in the ^{1}H NMR spectrum hinted at the formation of an in-ring N–*H* moiety. However, the ^{13}C NMR spectrum showed only two signals at 193.6 and 146.9 ppm instead of the expected three, both of which lacked the multiplet formation that would be expected from coupling to the ^{19}F atoms, indicating the formation of a smaller or higher symmetry product and absence of ^{19}F atoms. Single-crystal diffractometry revealed the formation of 2,3,5,6-tetrahydro-2,6-dithioxo-4*H*-1,3,5-thiadiazin-4-one (in the form of two tautomers: **8a** and **8b**) instead of the desired reaction product. This product can be made directly from carbonyl diisothiocyanate and H_2S which is an alternative synthetic route (see Scheme 2).[5]

Next, we tried a substitution reaction with sodium fluoride in acetone starting from compound **5**, see below, but we found that it reacts with acetone to give decomposition products which could not yet been identified. Silver fluoride dissolved in acetonitrile was another F$^-$ ion source we tried for the halogen atom exchange. A reaction was observed and AgCl proven as a side product by powder X-ray diffraction. However, only starting
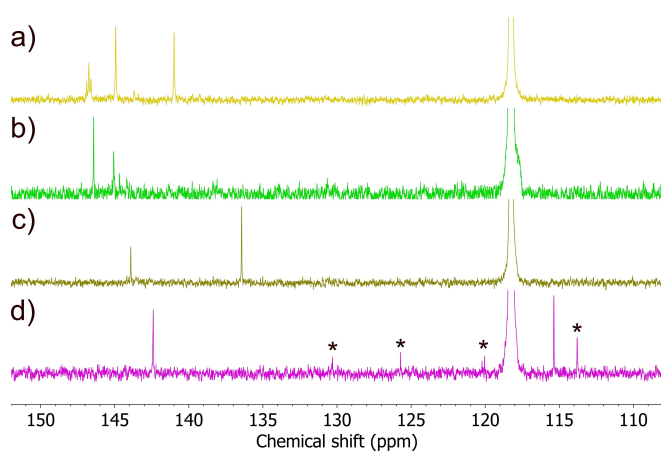

Figure 1. Sections of ^{13}C NMR spectra of the compounds **1** (a), **2** (b), **3** (c), and **4** (d). The latter spectrum also shows signals of decomposition, which are marked with asterisks.

Chem. Eur. J. **2023**, *29*, e202203983 (2 of 8)

© 2023 The Authors. Chemistry - A European Journal published by Wiley-VCH GmbH

Chemistry–A European Journal

Research Article
doi.org/10.1002/chem.202203983

Chemistry Europe
European Chemical
Societies Publishing

2,3,5,6-Tetrahydro-2,6-dithioxo
-4H-1,3,5-thiadiazin-4-one

Scheme 2. Reaction of carbonyl diisothiocyanate with hydrogen sulfide to 2,3,5,6-tetrahydro-2,6-dithioxo-4H-1,3,5-thiadiazin-4-one (**8**) and its tautomerism. For more details see Supporting Information.

material **5** alongside with compound **8** in small amounts were detected as reaction products. We assume that while the product in principle should be stable, see quantum chemical calculations below, the F$^-$ ion reacts predominantly with the C=O group and thus new synthetic strategies will be necessary to isolate the so far elusive 6-fluoro-2,3-dihydro-2-thioxo-4H-1,3,5-thiadiazin-4-one.

The reaction of carbonyl diisothiocyanate with HCl has been described previously and we were able to reproduce the procedure.[14] Dry HCl was passed through a solution of carbonyl diisothiocyanate in diethyl ether at 0 °C upon which the solution turned yellow and turbid. Subsequently, the solution was allowed to warm to room temperature and stirred for additional 20 h after which the volatiles were removed under reduced pressure and compound **5** was isolated in 96 % yield as a bright yellow powder. A singlet in the ^{1}H NMR spectrum at 13.0 ppm showed formation of in-ring N–H motif and three resonances in the ^{13}C NMR spectrum were attributed to the three carbon atoms at 190.4 ppm (C=S), 167.5 ppm (C–Cl), and 150.8 ppm (C=O), respectively. Single crystals suitable for X-ray diffraction were grown by recrystallization from THF/n-hexane.

For the reaction of carbonyl diisothiocyanate with HBr, ten equivalents of HBr were freshly evolved and dried by passing through a U-tube packed with P$_4$O$_{10}$ and subsequently through a solution of carbonyl diisothiocyanate in diethyl ether at 0 °C. During the reaction the solution turned yellow and turbid. Workup was similar to the one of compound **5** and compound **6** was obtained as a bright yellow powder, isolated in 68 % yield. It is likely that the yield can be increased by longer reaction times and use of more equivalents of HBr. Again, ^{1}H and ^{13}C NMR spectra showed the expected resonances at 13.0 ppm (N–H), 191.6 ppm (C=S), 157.7 ppm (C–Br), and 149.4 ppm (C=O). Single crystals suitable for X-ray diffraction were grown by recrystallization from THF.

Synthesizing compound **7** proved more difficult. Similarly to above, 40 equiv. HI were freshly evolved and dried by passing through a U-tube packed with P$_4$O$_{10}$ and subsequently through a solution of carbonyl diisothiocyanate in diethyl ether. Various temperatures in the range from −95 °C to 0 °C were tested but in all cases the reaction mixture immediately turned brown. During syntheses, compound **7** appeared as brown powder, decomposing faster than we were able to isolate. It is likely that the brown color of the powder originates from elemental iodine (see Figure S23). The reaction was also performed in dichloromethane instead of diethyl ether, however, the results were similar.

To get hold of compound **7** we tried the metathesis starting from compound **5** and NH$_4$I. The reaction was performed in tetrahydrofuran at room temperature during which the reaction mixture turned turbid and the color changed from yellow to brown. Filtration afforded NH$_4$Cl as side product with a deep red filtrate which contained iodine. No traces of compound **7** could be detected. The solvent was switched to sulfur dioxide, but only starting materials were detected by powder X-ray diffraction.

Molecular structures in the single crystals and their H-bonding interactions

Carbonyl diisocyanate adds two equivalents of hydrogen halide to form the carbonyl bis(carbamoylhalides) **1–4**. Whereas we were able to grow crystals for compounds **1–3**, compound **4** was too labile and we were not able to isolate crystals suitable for X-ray diffraction. However, at ambient temperature and pressure both compounds **2** and **3** also slowly decompose under elimination of the respective hydrogen halide manifesting in the formation of gas bubbles under dry paratone oil (see Figure S6).

In contrast, carbonyl diisothiocyanate adds only one equivalent of hydrogen halide and an intramolecular ring closure leads to substituted thiadiazine rings. The reaction products with HF and HI were either not accessible or isolable, respectively, and we were only able to isolate compounds **5** and **6** as reaction products.

Compound **1** crystallizes in the orthorhombic crystal system with the non-centrosymmetric space group $P2_12_12_1$ and one crystallographically independent molecule in the unit cell. The molecule adopts a linear conformation, see Figure in Table 1, approximating point group symmetry C_{2v}. However, in the crystal structure there are small distortions: All atoms but the central C=O moiety and the H atoms lie in one plane and due to the H-bonding the central C=O moiety is tilted out of the

Table 1. Molecular structures of compounds **1** (a) and **2** (b, **3** shows a similar conformer) as obtained from single-crystal X-ray diffraction. Displacement ellipsoids are drawn with 75 % probability level at 100 K, H-atoms isotropic with arbitrary radius. The table contains observed bond length [Å] and angles [°] of compounds **1**, **2**, and **3**.

	1 (X = F)	2 (X = Cl)	3 (X = Br)
C1–X1	1.3362(9)	1.772(4)	1.938(5)
C3–X2	1.3384(9)	1.751(4)	1.922(5)
C1–O1	1.1871(9)	1.186(5)	1.181(6)
C2–O2	1.2147(9)	1.206(4)	1.207(6)
C3–O3	1.1859(10)	1.195(4)	1.193(6)
N1–C1–X1	108.67(6)	108.7(3)	109.3(3)
N2–C3–X2	108.68(6)	110.6(3)	112.0(3)
N1–C2–N1	112.27(6)	114.7(3)	114.1(4)

Chemistry–A European Journal

Research Article
doi.org/10.1002/chem.202203983

Chemistry
Europe
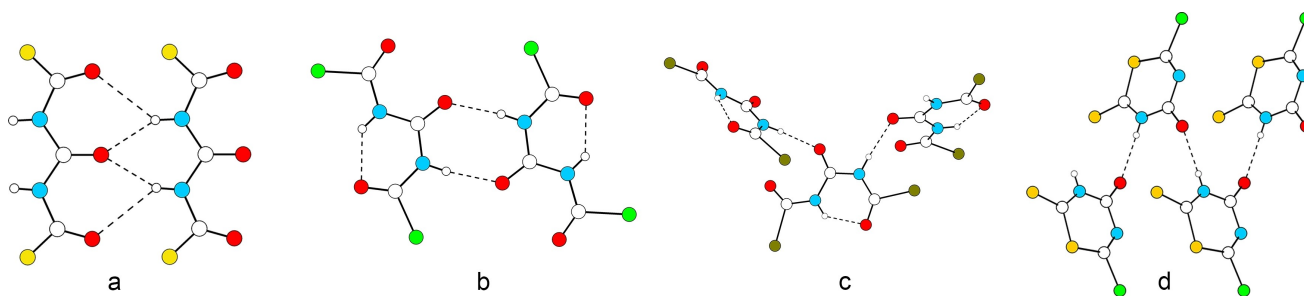European Chemical
Societies Publishing

Figure 2. Sections of the differing H-bonding networks in compounds **1** (a), **2** (b), **3** (c), and the isotypic crystal structures of compounds **5** and **6** (d). Color code: C white, N blue, O red, H small white, F gold, Cl green, Br brown. Atoms drawn isotropic with arbitrary radii.

plane by 3.05(11)° (see Figure S25). If calculated as a single molecule in the gas-phase, C_{2v} symmetry results. Measured interatomic distances (see Table 1) of the carbamoyl fluoride moiety are comparable to the unsubstituted carbamoyl fluoride (NH_2COF).[15]

Compound **1** forms intermolecular H-bonds from the N–H groups to the central C=O moiety of an adjacent molecule with H···O distances of 2.16(2) & 2.15(2) Å, thus forming sheets perpendicular to the [100] axis (see Figure 2). The resulting sheets are puckered with the central C=O moiety bent out of the molecular plane by the H-bonds. Those sheets run parallel in pairs which are shifted with respect to each other by $\frac{1}{2}a$ due to the 2_1 screw axes of the space group, resulting in rod symmetry $\not p112_1$ (rod-group no. 9). The sheets are not interconnected by H-bonds.

Compound **2** crystallizes in the triclinic space group $P\bar{1}$ and with one crystallographically independent molecule in the unit cell. In contrast to compound **1**, the structure exhibits an intramolecular H-bond N1–H1···O3 thus forming a six-membered ring, see Figure in Table 2. The molecule is almost planar and approximates point group C_s. The main deviation is the torsion around the C1–N1 bond. Whereas the ring is close to

planarity, the terminal (C=O)–Cl moiety is tilted out of plane with a O1–C1–C2–O2-torsion angle of 3.2(3)°. When the molecule is calculated as a single molecule, C_s symmetry is found.
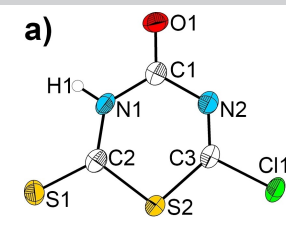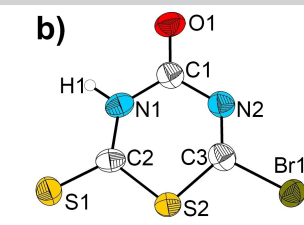
Testament to its different molecular structure, the H-bonding network and packing in compound **2** is different from **1**, too. Additional to the intramolecular H-bonds, intermolecular H-bonds are present: From N2–H2 to O2 of the adjacent molecule with d(N–H···O) = 2.007(2) Å. Through these bonds, discrete and almost planar pairs are formed that are not further connected to other pairs.

The molecular structure of compound **3** in the solid state also exhibits an intramolecular H-bond and thus similar conformation to compound **2**. However, the packing is different. It crystallizes with the non-centrosymmetric tetragonal space group $P4_1$ and one crystallographically independent molecule in the unit cell. Again, the molecule is almost planar with approximately point group C_s. Whereas in molecule **2** the ring is planar with a tilted residue, here the atoms of the "linear" Br1 to N1 moiety lie in one plane with the in-ring (C3=O3)–Br motif tilted out of plane with a torsion angle O2–C2–C3–O3 of 7.1(7)°. This is probably a symptom of the different H-bond connectivity.

Whereas the structures of molecules **3** and **2** are similar, their H-bonding and thus the crystal structures are different. In compound **3** the N2–H2 moiety is also connected to O3 of a neighboring molecule with a H···O distance of 2.029(3) Å. However, instead of dimers, screws with ideal $\not p4_1$ rod-group symmetry that extend along the [001] axis are formed. Thus, every individual molecule of **3** is connected to two further molecules. The individual rods are not interconnected by further H-bonds.

For compounds **1**–**3**, the C–X bond lengths (see Table 1) are in the range of single bonds and comparable to related compounds, for example, carbamoyl fluoride with 1.351(1) Å,[15] carbonyl chloride with 1.74(2) Å,[16] oxalyl chloride with 1.697 Å, and oxalyl bromide with 1.843–1.961 Å.[17,18] Similarly, all C–N bond lengths indicate single bond character. In all cases, the C=O distances are in the range of double bonds. For carbonyl groups not taking part in H-bonding, the distances average d(C=O) = 1.185 Å, which is comparable to carbonyl dichloride with 1.15(2) Å.[16] The central C=O moiety exhibits systematically longer bonds by approximately 0.2 Å in comparison to the

Table 2. Molecular structures of compounds **5** (a) and **6** (b) as obtained from single-crystal X-ray diffraction. Displacement ellipsoids drawn with 75% probability level at 100 K, H-atoms isotropic with arbitrary radius. The table contains selected bond lengths of compounds **5** and **6**, and compounds from Ref. [19].

	5 (X = Cl)	6 (X = Br)	Ref. [19]
C1–O1	1.205(3)	1.205(5)	–
C2–S1	1.637(2)	1.642(5)	1.614–1.640
C3–X1	1.721(2)	1.893(4)	–
C3–N2	1.261(3)	1.260(6)	1.284–1.293
C2/C3–S2	1.742(2)/ 1.733(2)	1.735(4)/ 1.727(5)	1.733–1.768
N1–C1–N2	119.8(2)	120.0(4)	123.1–128.3
C2–S2–C3	100.9(1)	100.7(2)	104.07–105.13

Chem. Eur. J. **2023**, *29*, e202203983 (4 of 8)

© 2023 The Authors. Chemistry - A European Journal published by Wiley-VCH GmbH

Chemistry–A European Journal

Research Article
doi.org/10.1002/chem.202203983

Chemistry Europe
European Chemical
Societies Publishing

shorter terminal C=O moieties, due to the former being part of extended H-bonding interactions. If part of the intramolecular H-bonding, the C3=O3 bond in **2** and **3** averages 1.194 Å which is in between the values discussed above.

Compounds **5** and **6** crystallize isotypically in the monoclinic crystal system with the space group $P12_1/n1$ and with one crystallographically independent molecule in the unit cell. The molecule is almost planar with a slight concave bend which is due to the O1-atom taking part in hydrogen bond interactions. For molecule **5**, the torsion angle O1–C1–C3–S2 of 6.4(3)° is the largest deviation from planarity. In molecule **6** the bend is slightly larger with a torsion angle O1–C1–C3–S2 of 10.0(6)°. If the molecule is calculated in the gas phase, it adopts ideal C_s symmetry.

For molecules **5** and **6** the bond lengths in the thiadiazine ring are similar within the tripled standard uncertainty. All interatomic distances correspond to single bonds with the exception of the N2=C3 bond which, with a length of 1.261 Å, is in the typical range of a C=N double bond.

Whereas a crystal structure comprising the saturated six membered tetrahydro thiadiazine ring with its oxygen and sulfur substituents has already been described, this unsaturated and halogen substituted motif is hitherto unknown.[20] Furthermore, in all other reported cases the thiadiazine ring is either part of a condensed ring system[19] or includes carbon atoms with four bonds.[21,22] Regardless of this, the interatomic distances are comparable with our values.

Each molecule of compounds **5** and **6**, respectively, is connected to two adjacent molecules through N–H···O H-bonds, 2.14(3) Å in compound **5** and 2.063(3) Å in compound **6**. The resulting strands resemble puckered sheets extending along [010] exhibiting rod-group symmetry ꝓ112₁.

IR spectroscopy

To get more insight into the solid state structures and the respective vibration modes, IR spectra were recorded and supplemented with quantum chemical calculations, see Figure 3 for compounds **1**–**3** and the Supporting Information for compounds **5** and **6**. The crystal structures of compounds **1**–**3**, **5**, and **6** were optimized in with the CRYSTAL17 program suite applying the PBE0/def2-TZVP level of theory for accurate simulation of IR and Raman spectra; for details see the Supporting Information. Optimization of the crystal structures with quantum chemical calculations reproduced the measured crystal structures within close margins.

All compounds have NH groups that are, to different degrees, participating in H-bond interactions. For compound **1**, the stretching vibration of the N–H bonds is observed from 3200–3300 cm^{-1}, whereas for compounds **2** and **3** no bands in the region above 3000 cm^{-1} are observed. It is likely that these bands are broadened due to extensive H-bonding. Evidence lies in the fact that for compounds **1**–**3** N–H rocking and bending vibrations can be found: For compound **1** at 1555 cm^{-1} (calc. 1626 and 1595 cm^{-1}), for compound **2** at 1486 cm^{-1} (calc. 1578 and 1549 cm^{-1}) and for compound **3** at 1507 cm^{-1} (calc. 1576 and 1540 cm^{-1}). In all cases the two calculated bands are merged probably due to H-bonding and give only one band. N–H wagging modes can also be observed for compound **1** at 691 cm^{-1} (broad band, calc. 782 and 761 cm^{-1}), compound **2** at 875, 850 and 794 cm^{-1} (calc. 913, 884, and 855 cm^{-1}), and compound **3** at 759, 687 cm^{-1} (calc. 805, 776, and 747 cm^{-1}, the latter two only giving one observed signal). In all cases combination with other vibration modes is present, for a full assignment please see the Supporting Information.

The position of the C=O stretching vibration within the IR spectra is dependent on the type of H-bonding in which the group participates. For compound **1** the distinction can be
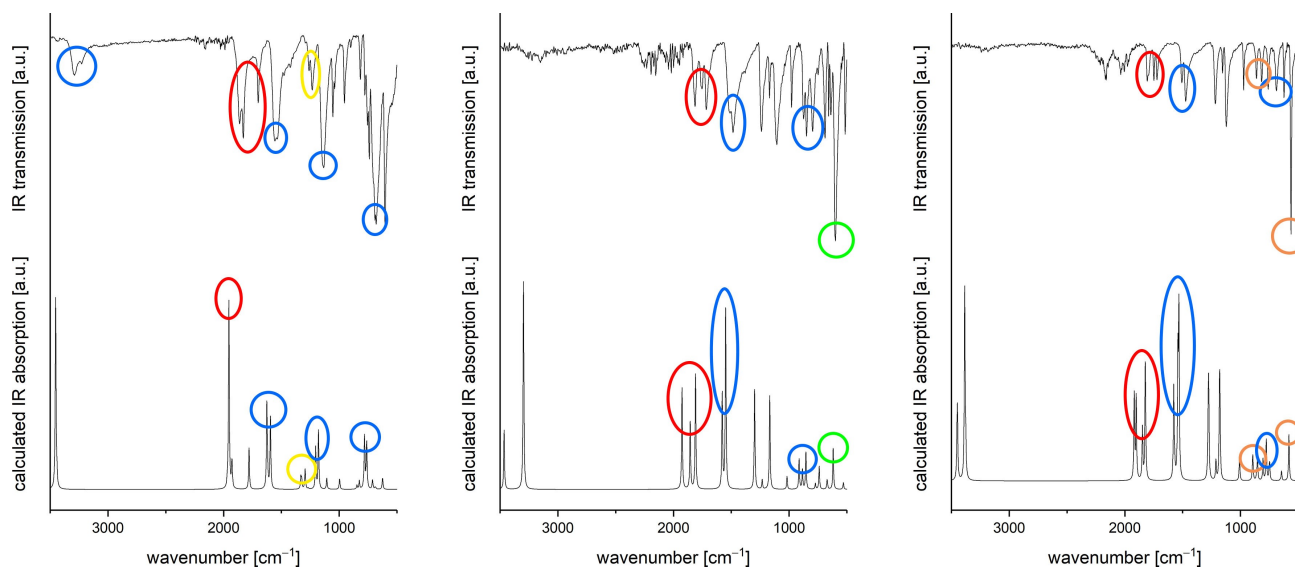

Figure 3. Recorded and calculated IR spectra of compounds **1** (left), **2** (middle), and **3** (right). Color code: N–H vibration band blue, C=O red, C–F yellow, C–Cl green, C–Br brown.

Chemistry–A European Journal

Research Article
doi.org/10.1002/chem.202203983

Chemistry
Europe
European Chemical
Societies Publishing

made between the outer carbamoyl groups and the "urea" type moiety: At 1861 cm^{-1} (calc. 1953 cm^{-1}) all C=O stretching vibrations are in phase, whereas at 1828 cm^{-1} (calc. 1926 cm^{-1}) only the carbamoyl C=O groups participate in the mode. The urea-type C=O moiety yields a band shifted to lower wavenumbers at 1698 cm^{-1} (calc. 1779 cm^{-1}). For compound **2** all three carbonyl moieties give distinct bands: C1=O1 1812 cm^{-1} (calc. 1925 cm^{-1}), C2=O2 1715 cm^{-1} (calc. 1809 cm^{-1}), and C3=O3 1752 cm^{-1} (calc. 1855 cm^{-1}). Similarly, the IR spectrum of compound **3** shows three distinct signals, the assignment of which is not as pronounced due to the differing topology of the H-bonding. At 1805 and 1748 cm^{-1} (calc. 1918, 1901, and 1847 cm^{-1}) C1=O1 and C2=O2 vibrate combined in- and out-of-phase, respectively. The C3=O3 stretching vibration can be observed at 1721 cm^{-1} (calc. 1820 cm^{-1}).

In compound **1**, the C–F stretching vibration gives two relatively weak bands at 1260 and 1233 cm^{-1} (calc. 1331, 1294 cm^{-1}) which are in the expected range. These vibrations are substantially coupled to vibrations of the molecule scaffold. In comparison, the corresponding C–Cl and C–Br stretching vibration in compounds **2** and **3** yields the strongest bands of the spectra at 599 and 562 cm^{-1}, respectively (calc. 618 and 580 cm^{-1}, resp.), also coupled to vibrations of the molecule scaffold. Again, the bands are in the expected range for C–Cl and C–Br stretching vibrations.

While we were unable to crystallize carbonyl bis(carbamoyliodide) (**4**), we were able to collect an IR spectrum which, taking into account the findings above, yields some insight into its structure (see Figure S15). First, the absence of a band above 3000 cm^{-1} is not necessarily indicative for missing NH moieties, as a strong band at 1466 cm^{-1} could be attributed to N–H rocking and/or bending vibrations. Similar to compound **3**, the pronounced triad of bands at 1795, 1738 and 1705 cm^{-1} could indicate three different C=O stretching modes. The strongest band of the spectrum is at 553 cm^{-1}. Bearing in mind the value for the C–Br stretching vibration, this band can be assigned to the C–I stretching vibration. We have tentatively modeled the crystal structure of compound **4** assuming it crystallizes isotypically to compound **3** and subsequently calculated the IR spectrum. While there are some similarities, especially the deviation between the three recorded bands for the three C=O moieties and the calculated ones is substantial (see Figure S15). Therefore, we assume that both compounds adopt different crystal structures.

Compounds **5** and **6** are isotypic and give very similar IR spectra. For both, signals for the N–H stretching vibration can be observed above 3000 cm^{-1}. N–H wagging vibrations lie at 1453 cm^{-1} (calc. 1535 and 1530 cm^{-1} for compound **5**, 1534 and 1529 cm^{-1} for compound **6**). Due to the width of the signals, the N–H out-of-plane rocking vibrations computed at ~850 cm^{-1} cannot be assigned.

For both compounds **5** and **6**, the band of the sole C=O moiety is at 1686 cm^{-1} which in both cases are two modes that are not resolved (calc. 1811 and 1793 cm^{-1} for compound **5**, and 1807 and 1791 cm^{-1} for compound **6**). In-ring imine C=N stretching vibrations are observed at 1564 and 1553 cm^{-1} for compounds **5** and **6**, respectively (calc. 1662 and 1663 cm^{-1} for

compound **5**, 1649 and 1648 cm^{-1} for compound **6**), in agreement with the bond length as observed from single-crystal diffraction. The C=S moieties are not part of the H-bond interactions, the stretching vibrations yield sharp bands at 1050 for compound **5** and 1044 cm^{-1} for compound **6** (calc. 1090 and 1086 cm^{-1}, resp.). Stretching vibrations of the C–Cl and C–Br moiety give narrow bands at 901 cm^{-1} for compound **5** (calc. 939 and 938 cm^{-1} and 862 cm^{-1} for compound **6** (calc. 903 and 898 cm^{-1}), respectively.

Conformer analysis: Open chain *vs.* intramolecular H-bond

During single-crystal analysis it became apparent that compounds **1** and **2** exhibit different crystal structures. Whereas compound **1** shows a linear form, compounds **2** and **3** show additional intramolecular H-bonding. The energy differences between those rotamers were calculated by means of density functional theory with the Turbomole code on the PBE0/def2-TZVP level of theory and COSMO with default parameters for modelling solvent effects (for details and for results without COSMO as well as with other functionals see Supporting Information).

First, the molecular structures of **1**–**4** were optimized in the respective open chain form, the native state of molecule **1** in the single crystal. All optimizations converged into energetic minima as evident by the absence of imaginary frequencies. The energies for the reactions in Scheme 3 given below are Gibbs energies calculated for 300 K with frequencies scaled by 0.989. Energies without thermal contributions are given in the supplement, also for other levels of calculations. Moreover, we performed a relaxed potential energy scan by rotation around the C2–N2 bond in 5° increments which after rotation by 180° results in the structure with the intramolecular H-bond (see Figure 4). Geometries of all points were optimized with the above mentioned angle being fixed.

The results for molecules **1**–**4** were similar and showed a net energy difference of circa 10 kJ/mol favoring the conformer with the intramolecular H-bond. A rotation barrier of 40 kJ/mol (molecule **1**), or 35 kJ/mol (molecules **2**–**4**) has to be overcome, which can easily be achieved at room temperature. As this analysis cannot rationalize the two conformers, we assumed it to be possible that the different crystallization conditions are responsible and that under suitable circumstances both conformers could in principle be isolated individually for the investigated molecules. To test this hypothesis, we dissolved a
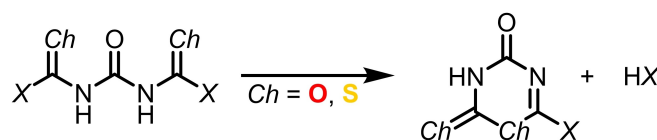
Scheme 3. Hypothetical reaction of the carbonyl bis(carbamoylhalides) to the corresponding substituted thiadiazines under loss of 1 equiv. HX with X = F–I. Calculations show the former motif stable for Ch = O and the latter for Ch = S.

Chemistry–A European Journal

Research Article
doi.org/10.1002/chem.202203983

Chemistry Europe
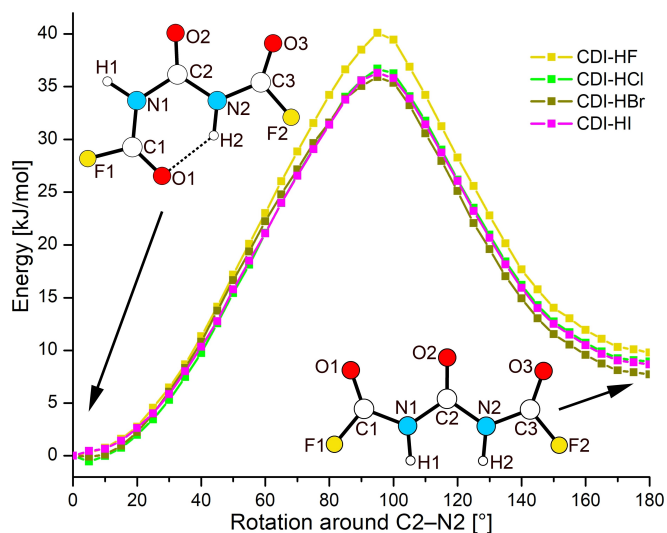European Chemical
Societies Publishing

Figure 4. Relative energies of the two shown conformers computed for molecules **1**, **2**, **3**, and **4**. The two conformers are related through the rotation around the N2–C2 bond.

small amount of compound **1** in different solvents (DCM, THF, MeCN) and tried its recrystallization under different conditions. However, we were unable to obtain crystals suitable for X-ray diffraction.

Addition of 2 equiv. HX for carbonyl diisocyanate *vs.* addition of 1 equiv. HX for carbonyl diisothiocyanate

Quantum chemical calculations were also performed to better understand the differing reaction patterns between carbonyl diisocyanate and carbonyl diisothiocyanate again applying the Turbomole code. We investigated the hypothetical reactions shown in Scheme 3.

The carbonyl bis(carbamoyl halides) (Ch=O) and bis((thio)-carbamoylhalides) (Ch=S) were decomposed in silico to the oxa- or thiadiazines compounds alongside their corresponding hydrogen halides. The energies of these reactions will indicate for which of the chalcogen atoms the carbamoyl or the thiadiazine motif is more stable. Our calculations indicate that for Ch=O these reactions are endergonic whereas for Ch=S they are exergonic. This is in accordance with our experimental results as for Ch=O the carbamoyl moiety and for Ch=S the thiadiazine ring forms. For Ch=O and X=F the energy difference is $+61.1$ kJ/mol which is about 40% higher than for X=Cl–I (Cl = $+34.9$, Br = $+40.1$, I = $+38.8$ kJ/mol). For Ch=S the value for X=F is least exergonic with -28.4 kJ/mol with the other reactions being significantly more exergonic (Cl = -43.9, Br = -39.6 kJ/mol, I = -36.3 kJ/mol).

Clearly, the differing reaction patterns originate from the O versus the S atoms of the iso(thio)cyanate groups of the starting materials. To get a clearer picture, we took the thiadiazine framework from compound **5** as a model and replaced either

the S1 or the S2 positions with oxygen atoms in silico (see Scheme 4).

The replacement of the terminal S1 position with an O atom (Scheme 4 b) is exergonic with -214.4 kJ/mol. In contrast, replacement of the in-ring S2 position with an O atom (Scheme 4 a) leads to the much lower energy gain of merely -124.4 kJ/mol leaving a difference of the respective molecules of -90 kJ/mol. The calculations clearly favor the in-ring sulfur atom with single bonds concomitant with the doubly bonded ex-ring oxygen atom over the in-ring oxygen with ex-ring sulfur atoms, which is in accordance with both our experimental findings and chemical intuition.

Thus, the calculations can explain the differing reactivity patterns of carbonyl diisocyanate versus carbonyl diisothiocyanate quite well. Also, the trend in stability of the carbonyl bis(carbamoylhalides) compounds towards decomposition through abstraction of HX can be reproduced, see the Supporting Information for details. However, the situation is less clear for the thiadiazines. Whereas the general calculated trend towards abstraction of dihalides could be an indication for the instability of the iodinated compound, the so far missing isolation of 6-fluoro-2,3-dihydro-2-thioxo-4H-1,3,5-thiadiazin-4-one cannot be explained thus far (see Supporting Information for details), as the compound itself should be stable towards the decomposition paths calculated by us.

Reacting carbonyl diisothiocyanate with HF yielded compound **8** which crystallizes in form of two different tautomers (see Supporting Information for details). In principle, this would be the reaction product of carbonyl diisothiocyanate with H$_2$S leading to the question where this particular building block stems from. We can speculate that the F$^-$ ion as a hard nucleophile could attack at the carbonyl group rather than the isothiocyanate substituents, leading to an intermediate formation of HSCN. Acting as a soft nucleophile, it would react with another carbonyl diisothiocyanate molecule, this time at the isothiocyanate substituent, leading to ring closure. Then, HCN is abstracted leaving compound **8** after all volatiles were removed in vacuo. We have also tried to isolate crystals directly from the reaction medium anhydrous HF to get access to the fluorine substituted compound, but solely compound **8** was isolated. However, when HF is removed a red solid is obtained showing the typical color of pararhodane (SCN)$_x$, which is probably a strong thermodynamic minimum in this system.
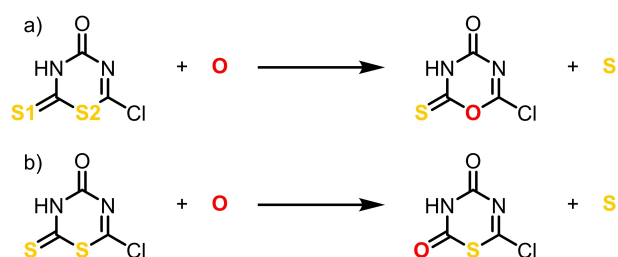
Scheme 4. In silico replacement of the S1 and S2 with O atoms. Calculations favor in-ring sulfur and ex-ring oxygen molecules.

Chem. Eur. J. **2023**, 29, e202203983 (7 of 8)

© 2023 The Authors. Chemistry - A European Journal published by Wiley-VCH GmbH

Conclusion

The related compounds carbonyl diisocyanate, $CO(NCO)_2$, and carbonyl diisothiocyanate, $CO(NCS)_2$, react differently towards archetypical nucleophiles. While the former adds two equivalents of HF, HCl, HBr, or HI to form the respective carbonyl bis(carbamoylhalides), the latter adds only one equivalent of HX under ring closure yielding substituted thiadiazines which were only observed for reaction with HCl and HBr. Quantum mechanical calculations reveal that this differing reactivity is likely a thermodynamically controlled process driven by the tendency of oxygen atoms to form double bonds versus sulfur atoms to form single bonds with carbon atoms. Both substance classes are reactive towards nucleophilic substitution of the halogen atom and we are currently in the process of testing their aptness for further chemical transformations.

Experimental Section

Experimental details, tables for single-crystal X-ray data including refinements and additional figures, Raman, IR and NMR spectra, computational data, and discussion of the crystal structures of compound **8** can be found in the Supporting Information.

Deposition Number(s) 2228316 (**1**), 2228314 (**2**), 2228313 (**3**), 2228315 (**5**), 2228319 (**6**), 2228317 (**8 a**) and 2228318 (**8 b**) contain(s) the supplementary crystallographic data for this paper. These data are provided free of charge by the joint Cambridge Crystallographic Data Centre and Fachinformationszentrum Karlsruhe Access Structures service.

Acknowledgements

Conflict of Interest

The authors declare no conflict of interest.

Data Availability Statement

The data that support the findings of this study are available in the supplementary material of this article.

[1] L. Cotarca, C. Lange, K. Meurer, J. Pauluhn, in *Ullmann's Encycl. Ind. Chem.*, Wiley-VCH Weinheim, Germany, **2019**, pp. 1–30.
[2] E. Nachbaur, *Monatsh. Chem.* **1966**, *97*, 361–367.
[3] T. M. Klapötke, B. Krumm, S. Rest, R. Scharf, J. Schwabedissen, H.-G. Stammler, N. W. Mitzel, *J. Phys. Chem. A* **2016**, *120*, 4534–4541.
[4] J. Pfeiffer, C. Trost, A. Pachkovska, F. Tambornino, *Inorg. Chem.* **2021**, *60*, 10722–10728.
[5] R. Bunnenberg, J. C. Jochims, *Chem. Ber.* **1981**, *114*, 2075–2086.
[6] B. Anders, H. Malz, *Verfahren zur Herstellung von Acylsenfoelen*, **1966**.
[7] E. L. Martin, *Org. Synth.* **1971**, *51*, 70.
[8] R. Malachowski, L. Jurkiewicz, J. Wojtowicz, *Ber. Dtsch. Chem. Ges.* **1937**, *70*, 1012–1016.
[9] X. Zeng, M. Gerken, H. Beckers, H. Willner, *Inorg. Chem.* **2010**, *49*, 9694–9699.
[10] T. Curtius, K. Heidenreich, *Ber. Dtsch. Chem. Ges.* **1894**, *27*, 2684–2685.
[11] R. Bunnenberg, J. C. Jochims, H. Härle, *Chem. Ber.* **1982**, *115*, 3587–3596.
[12] B. Akteries, J. C. Jochims, *Chem. Ber.* **1986**, *119*, 1133–1143.
[13] B. Akteries, J. C. Jochims, *Chem. Ber.* **1986**, *119*, 83–95.
[14] B. Akteries, J. C. Jochims, *Chem. Ber.* **1986**, *119*, 669–682.
[15] A. F. Baxter, K. O. Christe, R. Haiges, *Struct. Chem.* **2017**, *28*, 303–307.
[16] B. Zaslow, M. Atoji, W. N. Lipscomb, *Acta Crystallogr.* **1952**, *5*, 833–837.
[17] P. Groth, O. Hassel, C. Römming, A. Block-Bolten, J. M. Toguri, H. Flood, *Acta Chem. Scand.* **1962**, *16*, 2311–2317.
[18] E. Damm, O. Hassel, C. Rømming, R. B. Jensen, C. T. Pederson, E. Larsen, *Acta Chem. Scand.* **1965**, *19*, 1159–1165.
[19] A. Peña-Hueso, A. Esparza-Ruiz, I. Ramos-García, A. Flores-Parra, R. Contreras, *J. Organomet. Chem.* **2008**, *693*, 492–504.
[20] I. Bélai, P. Sohár, K. Maekawa, L. Párkányi, G. Matolcsy, *J. Heterocycl. Chem.* **1981**, *18*, 283–286.
[21] A. R. Katritzky, A. V. Vakulenko, Y. Xu, P. J. Steel, *J. Org. Chem.* **2002**, *67*, 4960–4962.
[22] J. S. Davidson, S. J. Rettig, J. Trotter, *Acta Crystallogr. Sect. C* **1999**, *55*, 434–436.

3.5 Intra- and Intermolecular Hydrogen Bonding in *N,N'*-Carbonyl bis(carbamates), -(*S*-thiocarbamates) and *N,N'*-biscarbamoyl ureas

Jonathan Pfeiffer, Martin Möbs, Sascha Reith, Mirko Tallu, Frank Tambornino

Abstract: *The three structural related compound classes of N,N'-biscarbamoyl ureas, N,N'-carbonyl bis(carbamates) and N,N'-carbonyl bis(S-thiocarbamates) have been intensively studied. ^{13}C NMR spectroscopy shows a specific chemical shift for each compound class. In the solid state the molecules undergo intramolecular ring formation and additionally intermolecular dimer or strand building both via hydrogen bonds. The influence of the organic groups is showcased by Hirshfeld surface analysis and the study is rounded off by findings from IR spectroscopy.*

Zusammenfassung:

Die drei strukturell verwandten Verbindungsklassen der *N,N'*-Biscarbamoylharnstoffe, *N,N'*-Carbonylbis(carbamate) und *N,N'*-Carbonylbis(*S*-thiocarbamate) wurden eingehend untersucht. ^{13}C-NMR-Spektroskopie zeigt spezifische chemische Verschiebungen für jede Verbindungsklasse. Im Festkörper unterlaufen die Moleküle über Wasserstoffbrückenbindungen einer intramolekularen Ringbildung und zusätzlich einer intermolekularen Formie-

rung von Dimeren oder Strängen. Der Einfluss der organischen Gruppen wird durch Hirshfeld Oberflächen Analyse gezeigt und die Studie wird durch Befunde aus IR-Spektroskopie abgerundet.

Beiträge der Autoren:

In einem Forschungspraktikum wurden von MÖBS, REITH und TALLU unter Betreuung und Anleitung von TAMBORNINO und mir Synthesen der Verbindungen **2** und **3** durchgeführt. Synthesen der Verbindungen **1** wurden von mir ausgeführt. Sämtliche analytischen Daten (^{1}H & ^{13}C{^{1}H}-NMR-Spektroskopie, Elementaranalytik, MS, IR-Spektroskopie) aller Verbindungen wurden von mir vervollständigt. SC-XRD Messungen wurden von TAMBORNINO durchgeführt. Die Strukturlösung und -verfeinerung wurde von TAMBORNINO oder mir ausgeführt. Hirshfeld Analyse wurde von mir vorgenommen. Das Manuskript und die *Supporting Information* wurden von mir geschrieben und zusammen mit TAMBORNINO überarbeitet.

Intra- and intermolecular hydrogen bonding in *N,N*'-Carbonyl bis(carbamates), -(*S*-thiocarbamates) and *N,N*'-biscarbamoyl ureas

Jonathan Pfeiffer , Martin Möbs , Sascha Reith , Mirko Tallu , Frank Tambornino [*]

Fachbereich Chemie, Philipps-Universität Marburg, Hans-Meerwein-Straße 4, 35043 Marburg, Germany

A B S T R A C T

The three structural related compound classes of *N,N*'-biscarbamoyl ureas, *N,N*'-carbonyl bis(carbamates) and *N,N*'-carbonyl bis(*S*-thiocarbamates) have been intensively studied. ^{13}C NMR spectroscopy shows a specific chemical shift for each compound class. In the solid state the molecules undergo intramolecular ring formation and additionally intermolecular dimer or strand building both via hydrogen bonds. The influence of the organic groups is showcased by Hirshfeld surface analysis and the study is rounded off by findings from IR spectroscopy.
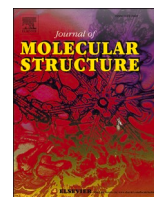
1. Introduction

Urea, $CO(NH_2)_2$, was discovered as early as in 1727 by Boerhaave during investigations of urine, and he named the new compound "*sal nativus urinae*" [1,2]. About 50 years later, Rouelle obtained it through alcohol extraction of urine[2,3] and 1797 urea was first crystalized from nitric acid as its nitrate salt [2,4,5]. Without knowing it, Davy synthesized urea form phosgene and ammonia in 1812 [6]. The significant discovery to synthesize urea from silver cyanate and ammonium chloride by Wöhler[7] shackled the "vitalism" theory as it is commonly regarded as the first organic compound to be synthesized from inorganic starting materials. In 1848 Wiedemann then discovered a new substance by heating nitric acid with urea. In this condensation reaction, which proceeds under elimination of ammonium nitrate, biuret, $CO(NH_2)_2NH$, was synthesized [8–10]. Shortly after, in 1872, Schmidt discovered the corresponding triuret, $CO(NHCO(NH_2))_2$, by reacting phosgene with urea [11] (see Fig. 1).

Derivatives of symmetrically substituted triuret, *N,N*'-biscarbamoyl ureas $(CO(NHCO(NR_2))_2)$, can be synthesized through different synthetic approaches. The first reported procedure is the reaction of phosgene with disubstituted cyanamides (Fig. 2a), which form derivatives of trichlorodiazapentadiene chloride salts. These compounds can then be hydrolysed to *N,N*'-biscarbamoyl ureas [12,13]. A similar synthesis starts from trichloromethyl chloroformate (diphosgene) and substituted *N,N*-ureas (Fig. 2b). This reaction also proceeds with the formation of trichlorodiazapentadiene chloride salts as intermediate species [14]. A different approach is realized by using carbonyl diisocyanate as precursor which then acts as electrophile towards primary and secondary amines which in turn act as nucleophiles (Fig. 2c) [15]. One reaction is reported using urea and *n*-butyl isocyanate (Fig. 2d) [16]. To gain access to asymmetrically substituted *N,N*'-biscarbamoyl ureas, a reaction between substituted *N,N*-biurets and chlorosulfonyl isocyanate is possible (Fig. 2e) [17]. In one example, specifically cumidinyl biuret and carbamoyl chlorides are used towards the formation of *N,N*'-biscarbamoyl urea (Fig. 2f) [18].

Structurally related to *N,N*'-biscarbamoyl ureas are *N,N*'-carbonyl bis(carbamates) with the general formula $CO(NHCOOR)_2$. Those differ from the aforementioned substance class by formally changing the amine to an alkoxy group. These compounds have been known since 1897[19] and can be synthesized from phosgene and carbamates (Fig. 3a) [19–21]. A second synthetic approach is, once more, from carbonyl diisocyanate and alcohols (Fig. 3b). Furthermore, thiols can also be used in this reaction to

---

* Corresponding author.

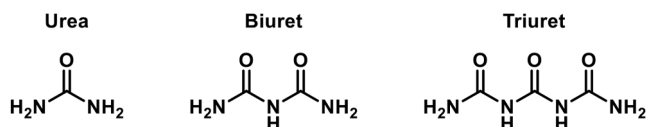*E-mail address:* Frank.Tambornino@chemie.uni-marburg.de (F. Tambornino).

Fig. 1. Molecular structures of urea, biuret and triuret.

synthesize *N,N'*-carbonyl bis(*S*-thiocarbamates), offering the thus far sole access route to this compound class [15].

Despite being known for over one hundred years with well-established syntheses, these three types of compounds, *N,N'*-biscarbamoyl ureas, *N,N'*-carbonyl bis(carbamates) and *N,N'*-carbonyl bis(*S*-thiocarbamates), have not been structurally characterized, yet. In literature, solely the crystal structures of one *N,N'*-biscarbamoyl urea[22] and of two *N,N'*-carbonyl biscarbamates[23] are described (Fig. 4). The first one is *N*-(4-methoxyphenylcarbamoyl)-*N'*-(4-methylbenzenesulfonylcarbamoyl) urea (**A**), synthesized from a sulfonyl chloride, sodium cyanate and 4-methoxyphenyl aniline. The biscarbamates are di(2,2,2-trinitroethyl) *N,N'*-carbonyl (**B**) and di(2-fluoro-2,2-dinitroethyl) *N,N'*-carbonyl biscarbamate (**C**), which were synthesized from carbonyl diisocyanate. Recently, we were able to determine the molecular motifs of the structurally related carbonyl bis(carbamoylhalides), CO(NHCO*X*)₂ (*X*=F, Cl, Br), in a comprehensive study [24].

In this study we aim to broaden the understanding of tricarbonyl group containing compounds in the solid state. We present their crystal structures, in-depth Hirshfeld surface analyses alongside a full characterisation by modern methods. All molecules form hydrogen bonds in the solid state to form an intramolecular six-membered ring and intermolecular connections to neighbouring molecules, enabling extended hydrogen bonding networks.

2. Experimental

2.1. Syntheses and crystallization

General Syntheses. All syntheses were carried out according to modified literature procedures. A 1 M solution of the respective nucleophile (HO−R, HS−R, HNR₁R₂) (2 mL) was added dropwise to a chilled (0 °C) 1 M solution of carbonyl diisocyanate in THF (1 mL). The solution was allowed to warm to room temperature and stirred for 16 to 18 h. The solvent was evaporated under reduced pressure and the reaction product obtained as powder. Further purification included washing the product subsequently with diethyl ether and *n*-hexane. For more details see the Supporting Information. The compounds were crystallized either from saturated solutions under evaporation of the solvent, or by layering a solution with an anti-solvent.

2.2. Analytical data

All analytical data can be found in the Supporting Information including ¹H NMR and ¹³C NMR spectra, with assignment of the signals, as well as IR spectra. Furthermore, elemental analyses and mass spectrometry data are given. Details of crystal data, data collection and refinement details are summarized in tables (see Supporting Information Table S 1 – S 3).
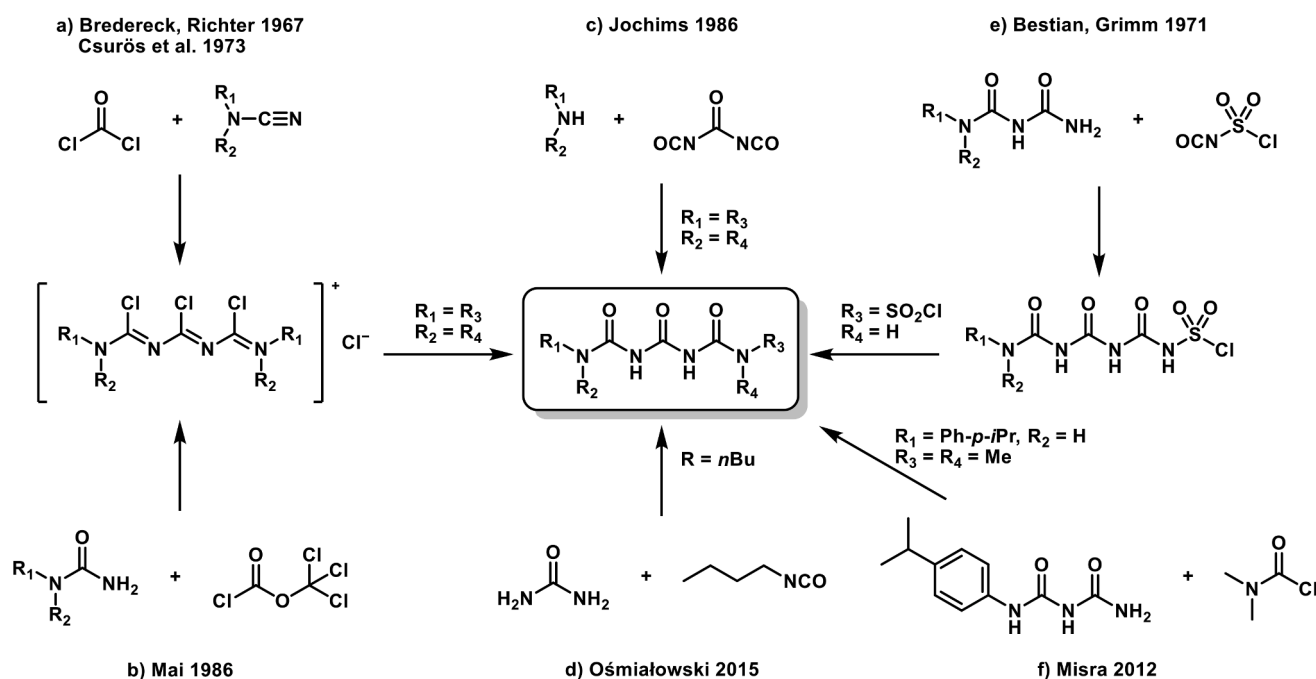
Fig. 2. Syntheses of *N,N'*-biscarbamoyl ureas described in literature. Reaction pathways a, b, c, and d lead to symmetrical products, whereas e and f afford asymmetrical derivatives.
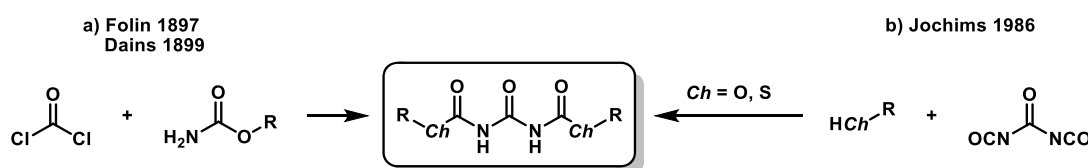
Fig. 3. Syntheses of *N,N'*-carbonyl bis(carbamates) (a,b) and *N,N'*-carbonyl bis(*S*-thiocarbamates) (b).
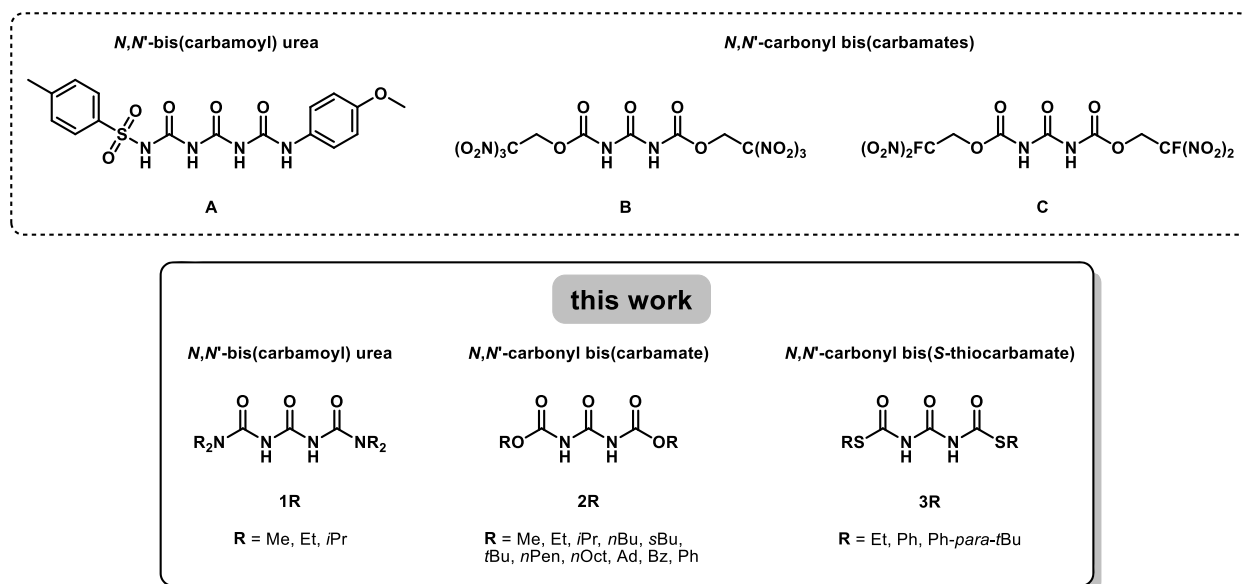
Fig. 4. Structural formulas of the molecules presented in this work: *N,N'*-bis(carbamoyl) urea **1R**, *N,N'*-carbonyl bis(carbamate) **2R** and *N,N'*-carbonyl bis(*S*-thiocarbamates) **3R**.

3. Results and discussion

We were able to synthesize and fully characterize in summary 17 compounds (three *N,N'*-biscarbamoyl ureas, eleven *N,N'*-carbonyl bis (carbamates), three *N,N'*-carbonyl bis(*S*-thiocarbamates)). Out of these compounds we were able to crystalize twelve. Despite the starting material, carbonyl diisocyanate, being highly moisture sensitive, the products are unsensitive towards air and moisture, which makes the

handling much more facile.

3.1. Nuclear magnetic resonance spectroscopy

^{1}H- and ^{13}C NMR spectroscopy analyses were carried out for all molecules (see Supporting Information). To compare the three different types of compounds, we chose **1Et, 2Et** and **3Et** as representatives (Fig. 5). In the ^{1}H NMR spectrum, the chemical shift for N–*H* is 9.05 ppm
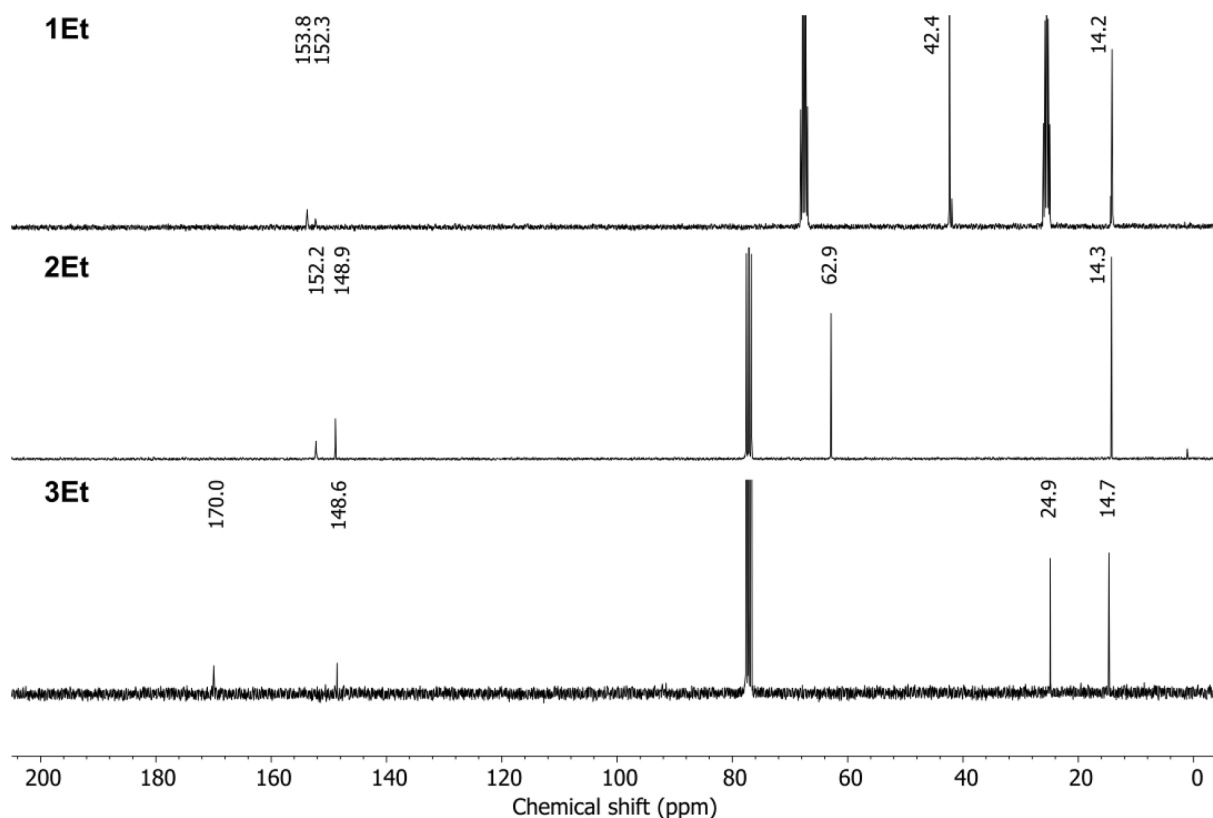
Fig. 5. ^{13}C NMR spectra of **1Et** in THF-d8 and, **2Et** and **3Et** in CDCl$_3$ at room temperature.

for **2Et** and 9.32 ppm for **3Et**. Exact comparison with **1Et** (10.28 ppm) is possible, albeit with the caveat of a different solvent (THF-d8 vs. CDCl₃). Regardless, all shifts are in the range of typical secondary amines. A better comparison is possible with ^{13}C NMR spectroscopy. The chemical shift of the central *C=O* moiety is in the same range for all molecules: 152.3 ppm (**1Et**), 152.2 ppm (**2Et**) and 148.6 ppm (**3Et**). They are, compared to the shifts of literature known carbonyl bis(carbamoylhalides), CO(CO*X*)₂ (*X*=F, Cl) with 146.7 ppm and 146.4 ppm, slightly downfield shifted. The respective signals in the ^{13}C NMR spectra for the second carbonyl group are, depending on the substituent, shifted differently. For **1Et** the shift of 153.8 ppm is nearly the same as for the central carbonyl group, which is to be expected for an amide substitution. The signal of **2Et** is found at 148.9 ppm, thus shifted upfield, which is due to the alkoxy substitution. The largest shift is found for the *C=O* moiety in **3Et** in which a downfield shift to 170.0 ppm is caused by the strong influence of the sulfide group. The same influence of the substituent is visible in the shift of the ^{13}C NMR signal for the *CH₂* group: It is 42.4 ppm (**1Et**), 62.9 ppm (**2Et**) and 24.9 ppm (**3Et**), while the *CH₃* group is in all cases detected at ~14 ppm.

3.2. Crystal structure description

N,N'-Bis(methylcarbamoyl) urea

1Me crystallizes with two independent molecules in the asymmetric unit in the orthorhombic space group $P2_12_12_1$ with eight molecules in the unit cell ($Z = 8$). The molecules are arranged as six-membered rings *via* an intramolecular hydrogen bond (O3···H–N1) over the O3–C3–N2–C2–N1 unit (Fig. 6, left). Two crystallographically independent molecules form a dimer with two intermolecular hydrogen bonds (O1A···H–N2B and O2B···H–N2A). These dimers build strands in [010] direction and stack along the [100] axis (Fig. 10). The carbonyl group C2=O2 do not participate in any hydrogen bonds. The graph-set notation is $N_1 = [R_2^2(8)]_{O1}[S(6)]_{O3}$.

N,N'-Bis(ethylcarbamoyl) urea

1Et also crystallizes in the orthorhombic space group $P2_12_12_1$. The unit cell contains four molecules ($Z = 4$) with one independent molecule in the asymmetric unit. Again, the intramolecular hydrogen bond O3···H–N1 leads to an intramolecular six-membered ring (Fig. 7 left). The intermolecular hydrogen bonds in the crystal structure result in chains of molecules along [100] (Fig. 7 middle). In contrast to **1Me** and **2Me**, here one molecule is connected to two different molecules. O2 forms one hydrogen bond O2···H–N2 and a short contact O2···H–C10 to a hydrogen atom of –CH₂– in the ethyl group. The other way around H–N1 and H–C10 are connecting to O2 of another molecule. This gives the $N_1 = [S(6)]_{O3}[C(6)]_{O2}$ graph-set notation. C2=O2 is oriented *cis* to C1=O1 and, interestingly, O1 is not part of the hydrogen bond network, which is not observed in any of the other discussed molecular structures.

Dimethyl *N,N'*-carbonyl bis(carbamate)

2Me crystallizes in the monoclinic space group $P2_1/c$ with two independent molecules in the asymmetric unit and $Z = 4$. The molecules form dimers in the crystal structure *via* two intermolecular hydrogen bonds (Fig. 6). The central oxygen atoms of each molecule are connected to a hydrogen atom of one H–N group (O1A···H–N2B/O1B···H–N2A) from the other molecule. These dimers form layers in the {102} plane and stack in [001] direction (Fig. 10). C1=O1 and C2=O2 are oriented *cis* to one another. Additionally, together with the N1–C1–N2–C3–O3 framework the intramolecular hydrogen bond (O3···H–N1) completes a six-membered ring. This gives the $N_1 = [R_2^2(8)]_{O1}[S(6)]_{O3}$ graph-set
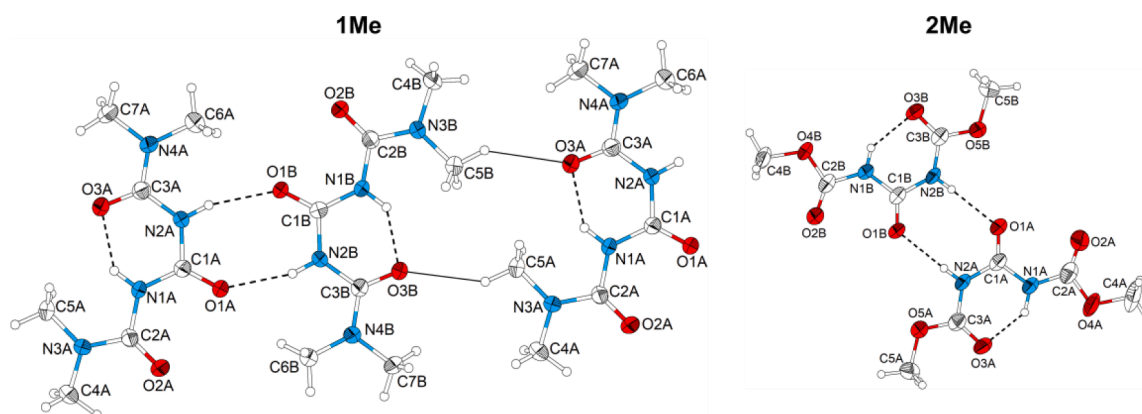
Fig. 6. Molecular structures of **1Me** and **2Me** in the single crystal showcasing the dimer formation. For **1Me** additional short contacts H–C are indicated by thin black lines, highlighting the formation of sheets in the extended crystal structure (see Fig. 10). Ellipsoids are drawn with 75 % probability level and hydrogen atoms with arbitrary radius.
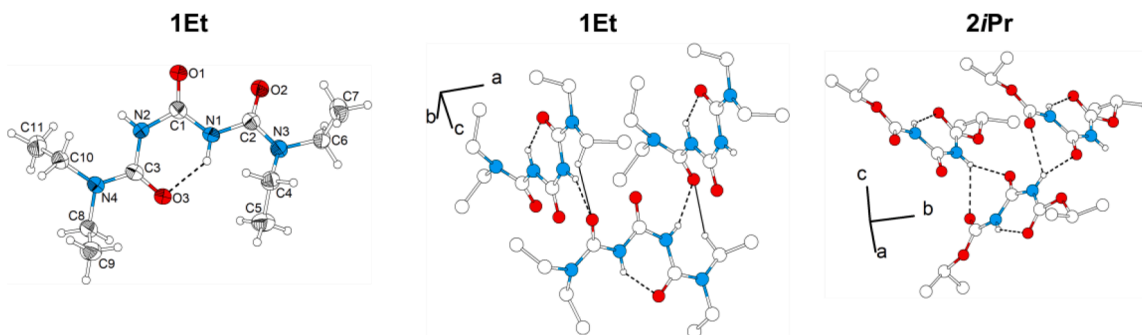
Fig. 7. Left: Molecular structure of **1Et** in the single crystal. Ellipsoids are drawn with 75 % probability level and hydrogen atoms with arbitrary radius. Middle and right: The hydrogen bonds forming a chain are shown for **1Et** (along [100], middle) and for **2iPr** (along [010], right). Short contacts H–C in **1Et** are indicated by thin black lines. Atoms are drawn in arbitrary units and hydrogen atoms are neglected for visibility.
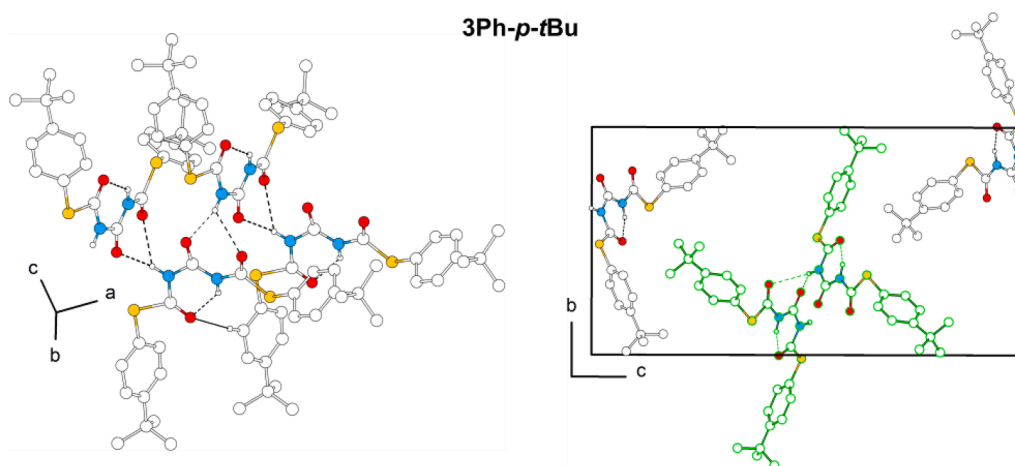
Fig. 8. Hydrogen bond connection and short contact H–C (indicated by thin black line) of **3Ph-*p-t*Bu** forming chains along [100]. These chains, highlighted in green, build a windmill like shape in the unit cell. Atoms are drawn with arbitrary radius and hydrogen atoms are neglected for visibility.

notation.

Diethyl *N,N'*-carbonyl bis(carbamate)

2Et crystallizes in the monoclinic space group $P2_1/c$ with one molecule in the asymmetric unit and four molecules in the unit cell ($Z =$ 4). The molecular structure of **2Et** (Fig. 9) in the solid state exhibits similar hydrogen bonding as **2Me**. It also shows one intramolecular and two intermolecular hydrogen bonds thus forming a dimer ($N_1 =$ $[R_2^2(8)]_{O1}[S(6)]_{O3}$). Stacking in [010] direction of the dimers is observed (Fig. 10).

Di*iso*propyl *N,N'*-carbonyl bis(carbamate)

2iPr crystallizes in the monoclinic crystal system with space group $P2_1/c$ with one independent molecule in the asymmetric unit and $Z = 4$. The molecule includes an intramolecular H-bond akin to **2Me** and **2Et** (Fig. 9). In contrast to those, **2iPr** does not form dimers. Instead, each molecule of **2iPr** is connected, similar to **1Et**, to two adjacent molecules (Fig. 7). The first connection is from O1 and O2 to H–N2 (O1/ O2⋯H–N2) of the first molecule. The second connection is from H–N2 to O1 and O2 (N2–H⋯O1/O2) of the second molecule. This gives two graph-set network notations $N_1 = [S(6)]_{O3}[C(6)]_{O2}[C(4)]_{O1}$ and $N_2 = [R_1^2(6)]_{O1}^{O2}$. In contrast to **1Et**, here the O1 atom is part of the hydrogen bonding network. Through these connections a chain along [010] is created (Fig. 7). Once again, *cis* conformation of the carbonyl groups (C1=O1/C2=O2) is observed.

Di*tert*butyl *N,N'*-carbonyl bis(carbamate)

2tBu crystalizes in the monoclinic space group *C2/c*. The asymmetric unit contains one molecule, and eight molecules in the unit cell ($Z = 8$). Similar to all other structures, an intramolecular hydrogen bond (O3⋯H–N1) is present, and the molecule shows the same conformation (Fig. 9). Akin to **2Me**, this molecule forms dimers. It is connected to one symmetry generated molecule *via* two hydrogen bonds (2 × O1⋯H–N2). This concludes to the $N_1 = [R_2^2(8)]_{O1}[S(6)]_{O3}$ graph-set notation. The molecules are stacked in the [010] direction, so that *tert*-butoxy groups are pointing towards each other (Fig. 10).

Dioctyl *N,N'*-carbonyl bis(carbamate)

2nOct crystallizes in space group $P\bar{1}$ with two molecules in the unit cell ($Z = 2$). The asymmetric unit contains one independent molecule. It forms dimers through intermolecular hydrogen bonds (O1⋯H–N2/ N2–H⋯O1). An intramolecular hydrogen bond (O3⋯H–N1) forms with the C3–N2–C1–N1 the motif of a six membered ring (Fig. 9), similar to **2Me** ($N_1 = [R_2^2(8)]_{O1}[S(6)]_{O3}$). The octyl groups are arranged next to each other, so that the dimers stack in [100] direction (Fig. 10) and the carbonyl groups are oriented *cis* to one another.

Diadamantyl *N,N'*-carbonyl bis(carbamate)

2Ad crystallizes in the monoclinic space group $P2_1/n$. The unit cell contains two molecules ($Z = 2$) with one independent molecule in the asymmetric unit. In contrast to the molecular structures above, the central tricarbonyl unit exhibits a different structural conformation (Fig. 9). In this molecule the carbonyl groups C1=O1 and C2=O2 are oriented *trans* to each other, the result of a rotation around the N1–C2 bond. This feature is most likely caused by the bulky adamantly group. Nonetheless, one intramolecular and two intermolecular hydrogen bonds are present. The molecule is connected to two different molecules ($N_1 = [S(6)]_{O3}[C(4)]_{O1}$), similar to **2iPr**. One intermolecular hydrogen bond connects from N2–H to O1 and the other from O1 to H–N2 (N2–*H*⋯O1/O1⋯*H*–N2). These connections are forming a chain like structure in [010] direction (Fig. 10).

Dibenzyl *N,N'*-carbonyl bis(carbamate)

2Bz crystallizes in the triclinic space group $P\bar{1}$ with two molecules per unit cell ($Z = 2$). The molecule forms the H-bonded intramolecular six-membered ring (Fig. 9) and a dimer with O1⋯H–N2 bonds. The graph-set notation is $N_1 = [R_2^2(8)]_{O1}[S(6)]_{O3}$. The dimers are stacked in [100] direction (Fig. 10). C2=O2 and C1=O1 are oriented *cis* towards each other. The major part of the molecule is planar, with a phenyl group (C5 – C10) rotating out of the plane around the O4–C4 bond with a torsion angle of 119° Thus, this group is orthogonal tilted with respect to this plane. The benzyl groups align in shifted π-stacking (Fig. 10).

Diphenyl *N,N'*-carbonyl bis(carbamate)

2Ph crystallizes in the monoclinic space group $P2_1/n$ with four molecules in the unit cell ($Z = 4$). Again, one independent molecule forms dimers with its symmetry generated entity. The dimers are stacked in [010] direction (Fig. 10). Here the carbonyl groups C1=O1 and C2=O2 are oriented *trans* towards another (Fig. 9), like in **2Ad**. The C3–N2–C1–N1 motif along with the O3⋯*H*–N1 hydrogen bond forms a six membered ring. This concludes to the $N_1 = [R_2^2(8)]_{O1}[S(6)]_{O3}$ graph-set notation. The phenyl groups exhibit shifted π-stacking (Fig. 10).

Diphenyl *N,N'*-carbonyl bis(*S*-thiocarbamate)

3Ph crystallizes with three crystallographically independent molecules in space group $P\bar{1}$ and $Z = 6$. Molecule 1 forms a dimer with its symmetry generated neighbour molecule, while molecules 2 and 3 together form a second dimer (Fig. 9) to give the overall $N_1 = [R_2^2(8)]_{O1}[S(6)]_{O3}$ graph-set notation. The molecular structure is highly disordered. For molecules 1 and 2 we observe a different tilting of the phenyl groups of about 4°. For molecule 3 we observe a rotational disorder involving one complete *S*-thiocarbamate group: The positions of O2C and S1C are disordered, so that both atom sides are occupied to 50 % by oxygen and sulphur (S1C/O4C and O2C/S2X). This leads to C2=O2
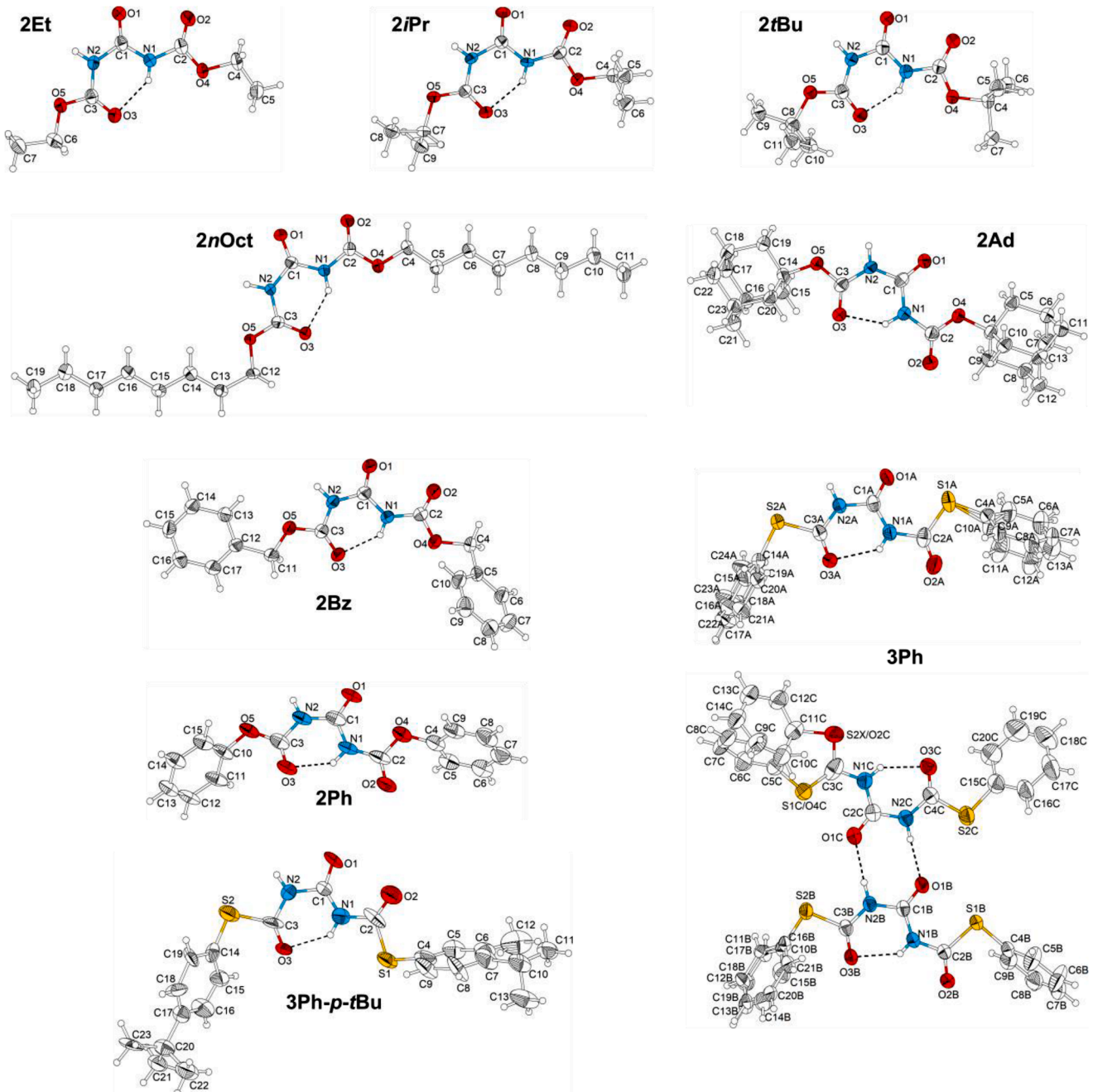
Fig. 9. Molecular structures of **2Et, 2*i*Pr, 2*t*Bu, 2*n*Oct, 2Ad, 2Bz, 2Ph, 3Ph** and **3Ph-*p*-*t*Bu** in the single crystal. **3Ph** is shown with the disorder at the phenyl rings and one C(=O)–SPh unit. Ellipsoids of **2Et, 2*i*Pr, 2*t*Bu, 2*n*Oct** and **2Ad** are drawn with 75 % probability level. Ellipsoids of **2Bz, 2Ph, 3Ph** and **3Ph-*p*-*t*Bu** are drawn with 50 % probability level. Hydrogen atoms are drawn with arbitrary radius.
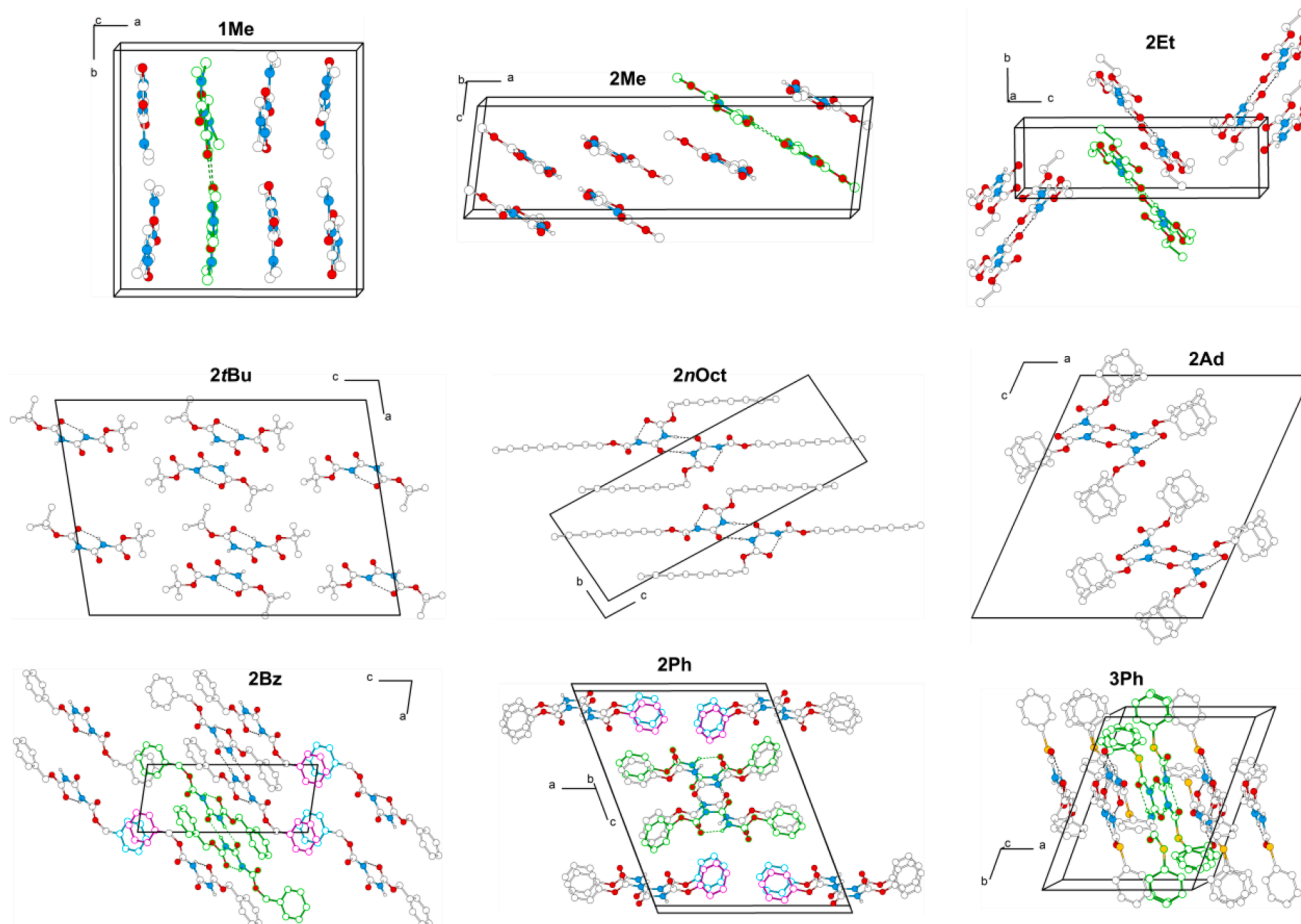
Fig. 10. Unit cells and crystal packing of **1Me, 2Me, 2Et, 2tBu, 2nOct, 2Ad, 2Bz, 2Ph** and **3Ph**. Dimers are highlighted in green. In **2tBu, 2nOct** and **2Ad** non-polar regions formed by the alkyl groups are visible. π-stacking of **2Bz** and **2Ph** is highlighted in purple and blue.

Table 1
Selected bond lengths [Å] of the molecular structures in the single crystal of **1Me, 1Et, 2Me, 2Et, 2iPr, 2tBu, 2nOct, 2Ad** and **2Bz**.

| bond	1Me	1Et	2Me	2Et	2iPr	2tBu	2nOct	2Ad	2Bz
C1=O1	1.218(3)/1.222(3)	1.213(2)	1.213(2)/1.217(2)	1.216(2)	1.213(2)	1.215(1)	1.220(2)	1.222(6)	1.212(2)
C2=O2	1.212(3)/1.215(3)	1.227(2)	1.183(2)/1.192(2)	1.192(2)	1.197(2)	1.198(1)	1.195(3)	1.207(6)	1.194(2)
C3=O3	1.243(3)/1.240(3)	1.234(2)	1.212(2)/1.212(2)	1.216(2)	1.220(2)	1.214(1)	1.209(3)	1.216(6)	1.203(2)
C1–N1	1.371(3)/1.365(3)	1.368(3)	1.375(2)/1.371(2)	1.369(2)	1.370(2)	1.369(1)	1.373(3)	1.373(5)	1.364(2)
C1–N2	1.397(3)/1.394(3)	1.402(3)	1.387(2)/1.388(2)	1.386(2)	1.392(2)	1.395(1)	1.384(3)	1.387(6)	1.384(2)
O1···H–N2	2.079(2)/2.079(2)	2.236(3)[a]	2.062(2)/2.068(2)	1.955(2)	2.133(2)	2.056(11)	1.919(3)	2.028(3)	1.987(2)

[a] for this compound the numbering is O2···H–N2.

being either in *cis* or *trans* orientation to C1=O1, and the phenyl group to be flipped. In molecule 1 and 2 C1=O1 and C2=O2 are oriented *trans* to each other. Stacking of the molecules along one axis or π-stacking is not observed due to the disorder, but all phenyl groups are pointing in [010] direction, forming a non-polar region along the [100] axis (Fig. 10).

Di-*para-tert*butyl phenyl *N,N*'-carbonyl bis(*S*-thiocarbamate)

3Ph-*p-t*Bu crystallizes in the orthorhombic space group $P2_12_12_1$ with two molecules in the unit cell ($Z = 2$) and one independent molecule in the asymmetric unit. It forms an intramolecular hydrogen bond (O3···*H*–N1), which builds a six-membered ring with the C3–N2–C1–N1 motif (Fig. 9). The molecules form strands *via* hydrogen bonds along [100], looking like a windmill (Fig. 8). One molecule is connected to two different molecules with O1 and O2 connected to *H*–N2 of the first and with *H*–N2 to O1 and O2 of the second molecule (Fig. 8), exactly like in **2iPr** ($N_1 = [S(6)]_{O3}[C(6)]_{O2}[C(4)]_{O1}$ and $N_2 = [R_1^2(6)]_{O1}^{O2}$). Additionally, a short contact between O3 and the *ortho* hydrogen atom of one phenyl ring (H–C19) is formed.

3.3. Comparative crystal structure discussion

All compounds have in common, that they exhibit an intramolecular hydrogen bond forming a six membered ring. This is similar to the literature-known compounds *N*-(4-methoxyphenylcarbamoyl)-*N*'-(4-methylbenzenesulfonylcarbamoyl) urea (**A**), di(2,2,2-trinitroethyl) *N,N*'-carbonyl biscarbamate (**B**) and di(2-fluoro-2,2-dinitroethyl) *N,N*'-carbonyl biscarbamate (**C**). The biscarbamoyl urea **A** even shows two intramolecular rings. The intramolecular ring conformer is more stable than an "open chain" conformer as has been proven before by discussing the molecular structures of carbonyl bis(carbamoylhalides), findings which are supported by DFT calculations [24]. The same results can be applied to the compounds discussed in this work. Additionally, all compounds exhibit intermolecular hydrogen bonds forming either dimers that are not further connected (with the notable exception of **1Me**), or chains. From the literature compounds only **C** forms dimers. In contrast, **A** and **B** exhibit more complex 3D hydrogen bonding networks,

Table 2

Selected bond and torsion angles [°] of the molecular structures in the single crystal of **1Me, 1Et, 2Me, 2Et, 2iPr, 2tBu, 2nOct, 2Ad** and **2Bz**.

angle	1Me	1Et	2Me	2Et	2iPr	2tBu	2nOct	2Ad	2Bz
N1–C1–N2	114.4(2)/115.1(2)	114.4(2)	114.3(1)/114.3(1)	114.8(1)	114.8(2)	114.0(8)	115.2(3)	115.0(3)	114.8(1)
O2–C2–N1–C1	3.9(4)/6.7(3)	24.4(3)	2.5(3)/2.5(3)	2.0(2)	2.6(3)	5.4(2)	0.2(4)	167.1(4)	4.7(3)
C1–N2–C3–O3	5.5(4)/2.9(4)	0.8(3)	0.0(3)/1.5(3)	1.9(2)	2.2(3)	0.2(2)	4.8(4)	0.6(7)	2.7(3)

so that comparison with **C** is best suited. A general trend for forming dimers or chains depending on the alkyl or aryl group cannot be discerned. For example, **2Et** and **2tBu** are in dimeric form, while **2iPR** forms chains, although the substituent *i*Pr lies in between the former two regarding the respective steric demand.

N,N`-Biscarbamoyl ureas

In **1Me** and **1Et** the hydrogen bond formation is contrary to each other. In **1Et**, C1=O1 is not part of a hydrogen bond and thus this group exhibits the shortest interatomic C=O distance with 1.213(2) Å. The interatomic distances C2=O2 and C3=O3, with both carbonyl groups part of hydrogen bonds, are longer with 1.227(2) Å and 1.234(2) Å, respectively (see Table 1). In **1Me**, C2=O2 is the shortest bond with 1.212(3) Å and 1.215(3) Å (two crystallographically independent molecules in the unit cell). As C3=O3 is involved in two hydrogen bonds it is overall the longest bond with 1.243(3) Å and 1.240(3) Å, respectively. Compared to **A**, in which every C=O bond is part of the hydrogen bonding network (**A**: 1.228(4) Å, 1.215(3) Å, and 1.217(4) Å), the distances in **1Me** and **1Et** are similar. C1–N1/2 distances (**1Me**: 1.365(3) – 1.397(3) Å, **1Et**: 1.368(3) Å/1.402(3) Å) are longer than in **A** (1.357(4) Å /1.387(4) Å), but still in single bond range. In all cases C1–N1 is shorter then C1–N2.

The central six membered ring in **1Me** is nearly planar, as torsion angles of O2–C2–N1–C1 and C1–N2–C3–O3 are 3.9(4)°, 6.7(3)°, and 5.5(4)°, 2.9(4)° (see Table 2). In **1Et** the central motif is not planar with a torsion angle of O2–C2–N1–C1 resulting in a tilt of 24.4(3)° out of the plane, caused by O2 being part of a hydrogen bond. The central N1–C1–N2 angles (**1Me**: 114.4(2)° and 115.1(2)°, **1Et**: 114.4(2)°) are in accordance with literature compounds (**A**: 116.9(3)°).

N,N`-Carbonyl bis(carbamates)

In all cases an intermolecular hydrogen bond O1⋯H–N2 is formed. The distances are in the same range (1.919(3) Å to 2.133(2) Å; Table 1) as for the literature compound **C** (2.096(4) Å). According to the sum of the van der Waals radii (r_{vdW}(H+O)=2.70 Å [25]) these interactions can be considered as strong hydrogen bonds. The C=O distances are in the range of double bonds. C1=O1 and C3=O3 are elongated due to those being part of hydrogen bonds. Their average distances ($d_{(C1=O1)}$=1.216 Å and $d_{(C3=O3)}$=1.213 Å) are in between the bond lengths of **C** (1.245(3) Å and 1.193(4) Å). The shorter C2=O2 distance is in average $d_{(C2=O2)}$=1.195 Å, which is slightly longer than in **C** (1.189(3) Å), but still follows the trend. In all cases every C–N distance is in single bond range.

The N1–C1–N2 angle is about 115° for all compounds. This in accordance with **B** and **C** (113.8(3)° and 116.2(3)°). The core unit of all molecules (C2(=O2)–N1–C1(=O1)–N2–C3(=O3)) is nearly planar with torsion angles O2–C2–N1–C1 and C1–N2–C3–O3 of 0.0(3)° in **2Me** up to 5.4(2)° in **2tBu** (Table 2). Only the O2–C2–N1–C1 torsion angle of **2Ad** (167.1(4)°) is an outlier. Here, the bulky adamantyl group is tilted out of the plane due to its high steric demand.

N,N`-Carbonyl bis(*S*-thiocarbamates)

Due to the abundant disorder and the low single crystal quality, the discussion of bond lengths and angles of **3Ph** and **3Ph-*p-t*Bu** must be treated with caution. The C1=O1 distance in **3Ph** ranges from 1.217(4) Å to 1.221(3) Å and thus is in agreement with the **2R** molecules. In **3Ph-*p-t*Bu**, the C1=O1 bond is longest with 1.230(3) Å. In contrast, C2=O2 (1.190(3) Å) is among the shortest bonds, while C3=O3 (1.164(3) Å) is by far the shortest one. Both carbonyl bonds in **3Ph** (C2=O2: 1.198(4) –

1.202(2) Å, C3=O3: 1.208(4) – 1.214(4) Å) are in better accordance with compounds **1R** and **2R**. Here, C–N bonds exhibit the shortest value (1.322(3) Å) up to the longest (1.455(3) Å) one. Both extremes are detected in **3Ph-*p-t*Bu**. The core motif of both structures is tilted out of planarity by a torsion angle up to 7.7(5)° and 3.7(3)° in **3Ph** and 7.4(4)° in **3Ph-*p-t*Bu**.

3.4. Comparative hirshfeld-surface analysis

To get more insight into the crystal packing, we performed a Hirshfeld surface analysis of all structures except **2Ph** and **3Ph**, because of their poor datasets and disorder (see above). Also, we generated their respective fingerprint plots. The contribution of each atomic surface interaction is determined from the d_e versus d_i values. All values are listed in the Supporting Information in Table S 4. The most prominent interaction, which is observed in every compound of this work, is the intermolecular O⋯H–N hydrogen bond. These, and all other O⋯H/H⋯O contacts result in sharp spikes (see Fig. 11, green circles), which are shortest at ≈1.9 Å. The bright blue-greenish regions represent mostly all H⋯H contacts, showing that van der Waals interactions are the most common. The tip between the two spikes (see Fig. 11, red circle) is formed by the shortest H⋯H contacts being around ≈2.2 Å.

A closer look into the fingerprint plots, by breaking them down into specific contacts (see Fig. 12), reveals the influence of the aryl or alkyl group. The relative amount of nonpolar interactions (H⋯H and C⋯H) is increasing with bigger alkyl groups (meaning more $(CH_x)_n$ groups). It is lowest for **2Me** with 33.5 % and the highest for **2nOct** (75.3 %) and **2Ad** (74.9 %). This is, as expected, attributed to increasing number of van der Waals interactions. The nonpolar interactions for **1Me** (55.1 %) and **1Et** (71.1 %) are compared to **2Me** (33.5 %) and **2Et** (49.8 %) nearly one third higher, which indicates the impact of doubling the alkyl groups. For the aryl containing molecules, **2Bz** and **3Ph-*p-t*Bu**, a much higher C⋯C value (20.0 % and 17.3 %) is testament to the observed π-stacking.

The amount of polar interactions H⋯O, H⋯N and C⋯O (Fig. 12 only shows H⋯O) decreases with increasing sizes of the alkyl groups. With 59.1 % for **2Me**, those make up the main interactions, while for **2Et** polar (43.4 %) and non-polar (49.8 %) interactions nearly keep in balance. From **2iPr** to **2Ad** the polar interactions are decreasing further to ca. 25 %. Very prominent for **3Ph-*p-t*Bu** is the effect of the sulphur atom with an H⋯S amount of 8.7 % (see Fig. 12). Despite the bulky group it still is half the value than for H⋯O (17.3 %).

Like our chemical intuition suggests and as indicated above, there is a discernible trend. The bigger the alkyl/aryl group, the higher is the influence of nonpolar interactions in the form of van der Waals forces. The other way around holds also true: the smaller the substituent, the more the number of polar interactions increases. Unfortunately, we were not able to crystallize **1iPr** and **3Et** to understand the trends clearer and the influence of the nucleophilic group, which would make the three molecule classes *N,N`*-biscarbamoyl ureas, *N,N`*-carbonyl bis(carbamates), and *N,N`*-carbonyl bis(*S*-thiocarbamates) more comparable.

3.5. Infrared spectroscopy

Knowing the crystal structures of the compounds it is possible to assign some bands in the IR spectra of the molecules. In Fig. 13 the IR spectra of **1Et, 2Et** and **3Et** are as representatives compared to each
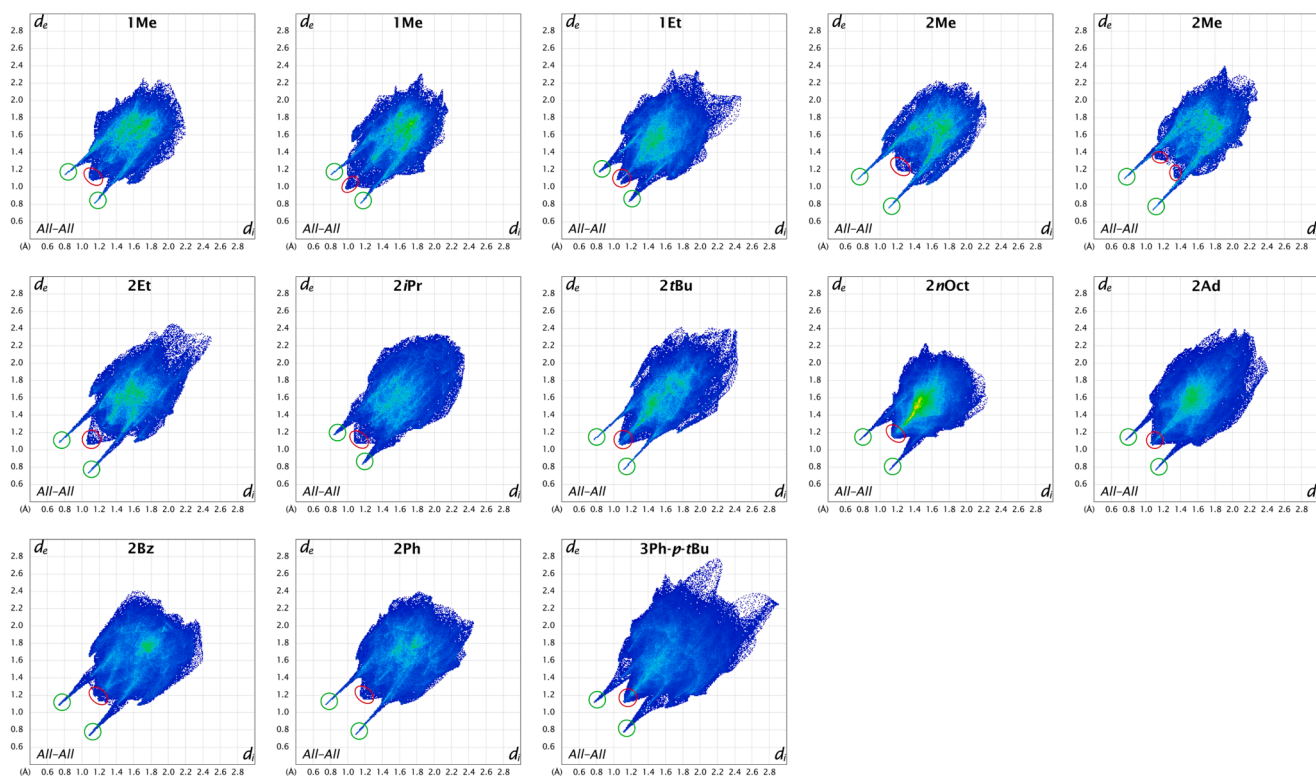
Fig. 11. Hirshfeld surface analysis plotted as fingerprint plots for **1Me, 1Et, 2Me, 2Et, 2*i*Pr, 2*t*Bu, 2*n*Oct, 2Ad, 2Bz, 2Ph**, and **3Ph-*p-t*Bu**. Short O···H/ H···O contacts are marked with green circles and short H···H contacts with red circles. Bright blue-greenish areas represent the highest number of H···H contacts.

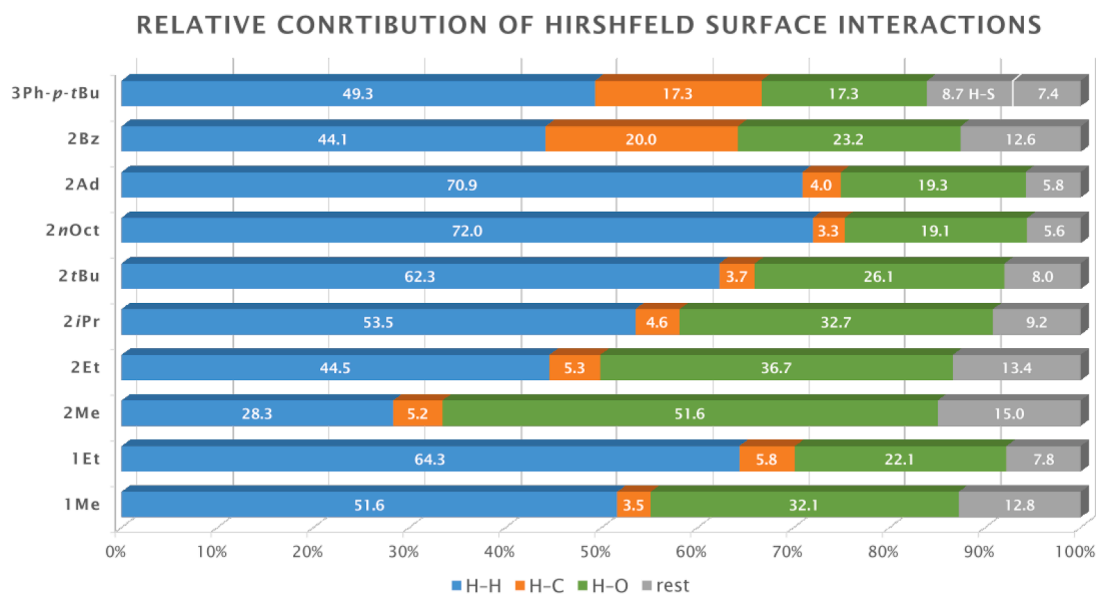**Fig. 12.** Relative contributions of the H···H (blue), H···C (orange) and H···O (green) contacts to the Hirshfeld surface interactions of **1Me, 1Et, 2Me, 2Et, 2*i*Pr, 2*t*Bu, 2*n*Oct, 2Ad, 2Bz** and **3Ph-*p-t*Bu**.
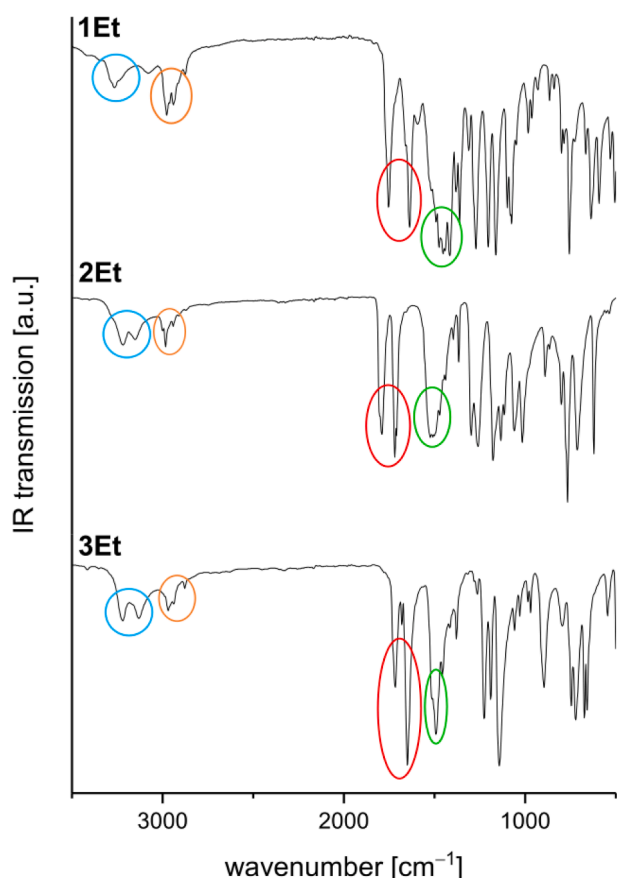
Fig. 13. Comparison of the infrared spectra of **1Et**, **2Et** and **3Et**. Characteristic vibration modes are marked in circles: blue N–H, orange C–H, red C=O and green N–H/C–H. Measurements were performed at room temperature on an ATR device from the neat powder samples.

other. IR spectra of all compounds are in the Supporting Information. Marked in blue are N–H stretching vibrations in the region of 3200 cm^{-1}. For **1Et** only one vibration mode is detected, albeit a small shoulder could also be discernible. For **2Et** and **3Et** two vibration modes for both N–H groups participating in different hydrogen bonds are found. At ca. 2975 cm^{-1} the C–H stretching vibrations of the ethyl group are present (orange circle). For all three compounds two signals for the C=O stretching vibrations (red circle) are detected. The C=O stretching vibration of the central N–(C=O)–N moiety is at 1754 cm^{-1} **1Et**, 1792 cm^{-1} **2Et** and 1717 cm^{-1} **3Et**. The other C=O stretching vibration is detected at lower wavenumbers of 1637 cm^{-1} for **1Et**, 1718 cm^{-1} for **2Et** and 1649 cm^{-1} for **3Et**. The shift to lower frequencies is evidence for both C=O groups participating in hydrogen bonds, so that two individual signals can be observed. In the region in between 1500 cm^{-1} to 1400 cm^{-1} a broad absorption (green circle) is formed due to the combination of N–H and C–H deformation vibrations. Below 1300 cm^{-1}, in the fingerprint region, compound specific C–N, C–O and C–S vibrations, as well as C–C and C–H vibrations are present. It was not possible to crystallize **3Et**, but from the IR spectra it can be assumed, that the molecule exhibits a similar structure as **2Et**, maybe even isostructural.

4. Conclusion

Within this work, we disclose our findings regarding the synthesis characterization (spectroscopic and crystallographic incl. Hirshfeld analysis) of the hitherto overlooked compound classes *N,N'*-biscarbamoyl ureas, *N,N'*-carbonyl bis(carbamates) and *N,N'*-carbonyl bis(*S*-thiocarbamates). Thus we close an obvious an long-standing gap in the structural chemistry of urea derived molecules. We show that these

types of compounds can be differentiated in ^{13}C NMR spectroscopic analysis, most conveniently by the carbon atom substituted with an amide, alkoxide or sulfide group. In the solid state, the substitution group plays a role in the formation of dimers or chains of the molecules, and in the stacking of the molecules in the extended crystal structure. Although an obvious trend is absent, through Hirshfeld surface analysis this effect is showcased by an increasing amount of non-polar van der Waal forces with increasingly bulkier aryl or alkyl groups. The molecules interconnected by strong N–H···O hydrogen bonds, which form an intramolecular six-membered ring and intermolecular dimers or strands. The short contacts are shown by spikes in the fingerprint plots. IR spectroscopy completes the insight of the hydrogen bond network with the detection of two separate vibration modes for the C=O and N–H bonds, respectively. In future work we will aim to establish those compounds as building blocks in supramolecular architectures towards crystal engineering.

CRediT authorship contribution statement

Jonathan Pfeiffer: Data curation, Investigation, Writing – original draft, Writing – review & editing. **Martin Möbs:** Investigation. **Sascha Reith:** Investigation. **Mirko Tallu:** Investigation. **Frank Tambornino:** Conceptualization, Funding acquisition, Supervision, Writing – review & editing.

Declaration of competing interest

The authors declare that they have no known competing financial interests or personal relationships that could have appeared to influence the work reported in this paper.

Data availability

Data is in the Supporting Information.

Acknowledgements

Supplementary materials

Supplementary material associated with this article can be found, in the online version, at doi:10.1016/j.molstruc.2024.138198.

References

[1] H. Boerhaave, Elementa chemiae, quae anniversario labore docuit in publices privatiaque scholis, Leiden (1732).
[2] F. Kurzer, P.M. Sanderson, Urea in the history of organic chemistry: isolation from natural sources, J. Chem. Educ. 33 (1956) 452.
[3] H. Rouelle, Observations sur l'urine humaine, & sur celle de vache & de cheval, comparées ensemble, J. Médecine, Chir. Pharm. 40 (1773) 48–71.
[4] W. Cruickshank, The results of the trials of various acids, and some other substances, in the treatment of the Lues Veneres and some observation on the nature of sugar, in: an Account, Two Cases Diabetes Mellit II (1797).
[5] L.-N. Vauquelin, A.F. de Fourcroy, Extrait d'un premier mémoire des cit. Fourcroy et Vaulquelin, pour servir à l'histoire naturelle, chimique et médicale de l'urine humaine, contenant quelques faits nouveaux sur son analyse et son altération spontanée, Ann. Chim. 31 (1799) 48–71.
[6] J. Davy, On a gaseous compound of carbonic oxide and chlorine, Philos. Trans. R. Soc. Lond. 102 (1812) 144–151.
[7] F. Wöhler, Ueber künstliche Bildung des Harnstoffs, Ann. Phys. Chem. 88 (1828) 253–256.
[8] G. Wiedemann, Ueber eine neue, aus dem Harnstoff entstehende Verbindung, J. Prakt. Chem. 43 (1848) 271–280.
[9] G. Wiedemann, Ueber ein neues Zersetzungsprodukt des Harnstoffs, Ann. Phys. Chem. 150 (1848) 67–84.

[10] G. Wiedemann, Biuret. Zersetzungsprodukt des Harnstoffs, Ann. Chem. Pharm. 68 (1848) 323–326.

[11] E. Schmidt, Über die Einwirkung von flüssigen Phosgen auf Amide, Chem. Zentralblatt 43 (1872) 195–197.

[12] K. Bredereck, R. Richter, Verfahren zur Herstellung von Diazapentadienderivaten, DE1256646B, 1967.

[13] Z. Csurös, R. Soós, Á. Antus-Ercsényi, I. Bitter, J. Tamás, Acylation of disubstituted cyanamides with phosgene, Acta Chim. Acad. Sci. Hungaricae 76 (1973) 81–94.

[14] K. Mai, G. Patil, Action of Trichloromethyl Chloroformate on Sustituted Ureas: preparation of Some Alkylcarbamoylureas, Synth. Commun. 16 (1986) 1823–1826.

[15] B. Akteries, J.C. Jochims, Carbonyl diisocyanate: a new preparation and some reactions, Chem. Ber. 119 (1986) 83–95.

[16] K. Mroczyńska, M. Kaczorowska, E. Kolehmainen, I. Grubecki, M. Pietrzak, B. Ośmiałowski, Conformational equilibrium in supramolecular chemistry: dibutyltriuret case, Beilstein J. Org. Chem. 11 (2015) 2105–2116.

[17] H. Bestian, D. Grimm, Verfahren zur Herstellung von carbamoylsubstituierten Kohlensäureamidderivaten, DE1668004A1, 1971.

[18] D.V. Singh, K. Adeppa, K. Misra, Mechanism of isoproturon resistance in Phalaris minor: in silico design, synthesis and testing of some novel herbicides for regaining sensitivity, J. Mol. Model. 18 (2012) 1431–1445.

[19] O. Folin, Über Urethane, Chem. Zentralblatt 68 (1897) 23–25.

[20] F.B. Dains, On the isourea ethers and other derivatives of ureas, J. Am. Chem. Soc. 21 (1899) 136–192.

[21] V. Kerrigan, K.W. Pearson, Manuf. Carbonyl Bisurethanes (1967) GB1107538.

[22] A. Das Mahapatra, A. Shaik, V. Thiruvenkatam, B. Datta, Supramolecular architecture in sulfonylurea, sulfonyldiurea and sulfonyltriurea drugs: synthesis, X-ray structure and Hirshfeld surface analysis, J. Mol. Struct. 1233 (2021) 130158.

[23] T.M. Klapötke, B. Krumm, S.F. Rest, M. Sućeska, Polynitro containing energetic materials based on carbonyldiisocyanate and 2, 2-Dinitropropane-1, 3-diol, Z. Anorg. Allg. Chem. 640 (2014) 84–92.

[24] J. Pfeiffer, H. Günther, L. Völlinger, D. Botros, B. Scheibe, M. Möbs, F. Kraus, F. Weigend, F. Tambornino, Double addition vs. ring closure: systematic reactivity study of $CO(NCO)_2$ and $CO(NCS)_2$ towards Hydrogen Halides, Chem. – A Eur. J (2023) e202203983.

[25] S. Alvarez, A cartography of the van der Waals territories, Dalt. Trans. 42 (2013) 8617–8636.
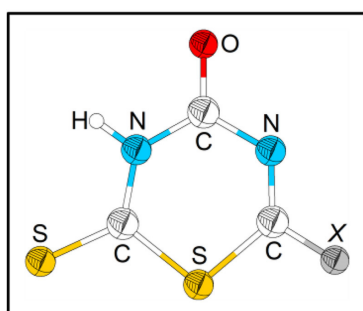
3.6 Synthesis, Crystal Structure Study and Spectroscopic Analysis of Substituted 2,3-dihydro-2-thioxo-4*H*-1,3,5-thiadiazin-4-ones

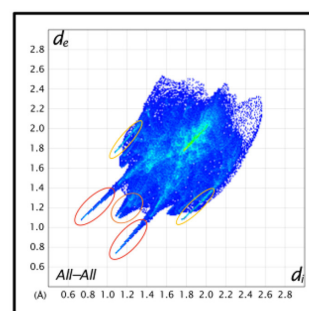Jonathan Pfeiffer, Clemens Trost, Frank Tambornino

2,3-dihydro-2-thioxo-4*H*-1,3,5-thiadiazin-4-ones

synthesis

crystal packing

Hirshfeld surface

hydrogen bonding

Abstract:

A variety of substituted 2,3-dihydro-2-thioxo-4H-1,3,5-thiadiazin-4-ones was synthesized from carbonyl diisothiocyanate and different nucleophiles, like water, alcohols, thiols, and amines. A comprehensive crystal structure analysis of the resulting thiadiazines is presented together with analysis of their nuclear magnetic resonance and infrared spectra. The central thiadiazine motif of each molecules forms a planar albeit slightly irregular hexagon. Independent of the substituent, all molecules form dimers in the solid state which are held together via hydrogen bonds. Hirshfeld surface analysis shows mostly short polar interactions, with increasing non-polar interactions depending on the size of the side chain.

Zusammenfassung:

Eine Vielzahl von substituierten 2,3-Dihydro-2-thioxo-4*H*-1,3,5-thiadiazin-4-onen wurde aus Carbonyldiisothiocyanat und verschiedenen Nukleophilen wie Wasser, Alkoholen, Thiolen und Aminen synthetisiert. Eine umfassende Kristallstrukturanalyse der resultierenden Thiadiazine wird zusammen mit der Analyse ihrer Kernspinresonanz und Infrarot-Spektren präsentiert. Das zentrale Motiv der Thiadiazine jedes Moleküls bildet ein planares, leicht unregelmäßiges Hexagon. Unabhängig des Substituenten bilden alle Moleküle Dimere im Festkörper, welche über Wasserstoffbrückenbindungen zusammengehalten werden. Hirs-

hfeld Oberflächen Analyse zeigt überwiegend kurze polare Wechselwirkungen mit zunehmend größeren unpolaren Wechselwirkungen abhängig von der Größe der Seitenkette.

Beiträge der Autoren:

Die Publikation enthält Ergebnisse der Masterarbeit von CLEMENS TROST.[130] Synthese und Charakterisierung aller Verbindungen **1-4**, außer NMR- und IR-Spektroskopie von **4Et** und **4iPr**, wurde von TROST durchgeführt. SC-XRD Analyse mit Strukturlösung und -verfeinerung wurde von mir und TAMBORNINO vorgenommen. Hirshfeld Analyse wurde von mir durchgeführt. Das Manuskript und die *Supporting Information* wurden von mir geschrieben und zusammen mit TAMBORNINO überarbeitet.
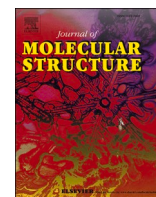
Synthesis, crystal structure study and spectroscopic analysis of substituted 2,3-dihydro-2-thioxo-4H-1,3,5-thiadiazin-4-ones

Jonathan Pfeiffer , Clemens Trost , Frank Tambornino [*]

Fachbereich Chemie, Philipps-Universität Marburg, Hans-Meerwein-Straße 4, Marburg 35043, Germany

ABSTRACT

A variety of substituted 2,3-dihydro-2-thioxo-4H-1,3,5-thiadiazin-4-ones was synthesized from carbonyl diiso-thiocyanate and different nucleophiles, like water, alcohols, thiols, and amines. A comprehensive crystal structure analysis of the resulting thiadiazines is presented together with analysis of their nuclear magnetic resonance and infrared spectra. The central thiadiazine motif of each molecules forms a planar albeit slightly irregular hexagon. Independent of the substituent, all molecules form dimers in the solid state which are held together *via* hydrogen bonds. Hirshfeld surface analysis shows mostly short polar interactions, with increasing non-polar interactions depending on the size of the side chain.

1. Introduction

Hexagonal heterocycles with two nitrogen atoms in the 3 and 5 position, and one sulphur atom in the 1 position, are called 1,3,5-thiadiazines. Thiadiazines with various substitutions are well known in literature, even though the fully unsubstituted tetrahydro-2H-1,3,5-thiadiazine **I** is still unknown. Scheme 1 displays a selection of possible substitution patterns for 1,3,5-thiadiazines, which relate to this work.

Molecules with alkyl or aryl substituents at the nitrogen atom positions 3 and 5 (see Scheme 1 for numbering), disubstituted tetrahydro-2H-1,3,5-thiadiazines **I**, can be synthesized from amines, formaldehyde and a sulphur source like hydrogen sulphide or sodium hydrosulphide [1–6]. Similar to **I**, the unsubstituted 3,4-dihydro-2H-1,3,5-thiadiazine **II**, which bears a C=N double bond, needs to be synthesized yet. Preparation of molecules **II** which are substituted at the nitrogen atom position 3 and carbon atom position 6 with alkyl or aryl groups is possible from primary thioamides and bis(benztriazolylmethyl)amines [7]. The next 1,3,5-thiadiazine in Scheme 1 shows a carbonyl group at the NCN carbon atom position 4 and is called tetrahydro-4H-1,3,5-thiadiazin-4-one **III**. In contrast to the molecules discussed before, the *N*-unsubstituted molecule can be synthesized from urea, formaldehyde or bis(dimethylamino)methane and hydrogen sulphide [8,9]. *N*-substitution at the nitrogen atoms with an alkyl group is possible by starting from the corresponding substituted urea derivative [10]. Instead of the introduction of a carbonyl function, a thiocarbonyl group can also be introduced albeit at a different position which is the NCS carbon atom 2,

leading to tetrahydro-2H-1,3,5-thiadiazine-2-thione **IV**. Reports on the *N*-unsubstituted molecule are not found in literature, yet. However, the molecule framework is of pharmaceutical interest and concludes to a variety of alky or aryl *N*-disubstituted examples. Synthesis is achieved by reaction of potassium dithiocarbamate with formaldehyde and a primary amine [11–15]. The challenge to combine the three features C=N, C=O and C=S in one ring system to gain access to 2,3-dihydro-2-thioxo-4H-1,3,5-thiadiazin-4-one **V** has been possible, but with a completely new synthesis approach. Here, carbonyl diisothiocyanate is reacted with nucleophiles like alcohols, thiols, amines or halides (Scheme 2). This leads to a functionalization in the 6 position resulting in either ether, thioether or tertiary amine [16,17].

Crystal structures of 1,3,5-thiadiazines with various substitutions, more than shown here, are known very well. For the discussed substituted thiadiazines **I**, four structures are described with phenyl [5], *para*-toluyl [5], 2-chloropropyl[18] and *para*-ethylcarboxyphenyl[19] groups. All crystallize in chair conformation and the side chains are in axial positions. Only one example for **II** was crystallized with a phenyl group at the carbon atom position 6 and a *para*-methoxyphenyl group at the nitrogen atom position 3 [7]. The molecule forms a half-chair conformation with the N–R[1] tilted out of the plane. Crystal structures for compounds of type **III** are, until now, unknown. Solely, their CHN analysis and melting points have been reported [10]. For thiadiazines **IV**, three crystal structures with R[1]=benzyl and R[2]=butyl [20], R[1]=mesityl and R[2]=carboxymethyl [21], and R[1]=furfurylmethyl and R[2]=carboxyethyl[22] are reported. All three compounds crystallize with
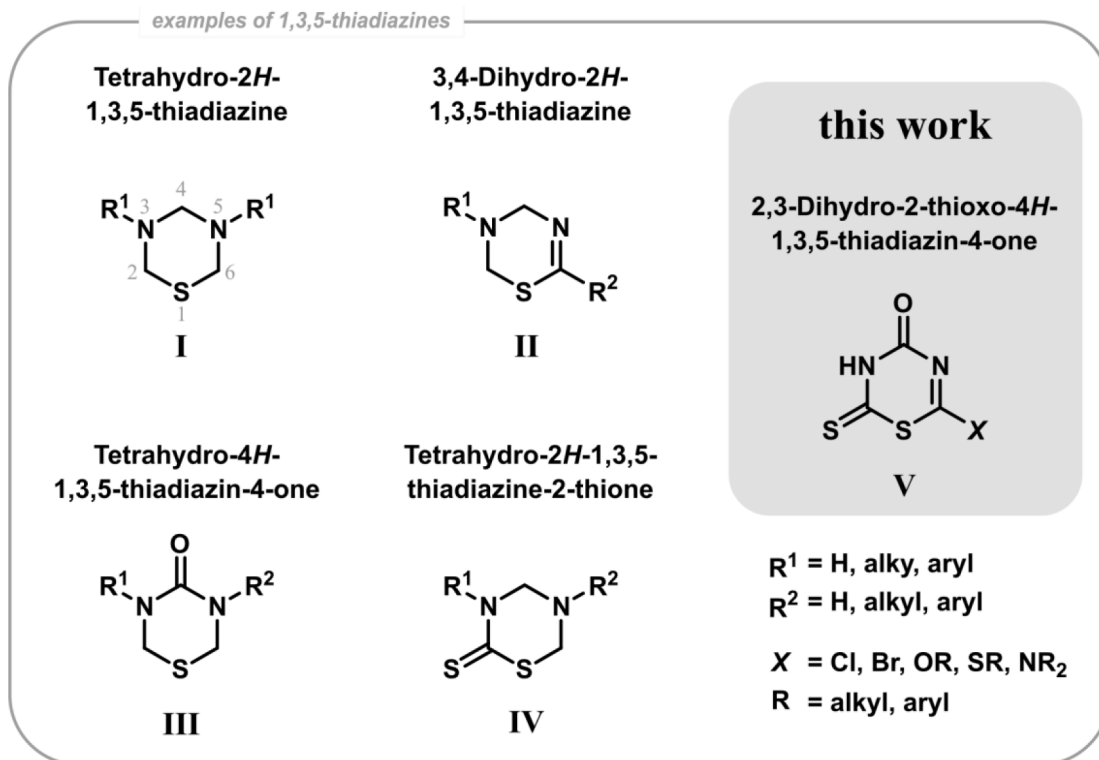
Scheme 1. Selected examples of 1,3,5-thiadiazines with different substitution patterns and position numbering.
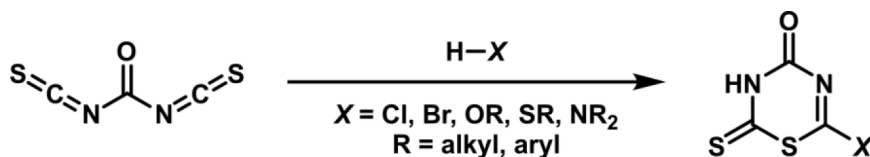
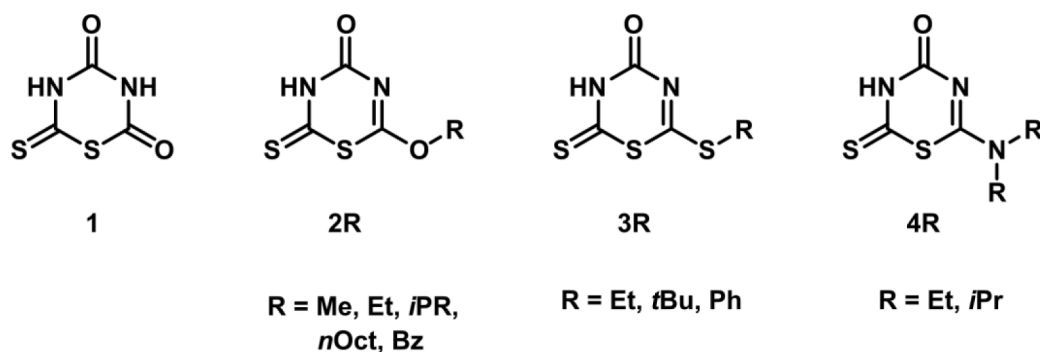**Scheme 2.** Synthesis of substituted 2,3-dihydro-2-thioxo-4*H*-1,3,5-thiadiazin-4-ones from carbonyl diisothiocyanate.

Scheme 3. Structural formulas and nomenclature of 1,3,5-thiadiazine molecules presented in this work.

half-chair conformation with the N–R^2 group being tilted out of plane. The crystal structures of compound type **V** were long elusive and only recently we were able to determine the structures with chlorine and bromine substitution [23]. However, structures including other substituents are missing so far.

This fact was incentive for us to study the crystal structures of alkoxy, sulfanyl and amine substituted 2,3-dihydro-2-thioxo-4*H*-1,3,5-thiadiazin-4-ones (Scheme 3). We present a comprehensive molecular and structural analysis of the compounds illustrated in Scheme 3, including NMR and IR spectroscopy, single crystal X-ray diffraction and Hirshfeld surface analysis.

2. Results and discussion

2.1. Experimental

2.1.1. General synthesis

Syntheses were carried out after modified literature procedure [16]. To a 1 molar solution of nucleophilic substrate in THF neat carbonyl diisothiocyanate was added dropwise at room temperature. The
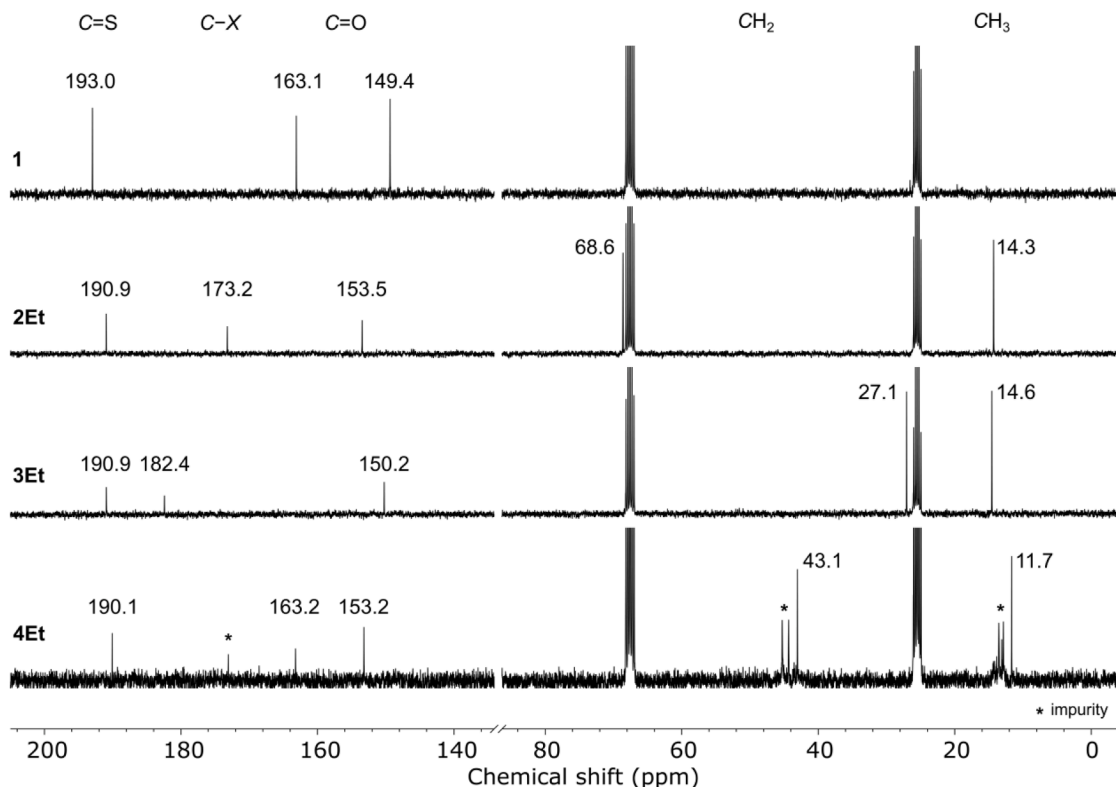
Fig. 1. Comparison of the ^{13}C NMR spectra of 1, 2Et, 3Et and 4Et in THF-d8 at room temperature.

resulting solution was stirred for 16 h. After evaporation of the solvent, the product was obtained as a solid. Reactions with amines were carried out in diethyl ether and at −78 °C. For detailed synthetic procedures see Supporting Information. As amines are more reactive than alcohols and thiols, reactions were hard to control, e.g. reaction occurred in the gas phase above the solution even at −78 °C. This led to mostly impure

reaction products, which could not be purified completely.

2.2. NMR spectroscopy

All compounds can be identified by ^{13}C NMR spectroscopy. They exhibit a characteristic set of three signals for the carbon atoms of the
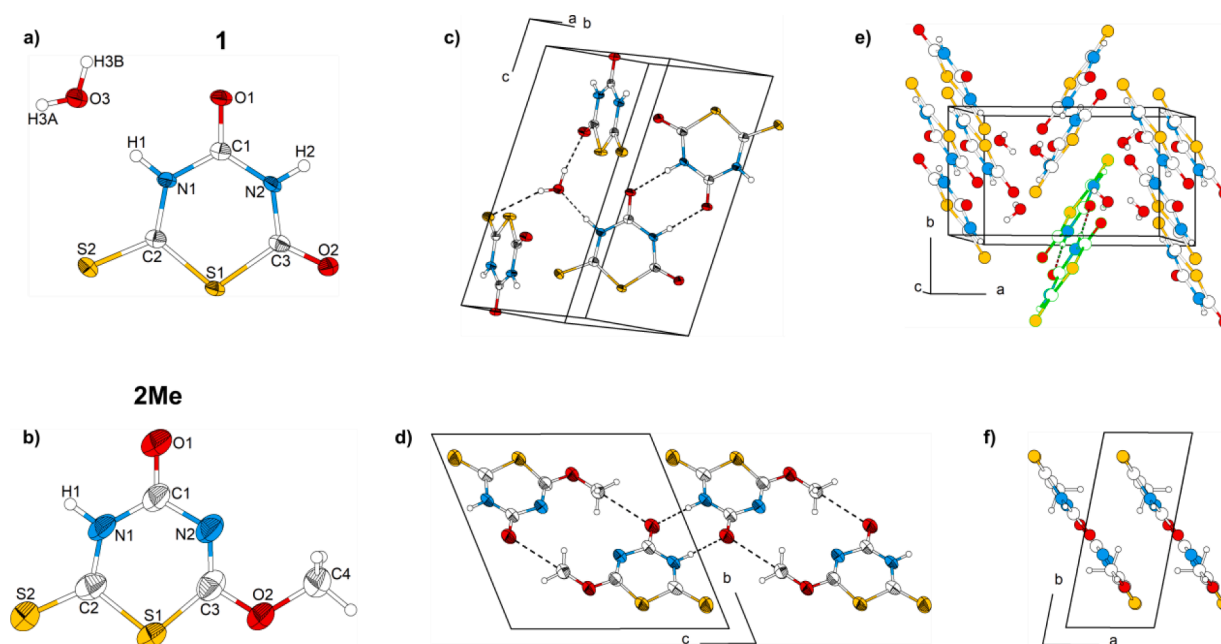
Fig. 2. Crystal structures of 1 and 2Me in the solid state. a) molecular structure of 1, b) molecular structure of 2Me, c) hydrogen bonding network of 1 in the unit cell, viewed approximately along [110] with Etter's graph set notation $N_1 = [R_2^2(8)]_{O1}[C_2^2(8)]_{O3}^{O2}[C_2^2(6)]_{O3}^{S2}$, d) hydrogen bonding network of 2Me in the unit cell viewed along [100] with Etter's graph set notation $N_1 = [R_2^2(8)]_{O1}$, e) dimer formation of 1 in approximately the [001] direction, f) dimer strands of 2Me in [001] direction. Ellipsoids are drawn with 75% probability level and hydrogen atoms with arbitrary radius.

Fig. 3. Molecular structure in the solid state of 2Bz (a) with the stacking of the two independent molecules in the crystal structure (b, c). Ellipsoids are drawn with 75% probability level and hydrogen atoms with arbitrary radius.

thiadiazine ring. In Fig. 1 the ^{13}C NMR spectrum of **1** is shown with its comparison to the NMR spectra of **2Et, 3Et** and **4Et,** as representatives for alkoxy, sulfanyl and amine substituted thiadiazines. The signal for the C=S carbon atom of **1** is at 193.0 ppm and for the three other compounds at ~190 ppm. Its chemical shift is not affected by the different substituents in position 6. The signal for the carbon atom of the C=O group is at ~153 ppm for **2Et** and **4Et,** and slightly high field shifted to 149.4 ppm for **1** and to 150.2 ppm for **3Et.** This is comparable

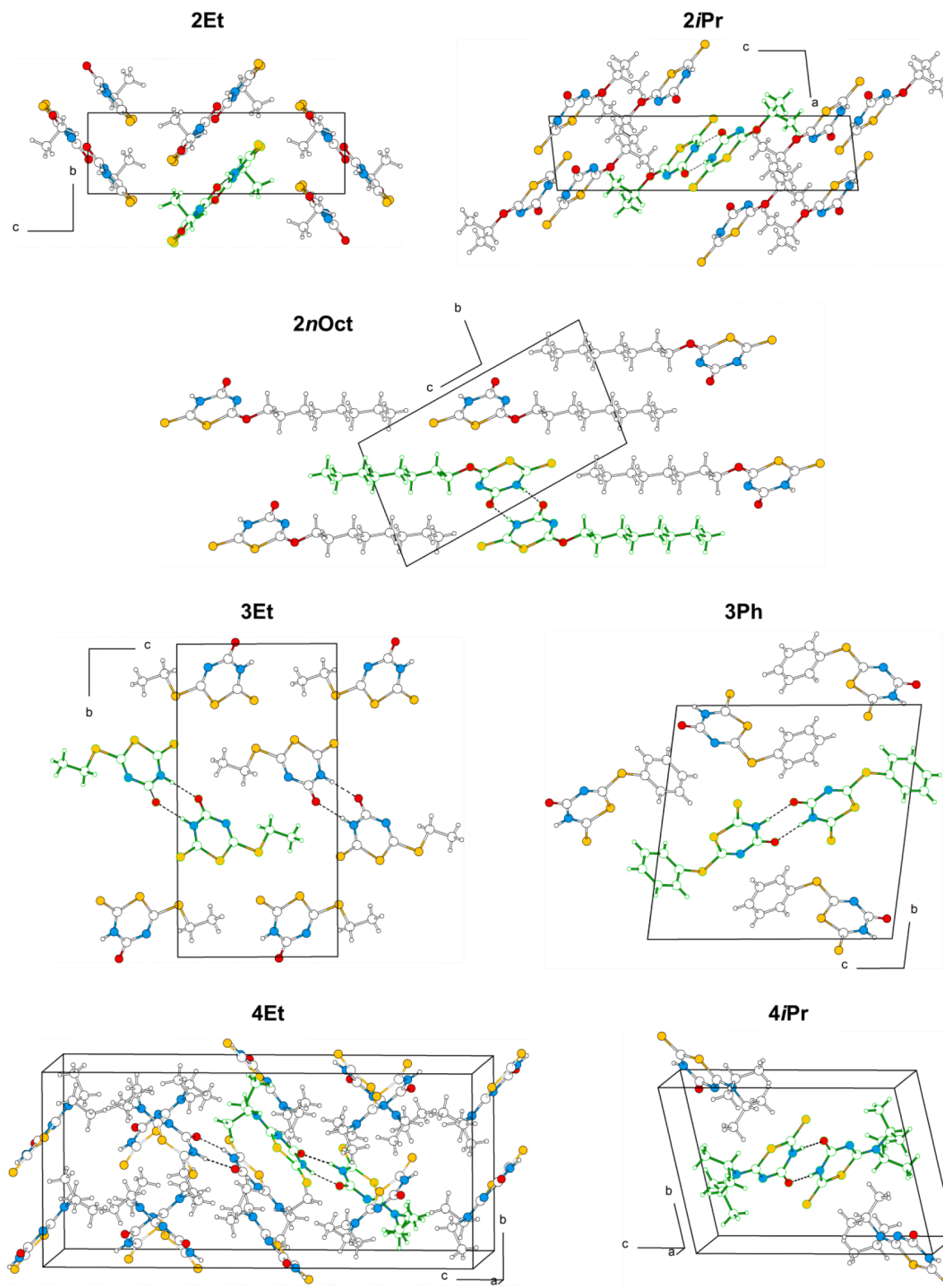to the halide substituted thiadiazines [23]. For those a ^{13}C NMR shift of the C=S carbon atom is reported to be at 190.4 ppm (Cl) and 191.6 ppm (Br), and for the C=O carbon atom at 150.8 ppm (Cl) and 149.4 ppm (Br). The ^{13}C NMR shift for the carbon atom in position 6 is depending on the heteroatom of the corresponding nucleophile X. In **1,** the shift of the second C=O group is located at 163.1 ppm. For the alkoxy group the signal is in between the two other carbon atoms at 173.2 ppm. The sulfanyl group shifts the signal into low field to 182.4 ppm, while the

Fig. 4. Molecular structures of 2Et, 2iPr, 2nOct, 3Et, 3Ph, 4Et and 4iPr in the solid phase. Ellipsoids are drawn with 75% probability level, except for 3Ph which is drawn with 50% probability level. Hydrogen atoms are drawn with arbitrary radius. All compounds crystallize in the form of dimers with Etter's graph set notation $N_1 = [R_2^2(8)]_{O1}$.

Fig. 5. Depiction of the unit cells for the molecules 2Et, 2*i*Pr, 2*n*Oct, 3Et, 3Ph, 4Et and 4*i*Pr with the stacking of molecules in the extended crystal structure. Selected dimers of two molecules are highlighted in green. Atoms are drawn with arbitrary radius.

amine group shifts it high field to 163.2 ppm. This is to be expected an also comparable to the halide substituted thiadiazines. Additionally, the shift for the CH_2 of the ethyl group is differently located at 68.6 ppm for **2Et**, 27.1 ppm for **3Et** and 43.1 ppm for **4Et**. As stated above, compounds **4** are impure and contain side products as shown by additional signals in the ^{13}C NMR spectrum.

In the ^{1}H NMR spectrum of **1** two N–*H* signals at 12.56 ppm and 11.62 ppm are detected. All other compounds of **2, 3** and **4** only show one N–*H* signal at approximately 12.5 ppm. The signals of the ethyl group are detected at 4.59 ppm and 1.38 ppm for **2Et**, 3.32 ppm and 1.38 ppm for **3Et**, and 3.72 ppm and 1.32 ppm for **4Et**. NMR spectra of all compounds are shown in the Supporting Information.

Table 1

Selected bond lengths and bond angles of all compounds reported in this study in the solid state as derived from single crystal X-ray diffraction.

bond [Å]	1	2Me	2Et	2iPr	2nOct	2Bz	3Et	3Ph	4Et	4iPr
C1=O1	1.216(2)	1.223(4)	1.225(2)	1.223(5)	1.226(3)	1.212(5) / 1.218(5)	1.248(2)	1.232(6) / 1.221(7)	1.229(2) / 1.235(2)	1.231(3) / 1.228(3)
C2=S2	1.649(2)	1.635(4)	1.639(2)	1.647(4)	1.634(3)	1.641(4) / 1.641(4)	1.642(2)	1.626(5) / 1.649(6)	1.642(2) / 1.648(2)	1.643(3) / 1.637(2)
C−N	1.353(2) – 1.387(3)	1.356(4) –1.395(4)	1.356(2) – 1.394(3)	1.349(5) – 1.400(5)	1.350(4) – 1.397(3)	1.350(5) – 1.409(5)	1.352(2) – 1.399(2)	1.362(8) – 1.406(8)	1.344(2) – 1.411(2)	1.337(3) – 1.407(3)
C3=N2	–	1.278(4)	1.287(2)	1.277(5)	1.275(3)	1.273(5) / 1.290(5)	1.288(2)	1.282(7) / 1.299(7)	1.316(2) / 1.315(2)	1.310(3) / 1.317(3)
C2−S1	1.740(2)	1.749(4)	1.746(2)	1.750(4)	1.755(2)	1.730(4) / 1.737(4)	1.740(2)	1.752(5) / 1.737(6)	1.745(2) / 1.734(2)	1.748(2) / 1.758(3)
C3−S1	1.770(2)	1.759(4)	1.7618(2)	1.764(4)	1.768(3)	1.767(4) / 1.743(4)	1.763(2)	1.746(5) / 1.752(6)	1.781(2) / 1.774(2)	1.791(3) / 1.794(2)
C3−X	1.212(2)	1.313(5)	1.313(2)	1.315(5)	1.320(3)	1.332(5) / 1.326(5)	1.729(2)	1.751(6) / 1.744(6)	1.328(2) / 1.323(3)	1.332(3) / 1.321(3)
O1···H1	1.86(2)	1.96(3)	1.99(3)	2.14(5)	2.02(3)	1.99(3) / 2.00(3)	1.98(2)	1.93(4) / 1.94(4)	1.94(2) / 1.99(2)	1.97(1) / 1.94(2)

angle [°]										
N1−C1−N2	118.9 (1)	121.4 (3)	121.1 (2)	120.6 (4)	120.9 (2)	120.8(4) / 121.0 (4)	120.6 (1)	122.0(5) / 121.5 (5)	128.2(1) / 121.9 (1)	121.8(1) / 121.2 (1)
C2−S1−C3	104.6 (1)	101.2 (2)	100.8 (1)	101.0 (2)	100.7 (1)	100.8(2) / 100.3 (2)	101.2 (1)	101.2(3) / 101.5 (3)	101.4(1) / 102.2 (1)	102.0(1) / 102.0 (1)
C3−X − C4−C5	–	–	88.2(2)	79.9(4)	3.5(2)	14.2(3) / 13.5(3)	2.3(1)	87.0(5) / 81.8(5)	82.1(2) / 85.1(2)	108.9(2) / 105.3 (2)

2.3. Crystal structure description

2.3.1. 6-thioxo-1,3,5-thiadiazinane-2,4-dione

1 crystallizes with one independent molecule in the asymmetric unit and four molecules per unit cell ($Z = 4$) (Fig. 2) in the monoclinic space group $P2_1/n$. Additionally, the crystal structure includes one molecule water per formula unit. The molecule forms dimers with two hydrogen bonds H2···O1 and O1···H2. In addition, hydrogen bonds to the water molecule are present, so that each water molecule is connected to three different molecules (Fig. 2). H1 connects to the oxygen atom O3 of the water molecule (H1···O3). O2 and S2 build short contacts to the hydrogen atoms of the water molecule (O2···H3B & S2···H3A).

2.3.2. 6-methoxy-2-thioxo-2,3-dihydro-4H-1,3,5-thiadiazin-4-one

2Me crystallizes with one independent molecule in the asymmetric unit and two molecules per unit cell ($Z = 2$) in the triclinic crystal system with the space group $P\bar{1}$. The molecules forms strands along [001] direction. Each molecule is connected to one additional molecule with two hydrogen bonds (O1···H1/ H1···O1) and to another molecule with short contacts from the oxygen atom O1 to the CH_3 group and vice versa. The strands stack in [100] direction of the crystal (Fig. 2).

2.3.3. 6-ethoxy-2-thioxo-2,3-dihydro-4H-1,3,5-thiadiazin-4-one

2Et crystallizes in the monoclinic space group $P2_1/n$ with four molecules in the unit cell ($Z = 4$). One independent molecule per asymmetric unit (Fig. 4) is connected to other molecules similar to **2Me**. The two hydrogen bonds O1···H1 and H1···O1 are formed with one molecule and a short contact from O1 to the CH_2 unit of the ethyl group of another molecule is present. Strands are built in [100] direction, which stack in [010] direction (Fig. 5).

2.3.4. 6-isopropoxy-2-thioxo-2,3-dihydro-4H-1,3,5-thiadiazin-4-one

2iPR crystallizes in the space group $P2_1/n$ with one independent molecule and four molecules in the unit cell (Fig. 4). The molecule forms isolated dimers via O1···H1 and H1···O1 hydrogen bonds (Fig. 5) which stack in [100] direction.

2.3.5. 6-octyloxy-2-thioxo-2,3-dihydro-4H-1,3,5-thiadiazin-4-one

2nOct crystallizes with one independent molecule (Fig. 4) in the triclinic crystal system with the space group $P\bar{1}$ and two molecules in the unit cell ($Z = 2$). The molecules also forms isolated dimers, which are formed by hydrogens bonds from O1 and H1 to H1 and O1 (O1···H1 & H1···O1), respectively. The dimers stack in [100] direction (Fig. 5). The octyl groups are orientated towards each other, like a surfactant arrangement with polar and non-polar regions.

2.3.6. 6-benzyloxy-2-thioxo-2,3-dihydro-4H-1,3,5-thiadiazin-4-one

2Bz crystallizes in the space group $P2_1/c$. In the asymmetric unit are two independent molecules with eight molecules in the unit cell ($Z = 8$, Fig. 3). The molecules form dimers with their symmetry generated individuums *via* hydrogen bonds (O1A···H1A & H1A···O1A / O1B···H1B & H1B···O1B). In the extended structure the phenyl rings of two molecules A stack above another, while molecule B stacks alternating phenyl group and thiadiazine ring (Fig. 3).

2.3.7. 6-ethylthio-2-thioxo-2,3-dihydro-4H-1,3,5-thiadiazin-4-one

3Et crystallizes in the monoclinic crystal system with the space group $P2_1/c$. In the unit cell are four molecules ($Z = 4$) with one independent molecule (Fig. 4). The molecule forms isolated dimers, which stack in [100] direction (Fig. 5). Dimers are built by hydrogen bonds from O1 to H1 and H1 to O1 (O1···H1 & H1···O1).

2.3.8. 6-phenylthio-2-thioxo-2,3-dihydro-4H-1,3,5-thiadiazin-4-one

3Ph crystallizes in the space group $P\bar{1}$ of the triclinic crystal system with four molecules in the unit cell and two independent molecules in the asymmetric unit (Fig. 4). Isolated dimers are formed *via* hydrogen bonds (O1A···H1B & H1A···O1B). The phenyl rings are tilted out of the plane from the thiadiazine ring by 82° and 99°, respectively. In the crystal structure π-stacking is not observed, but an offset arrangement from the phenyl groups (Fig. 5).

2.3.9. 6-diethylamino-2-thioxo-2,3-dihydro-4H-1,3,5-thiadiazin-4-one

4Et crystallizes in the orthorhombic crystal system with the space group *Pbca*. In the asymmetric unit are two independent molecules (Fig. 4) and the unit cell contains eight molecules ($Z = 8$). The molecules form isolated dimers with two hydrogen bonds from O1A to H1B and H1A to O1B (O1A···H1B & H1A···O1B). One ethyl group of molecule B is disordered with an occupation of 0.553(6).
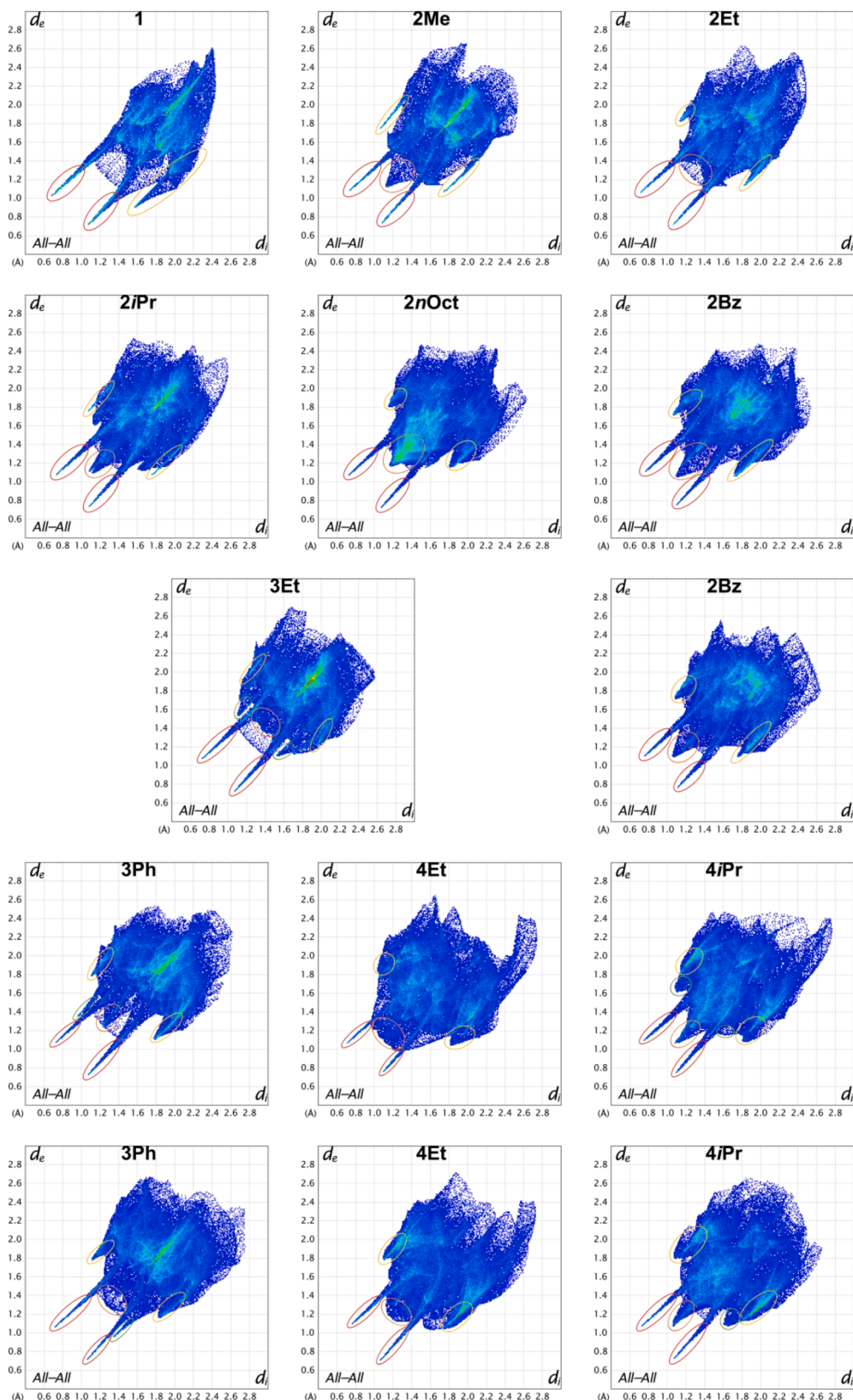
Fig. 6. Fingerprint plots generated from Hirshfeld surface analysis. Short contacts are marked with circles: red: H–H, yellow: H–S, orange: H–H, green: H–N.

2.3.10. 6-diisopropylamino-2-thioxo-2,3-dihydro-4H-1,3,5-thiadiazin-4-one

4iPr crystallizes with four molecules in the unit cell and in the space group $P\bar{1}$. Two independent molecules (Fig. 4) in the asymmetric unit form isolated dimers with their symmetry generated equivalent. One dimer is formed by the hydrogen bonds O1A···H1A and H1A···O1A, and the second dimer by the O1B···H1B and H1B···O1B hydrogen bonds. The dimers stack in [100] direction (Fig. 5).

Relative Contribution of Hirshfeld Surface Interactions
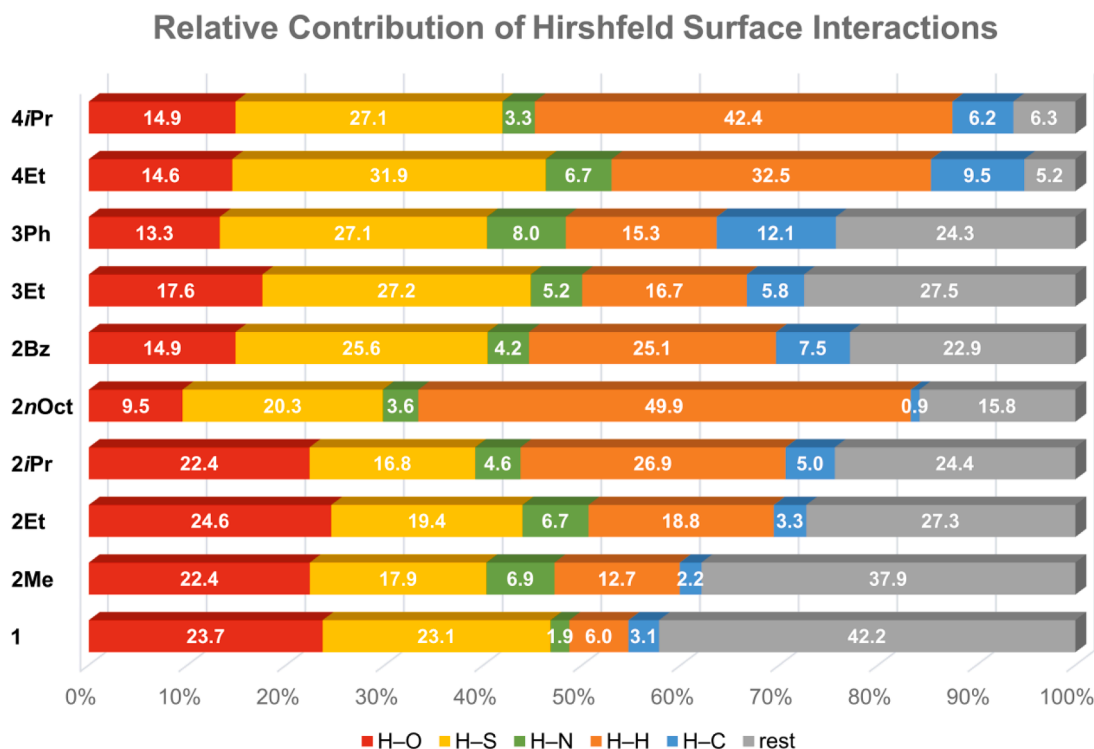
Fig. 7. Relative contribution of interactions to the Hirshfeld surface. A complete list of all relative contributions is in Table S4.

All molecules share the same Etter's graph-set notation[24] $N_1 = [R_2^2(8)]_{O1}$ for the hydrogen bond network, as all of them form isolated dimers. An exception here is **1**, which in addition forms a more complex network through the co-crystallized water molecule. The notation is $N_1 = [R_2^2(8)]_{O1}[C_2^2(8)]_{O3}^{O2}[C_2^2(6)]_{O3}^{S2}$.

2.4. Comprehensive crystal structure discussion

In literature, the solid-state structures of the thiadiazines bearing a halide (chlorine and bromine) substituent in the 6 position, are reported [23]. All molecules exhibit planar six membered rings, which can be derived from cyanuric acid. Only the alkyl or aryl groups are tilted out of the plane, considered from the $C3-X-C4-C5$ torsion angles. In **2Me** the ethyl group and in **3Ph** the phenyl ring are, with 88.2(2)° and 87.0 (5)°, nearly orthogonally aligned to the ring plane. In contrast, **2nOct** and **3Et** keep near planarity with torsion angles of only 3.5(2)° and 2.3 (1)°. In the ring system itself, the hexagon is slightly irregular. The N1–C1–N1 angle is on average 121°, which is nearly ideal for a hexagon, while the C2–S1–C3 angle is sharper with a medium value of 101° This feature is also observed in literature known compounds (N1–C1–N1: ≈120° and C2–S1–C3: ≈100°[23]).

All relevant interatomic distances are compiled in Table 1. The average C1=O1 bond lengths ($d_{(C=O)}$=1.226 Å) are overall longer than reported in the literature (d=1.205 Å[23]). The C2=S2 bond lengths are with a medium value of $d_{(C=S)}$=1.641 Å in between the literature known compounds (Cl: 1.637(2) Å, Br: 1.642(5) Å[23]) and similar within 3σ range. All C–N single bonds lie, with a range from 1.337 Å to 1.411 Å, in the typical margin of a single bond between carbon and nitrogen (d=1.46 Å[25]). In comparison, the C3=N2 double bond concludes to an average of $d_{(C=N)}$=1.293 Å, which is longer than reported in literature (1.261 Å[23]), but still in carbon nitrogen double bond range (d=1.267 Å[25]). Interestingly, a trend of increasing bond lengths from **1** to **2** to **3** is observed. The average for the C2/C3–S1 bonds is at $d_{(C-S)}$=1.756 Å. This is longer than in literature (1.727(5) to 1.742(2) Å[23]), but still shorter as a typical S–N single bond (d=1.78 Å[25]). The bond lengths from C3 to the alkoxy (d=1.320 Å), sulfanyl (d=1.741 Å) or amino

(d=1.326 Å) group (C3–X) are all in range for an C–O (d=1.38 Å[25]), C–S (1.46 Å[25]) or C–N (1.78 Å[25]) single bond.

As described, all compounds form dimers *via* hydrogen bonds (N1–H1···O1) to a neighbouring molecule, which can either be a symmetry generated one or crystallographically independent. The distance is shortest in **1**, but approximately around $d_{(H···O)}$≈2.0 Å for the molecules **2**, **3** and **4**. This is shorter than in the chloride (2.14(3) Å[23]) and bromide (2.063(3 Å[23]) substituted thiadiazines, which are connected to two molecules and thus form strands instead of dimers.

2.5. Comparative hirshfeld surface analysis

For a better insight into the crystal packing, the Hirshfeld surfaces were calculated and the 2D fingerprint plots generated from it. d_i is plotted against d_e to determine the specific contribution of every interaction to the Hirshfeld surface. In the fingerprint plots, dark blue indicates very few interactions, light blue more interactions, with yellow and subsequently red indicating a very high number of interactions. In all fingerprint plots (see Fig. 6) two sharp spikes (red circles) represent H···O hydrogen bonds, which are the shortest surface contacts at a minimum of ≈1.8 Å. This is much shorter than the sum of their van der Waals radii ($\sum r_{vdW}(H + O)$=2.7 Å[26]) as is expected for hydrogen bonding. In between the two spikes, a smaller tip (orange circle) for the shortest H···H interactions is formed. In **1**, **2Et**, **3Et** and **4Et** there is no such tip which is caused in **1** by the absence of an alkyl/aryl group and in **2Et**, **3Et** and **4Et** by the absence of short H···H contacts. In these three compounds, the shortest H···H contacts are around ≈2.8 Å, while in all other molecules the value is at ≈2.4 Å, corresponding to the sum of their van der Walls radii[26]. In **2nOct** the region for short H···H contacts is bright blue, indicating a high number of contacts. This high number stems from the alignments of the octyl groups as indicated above. On the side of the plots a "*wing like*" shape (yellow circle) is present, representing H···S interactions. Interestingly, in **1** the wing is one sided, meaning there are only contacts from sulphur atoms inside the surface to hydrogen atoms outside the surface, but not the other way around. The interaction of the sulphur atom to the hydrogen atom of the
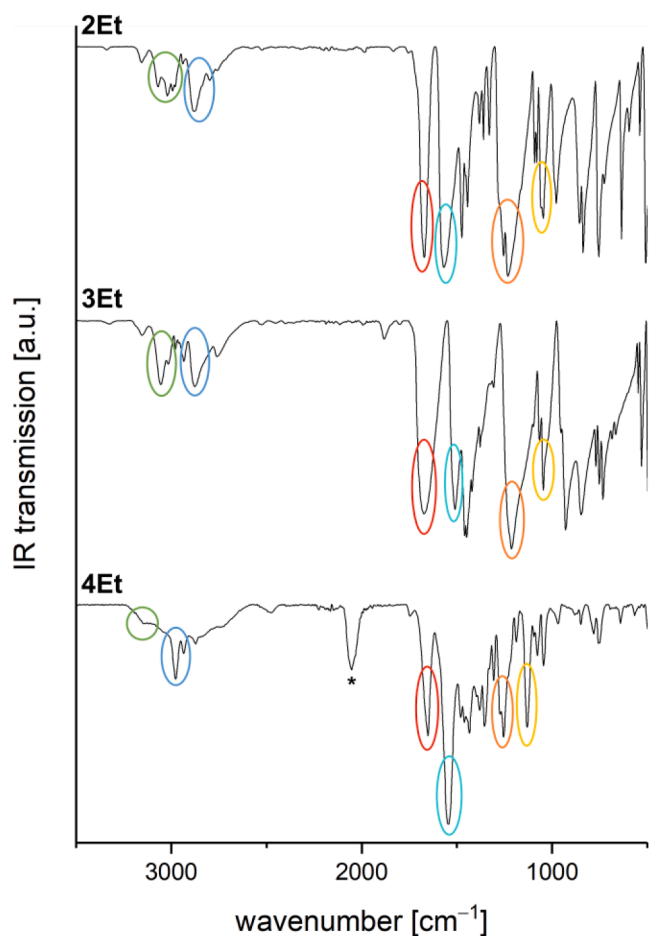
Fig. 8. IR spectra of 2Et, 3Et and 4Et compared to each other. Vibration bands are marked with circles: green N–H, blue C–H, red C=O, turquoise C=N, orange C–N, yellow C=S. Measurements were performed on neat powder samples with an ATR device at room temperature. Asterisk indicates unidentified side product.

co-crystallized water molecule is the reason for this effect, as the water molecule is not included in the calculation of the Hirshfeld surface for the thiadiazine. The shortest contacts are present in **1** with ≈2.6 Å and in the other molecules they get as short as ≈2.9 Å. The sum of the van der Waals radii is $\sum r_{vdW}(H + S)$=3.09 Å [26], leading to the assumption of the presence of attractive polar interactions. Only in **3Et**, **3Ph** and **4iPr** the interactions of H···N lead to the formation of small tips (green circle). In **3Et** and **4iPr** the shortest interactions are around ≈2.7 Å and in **3Ph** even shorter at ≈2.4 Å, which is shorter than the sum of the van der Waals radii ($\sum r_{vdW}(H + N)$=2.86 Å[26]).

Based on **2Et**, **3Et** and **4Et**, the variation in crystal packing from the differently substituted thiadiazine rings is apparent (Fig. 7). **2Et** (50.0%), **3Et** (50.7%) and **4Et** (53.2%) show overall the highest values of polar interactions (H···O, H···S, H···N). The H···O interactions decrease from **2Et** (24.6%) over **3Et** (17.6%) to **4Et** (14.6%). In contrast H···S interactions increase (**2Et**: 19.4%, **3Et**: 27.2%, **4Et**: 31.9%), while H···N interactions keep the balance with 6.7% (**2Et**), 8.0% (**3Et**) and 6.7% (**4Et**). The non-polar interactions (H···H, H···C) are in **2Et** (22.1%) and **3Et** (22.5%) even but doubled in **4Et** (42.0%) compared to them. This is to be expected as in **4Et** two ethyl groups instead of one are contributing to the Hirshfeld surface interactions.

Inside the compound class **2** the influence of the size of the alky group is shown. The number of polar interactions decreases with bigger groups from **2Et** (50.0%) over **2iPr** (43.8%) to **2nOct** (33.4%). The long alkyl chain in **2nOct** also causes a drastically increase of non-polar interactions up to 50.8%, meaning that mostly van der Waals forces are

responsible for molecule packing. Macroscopically this is evident by the crystals of **2nOct** being very soft, as detected during crystal mounting. A little outstanding is **2Bz** with its unique molecule stacking. Polar interactions sum up to 44.7% and non-polar interactions to 32.6%. H···C interactions are only at 7.5%, which point out the missing π-stacking. In **3Ph** π-stacking is not observed either, but the phenyl rings are arranged offset from each other, which leads to at least 12.1% of H···C interactions.

In all molecules a high value of other interactions, not shown in Fig. 7, are also present. The value is highest in **1** and decreases in all following molecules. The main contributions originate from S···S, S···O and S···C interactions with values from 6% to 10%. A detailed list of all relative contributions to the Hirshfeld surface is in Table S4.

2.6. Vibrational infrared spectroscopy

In the IR spectra characteristic vibrational bands for the functional groups in the compounds can be assigned. In Fig. 8 the spectra of **2Et**, **3Et** and **4Et** are illustrated as representatives of the compound classes. All full spectra can be found in the Supporting Information. Above 3000 cm^{-1} absorption for the N–H stretching vibrations (green circles) are found. In **4Et** those are not clearly resolved. Right next to it are the C–H stretching vibrations (blue circles) from the ethyl groups at 2870 cm^{-1} (**2Et**, **3Et**) and 1976 cm^{-1} (**4Et**). The outer ring double bond stretching vibrations of C=O (red circle) generate strong bands at 1670 cm^{-1} for **2Et** and **3Et** and 1650 cm^{-1} for **4Et**. They are shifted to lower frequencies caused by the hydrogen bonding compared to the halide substituted thiadiazines (1686 cm^{-1}[23]). The other outer ring C=S stretching vibration (yellow circles) for **2Et** and **3Et** are located at 1046 cm^{-1} and at 1130 cm^{-1} for **4Et**. Also, a strong band for the inner ring C=N imine vibration (turquoise circles) is found at 1562 cm^{-1} (**2Et**), 1511 cm^{-1} (**3Et**) and 1545 cm^{-1} (**4Et**). The last strong absorption belongs to the C–N stretching vibrations (orange circles), which are at 1227 cm^{-1} for **2Et**, 1211 cm^{-1} for **3Et** and 1253 cm^{-1} for **4Et**.

3. Conclusion

We present an extensive study of substituted 2,3-dihydro-2-thioxo-4H-1,3,5-thiadiazin-4-ones including synthesis, crystal structure, spectroscopic and Hirshfeld surface analysis. All molecules can be synthesized from carbonyl diisothiocyanate and a nucleophile (**2**: alcohol, **3**: thiol, **4**: amine). Identification via ^{13}CNMR spectroscopy is easily achieved through specific chemical shifts of the thiadiazine ring carbon atoms with ~190 ppm for C=S, ~153 ppm for C=O and C–X in between, the latter depending on the substituent. In our findings, the thiadiazine ring motif is planar in all molecules. This central motif partakes in hydrogen bonding. Two molecules form dimers in the solid state, regardless of the nature of the substituent. These dimers stack in a variety of motifs depending on the alky or aryl rest of the substituted group. This causes unique fingerprint plots calculated from the Hirshfeld surfaces with two spikes and a tip in between them, as well as a "*wing like*" shape, which represent H···O, H···H and H···S short contacts, respectively. Two trends are observed: First a decrease of H···O interactions, alongside an increase of H···S from molecules class **2** to **4** and second an increase of non-polar interactions depending on the increasing size of the side chain. Effects of crystal packing are visible in the IR spectra which complement our study. Here a shift of C=O stretching vibrations to lower frequencies is visible as a sign of these groups participating in the hydrogen bonding.

CRediT authorship contribution statement

Jonathan Pfeiffer: Writing – original draft, Investigation. **Clemens Trost:** Investigation. **Frank Tambornino:** Supervision, Conceptualization.

Declaration of competing interest

The authors declare the following financial interests/personal relationships which may be considered as potential competing interests: Frank Tambornino reports financial support was provided by German Research Foundation. Jonathan Pfeiffer reports financial support was provided by Chemical Industry Fund. If there are other authors, they declare that they have no known competing financial interests or personal relationships that could have appeared to influence the work reported in this paper.

Data availability

All data is presented in the Supporting Information

Supplementary materials

Supplementary material associated with this article can be found, in the online version, at doi:10.1016/j.molstruc.2024.138079.

References

[1] D. Collins, J. Graymore, The action of hydrogen sulphide on certain aromatic amines in the presence of formaldehyde, J. Chem. Soc. (1953) 4089, https://doi.org/10.1039/jr9530004089.

[2] M. Torres, J.C. Vega, Reactions of dichloromethane with thioanions. 2. formation of 5-alkyl-1,3,5-dithiazinanes, 3,5-dialkyl-1,3,5-thiadiazinanes, and 1,3,5-trialkyl-1,3,5-triazinanes by reaction of dichloromethane with sodium sulfide and monoalkylamineS, Phosphorus. Sulfur. Silicon Relat. Elem. 106 (1995) 125–130, https://doi.org/10.1080/10426509508027897.

[3] A. Flores-Parra, S.A. Sánchez-Ruíz, New 1,3,5-heterocyclohexanes: dioxazines, oxadiazines, thiadiazines, oxathiazines and triazines and their amination, transamination and disproportionation reactions, Heterocycles 51 (1999) 2079–2092, https://doi.org/10.3987/COM-99-8583.

[4] J.M. Bakke, J.B. Buhaug, Hydrogen sulfide scavenging by 1,3,5-Triazinanes. Comparison of the Rates of Reaction, Ind. Eng. Chem. Res. 43 (2004) 1962–1965, https://doi.org/10.1021/ie030510c.

[5] V.R. Akhmetova, Z.T. Niatshina, G.R. Khabibullina, I.S. Bushmarinov, A.O. Borisova, Z.A. Starikova, L.F. Korzhova, R.V. Kunakova, Synthesis, crystal structure, and interconversions of new N-aryl-1,3,5-dithiazinanes, 1,3,5-thiadiazinanes, and 1,5-dithia-3,7-diazacyclooctanes, Russ. Chem. Bull. 59 (2010) 1002–1009, https://doi.org/10.1007/s11172-010-0196-y.

[6] G.R. Khabibullina, D.K. Yapparova, A.G. Ibragimov, V.R. Akhmetova, Sodium sulfide in the synthesis of N-Alkyl-1,3,5-dithiazinanes and 1,3,5-Thiadiazinanes, Russ. J. Gen. Chem. 91 (2021) 1453–1458, https://doi.org/10.1134/S1070363221080053.

[7] A.R. Katritzky, A.V. Vakulenko, Y.J. Xu, P.J. Steel, Synthesis of 3,4-Dihydro-2H-1,3,5-thiadiazines, J. Org. Chem. 67 (2002) 4960–4962, https://doi.org/10.1021/jo020033s.

[8] V.R. Akhmetova, R.R. Khairullina, I.S. Bushmarinov, T.V. Tyumkina, V.M. Yanybin, Multicomponent reactions of urea and its derivatives with CH2O and H2S in the synthesis of 1,3,5-thiadiazinane-4-(thi)ones and macroheterocycles, Arkivoc 2011 (2011) 149–162, https://doi.org/10.3998/ark.5550190.0012.811.

[9] R.R. Khairullina, T.V. Tyumkina, S. Meshcheryakova, G. Ibragimov, Catalytic cyclothiomethylation of diamides and dihydrazides of (Thio)carbonic acid using bis(dimethylamino)methane, H2S, and Na2S·9H2O, Russ. J. Org. Chem. 56 (2020) 276–280, https://doi.org/10.1134/S1070428020020165.

[10] M.C. Seidel, F.E. Boettner, The preparation of 3,5-disubstituted tetrahydro-4H-1,3,5-oxadiazine-4-thiones, tetrahydro-4H-1,3,5-thiadiazin-4-ones, and tetrahydro-4H-1,3,5-thiadiazine-4-thiones, J. Heterocycl. Chem. 9 (1972) 231–234, https://doi.org/10.1002/JHET.5570090211.

[11] T. Aboul-Fadl, A. El-Shorbagi, New prodrug approach for amino acids and amino-acid-like drugs, Eur. J. Med. Chem. 31 (1996) 165–169, https://doi.org/10.1016/0223-5234(96)80450-8.

[12] T. Aboul-Fadl, A. El-Shorbagi, New carriers for representative peptides and peptide drugs, Arch. Pharm. (Weinheim). 330 (1997) 327–332, https://doi.org/10.1002/ardp.19973301103.

[13] M.A. Hussein, M. Hashem, Synthesis of new 3-substituted-5-(2-hydroxyethyl)-3,4,5,6-tetrahydro-2H-l, 3,5-thiadiazine-2-thione derivatives with potential antimicrobial activity, Arch. Pharm. (Weinheim). 341 (2008) 370–376, https://doi.org/10.1002/ARDP.200700195.

[14] A.A. Radwan, A. Al-Dhfyan, M.K. Abdel-Hamid, A.A. Al-Badr, T. Aboul-Fadl, 3,5-Disubstituted thiadiazine-2-thiones: new cell-cycle inhibitors, Arch. Pharm. Res. 35 (2012) 35–49, https://doi.org/10.1007/s12272-012-0104-0.

[15] H. Ali, R. Khan, X. Pan, F. Shaheen, A. Jabeen, A. Rauf, M. Shah, U. Rashid, Y.S. Al-Awthan, O.S. Bahattab, M.A. Al-Duais, M.S. Mubarak, Synthesis, characterization, anticancer, anti-inflammatory activities, and docking studies of 3,5-disubstituted thiadiazine-2-thiones, Green Process. Synth. 12 (2023), https://doi.org/10.1515/gps-2022-8136.

[16] R. Bunnenberg, J.C. Jochims, Carbonyldiisothiocyanat, Chem. Ber. 114 (1981) 2075–2086, https://doi.org/10.1002/cber.19811140609.

[17] R. Bunnenberg, J.C. Jochims, H. Härle, Zur darstellung und chlorierung von carbonyl-diisothiocyanat, Chem. Ber. 115 (1982) 3587–3596, https://doi.org/10.1002/cber.19821151111.

[18] A. Xotlanihua-Flores, P. Montes-Tolentino, S.A. Sánchez-Ruíz, G.V. Suárez-Moreno, J.C. Gálvez-Ruiz, R. Contreras, A. Flores-Parra, New N-[2-chloropropyl]-heterocyclohexanes. NMR long range shielding effects of chlorine substituent. Use of BH3 as freezing conformational agent, J. Mol. Struct. 1106 (2016) 322–330, https://doi.org/10.1016/j.molstruc.2015.10.087.

[19] V.R. Akhmetova, G.R. Nadyrgulova, Z.T. Niatshina, R.R. Khairullina, Z.A. Starikova, A.O. Borisova, M. Yu. Antipin, R.V. Kunakova, U.M. Dzhemilev, cyclothiomethylation of functional substituted anilines by CH2O and H2S, Heterocycles 78 (2009) 45, https://doi.org/10.3987/COM-08-11432.

[20] M. Arfan, M.N. Tahir, M.I.A. Shah, M.S. Iqbal, 3-Benzyl-5-butyl-1,3,5-thiadiazinane-2-thione, Acta Crystallogr. Sect. E Struct. Reports Online 65 (2009) o468, https://doi.org/10.1107/S1600536809003882. –o468.

[21] R. Pérez, M. Suárez, E. Ochoa, H. Rodríguez, N. Martín, C. Seoane, H. Novoa, N. Blaton, O.M. Peeters, C. De Ranter, A joint theoretical and experimental structural study of 5-carboxyethyl-3-(2′-furfurylmethyl) tetrahydro-2H-1,3,5-thiadiazine-2-thione, Tetrahedron 57 (2001) 7361–7367, https://doi.org/10.1016/S0040-4020(01)00696-2.

[22] M. Arfan, M.N. Tahir, M.I.A. Shah, R. Khan, M.S. Iqbal, 2-[6-Thioxo-5-(2,4,6-trimethylphenyl)-1,3,5-thiadiazinan-3-yl]acetic acid, Acta Crystallogr. Sect. E Struct. Reports Online 65 (2009) o902, https://doi.org/10.1107/S1600536809011027. –o902.

[23] J. Pfeiffer, H. Günther, L. Völlinger, D. Botros, B. Scheibe, M. Möbs, F. Kraus, F. Weigend, F. Tambornino, Double addition vs . ring closure: systematic reactivity study of CO(NCO)2 and CO(NCS)2 towards hydrogen halides, Chem. – A Eur. J. 29 (2023) e202203983, https://doi.org/10.1002/chem.202203983.

[24] M.C. Etter, J.C. MacDonald, J. Bernstein, Graph-set analysis of hydrogen-bond patterns in organic crystals, Acta Crystallogr. Sect. B Struct. Sci. 46 (1990) 256–262, https://doi.org/10.1107/S0108768189012929.

[25] P. Pyykkö, M. Atsumi, Molecular double-bond covalent radii for elements Li–E112, Chem. – A Eur. J. 15 (2009) 12770–12779, https://doi.org/10.1002/chem.200901472.

[26] S. Alvarez, A cartography of the van der Waals territories, Dalt. Trans. 42 (2013) 8617–8636, https://doi.org/10.1039/c3dt50599e.

3.7 Thiocarbonyl pseudohalides – the curious case of thiocarbonyl dithiocyanate

Jonathan Pfeiffer, Hennes Günther, Patrick Fuzon, Florian Weigend, and Frank Tambornino

submitted
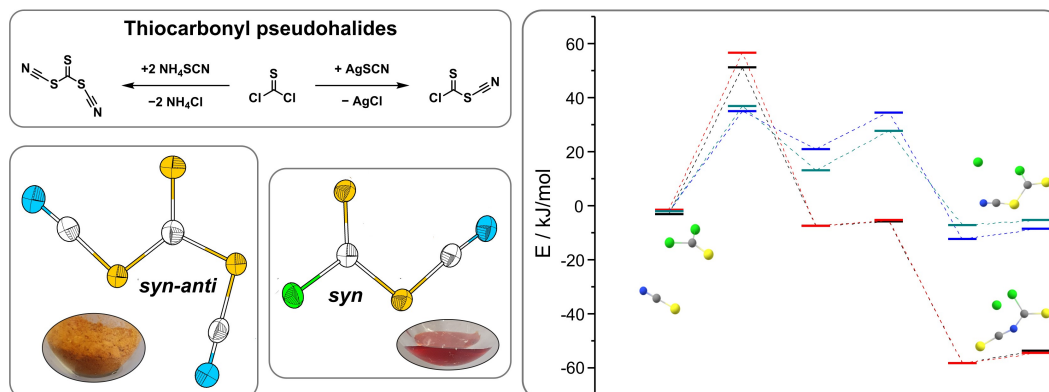
Abstract: *Thiocarbonyl dithiocyanate (**1**) and chlorothiocarbonyl thiocyanate (**2**) were synthesized from thiophosgene and ammonium or silver thiocyanate, respectivley. The crystal structures show a syn-anti (**1**) and syn (**2**) conformation, which are confirmed by vibrational spectroscopy and DFT calculations. Further calculations explain the isolation of the kintetic reaction products by a lower transition state. Reaction of **1** with ethanole gave a dithiobiuret derivative (**3**), which can be used for the complexation of nickel (**4**).*

Zusammenfassung:

Thiocarbonyldithiocyanat (**1**) und Chlorthiocarbonylthiocyanat (**2**) wurden aus je Thiophosgen und Ammonium- oder Silberthiocyanat synthetisiert. Die Kristallstrukturen zeigen *syn-anti* (**1**) und *syn* (**2**) Konformation, welche durch Schwingungsspektroskopie und DFT Rechnungen bestätigt werden. Weitere Berechnungen erklären die Isolation der kinetischen Reaktionsprodukte über einen geringeren Übergangszustand. Die Reaktion von **1** mit Ethanol erzeugte ein Dithiobiuret-Derivat (**3**), welches zur Komplexierung von Nickel (**4**) verwendet werden kann.

Beiträge der Autoren:

Fuzon und Günther führten ein Forschungspraktikum unter meiner Anleitung und Betreuung durch, welche in der Synthese von **1** und **4** endeten. Die Synthese von **1** wurde von mir optimiert, sowie Verbindung **2** dargestellt. SC-XRD Analytik wurde von Tambornino durchgeführt. Strukturlösung und -verfeinerung erfolgte durch mich unterstützt durch Tambornino. PXRD wurde von mir durchgeführt und Rietveld Verfeinerung von Tambornino. Jegliche Analytik der Verbindungen **1**, **2** und **3** wurden von mir und von Verbindung **4** von Günther durchgeführt. Die Auswertung der Analytik erfolgte durch mich. DFT Rechnungen mit Crystal17 wurden von mir und mit Turbomole von Weigend durchgeführt. Das Manuskript und die *Supporting Information* wurden von mir in Hauptarbeit, Tambornino und Weigend erstellt.

Thiocarbonyl pseudohalides − the curious case of thiocarbonyl dithiocyanate

Jonathan Pfeiffer, Hennes Günther, Patrik Fuzon, Florian Weigend, and Frank Tambornino*

Department of Chemistry, Philipps University Marburg,

E-mail: Frank.Tambornino@chemie.uni-marburg.de

Abstract

Thiocarbonyl dithiocyanate (**1**) and chlorothiocarbonyl thiocyanate (**2**) were synthesized from thiophosgene and ammonium or silver thiocyanate, respectivley. Their crystal structures show *syn-anti* (**1**) and *syn* (**2**) conformations, which were confirmed in the bulk phases by powder X-ray diffraction, vibrational spectroscopy and DFT calculations. Further calculations explain the isolation of the kintetic reaction products by a lower transition stateas opposed to the thermodynamic reaction products. Reaction of **1** with ethanol gave a dithiobiuret derivative (**3**). In a proof-of-principle study we show that it in turn can be used as ligand for the complexation of Ni^{2+} (**4**).

Introduction

Phosgene is among the most widely known chemicals, even amidst non-chemists. In chemical industry it is the principal C=O building block and can be seen as the parental compound towards many small molecules. Carbonyl pseudohalides are derived from phosgene by formal substitution of the chlorine atoms for pseudohalogen groups. If only one chlorine atom is

1

exchanged chlorocarbonyl pseudohalides result. In a more general sense those are part of the family of halogenocarbonyl pseudohalides, of which quite a few compounds are known.[1–6] In contrast, only a handfull of carbonyl dipseudohalides are described in literature. Those are carbonyl dicyanide,[7,8] carbonyl diazide,[9] carbonyl diisocyanate[10,11] and carbonyl diisothiocyanate.[12,13]

Carbonyl diisocyanate and -diisothiocyanat can conveniently be synthesized from phosgene or related compounds (diphosgene, triphosgene, fluorophosgene) by a variety of synthetic protocols. All carbonyl pseudohalides are highly moisture and temperature sensitive, and additionally, in the case of carbonyl diazide, explosive. Nonetheless, crystal structures of carbonyl diazide,[8] carbonyl diisocyanate[11] and carbonyl diisothiocyanate[13] were determined (see Figure 1), alongside their spectroscopic signatures and quantum chemical calculations.
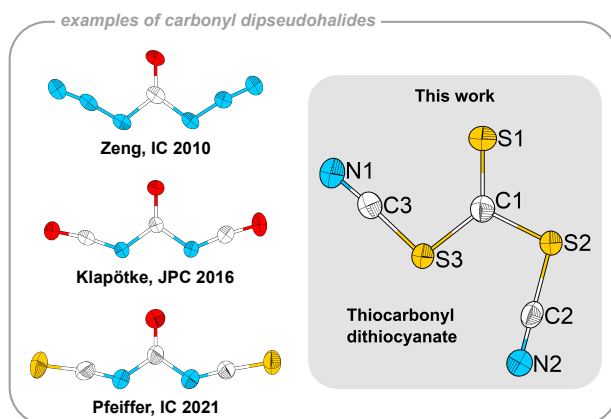
Figure 1: Molecular structures of literature known carbonyl diazide, diisocyanate and diisothiocyanate in comparison with thiocarbonyl dithiocyanate **1** presented in this work. Thermal displacement ellipsoids are drawn with 75 % probability level. Color code: nitrogen blue, oxygen red, carbon white, sulfur yellow.

All three can theoretically exist in three different rotational conformers: *syn-syn*, *syn-anti* and *anti-anti* (always interpreted as the position of the cumulene with respect to the carbonyl group). For carbonyl diazide[8,14] and carbonyl diisocyanate[11,15] a conformer equilibrium in the gas and liquid phase between the preferred *syn-syn* and less preferred *syn-anti* conformer is present (62:38 and 66(3):34(3), respectively), while no trace of a *anti-anti* positioning is

found. This is corroborated by quantum chemical calculations which predict the *anti-anti* arrangement to be unstable. In the solid state, exclusively the energetically preferred *syn-syn* conformer is observed.[8,11] However, the spectroscopic investigation of the less stable *syn-anti* conformer of carbonyl diisothiocyanate was performed in an argon matrix. The isolation of this conformer was based on the decarbonylation of oxalyl diisothiocyanat, where the isothiocyanate moieties were pre-aligned in the desired conformation.[16] Of the halogenocarbonyl (iso)thiocyanates, fluoro and chlorocarbonyl (iso)thiocyanate are known.[17,18] All four compounds exhibit an equilibrium in the gas phase between *syn* and *anti* conformation with the *syn* arrangement being preferred. The solid state structures reveal this preference as well (see Figure 3). In addition, an isomerization from the carbonyl thiocyanate to the thermodynamically more stable isothiocyanate is observed.

An obvious gap within this line of chemistry is the synthesis and characterization of thiocarbonyl pseudohalide compounds. Hitherto, only the synthesis of thiocarbonyl dithiocyanate has been reported, togehter with relatively little analytical data.[19]

In context of our investigation of carbonyl pseudohalides, we revisited the reaction between thiophosgene and ammonium thiocyanate. The sole product of this reaction is the kinetic product thiocarbonyl dithiocyanate (as opposed to the thermodynamically more stable thiocarbonyl diisothiocyanate, *vide infra* for quantum chemical calculations) and we comprehensively investigated its structure, spectroscopic signatures, properties, and reactivity. Surprisingly, we found this compound to be exhibit the *syn-anti* arrangement as preferred conformer in the solid state. This stable conformer and the fact that the pseudohalide is bound to the thiocarbonyl group *via* its S atom made us curious. Reaction path calculations show that thiocarbonyl dithiocyanate is indeed the kinetic reaction product. During our quest towards the thermodynamic product, thiocarbonyl diisothiocanate, we synthesized chlorothiocarbonyl thiocyanate as the first member of a halogenothiocarbonyl pseudohalide and discuss its structure and spectroscopic signatures. Furthermore, we explored the reactiv-

3

ity of thiocarbonyl dithiocyanate towards ethanol as stereotypical nucleophile which formed an unprecedented thiobiuret congener (thioimidodicarbonic-O,O-diethyl ester). In a proof of principle reaction we show that it in turn can act as ligand towards nickel as a representative of group 10 elements.

Results and discussion

Synthesis and crystal structure of thiocarbonyl dithiocyanate

Our first attempts to synthesize thiocarbonyl diisothiocyanate, $CS(NCS)_2$, started from thiophosgene and ammonium thiocyanate (see Scheme 1), following a procedure akin to the synthesis of the parent compound carbonyl diisothiocyanate.[13]
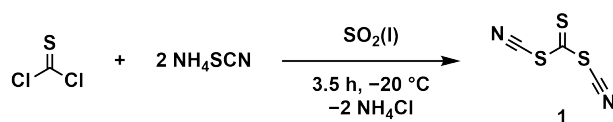
Scheme 1: Synthesis of thiocarbonyl dithiocyanate **1**.

Ammonium chloride was identified as side product of the reaction by powder X-ray diffraction. The ^{13}C-NMR spectrum of the reaction mixture showed two signals at 188.6 ppm and 105.5 ppm, which is quite dissimilar to carbonyl diisothiocyanate (151.0 and 140.2 ppm). Whereas a significant shift of the signal for the C=S-moitey is expected (substitution of O for S), only a small difference for the NCS group would be sensible. However, a difference of 45 ppm indicates a substantial change in chemical surrounding. Literature research revealed that instead of our desired product, thiocarbonyl dithiocyanate (**1**) was obtained.[19] For **1** the chemical shift of C=S is at 188.6 ppm, which is shifted low field compared to thiophosgene (169.7 ppm[20]) due to the thioccyanate substitution. The signal for the thiocyanate carbon atom (105.5 ppm) is similar to the shift of related compounds CO(SCN)F and CO(SCN)Cl.[17,18] With this knowledge in hand we were able to modify and simplify the liter-

ature known synthesis[19] and increase the yield up to 87 %. Subsequently, the procedure got safer and more facile through the substitution of extraction with boiling tetrachloromethane with dichloromethane (see Supporting Information). **1** is a temperature sensitive orange solid, which decomposes above $-20\,°C$ to give pararhodane $(SCN)_x$.

Single crystals of **1** suitable for X-ray diffraction were grown at $-78\,°C$ from a saturated solution in dichloro methane. **1** crystallizes in the space group $P2_1/n$ [$a = 5.9384(2)\,Å$, $b = 5.7917(2)\,Å$, $c = 17.6562(6)\,Å$, $\beta = 97.103(3)°$] with one independent molecule in the asymmetric unit and four molecules per unit cell ($Z=4$). Interestingly, one $-SCN$ group is in *syn* position to C=S and one is *anti* to it, leading to the overall *syn-anti* conformer (see Figure 1). This is different to the related compounds carbonyl diisocyanate, carbonyl diisothiocyanate and carbonyl diazide, which crystallize in the *syn-syn* conformer.[8,11,13] This is also the crystal structure of the bulk solid phase, as has been proven by powder X-ray diffraction and subsequent Rietveld analysis, see Figure 2.
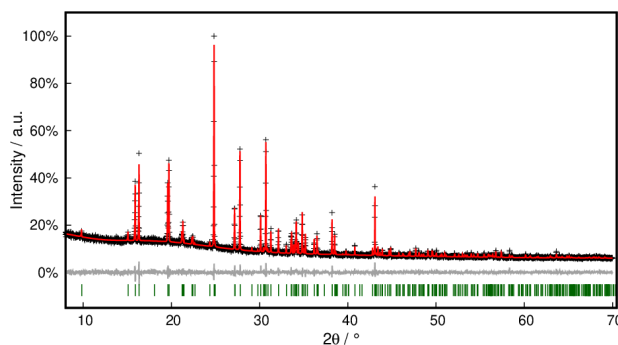
Figure 2: Rietveld refinement of thiocarbonyl dithiocyanate. Black crosses display measured data, the red line represents the refined model, green bars indicate Bragg positions, and the grey line displays the difference plot.

Synthesis and crystal structure of thiocarbonyl chloro thiocyanate

In an endeavor to synthesize thiocarbonyl diisothiocyanate, many different strategies were employed, e.g., synthesis from thiophosgene and sodium thiocyanate, or isomerization of **1** with UV light. Details for all attempted but ultimately unsuccessful syntheses can be found

in the Supporting Information.

As sulfur exhibits a pronounced argentophilicity, we used Ag[SCN] as starting material, envisaging that through the encumbering of the S-terminus of [SCN]$^-$, the N-terminus would act as the nucleophile. ^{13}C-NMR spectra of the crude reaction mixture showed three signals. Resonances at 178.7 ppm and 107.1 ppm were attributed to two carbon atoms of chlorothiocarbonyl thiocyanate, CS(SCN)Cl (**2**), with the resonance at 170.5 ppm being indicative of remaining thiophosgene. Synthesis optimization (see Scheme 2) and purification of **2** through repeated trap-to-trap condensation cycles yielded a deep red oil in 23 % yield. Akin to **1**, the compound is temperature sensitive and decomposes above $-20\,^\circ$C to give pararhodane.
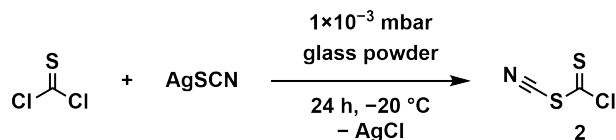
Scheme 2: Synthesis of chlorothiocarbonyl thiocyanate **2**.

As **2** is a liquid, it was crystallized in a capillary directly on the goniometer of the diffractometer. It crystallizes with eight molecules per unit cell (Z=8) in $P2_1/c$ [$a = 6.3005(2)\,$Å, $b = 22.0171(5)\,$Å, $c = 7.4131(2)\,$Å, $\beta = 104.256(2)^\circ$]. Two crystallographically independent molecules are in the asymmetric unit, see Figure 3. Here, the $-$SCN group is in *syn* position to C=S, as is also observed for CO(SCN)F and CO(SCN)Cl.[17,18]

Interatomic distances in **1**, **2**, are compiled in Table 1, together with the structurally related molecules CSCl$_2$, CO(SCN)Cl and the anion in K$_2$CS$_3$, CS$_3{}^{2-}$. The C=S bond lengths are 1.618(3) Å (**1**) and 1.602(3) Å (**2**) indicating double bond character. They are the same in the 3σ range for CSF$_2$ (1.589(3) Å[21]) and CSCl$_2$ (1.604(5) Å[22]) as derived from gas phase electron diffraction and microwave spectroscopy (see Table 1). The C$-$SCN bond lengths are in single bond range with 1.762(3) Å in **1** and 1.766(3) Å in **2**. As is charac-
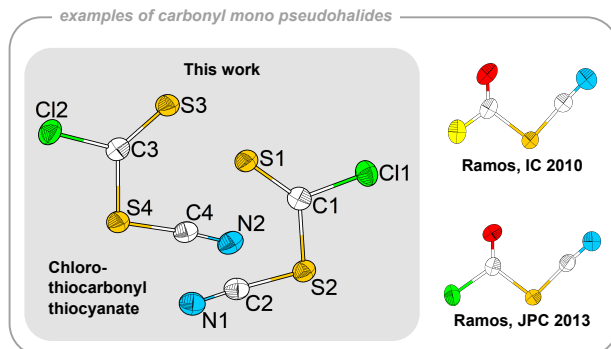
6

Figure 3: Molecular structures of literature known fluoro- and chlorocarbonyl thiocyanate in comparison to chlorothiocarbonyl thiocyanate (**2**) presented in this work. Ellipsoids are drawn with 50 % probability level. Color code: nitrogen blue, oxygen red, carbon white, sulfur yellow, fluorine bright yellow, chlorine green.

teristic for thiocyanate compounds, both **1** and **2** exhibit short bond lengths for $S-CN$ [17,18] with approximately 1.70 Å, indicating some double bond character, while the $C\equiv N$ bonds ($\approx$1.14 Å in **1** and $\approx$1.15 Å in **2**) are in typical triple bond range. In **2**, the $C-Cl$ distances of 1.742(2) Å and 1.738(2) Å are similar to those in $CSCl_2$ (1.730(3) Å [22]) and $CO(SCN)Cl$ (1.746(1) Å [18]). From Hirshfeld surface analysis short intermolecular contacts are detected (see Supporting Informations for more details). In **1**, N···S contacts from N1···S2 (3.028 Å) and N2···S3 (3.149 Å) are shorter than their combined van der Waals radii (3.35 Å [23]). In addition, short contacts between nitrogen and carbon from N1···C2, N2···C2 and N2···C3 (3.059 Å to 3.197 Å) are also shorter than the sum of their van der Waals radii ($d_{\Sigma(vdW)} =$ 3.25 Å [23]). The packing situation is similar in **2**. Here the distances of N2···S2 (3.096 Å) and N1···S4 (3.142 Å) are shorter than their combined van der Waals radii. Additionally, chlorine and sulfur atoms (S1···Cl1: 3.412 Å and S3···Cl2: 3.425 Å) exhibit weak short contacts ($d_{\Sigma(vdW)} = 3.55$ Å [23]).

Table 1: Comparison of bond lengths in **1** and **2** to thiophosgene,[22] chlorocarbonyl thiocyanate[18] and trithiocarbonate.[24]

bond	**1** [Å]	**2** [Å]	CSCl$_2$ [Å][a]	CO(SCN)Cl [Å]	CS$_3{}^{2-}$ [Å][b]
C=S	1.618(3)	1.602(3) / 1.602(3)	1.604(5)	–	1.713(1)–1.717(2)
C–SCN	1.762(3) / 1.762(3)	1.765(3) / 1.766(3)	–	1.781(1)	1.726(3)–1.728(3)
S–CN	1.705(3) / 1.696(3)	1.704(3) / 1.700(3)	–	1.697(1)	–
SC≡N	1.145(4) / 1.144(4)	1.147(4) / 1.150(5)	–	1.146(2)	–
C–Cl	–	1.742(2) / 1.738(2)	1.730(3)	1.746(1)	–

[a] from gas-phase electron diffraction. [b] from K$_2$CS$_3$.

Vibrational spectroscopy

For both **1** and **2**, vibrational spectra were recorded. For Raman spectroscopy the samples were cooled to avoid decomposition and to measure the spectrum of **2** in the solid state. Additionally, solid state spectra for both compounds were calculated at DFT level with the PBE0 functional with the Crystal17 code.[25] A detailed band assignment can be found in the Supporting Information (Tables S8 and S10).

In the Raman spectrum of **1** (see Figure 4a), two bands of the ν_s(C≡N) stretching modes are detected: $2152\,\mathrm{cm}^{-1}$ for the SCN group in *syn* position and $2166\,\mathrm{cm}^{-1}$ for the SCN group in *anti* position.

This clear detection of both modes further supports the conclusion, that the *syn-anti* conformer is the sole species in the sample. The ν_s(C=S) stretching mode of the thiocarbonyl group is located at $1080\,\mathrm{cm}^{-1}$. Deformation bending of the core S–C–S unit is found at $832\,\mathrm{cm}^{-1}$. A scissoring deformation mode δ(S–C≡N) of the *syn* SCN group is found at $495\,\mathrm{cm}^{-1}$. A combination of whole molecule rocking, δ(S–C≡N) twisting (*anti*) and δ(S–C≡N) twisting (*syn*) is found at $384\,\mathrm{cm}^{-1}$. Two bands for a bending vibration for both SC–SCN parts can be detected at $264\,\mathrm{cm}^{-1}$ and $244\,\mathrm{cm}^{-1}$, respectively. At low wavenumbers of $155\,\mathrm{cm}^{-1}$, the whole molecule shows a combined bending and rocking mode.
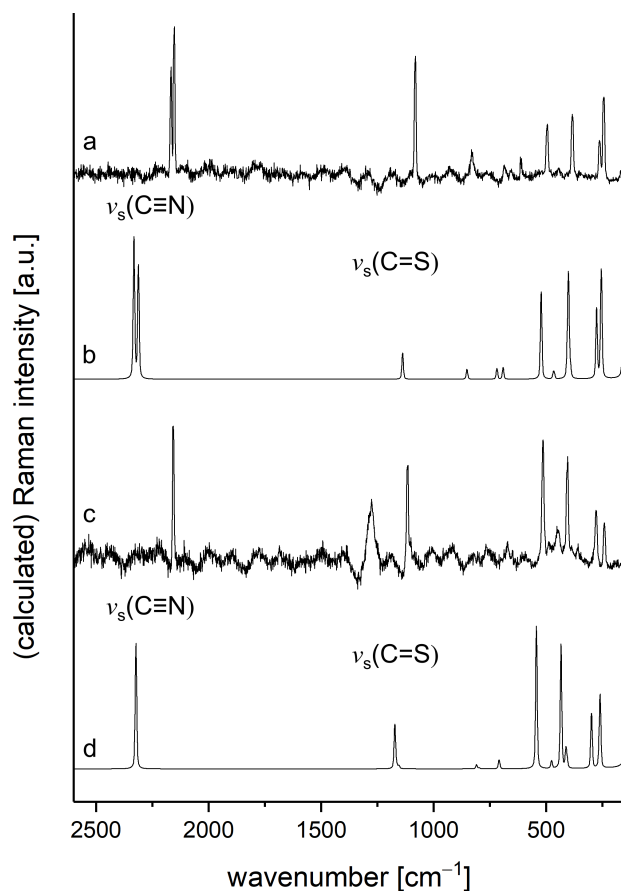
Figure 4: Comparison of the measured (underground corrected) and calculated Raman spectra of **1** (a, b) and **2** (c, d). Spectra were measured with a 633 nm Laser at $-25\,°C$ for **1** and $-75\,°C$ for **2**. For a full assignment of bands and the uncorrected spectra see SI.

Vibrational mode assignments for the Raman spectrum of **2** (see Figure 4c), measured at $-75\,°C$, are similar to **1**. At $2158\,\mathrm{cm^{-1}}$ the band for the only occurring $\nu_s(C\equiv N)$ stretching vibration, located *syn* to the $C=S$ group, is found. The stretching vibration for the thiocarbonyl group $\nu_s(C=S)$ is at $1115\,\mathrm{cm^{-1}}$, which is at slightly higher wavenumbers as for **1**. Scissoring vibration modes of the SCN group are found at $513\,\mathrm{cm^{-1}}$. The core $S-C-Cl$ unit exhibits a wagging vibration mode at $448\,\mathrm{cm^{-1}}$. At $404\,\mathrm{cm^{-1}}$ $\delta(S-C\equiv N)$ bending and at $277\,\mathrm{cm^{-1}}$ whole molecule bending is observed. The $SC-SCN$ unit shows a rocking vibration at $240\,\mathrm{cm^{-1}}$. A distictive $C-Cl$ vibration mode is not found or supported by calculations.

Measurement and assignment of the IR spectra is less straightforward. As the spectra

9

were measured at room temperature, it is likely that most bands stem from already de-composed products. Bands with highest intensity are at $1087\,\mathrm{cm}^{-3}$ and $827\,\mathrm{cm}^{-3}$ for **1** and $1124\,\mathrm{cm}^{-3}$ and $748\,\mathrm{cm}^{-3}$ for **2**, and correspond to $\mathrm{C{=}S}$ and $\mathrm{S{-}C{-}S}$ in plane rocking modes. The full spectra and corresponding assignments can be found in the Supporting Information (Figure S9, Tables S7 and S9).

Thermodynamic stability and reaction path analysis

For investigating the thermodynamic stability, we calculated[26] the energies of all isomers of **1** with $-\mathrm{SCN}$ and $-\mathrm{NCS}$ connection, in the three configurations *syn-syn*, *syn-anti*, *anti-anti* (*ss*, *sa*, *aa*) and analogous compounds in which the sulfur atom (E') that binds directly to the central carbon atom, as well as the other two sulfur atoms (E) of the pseudohalide group, are exchanged with oxygen, see Figure 5. The PBE0 functional[25] was employed with def2-TZVP bases.[27] Further, the conductor-like screening model (COSMO) was used in a very recent implementation[28] with infinite dielectric constant. Further details can be found in the Supporting Information.

Energies relative to the most stable isomer (electronic energies plus thermal contributions for the free enthalpy at 300 K according to the harmonic-oscillator-rigid-rotor model, separate listing in Table S11) reveal the following trends. Regardless of whether E or E' is S or O, the thermodynamic stability is primarily determined by the position of E. The occupation of the two terminal positions by E ($-\mathrm{NCE}$) is favourable over N ($-\mathrm{ECN}$) occupying them by $\approx100\,\mathrm{kJ\,mol}^{-1}$ (E=S) or $\approx300\,\mathrm{kJ\,mol}^{-1}$ (E=O); in particular, **1** is $\approx100\,\mathrm{kJ\,mol}^{-1}$ higher in energy than the global minimum structure. The isomers with one terminal E and one terminal N are energetically in-between. The choice of E' as O or S has no major influence on the energies. The energy differences between *ss*, *sa* and *aa* are comparably small, $10\,\mathrm{kJ\,mol}^{-1}$ to $20\,\mathrm{kJ\,mol}^{-1}$, with *aa* always being highest in energy. We further note: The energetic sequences at MP2 level are the same, but energy differences are smaller by a factor of 1.7,
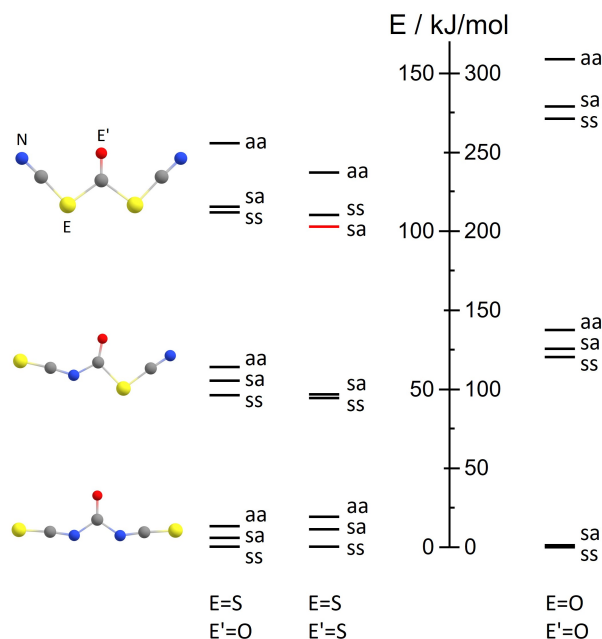
as exemplarily investigated for E=E'=S.

Figure 5: Energies [kJ mol^{-1}] relative to the corresponding most stable isomers for the title compound and related compounds. *aa*, *sa* and *ss* denote the configurations (*anti-anti*, *syn-anti*, *syn-syn*), the three *ss*-isomers for E'=O, E=S are graphically shown. The bar representing the energy of compound **1** is drawn in red.

Without COSMO, the differences for different elements occupying the terminal positions become larger by ≈10 %. The above findings also apply when one of the NCS groups is replaced with Cl, yielding, e.g., compound **2**. The two isomers with S in the terminal position (–NCS) are the most stable here, with *anti* (*a*) and *syn* (*s*) being almost degenerate, while the two isomers with N in the terminal position (–SCN, compound **2**) are about $50\,\mathrm{kJ\,mol^{-1}}$ higher. The observation that E=C=N–R (two double bonds) is much more stable than N≡C–E–R (one triple and one single bond) is not too surprising: N–R, like E, is able to form a double bond with C, so the electronic situation of E=C=N–R is quite similar to that of highly stable CO_2.

Obviously, both **1** and **2** are clearly disadvantaged thermodynamically, so that their existence is more likely to be due to kinetic reasons. It is therefore helpful to examine the energy

11

profiles for the subsequent exchange of the two Cl^- in $CSCl_2$ with $(SCN)^-$. Calculated[29] energy profiles (including thermal contributions for T=300 K) for the first step are shown in Figure 6 (corresponding numbers are listed in Table S12).
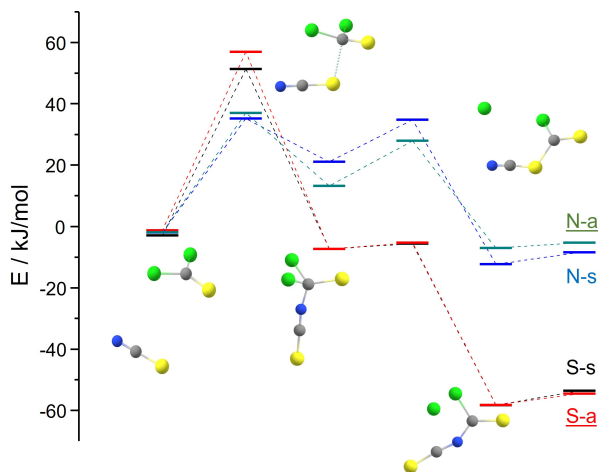
Figure 6: Energy profiles for exchanging one Cl^- in $CSCl_2$ with $(SCN)^-$ for different isomers of the target system. The states on the left are minima with slightly ($\approx 2\,\mathrm{kJ\,mol^{-1}}$) lower energies than the separated systems $CSCl_2$ plus $(SCN)^-$ which define the relative energy=0; analogously, the structures on the right are minima and refer to the penultimate bar at the right-hand side, while the last bar represents the separated systems CS(SCN)Cl and CS(NCS)Cl plus Cl^-. The colours of the bars indicate the following products. Green: N in terminal position, *anti*-configuration (N-a), blue: N in terminal position, *syn*-configuration (N-s), red: S in terminal position, *anti*-configuration (S-a), black: S in terminal position, *syn*-configuration (S-s). The product structures of which an image is shown are underlined.

The reactions to products in which N occupies the terminal position (blue and green bars in Figure 6) are only slightly exothermic, $-9\,\mathrm{kJ\,mol^{-1}}$ for *syn* (s) or $-5\,\mathrm{kJ\,mol^{-1}}$ for *anti* (a) and have a moderate energy barrier of ca. $35\,\mathrm{kJ\,mol^{-1}}$ (similar for s and a) between the initial state and an intermediate state ca. $20\,\mathrm{kJ\,mol^{-1}}$ above the initial state in which both SCN and Cl are bonded to C. Cl^- then leaves the system *via* a barrier of $15\,\mathrm{kJ\,mol^{-1}}$ higher than this intermediate state. The differences between *syn* and *anti* are $2\,\mathrm{kJ\,mol^{-1}}$ for the crucial first barrier, for the subsequent states the differences amount to $\approx 10\,\mathrm{kJ\,mol^{-1}}$. A different picture emerges for the reactions to products with S occupying the terminal position (black and red bars in Figure 6). The energy gain is much larger ($\approx -50\,\mathrm{kJ\,mol^{-1}}$), but also

the decisive first barrier is significantly higher at $50\,\mathrm{kJ\,mol^{-1}}$ for *syn* and 57 for *anti*, than for N in the terminal positions. This indicates a kinetic preference for the latter. As an aside, it is noted that for S in terminal position, Cl^- is released with virtually no barrier.

The energy profiles for the second step, Figure 7 (numbers listed in Table S13), show very similar features, the difference between the barrier heights is even slightly larger than in the first step. Thus, for the entire process, the formation of isomers with S in the terminal position comes with an energy gain by more than $100\,\mathrm{kJ\,mol^{-1}}$, but two barriers of almost $60\,\mathrm{kJ\,mol^{-1}}$ have to be overcome, whereas for N in the terminal position the energy gain is less than $10\,\mathrm{kJ\,mol^{-1}}$, but the two barriers are only slightly more than half as high.
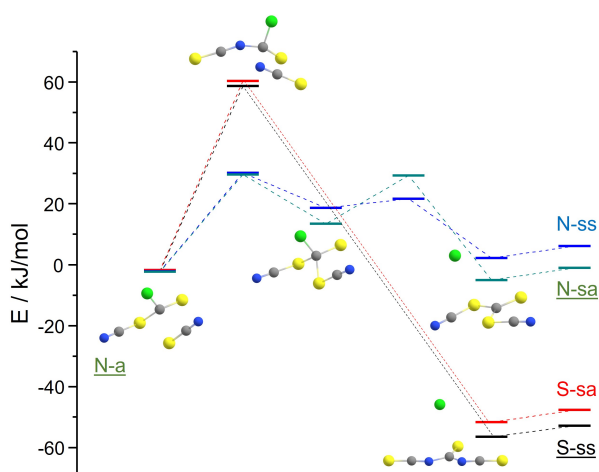
Figure 7: Energy profiles for exchanging Cl^- in CS(SCN)Cl and CS(NCS)Cl with $(SCN)^-$ for different isomers. See also Figure 5. Green: Path from (N-a) to (N-sa), blue: from (N-s) to (N-ss), red: from (S-a) to (S-sa), black: from (S-s) to (S-ss).

Finally, we investigate the barriers for the conversion from *ss* to *sa* to *aa* for E=E'=S with N as well as S in terminal position. For N in terminal position, the conversion is realized by a rotation around the S−C axis, with barriers about $20\,\mathrm{kJ\,mol^{-1}}$ for the conversion from *sa* to *ss* and about $30\,\mathrm{kJ\,mol^{-1}}$ for that from *sa* to *aa*, see Table 2. The higher energies for the transition states, where the rotated −SCN unit is oriented perpendicular to the plane spanned by the residue, are in line with a decreasing bond order[30] for the bond from the

central C atom to the S atom of the rotating group from 1.07 for *ss* to 0.92 for the transition states. This may be rationalized by subtle changes in the p-type lone pair at S. While the planar configurations allow a slight delocalization from this p-orbital perpendicular to the plane to the central C atom, this is not so easily possible for the transition state with the rotated $-$SCN group. In contrast, for S in terminal position, the conversion from *aa* to *sa*, as well as from *sa* to *ss* is realized by only changing the $C-N-C$ angle, i.e. without leaving planarity, and without significant energy barriers ($\approx 5\,\text{kJ mol}^{-1}$), since there is no p-type lone pair at N in this case. Note that the barriers are even slightly lower than the energies for *aa* and *sa* when the thermal corrections are applied.

Table 2: Relative energies [kJ mol^{-1}] for the conversion of $CS(SCN)_2$ from *ss* via *sa* to *ss* configuration for S and N in terminal position. "trans1" denotes the transition state between *ss* and *sa*, trans2 that between *sa* and *aa*. "elec" denotes the electronic energy, "therm" the thermal contribution to the free enthalpy according to the harmonic-oscillator-rigid-rotor model for T=300 K, "sum" the sum of both.

	S terminal			N terminal		
	elec	therm	sum	elec	therm	sum
ss	0.0	0.0	0.0	3.8	0.0	3.8
trans1	6.5	−2.5	4.0	21.9	−2.6	19.3
sa	5.6	−0.2	5.4	0.0	0.0	0.0
trans2	10.2	−2.5	7.7	30.4	−2.6	27.8
aa	9.6	−0.1	9.5	17.1	−0.1	17.0

Further reactivity studies

The reactivities of carbonyl pseudohalides show pronounced differences with variation of the substituent. Whereas carbonyl diisocyanate adds two equivalents of nucleophile, carbonyl diisothiocyanate adds only one equivalent under intramolecular ring formation.[31–34] In both instances, the pseudohalide of the starting material is bound *via* the N-terminus. In contrast, for **1** the [SCN]$^-$-unit is bound *via* the S-terminus, and we were interested in how this affects

the reactivity towards nucleophiles. To study this, we reacted **1** with ethanol according to a previous published procedure (see Scheme 3).[19] The product is thioimidodicarbonic-*O,O*-diethyl ester (**3**) which is formed under loss of one equivalent of thiocyanic acid (HSCN) and subsequent isomerization. If this isomerization proceeds *via* an inter- or intramolecular pathway cannot be distinguished at the moment.
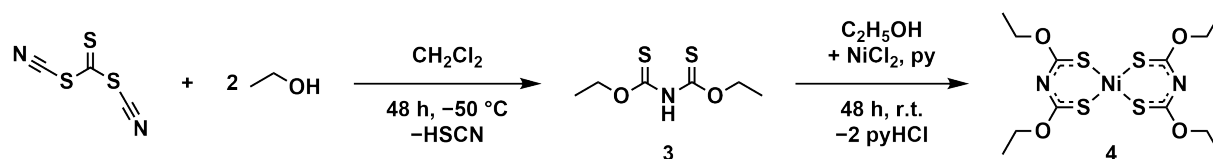
Scheme 3: Reactivity of **1** towards ethanol to form thioimidodicarbonic-*O,O*-diethyl ester **3** and subsequent salt metathesis with nickel chloride to form bis(*O,O*-diethyl-1,3-dithioimidodicarbonato)nickel **4**.

The ^{13}C-NMR spectrum thioimidodicarbonic-*O,O*-diethyl ester (**3**) only shows one low field signal at 186.1 ppm which we assign to the C=S group. ^{13}C-NMR signals of the ethyl groups are at 69.6 ppm and 13.8 ppm. **3** was crystallized by slow evaporation of the solvent from a saturated solution of **3** in *n*-hexane on air. It crystallizes in the monoclinic space group $P2_1/c$ [$a = 7.1491(3)$ Å, $b = 17.1140(6)$ Å, $c = 7.6929(4)$ Å, $\beta = 98.302(4)°$] with four molecules in the unit cell (Z=4) and one independent molecule in the asymmetric unit. Both thiocarbonyl groups are oriented *cis* to the N−H moiety (see Figure 8). Dimers are formed by hydrogen bonds connecting N1−H to S2=C2 (2.589(6) Å), the latter from a symmetry generated pendant. The C1=S1 bond with 1.650(3) Å is shorter than the C2=S2 bond (1.661(3) Å), which is due to the latter taking part in hydrogen bonding. Both bonds are longer than in **1** and **2**, but shorter than in dithiobiuret (1.673(3) Å / 1.702(3) Å[35]). Both C−N bonds (1.388(3) Å / 1.374(3) Å) are in single bond range and comparable to dithiobiuret (1.367(4) Å / 1.386(4) Å).[35]
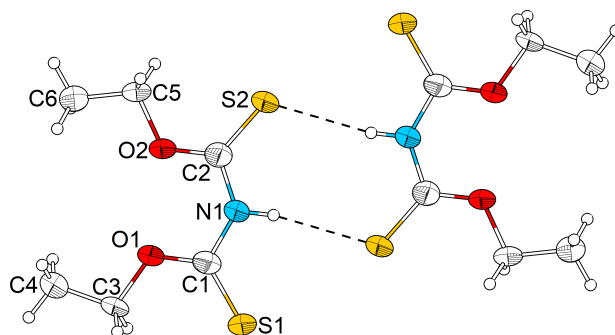
Figure 8: Molecular structure of thioimidodicarbonic-O,O-diethyl ester **3** in the solid state and the formation of dimers *via* intermolecular S···H−N hydrogen bonds. Ellipsoids are drawn with 75 % probability level and hydrogen atoms with arbitrary radius.

The molecular framework of **3** is unique in the way, that it can, thus far, solely be prepared starting from **1**. It exhibits one acidic H-atom which resides at the N−H group and two sulphur atoms which, through rotation about the N1−C1 and N1−C2 bonds would be brought in direct vicinity. Rotation and deprotonation together enable for **3** to act as an anionic bidentate ligand, connecting through both sulphur atoms.

To test this hypothesis, we reacted **3** with nickel chloride and pyridine as non-nucleophilic base. This salt metathesis reaction proceeded in ethanol under precipitation of bis(O,O-diethyl-1,3-dithioimidodicarbonato)nickel (**4**), [Ni((SC(OEt))$_2$N)$_2$], while pyridinium hydrochloride remained in solution. The brown powdery product was recrystallized from acetonitrile, upon which single crystals suitable for X-ray diffraction were obtained. In the ^{13}C-NMR spectrum the chemical shift of the C=S atom is shifted low field compared to **3** to 192.5 ppm. Signals for the ethyl group (69.3 ppm and 14.4 ppm) are not influenced by the metal center.

4 crystallizes in space group $P2_1/c$ [$a = 18.8725(4)$ Å, $b = 7.0820(2)$ Å, $c = 14.8003(3)$ Å, $\beta = 112.929(1)°$] with four molecules in the unit cell (Z=4) and two independent molecules in the asymmetric unit. It is the first crystal structure of this type of complex, since only dithiobiuret derivative complexes are known.[36–41] The nickel atom in **4** is coordinated in a square planar geometry by four sulfur atoms (see Figure 9). The ligand backbone is tilted

out of the coordination plane by 22°. The C=S bond lengths are in the range of 1.706(3) Å to 1.712(3) Å which is in between the values for a carbon sulfur single (1.78 Å [42]) and double (1.61 Å [42]) bond. The same applies to the C−N bonds with 1.319(4) Å to 1.327(4) Å compared to the single (1.46 Å [42]) and double (1.27 Å [42]) bond values. This is indicative for an electron delocalization over the S−C−N−C−S moiety. Ni−S distances are ranging from 2.165(5) Å to 2.169(7) Å, which is comparable to literature known complexes. [36–41]
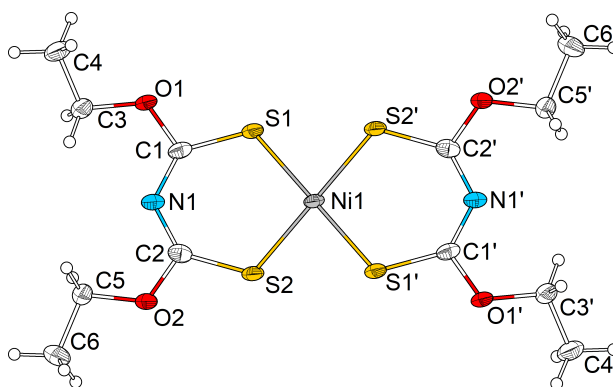
Figure 9: Molecular structure of bis(O,O-diethyl-1,3-dithioimidodicarbonato)nickel **4** of one independent molecule. Ellipsoids are drawn with 75 % probability level and hydrogen atoms with arbitrary radius.

Conclusion

The reaction of thiophosgene with ammonium thiocyanate in SO_2 yields thiocarbonyl dithiocyanate (**1**). A similar reaction with silver thiocyanate as starting material resulted in formation of the mono-substituted variant chlorothiocarbonyl thiocyanate (**2**). As deduced from both single crystal and powder X-ray diffraction we found that **1** crystallizes in its *syn-anti* conformer which is in contrast to the hitherto reported carbonyl dipseudohalides that crystallize as their respective *syn-syn* conformer. Only one conformer for **1** and **2** was also observed in vibrational spectroscopy, which corroborates the structural findings. DFT calculations revealed the *syn-anti* conformer for **1** being the energetically favored species. Furthermore,

the thiocyanate isomer is the kinetic reaction product, which is about $100\,\mathrm{kJ\,mol^{-1}}$ higher in energy than the thermodynamical reaction product, thiocarbonyl diisothiocyanate. The isolation of only $-\mathrm{SCN}$ substituted compounds **1** and **2** emerges from a significantly higher transition state for the $-\mathrm{NCS}$ substitution. Lastly, the reaction of **1** with ethanol led to the formation of ethoxy substituted dithiobiuret **3**, which can further be used as complexating ligand for nickel (**4**). Currently, we are investigating the syntheses of compounds similiar to **3** and their aptness to function as ligands for the complexation of other transition metals.

Acknowledgement

Supporting Information Available

The following files are available free of charge.

- Supporing Information: The Supporting Information contains detailed experimental procedures, NMR, IR and Raman spectra as well as details on crystallography, Hirshfeld analysis and quantum mechanical calculations.

- CCDC 2343032–2343036 contain the supplementary crystallographic data for this paper.

References

(1) Verbeek, W.; Sundermeyer, W. Preparation of Carbonyl and Fluorocarbonyl Pseudo-halides in Molten Salts. *Angew. Chem. Int. Ed.* **1967**, *6*, 871–872.

(2) Haas, A.; Reinke, H. Halogencarbonylschwefel-pseudohalogenide. *Angew. Chem.* **1967**, *79*, 687–688.

(3) Haas, A.; Reinke, H. Pseudohalogenverbindungen, XII Halogencarbonylsulfenyl-pseudohalogenide. *Chem. Ber.* **1969**, *102*, 2718–2727.

(4) Jäckh, C.; Sundermeyer, W. Darstellung und Reaktionen von Carbonylhalogeniden und -pseudohalogeniden. *Chem. Ber.* **1973**, *106*, 1752–1757.

(5) Appel, R.; Siray, M. Cyanformylchlorid. *Angew. Chem.* **1983**, *95*, 807–807.

(6) Mack, H. G.; Della Védova, C. O.; Willner, H. Structures and conformations of carbonyl isocyanates and carbonyl azides. An experimental and theoretical investigation. *J. Mol. Struct.* **1993**, *291*, 197–209.

(7) Malachowski, R.; Jurkiewicz, L.; Wojtowicz, J. Über das Carbonylcyanid (I. Mitteil.). *Ber. Dtsch. Chem. Ges.* **1937**, *70*, 1012–1016.

(8) Zeng, X.; Gerken, M.; Beckers, H.; Willner, H. Synthesis and Characterization of Carbonyl Diazide, $OC(N_3)_2$. *Inorg. Chem.* **2010**, *49*, 9694–9699.

(9) Curtius, T.; Heidenreich, K. Stickstoffkohlenoxyd und Diharnstoff. *Ber. Dtsch. Chem. Ges.* **1894**, *27*, 2684–2685.

(10) Nachbaur, E. Darstellung und Eigenschaften von Carbonylisocyanat. *Monatsh. Chem.* **1966**, *97*, 361–367.

(11) Klapötke, T. M.; Krumm, B.; Rest, S.; Scharf, R.; Schwabedissen, J.; Stammler, H.-G.; Mitzel, N. W. Carbonyl Diisocyanate $CO(NCO)_2$: Synthesis and Structures in Solid State and Gas Phase. *J. Phys. Chem. A* **2016**, *120*, 4534–4541.

(12) Dixon, A. E. The action of metallic thiocyanates upon carbonyl chloride. *Proc. Chem. Soc.* **1902**, *18*, 240.

(13) Pfeiffer, J.; Trost, C.; Pachkovska, A.; Tambornino, F. A Crystallographic, Spectroscopic, and Computational Investigation of Carbonyl and Oxalyl Diisothiocyanate. *Inorg. Chem.* **2021**, *60*, 10722–10728.

(14) Nolan, A. M.; Amberger, B. K.; Esselman, B. J.; Thimmakondu, V. S.; Stanton, J. F.; Woods, R. C.; McMahon, R. J. Carbonyl Diazide, $OC(N_3)_2$: Synthesis, Purification, and IR Spectrum. *Inorg. Chem.* **2012**, *51*, 9846–9851.

(15) Liu, Q.; Li, H.; Wu, Z.; Li, D.; Beckers, H.; Rauhut, G.; Zeng, X. Photolysis of Carbonyl Diisocyanate: Generation of Isocyanatocarbonyl Nitrene and Diazomethanone. *Chem. - Asian J.* **2016**, *11*, 2953–2959.

(16) Pfeiffer, J.; Wagner, J. P.; Tambornino, F. Photolytic Decarbonylation of Oxalyl Diisothiocyanate in Solid Argon Matrices to syn-anti Carbonyl Diisothiocyanate and Its Isomerization. *Eur. J. Inorg. Chem.* **2023**, *26*, e202300290.

(17) Ramos, L. A.; Ulic, S. E.; Romano, R. M.; Erben, M. F.; Lehmann, C. W.; Bernhardt, E.; Beckers, H.; Willner, H.; Della Védova, C. O. Vibrational spectra, crystal structures, constitutional and rotational isomerism of FC(O)SCN and FC(O)NCS. *Inorg. Chem.* **2010**, *49*, 11142–11157.

(18) Ramos, L. A.; Ulic, S. E.; Romano, R. M.; Erben, M. F.; Vishnevskiy, Y. V.; Reuter, C. G.; Mitzel, N. W.; Beckers, H.; Willner, H.; Zeng, X.; Bernhardt, E.; Ge, M.; Tong, S.; Védova., C. O. D. Spectroscopic Characterization and Constitutional and Rotational Isomerism of ClC(O)SCN and ClC(O)NCS. *J. Phys. Chem. A* **2013**, *117*, 2383–2399.

(19) Bunnenberg, R.; Jochims, C. Thiocarbonyl-dithiocyanat und sein S-Oxid. *Chem. Ber* **1981**, *114*, 1132–1136.

(20) Gombler, W. ^{13}C- und ^{19}F-NMR-spektren von verbindungen des typs E=CXY (E =

O, S, Se; X, Y = Halogen, SCF$_3$). *Spectrochim. Acta Part A Mol. Spectrosc.* **1981**, *37*, 57–61.

(21) Christen, D.; Oberhammer, H.; Zeil, W.; Haas, A.; Darmadi, A. The molecular structure of seleno- and thiocarbonyl difluoride. *J. Mol. Struct.* **1980**, *66*, 203–210.

(22) Nakata, M.; Fukuyama, T.; Kuchitsu, K. Molecular structure of thiocarbonyl chloride as studied by gas electron diffraction. *J. Mol. Struct.* **1982**, *81*, 121–129.

(23) Mantina, M.; Chamberlin, A. C.; Valero, R.; Cramer, C. J.; Truhlar, D. G. Consistent van der Waals Radii for the Whole Main Group. *J. Phys. Chem. A* **2009**, *113*, 5806–5812.

(24) James, C. M. Synthesis and Characterisation of Inorganic Trithiocarbonates, Perthiocarbonates and Related 1,1-Dithiolate Compounds. Ph.D. thesis, Universität zu Köln, 2021.

(25) Perdew, J. P.; Ernzerhof, M.; Burke, K. Rationale for mixing exact exchange with density functional approximations. *J. Chem. Phys.* **1996**, *105*, 9982–9985.

(26) TURBOMOLE v. 7.8 (University of Karlsruhe and Forschungszentrum Karlsruhe GmbH, 1989-2007, TURBOMOLE GmbH since 2007. Available from https://turbomole.org, 2024).

(27) Weigend, F.; Ahlrichs, R. Balanced basis sets of split valence, triple zeta valence and quadruple zeta valence quality for H to Rn: Design and assessment of accuracy. *Phys. Chem. Chem. Phys.* **2005**, *7*, 3297–3305.

(28) Pausch, A. Consistent analytical second derivatives of the Kohn–Sham DFT energy in the framework of the Conductor-like screening Model (COSMO) through Gaussian charge distributions. *J. Chem. Theory Comput.* **2024**, preprint.

(29) Plessow, P. Reaction Path Optimization without NEB Springs or Interpolation Algorithms. *J. Chem. Theory Comput.* **2013**, *9*, 1305–1310.

(30) Mayer, I. Charge, bond order and valence in the AB initio SCF theory. *Chem. Phys. Lett.* **1983**, *97*, 270–274.

(31) Akteries, B.; Jochims, J. C. Carbonyl diisocyanate: A new preparation and some reactions. *Chem. Ber.* **1986**, *119*, 83–95.

(32) Bunnenberg, R.; Jochims, J. C. Carbonyldiisothiocyanat. *Chem. Ber.* **1981**, *114*, 2075–2086.

(33) Pfeiffer, J.; Günther, H.; Völlinger, L.; Botros, D.; Scheibe, B.; Möbs, M.; Kraus, F.; Weigend, F.; Tambornino, F. Double Addition *vs.* Ring Closure: Systematic Reactivity Study of CO(NCO)$_2$ and CO(NCS)$_2$ towards Hydrogen Halides. *Chem. – A Eur. J.* **2023**,

(34) Pfeiffer, J.; Möbs, M.; Reith, S.; Tallu, M.; Tambornino, F. *J. Mol. Struct., submitted.*

(35) Spofford, W. A.; Amma, E. L. Crystal and molecular structure of dithiobiuret. *J. Cryst. Mol. Struct.* **1972**, *2*, 151–158.

(36) Luth, H.; Hall, E. A.; Spofford, W. A.; Amma, E. L. The crystal and molecular structure of bis(dithiobiureto)nickel(II). *J. Chem. Soc. D Chem. Commun.* **1969**, 520b–521.

(37) Uechi, T.; Ueda, I.; Matsumoto, N.; Kida, S. Syntheses and molecular structure of bis(1-substituted-2,4-dithiobiuretato)-nickel(II) complexes. *Inorg. Chim. Acta* **1979**, *33*, 87–93.

(38) Pignedoli, A.; Peyronel, G.; Antolini, L. The crystal and molecular structure of bis(2,4-dithiobiureto)nickel(II) diperchlorate–ethanol, Ni(HDTB)$_2$ (ClO$_4$)$_2$.EtOH. *Acta Crystallogr. Sect. B Struct. Crystallogr. Cryst. Chem.* **1973**, *29*, 1490–1499.

(39) Billson, T. S.; Crane, J. D.; Sinn, E.; Teat, S. J.; Wheeler, E.; Young, N. A. Shape selective solvent inclusion within the lattice of bis(N^1,N^1,N^5,N^5-tetrabenzyl-2,4-dithiobiureto)nickel(II). *Inorg. Chem. Commun.* **1999**, *2*, 527–529.

(40) Ramasamy, K.; Malik, M. A.; O'Brien, P.; Raftery, J. Metal complexes of thiobiurets and dithiobiurets: Novel single source precursors for metal sulfide thin film nanostructures. *Dalt. Trans.* **2010**, *39*, 1460–1463.

(41) Ramasamy, K.; Malik, M. A.; O'Brien, P.; Raftery, J.; Helliwell, M. Nickel sulfide thin films from thio- and dithiobiuret precursors. *Chem. Mater.* **2010**, *22*, 6328–6340.

(42) Pyykkö, P.; Atsumi, M. Molecular Double-Bond Covalent Radii for Elements Li–E112. *Chem. – A Eur. J.* **2009**, *15*, 12770–12779.

4 Monographischer Teil

4.1 Syntheseversuche zu Carbonyldipseudohalogeniden

In den folgenden Abschnitten sollen die Syntheseversuche zu den höheren Homologen von Carbonyldiisocyanat (OC(NCO)$_2$) erläutert werden. In Schema 4.1 sind die relevanten Homologen farblich hervorgehoben. Dargestellt sind jeweils nur die *Iso*cyanat-Homologen, welche ein Konstitutionsisomer der Cyanat-Homologen sind. Der synthetische Fokus wurde auf Carbonyldi(iso)selenocyanat (CO(NCSe)$_2$ (violett)/CO(SeCN)$_2$), Thiocarbonyldiisocyanat (CS(NCO)$_2$ (hellblau)), Thiocarbonyldiisothiocyanat (CS(NCS)$_2$ (hellgrün)) und Thiocarbonyldi(iso)selenocyanat (CS(NCSe)$_2$ (kirschrot)/CS(SeCN)$_2$) gelegt. Syntheseversuche zu den Selenocarbonyl-Homologen (untere Reihe) wurden in der Bearbeitungszeit dieser Promotion nicht durchgeführt und sind noch ausstehend. In den folgenden Abschnitten wird auf die analytischen Ergebnisse der Reaktionen und deren Beobachtungen eingegangen. Die detaillierten Versuchsbeschreibungen sind in Abschnitt 6.4.1 zu finden.
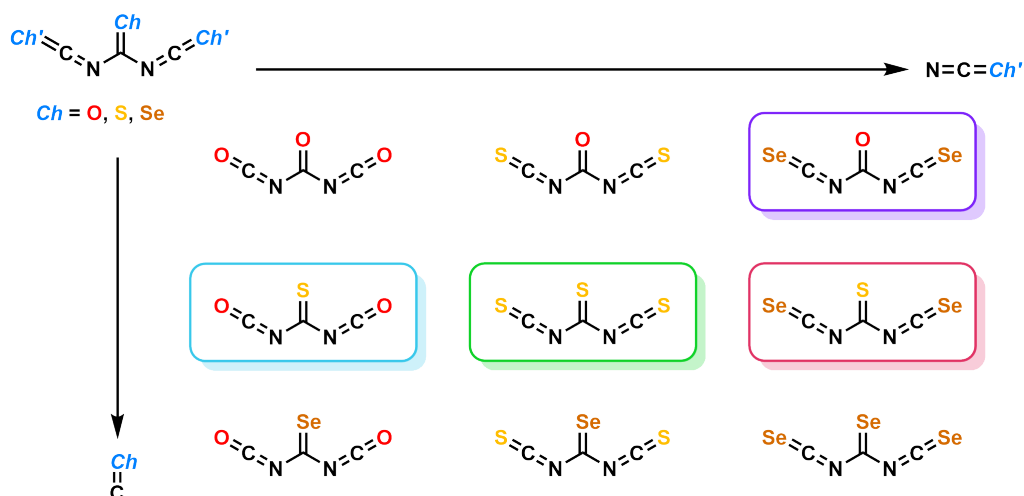
Schema 4.1: Höhere Homologe von Carbonyldiisocyanat mit farblicher Hervorhebung der für den monographischen Teil relevanten Moleküle.

4.1.1 Carbonyldi(iso)selenocyanat

Als erstes wurde versucht Carbonyldiisoselenocyanat (CO(NCSe)$_2$) darzustellen, um die oberste Reihe (Schema 4.1) der Carbonylisocyanate zu vervollständigen. Hierbei muss beachtet werden, dass die Entstehung von Carbonyldiselenocyanat (CO(SeCN)$_2$) im Rahmen der Möglichkeiten liegt, wie es bereits in Abschnitt 3.7 für Thiocarbonyldi(iso)thiocyanat gezeigt wurde. Die dazu durchgeführten, synthetischen Herangehensweisen sind in Schema 4.2 dargestellt und eine Übersicht der Reaktionsbedingungen ist in Tabelle 4.1 gegeben. Es kann davon ausgegangen werden, dass beide Moleküle (CO(NCSe)$_2$ oder CO(SeCN)$_2$) thermisch instabil sind, weshalb alle Reaktionen bei tiefen Temperaturen durchgeführt wurden. Dazu wurden im Allgemeinen Edukt und Reaktant miteinander reagiert, Nebenprodukte abfiltriert und das Filtrat zur Analyse aufgearbeitet.
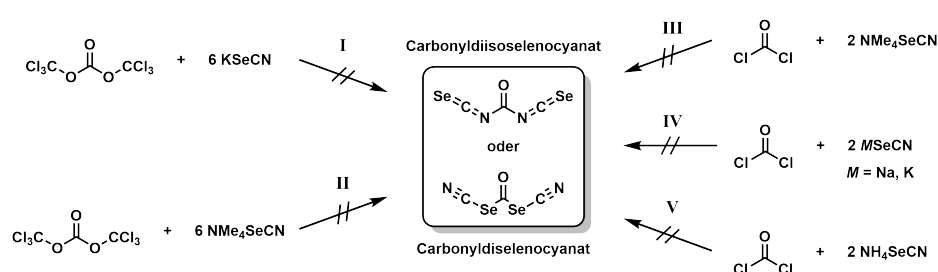
Schema 4.2: Syntheseversuche zur Darstellung von Carbonyldiisoselenocyanat oder Carbonyldiselenocyanat.

Zunächst wurden Synthesen ausgehend von Triphosgen vorgenommen, welches mit Kaliumselenocyanat (KSeCN) umgesetzt wurde (**I**). Die Reaktionslösungen trübten und färbten sich von gelb bis orange-rot, was ein erster optischer Hinweis auf die Entstehung von Zerfallsprodukten wie rotem Selen[133] ist. Mittels ^{13}C{^{1}H}-NMR-Spektroskopie konnten nur die Zerfallsprodukte (SeCN)$_2$ (97.8 ppm) in **Ia** und Se(CN)$_2$ (90.4 ppm) in **Ib**[134] detektiert werden. Durch PXRD wurde das Nebenprodukt KCl nachgewiesen. Es gab keine Hinweise der Synthese der gewünschten Produkte. Eine Reaktion hat stattgefunden, führte jedoch nicht zu CO(NCSe)$_2$ oder CO(SeCN)$_2$.

Die Selenocyanatquelle wurde aufgrund der besseren Löslichkeit von NMe$_4$SeCN in THF (**II**) geändert. Die Reaktionslösung verfärbte sich unmittelbar nach beendeter Zugabe über 30 min von gelb zu dunkelrot (Abbildung 4.1). Der erhaltene nach Aufarbeitung orangene Feststoff zerfiel beim Lösen in deuteriertem THF-d$_8$, CD$_3$CN oder Pyridin-d$_5$ unter Rotfärbung des Feststoffes. Die Rotfärbungen sind erneut ein Hinweis auf die Bildung von rotem Selen als Zerfallsprodukt.[133] Durch ^{13}C{^{1}H}-NMR-Spektroskopie in CDCl$_3$ wurde lediglich das Edukt Triphosgen[135] (141.1 & 108.5 ppm) und (SeCN)$_2$[134] (97.3 ppm) nachgewiesen. Im Röntgenpulverdiffraktogramm sind Reflexe von NMe$_4$Cl und grauem

Selen zu finden. Erneut gab es keine Hinweise auf die Bildung von $CO(NCSe)_2$ oder $CO(SeCN)_2$. Eine Reaktion hat stattgefunden, welche nicht zum gewünschten Produkt führte.

Tabelle 4.1: Reaktionsübersicht zu Syntheseversuchen von Carbonyldiisoselenocyanat oder Carbonyldiselenocyanat.

Nummer	Edukt	Reaktant	Lösungsmittel	Temperatur
Ia			THF	0 °C
Ib	$CO(OCCl_3)_2$	KSeCN	THF	–78 °C
Ic			Toluol	–78 °C
II	$CO(OCCl_3)_2$	NMe_4SeCN	THF	–78 °C
IIIa	$COCl_2$	NMe_4SeCN	THF	–78 °C
IIIb			SO_2	–25 °C
IVa	$COCl_2$	NaSeCN	THF	–78 °C
IVb		KSeCN	SO_2	–78 °C
Va	$COCl_2$	NH_4SeCN	THF-d_8	RT
Vb			SO_2	–30 °C

Die Detektion des Reaktants (Triphosgen) in Versuch **II** lässt schließen, dass Triphosgen für diese Syntheseversuche nicht ausreichend reaktiv ist. Daher wurde Phosgen als neues Edukt gewählt. $COCl_2$ und NMe_4SeCN reagieren (**IIIa**) unter Gelbfärbung miteinander. Es wurde ein gelber Feststoff abfiltriert, welcher sich beim Erwärmen unter grünrötlichem Farbumschlag vermutlich zersetzte. Das gelbe Filtrat verfärbte sich beim Erwärmen auf 0 °C orange und der Ausfall eines grauen Feststoffes (Se_{grau}) konnte beobachtet werden. In den Rückständen des Filtrates wurden lediglich die Zerfallsprodukte $Se(CN)_2$ (90.7 ppm), $(SeCN)_2$ (98.2 ppm)[134] und $Se(SeCN)_2$ (101.7 ppm) mittels $^{13}C\{^1H\}$-NMR-Spektroskopie und $Se(SeCN)_2$ mittels PXRD nachgewiesen. Die Reaktion mit NaSeCN als Reaktant (**IVa**) führte unter Agglomeration von THF und Natriumsalzen, sichtbar durch eine zähflüssige Reaktionslösung (Abbildung 4.1 d), zu dem gleichen Ergebnis. Zusätzlich konnten erhaltene rote Kristalle mittels SC-XRD als $Se(SeCN)_2$ identifiziert werden. Weder in **IIIa**, noch **IVa** wurden Hinweise auf die Bildung von $CO(NCSe)_2$ oder $CO(SeCN)_2$ erhalten.

Bisher konnte einsetzende Zersetzung bereits bei der Filtration oder dem Entfernen des Lösungsmittels beobachtet werden. Um eine Isolation der Reaktionsprodukte zu vereinfachen wurde deshalb zu Schwefeldioxid (SO_2) als Lösungsmittel, nach dem Vorbild der Synthese von Carbonyldiisothiocyanat[68] (Abschnitt 1.2.2), gewechselt. SO_2 kann mit seinem Sdp. von –10 °C[136] im Eisbad verdampft oder bei –40 °C im Vakuum entfernt werden.

Abbildung 4.1: Reaktionslösung der Umsetzung von CO(OCCl₃)₂ mit NMe₄SeCN in THF (**II**) direkt nach beendetem Zusammengeben der Edukte (a) und 3 min später (b). Isolierter Reaktionsrückstand von **II** bestehend aus CO(OCCl₃)₂ und (SeCN)₂ (c). Zähflüssige Reaktionslösung von **IVa** während der Filtration (d).

Aus der Reaktion zwischen $COCl_2$ und KSeCN (**IVb**) konnten weder Edukte, noch Produkte oder Zerfallsprodukte nachgewiesen werden. Die Löslichkeit von KSeCN scheint für eine Reaktion zu gering in SO_2. Deshalb wurde NH_4SeCN mit einer höheren Löslichkeit in SO_2 als neuer Reaktant gewählt. Es wurde zunächst im NMR-Rohr eine Testreaktion (**Va**) durchgeführt, welche im $^{13}C\{^1H\}$-NMR-Spektrum zwei Resonanzsignale bei 185.3 ppm und 98.1 ppm aufweist (Abbildung 4.2). Diese Signale sind erstmals ein Hinweis auf die Bildung eines Produktes und könnten im Vergleich zu $CS(SCN)_2$ (189.8 & 106.2 ppm[78]) $CO(SeCN)_2$ zugeordnet werden. Hier könnte ein Trend der schweren Pseudohalogenide, keine *iso*-Konstitution zu bevorzugen, erkennbar sein. Da es allerdings keine vergleichbaren NMR-Daten für organische Selenocyanatverbindungen in der Literatur gibt, bleibt eine exakte Aussage ohne weitere Analytik unmöglich.
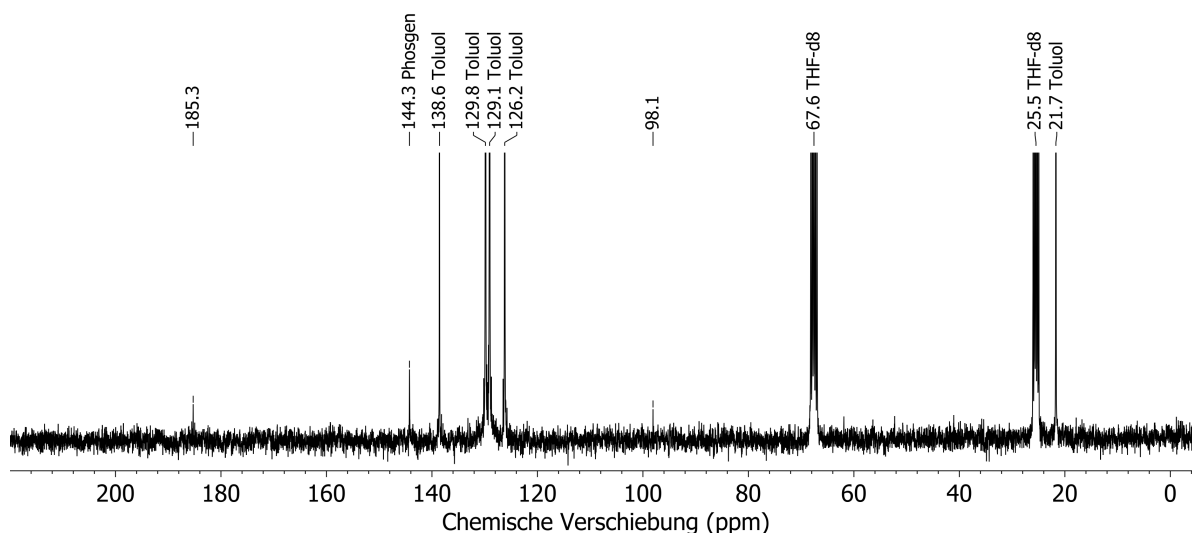
Abbildung 4.2: $^{13}C\{^1H\}$-NMR-Spektrum der Reaktion von $COCl_2$ mit NH_4SeCN in THF-d₈ (**Va**).

Die Reaktion wurde im größerem Maßstab (15 mmol) in SO$_2$ durchgeführt (**Vb**) und in dem gelben Rückstand des Filtrates Se(SeCN)$_2$ (102.9 ppm) und (SeCN)$_2$ (98.2 ppm)[134] mittels ^{13}C{^{1}H}-NMR-Spektroskopie detektiert. Es wurden keine Resonanzsignale bei 185 ppm und 98 ppm gefunden. Während der Reaktionsdurchführung von **Vb** ist aufgefallen, dass die Masse des abfiltrierten Rückstandes (7.0 g) wesentlich größer war als die theoretisch zu erwartende Masse der Nebenprodukte (3.8 g). Es ist anzunehmen, dass das Reaktionsprodukt schlecht löslich in SO$_2$ ist und aus der Lösung ausfällt. Dies wird zusätzlich unterstützt durch die Beobachtung, dass der abfiltrierte Feststoff sich bei Raumtemperatur rasch tiefrot verfärbte. Aus diesem Grund wurde die Reaktion ohne Abfiltration der Nebenprodukte wiederholt und versucht das Rohprodukt direkt mit Ethanol zu einem Folgeprodukt nach ähnlichen Synthesen aus der Literatur[137] umzusetzen (Schema 4.3). Dabei ist ein schwarzer Feststoff präzipitiert, welcher durch PXRD als NH$_4$Cl und graues Selen identifiziert werden konnte. Aus der roten Reaktionslösung wurden mittels ^{13}C{^{1}H}-NMR-Spektroskopie und PXRD die Nebenprodukte NH$_4$Cl, (SeCN)$_2$ (99.8 ppm)[134] und Se(SeCN)$_2$ (107.3 ppm) detektiert. Es konnten jedoch keine Hinweise auf ein Folgeprodukt erhalten werden.
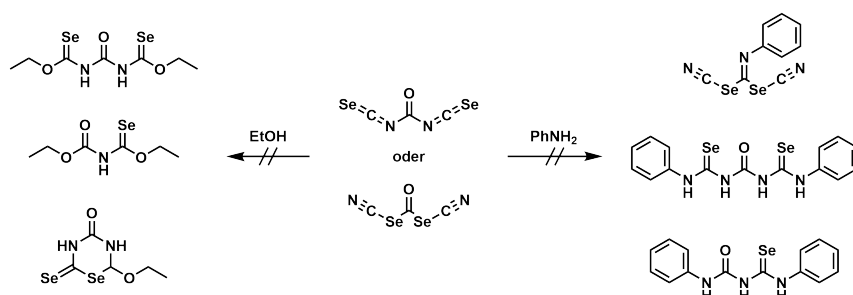
Schema 4.3: Denkbare Reaktionsprodukte aus der *in situ* Synthese von Carbonyldiisoselenocyanat oder Carbonyldiselenocyanat mit Ethanol und Anilin als indirekter Nachweis selbiger.

Aufgrund der aufwendigen Synthese von NH$_4$SeCN wurde zuletzt stattdessen nochmals NMe$_4$SeCN verwendet (**IIIb**). Bei der Reaktion wurde auf jegliche Aufarbeitung verzichtet und Analytik direkt aus dem gelben Rohprodukt vorgenommen. Dieses verfärbt sich bei RT zunächst rot und zerfällt weiter zu einer schwarzen „verkohlten" Masse (Abbildung 4.3), welche sich im PXRD als Mischung aus grauem Selen und NMe$_4$Cl herausstellte. Bei dem Versuch den Rückstand in Chloroform (CHCl$_3$), Acetonitril (CH$_3$CN), Dimethoxyethan, Toluol, THF, Diethylether (Et$_2$O) und Aceton bei −78 °C zu lösen, konnte kein Feststoff in Lösung gebracht werden. Alle Suspensionen verfärbten sich schnell orange-rot und im ^{13}C{^{1}H}-NMR-Spektrum konnten keine Resonanzsignale außer die der Lösungsmittel detektiert werden. Bei dem langsamen Erwärmen auf Raumtemperatur entfärbten sich die Suspensionen und die Bildung eines roten oder grauen Feststoffes war zu beobachten

(Abbildung 4.3). Zuletzt wurde versucht ein Folgeprodukt für einen indirekten Nachweis, wie in der Literatur für ähnliche Moleküle beschrieben,[137–140] zu erhalten. Dazu wurde das Rohprodukt mit Anilin umgesetzt (Schema 4.3). Durch NMR-Spektroskopie konnte kein eindeutiges Folgeprodukt identifiziert werden.
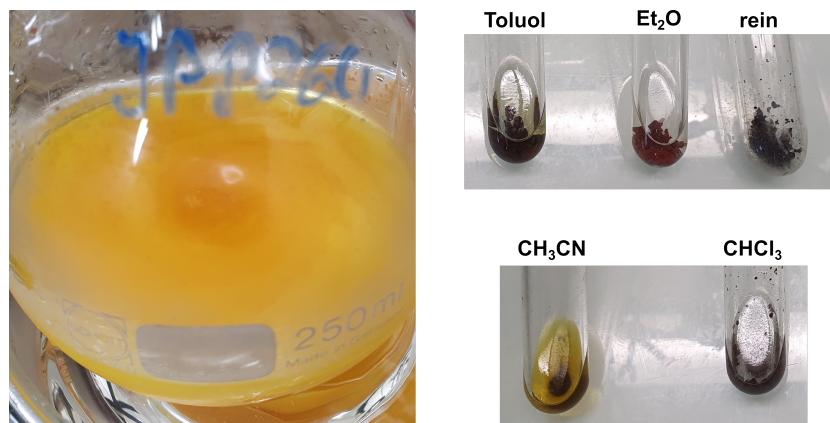

Abbildung 4.3: Reaktionslösung der Umsetzung von $COCl_2$ mit NMe_4SeCN in SO_2 ($\mathbf{IIIb}$, links) und Suspensionen des Rohprodukts nach Löslichkeitstest (rechts).

Zusammenfassend konnte kein reines Produkt isoliert werden. Dennoch wird davon ausgegangen, dass Carbonyldiselenocyanat ($CO(SeCN)_2$) in den Reaktionen $\mathbf{IIIb}$, $\mathbf{Va}$ und $\mathbf{Vb}$ synthetisiert werden konnte. Die $^{13}C\{^1H\}$-NMR spektroskopischen Resonanzsignale von 185.3 ppm und 98.1 ppm sprechen für die Synthese, auch wenn keine Kopplung zu ^{77}Se aufgrund eines schlechten Signal-zu-Rausch Verhältnisses erkennbar ist. Es deutet sich zudem ein Trend an, dass die Pseudohalogenide mit zunehmend schwererem Chalkogenatom (O<S<Se) die *iso*-Konstitution nicht bevorzugt bilden. Die Annahme der erfolgreichen Synthesen wird zusätzlich unterstützt durch die Beobachtung, dass die erhaltenen Feststoffe sich sowohl beim Erwärmen, als auch beim Lösen mit rotem Farbumschlag zersetzen. Die rote Farbe kann durch das Entstehen von rotem Selen oder den ebenfalls rötlichen Verbindungen $(SeCN)_2$ und $Se(SeCN)_2$, welche mittels $^{13}C\{^1H\}$-NMR-Spektroskopie und PXRD nachgewiesen werden konnten, stammen. Es muss davon ausgegangen werden, dass $CO(SeCN)_2$ nur bei tiefen Temperaturen ($<$ –30 °C) als Feststoff stabil ist. Eine weitere Herangehensweise Carbonyldiisoselenocyanat ($CO(NCSe)$) möglicherweise zu synthetisieren, kann aus der Literatur abgeleitet werden. In dieser wird ein primäres Amin mit Kohlenstoffdiselenid (CSe_2) in Gegenwart von Quecksilberchlorid ($HgCl_2$) und Triethylamin (NEt_3) umgesetzt, um eine Isoselenocyanat-Gruppe zu bilden.[141] Die Synthese könnte auf Harnstoff übertragen werden, um sowohl die Carbonylfunktion, als auch die Isoselenocyanat-Gruppen einzubauen.

Syntheseversuche zu *tert*-Butylcarbonyl(iso)selenocyanat

Die Ergebnisse der Syntheseversuche zu Carbonyldi(iso)selenocyanat sind nicht eindeutig aussagekräftig, deshalb wurde versucht ein Carbonyl(iso)selenocyanat (CO(NCSe)R oder CO(SeCN)R) zu erhalten. Diese Verbindungen sind bereits als nicht isolierte Zwischenstufen beschrieben. In der Literatur werden sie *in situ* dargestellt und mit Aminen oder Alkoholen umgesetzt,[137–140] wie es zuvor für einen indirekten Nachweis mit Ethanol und Anilin getestet wurde. Dazu wird Kaliumselenocyanat in Aceton oder Ethanol mit einem Säurechlorid umgesetzt und durch Zugabe eines Amins weiter reagiert (Schema 4.4). Zu diesem Zweck wurde Pivalinsäurechlorid (*t*BuCOCl) als Ausgangssubstanz gewählt, um *tert*-Butylcarbonylisoselenocyanat (CO(NCSe)^{t}Bu) erstmals zu isolieren. In Tabelle 4.2 sind die durchgeführten Reaktionen aufgelistet und werden im Folgenden besprochen.
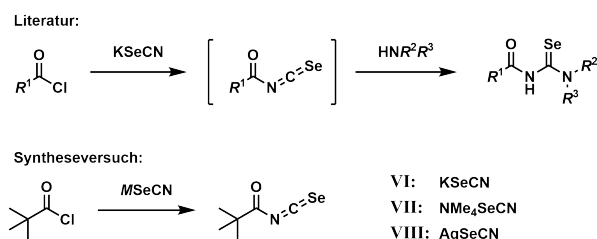
Schema 4.4: Reaktionsverlauf der *in situ* Darstellung von Carbonylisoselenocyanaten nach Literaturangaben[137–140] und Syntheseversuche zur Isolierung von *tert*-Butylcarbonylisoselenocyanat.

Die Literaturvorschriften mit Aceton[137,139,140] als Lösungsmittel wurden zunächst getestet (**VIa**). Im NMR-Rohr wurde KSeCN in Aceton-d$_6$ gelöst und mit *t*BuCOCl versetzt. Es wurde ein ^{13}C{^{1}H}-NMR-Spektrum nach sofortiger Zugabe (24 min Messzeit, Abbildung 4.5) und eines nach 24 h aufgenommen. Direkt nach der Zugabe sind keine Resonanzsignale der Edukte mehr vorhanden. Die Resonanzsignale bei 171.8 (C=O), 143.8 (N=C=Se), 44.8 (C(CH$_3$)$_3$) und 26.4 ppm (CH$_3$) könnten dem gewünschten Isoselenocyanat-Produkt zugeordnet werden. Das Resonanzsignal bei 210.2 ppm kann CSe$_2$[86] und bei 69.4 ppm nicht zugeordnet werden. Nach 24 Stunden ist das entstandenen Produkt vollständig zerfallen, woraus sich schließen lässt, dass es in Lösung bei Raumtemperatur nicht stabil ist. Der Versuch **VIa** wurde in größerem Maßstab (2.1 mmol) wiederholt und versucht ein Produkt aus der roten Reaktionslösung (Abbildung 4.4) über Filtration und Entfernung des Lösungsmittels im Vakuum zu isolieren. Ein gelber Feststoff wurde erhalten, welcher im ^{13}C{^{1}H}-NMR-Spektrum lediglich je zwei Resonanzsignale bei 210 ppm und 69 ppm mit einem zusätzlichen Resonanzsignal bei 55.6 ppm zeigt. CO(NCSe)^{t}Bu wurde nicht detektiert.

Tabelle 4.2: Reaktionsübersicht zu den Syntheseversuchen von *tert*-Butylcarbonyliso-selenocyanat oder *tert*-Butylcarbonylselenocyanat.

Nummer	Edukt	Reaktant	Lösungsmittel	Temperatur
VIa			Aceton	RT
VIb			Ethanol	78 °C
VIc	CO(^{t}Bu)Cl	KSeCN	THF	RT
VId			THF	66 °C
VIIa	CO(^{t}Bu)Cl	NMe$_4$SeCN	THF	RT
VIIb			CD$_3$CN	RT
VIIIa	CO(^{t}Bu)Cl	AgSeCN	THF	RT
VIIIb			–	–20 °C

Darauffolgend wurde die Literaturvorschrift mit Ethanol[138] als Lösungsmittel angewendet (**VIb**). Beim Zutropfen von *t*BuCOCl in die ethanolische Lösung von KSeCN fiel sofort ein roter Niederschlag aus (Abbildung 4.4), was auf die Bildung von rotem Selen[133] zurück-geführt werden kann. Es wurde ein ^{13}C{^{1}H}-NMR-Spektrum der Lösung als Reaktionskon-trolle aufgenommen (Abbildung 4.5). In diesem sind Resonanzsignale bei 178.3 (*C*=O), 111.3 (Se−*C*≡N), 60.2 (*C*(CH$_3$)$_3$) und 26.6 ppm (*C*H$_3$), welche dem Selenocyanat-Produkt zugeordnet werden könnten. Zwei Resonanzsignale bei 38.4 und 13.6 ppm sind nicht zu-ordenbar. Nach Aufarbeitung konnten keine Resonanzsignale mehr detektiert werden.
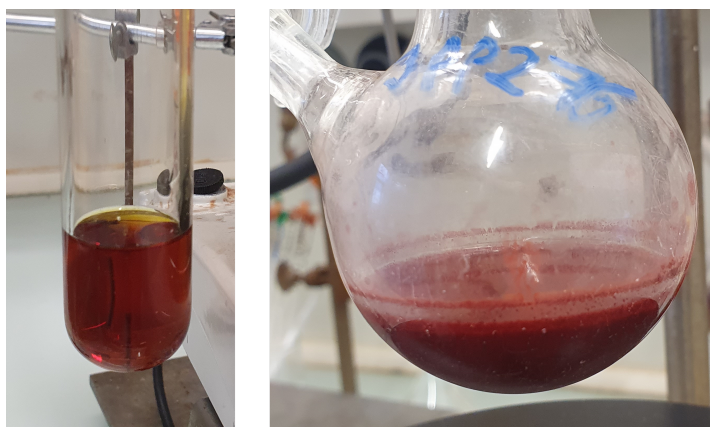
Abbildung 4.4: Reaktionslösungen der Syntheseversuche **VIa** (links) und **VIb** (rechts).

Ethanol und Aceton sind nach eigener Erfahrung, wie die Reaktionsverläufe zeigen, für diese Reaktionen keine geeigneten Lösungsmittel. Es wurde THF als Solvens gewählt (**VIc**). In einer Testreaktion im NMR-Maßstab konnten Resonanzsignale mit der gleichen chemischen Verschiebung wie in **VIa** (171.4, 144.0, 44.7 und 26.4 ppm) detektiert werden (Abbildung 4.5). Die Reaktion wurde in einem größeren Ansatz (5.0 mmol) wiederholt und es wurde ein gelber Feststoff isoliert, welcher sich bei Raumtemperatur rot verfärbte. Im

Verlauf der Reaktionsdurchführung erschwerte Agglomeration in Form einer zähflüssigen Reaktionslösung die Aufarbeitung. Es wurde gerade ausreichend Produkt für eine NMR spektroskopische Analyse gewonnen, in welcher erneut der selbe Signalsatz detektiert wurde.

Um zu überprüfen, ob bei höheren Temperaturen tatsächlich das Selenocyanat-Produkt entsteht, wie in **VIb** vermutet, wurde eine Reaktion in siedendem THF durchgeführt (**VId**). In einer Reaktionskontrolle mittels $^{13}C\{^1H\}$-NMR-Spektroskopie wurde wiederum der Signalsatz identisch zu **VIa** und **VIc** detektiert. Allerdings konnten nach Aufarbeitung erneut keine Resonanzsignale mehr detektiert werden.
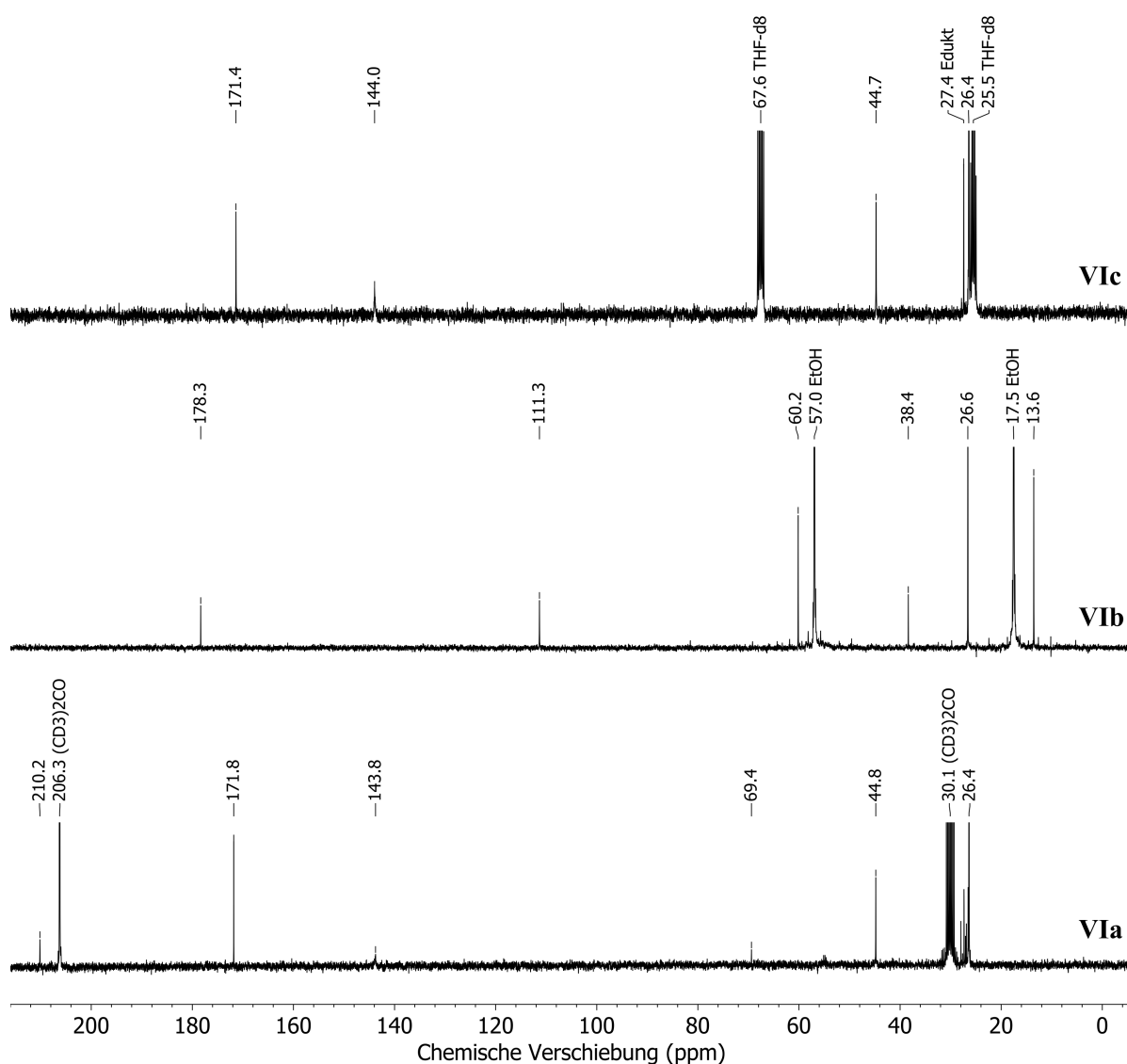
Abbildung 4.5: $^{13}C\{^1H\}$-NMR-Spektren der Reaktionen **VIa** in Aceton-d_6, **VIb** in C_2H_5OH und **VIc** in THF-d_8. Das Spektrum aus Reaktion **VIc** zeigt keine Bildung von Nebenprodukten und nur Signale von CO(NCSe)^{t}Bu.

Die Agglomeration bereitete Schwierigkeiten bei der Aufarbeitung der Reaktionen, weshalb versucht wurde NMe$_4$SeCN zu verwenden. Sowohl in THF (**VIIa**), als auch in CD$_3$CN (**VIIb**) konnte jedoch mittels ^{13}C{^{1}H}-NMR-Spektroskopie nur ein sehr geringer Umsatz festgestellt werden. Aus diesem Grund wurde zuletzt AgSeCN (**VIIIa**) verwendet, obwohl dessen Löslichkeit in THF wie in Wasser[142] ebenfalls gering sein sollte. Selbst nach drei Tagen Reaktionszeit konnten keine Resonanzsignale des Produktes im ^{13}C{^{1}H}-NMR-Spektrum detektiert werden. Durch PXRD wurden Reflexe schwacher Intensität von AgCl gefunden. Dies ist zumindest ein Hinweis auf einen geringen Umsatz. Die Reaktion wurde ohne Lösungsmittel wiederholt (**VIIIb**), es konnte allerdings nur Edukt durch PXRD nachgewiesen werden.

Zusammenfassend zeigen die Reaktionen, dass *tert*-Butylcarbonylisoselenocyanat (CO(NCSe)^{t}Bu) in Lösung dargestellt werden kann. Es zerfällt bei Raumtemperatur in Lösung und beim Versuch der Isolation durch Entfernen des Lösungsmittels. An dieser Stelle bietet sich an, die Synthese nochmals in Schwefeldioxid (Sdp.: −10 °C[136]) als Lösungsmittel durchzuführen, da dieses bei Raumtemperatur durch Verdampfung gasförmig entfernbar ist und kein Vakuum angelegt werden muss. Es kann keine Aussage darüber getroffen werden, ob das alleinige Anlegen von Vakuum oder grundsätzlich das Entfernen des Lösungsmittels den Zerfallsprozess begünstigt. Mit den bisherigen Erkenntnissen kann davon ausgegangen werden, dass CO(NCSe)^{t}Bu als Reinstoff nicht stabil ist.

4.1.2 Thiocarbonyldiisocyanat

Das erste Thiocarbonyl-Homologe von Carbonyldiisocyanat ist das Thiocarbonyldiisocyanat (CS(NCO)$_2$). Für die Synthese der Thiocarbonyl-Verbindungen wurde das kommerziell erwerbliche Thiophosgen (CSCl$_2$) als C=S Synthon gewählt. In Schema 4.5 sind die fünf synthetischen Herangehensweisen zu den Syntheseversuchen dargestellt.
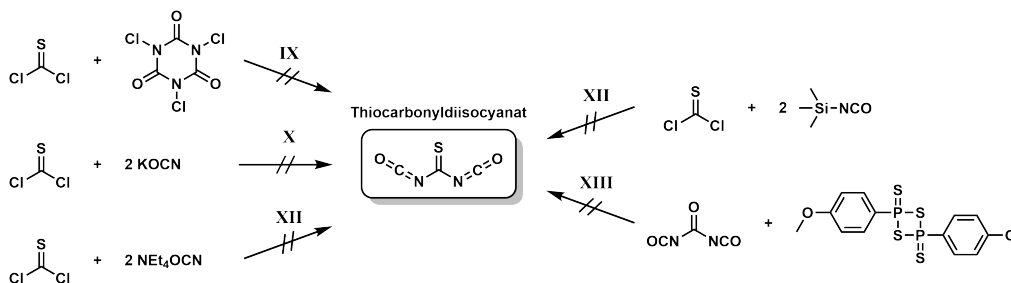
Schema 4.5: Syntheseversuche zur Darstellung von Thiocarbonyldiisocyanat.

Die Synthese von Carbonyldiisocyanat ist ausgehend von TCCA und Phosgen und wurde zunächst versucht zu übertragen. Dazu wurde Phosgen durch Thiophosgen substi-

tuiert (**IXa**). Die Synthese wurde analog wie für $CO(NCO)_2$ in Abschnitt 8.1.4 beschrieben durchgeführt. Es konnten im $^{13}C\{^1H\}$-NMR-Spektrum keine Resonanzsignale oberhalb 170 ppm entsprechend einer C=S Gruppe (vgl. CSCl$_2$: 169.7 ppm,[86] CS(SCN)$_2$: 189.8 ppm[78]) und somit kein Produkt detektiert werden. Das Lösungsmittel wurde zu Chloroform gewechselt und die Reaktion bei Raumtemperatur durchgeführt (**IXb**). Es konnten mittels $^{13}C\{^1H\}$-NMR-Spektroskopie das Edukt $CSCl_2$ und der Reaktant TCCA nachgewiesen werden. Aufgrund keiner ersichtlichen Reaktion nach 20 h Reaktionszeit wurde ein neuer Versuch mit erhöhter Reaktionstemperatur (**IXc**) durchgeführt. In den Reaktionsrückständen konnten weder Edukte noch Produkte detektiert werden.

Tabelle 4.3: Reaktionsübersicht zu den Syntheseversuchen von Thiocarbonyldiisocyanat.

Nummer	Edukt	Reaktant	Lösungsmittel	Temperatur
IXa			2-Chlornitrobenzol	120 °C – 170 °C
IXb	$CSCl_2$	TCCA	$CHCl_3$	RT
IXc			$CHCl_3/CH_3CN$	62 °C
Xa			THF	–78 °C → RT
Xb	$CSCl_2$	KOCN	–	0 °C
Xc			SO_2	–20 °C
XI	$CSCl_2$	NEt$_4$OCN	THF	–78 °C → RT
XIIa	$CSCl_2$	Me$_3$SiNCO	THF	66 °C
XIIb			SO_2	–78 °C
XIIIa			Toluol	111 °C
XIIIb	$CO(NCO)_2$	Lawessons Reagenz	$CDCl_3$	RT
XIIIc			THF-d$_8$	RT

Im Anschluss wurde die Synthese über Salzmetathese versucht. Dazu wurde $CSCl_2$ mit KOCN zuerst in THF umgesetzt (**Xa**). Die Löslichkeit von KOCN erwies sich als zu gering in THF, weshalb lediglich Edukt mittels $^{13}C\{^1H\}$-NMR-Spektroskopie und Reaktant durch PXRD nachgewiesen werden konnte. Eine solvensfreie Reaktion (**Xb**) lieferte das gleiche Ergebnis. Bei dem Syntheseversuch in flüssigem SO_2 (**Xc**) erwies sich die Löslichkeit als zu gering und es wurde ausschließlich Edukt detektiert. NEt$_4$OCN wurde als neuer Reaktant gewählt (**XI**), da es eine höhere Löslichkeit als KOCN in THF haben sollte. Dieser Ansatz führte wiederum nur zum Nachweis von NEt$_4$OCN. In keinem Versuch konnten Hinweise auf eine Reaktion zu $CS(NCO)_2$ gefunden werden.

Die Bildung von Trimethylsilylchlorid (($CH_3)_3$SiCl) als Triebkraft der Reaktion wurde getestet, indem $CSCl_2$ mit $(CH_3)_3$SiOCN umgesetzt wurde. In **XIIa** konnten weder Edukte, noch Produkte mittels $^{13}C\{^1H\}$-NMR-Spektroskopie nachgewiesen werden, wohingegen in

XIIb ausschließlich beide Edukte detektiert wurden. Zuletzt wurde ein neuer Ansatz ge-wählt und versucht mittels des Lawessons-Reagenz die Carbonylgruppe von $CO(NCO)_2$ in eine Thiocarbonylgruppe umzuwandeln (**XIII**). In allen drei Syntheseversuchen hat ei-ne Reaktion stattgefunden, was durch fehlende Resonanzsignale des Eduktes $CO(NCO)_2$ im $^{13}C\{^{1}H\}$-NMR-Spektrum ersichtlich ist. Allerdings konnten keine Resonanzsignale, wel-che $CS(NCO)_2$ zugeordnet werden können, detektiert werden. Stattdessen wurden Reso-nanzsignale unbestimmter Nebenprodukte im $^{13}C\{^{1}H\}$-NMR-Spektrum erhalten.

Eine weitere Strategie zur Synthese von $CS(NCO)_2$ ist Thiophosgen mit Ammoniumcya-nat (NH_4OCN) oder Silbercyanat (AgOCN) umzusetzen. Diese Synthesen wurden von HENNES GÜNTHER im Rahmen seiner Masterarbeit durchgeführt.[143] Es gelang ihm aus einer Reaktion mit Thiophosgen und Silbercyanat im $^{13}C\{^{1}H\}$-NMR-Spektrum bei einer chemischen Verschiebung von 182.7 ppm und 154.4 ppm zwei passende Resonanzsigna-le zu detektierten, aber es konnte kein Produkt isoliert werden. Durch *in situ* Umsetzung mit Ethanol erfolgte ein indirekter Nachweis durch die Bildung eines gezielten Reaktions-produktes (Schema 4.6). Es bleibt hierbei allerdings unklar ob *in situ* CS(NCO)Cl oder $CS(NCO)_2$ gebildet wurde, da beide mit Ethanol zum gleichen Produkt reagieren können.
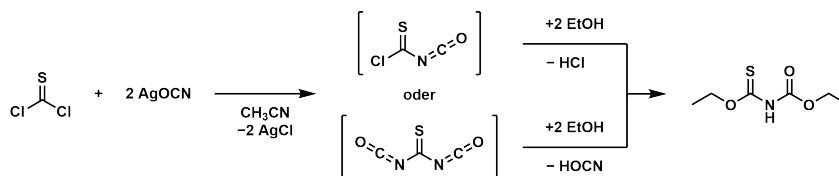
Schema 4.6: Synthese von Thiocarbonyldiisocyanat und *in situ* Umsetzung mit Ethanol als indirekter Nachweis aus der Masterarbeit[143] von HENNES GÜNTHER. Ebenfalls darge-stellt ist die mögliche Bildung von Chlorthiocarbonylisocyanat.

4.1.3 Thiocarbonyldiisothiocyanat

In Abschnitt 3.7 wurden die Untersuchungen zu Thiocarbonyldithiocyanat ($CS(SCN)_2$) pu-bliziert. Bei dem Versuch Thiocarbonyldiisothiocyanat ($CS(NCS)_2$) aus Thiophosgen und Ammoniumthiocyanat zu synthetisieren, wurde stattdessen $CS(SCN)_2$ erhalten. Die Dar-stellung von $CS(NCS)_2$ über andere Herangehensweisen zu verwirklichen sollen hier nur kurz zusammengefasst werden (Schema 4.7). Eine ausführliche Beschreibung der Syn-theseversuche ist in den *Supporting Information* (Abschnitt 8.1.7) von Abschnitt 3.7 zu fin-den. Es wurde versucht über Salzeliminierung ausgehend von Thiophosgen mit NaSCN, AgSCN oder IPrCuNCS die Darstellung von $CS(NCS)_2$ zu ermöglichen. Isomerisierung durch Bestrahlung mit UV-Licht (λ = 390 nm) des gelbfarbenen Feststoffes $CS(SCN)_2$ in Lösung war ebenso erfolglos. Die Amingruppen von Thioharnstoff mittels Thiophosgen zu

thiocarbonylieren gelang ebenfalls nicht. Zuletzt wurde versucht mittels des Lawessons-Reagenz die Carbonylgruppe von Carbonyldiisothiocyanat in eine Thiocarbonylgruppe umzuwandeln. Alle Syntheseversuche zu Thiocarbonyldiisothiocyanat ($CS(NCS)_2$) blieben erfolglos.
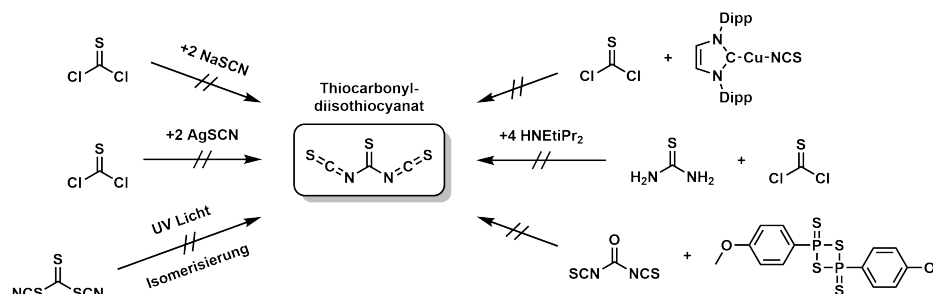
Schema 4.7: Syntheseversuche zur Darstellung von Thiocarbonyldiisothiocyanat.

4.1.4 Thiocarbonyldi(iso)selenocyanat

Die Synthese von Thiocarbonyldi(iso)selenocyanat ($CS(NCSe)_2$ oder $CS(SeCN)_2$) wurde ausgehend von Phosgen und Ammoniumselenocyanat versucht (Schema 4.8). Es besteht hier wiederum die Möglichkeit beide Konstitutionsisomere, Isoselenocyanat und Selenocyanat, zu erhalten. Drei Syntheseversuche wurden unternommen (Tabelle 4.4). Nach diesen Versuchen wurden zunächst die im Abschnitt Syntheseversuche zu *tert*-Butylcarbonyl(iso)selenocyanat erläuterten Synthesen durchgeführt. Die daraus erhaltenen Erkenntnisse sollten dann auf die Synthese von Thiocarbonyldi(iso)selenocyanat angewendet werden. Da bereits CO(SeCN) nicht isoliert werden konnte, wurden weitere Syntheseversuche erstmals ausgelassen.
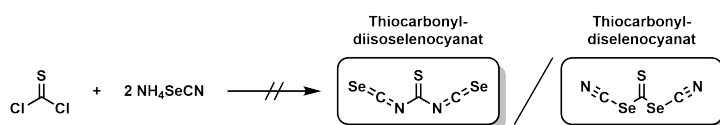
Schema 4.8: Syntheseversuche zur Darstellung von Thiocarbonyldiisoselenocyanat oder Thiocarbonyldiselenocyanat.

Die Synthese wurde zunächst im NMR-Maßstab je einmal in CD_3CN (XIVa) und in THF-d_8 (XIVb) durchgeführt. In beiden Fällen wurden im $^{13}C\{^1H\}$-NMR-Spektrum jeweils zwei Resonanzsignale detektiert (Abbildung 4.6). Die ersten Resonanzsignale bei 183.5 ppm und 185.8 ppm könnten einem $C{=}S$ Kohlenstoffatom (vgl. $CS(SCN)_2$: 189.8 ppm[78]) zugeordnet werden. Die zweiten Resonanzsignale bei 104.1 ppm und 103.2 ppm könnten

Tabelle 4.4: Reaktionsübersicht zu den Syntheseversuchen von Thiocarbonyldiisoseleno-cyanat oder Thiocarbonyldiselenocyanat.

Nummer	Edukt	Reaktant	Lösungsmittel	Temperatur
XIVa			CD_3CN	RT
XIVb	$COCl_2$	NH_4SeCN	THF-d_8	RT
XIVc			SO_2	−25 °C

im Vergleich mit den NMR-Daten aus Syntheseversuch **Va** (98.1 ppm) auf eine Seleno-cyanatgruppe (Se−*C*≡N) zurückzuführen sein. Es ist kein solvatisiertes Selenocyanat-Anion (vgl. Se*C*N⁻: 121.8 ppm[144]), aber eine exakte Interpretation der chemischen Verschiebungen bleibt aufgrund fehlender Literaturdaten wage. Die Synthese wurde in einem größeren Maßstab (4.6 mmol) in flüssigem Schwefeldioxid wiederholt. Es konnte aus dem Filterkuchen das Nebenprodukt NH_4Cl durch PXRD nachgewiesen werden. Mittels $^{13}C\{^1H\}$-NMR-Spektroskopie konnten jedoch nur $Se(CN)_2$ (90.5 ppm)[134] und SCSe (200.6 ppm)[145] detektiert werden. Wie zuvor für Carbonyldi(iso)selenocyanat beschrieben, war die Isolierung des Produktes nicht möglich und die Synthese wurde nicht weiter verfolgt.
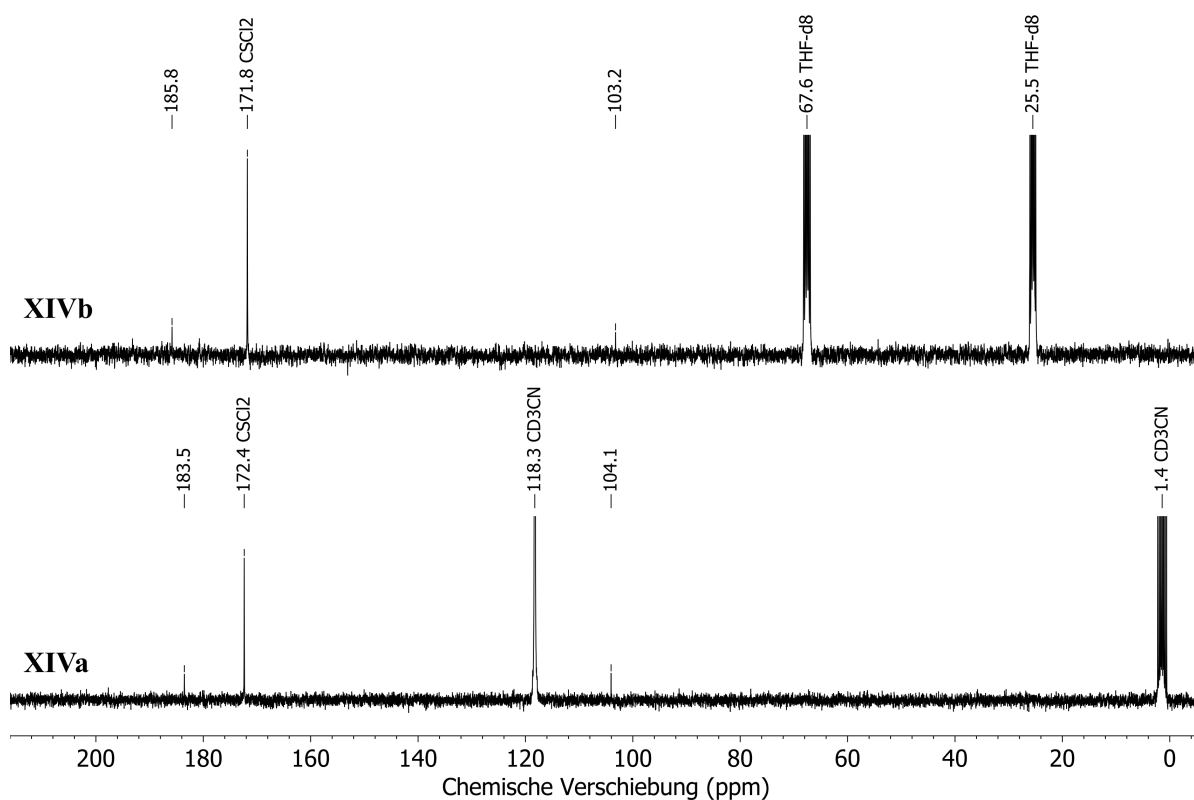
Abbildung 4.6: $^{13}C\{^1H\}$-NMR-Spektren der Reaktionen **XIVa** in CD_3CN und **XIVb** in THF-d_8.

4.2 Synthese von Oxalylchloridisothiocyanat und Chlorcarbonylisothiocyanat

In Abschnitt 3.1 konnte die Molekülstruktur von $(CONCS)_2$ aufgeklärt werden. Die Literatur beschreibt zusätzlich die Synthese einer einfachen Substitution von Oxalylchlorid $((COCl)_2)$ zu Oxalylchloridisothiocyanat $(Cl(CO)_2NCS)$ und dessen Decarbonylierung mit Aktivkohle zu Chlorcarbonylisothiocyanat $(CO(NCS)Cl)$[44] (Schema 4.9). Die Synthesen wurden zur Bestimmung der Molekülstrukturen im Festkörper reproduziert.
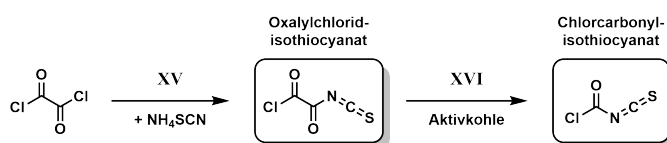
Schema 4.9: Synthese von Oxalylchloridisothiocyanat und dessen Decarbonylierung zu Chlorcarbonylisothiocyanat.

Aus dem ersten Syntheseschritt $(\mathbf{XV})$ wurde ein gelber Feststoff (Abbildung 4.7) erhalten. Dessen $^{13}C\{^{1}H\}$-NMR-Spektrum beinhaltet mehr Resonanzsignale als erwartet wurden (Abbildung 4.8). $Cl(CO)_2NCO$ wurde bei einer chemischen Verschiebung von 162.3 ppm ($N=C=S$), 153.7 ppm ($C=O$) und 153.4 ppm ($C=O$) detektiert.[44] Dazu sind Resonanzsignale geringer Intensität von der zweifachen Substitution zum $(CONCS)_2$ (156.8 ppm & 154.7 ppm) vorhanden,[44] welches als Nebenprodukt entstanden ist. Der dritte Signalsatz bei 184.4 ppm, 181.9 ppm und 167.5 ppm konnte 2-Chlorthiazol-4,5-dion (Abbildung 4.9), welches durch SC-XRD identifiziert wurde, zugeordnet werden. Weder das Molekül selbst, noch dessen Signalsatz im $^{13}C\{^{1}H\}$-NMR-Spektrum finden eine Erwähnung in der Literatur.[44,45] Das Entstehen dieses Moleküls bleibt ungeklärt, so dass versucht wurde mit einer anderen Synthese ausgehend von Oxalylchlorid und Silberthiocyanat[45] dessen Bildung zu verhindern. Nach dieser Synthese wurden die gleichen drei Produkte mittels $^{13}C\{^{1}H\}$-NMR-Spektroskopie (Abbildung 8.2) nachgewiesen.
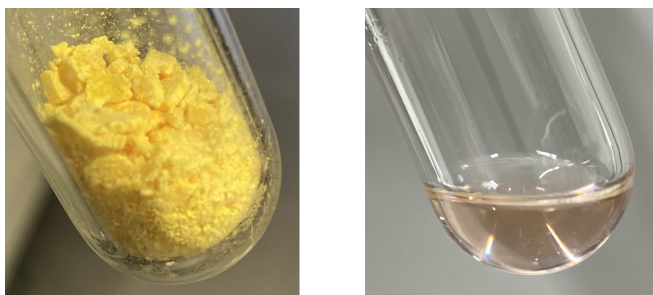
Abbildung 4.7: 2-Chlorthiazol-4,5-dion (links) und Chlorcarbonylisothiocyanat (rechts). Bilder zur Verfügung gestellt von SVEN RINGELBAND.
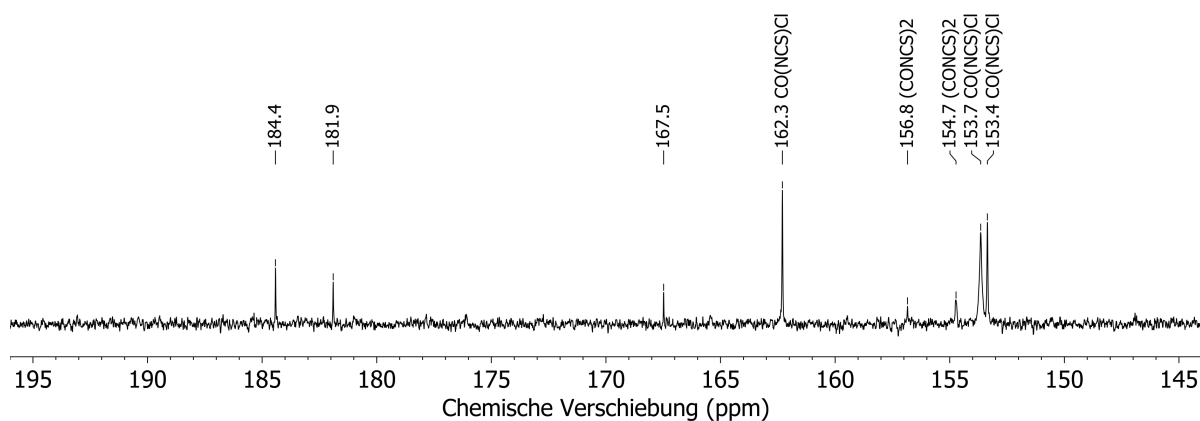
Abbildung 4.8: Ausschnitt aus dem ^{13}C{^{1}H}-NMR-Spektrum von Cl(CO)$_2$NCS in THF-d$_8$. Das vollständige Spektrum ist in Abbildung 8.1 abgebildet.

2-Chlorthiazol-4,5-dion kristallisiert im monoklinen Kristallsystem mit der Raumgruppe *P*2$_1$/*n* und den Gitterparamatern *a* = 5.8002(2) Å, *b* = 6.3811(2) Å, *c* = 13.5134(5) Å und β = 98.753(3)°. In der asymmetrischen Einheit befindet sich ein Molekül (*Z′* = 1) und vier in der Elementarzelle (*Z* = 4). Das Molekül ist nahezu planar mit dem größten Torsionswinkel von 4.7(7)° (O1−C1−C3−Cl1). Die C=O Bindungen sind 1.195(2) Å und 1.198(2) Å lang und damit identisch zu den C=O Bindungen in (CON$_3$)$_2$[80] und (CONCS)$_2$ (Abschnitt 3.1). Die C1−C2 Bindungslänge beträgt 1.558(2) Å und ist gleich zu der C−C Bindung in (CONCS$_2$) (1.554(3) Å). Durch das Ringsystem sind die restlichen Bindungslängen besser vergleichbar mit dem Chlor substituierten 1,3,5-Thiadiazin aus Abschnitt 3.4. In diesem betragen die C−S Bindungslängen 1.742(2) Å und 1.733(2) Å, wohingegen in 2-Chlorthiazol-4,5-dion C2−S1 1.782(2) Å und C3−S1 1.760(2) Å lang ist. Die C1−N1 Einfachbindung (1.414(3) Å) ist geringfügig länger als im Thiadiazin (1.392(3) Å & 1.404(3) Å). Gleiches gilt für die C3=N1 Doppelbindung mit 1.281(2) Å im Vergleich zu 1.261(3) Å des Thiadiazins. Die Verlängerung aller Bindungslängen ist auf das gespanntere Fünfringsystem im Vergleich zum Sechsring zurückzuführen. Gegensätzlich dazu ist die C3−Cl1 Bindungslänge mit 1.697(2) Å verkürzt (1.721(2) Å).
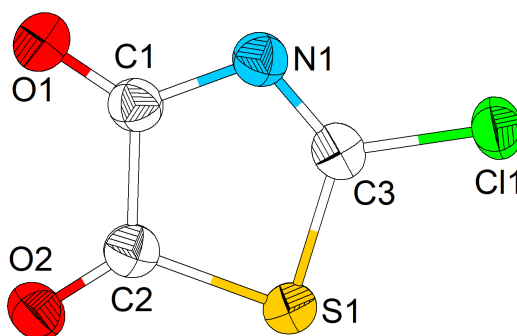
Abbildung 4.9: Molekülstruktur im Festkörper von 2-Chlorthiazol-4,5-dion. Ellipsoide sind mit einer Aufenthaltswahrscheinlichkeit von 75 % dargestellt.

Kristalle wurden durch Sublimation und Diffusionskristallisation erhalten und in beiden Fällen als 2-Chlorthiazol-4,5-dion identifiziert. Es stellte sich die Frage, ob der erhaltene Feststoff ausschließlich aus 2-Chlorthiazol-4,5-dion oder einer Mischung der durch NMR-Spektroskopie ermittelten drei Verbindungen ist. Aus den Daten der Molekülstruktur wurden mittels DFT Rechnungen IR- und Raman-Schwingungsbanden berechnet und mit dem gemessenen IR- und Raman-Spektrum verglichen (Abbildung 4.10). Der Vergleich zeigt, dass es sich bei dem Feststoff ausschließlich um 2-Chlorthiazol-4,5-dion handelt. Ausschlaggebend hier ist die ν_s(C3−N1) Streckschwingung bei 1500 cm^{-1} mit Schulter im Raman-Spektrum bei 1527 cm^{-1}, welche nur im Fünfringsystem von 2-Chlorthiazol-4,5-dion existiert. Weder $CO(NCS)_2$ noch $(CONCS)_2$ weisen diese Schwingung auf (Abschnitt 3.1) und somit ist diese in $Cl(CO)_2NCS$ ebenfalls nicht zu erwarten. Die zweite ν_s(C1−N1) Streckschwingung ist im IR-Spektrum bei 1142 cm^{-1} lokalisiert. Bei 1750 cm^{-1} werden die symmetrischen und asymmetrischen ν(C=O) Streckschwingungen inklusive Schulter bei 1770 cm^{-1} detektiert. Alle detektierten Banden können den spezifischen, berechneten Banden zugeordnet werden, so dass das Vorliegen einer zweiten Verbindung ausgeschlossen werden kann.
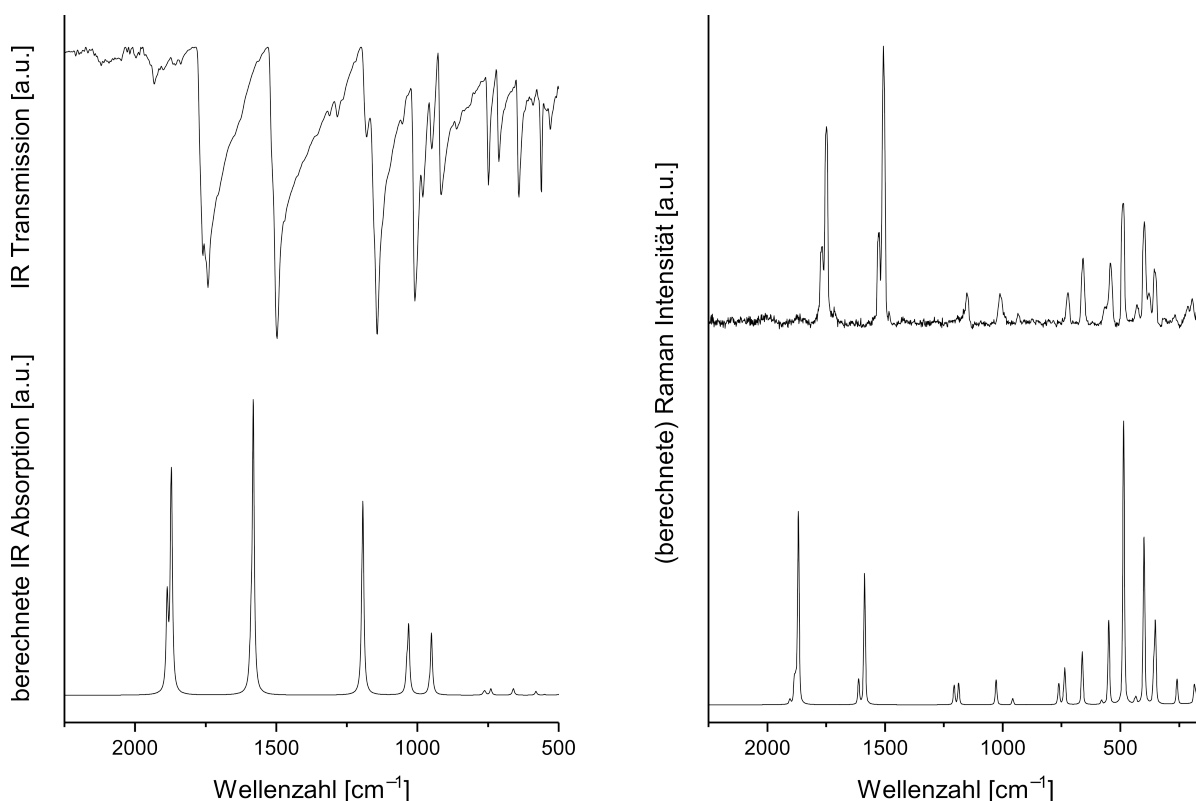
Abbildung 4.10: Vergleich des gemessenen IR- und Raman-Spektrums mit den aus DFT Analyse berechneten Spektren. Das gemessene Raman-Spektrum ist untergrundkorrigiert. Die vollständigen, gemessenen Spektren sind in Abbildung 8.16 und Abbildung 8.17 abgebildet.
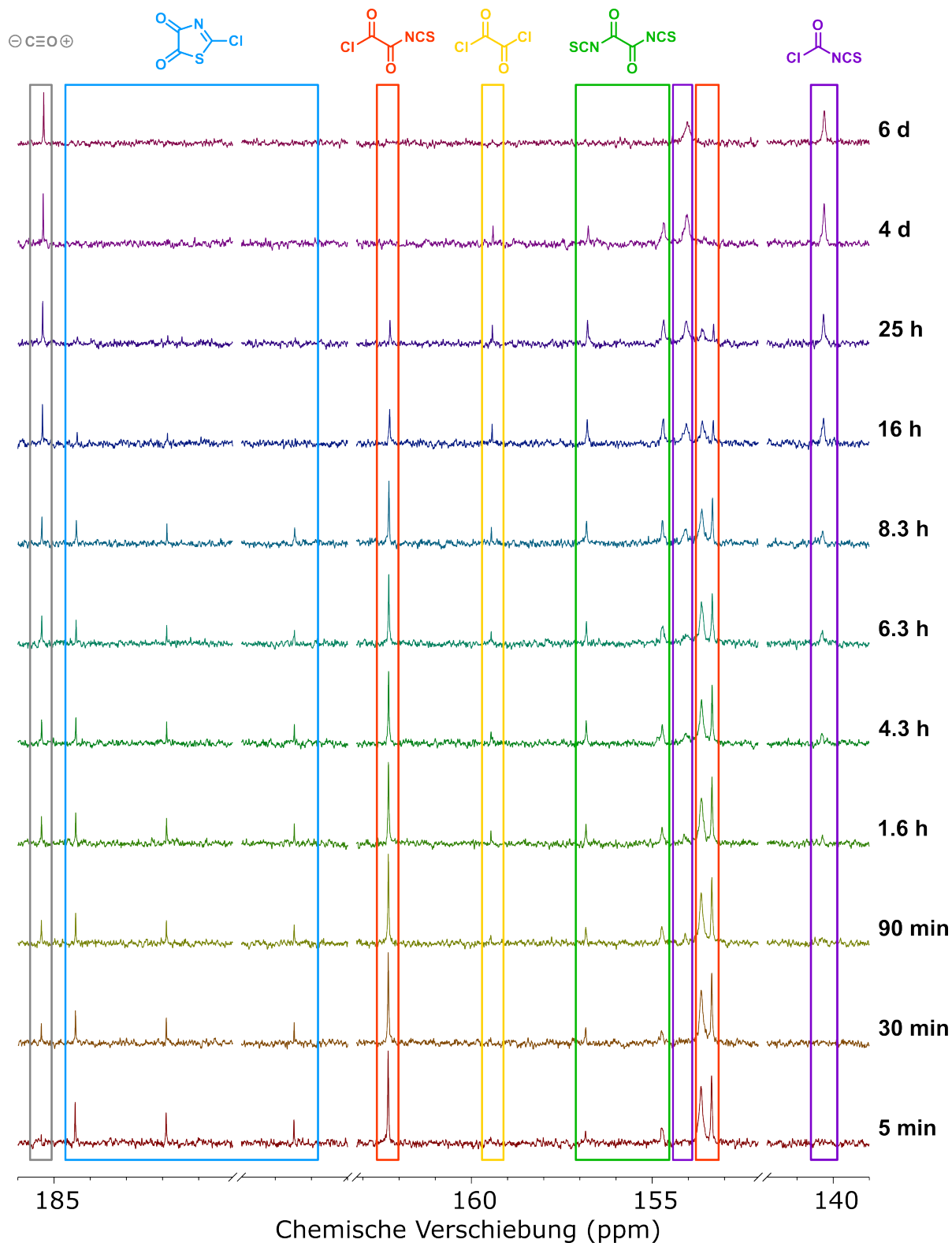
Abbildung 4.11: Zerfall von 2-Chlorthiazol-4,5-dion (blau) und Oxalylchloridisothiocyanat (orange) in Kohlenstoffmonoxid (grau) und Chlorcarbonylisothiocyanat (lila) und Dissoziation in Oxalylchlorid (gelb) und Oxalyldiisothiocyanat (grün) mittels $^{13}C\{^1H\}$-NMR-Spektroskopie in THF-d$_8$ beobachtet.

Die Erkenntnisse der schwingungsspektroskopischen Analysen lassen den Rückschluss zu, dass $Cl(CO)_2NCS$ erst in Lösung durch Ringöffnung und Umlagerung von 2-Chlorthiazol-4,5-dion entsteht. Wie dieser Reaktionsmechansimus von statten geht, kann ohne DFT Rechnungen nicht vorhergesagt werden. Es wurde versucht die Umlagerung mittels zeitabhängiger $^{13}C\{^{1}H\}$-NMR-Spektroskopie zu beobachten. Dazu wurde eine Lösung von 2-Chlorthiazol-4,5-dion luftdicht im NMR-Rohr verschlossen und wiederholt NMR spektroskopische Messungen durchgeführt (Abbildung 4.11). Anstelle der Umlagerung wurde der Zerfall beider Moleküle beobachtet. Direkt nach dem Lösen werden 2-Chlorthiazol-4,5-dion (184.4, 181.9 & 167.5 ppm), $Cl(CO)_2NCS$ (162.3, 153.6 & 153.3 ppm)[44] und Spuren von $(CONCS)_2$ (156.8 & 154.7 ppm)[44] detektiert. Bereits nach 30 min ist die Bildung von CO (189.8 ppm)[146] zu beobachten und nach 90 min werden erstmals CO(NCS)Cl (154.1 & 140.3 ppm)[44] und $(COCl)_2$ (159.4 ppm) detektiert. Die Signalintensität der zu 2-Chlorthiazol-4,5-dion gehörigen Resonanzsignale nimmt bereits nach 30 min ab, während für die Resonanzsignale von $Cl(CO)_2NCS$ erst nach 1.6 h eine Verringerung der Intensität festzustellen ist. Ersteres wird nach 24 h und letzteres nach 4 d nicht mehr detektiert. Nach 6 d sind nur noch CO und CO(NCS)Cl vorhanden.

Anhand dieser Beobachtungen kann davon ausgegangen werden, dass 2-Chlorthiazol-4,5-dion und $Cl(CO_2)NCS$ in einem Gleichgewicht zueinander stehen. Diese zerfallen entweder zu CO und CO(NCS)Cl oder dissoziieren in $(COCl)_2$ und $(CONCS)_2$ (Schema 4.10). Optisch ist zunehmend die Bildung eines roten Niederschlages und eine Rotfärbung der Lösung zu beobachten. Dies lässt auf die Bildung von Pararhodan $((SCN)_n)$ und die damit verbundene Zersetzung der Moleküle schließen.
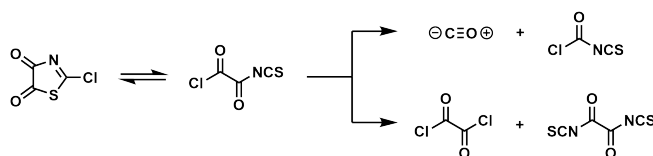
Schema 4.10: Zerfall und Dissoziation von 2-Chlorthiazol-4,5-dion und Oxalylchloridisothiocyanat.

Im Anschluss wurde die Decarbonylierung mittels Aktivkohle ($\mathbf{XVI}$, Schema 4.9) getestet. Chlorcarbonylisothiocyanat (CO(NCS)Cl) konnte als schwach rosafarbene Flüssigkeit (Abbildung 4.7) erhalten und mittels $^{13}C\{^{1}H\}$-NMR-Spektroskopie (Abbildung 4.12) nachgewiesen werden. Charakterisierung und Reaktivität der Moleküle, $Cl(CO)_2NCS$ und CO(NCS)Cl, wurde nicht weiter verfolgt und als Thema der Masterarbeit von SVEN RINGELBAND ausgegliedert.[147]
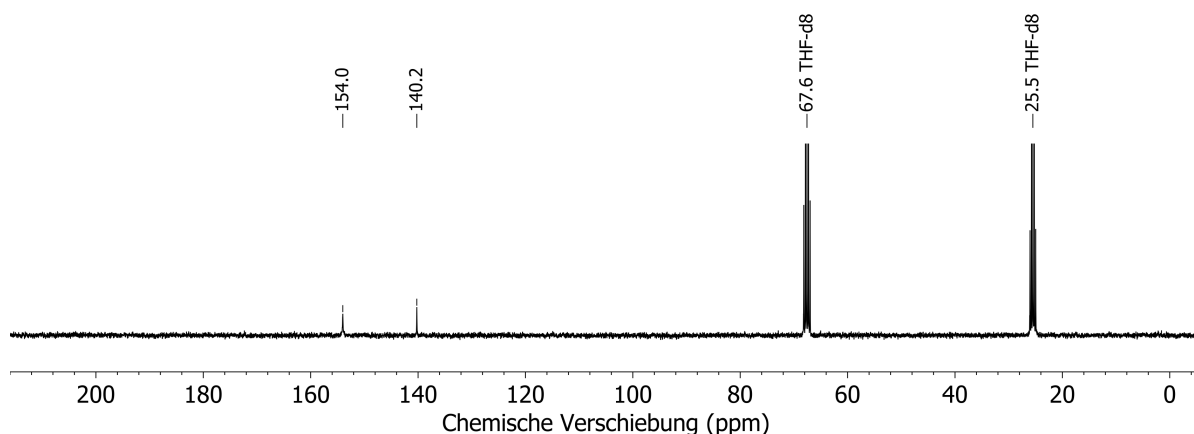
Abbildung 4.12: ^{13}C{^{1}H}-NMR-Spektrum von Chlorcarbonylisothiocyanat in THF-d$_8$.

## 4.3 [2+4]-Cycloadditionen von Carbonyldiisocyanat

In Abschnitt 1.4.3 wurde die Reaktivität von Carbonyldiisocyanat gegenüber Mehrfachbindungen in einer [2+4]-Cycloaddition beschrieben. In Vorarbeiten zur Bachelorarbeit von CELINA JAKOBI wurden drei Reaktionen dieser Art nach Literaturvorschriften[121,122] durchgeführt. Dazu wurde CO(NCO)$_2$ jeweils mit Cyclohexanon, *N,N'*-Dicyclohexylcarbodiimid und Phenylisocyanat umgesetzt. Die erhaltenen Produkte (Schema 4.11) wurden NMR spektroskopisch nachgewiesen (Abbildung 8.3, Abbildung 8.4 und Abbildung 8.5), konnten durch Elektrosprayionisation (ESI)-MS jedoch nicht gefunden werden. Kristallisation zur Untersuchung der Molekülstruktur im Festkörper setzte nicht ein. Die Reaktionen galten lediglich zur Überprüfung der Reproduzierbarkeit der Literaturvorschriften und wurden nicht weiter verfolgt.
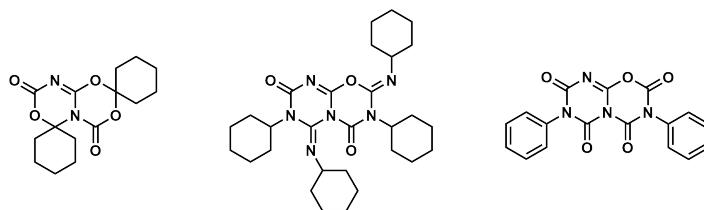
Schema 4.11: Von links nach rechts: Reaktionsprodukte der [2+4]-Cycloadditionen von Carbonyldiisocyanat mit Cyclohexanon, *N,N'*-Dicyclohexylcarbodiimid und Phenylisocyanat.

In ihrer Bachelorarbeit hat CELINA JAKOBI die [2+4] Cycloaddition von Carbonyldiisocyanat mit C–C Mehrfachbindungen untersucht,[148] welche unter meiner Anleitung und Betreuung durchgeführt wurde. Mit C=C Doppelbindungen konnte keine Reaktivität festgestellt werden, während mit C≡C Dreifachbindungen die Reaktionsprodukte nicht eindeutig identifiziert werden konnten. Dahingegen konnte aus der Reaktion mit Dimethylsulfoxid (SO(CH$_3$)$_2$) eine Reaktion mit der S=O Doppelbindung unter Abspaltung von

Kohlenstoffdioxid zum Carbonylbis(dimethylsulfimin) ($CO(NS(CH_3)_2)_2$) festgestellt werden (Schema 4.12). Die gleiche Reaktion sollte bei Verwendung von Carbonyldiisothiocyanat unter Abspaltung von Carbonylsulfid (COS) einsetzen. Diese wurde als explosionsartig beschrieben.[67]
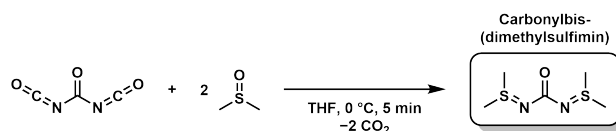
Schema 4.12: Synthese von Carbonylbis(dimethylsulfimin) entnommen aus der Bachelorarbeit von CELINA JAKOBI.[148]

4.4 Reaktivität von Carbonyldiisocyanat gegenüber Lithiumorganylen

In Abschnitt 3.5 und Abschnitt 3.6 konnte die Reaktivität von Carbonyldiisocyanat gegenüber Nukleophilen gezeigt werden, welche zu von Triuret ableitbaren Verbindungen der allgemeinen Formel $CO(NHCONu)_2$ (Nu = OR, SR, NR_2) führt. Bisher gibt es keine Versuche zur Reaktivität gegenüber nukleophilen Kohlenstoffatomen, die Diacylharnstoffe ($CO(NHCOR)_2$) bilden würden. Deshalb wurde $CO(NCO)_2$ mit den Lithiumorganylen MeLi (XVII) und nBuLi (XVIII) in Diethylether umgesetzt, um die deprotonierte Form von Diacetylharnstoff bzw. Dibutyrylharnstoff zu erhalten (Schema 4.13). Die Reaktionen wurden zusätzlich unter der Zugabe von 12-Krone-4 zur Sequestrierung des Lithium-Kations durchgeführt (Tabelle 4.5).
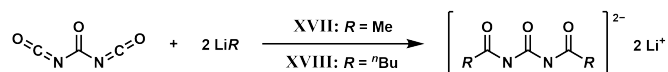
Schema 4.13: Syntheseversuche zur Umsetzung von Carbonyldiisocyanat mit Lithiumorganylen.

Aus allen vier Reaktionen wurden pulverförmige Feststoffe erhalten, die für eine stattgefundene Reaktion sprechen. Die Rückstände aus den Reaktionen XVII waren in gängigen Lösungsmitteln (CH_3CN, THF, CH_2Cl_2, Aceton, EtOAc) unlöslich. Es konnte lediglich ein geringer Teil in Pyridin-d_5 für die NMR spektroskopische Analyse gelöst werden. Das Pulver aus XVIIa zeigte pyrophores Verhalten an Luft und bei Zugabe von Chloroform wurde eine Reaktion beobachtet. Beide Beobachtungen deuten daraufhin, dass sich nicht abreagiertes, reines Methyllithium im isolierten Pulver befunden haben könnte. Im $^{13}C\{^1H\}$-NMR-Spektrum sind Resonanzsignale für die C=O Kohlenstoffe bei un-

Tabelle 4.5: Reaktionsübersicht zu den Syntheseversuchen zur Umsetzung von Carbonyl-diisocyanat mit Lithiumorganylen.

Nummer	Edukt	Reaktant	Additiv
XVIIa	CO(NCO)$_2$	MeLi	–
XVIIb			12-Krone-4
XVIIIa	CO(NCO)$_2$	*n*BuLi	–
XVIIIb			12-Krone-4

gefähr 173 ppm und 150 ppm[149] zu erwarten. Aufgrund der geringen Löslichkeit konnte nur ein Resonanzsignal bei 16.0 ppm (Abbildung 8.6) in **XVIIa**, welches einer Methylgruppe entspricht, und ausschließlich 12-Krone-4 (71.4 ppm) (Abbildung 8.7) in **XVIIb** detektiert werden. Im Pulver aus **XVIIIa** konnten sowohl im ^{1}H-NMR, als auch ^{13}C{^{1}H}-NMR-Spektrum Hinweise auf eine Butylgruppe gefunden werden (Abbildung 4.13). Die chemischen Verschiebungen in letzterem (68.7, 42.9, 26.6 & 14.7 ppm oder 68.4, 40.3, 26.3 & 14.4 ppm) sind im Vergleich zu Pentanamid (34.8, 27.3, 21.8 & 13.7 ppm[150]) zu sehr im Tieffeld gelegen, als dass sie dem gesuchten Produkt zugeordnet werden könnten. In den NMR-Spektren von **XVIIIb** wurde erneut ausschließlich 12-Krone-4 detektiert (Abbildung 8.9).
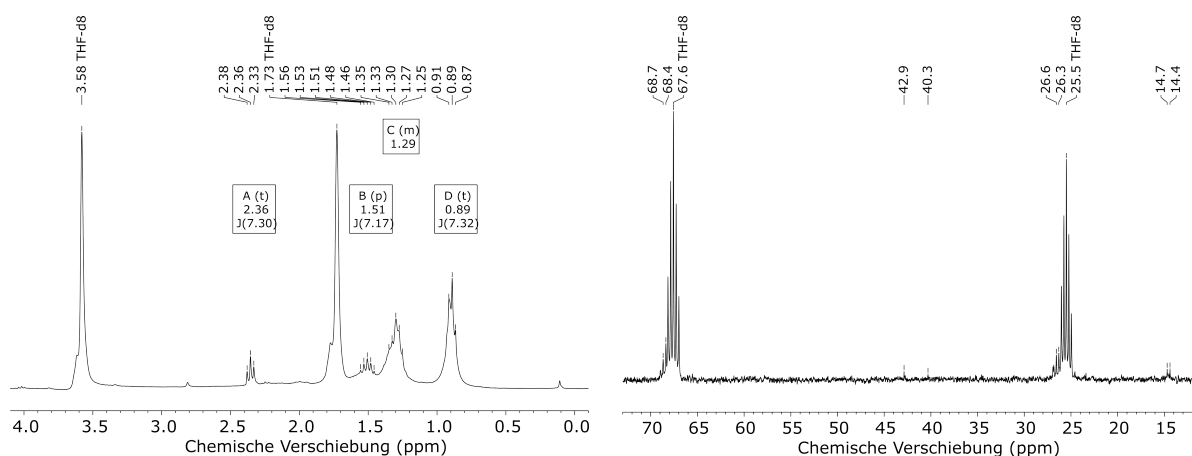

Abbildung 4.13: Ausschnitt aus dem ^{1}H-NMR (links) und ^{13}C{^{1}H}-NMR-Spektrum (rechts) des Pulvers aus Reaktion **XVIIIa** in THF-d$_8$. Die vollständigen Spektren sind in Abbildung 8.8 abgebildet.

Zur besseren Einsicht wurden IR-Spektren zur Detektion von C=O Streckschwingungsbanden aufgenommen. Diese werden bei ca. 1750 cm^{-1} erwartet.[151] In den IR-Spektren der Pulver (Abbildung 4.14) konnten keine Banden, welche einer C=O Schwingung im Bereich 1700 cm^{-1} entsprechen, gefunden werden. Banden im Bereich von 3000 cm^{-1}, 1600 cm^{-1} und 1400 cm^{-1} können den Lösungsmitteln Diethylether und *n*-Hexan zugeordnet werden.[152] Die unteren beiden Spektren weisen zudem je eine scharfe Bande

bei $1082\,\text{cm}^{-1}$ auf, welche 12-Krone-4 zuzuordnen ist.[152] Die Bande bei $2200\,\text{cm}^{-1}$ liegt im Bereich einer $N{=}C{=}O$ Streckschwingung[153] und könnte einem Nebenprodukt wie LiOCN entstammen. Weder die NMR, noch IR spektroskopischen Daten geben ausreichend Hinweise auf eine erfolgreiche Synthese. Die Herangehensweise wurde deshalb leicht abgeändert.
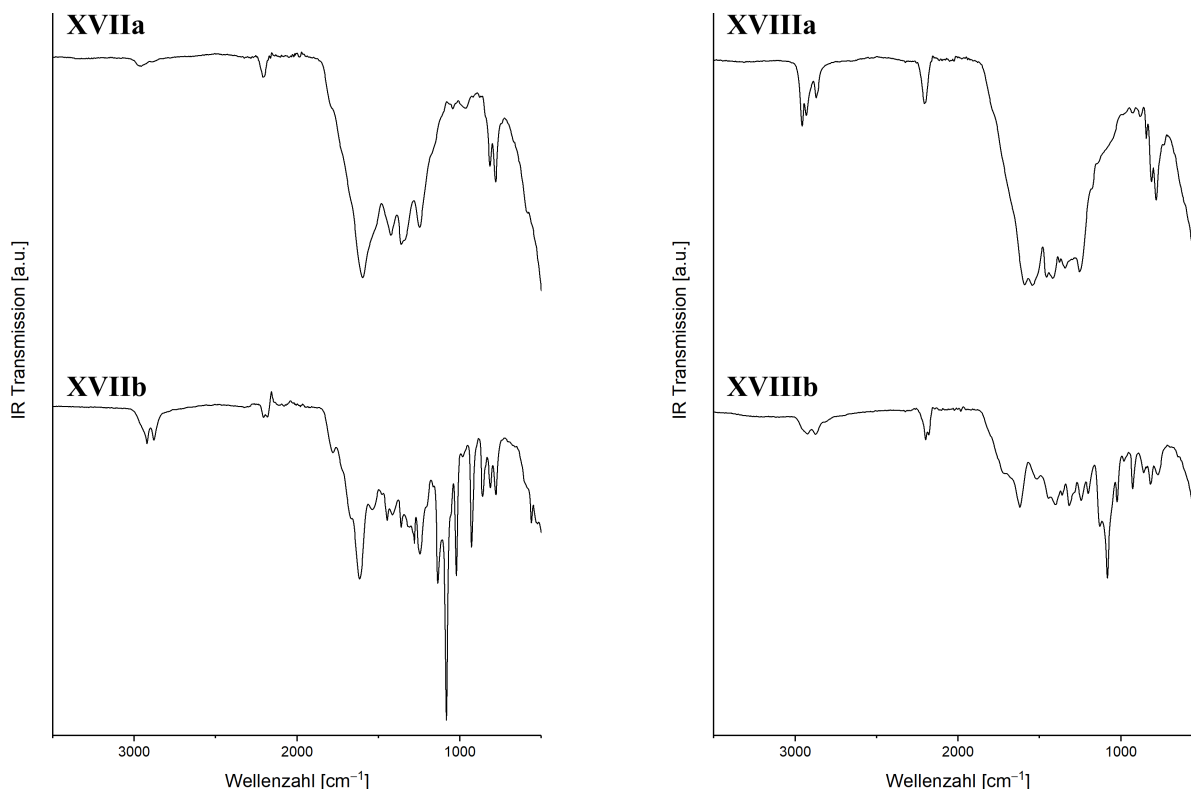

Abbildung 4.14: IR-Spektren von den Pulvern der Reaktionen **XVII** (links) und **XVIII** (rechts).

Aus der Reaktion von $CO(NCO)_2$ mit Methanol[72] wird das bekannte Dimethyl-*N,N'*-carbonylbis(carbamat) erhalten. In einer Umsetzung mit Lithiummethanolat (LiOMe) wurde versucht das Strukturmotiv in seiner deprotonierten Form zu bilden (Schema 4.14). Erneut wurde eine Reaktion ohne (**XIXa**) und mit (**XIXb**) 12-Krone-4 durchgeführt. In den erhaltenen Pulvern konnte im $^{13}\text{C}\{^1\text{H}\}$-NMR-Spektrum (Abbildung 8.10 und Abbildung 8.11) jeweils ein Resonanzsignal entsprechend einer Methoxygruppe bei $53.0\,\text{ppm}$, aber keine Resonanzsignale einer Carbonylgruppe detektiert werden.
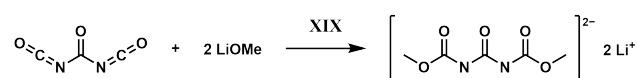

Schema 4.14: Syntheseversuche zur Umsetzung von Carbonyldiisocyanat mit Lithiummethanolat.

Es ist nicht auszuschließen, dass Carbonyldiisocyanat mit Lithiumorganylen reagiert, die dabei gebildeten anionischen Moleküle allerdings zu instabil sind und sich zersetzen. Hier hätte nach der Zugabe des Lithiumorganyls eine Säure zugegeben werden können, um eine Protonierung zu bereits bekannten Molekülen zu erreichen. Diese Reaktionsführung ist dann ein direkter Nachweis für die gesuchte Reaktivität. Gleichzeitig könnte versucht werden Diacylharnstoffe oder Carbonylbis(carbamate) einfach oder zweifach zu deprotonieren, um die Existenz dieser Anionen zu validieren.

4.5 Koordinationsverhalten von Carbonyldiisocyanat gegenüber Übergangsmetallbisamiden

Carbonyldiisocyanat kann in verschiedenen Resonanzstrukturen vorliegen und besitzt freie Elektronenpaare mit denen es potentiell an Metalle koordinieren könnte (Schema 4.15). Dabei ist eine einfache Koordination über das Carbonylsauerstoffatom oder eine zweifache Koordination entweder jeweils über das Sauerstoffatom der Carbonyl- und Isocyanatgruppe, oder über das Carbonylsauerstoffatom und das Isocyanatstickstoffatom denkbar. Ein Koordinationsverhalten, wie es für Carbonyldicyanid beobachtet wurde (Abschnitt 1.4.2), ist auch im Rahmen des Erwartbaren. Bisher gibt es keine Untersuchungen bezüglich des Koordinationsverhaltens von Carbonyldiisocyanat oder -diisothiocyanat.
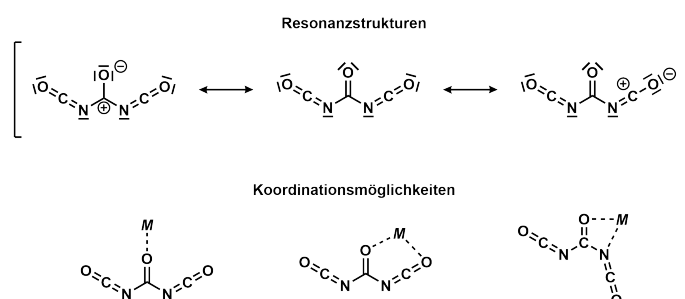

Schema 4.15: Ausgewählte Resonanzstrukturen von Carbonyldiisocyanat und potentielle Koordinationsmöglichkeiten an Metallzentren.

Das Koordinationsverhalten von Carbonyldiisocyanat wurde untersucht, indem es mit Übergangsmetallkomplexen umgesetzt wurde. Dazu wurden die Eisenbisamid-Komplexe $Fe(N(TMS)_2)_2$ (Trimethylsilyl (TMS)) und $Fe(N(Dipp)(TMS))_2$ (2,6-Diisopropylphenyl (Dipp)) gewählt, da diese erstens freie Koordinationsstellen besitzen und zweitens in unpolaren Lösungsmitteln wie Toluol löslich sind. Für die Untersuchungen ist ein unpolares Lösungsmittel notwendig, da polare Lösungsmittel wie THF oder Diethylether in Konkurrenz als Liganden zu Carbonyldiisocyanat stehen.

In der Umsetzungen mit $Fe(N(TMS)_2)_2$ konnte eine Reaktion beobachtet werden, führte aber nicht zur verwertbaren analytischen Ergebnissen. Im $^{13}C\{^1H\}$-NMR-Spektrum konnten keine Signale und mittels IR-Spektroskopie nur Banden des Eduktes detektiert werden.

Die Reaktion mit $Fe(N(Dipp)(TMS))_2$ führte dagegen zu unerwarteten Ergebnissen. Es konnten grün-türkise Kristalle aus der Reaktionslösung kristallisiert werden. Mittels SC-XRD wurde die Struktur ermittelt, welche offenbarte, dass die Liganden am Eisenion (N(Dipp)(TMS)) mit $CO(NCO)_2$ zu einem *N,N'*-Carbamoylharnstoff (*N,N'*-Bis(**d**iisopropylphenyl)-*N,N'*-di**t**rimethylsilyl**c**arbamoyl**h**arnstoff (DTCH)), welches ein substituiertes Biuret ist, reagiert haben (Schema 4.16). Bei der Reaktion ist formal Eisen(II)cyanat als Nebenprodukt entstanden und der Eisen(II)-Komplex $Fe(DTCH)_2$ wurde als Produkt isoliert.
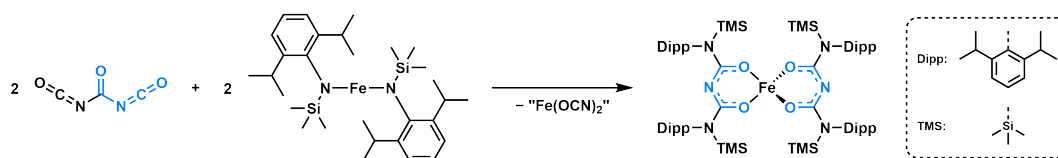
Schema 4.16: Reaktionsverlauf von Carbonyldiisocyanat mit $Fe(N(Dipp)(TMS))_2$ zum ersten Eisen-Biuretderivat-Komplex $Fe(DTCH)_2$.

Die Synthesen wurden versucht auf weitere Übergangsmetalle und Carbonyldiisothiocyanat zu übertragen. Dazu wurden $CO(NCO)_2$ und $CO(NCS)_2$ mit $M(N(Dipp)(TMS))_2$ (M = Fe, Co, Ni) in Toluol umgesetzt. Die Synthese von $Fe(DTCH)_2$ konnte reproduziert werden. Aus den restlichen Synthesen konnten keine Kristalle gewonnen werden, obwohl in allen Fällen eine Reaktion durch einen Farbumschlag und Gasentwicklung beobachtet wurde. Bei den Reaktionen von $CO(NCS)_2$ mit $Ni(N(Dipp)(TMS))_2$ und $Fe(N(Dipp)(TMS))_2$ hat eine Polymerisation stattgefunden, so dass ein Gel erhalten wurde. Aus den Rückständen des Gels mit $Ni(N(Dipp)(TMS))_2$ konnte mittels *Liquid Injection Field Desorption Ionization* (LIFDI) MS (Abbildung 4.15) der gesuchte Komplex detektiert werden. Dieser hat eine berechnete Masse von $1222.60927 \, g \, mol^{-1}$ und wurde bei einem Masse-zu-Ladung-Verhältnis von *m/z* 1222.61211 detektiert. Es gibt aufgrund fehlender Kristallisation keine weiteren Hinweise auf die erfolgreiche Synthese. Es ist anzunehmen, dass die Reaktion und Kristallisation sehr langsam erfolgen, da nach sechs Wochen erstmals winzige Kristallite im Reproduktionsversuch beobachtet werden konnten. Eine Erhöhung der Kristallisationszeit oder Konzentration könnte bei allen Versuchen zu den gewünschten Produkten führen.
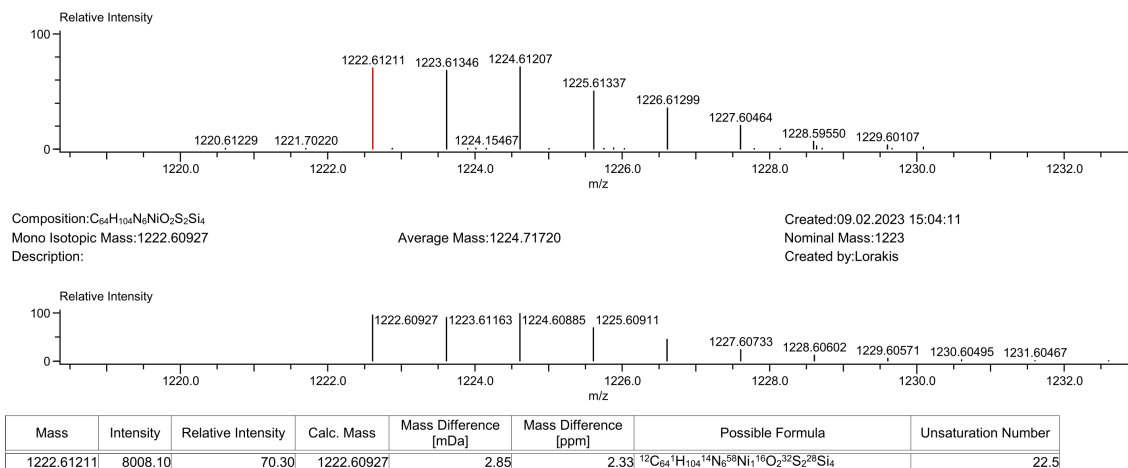
Abbildung 4.15: Hochauflösung des LIFDI Massenspektrums aus den Rückständen der Umsetzung von CO(NCS)$_2$ mit Ni(N(Dipp)(TMS))$_2$.

Fe(DTCH)$_2$ kristallisiert im monoklinen Kristallsystem mit der Raumgruppe *C*2/*c*. In der asymmetrischen Einheit befindet sich ein halbes Individuum (*Z'* = 0.5) und in der Elementarzelle sind vier Moleküle (*Z* = 4). Die Gitterparameter sind *a* = 31.9731(11) Å, *b* = 9.8071(5) Å, *c* = 23.2858(8) Å und β = 105.638(3)°. In der Literatur sind einige Komplexe mit Biuret als Ligand beschrieben. Diese weisen alle eine oktaedrische Koordination von zwei Biuret-Molekülen und je zwei Gegenionen oder Wassermolekülen auf.[154–157] Fe(DTCH)$_2$ ist der erste Komplex mit sowohl einem substituierten Biuret-Liganden, als auch tetraedrischer Koordination. Das Eisenion ist verzerrt tetraedrisch von zwei Liganden über je zwei Sauerstoffatome koordiniert Abbildung 4.16. Die Koordination wird durch die Parameter τ_4 = 0.78 und τ'_4 = 0.67 verdeutlicht. Für beide Parameter entspricht ein Wert von 1 einer tetraedrischen und 0 einer quadratisch-planaren Koordination. Die berechneten Werte ergeben somit eine zur tetraedrischen Anordnung ähnliche Koordination.

Der Ligand ist im Vergleich zu den Komplexen der Literatur ein anionisches Biuret-Derivat. Dies ermöglicht eine Deloklalisierung der Elektronen über das O1−C1−N1−C2−O2 Gerüst, was in den Bindungslängen (Tabelle 4.6) deutlich wird. Die C=O Bindungen (1.289(2) Å & 1.286(2) Å) sind länger als in Biuret (1.241(3) Å & 1.231(3) Å[21]) oder dem Komplex [Ni(Biuret)$_2$(H$_2$O)$_2$]Cl$_2$ (1.243(4) Å − 1.245(4) Å[156]). Dahingegen sind die C−N Bindungen mit 1.332(2) Å und 1.338(2) Å kürzer als in Biuret (1.380(3) Å & 1.384(3) Å[21]) oder dem Nickel-Komplex (1.375(5) Å − 1.385(4) Å[156]). Sowohl die Werte für die C=O als auch die C−N Bindungen liegen damit zwischen der Bindungslänge einer typischen Doppel- (r_{kov}(C=O): 1.24 Å, r_{kov}(C=N): 1.27 Å[158]) oder Einfachbindung (r_{kov}(C−O): 1.38 Å, r_{kov}(C−N): 1.46 Å[158]). Beide Bindungen weisen einen höheren Doppelbindungscharakter auf, was für eine Delokalisierung der negativen Ladung am Ligandsystem spricht. Die Fe−O Bindungslängen von 1.969(1) Å und 1.973(1) Å sind vergleichbar zu den den Ni−O
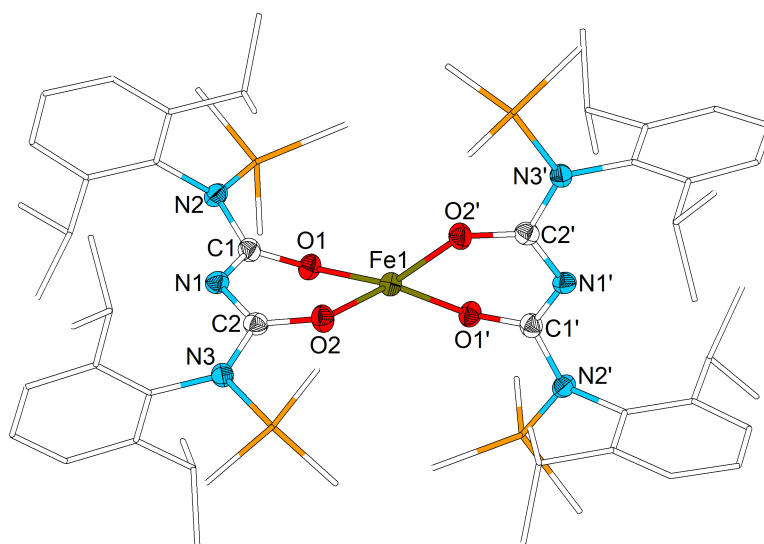
Abbildung 4.16: Molekülstruktur im Festkörper von Fe(DTCH)$_2$. Ellipsoide sind mit einer Aufenthaltswahrscheinlichkeit von 50 % dargestellt. Der Übersichtlichkeit halber sind das Ligandenrückgrat in *stick and wire* Model und Wasserstoffatome nicht abgebildet.

Bindungslängen mit 2.015(3) Å – 2.024(2) Å.[156] An den Bindungswinkeln ist die unterschiedliche Koordination erkenntlich. Während im Nickel-Komplex alle Winkel mit ca. 90° der oktaedrischen Koordination entsprechen, wird in Fe(DTCH)$_2$ die Verzerrung der tetraedrischen Koordination deutlich. Der O1 – Fe1 – O2 Winkel innerhalb des selben Liganden beträgt 87.88(5)° und der ligandenübergreifende O1 – Fe1 – O2 Winkel 142.87(4)°. Dies führt ebenso zu einer Verdrehung innerhalb des Liganden weg von der Planarität, welches durch den O1 – C1 – C2 – O2 Torsionswinkel von 35.9(1)° ersichtlich ist.

Tabelle 4.6: Ausgewählte Bindungslängen und Bindungswinkel von Fe(DTCH)$_2$ im Vergleich zu Biuret[21] und [Ni(Biuret)$_2$(H$_2$O)$_2$]Cl$_2$.[156]

Bindung [Å]	Fe(DTCH)$_2$	Biuret[21]	[Ni(Biuret)$_2$(H$_2$O)$_2$]Cl$_2$[156]
Fe1 – O1/O2	1.969(1)/1.973(1)	–	2.015(3)–2.024(2)
C1 – O1/C2 – O2	1.289(2)/1.286(2)	1.241(3)/1.231(3)	1.243(4)–1.245(4)
N1 – C1/C2	1.332(2)/1.338(2)	1.380(3)/1.384(3)	1.375(5)–1.385(4)
C1 – N2/C2 – N3	1.367(2)/1.360(2)	1.315(3)/1.330(3)	1.314(6)–1.333(4)

Winkel [°]	Fe(DTCH)$_2$	Biuret	[Ni(Biuret)$_2$(H$_2$O)$_2$]Cl$_2$[156]
O1 – Fe1 – O2	87.88(5)/142.87(4)	–	87.61(9)/87.54(8)
O1 – Fe1 – O1	106.91(7)	–	91.35(9)
O2 – Fe1 – O2	100.66(7)	–	93.51(8)
C1 – N1 – C2	118.4(1)	128.0(2)	127.3(3)/127.3(3)
O1 – C1 – C2 – O2	35.9(1)	4.6(3)	1.4(3)/0.9(3)

4.6 Weitere Verbindungen und Molekülstrukturen

Im Laufe der Bearbeitungszeit dieser Dissertation konnten einige Molekülstrukturen im Festkörper bestimmt werden, welche keine direkte Relevanz für die Synthesen der CD*PsH* haben. Sie geben dennoch Hinweise auf in Lösung vorliegende Spezies bei den Studien zur Reaktivität von CD*PsH* gegenüber Nukleophilen. Im Besonderen sind es Nebenprodukte aus Reaktionen mit Carbonyldiisocyanat und Carbonyldiisothiocyanat. Sie sollen deshalb hier vorgestellt werden.

4.6.1 2,4,6-Trioxo-1,3,5-oxadiazin

Aus der Reaktion zwischen Carbonyldiisocyanat und Wasser entsteht 2,4,6-Trioxo-1,3,5-oxadiazin.[69,72] Die Synthese konnte reproduziert (Schema 4.17) und eine vollständige Analytik erhalten werden. Im Anhang sind das ^{1}H- und ^{13}C{^{1}H}-NMR-Spektrum (Abbildung 8.13), sowie das IR-Spektrum (Abbildung 8.19) abgebildet. Es konnte aus Schwefeldioxid durch langsames Verdampfen zufällig kristallisiert werden. Es wurde ein einziger Kristall gewonnen, welcher mittels SC-XRD untersucht wurde. Während der Messung kam es zu einem Gerätefehler, welcher zur Zersetzung dieses Kristalls und zu einem unvollständigen Datensatz führte. Erneute Kristallisation war nicht möglich. Die nachfolgende Diskussion der Molekülstruktur ist vorsichtig vor allem im Bezug auf die Bindungslängen als nicht endgültig zu betrachten. Die Identität ist durch die zusätzliche Analytik gewährleistet.
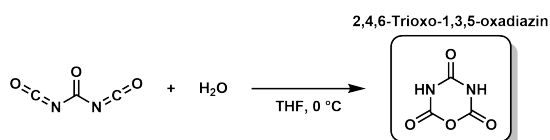
Schema 4.17: Synthese von 2,4,6-Trioxo-1,3,5-oxadiazin aus Carbonyldiisocyanat und Wasser.

2,4,6-Trioxo-1,3,5-oxadiazin (Abbildung 4.17) kristallisiert im orthorhombischen Kristallsystem mit der Raumgruppe *Pnma* und vier Molekülen pro Elementarzelle (Z = 4). In der asymmetrischen Einheit befindet sich ein halbes Molekül (Z' = 0.5). Die Gitterparameter sind a = 8.0350(8) Å, b = 11.9026(10) Å und c = 4.8887(5) Å. Es kristallisiert isotyp zu dem literaturbekannten 3,5-Dimethyl-2,4,6-trioxo-1,3,5-oxadiazin.[159] Das Molekül ist planar mit einem Torsionswinkel C1−N1−C2−O2 von 0.5(14) Å. Die C=O Bindungslängen betragen 1.242(13) Å (C1=O1) und 1.222(12) Å (C2=O3) und sind damit länger als in der Literatur (1.201(2) Å & 1.192(2) Å[159]) beschrieben. Die C−N Bindungen sind mit 1.350(10) Å (C1−N1) und 1.328(12) Å (C2−N1) dazu gegensätzlich kürzer als

zur Vergleichsverbindung (1.380(1) Å & 1.359(1) Å[159]). Einzig die C2−O2 Bindungslänge (1.362(10) Å) zeigt im Rahmen der Standardabweichung keine Differenz (1.366(1) Å[159]).
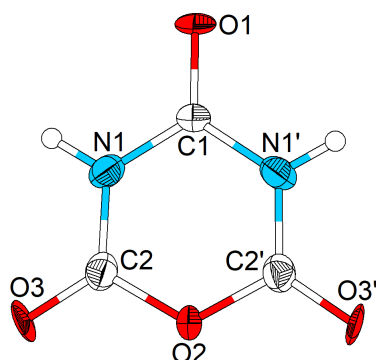

Abbildung 4.17: Molekülstruktur im Festkörper von 2,4,6-Trioxo-1,3,5-oxadiazin. Ellipsoide sind mit einer Aufenthaltswahrscheinlichkeit von 50 % und Wasserstoffatome mit willkürlichem Radius dargestellt.

4.6.2 Isocyanursäure und Biuret

Bei dem Versuch die Koordination von Carbonyldiisocyanat an Lithiumchlorid zu testen, sind in einem NMR-Rohr durch langsames Verdampfen des Lösungsmittels Kristalle gewachsen. Diese wurden röntgendiffraktometrisch analysiert und stellten sich als eine Verbindung aus **I**so**c**yanur**s**äure (ICS) und Biuret (**I**mido**dic**arbonsäure**dia**mid (IDC-DA)) heraus (Abbildung 4.18). Die Moleküle Isocyanursäure×Biuret×H$_2$O (ICS-IDCDA) kristallisieren zusammen in der Raumgruppe *P*$\overline{1}$ des triklinen Kristallsystems. Die asymmetrische Einheit besteht aus je zwei Molekülen Isocyanursäure und Biuret, sowie einem Molekül Wasser (*Z*′ = 1). In der Elementarzelle befinden sich insgesamt zehn Moleküle (*Z* = 2). Die Gitterparameter ergeben sich zu *a* = 8.260(4) Å, *b* = 10.905(4) Å, *c* = 11.919(5) Å, α = 67.17(3) °, β = 79.78(3) ° und γ = 69.80(3) °. Die Moleküle sind über Wasserstoffbrückenbindungen (H-Brücken) miteinander vernetzt und spannen eine Ebene [0.75 −0.26 −0.60] auf. Die zwei ICS-Moleküle sind über zwei intermolekulare H-Brücken (O3···HN7 & O6···HN5) miteinander verknüpft. Beide IDCDA-Moleküle weisen eine intramolekulare H-Brücke (O2···HN1 & O10···HN10) auf und sind miteinander über zwei intermolekulare Bindungen (O1···HN10 & O9···HN1) verbrückt. Jedes ICS-Molekül weist vier H-Brücken zu drei IDCDA-Molekülen (4×1: O4···HN12 & O2···HN6, O7···HN3 & O10···HN8; 2×2: O3···HN2 & O1···HN4, O6···HN11 & O9···HN9) auf. Zuletzt werden die beiden ICS-Moleküle über das Wassermolekül miteinander (O5···HO11 & O8···HO11) verknüpft. In Summe ergeben sich so 16 verschiedene Wasserstoffbrückenbindungen und ein komplexes H-Brücken-Netzwerk.
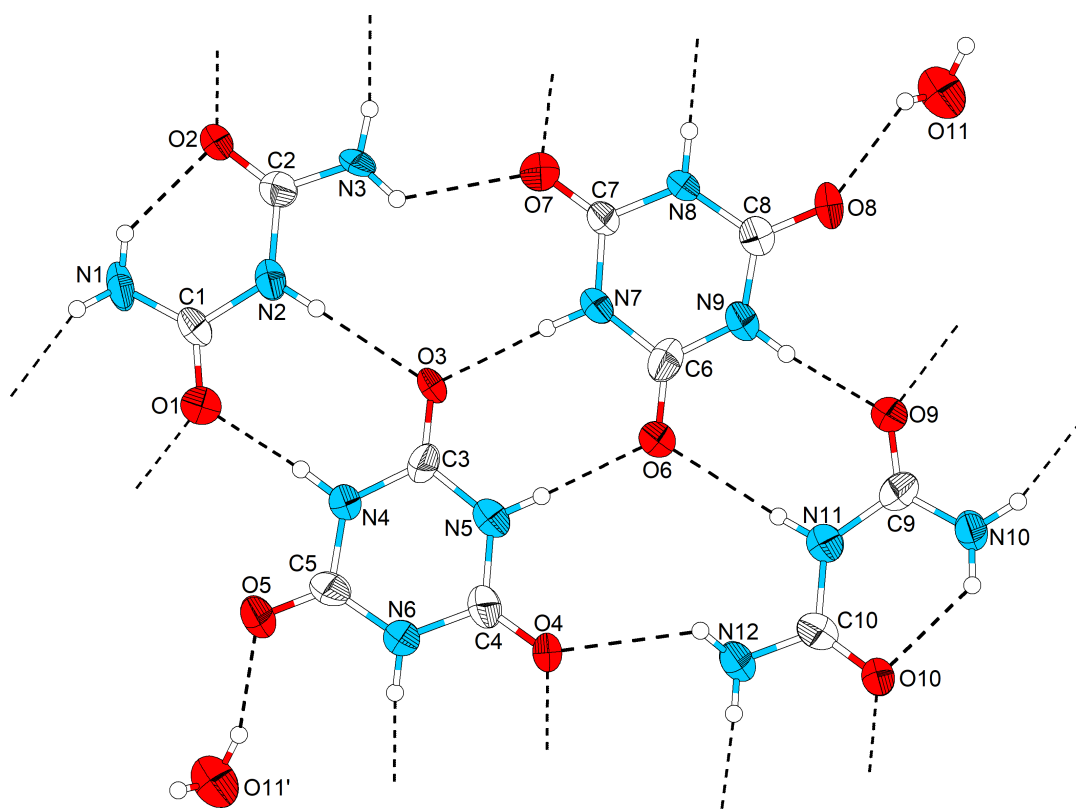
Abbildung 4.18: Molekülstruktur im Festkörper von Isocyanursäure×Biuret×H_2O. Ellipsoide sind mit einer Aufenthaltswahrscheinlichkeit von 50 % und Wasserstoffatome mit willkürlichem Radius dargestellt.

Die Qualität des Datensatzes (R_{int} = 24.57 %, R_1 = 10.04 %, wR_2 = 40.00 %) ist für eine ausführliche Bindungsanalyse unzureichend, weshalb die Werte der Bindungslängen in Tabelle 4.7 den Literaturwerten von Isocyanursäure und Biuret gegenübergestellt sind. In ICS-IDCDA sind sowohl die C=O (1.213 Å – 1.251 Å), als auch C–N (1.297 Å – 1.417 Å) Bindungslängen über einen größeren Bereich verteilt, als es den Literaturangaben (C=O: 1.216 Å – 1.241 Å & C–N: 1.315 Å – 1.384 Å[21,160]) zu entnehmen ist. Dies kann zum einen von dem Datensatz selbst oder zum anderen von dem ausgedehnten Wasserstoffbrückennetzwerk in ICS-IDCDA herbeigeführt sein. Alle Bindungslängen befinden sich dennoch im Bereich für Einfach- oder Doppelbindungen (r_{kov}(C=O): 1.24 Å, r_{kov}(C–N): 1.46 Å[158]). Die Abstände der Atome zwischen denen H-Brücken gebildet werden überspannen einen Bereich von ca. 1.89 Å – 2.45 Å. Die intermolekularen Atomabstände sind deutlich größer als in den vergleichbaren Molekülstrukturen (max. 2.050 Å[21,160]), aber immer noch kleiner als die Summe der Van-der-Waals Radien (r_{VdW}(H–O): 2.70 Å[161]).

Tabelle 4.7: Bindungslängen von ICS-IDCDA den Werten von Isocyanursäure[160] und Biuret[21] im Vergleich gegenübergestellt.

Bindung [Å]	ICS-IDCDA	Isocyanursäure[160]	Biuret[21]
$C=O_{ICS}$	1.213(13)–1.251(16)	1.2165(5)/1.2230(3)	–
$C-N_{ICS}$	1.343(14)–1.394(11)	1.3692(4)–1.3727(4)	–
$C=O_{IDCDA}$	1.214(15)–1.244(11)	–	1.231(3)/1.241(3)
$C-N_{IDCDA}$	1.297(11)–1.417(17)	–	1.315(3)–1.384(3)
$O{\cdots}H_{intra}$	2.023(9)/2.061(8)	–	1.920(20)
$O{\cdots}H_{inter}{}^a$	2.222(9)/2.431(9)	–	1.947(18)–2.050(17)
$O{\cdots}H_{inter}{}^b$	2.013(7)/2.015(7)	1.8823(8)/1.9019(5)	–
$O{\cdots}H_{inter}{}^c$	1.886(6)–2.445(6)	–	–

a: IDCDA···IDCDA, b: ICS···ICS, c: ICS···IDCDA

4.6.3 Monosubstituierte Derivate der Isocyanursäure

Aus Umsetzungen von Carbonyldiisocyanat mit Nukleophilen konnten zwei Molekülstrukturen der *N*-monosubstituierten ICS erhalten werden. Zum einen wurde *N,N*-Diethyl-2,4,6-trioxo-1,3,5-triazin-1-carboxamid (ICS-CONEt$_2$) und zum anderen *S*-Phenyl-2,4,6-trioxo-1,3,5-triazin-1-carbothioat (ICS-COSPh; Abbildung 4.19) kristallisiert. Beide Moleküle können durch das Trimer von CO(NCO)$_2$ entstanden sein. Es bildet sich bereits bei Raumtemperatur und reagiert mit Nukleophilen zu Isocyanursäure und Imidodicarbonsäure-Derivaten,[72] welche wiederum miteinander zu den erhaltenen Molekülen reagiert sein könnten.

ICS-CONEt$_2$ kristallisiert in der Raumgruppe *P*2$_1$2$_1$2$_1$ im orthorhombischen Kristallsystem. In der Elementarzelle befinden sich vier Moleküle (*Z* = 4) und ein unabhängiges Molekül in der asymmetrischen Einheit (*Z'* = 1). Die Gitterparameter sind *a* = 7.536(3) Å, *b* = 9.971(3) Å und *c* = 13.053(5) Å. Ein Molekül ist mit zwei benachbarten Molekülen über jeweils eine H-Brücke ausgehend von O4 (O4···HN1/2) verbunden und über N1H und N2H (HN1···O4 & HN2···O4) zu nochmals zwei Molekülen verbrückt (Abbildung 8.24). Dadurch wird ein Netzwerk in der ausgedehnten Kristallstruktur erzeugt.

ICS-COSPh kristallisiert im monoklinen Kristallsystem mit der Raumgruppe *P*2$_1$/*c*. Die Struktur weist vier Moleküle pro Elementarzelle (*Z* = 4) und ein unabhängiges Molekül in der asymmetrischen Einheit (*Z'* = 1) auf. Die Gitterparameter belaufen sich auf *a* = 11.070(2) Å, *b* = 8.311(1) Å, *c* = 11.778(3) Å und β = 92.65(2)°. Ein Molekül bildet jeweils ein Dimer über zwei Wasserstoffbrückenbindungen zu einem Symmetrie generierten Molekül (N1H···O1 & O1···HN1). Zusätzlich findet eine Vernetzung zu zwei benachbarten Dimeren über je eine weitere H-Brücke (N2H···O2 & O2···HN2) statt (Abbildung 8.24).
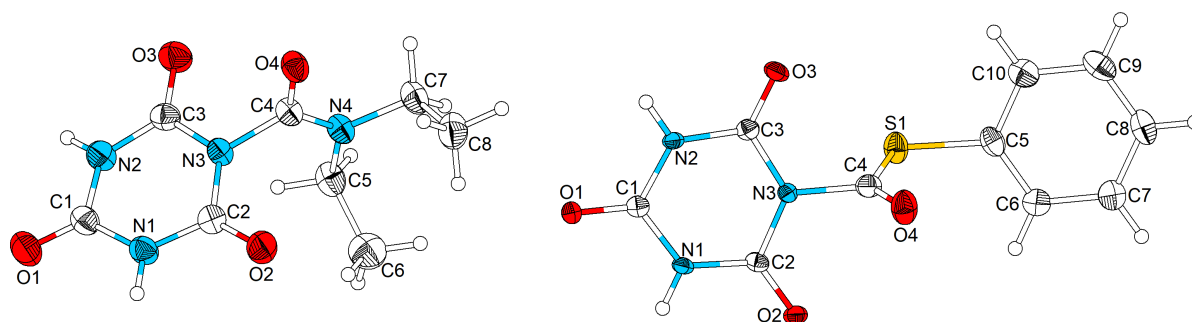
Abbildung 4.19: Molekülstruktur im Festkörper von ICS-CONEt$_2$ (links) und ICS-COSPh (rechts). Ellipsoide sind mit einer Aufenthaltswahrscheinlichkeit von 50 % und Wasserstoffatome mit willkürlichem Radius dargestellt.

Tabelle 4.8 ist zu entnehmen, dass die C=O und C−N Bindungslängen der Ringe vergleichbar mit Isocyanursäure[160] (Tabelle 4.7) sind. Die C=O$_{Ring}$ Bindungen sind in ICS-CONEt$_2$ (1.190(5) Å – 1.210(5) Å) und ICS-COSPh (1.197(3) Å – 1.222(3) Å) etwas kürzer als in ICS (1.2165(5) Å – 1.2230(3) Å[160]), die C−N$_{Ring}$ Bindungen mit 1.368(5) Å – 1.400(4) Å (ICS-CONEt$_2$) und 1.363(3) Å – 1.401(3) Å (ICS-COSPh) dagegen länger (ICS: 1.3692(4) Å – 1.3727(4) Å[160]). Dies ist auf die Substitution an N3 zurückzuführen. Die C4=O4 Doppelbindungen sind 1.227(4) Å (ICS-CONEt$_2$) und 1.194(4) Å (ICS-COSPh) lang und vergleichbar mit Biuret (1.231(3) Å – 1.241(3) Å[21]). Sie ist in ICS-COSPh durch den Einfluss des Sulfidrests kürzer. Die N3−C4 Bindungen sind aufgrund elektrostatischer Abstoßung des freien Elektronenpaars an N3 und den Elektronen der C4=O4 Doppelbindung auf 1.467(5) Å in ICS-CONEt$_2$ und 1.481(4) Å in ICS-COSPh verlängert. Die substituierten Gruppen sind aus der Ebene des Isocyanursäure-Ringes (C2N3−C4O4) um 92.0(4) ° in ICS-CONEt$_2$ und 72.3(4) ° in ICS-COSPh gedreht. Die H-Brücken Abstände zeigen keine Abweichungen zu Literatur.[21,160]

Tabelle 4.8: Bindungslängen von ICS-CONEt$_2$ und ICS-COSPh

Bindung [Å]	ICS-CONEt$_2$	ICS-COSPh
C=O$_{Ring}$	1.190(5)–1.210(5)	1.197(3)–1.222(3)
C−N$_{Ring}$	1.368(5)–1.400(4)	1.363(3)–1.401(3)
C4−N3	1.467(5)	1.481(4)
C4=O4	1.227(4)	1.194(4)
C4−*X*	1.314(4)[a]	1.735(3)[b]
O···H$_{inter}$	1.958(1)/2.015(1)	1.963(1)

a: *X* = N4, b: *X* = S1

4.6.4 Derivate des Harnstoffs und Biurets

Neben den Isocyanursäure-Derivaten wurde ebenfalls ein monosubstituiertes Harnstoff-Derivat, *N*-(*S*-Benzyldithiocarboxy)**c**arbonyl**dia**mid (CDA-CSSBz) erhalten. Dieses kristallisierte beim Versuch Kristalle von 6-Phenylthio-2-thioxo-2,3-dihydro-4*H*-1,3,5-thiadiazin-4-on zu züchten. Diese Thiadiazine zeigen bereits bei milden Bedingungen eine Ringöffnung[67] und dies könnte zu der Bildung von CDA-CSSBz geführt haben. CDA-CSSBz (Abbildung 4.20) kristallisiert in der Raumgruppe *P*2$_1$/*n* im monoklinen Kristallsystem und mit einem unabhängigen Molekül in der asymmetrischen Einheit (*Z*′ = 1). In der Elementarzelle sind vier Moleküle (*Z* = 4). Die Gitterparameter sind *a* = 4.6898(4) Å, *b* = 34.396(2) Å,
c = 6.5734(6) Å und β = 104.748(7)°. Das Molekül bildet über eine intramolekulare H-Brücke einen Sechsring (S1···HN1). Über jeweils zwei intermolekulare H-Brücken zu je zwei benachbarten Molekülen (O1···HN1/2, N1H···O1 & N2H···O1) wird eine Kette gebildet. Der Phenylring ist um 103.0(2)° aus der Ebene der Kette (C2S2−C3C4) gedreht und zeigt kein π-*stacking*.
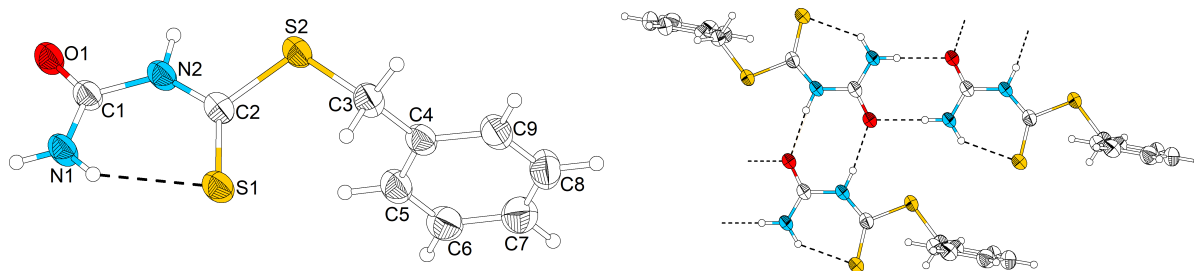

Abbildung 4.20: Molekülstruktur im Festkörper von CDA-CSSBz und Verknüpfung der Moleküle über Wasserstoffbrückenbindungen. Ellipsoide sind mit einer Aufenthaltswahrscheinlichkeit von 50 % und Wasserstoffatome mit willkürlichem Radius dargestellt.

Ebenso wurde das tetrasubstituierte Biuret, *N,N,N',N'*-Tetraisopropylimidodicarbonsäurediamid (IDCDA-*i*Pr) erhalten. Dieses ist ein Reaktionsprodukt des zuvor beschriebenen Trimers von CO(NCO)$_2$ mit Nukleophilen, welches nicht gezielt dargestellt wurde. IDCDA-*i*Pr (Abbildung 4.21) kristallisiert im orthorhombischen Kristallsystem mit der Raumgruppe *Pbca*. In der Elementarzelle befinden sich acht Moleküle (*Z* = 8) mit einem unabhängigen Molekül in der asymmetrischen Einheit (*Z*′ = 1). Die Gitterparameter sind *a* = 12.3349(13) Å, *b* = 10.7196(11) Å und *c* = 24.619(4) Å. Das Molekül bildet ein isoliertes Dimer mit einem Symmetrie generierten Selbst über zwei intermolekulare H-Brücken (O2···HN1 & N1H···O2). Es weicht im Vergleich zu Biuret[21] von der Planarität ab, indem die C1O1N2-Gruppe um 67.5(2)° (N3C3−N1C1) verdreht ist.
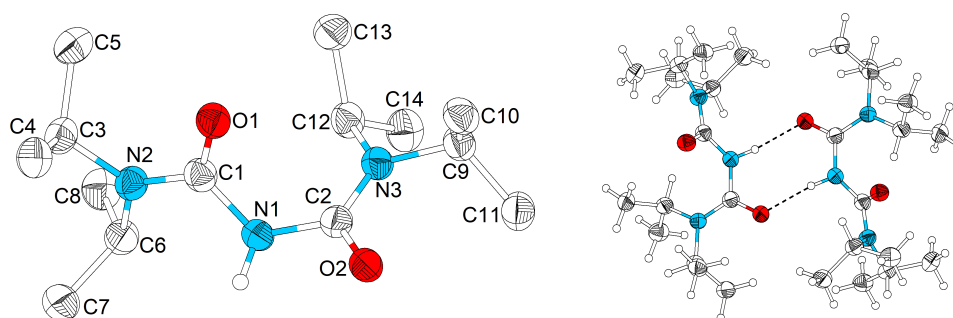
Abbildung 4.21: Molekülstruktur im Festkörper von IDCDA-*i*Pr und Verknüpfung der Moleküle über Wasserstoffbrückenbindungen.. Ellipsoide sind mit einer Aufenthaltswahrscheinlichkeit von 50 % und Wasserstoffatome mit willkürlichem Radius dargestellt.

Die Bindungslängen von CDA-CSSBz und IDCDA-*i*Pr (Tabelle 4.9) sind vergleichbar mit Biuret[21] (Tabelle 4.7). Die C=O Bindungen (CDA-CSSBz: 1.238(3) Å, IDCDA-*i*Pr: 1.226(2) Å & 1.236(2) Å) sind innerhalb der 3σ-Standardabweichung identisch (Biuret: 1.231(3) Å & 1.241(3) Å[21]). Die C−N Einfachbindungen von CDA-CSSBz (1.318(2) Å – 1.403(3) Å) und IDCDA-*i*Pr (1.342(2) Å – 1.414(2) Å) sind länger als in Biuret (1.315(3) Å – 1.384(3) Å[21]), was durch unterschiedliche Substituenten an den Stickstoffatomen zu erwarten ist. In CDA-CSSBz ist die C−S Bindung (1.760(2) Å) zu ICS-COSPh (1.735(3) Å) und die C=S Bindung (1.654(2) Å) zu Monothiobiuret (1.697(2) Å & 1.708(2) Å[162]) vergleichbar. Intermolekulare H-Brücken zeigen keine Abweichungen zur Literatur.[21] Die intramolekulare H-Brücke in CDA-CSSBz ist deutlich innerhalb der Summe der Van-der-Waals Radien (r_{VdW}(H−S): 3.09 Å[161]).

Tabelle 4.9: Bindungslängen von CDA-CSSBz, IDCDA-*i*Pr und TIDCDA-NH$_4$SCN.

Bindung [Å]	CDA-CSSBz	IDCDA-*i*Pr	TIDCDA-NH$_4$SCN
C=O	1.238(3)	1.226(2)/1.236(2)	1.237(2)
C=S	1.654(2)	–	1.710(2)
C−N	1.318(2)–1.403(3)	1.342(2)–1.414(2)	1.314(3)–1.402(3)
C−S	1.760(2)	–	–
N=CS	–	–	1.170(3)
NC=S	–	–	1.645(2)
$X\cdots$H$_{intra}$	2.311(6)[a]	–	1.975(26)[b]
$X\cdots$H$_{inter}$	2.015(1)/1.978(1)[b]	1.963(1)[b]	2.159(2)–2.489(29)[c]
S$\cdots$H$_{inter}$	–	–	2.446(32)–2.705(28)

a: X = S, b: X = O, c: X = N

Carbonyldiisothiocyanat wurde mit Ammoniak umgesetzt um 2-Imino-6-thioxo-1,3,5-thia-diazin-4-on zu erhalten. Beim Einleiten von Ammoniak in die Reaktionslösung bildete sich zuerst ein Feststoff, welcher sich beim weiteren Einleiten wieder auflöste. Nach Aufreinigung wurde ein gelbes Pulver erhalten, welches durch SC-XRD als Gemisch aus Mono-thiobiuret (**T**hio**i**mido**d**i**c**arbonsäure**dia**mid (TIDCDA)) und Ammoniumthiocyanat herausstellte. Es kann angenommen werden, dass sich beim Reaktionsverlauf zunächst 2-Imino-6-thioxo-1,3,5-thiadiazin-4-on mit einem Äquivalent Ammoniak bildet und aus der Lösung ausfällt. Bei weiterer Sättigung der Lösung mit Ammoniak zerfällt es durch den Überschuss zu TIDCDA und NH$_4$SCN, welche sich wieder im Lösungsmittel auflösen.
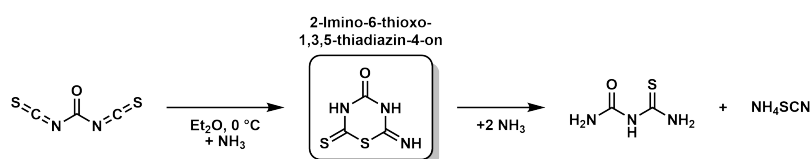
Schema 4.18: Syntheseversuch von 2-Imino-6-thioxo-1,3,5-thiadiazin-4-on und Zerfall zu Thioimidodicarbonsäurediamid und Ammoniumthiocyanat.

TIDCDA×NH$_4$SCN kristallisieren zusammen im monoklinen Kristallsystem und der Raumgruppe $P2_1/n$. Es befindet sich je ein Molekül in der asymmetrischen Einheit ($Z' = 1$) und es sind je vier Moleküle pro Elementarzelle ($Z = 4$). Das TIDCDA-Molekül bildet eine intramolekulare Wasserstoffbrückenbindung (O1···HN3) aus. Dazu kommen fünf weitere H-Brücken vom NH$_4^+$-Kation zum Stickstoffatom des NCS$^-$-Anions (N5H···N4), zu Schwefelatomen von drei TIDCDA-Molekülen (3×N5H···S1) und zum Sauerstoffatom eines TIDCDA-Moleküls (N5H···O1). Das NCS$^-$-Anion bildet über das Stickstoffatom drei H-Brücken zu zwei TIDCDA-Molekülen (N4···HN1 & N4···HN2, N4···HN3) neben der Bindung zum NH$_4^+$-Kation. Über das Schwefelatom werden zwei H-Brücken zu zwei TIDC-DA-Molekülen (S2···HN2 & S2···HN3) geformt.

Alle Bindungslängen des TIDCDA-Moleküls (Tabelle 4.9) zeigen keine signifikanten Abweichungen zu den Literaturwerten.[162] Die C=S Doppelbindung ist mit 1.710(2) Å geringfügig länger (1.697(2) Å & 1.708(2) Å[162]). Alle C−N Einfachbindungen (1.314(3) Å – 1.402(3) Å) sind im Bereich der Literaturangaben (1.307(2) Å – 1.396(2) Å[162]). Die C=O Doppelbindung liegt mit 1.237(2) Å ebenfalls zwischen den beiden Werten der Literatur (1.234(2) Å & 1.240(2) Å[162]). Für NH$_4$SCN sind keine Abweichungen im Vergleich zur Literatur zu beobachten. Die N=CS (1.170(3) Å) und NC=S (1.645(2) Å) Doppelbindungen innerhalb des Thiocyanat-Anions sind identisch zur Literatur (1.172 Å & 1.649 Å[163]). Die genannten Wasserstoffbrückenbindungen befinden sich alle innerhalb der Summe der Van-der-Waals Radien (r_{VdW}(H−N): 2.86 Å, r_{VdW}(H−O): 2.70 Å, r_{VdW}(H−S): 3.09 Å[161]) und sind verantwortlich für die Packung der Moleküle.
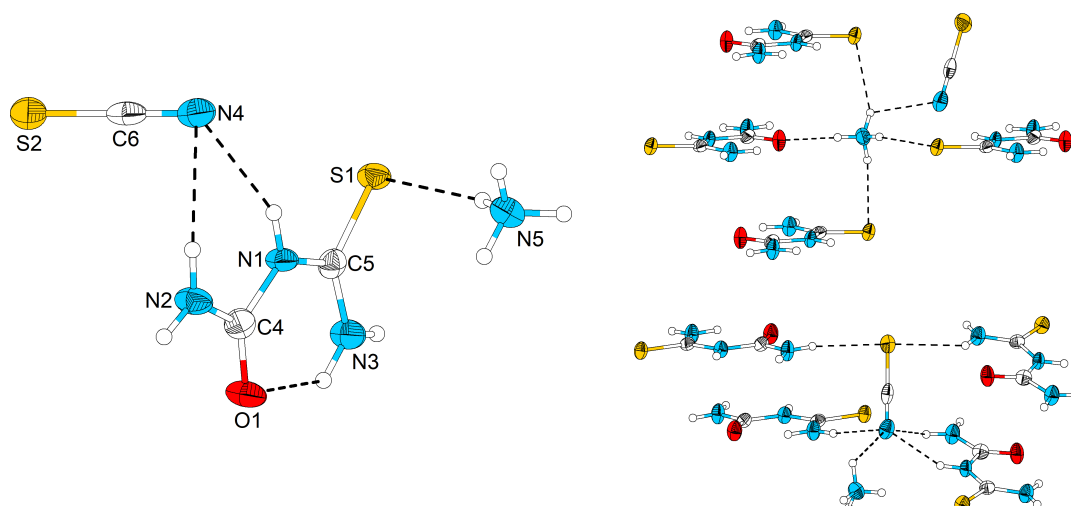
Abbildung 4.22: Molekülstruktur im Festkörper von TIDCDA-NH₄SCN und Wasserstoff-brückenbindungen des NH₄-Kations, sowie des SCN⁻-Anions. Ellipsoide sind mit einer Aufenthaltswahrscheinlichkeit von 75 % und Wasserstoffatome mit willkürlichem Radius dargestellt.

4.6.5 Tetramethylammoniumselenocyanat

Tetramethylammoniumselenocyanat (NMe₄SeCN) wurde aus Ammoniumchlorid und Kaliumselenocyanat als Edukt für weitere Synthesen nach abgewandelter Literaturvorschrift[164] hergestellt. Im Zuge der Synthese wurde ebenfalls die bisher unbekannte Molekülstruktur im Festkörper (Abbildung 4.23) bestimmt. NMe₄SeCN kristallisiert in der Raumgruppe $P2_1/c$ des monoklinen Kristallsystems. In der Elementarzelle befinden sich vier Moleküle (Z = 4) mit einem unabhängigem Molekül in der asymmetrischen Einheit (Z' = 1). Die Gitterparameter sind a = 7.8656(5) Å, b = 8.6002(4) Å, c = 11.9513(8) Å und β = 95.374(5)°. Das SeCN⁻-Anion ist verzerrt kubisch von acht NMe₄⁺-Kationen eingeschlossen und das NMe₄⁺-Kation unregelmäßig von acht SeCN⁻-Anionen umgeben (Abbildung 4.24). Das Selenocyanat-Anion ist mit 179.6(6)° linear, wie es auch für NH₄SeCN (179.38(15)°[144]) berichtet wird. Die Bindungslängen C≡N (1.158(8) Å) und C≡Se (1.808(6) Å) entsprechen den Literaturangaben (1.158(2) Å & 1.810(2) Å[144]).

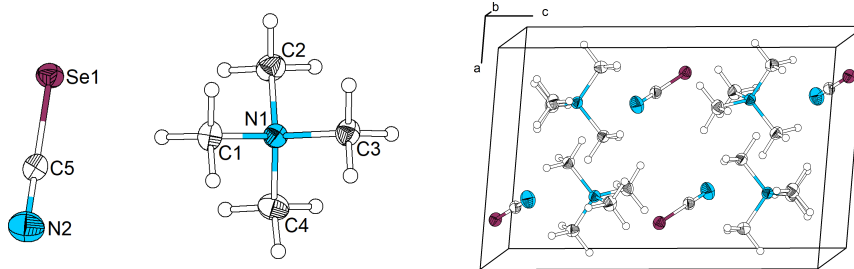**Abbildung 4.23:** Molekülstruktur im Festkörper und Packung der Elementarzelle von Tetra-methylammoniumselenocyanat. Ellipsoide sind mit einer Aufenthaltswahrscheinlichkeit von 50 % und Wasserstoffatome mit willkürlichem Radius dargestellt.
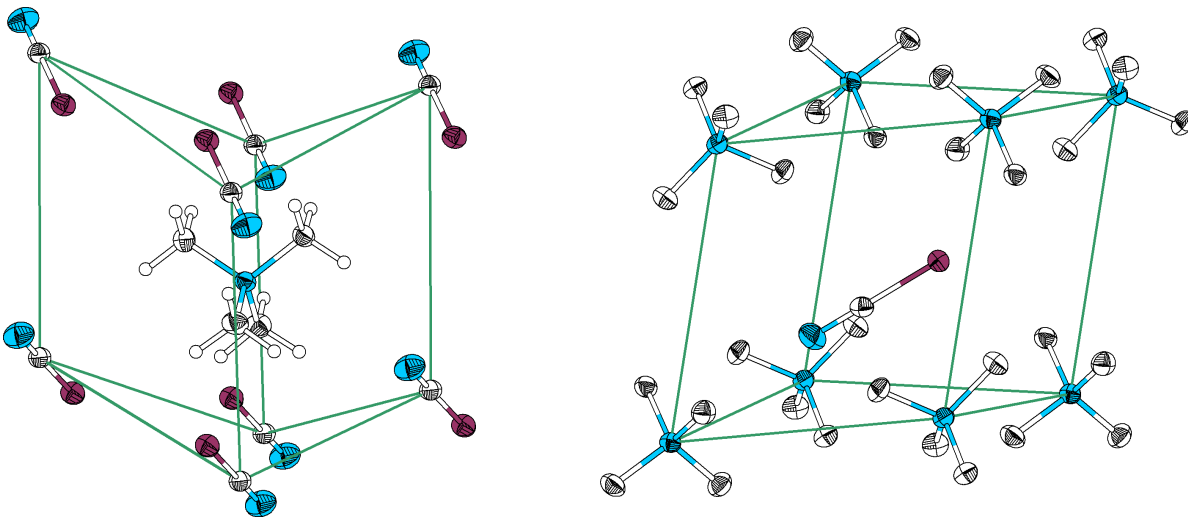

Abbildung 4.24: Umgebung des NMe$_4^+$-Kations (links) und SeCN$^-$-Anions (rechts) im Fest-körper von NMe$_4$SeCN. Der Umgebungspolyeder ist mit grünen Linien hervorgehoben.

5 Zusammenfassung

Der Fokuspunkt der Forschung in dieser Dissertation war die Synthese und Charakterisierung (erster Teil), sowie die Reaktivität (zweiter Teil) von Carbonyldipseudohalogeniden CD*PsH*. Die Kristallstrukturen von Carbonyldiisothiocyanat (CO(NCS)$_2$) und Oxalyldiisothiocyanat ((CONCS)$_2$) wurden ebenso wie ihre Hirshfeld Oberflächen und spektroskopischen Signaturen aufgeklärt (Abbildung 5.1 a).[165] Diese Erkenntnisse erweitern das Wissen über Syntheseverfahren, Konformation und Packung der Moleküle im Festkörper von kleinen Molekülen. Des Weiteren wurde eine Konformationsanalyse in Kooperation mit der Arbeitsgruppe SCHNELL (DESY in Hamburg) von Carbonyldiisothiocyanat mittels *chirped-pulse* Fourier-Transformation Mikrowellenspektroskopie durchgeführt, in welcher ein *syn-syn* zu *syn-anti* Verhältnis von 10:1 beobachtet wurde. Das *syn-syn* Konformer existiert dabei wie ein Boson in den zwei Kernspinisomeren *ortho* und *para* (Abbildung 5.1 b).[166]
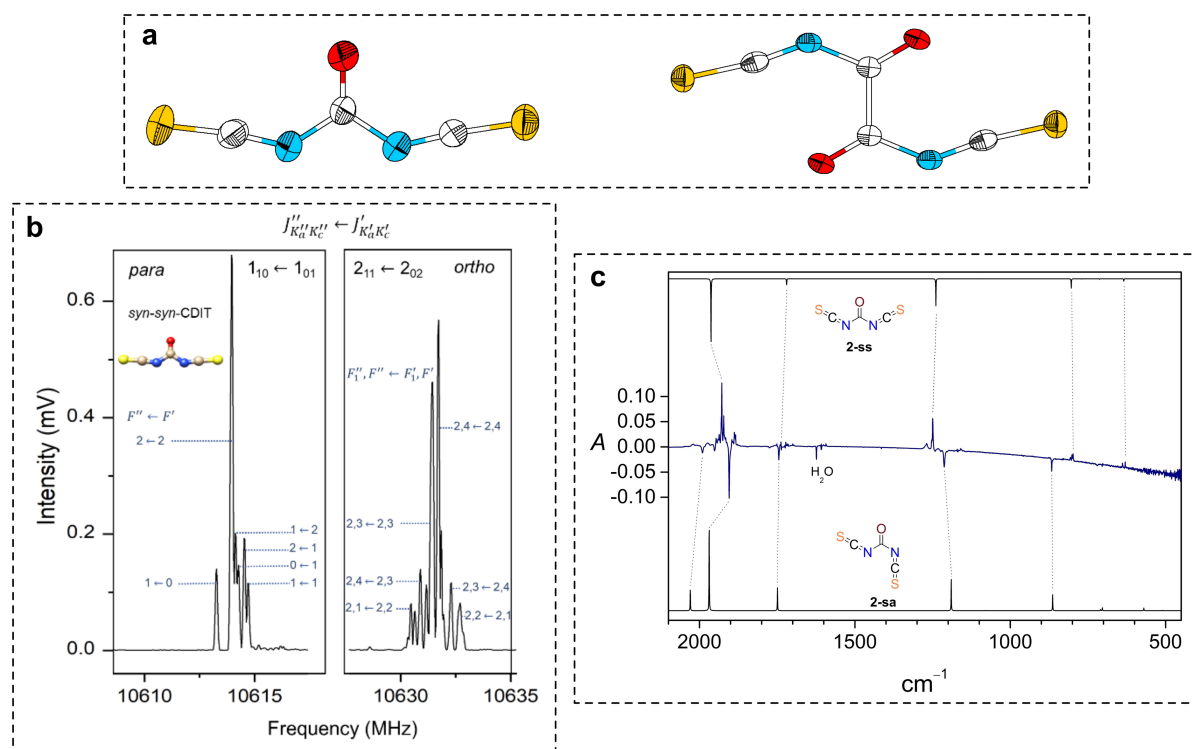
Abbildung 5.1: (a) Molekülstrukturen von Carbonyldiisothiocyanat und Oxalyldiisothiocyanat. (b) Rotationsübergänge von *para* und *ortho syn-syn* Carbonyldiisothiocyanat. (c) Differenz IR-Spektrum von *syn* und *anti* Carbonyldiisothiocyanat nach Bestrahlung von Oxalyldiisothiocyanat mit UV Licht und anschließendem Tempern.

Darüber hinaus wurde die photochemisch induzierte Zersetzung von Oxalyldiisothiocyanat in einer festen Argon-Matrix mittels IR-Spektroskopie in Zusammenarbeit mit der Ar-

beitsgruppe WAGNER (Eberhard Karls Universität Tübingen) untersucht. Bei Bestrahlung mit UV Licht wird Kohlenstoffmonoxid abgespalten und Carbonyldiisothiocyanat in seinem energetisch höherliegendem *syn-anti* Konformer gebildet. Tempern der Matrix nach Bestrahlung bei erhöhten Temperaturen (30 K) führt zu einer Konformationsänderung zum stabileren *syn-syn* Konformer (Abbildung 5.1 c).[167]

Viele Syntheseversuche von CD*PsH* wie z.B Carbonyldiselenocyanat oder Thiocarbonyldiisocyanat führten nicht zu isolierbaren Produkten. Carbonyldiselenocyanat ($CO(SeCN)_2$) wurde möglicherweise in Lösung durch ^{13}C-NMR-Spektroskopie bei einer chemischen Verschiebung von 185.3 ppm und 98.1 ppm beobachtet (Abbildung 5.2). Das erhaltene feste Produkt zersetzt sich jedoch oberhalb von –30 °C oder bei Solvatisierung. Aufgrund dessen wurde das alkylsubstituierte *tert*-Butylcarbonylisoselenocyanat ($CO(NCSe)t$Bu) synthetisiert, um die Existenz von Carbonylselenocyanaten zu überprüfen. Die Verbindung konnte als festes Rohprodukt aufgrund Zersetzung während dem Entfernen des Lösungsmittels nicht isoliert werden. In Lösung ist die Verbindung jedoch handhabbar und kann mittels ^{13}C-NMR-Spektroskopie mit Resonanzsignalen bei 171.4 ppm und 144.0 ppm detektiert werden.
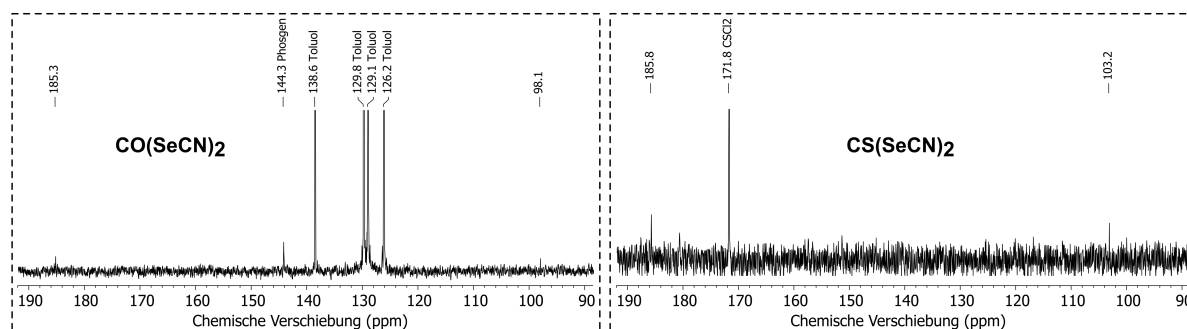

Abbildung 5.2: Ausschnitte aus den ^{13}C{^{1}H}-NMR-Spektren von Carbonyldiselenocyanat in THF-d$_8$ (links) und Thiocarbonyldiselenocyanat in THF-d$_8$ (rechts).

Die Synthese von Pseudohalogeniden mit Thiocarbonylgruppe wurde zuerst für Thiocarbonyldiisocyanat ($CS(NCO)_2$) versucht. Es konnte auf den durchgeführten Wegen nicht erhalten werden, aber es wurde in der Zwischenzeit von HENNES GÜNTHER (Arbeitsgruppe TAMBORNINO) in Lösung beobachtet und ein definiertes Folgeprodukt mit Ethanol erzeugt.[143] Die Synthese der anschließenden Verbindung Thiocarbonyldiisothiocyanat ($CS(NCS)_2$) führte zur Isolierung von dem bekannten, wenn auch bisher schlecht charakterisierten, Thiocarbonyldithiocyanat ($CS(NCS)_2$). Obwohl erstes das thermodynamisch stabilere Reaktionsprodukt ist, war es nicht möglich eine synthetische Herangehensweise, welche zu seiner Isolation führte, zu finden. DFT Rechnungen bestätigten, dass das kinetische Reaktionsprodukt Thiocarbonyldithiocyanat ($CS(NCS)_2$) über einen

niedrigeren Übergangszustand gebildet wird. Dessen Kristallstruktur wurde zusammen mit der des einfach substituierten Chlorthiocarbonylthiocyanats (CS(SCN)Cl) bestimmt (Abbildung 5.3).[168] Dies resultiert in der sechsten bekannten Molekülstruktur von CD*PsH*. Zuletzt wurden Versuche zur Synthese von Thiocarbonyldiselenocyanat (CS(SeCN)$_2$) unternommen, die zur möglichen Detektion durch ^{13}C-NMR-Spektroskopie mit Resonanzsignalen bei 185.8 ppm und 103.2 ppm führte (Abbildung 5.2). Die Verschiebungen stimmen mit den Beobachtungen zum Syntheseversuch von Carbonyldiselenocyanat (CO(SeCN)$_2$) überein und bekräftigen die oben genannten Schlussfolgerungen.
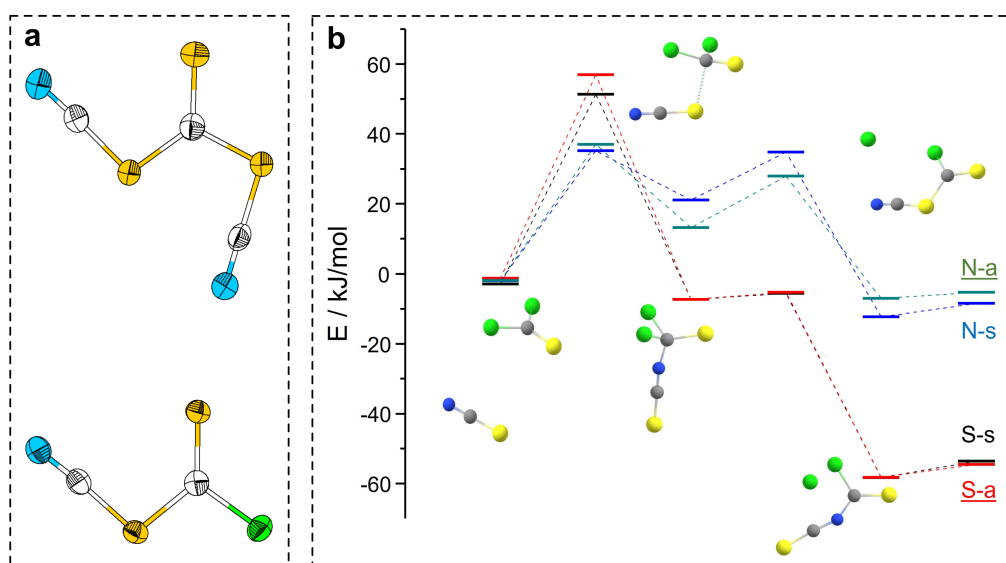

Abbildung 5.3: (a) Molekülstrukturen von Thiocarbonyldithiocyanat and Chlorthiocarbonyl-thiocyanat. (b) Energieprofile für den Austausch eines Chlorids von Thiophosgen gegen ein Thiocyanat mit Schwefel oder Stickstoff in der endständigen Position in ihren *syn* und *anti* Konformeren.

Zum Abschluss des ersten Teiles wurden Oxalylchloridisothiocyanat (Cl(CO)$_2$NCS) und Chlorcarbonylisothiocyanat (CO(NCS)Cl) synthetisiert. Im Verlauf der Synthese von Oxalylchloridisothiocyanat wurde ein Gleichgewicht von diesem und 2-Chlorothiazol-4,5-dion in Lösung festgestellt. Weitere Untersuchungen mit Einkristalldiffraktometrie und Schwingungsspektroskopie führte zu der Erkenntnis, dass nur letzteres im Festkörper vorliegt. Beide Verbindungen zersetzen sich in Lösung bei Raumtemperatur zu Chlorocarbonyl-isothiocyanat, welches genauer von SVEN RINGELBAND (Arbeitsgruppe TAMBORNINO) untersucht wurde.[147]

Der zweite Teil dieser Dissertation beschäftigt sich mit der Reaktivität von CD*PsH*. Carbonyldiisocyanat (CO(NCO)$_2$) und Carbonyldiisothiocyanat (CO(NCS)$_2$) reagieren mit Halogenwasserstoffen jeweils zu Carbonylbis(carbamoylhalogeniden) und halogensubstituierten 1,3,5-Thiadiazin-4-onen. Carbonyldiisocyanat addiert zwei Äquivalente des Nukleo-

phils, wohingegen Carbonyldiisothiocyanat unter intramolekularem Ringschluss nur ein Äquivalent addiert. Die verschiedenen Reaktionspfade sind thermodynamisch gesteuert. Während Sauerstoff die Bildung von *ex*-Ring Doppelbindungen mit Kohlenstoff präferiert, bevorzugt Schwefel *in*-Ring Einfachbindungen zu bilden.[169] Beide Verbindungsklassen zeigen im Festkörper ausgedehnte Netzwerke von Wasserstoffbrückenbindungen, welche im Detail anhand der Reaktionsprodukte zwischen Carbonyldiiso(thio)cyanat und Nukleophilen wie Alkoholen, Thiolen und Aminen erläutert wurden (Abbildung 5.4). *N,N'*-Carbonylbis(carbamate), -bis(*S*-thiocarbamate) und *N,N'*-Biscarbamoylharnstoffe werden jeweils in der Reaktion mit Carbonyldiisocyanat erzeugt.[170] Alle Moleküle bilden eine intramolekulare und zwei intermolekulare Wasserstoffbrückenbindungen zur Bildung von Dimeren oder Ketten. Aus der Reaktion von Nukleophilen mit Carbonyldiisothiocyanat entstehen substituierte 1,3,5-Thiadiazin-4-one, die alle über intermolekulare Wasserstoffbrückenbindungen Dimere bilden.[171] Dies steht im Gegensatz zu den Ketten bildenden halogensubstituierten 1,3,5-Thiadiazin-4-onen. Die weitere Packung der Moleküle aller Verbindungsklassen ist abhängig von der Größe der substituierten Gruppe, z.B. Methyl gegen Phenyl. Bei kleinen Alkylgruppen überwiegen polare Wechselwirkungen, während mit zunehmender Größe der Alkyl- oder Arylgruppe steigend unpolare Wechselwirkungen vorherrschen.
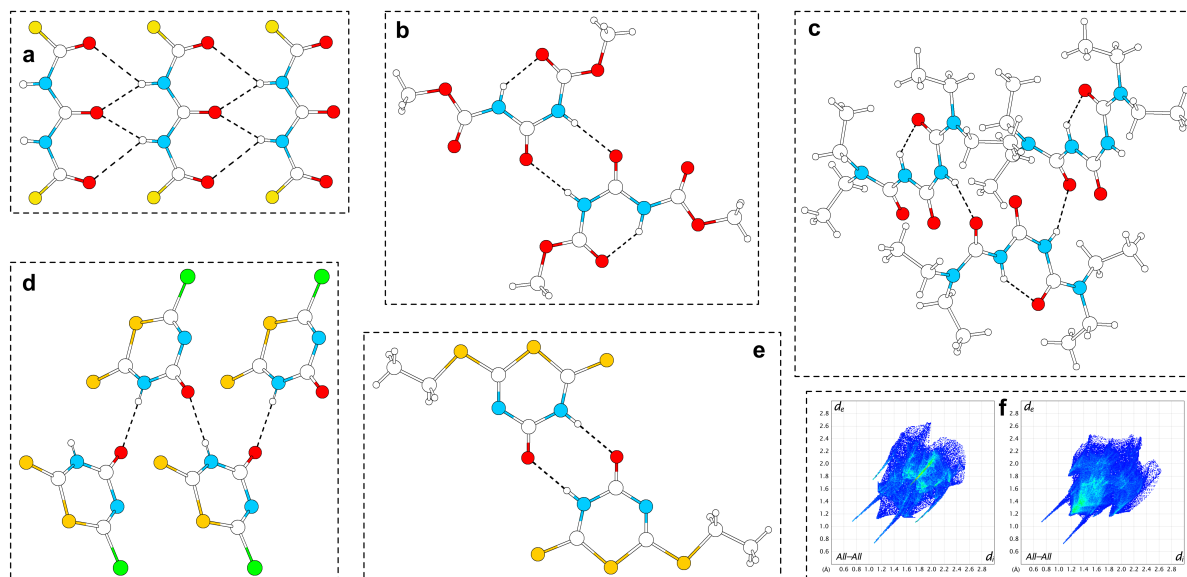
Abbildung 5.4: Beispiele von verschiedenen Wasserstoffbrückenbindungsnetzwerken im Festkörper der Reaktionsprodukte von Carbonyldiisocyanat (a-c) und Carbonyldiisothiocyanat (d-e) mit Nukleophilen. (a) Stränge, (b) Dimere, (c) Ketten, (d) Ketten, (e) Dimere, (f) Beispielhafte aus der Hirshfeld Oberfläche generierte *Fingerprint* Diagramme.

Einige Nebenprodukte der Reaktionen von Carbonyldiisocyanat und Carbonyldiisothiocyanat mit Nukleophilen konnten isoliert und als z.B. Derivate der Isocyanursäure und

des Biurets identifiziert werden. Diese könnten Hinweise auf mögliche reaktive Spezies in der Lösung während der Reaktion sein. Nukleophile Additionen von Organolithium-Verbindungen an Carbonyldiisocyanat wurden mit Methyllithium, *tert*-Butyllithium und Lithiummethanolat getestet, aber definierte Reaktionsprodukte wurden nicht erhalten. Es wird angenommen, dass die gebildeten Anionen zur Isolierung zu instabil sind, weshalb eine saure Aufarbeitung zur Protonierung dieser notwendig sein wird. Überraschend aufregend war das Ergebnis der Reaktion von Carbonyldiisocyanat mit Eisenbis(diisopropylphenyltrimethylsilylamid), in welcher eine Reaktion mit dem Liganden und die Kristallisation eines neuartigen Metallkomplexes erreicht wurde. Dieser neue Komplex mit einem substituiertem Biuret-Liganden und einem tetraedrisch koordiniertem Eisen ist der erste über den berichtet wird. Kristalle aus der selben Reaktion mit Cobalt oder Nickel, ebenso wie Carbonyldiisothiocyanat wurden nicht erhalten. Allerdings wurde ein äquivalenter Metallkomplex aus Nickel und Carbonyldiisothiocyanat durch Massenspektrometrie beobachtet. Dies beweist, dass die Reaktions- oder Kristallisationsbedingungen angepasst werden müssen, um mehr dieser Komplexe zu erhalten.

Zukünftige Perspektiven dieser Dissertation sind zunächst in Kooperation das Rotationsspektrum von Carbonyldiisocyanat, das IR-Spektrum von Oxalylchloridisothiocyanat beziehungsweise 2-Chlorthiazol-4,5-dion in fester Argon-Matrix und deren Verhalten bei Bestrahlung mit UV Licht zu untersuchen (Schema 5.1 a). Des Weiteren sollte die Isolierung einer reinen Probe und die Charakterisierung der Festkörper von Carbonyldiselenocyanat und Thiocarbonyldiselenocyanat durch Filtration über eine gekühlte Schlenk-Fritte oder
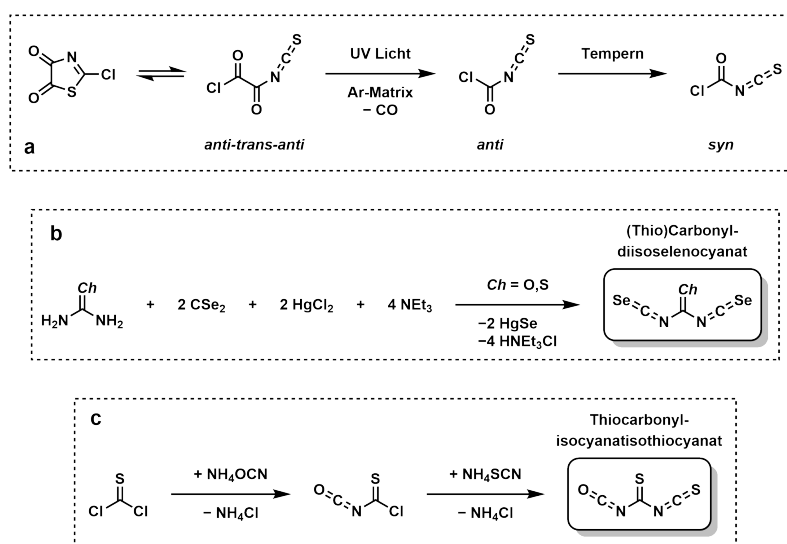
Schema 5.1: (a) Mögliches photochemisches Verhalten von 2-Chlorothiazol-4,5-dion in fester Argon-Matrix bei Bestrahlung mit UV Licht. (b) Neuer synthetischer Ansatz für die Synthese von (Thio)Carbonyldiisoselenocyanat. (c) Möglicher Weg zur Synthese von asymmetrischen Carbonyldipseudohalogeniden am Beispiel von Thiocarbonylisocyanatisothiocyanat.

die Verwendung von anderen Lösungsmitteln wie z.B. Dioxan möglich sein. Ein komplett neuer Ansatz wäre die Synthese ausgehend von (Thio)Harnstoff, Kohlenstoffdiselenid und Quecksilberchlorid (Schema 5.1 b). Darüber hinaus ist es lohnenswert einen Blick auf die fehlenden NMR spektroskopischen und Molekülstrukturdaten von Carbonyldicyanid $(CO(CN)_2)$, das in der Einleitung erwähnt wurde, zu werfen. Asymmetrische Carbonyldipseudohalogenide finden in dieser Dissertation keine Beachtung, obwohl Studien zu ihrer Synthese (Schema 5.1 c), Charakterisierung und Reaktivität das Wissen über Konformation und Kristallpackung von kleinen Molekülen deutlich verbessern würden. Abseits der Synthese von neuen Carbonylpseudohalogeniden ist auch die Untersuchung der Edukte Phosgen, Thiophosgen und Oxalylchlorid von Interesse. So sind bereits Experimente zur Neutronenbeugung an Phosgen und Thiophosgen am ISIS in Oxford geplant.

5.1 Summary

In this dissertation the synthesis and characterization (first part), as well as the reactivity (second part) of carbonyl dipseudohalides (CD*PsH*) were the focal point of research. The crystal structures of carbonyl diisothiocyanate (CO(NCS)$_2$) and oxalyl diisothiocyanate ((CONCS)$_2$) were elucidated alongside their Hirshfeld surfaces, as well as their spectroscopic signatures (Figure 5.5 a).[165] These findings extend the knowlegde about synthetic procedure, conformation and molecule packing in the solid state of small molecules. Furthermore, a conformer study of carbonyl diisothiocyanate was performed by chirped-pulse Fourier transform microwave spectroscopy in cooperation with the working group SCHNELL (DESY in Hamburg) and led to the observation of a *syn-syn* to *syn-anti* ratio of 10:1. The *syn-syn* conformer exists as two nuclear spin isomers *ortho* and *para* like a boson (Figure 5.5 b).[166] In addition, the photochemical induced decomposition of oxalyl diisothiocyanate in solid argon matrices was investigated with IR spectroscopy in collaboration with working group WAGNER (Eberhard Karls University Tübingen). Upon irradiation with UV light carbon monoxide is released and forms carbonyl diisothiocyanate in its less favored *syn-anti* conformer. Annealing the matrix after irradiation at higher temperature (30 K) leads to a conformer switch to the more stable *syn-syn* conformer (Figure 5.5 c).[167]
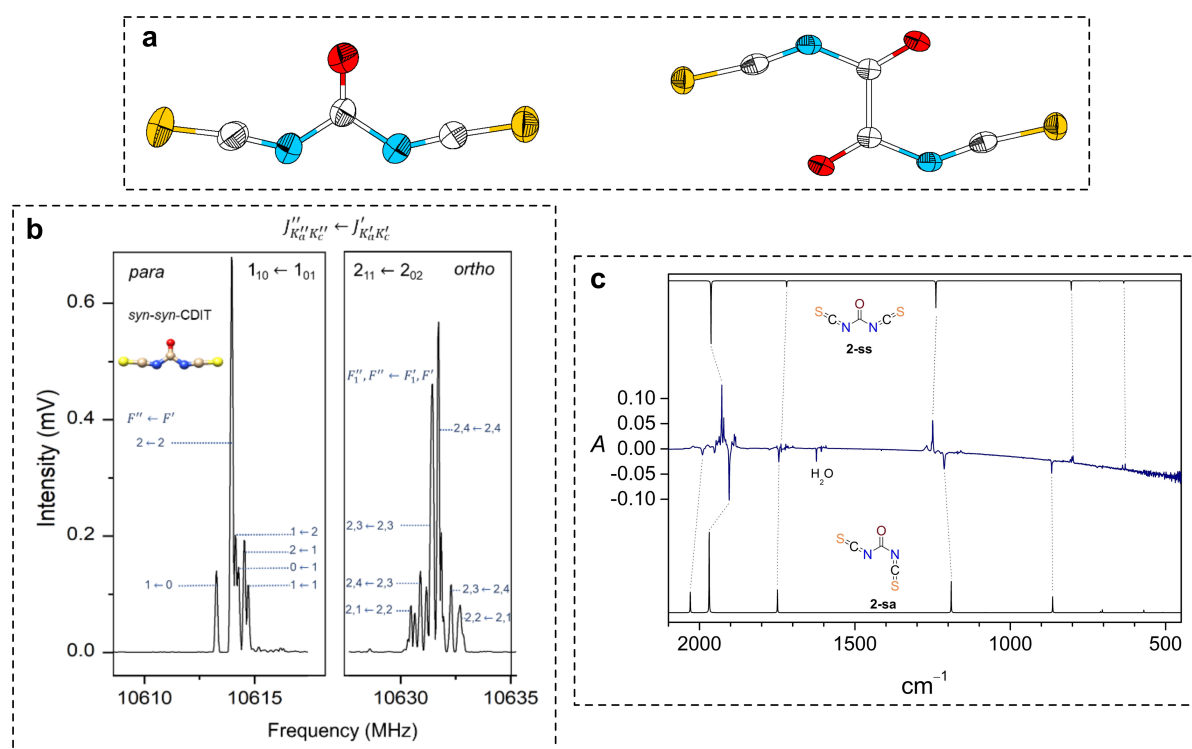

Figure 5.5: (a) Molecular structures of carbonyl diisothiocyanate and oxalyl diisothiocyanate. (b) Rotational transitions of *para* and *ortho syn-syn* carbonyl diisothiocyanate in its microwave spectrum. (c) Difference IR spectrum of *syn* and *anti* carbonyl diisothiocyanate after irradtion of oxalyl diisothiocyanate with UV light and subsequent annealing.

Many attempts to synthesize other carbonyl dipseudohalides (CD*PsH*) e.g. carbonyl di-selenocyanate or thiocarbonyl diisocyanate did not end in isolable products. Carbonyl diselenocyanate (CO(SeCN)) could possibly be observed in solution by ^{13}C-NMR spectroscopy with chemical shifts of 185.3 ppm and 98.1 ppm (Figure 5.6), but the collected solid product decomposes above $-30\,°C$ or during dissolution. Therefore, the alkyl substituted *tert*-butylcarbonyl isoselenocyanate (CO(NCSe)*t*Bu) was synthesized to confirm the existence of carbonyl selenocyanates. The isolation of this compound as crude solid was not possible due to decomposition during solvent removal, but it is manageable in solution and detectable by ^{13}C-NMR spectroscopy with signals at 171.4 ppm and 144.0 ppm.
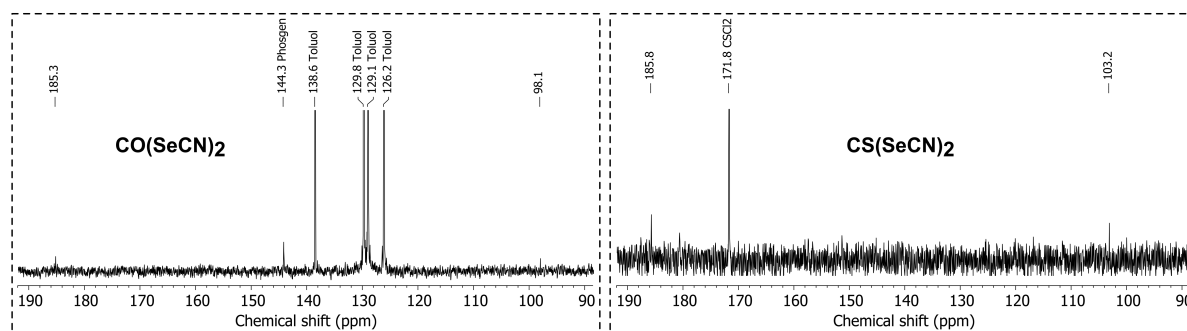

Figure 5.6: Excerpts from the ^{13}C{^{1}H}-NMR spectra of carbonyl diselenocyanate in THF-d$_8$ (left) and thiocarbonyl diselenocyanate in THF-d$_8$ (right).

The synthesis of thiocarbonyl group containing pseudohalides was first attempted for thiocarbonyl diisocyanate (CS(NCO)$_2$). It was not possible to synthesize this compound through the employed synthetic routes, but in the meantime HENNES GÜNTHER (working group TAMBORNINO) could observe it in solution and isolate a defined reaction product with ethanol.[143] The next compound is thiocarbonyl diisothiocyanate (CS(NCS)$_2$) from which the synthesis yielded in the isolation of the known, albeit hitherto poorly characterized, thiocarbonyl dithiocyanate (CS(SCN)$_2$). Despite the former being the thermodynamically more stable reaction product, it was not possible to find a synthetic pathway resulting in the isolation of the pure compound. DFT calculations confirmed that the kinetic reaction product thiocarbonyl dithiocyanate (CS(SCN)$_2$) is formed *via* a lower transition state. Its crystal structure was determined along with the monosubstituted chlorothiocarbonyl thiocyanate (CS(SCN)Cl, Figure 5.7),[168] which concludes to the sixth known structure of CD*PsH*. Lastly, an effort to synthesize thiocarbonyl diselenocyanate (CS(SeCN)$_2$) was made and resulted in the possible detection by ^{13}C-NMR spectroscopy with signals at 185.8 ppm and 103.2 ppm (Figure 5.6). The shifts match the observation made for the synthesis attempt of carbonyl diselenocyanate (CO(SeCN)$_2$) and underline the above stated conclusions.
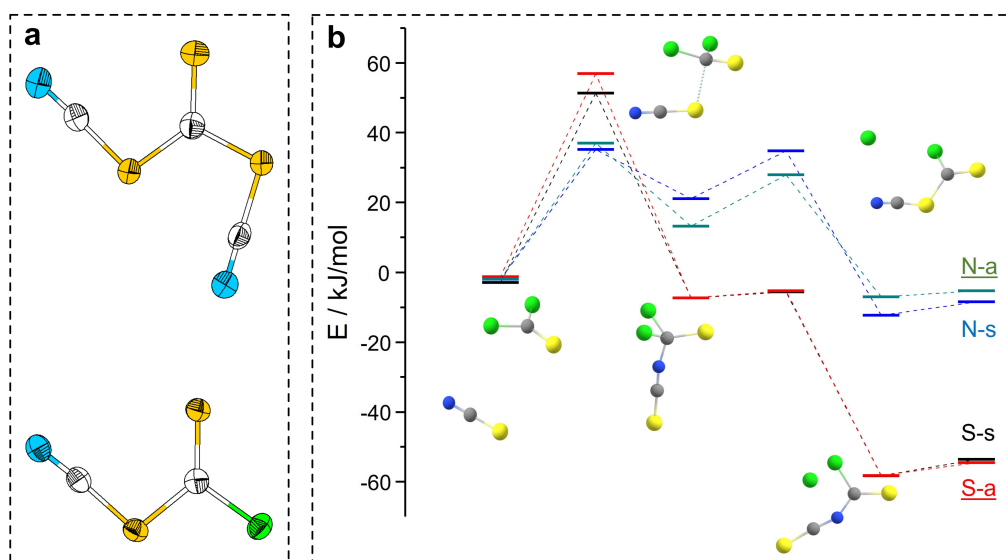
Figure 5.7: (a) Molecular structures of thiocarbonyl dithiocyanate and chlorothiocarbonyl thiocyanate. (b) Energy profiles for exchanging one chloride of thiophosgene with thiocyanate for sulfur or nitrogen in terminal position in their *syn* and *anti* conformation.

At the end of part one, oxalylchloride isothiocyanate (Cl(CO)$_2$NCS) and chlorocarbonyl isothiocyanate (CO(NCS)Cl) were synthesized. During the synthesize of oxalylchloride isothiocyanate an equilibrium with 2-chlorothiazol-4,5-dione in solution was observed. Further investigations with SC-XRD analysis and vibrational spectroscopy led to the conclusion that only the latter one exists in the solid state. Both compounds decompose in solution at room temperature to chlorocarbonyl isothiocyanate, which was extensivley studied by SVEN RINGELBAND (working group TAMBORNINO).[147]

The second part of this dissertation deals with the reactivity of CD*PsH*. Carbonyl diisocyanate (CO(NCO)$_2$) and -diisothiocyanate (CO(NCS)) react with hydrogen halides to form carbonyl bis(carbamoylhalides) and halogenido substituted 1,3,5-thiadiazine-4-ones, respectivley. Carbonyl diisocyanate adds two equivalents nucleophile, while carbonyl diisothiocyanate only adds one and undergoes intramolecular ring-closure. The different reaction pathways are thermodynamically driven by the preference of oxygen to form an ex-ring double bond versus the sulfur to form in-ring single bonds with carbon atoms.[169] Both compound classes show extended hydrogen bonding networks in the solid state, which were examined in detail by the reaction products between carbonyl diiso(thio)cyanate and nucleophiles e.g. alcohols, thiols and amines (Figure 5.8). *N,N'*-Carbonyl bis(carbamates), -bis(*S*-thiocarbamates) and *N,N'*-biscarbamoyl ureas are formed during the reaction with carbonyl diisocyanate, respectivley.[170] All molecules form an intramolecular hydrogen bond and intermolecular hydrogen bonds to form either dimers or chains. The reaction of nucleophiles with carbonyl diisothiocyanate yieldes substituted

1,3,5-thidiazine-4-ones, all of which form dimers *via* intermolecular hydrogend bonds.[171] This is in contrast to the chain forming halogenido substituted 1,3,5-thiadiazine-4-ones. Further packing of the molecules of all compound classes depends on the size of the substituted group, e. g. methyl versus phenyl. For small alkyl groups polar interactions predominate, while non-polar interactions dominate as the size of the alkyl or aryl groups increases.
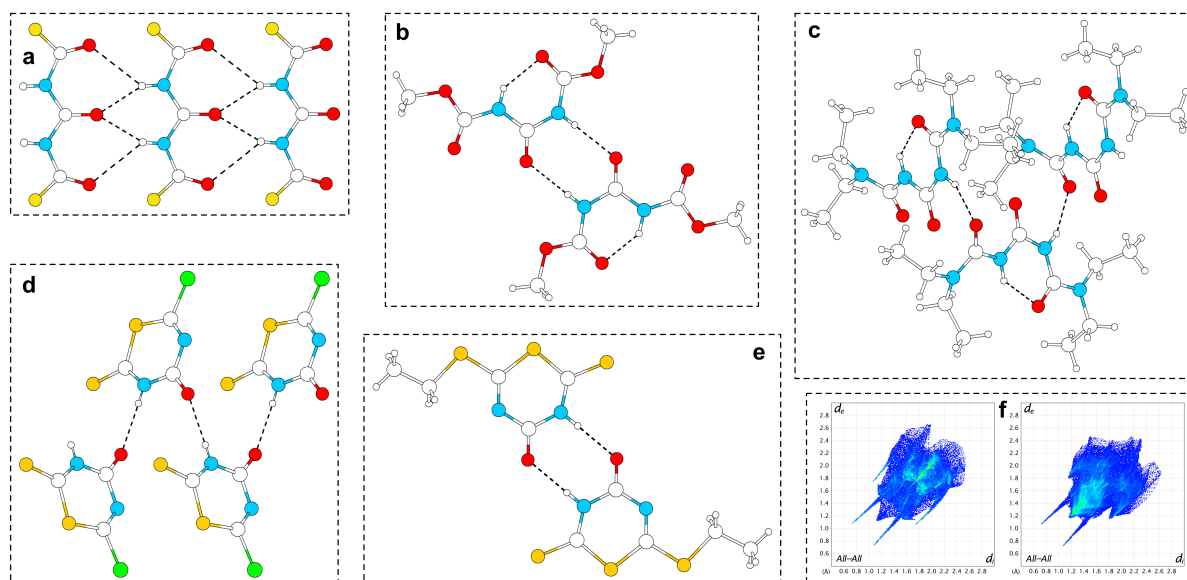

Figure 5.8: Examples of various hydrogen bonding networks in the solid state of reaction products from carbonyl diisocyanate (a-c) and carbonyl diisothiocyanate (d-e) with nucleophiles. (a) strands, (b) dimers, (c) chains, (d) chains, (e) dimers, (f) exemplary fingerprint plots generated from the Hirshfeld surface.

These reactions of carbonyl diisocyanate and carbonyl diisothiocyanate with nucleophiles led to the crystallisation of some side products like derivatives of isocyanuric acid and biuret, which could possibly hint at reactive species being present in solution during the reaction. Nucleophilic additions of organolithium compounds to carbonyl diisocyanate were tested with methyl lithium, *n*-butyl lithium and lithium methoxide, but defined reaction products were not collected. It is assumed that the formed anions are too unstable to isolate, therefore an acidious workup to protonate them is suggested. Surprisingly exciting was the result of the reaction of carbonyl diisocyanate with iron bis(diisopropylphenyltrimethyl-silyamide), in which a reaction with the ligands and crystallization of a new type of metal complex was observed. This new complex, featuring a substituted biuret ligand and tetrahedral coordination of iron, is the first one to be reported. While crystals of reactions with cobalt or nickel, as well as carbonyl diisothiocyanate were not obtained, the equivalent metal complex from nickel and carbonyl diisothiocyanate was observed in mass spec-

trometry. This proofs that the reaction or crystallization conditions need to be adjusted in order to obtain more of these complexes.

Future prospects of this dissertation are to investigate in collaboration the rotational spectrum of carbonyl diisocyanate, the IR spectrum of oxalyl chloride isothiocyanate or rather 2-chlorothiazol-4,5-dione in solid argon-matrix and its behaviour upon irradiation with UV light (Scheme 5.2 a). Further, the isolation of a pure sample and solid state characterization of carbonyl diselenocyanate and thiocarbonyl diselenocyanate should be possible by filtration over a cooled frit or the use of other solvents e.g. dioxane. A complete new approach would be the synthesis from (thio)urea, carbon diselenide and mercury chloride (Scheme 5.2 b). In addition, it is worth taking a look at the missing NMR spectroscopic and molecular structure data of carbonyl dicyanide ($CO(CN)_2$) mentioned in the introduction. In this work asymmetrical carbonyl dipseudohalides were not considered, but to study their synthesis (Scheme 5.2 c), characterization and reactivity should enhance the knowlegde of conformations and crystal packing of small molecules even further. Aside from the synthesis of new carbonyl pseudohalides an investigation of the starting materials phosgene, thiophosgene and oxalyl chloride is also of interest. For instance, neutron diffraction experiments of phosgene and thiophosgene at ISIS in Oxford are planned.
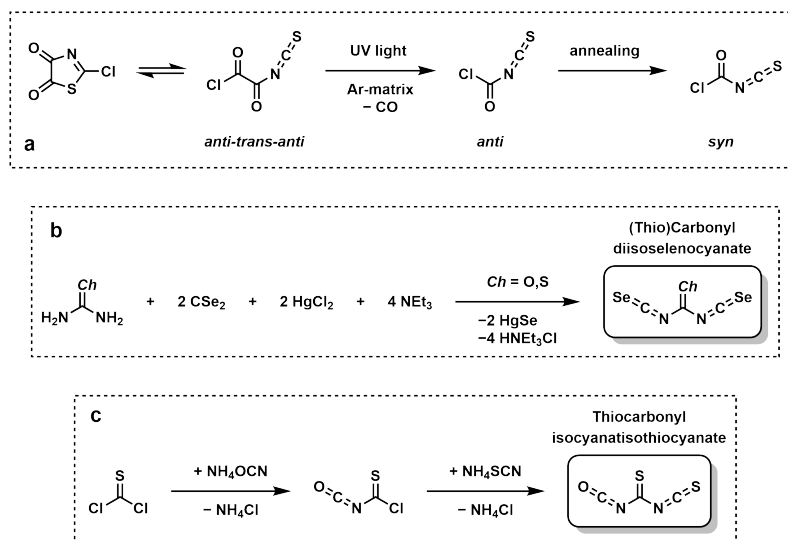
Scheme 5.2: (a) Possible photolytical behaviour of 2-chlorothiazol-4,5-dione in solid argon-matrix upon irradiation with UV light. (b) New synthetic approach towards the synthesis of (thio)carbonyl diisoselenocyanate. (c) Possible pathway for the synthesis of asymmetric carbonyl dipseudohalides illustrated by thiocarbonyl isocyanateisothiocyanate.

6 Experimenteller Teil

6.1 Arbeitstechniken

Alle Arbeiten wurden mit Standard-SCHLENK-Technik unter Argon-Schutzgasatmosphäre und Hochvakuum (1×10^{-3} mbar) oder in einer Glovebox mit Argonatmosphäre (MBRAUN UNILAB) durchgeführt. Verwendete Glasgeräte wurden zuvor ausgeheizt und sekuriert. Temperaturempfindliche Substanzen wurden Langzeit in einer Gefriertruhe von ARCTIKO bei –75 °C gelagert. Alle Lösungsmittel wurden mittels Standardprozedur absolutiert[172] und über Molekularsieb (3 Å oder 4 Å) gelagert. Chemikalien wurden kommerziell von ABCR, MERCK, SIGMA-ALDRICH, BLDPHARM, CARBOLUTION, TCI, FISHER SCIENTIFIC, ACROS ORGANICS, EURISOTOP oder GHC erworben und nach Standardprozeduren gereinigt[172] oder wie geliefert verwendet. Deuterierte Lösungsmittel wurden umkondensiert, entgast und über Molekularsieb (3 Å oder 4 Å) gelagert. Phosgen wurde aus Triphosgen nach einer Synthese von ECKERT und AUERWECK dargestellt,[29] bevor eine Phosgen-Gasflasche von SYNTHESIA käuflich erworben wurde. Carbonyldiisocyanat wurde nach eigener Vorschrift (veröffentlicht in Abschnitt 3.4) synthetisiert. Carbonyldiisothiocyanat[67] und Thiocarbonyldithiocyanat[78] wurden nach abgewandelten Literaturvorschriften hergestellt. NMe$_4$SeCN,[164] NH$_4$SeCN[144] und AgSeCN[144] wurden nach Literaturvorschrift synthetisiert. Fe(N(TMS)$_2$)$_2$ und Fe(N(Dipp)(TMS))$_2$ wurden von der Arbeitsgruppe WERNCKE zur Verfügung gestellt.

6.2 Fotografien

Fotografien wurden von mir persönlich falls nicht anders angegeben aufgenommen.

6.3 Analytische Methoden

6.3.1 Kernspinresonanzspektroskopie

Kernspinresonanz (*Nuclear Magnetic Resonance*, NMR) Spektroskopie (^{1}H, ^{13}C, ^{19}F) wurde an einem *AV III HD 250 MHz* oder *AV II 300 MHz* der Firma BRUKER durchgeführt. Die Service-Abteilung des Fachbereichs 15 Chemie der Philipps-Universität Marburg hat Messungen (^{1}H, ^{13}C, ^{15}N) an einem *AV III HD 300 MHz* oder *AV III 500 MHz* der Firma BRUKER durchgeführt. Multiplizitäten sind als Singulett (s), Dublett (d), Triplett (t), Quartett (q), Sextett (sext), Septett (hept) oder Multiplett (m) angegeben. Breite Resonanzsignale sind mit (br) gekennzeichnet.

6.3.2 Elementaranalyse

Elementaranalyse wurde von der Service-Abteilung des Fachbereichs 15 Chemie der Philipps-Universität Marburg an einem *CHN(S) Analysator vario MICRO CUBE* der Firma ELEMENTAR durchgeführt. Luftempfindliche Proben zuvor von mir in der Glovebox in Zinntiegel überführt und luftdicht verschlossen.

6.3.3 Massenspektrometrie

Massenspektrometrie (MS) wurde von der Service-Abteilung des Fachbereichs 15 Chemie der Philipps-Universität Marburg durchgeführt. Elektrosprayionisation (ESI) wurde an einem *Finnigan LTQ-FT Ultra* der Firma THERMO FISHER SCIENTIFIC in Methanol oder Acetonitril vorgenommen. *Liquid Injection Field Desorption Ionization* (LIFDI) wurde an einem *Accu-TOF-GCv* der Firma JEOL in THF, Chloroform, Dichlormethan oder Toluol vorgenommen.

6.3.4 Einkristallstrukturanalyse

Einkristallstrukturanalyse (*Single Crystal X-ray Diffraction*, SC-XRD) wurde an einem *IPDS II* oder *IPDS 2T* der Firma STOE mit jeweils Flächendetektorsystem und Mo-K_α Strahlung (λ = 0.710 73 Å) durchgeführt. Von FRANK TAMBORNINO wurden Messungen an einem *STADIVARI* der Firma STOE mit dem Flächendetektorsystem *Pilatus 300K* von DECTRIS und Cu-K_α Strahlung (λ = 1.541 86 Å) durchgeführt. Alle Geräte sind mit einem Kristall-Kühlsystem von OXFORD CRYOSYSTEMS ausgestattet. Erhaltene Daten wurden mit dem Programm *X-Area* von STOE ausgewertet.[173] Über die Implementierungen *SHELXT*[174] und *SHELXL*[175] innerhalb von *Olex2* (OLEXSYS)[176] wurden die Strukturen gelöst und verfeinert. Strukturen wurden mit *Diamond* von CRYSTAL IMPACT illustriert.[177]

6.3.5 Röntgenpulverdiffraktometrie

Röntgenpulverdiffraktometrie (*Powder X-ray Diffraction*, PXRD) wurde an einem *STADI MP* der Firma STOE mit Cu-K_α Strahlung (λ = 1.541 86 Å) und einem *MYTHEN 1K* Detektor durchgeführt. Proben wurden in Kapillaren in Reflexion oder als Flachträger zwischen Silikon-Klebeband in Transmission gemessen. Präparation wurde zuvor in einer Glove-Box vorgenommen.

6.3.6 Infrarotspektroskopie

Infrarot (IR) Spektroskopie wurde an einem *Alpha FT-IR* Spektrometer der Firma BRUKER mit Diamant ATR Einheit durchgeführt. Das Gerät befindet sich in einer MBRAUN UNI-LAB Glovebox unter Argon-Atmosphäre und wurde vom Arbeitskreis VON HÄNISCH zur Verfügung gestellt. Spektren wurden mit OriginPro aufgetragen.[178]

6.3.7 Raman Spektroskopie

Raman Spektroskopie wurde an einem *Monovista CRS+* der Firma SPECTROSCOPY & IMAGING GMBH, welches mit Lasern der Wellenlängen 488 nm, 532 nm, 633 nm und 785 nm ausgestattet ist, durchgeführt. Das Gerät wurde vom Arbeitskreis KRAUS zur Verfügung gestellt. Spektren wurden mit OriginPro aufgetragen.[178]

6.3.8 Quantenchemische Rechnungen

Periodische quantenchemische Rechnungen wurden mit dem *CRYSTAL17*[179] Programm auf den Marburger Rechenclustern MaRC2 oder MaRC3 durchgeführt. Die PBE0 Methode[180,181] wurde als Funktional und das *Triple-ζ-valence+polarization* (TZVP) Niveau als Basissatz zur Berechnung gewählt, welche von den Karlsruher def2-Basissätzen abgeleitet wurden.[182,183] Intermolekulare Van-der-Waals Wechselwirkungen wurden mit der Grimme empirischen D3 Dispersionskorrektur[184] mit Nulldämpfung berücksichtigt. Der reziproke Raum wurde mittels des Monkhorst-Pakets[185] mit k-Gitter abgetastet. Für die Auswertung der Coulomb- und Austauschintegrale (TOLINTEG) wurden für alle Berechnungen Toleranzfaktoren von 8, 8, 8, 8 und 16 verwendet. Gitterparameter und Atompositionen wurden vollständig unter Berücksichtigung der Raumgruppe optimiert, sowie Standard-DFT-Integrationsgitter und Konvergenzschwellen für die Optimierung aller Berechnungen verwendet. Harmonische Schwingungsfrequenzen, sowie IR und Raman Intensitäten wurden mit *CRYSTAL* berechnet.[186–189] Die Intensitäten wurden für polykristalline Pulver berechnet. Raman-Spektren wurden unter Verwendung eines Pseudo-Voigt-Bandenprofils (50:50 Lorentz:Gauß) und einer Halbwertsbreite von 8 cm^{-1} simuliert. Falls nicht anders angegeben wurde die Standard-Versuchsanordnung (T = 293.15 K, λ = 532 nm) berücksichtigt. Die Banden der IR- und Raman-Spektren wurden visuell mit dem Programm *Jmol*[190,191] auf `http://crysplot.crystalsolutions.eu/` zugeordnet und mit OriginPro[178] abgebildet.

6.4 Reaktionsdurchführungen

6.4.1 Syntheseversuche zu Carbonyldi(iso)selenocyanat
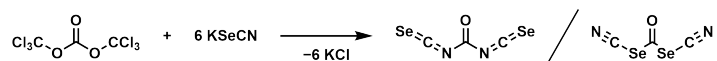
Ia: Triphosgen (1.5 g, 1.0 eq., 5.1 mmol) und Kaliumselenocyanat (4.35 g, 6.0 eq., 30.2 mmol) wurden in einen Kolben gegeben und bei 0 °C mit THF (40 mL) versetzt. Eine sofortige Rotfärbung über gelb wurde beobachtet. Nach 2.5 h wurde die Lösung filtriert. Das rote Filtrat wurde um die Hälfte eingeengt und mit *n*-Hexan (10 mL) versetzt. Es wurde filtriert. Im Filtrat war die Bildung eines schwarzen Feststoffes zu beobachten. Das Lösungsmittel wurde entfernt und ein roter Feststoff erhalten.

^{13}C{^{1}H}-NMR (75 MHz, CD$_3$CN): δ = 97.8 ((Se*C*N)$_2$) ppm.

Ib: Triphosgen (1.5 g, 1.0 eq., 5.1 mmol) wurde in THF (15 mL) gelöst und auf –78 °C gekühlt. Eine Suspension aus Kaliumselenocyanat (4.0 g, 5.5 eq., 27.8 mmol) in THF (45 mL) wurde über 30 min zugetropft. Nach 1 h wurde filtriert. Vom gelben Filtrat wurde in leichtem Unterdruck bei 35 °C THF abdestilliert. Der Rückstand wurde im Vakuum getrocknet.

^{13}C{^{1}H}-NMR (75 MHz, CDCl$_3$): δ = 90.4 (Se(*C*N)$_2$) ppm.
PXRD (Produkt): KCl

Ic: Kaliumselenocyanat (4.0 g, 5.5 eq., 27.8 mmol) wurde in Toluol (30 mL) suspendiert und auf –78 °C gekühlt. Triphosgen (1.5 g, 1.0 eq., 5.1 mmol) gelöst in Toluol (20 mL) wurde über 30 min zugetropft. Die Reaktionslösung wurde über 4.5 h auf –15 °C erwärmt, in welcher sie sich orange-rot färbte. Es wurde filtriert, das farblose Filtrat verworfen und der orangene Feststoff (3.9 g) getrocknet.

^{13}C{^{1}H}-NMR (75 MHz, Py-d$_5$): δ = 121.0 ([SeCN]$^-$) ppm.
PXRD (Produkt): KCl, KSeCN.
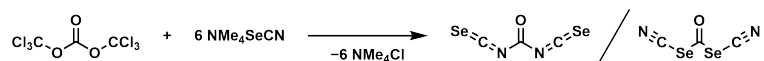
II: Tetramethylammoniumselenocyanat (1.8 g, 2.0 eq., 10.1 mmol) wurde in THF (20 mL) suspendiert und auf –78 °C gekühlt. Triphosgen (1.5 g, 1.0 eq., 5.1 mmol) gelöst in THF (10 mL) wurde über 30 min zugetropft. Die Lösung verfärbte sich von gelb zu dunkelrot 3 min nach beendeter Zugabe. Nach 30 min wurde filtriert und das Lösungsmittel vom orangen Filtrat bei 0 °C entfernt. Es wurde ein orangener Feststoff (1.4 g) erhalten.

^{13}C{^{1}H}-NMR (75 MHz, THF-d$_8$): δ = 141.1 (CO(OCCl$_3$)$_2$), 108.5 (CO(OCCl$_3$)$_2$), 97.3 ((SeCN)$_2$) ppm.
PXRD (Produkt): NMe$_4$Cl
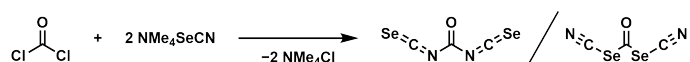
IIIa: Tetramethylammoniumselenocyanat (7.2 g, 1.7 eq., 40.2 mmol) wurde in THF (30 mL) suspendiert und Phosgen (2.4 g, 1.0 eq., 24.3 mmol) in THF (20 mL) gelöst. Beide Gemische wurde auf –78 °C gekühlt. Die Triphosgen-Lösung wurde zur Suspension gegeben. Nach 1.5 h wurde filtriert und das gelbe Filtrat in zwei Hälften geteilt. Für 24 h wurde die erste Hälfte bei 0 °C und die zweite Hälfte bei –25 °C gelagert. In beiden Hälften ist grauer Feststoff entstanden. Das Lösungsmittel der ersten Hälfte wurde entfernt und ein orangener Rückstand erhalten. Das Lösungsmittel der zweiten Hälfte wurde unter Unterdruck bei 0 °C – 30 °C abdestilliert. Es wurde ein orange-roter Rückstand erhalten.

^{13}C{^{1}H}-NMR (75 MHz, THF-d$_8$, Produkt erste Hälfte): δ = 90.7 (Se(CN)$_2$) ppm.
^{13}C{^{1}H}-NMR (75 MHz, THF-d$_8$, Produkt zweite Hälfte): δ = 101.7 (Se(SeCN)$_2$), 98.2 ((SeCN)$_2$), 56.2 ([N(CH$_3$)$_4$]$^+$) ppm.
PXRD (Produkt erste Hälfte): Se(CN)$_2$

IIIb: Schwefeldioxid (150 mL) wurde zuerst bei –78 °C und Phosgen (2.5 g, 1.0 eq., 27.8 mmol) dazu einkondensiert. Die Lösung wurde auf –25 °C erwärmt und Tetramethylammoniumselenocyanat (8.0 g, 1.8 eq., 44.9 mmol) portionsweise über 1.5 h hinzugeben. Nach 2 h wurde das Lösungsmittel bei –25 °C entfernt. Es wurde ein gelber Rückstand erhalten. Ein Löslichkeitstest wurde durchgeführt, indem jeweils etwas Feststoff bei –78 °C in THF, CHCl$_3$, CH$_3$CN, Dimethoxyethan, Toluol, Et$_2$O und Aceton gelöst wurde. Etwas Produkt wurde bei RT zur Zersetzung gelassen.

PXRD (Rohprodukt): Se, NMe$_4$Cl
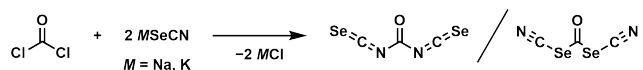
IVa: Phosgen (2.4 g, 1.0 eq., 24.3 mmol) wurde in THF (20 mL) gelöst und auf −78 °C gekühlt. Eine Lösung von Natriumselenocyanat (5.5 g, 1.8 eq., 43.0 mmol) in THF (40 mL) wurde über 40 min hinzugetropft. Nach 1.5 h wurde erfolglos versucht über einen Teflonschlauch mit Vorsatzfilter zu filtrieren. Die gelbe Reaktionslösung wurde auf RT erwärmt und filtriert. Ein zähflüssiges, orangenes Filtrat wurde erhalten. Es wurde Acetonitril (30 mL) hinzugegeben und filtriert. Vom orangenen Filtrat wurde das Lösungsmittel entfernt und ein gelber Feststoff erhalten. Im NMR-Rohr sind rote Kristalle (Se(SeCN)$_2$) gewachsen.

^{13}C{^{1}H}-NMR (75 MHz, CD$_3$CN): δ = 101.7 (Se(Se*C*N)$_2$), 97.6 ((Se*C*N)$_2$) ppm.

IVb: Schwefeldioxid (30 mL) wurde bei −78 °C in einen Stickstoffkolben kondensiert und Phosgen (1.7 g, 1.0 eq., 16.7 mmol) eingeleitet. Kaliumselenocyanat (4.3 g, 1.8 eq., 30.0 mmol) wurde portionsweise zugegeben. Die gelbe Suspension wurde filtriert und Schwefeldioxid vom Filtrat bei 0 °C abgedampft. Ein roter Feststoff (2.6 g) wurde erhalten.

^{13}C{^{1}H}-NMR (75 MHz, CD$_3$CN): δ = 114.3 ppm.
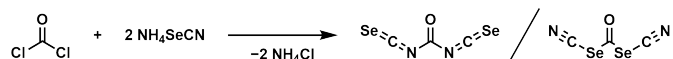
Va: Ammoniumselenocyanat (15 mg, 2.0 eq., 120 µmol) wurde im NMR-Rohr in THF-d$_8$ (0.7 mL) gelöst. Phosgen (15 % in Toluol, 43 µL, 1.0 eq., 60 µmol) wurde hinzugegeben. Sofortige Trübung und Gelbfärbung war zu beobachten.

^{13}C{^{1}H}-NMR (75 MHz, CD$_3$CN): δ = 185.3, 98.1 ppm.

**Vb:** Ammoniumchlorid (3.2 g, 4.0 eq., 60 mmol) und Kaliumselenocyanat (4.3 g, 2.0 eq., 30 mmol) wurden zusammen in einen Stickstoffkolben gefüllt. Bei –78 °C wurde Ammoniak (120 mL) einkondensiert. Die Reaktionslösung wurde für 18 h gerührt und langsam erwärmt. Bei RT wurde der Ammoniak vollständig entfernt. Auf den grauen Rückstand wurde bei –78 °C zuerst Schwefeldioxid (100 mL) und dann Phosgen (1.5 g, 1.0 eq., 15.0 mmol) kondensiert. Die gelbe Suspension wurde auf –30 °C erwärmt. Nach 3 h wurde in der Kälte filtriert. Es wurde ein orangener Feststoff (7.0 g) erhalten. Vom Filtrat wurde das Lösungsmittel bei –20 °C im Vakuum entfernt. Weil der Stickstoffkolben einen Riss aufwies, wurde der Rückstand möglichst schnell in THF (20 mL) gelöst und in einen neuen Stickstoffkolben überführt. Das Lösungsmittel wurde bei –20 °C im Vakuum entfernt. Es wurde ein gelber Feststoff erhalten.

^{13}C{^{1}H}-NMR (75 MHz, THF-d$_8$): δ = 102.9 (Se(SeCN)$_2$), 98.2 ((SeCN)$_2$) ppm.

In situ Folgereaktionen
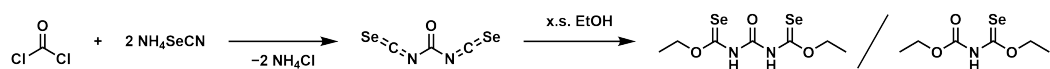
Schwefeldioxid (30 mL) wurde zuerst bei –78 °C in einen Schlenkkolben und danach Phosgen (0.8 g, 1.0 eq., 8.5 mmol) dazu kondensiert. Die Lösung wurde auf –30 °C erwärmt und Ammoniumselenocyanat (1.5 mg, 1.5 eq., 12.5 mol) portionsweise über 1 h dazugegeben. Im Laufe der Zugabe ist ein farbloser Feststoff entstanden. Die Suspension wurde bei –30 °C für 1.5 h gerührt. Das Lösungsmittel wurde im Vakuum entfernt und ein gelbes Pulver erhalten. Bei –45 °C wurde Ethanol (20 mL, 15.8 g, 20 eq., 0.34 mol) unter Rauchentwicklung und Bildung eines roten Feststoffes hinzugegeben. Die Lösung wurde über 20 h langsam auf RT erwärmt. Es wurde filtriert und ein schwarzer Filterkuchen, sowie ein rotes Filtrat erhalten. Das Lösungsmittel des Filtrats wurde im Vakuum entfernt und ein dunkelroter Feststoff erhalten.

^{13}C{^{1}H}-NMR (75 MHz, CD$_3$OD, Feststoff): δ = 107.3 (Se(SeCN)$_2$), 99.8 ((SeCN)$_2$) ppm.
PXRD (Feststoff): Se(SeCN)$_2$, NH$_4$Cl
PXRD (Filterkuchen): Se, NH$_4$Cl
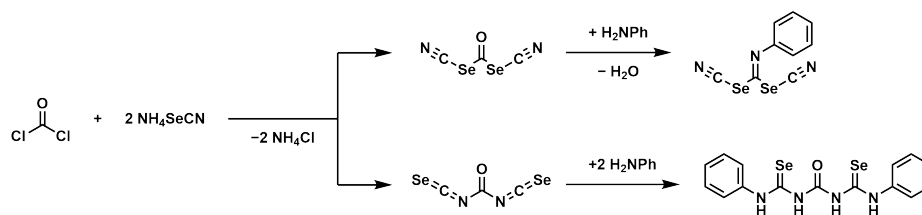
Etwas Rohprodukt aus **IIIb** wurde in Ethanol (8 mL) bei −78 °C suspendiert. Anilin (0.5 mL) wurde zugegeben und die Reaktionslösung über 18 h auf RT erwärmt. Die orange Suspension wurde filtriert und ein gelbes Filtrat erhalten. Die Lösung wurde eingeengt und *n*-Hexan zugegeben. Es bildeten sich zwei Phasen. Die obere, gelbe Phase wurde abdekantiert und das Lösungsmittel im Vakuum entfernt. Es wurde ein roter Rückstand erhalten. Von der unteren, orange-trüben, öligen Phase wurde das Lösungsmittel entfernt.

¹³C{¹H}-NMR (75 MHz, THF-d$_8$, obere Phase): δ = 147.9, 146.2 (Anilin), 143.5, 139.5, 139.1, 130.0, 129.9 (Anilin), 129.8, 129.5, 124.4, 124.2, 121.3, 120.7, 119.9, 119.7 (Anilin), 118.7, 117.1 (Anilin), 115.2, 64.3, 58.0 (Ethanol), 55.9 (N(*C*H$_3$)$_4^+$), 40.6, 32.6 (*n*-Hexan), 30.7, 23.6 (*n*-Hexan), 19.1 (Ethanol), 15.7, 15.0, 14.6 (*n*-Hexan), 14.5 ppm.

¹³C{¹H}-NMR (75 MHz, THF-d$_8$, untere Phase): δ = 148.1 (Anilin), 139.7, 129.8, 129.8 (Anilin), 124.3, 120.9, 118.4 (Anilin), 118.0, 116.0 (Anilin), 114.1, 58.0 (Ethanol), 39.7, 19.2 (Ethanol), 15.6, 14.8 ppm.

6.4.2 Syntheseversuche zu *tert*-Butylcarbonyl(iso)selenocyanat
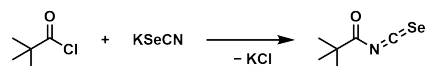
VIa: Pivalinsäurechlorid (0.25 mL, 1.0 eq., 2.1 mmol) und Kaliumselenocyanat (295 mg, 1.0 eq., 2.1 mmol) wurden jeweils in Aceton (5 mL) gelöst. Erstere Lösung wurde zur zweiten Lösung getropft und für 20 min gerührt. Es wurde über einen Teflonschlauch mit vorgebautem Filter filtriert. Vom roten Filtrat wurde das Lösungsmittel im Vakuum entfernt. Ein gelber Feststoff, welcher sich schnell rot färbte, wurde erhalten.

Kaliumselenocyanat (72 mg, 1.0 eq., 0.5 mmol) wurde in Aceton-d$_6$ (1 mL) gelöst und Pivalinsäurechlorid (60 µL, 1.0 eq., 0.5 mmol) zugegeben. Die Suspension wurde nach 5 min über eine Spritze mit Spritzenvorsatzfilter in ein NMR-Rohr überführt.

¹³C{¹H}-NMR (75 MHz, CO(CD$_3$)$_2$): δ = 210.1 (*C*Se$_2$), 209.9, 69.7, 69.3, 55.6 ppm.

¹³C{¹H}-NMR (75 MHz, CO(CD$_3$)$_2$, NMR-Maßstab): δ = 210.2 (*C*Se$_2$), 171.8 (*C*=O), 143.8 (N*C*Se), 69.4, 44.8 (*C*(CH$_3$)$_3$), 26.4 (*C*H$_3$) ppm.

¹³C{¹H}-NMR (75 MHz, CO(CD₃)₂, NMR-Maßstab nach 24 h): δ = 210.1 (*C*Se₂), 207.1, 193.9, 190.8, 187.5, 184.4, 176.5, 176.2, 174.6, 171.8, 112.8, 70.8, 69.4, 54.9, 51.6, 50.3, 45.6, 44.8, 41.5, 40.9, 40.2, 40.1, 27.9, 27.6, 27.5, 27.4, 27.3, 27.3, 27.0, 27.0, 26.9, 26.9, 26.3, 24.8, 24.5, 24.3 ppm.

VIb: Kaliumselenocyanat (360 mg, 1.0 eq., 2.5 mmol) wurde ein Ethanol (10 mL) gelöst und Pivalinsäurechlorid (0.31 mL, 1.0 eq., 2.5 mmol) zugegeben. Ein roter Niederschlag bildete sich sofort. Die Suspension wurde für 1 h zum Reflux erhitzt. Es wurde filtriert und ein gelbes Filtrat, sowie ein grauer Filterkuchen erhalten. Das Lösungsmittel vom Filtrat wurde im Vakuum entfernt und ein gelblich-brauner Feststoff erhalten.

¹³C{¹H}-NMR (75 MHz, C₂H₅OH, Reaktionskontrolle): δ = 178.3, 111.3, 60.2, 38.4, 26.6, 17.5, 13.6 ppm.
¹³C{¹H}-NMR (75 MHz, THF-d₈): δ = 69.5, 27.1, 25.8, 13.6 ppm.

VIc: Kaliumselenocyanat (720 mg, 1.0 eq., 5.0 mmol) wurde in THF (15 mL) gelöst und mit Pivalinsäurechlorid (0.62 mL, 1.0 eq., 5.0 mmol) versetzt. Nach 45 min wurde die gelbe, trübe, zähflüssige Lösung filtriert. Etwas Filtrat (4 mL) wurde entnommen, mit *n*-Hexan überschichtet und bei −75 °C gelagert. Es konnte keine Kristallisation beobachtet werden. Vom restlichen Filtrat wurde das Lösungsmittel im Vakuum entfernt und wenig gelber Feststoff erhalten. Der Feststoff verfärbt sich bei RT rot.

Kaliumselenocyanat (72 mg, 1.0 eq., 0.5 mmol) wurde in THF-d₈ (1.0 mL) im NMR-Rohr suspendiert und Pivalinsäurechlorid (60 μL, 1.0 eq., 0.5 mmol) zugegeben. Die gelbe Lösung wurde 2 min in ein Ultraschallbad gestellt.

¹³C{¹H}-NMR (75 MHz, THF, Reaktionskontrolle): δ = 170.2 (*C*=O), 142.8 (N*C*Se), 43.6 (*C*(CH₃)₃), 25.2 (*C*H₃) ppm.
¹³C{¹H}-NMR (75 MHz, THF-d₈): δ = 171.4 (*C*=O), 143.9 (N*C*Se), 44.8 (*C*(CH₃)₃), 28.0, 27.0, 26.9 (*C*H₃) ppm.
¹³C{¹H}-NMR (75 MHz, THF-d₈, NMR-Maßstab): δ = 171.4 (*C*=O), 144.0 (N*C*Se), 44.7 (*C*(CH₃)₃), 26.4 (Edukt), 26.4 (*C*H₃) ppm.

VId: Kaliumselenocyanat (720 mg, 1.0 eq., 5.0 mmol) wurde in THF (15 mL) gelöst und Pivalinsäurechlorid (0.62 mL, 1.0 eq., 5.0 mmol) zugegeben. Die Reaktionslösung wurde für 90 min zum Reflux erhitzt. Es wurde filtriert und ein rötliches Filtrat, sowie ein gelber Filterkuchen erhalten. Das Lösungsmittel vom Filtrat wurde im Vakuum entfernt und ein gelb-oranger Feststoff erhalten.

^{13}**C{^{1}H}-NMR** (75 MHz, THF, Reaktionskontrolle): δ = 170.5 (*C*=O), 143.1 (N*C*Se), 43.9 (*C*(CH$_3$)$_3$), 25.6 (*C*H$_3$) ppm.

^{13}**C{^{1}H}-NMR** (75 MHz, THF-d$_8$): δ = 207.0, 193.8, 171.4, 51.5, 44.8, 41.6, 28.0, 27.6, 27.4, 27.3, 27.0, 26.6, 26.4 ppm.

PXRD (Filterkuchen): KCl
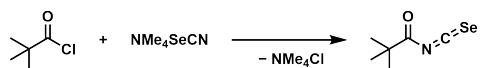
VIIa: Tetramethylammoniumselenocyanat (364 mg, 1.0 eq., 2.0 mmol) wurde in THF (5 mL) suspendiert und Pivalinsäurechlorid (0.25 mL, 1.0 eq., 2.0 mmol) zugegeben. Nach 1.5 h wurde die gelbe, trübe Lösung filtriert und ein farbloser Filterkuchen, sowie ein gelbes Filtrat erhalten. Das Lösungsmittel vom Filtrat wurde in Vakuum entfernt und ein orangenes Pulver erhalten.

^{13}**C{^{1}H}-NMR** (75 MHz, THF, Reaktionskontrolle): δ = 179.6 (Edukt), 170.5 (*C*=O), 49.5 (Edukt), 43.9 (*C*(CH$_3$)$_3$), 26.6 (Edukt), 25.6 (*C*H$_3$) ppm.

^{13}**C{^{1}H}-NMR** (75 MHz, THF-d$_8$): δ = 30.8 ppm.

VIIb: Tetramethylammoniumselenocyanat (90 mg, 1.0 eq., 0.5 mmol) wurde in CD$_3$CN (1.0 mL) im NMR-Rohr suspendiert und Pivalinsäurechlorid (60 µL, 1.0 eq., 0.5 mmol) zugegeben. Die gelbe Lösung wurde 2 min in ein Ultraschallbad gestellt.

^{13}**C{^{1}H}-NMR** (75 MHz, CD$_3$CN): δ = 181.4 (Edukt), 172.3 (*C*=O), 56.2 ([N(*C*H$_3$)$_4$]$^+$), 50.3 (Edukt), 41.4 (*C*(CH$_3$)$_3$), 27.8, 27.2 (Edukt), 26.8, 26.2 (*C*H$_3$), 24.7 ppm.
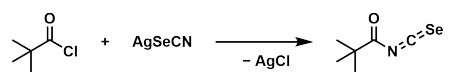
VIIIa: Silberselenocyanat (320 mg, 1.0 eq., 1.5 mmol) wurde in THF (6 mL) suspendiert und auf 0 °C gekühlt. Pivalinsäurechlorid (185 µL, 1.0 eq., 1.5 mmol) wurde zugegeben und der Stickstoffkolben abgedunkelt. Die Kühlung wurde entfernt und die Suspension für 3 d gerührt. Nach Filtration wurde ein rosa Filterkuchen und ein gelbes Filtrat erhalten. Das Lösungsmittel des Filtrats wurde im Vakuum entfernt und wenig orange-roter Feststoff erhalten.

PXRD (Filterkuchen): AgCl, AgSeCN

VIIIb: Silberselenocyanat (426 mg, 1.0 eq., 2.0 mmol) wurde mit dem gleichen Volumen Glaspulver vermengt und in ein Schlenkrohr gefüllt. Pivalinsäurechlorid (0.25 mL, 1.0 eq., 2.0 mmol) wurde in ein Schlenkrohr gegeben. Beide Kolben wurden über eine Etherbrücke miteinander verbunden und in flüssig Stickstoff eingefroren. Das System wurde unter Vakuum (1×10^{-3} mbar) gesetzt. Pivalinsäurechlorid wurde auf das Gemenge mit Silberselenocyanat kondensiert und gut vermischt. Die Apparatur wurde unter Vakuum für 24 h bei –20 °C aufbewahrt. Alle flüssigen Bestandteile wurden in ein neues Schlenkrohr wie zuvor kondensiert. Es wurde eine farblose Flüssigkeit erhalten.

^{13}C{^{1}H}-NMR (75 MHz, THF-d_8): δ = 181.5 (Edukt), 50.3 (Edukt), 27.4 (Edukt) ppm.
PXRD: AgSeCN

6.4.3 Syntheseversuche zu Thiocarbonyldiisocyanat
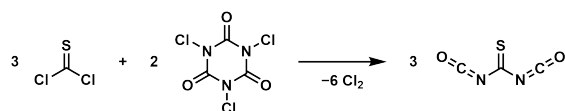
IXa: Trichlorisocyanursäure (3.1 g, 2.0 eq., 13.3 mmol) und 2-Chlornitrobenzol (15 g) wurden zusammen auf 100 °C erwärmt. Thiophosgen (1.5 mL, 3.0 eq., 19.6 mmol) wurde hinzugetropft. Über eine Destillierbrücke wurden entstehende Flüssigkeiten bei 0 °C in einem Vorlagekolben aufgefangen. Ein gelbes Gas bildete sich. Nach 30 min wurde auf 120 °C und nach weiteren 30 min auf 150 °C erhöht, sowie der Vorlagekolben auf –50 °C gekühlt. Ein leichter Argongasstrom wurde angelegt. Eine rötliche Flüssigkeit wurde aufgefangen. Nach 30 min wurde auf 170 °C erhöht und für 45 min destilliert. Es wurde ein rotes Destillat erhalten.

^{13}C{^{1}H}-NMR (75 MHz, CDCl$_3$): δ = 144.3, 143.3 (TCCA), 141.1, 133.2 (2-Chlornitrobenzol), 132.0 (2-Chlornitrobenzol), 130.3, 129.9 (2-Chlornitrobenzol), 127.7 (2-Chlornitrobenzol), 125.7 (2-Chlornitrobenzol), 97.6 ppm.

IXb: Trichlorisocyanursäure (1.5 g, 2.0 eq., 6.7 mmol) wurde in Chloroform (20 mL) suspendiert und Thiophosgen (0.77 mL, 3.0 eq., 10.0 mmol) zugegeben. Die Suspension erwärmte und verfärbte sich von rot zu gelb. Es wurde auf 0 °C gekühlt langsam auf RT erwärmt. Nach 20 h wurde filtriert. Es wurde ein farbloser Filterkuchen und ein gelbliches Filtrat erhalten. Das Filtrat wurde eingeengt.

¹³C{¹H}-NMR (75 MHz, CDCl₃, Filtrat): δ = 169.3 (CSCl₂), 158.8, 142.0, 135.4, 99.0, 29.5 ppm.

¹³C{¹H}-NMR (75 MHz, CD₃CN, Filterkuchen): δ = 144.8 (TCCA) ppm.

IXc: Trichlorisocyanursäure (1.6 g, 2.0 eq., 6.8 mmol) wurde in Chloroform (20 mL) suspendiert und Thiophosgen (0.78 mL, 3.0 eq., 10.2 mmol) zugegeben. Es wurde für 2 h zum Sieden erhitzt. Acetonitril (5 mL) wurde zugegeben und die sofortige Entwicklung eines gelben Gases beobachtet. Es wurde für weitere 2 h zum Sieden erhitzt. Die Reaktionslösung wurde fraktioniert destilliert und drei Fraktionen bei 62 °C, 65 °C und 82 °C erhalten. Es blieb ein roter Rückstand zurück.

¹³C{¹H}-NMR (75 MHz, CDCl₃, 1. Fraktion): δ = 137.4, 116.5 (Acetonitril), 77.4 (Chloroform), 2.0 (Acetonitril) ppm.

¹³C{¹H}-NMR (75 MHz, CDCl₃, 2. Fraktion): δ = 116.5 (CH₃CN), 77.4 (Chloroform), 1.7 (Acetonitril) ppm.

¹³C{¹H}-NMR (75 MHz, CDCl₃, 3. Fraktion): δ = 173.3, 140.9, 116.5 (Acetonitril), 77.4 (Chloroform), 1.5 (Acetonitril) ppm.
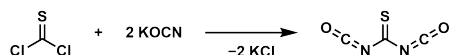
Xa: Thiophosgen (0.38 mL, 1.0 eq., 5.0 mmol) wurde in THF (30 mL) gelöst und auf –78 °C gekühlt. Kaliumcyanat (0.8 mg, 2.0 eq., 10.0 mmol) wurde zugegeben. Die Reaktionslösung wurde über 22 h auf RT erwärmen gelassen. Die orangene Suspension wurde filtriert. Es wurde ein farbloser Filterkuchen und ein gelbes Filtrat erhalten. Das Filtrat wurde auf 5 mL eingeengt.

¹³C{¹H}-NMR (75 MHz, THF-d₈, Filtrat): δ = 171.0 (CSCl₂), 149.6, 30.0 ppm.
PXRD (Filterkuchen): KOCN

Xb: Kaliumcyanat (4.0 g, 2.0 eq., 50.0 mmol) wurde auf 0 °C gekühlt und Thiophosgen (1.9 mL, 1.0 eq., 25 mmol) tropfenweise zugegeben. Die orangene Suspension wurde für 4 h gerührt. Das Gemisch wurde in THF aufgenommen und filtriert. Der Filterkuchen wurde mit THF gewaschen. Das gelbe Filtrat wurde bei 0 °C im Vakuum eingeengt.

¹³C{¹H}-NMR (75 MHz, THF-d₈, Filtrat): δ = 170.8 (CSCl₂) ppm.
PXRD (Filterkuchen): KOCN

Xc**:** Thiophosgen (0.38 mL, 1.0 eq., 5.0 mmol) wurde bei −20 °C in Schwefeldioxid gelöst und Kaliumcyanat (0.8 mg, 2.0 eq., 10.0 mmol) zugegeben. Nach 2.5 h wurde filtriert und ein farbloser Filterkuchen, sowie eine orangene Lösung erhalten. Schwefeldioxid wurde bei RT langsam abgedampft und eine rote Flüssigkeit gewonnen.

¹³C{¹H}-NMR (75 MHz, CDCl₃, Filtrat): δ = 170.6 (*C*SCl₂) ppm.
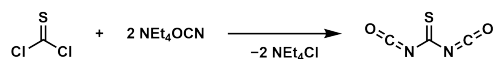
XI**:** Thiophosgen (0.26 mL, 1.0 eq., 3.4 mmol) wurde in THF (25 mL) gelöst und auf −78 °C gelöst. Tetraethylammoniumcyanat (1.2 g, 2.0 eq., 6.8 mmol) wurde hinzugegeben. Es wurde über 20 h langsam auf RT erwärmt. Die Suspension wurde filtriert und ein gelber Filterkuchen, sowie ein gelbes Filtrat erhalten. Das Filtrat wurde eingeengt.

¹³C{¹H}-NMR (75 MHz, THF-d₈, Filtrat): δ = 149.6 ppm.
¹³C{¹H}-NMR (75 MHz, D₂O, Filterkuchen): δ = 52.0 ([N(*C*H₂CH₃)₄]), 6.6 ([N(CH₂*C*H₃)₄]) ppm.
PXRD (Filterkuchen): NEt₄OCN
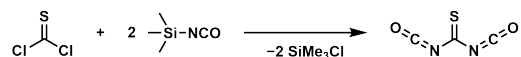
XIIa**:** Thiophosgen (0.15 mL, 1.0 eq., 2.0 mmol) und Trimethylsilylisocyanat (0.54 mL, 2.0 eq., 4.0 mmol) wurden in THF (15 mL) gelöst. Es wurde für 3.5 h zum Sieden erhitzt. Die gelbe Lösung wurde eingeengt.

XIIb**:** Thiophosgen (0.38 mL, 1.0 eq., 5 mmol) und Trimethylsilylisocyanat (0.68 mL, 1.0 eq., 5 mmol) wurden in flüssigem Schwefeldioxid bei −20 °C gelöst. Nach 3 h wurde bei RT Schwefeldioxid verdampft und die erhaltene rote Flüssigkeit für 1 h gerührt.

¹³C{¹H}-NMR (75 MHz, CDCl₃): δ = 170.5 (*C*SCl₂), 123.8 (O*C*N), 0.9 (Si(*C*H₃)₃) ppm.
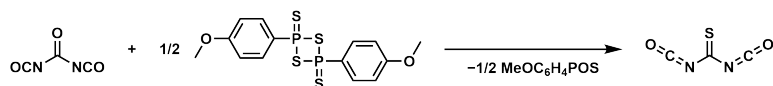
XIIIa: Lawessons-Reagenz (405.0 mg, 0.5 eq., 1.0 mmol) wurde in Toluol (3 mL) suspendiert und Carbonyldiisocyanat (224.0 mg, 1.0 eq., 2.0 mmol) in Toluol (2 mL) zugetropft. Die Suspension wurde für 2 h zum Sieden erhitzt. Die gelbe Lösung wurde auf 0 °C gekühlt und ein Niederschlag präzipitierte. Es wurde filtriert und ein farbloser Filterkuchen, sowie ein gelbes Filtrat erhalten. Toluol wurde bei 130 °C abdestilliert. Es wurde ein oranger, öliger Rückstand erhalten

^{13}**C{^{1}H}-NMR** (75 MHz, THF-d^8): δ = 207.3, 200.2, 165.2 (d, Lawessons), 150.5, 138.6, 134.1, 133.6, 133.3 (d, Lawessons), 129.8, 129.4, 129.2, 129.1, 126.6, 126.2, 124.5, 123.8, 115.2 (d, Lawessons), 56.2 (Lawessons), 30.7, 21.7 ppm.

XIIIb: Lawessons-Reagenz (140.0 g, 0.4 eq., 0.4 mmol) wurde in CDCl$_3$ (1 mL) suspendiert und Carbonyldiisocyanat (100.0 mg, 1.0 eq., 0.9 mmol) gelöst in CDCl$_3$ (1 mL) zugetropft. Es wurde bei RT für 2 d gerührt und über Kieselgur filtriert. Der Filterkuchen wurde mit CDCl$_3$ gewaschen.

^{13}**C{^{1}H}-NMR** (75 MHz, CDCl$_3$, Reaktionskontrolle): δ = 165.1 (d, Lawessons), 164.5, 156.7, 156.6, 139.8, 135.3, 135.1, 134.9 (d, Lawessons), 130.0, 120.6, 119.1, 115.1 (d, Lawessons), 114.8, 114.5, 114.5, 114.2, 55.9 (Lawessons) ppm.
^{13}**C{^{1}H}-NMR** (75 MHz, CDCl$_3$): δ = 165.1 (d, Lawessons), 164.8 (d), 164.5, 163.9, 156.7, 156.6, 153.3, 148.2, 144.1, 139.8, 135.2 (d), 134.9 (d, Lawessons), 134.5, 134.4, 134.2, 132.6, 132.4, 131.1, 130.0, 129.9, 125.4, 123.9, 120.6, 120.0, 119.1, 115.1 (d, Lawessons), 114.7 (d), 114.2, 55.8 (Lawessons) ppm.

XIIIc: Lawessons-Reagenz (140.0 g, 0.4 eq., 0.4 mmol) wurde in THF-d$_8$ (1 mL) suspendiert und Carbonyldiisocyanat (100.0 mg, 1.0 eq., 0.9 mmol) gelöst in THF-d$_8$ (1 mL) zugetropft. Es wurde bei RT für 2 d gerührt und über Kieselgur filtriert. Der Filterkuchen wurde mit THF-d$_8$ gewaschen.

^{13}**C{^{1}H}-NMR** (75 MHz, THF-d^8, Reaktionskontrolle): δ = 199.8, 197.9, 166.1 (d, Lawessons), 158.4, 154.5, 139.7, 135.9 (d, Lawessons), 134.6, 129.5, 122.5, 121.0, 115.6 (d, Lawessons), 115.3, 115.1, 56.33 (Lawessons) ppm.

6.4.4 Syntheseversuche zu Thiocarbonyldi(iso)selenocyanat
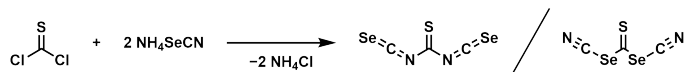
XIVa: Ammoniumselenocyanat (15 mg, 2.0 eq., 120 µmol) wurde in einem NMR-Rohr in CDCl$_3$ (0.6 mL) gelöst. Thiophosgen (5 µL, 1.0 eq., 60 µmol) wurde zugetropft und eine sofortige Präzipitation beobachtet.

^{13}C{^{1}H}-NMR (75 MHz, CD$_3$CN): δ = 183.5, 172.4 (*C*SCl$_2$), 104.1 ppm.

XIVb: Ammoniumselenocyanat (15 mg, 2.0 eq., 120 µmol) wurde in einem NMR-Rohr in THF-d$_8$ (0.6 mL) gelöst. Thiophosgen (5 µL, 1.0 eq., 60 µmol) wurde zugetropft und eine sofortige Präzipitation beobachtet.

^{13}C{^{1}H}-NMR (75 MHz, THF-d^8): δ = 185.8, 171.8 (*C*SCl$_2$), 103.2 ppm.

XIVc: Ammoniumselenocyanat (1.2 g, 2.0 eq., 9.3 mmol) wurde vorgelegt und Schwefeldioxid bei –78 °C aufkondensiert. Es wurde auf –65 °C erwärmt und zu der gelben Lösung Thiophosgen (0.35 mL, 1.0 eq., 4.6 mmol) getropft. Die Lösung wurde auf –30 °C erwärmt. Eine Trübung der Lösung setzte ein. Nach 2 h wurde filtriert und ein gelbes Filtrat erhalten. Schwefeldioxid wurde bei –40 °C im Vakuum entfernt. Ein orangener Feststoff wurde erhalten.

^{13}C{^{1}H}-NMR (75 MHz, CD$_3$CN): δ = 200.6 (S*C*Se), 90.5 (Se(*C*N)$_2$) ppm.
PXRD (Filterkuchen): NH$_4$Cl

6.4.5 Synthese von 2-Chlorthiazol-4,5-dion und Oxalylchloridisothiocyanat
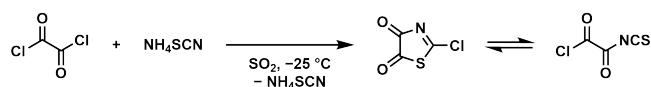
XV: Oxalylchlorid (1.6 mL, 1.0 eq., 18.7 mmol) wurde bei –25 °C in Schwefeldioxid (50 mL) gelöst und über 2 h Ammoniumthiocyanat (1.6 g, 1.2 eq., 21.6 mmol) portionsweise hinzugegeben. Nach weiteren 2 h bei –25 °C wurde filtriert und das Lösungsmittel vom Filtrat im Vakuum entfernt. Der Rückstand wurde von 10 °C auf einen Kühlfinger bei –22 °C sublimiert. 2-Chlorthiazol-4,5-dion (1.65 g, 11.0 mmol, 59 %) wurde als gelber, kristalliner Feststoff erhalten. Kristalle wurden durch Diffusionskristallisation bei –75 °C aus Dichlormethan und *n*-Hexan oder Sublimation gezüchtet.

^{13}C{^{1}H}-NMR (75 MHz, THF-d$_8$): δ = 184.4 (((*C*O)$_2$NCS)Cl), 181.9 (((*C*O)$_2$NCS)Cl), 167.5 (((CO)$_2$N*C*S)Cl), 162.3 (Cl(CO)$_2$N*C*S), 156.8 ((CON*C*S)$_2$), 154.7 ((*C*ONCS)$_2$), 153.7 (Cl(*C*O)$_2$NCS), 153.4 (Cl(*C*O)$_2$NCS) ppm.

CHNS gef. (theo.): C 24.37 (24.09), H 0.07 (0.00), N 9.51 (9.37), S 21.78 (21.44).
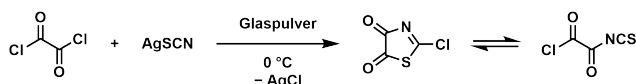
Silberthiocyanat (0.41 g, 1.0 eq., 2.5 mmol) wurde mit dem gleichen Volumen Glaspulver vermengt. Es wurde auf 0 °C gekühlt und Oxalylchlorid (0.22 mL, 1.0 eq., 2.5 mmol) zugegeben. Das Gemisch wurde für 24 h bei 4 °C aufbewahrt. Der Rückstand wurde in Chloroform (10 mL) aufgenommen. Nach Filtration wurde vom Filtrat das Lösungsmittel im Vakuum entfernt. Es wurde ein gelbe, zähflüssige Masse erhalten.

^{13}C{^{1}H}-NMR (75 MHz, THF-d$_8$): δ = 184.3 (((*C*O)$_2$NCS)Cl), 181.9 (((*C*O)$_2$NCS)Cl), 167.5 (((CO)$_2$N*C*S)Cl), 162.3 (Cl(CO)$_2$N*C*S), 156.8 ((CON*C*S)$_2$), 154.7 ((*C*ONCS)$_2$), 153.6 (Cl(*C*O)$_2$NCS), 153.3 (Cl(*C*O)$_2$NCS), 30.8 (Apiezon H) ppm.

6.4.6 Synthese von Chlorcarbonylisothiocyanat

XVI: 2-Chlorthiazol-4,5-dion (650 mg, 1.0 eq., 4.3 mmol) wurde mit Aktivkohle (85 mg) versetzt und für 4.5 h auf 85 °C erhitzt. Es wurde auf RT gekühlt und alle flüssigen Bestandteile wurden im Vakuum (1 × 10^{-3} mbar) und −196 °C abkondensiert. Chlorcarbonylisothiocyanat (421 mg, 3.5 mmol, 80 %) wurde als blass rosa Flüssigkeit erhalten.

^{13}C{^{1}H}-NMR (75 MHz, THF-d$_8$): δ = 154.0 (CO(N*C*S)Cl), 140.2 (*C*O(NCS)Cl) ppm.

6.4.7 Synthesen zu [2+4]-Cycloadditionen von Carbonyldiisocyanat

Umsetzung mit Cyclohexanon
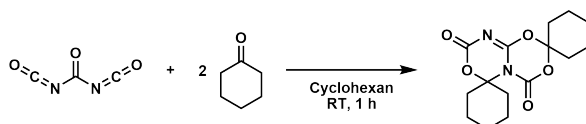
Cyclohexanon (1.4 mL, 3.1 eq., 13.6 mmol) wurde in Cyclohexan (15 mL) gelöst und Carbonyldiisocyanat (495 mg, 1.0 eq., 4.4 mmol) tropfenweise zugegeben. Eine sofortige Trübung und Bildung eines Niederschlages war zu beobachten. Nach 1 h wurde die zähflüssige Suspension filtriert. Der Filterkuchen wurde im Vakuum getrocknet und das Produkt als farbloses Pulver (615 mg, 2.0 mmol, 45 %) erhalten. Vom Filtrat und einer Lösung des Produktes in THF wurde an Luft das Lösungsmittel abdampfen gelassen. Es konnten keine Kristalle erhalten werden.

^{1}H-NMR (300 MHz, THF-d$_8$): δ = 2.52 (td, $^{3}J_{HH}$ = 13.33 Hz, $^{3}J_{HH}$ = 4.76 Hz), 2.23 (q, $^{3}J_{HH}$ = 6.29 Hz), 2.05 (m), 1.71 (m), 1.51 (q, $^{3}J_{HH}$ = 5.62 Hz), 1.30 (m) ppm.
^{13}C{^{1}H}-NMR (75 MHz, THF-d$_8$): δ = 155.9, 150.5, 143.8, 107.6, 95.7, 35.1, 33.9, 25.0, 23.1, 22.8 ppm.

Umsetzung mit *N,N'*-Dicyclohexylcarbodiimid
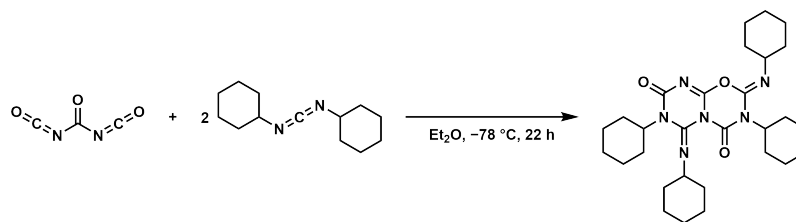
N,N'-Dicyclohexylcarbodiimid (1.3 mL, 2.0 eq., 8.6 mmol) wurde in Diethylether (10 mL) gelöst und auf −78 °C gekühlt. Carbonyldiisocyanat (480 mg, 1.0 eq., 4.3 mmol) gelöst in Diethylether (5 mL) wurde tropfenweise zugegeben. Es wurde für 22 h auf RT erwärmt, in welcher Zeit sich ein Niederschlag bildete. Es wurde filtriert und der Filterkuchen im Vakuum getrocknet. Das Produkt wurde als farbloses Pulver (660 mg, 1.3 mmol, 29 %) erhalten. Im gelblichen Filtrat präzipitierte beim Abkühlen auf 0 °C weiterer Feststoff. Es wurde bei −15 °C zur Kristallisation gelagert. Es konnten keine Kristalle erhalten werden.

^{1}H-NMR (300 MHz, THF-d_8): δ = 4.88 (p, $^3J_{HH}$ = 6.90 Hz), 4.76 (p, $^3J_{HH}$ = 6.90 Hz), 4.04 (hept, $^3J_{HH}$ = 6.34 Hz), 3.39 (hept, $^3J_{HH}$ = 6.00 Hz), 1.43 (dd, $^3J_{HH}$ = 8.66 Hz, $^3J_{HH}$ = 6.87 Hz), 1,15 (dd, $^3J_{HH}$ = 6.19 Hz, $^3J_{HH}$ = 5.07 Hz) ppm.
^{13}C{^{1}H}-NMR (75 MHz, THF-d_8): δ = 153.8, 151.8, 144.8, 135.0, 130.0, 51.4, 51.3, 49.7, 48.1, 24.2, 24.0, 19.5, 19.4 ppm.

Umsetzung mit Phenylisocyanat
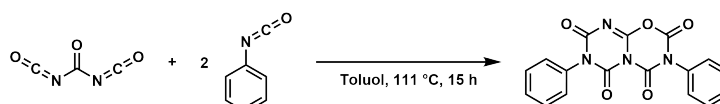
Carbonyldiisocyanat (220 mg, 1.0 eq., 2.0 mmol) und Phenylisocyanat (0.43 mL, 2.0 eq., 4.0 mmol) wurden in Toluol (15 mL) gelöst und für 15 h zum Sieden erhitzt. Nach dem Abkühlen wurde mit *n*-Hexan (15 mL) ausgefällt. Die Suspension wurde filtriert und der Filterkuchen im Vakuum getrocknet. Das Produkt wurde als farbloses Pulver (48 mg, 143 µmol, 7 %) erhalten. Das Filtrat wurde bei −75 °C zur Kristallisation gelagert. Es konnten keine Kristalle erhalten werden.

^{1}H-NMR (300 MHz, THF-d_8): δ = 7.51 (m), 7.44 (m), 7.35 (m), 7.26 (m) ppm.
^{13}C{^{1}H}-NMR (75 MHz, THF-d_8): δ = 152.2, 143.2, 134.5, 130.8, 129.9, 129.3, 129.2, 125.6, 121.4 ppm.

6.4.8 Syntheseversuche zu Carbonyldiisocyanat mit Lithiumorganylen

Umsetzung mit Methyllithium
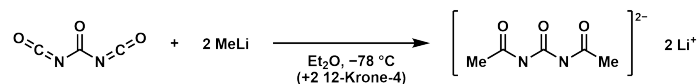
XVIIa: Zu einer 1 M Lösung von Carbonyldiisocyanat in Diethylether (1.0 mL, 1.0 eq., 1.0 mmol) gekühlt auf −78 °C wurde eine 0.5 M Lösung von Methyllithium in Diethylether (4.0 mL, 2.0 eq., 2.0 mmol) tropfenweise zugegeben. Es wurde für 22 h gerührt, in welcher Zeit ein Niederschlag präzipitierte. Der Feststoff wurde abfiltriert und im Vakuum getrocknet. Es wurde ein blass gelbes Pulver (91 mg, 0.6 mmol, 58 %) erhalten. Etwas Feststoff wurde in THF gelöst und mit *n*-Hexan überschichtet. Es konnten keine Kristalle erhalten werden. Das Pulver war schlecht bis nicht löslich in THF, Acetonitril, Dichlormethan, Aceton und Ethylacetat. Bei Kontakt mit Chloroform war eine Reaktion zu beobachten. An Luft ist das Pulver pyrophor.

^{1}H-NMR (300 MHz, Py-d$_5$): δ = 3.66 (s), 3.36 (Et$_2$O), 1.62 (s), 1.41 (s), 1.14 (Et$_2$O) ppm.
^{13}C{^{1}H}-NMR (75 MHz, Py-d$_5$): δ = 16.0 ppm.

XVIIb: Zu einer 1 M Lösung von Carbonyldiisocyanat in Diethylether (1.0 mL, 1.0 eq., 1.0 mmol) gekühlt auf −78 °C wurde 12-Krone-4 (0.3 mL, 2.0 eq., 2.0 mmol) gegeben. Eine 0.5 M Lösung von Methyllithium in Diethylether (4.0 mL, 2.0 eq., 2.0 mmol) wurde tropfenweise zugegeben. Es wurde für 22 h gerührt, in welcher Zeit ein Niederschlag präzipitierte. Der Feststoff wurde abfiltriert und im Vakuum getrocknet. Es wurde ein blass gelbes Pulver (252 mg, 0.5 mmol, 50 %) erhalten.

^{1}H-NMR (300 MHz, Py-d$_5$): δ = 3.66 (12-Krone-4) ppm.
^{13}C{^{1}H}-NMR (75 MHz, Py-d$_5$): δ = 71.4 (12-Krone-4) ppm.

Umsetzung mit *n*-Butyllithium
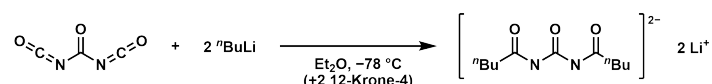
XVIIIa: Zu einer 1 M Lösung von Carbonyldiisocyanat in Diethylether (1.0 mL, 1.0 eq., 1.0 mmol) gekühlt auf –78 °C wurde eine 0.5 M Lösung von *n*-Butyllithium in *n*-Hexan (4.0 mL, 2.0 eq., 2.0 mmol) tropfenweise zugegeben. Es wurde für 20 h gerührt, in welcher Zeit ein Niederschlag präzipitierte. Der Feststoff wurde abfiltriert und im Vakuum getrocknet. Es wurde ein blass gelbes Pulver (145 mg, 0.6 mmol, 60 %) erhalten. Etwas Feststoff wurde in THF gelöst und mit *n*-Hexan überschichtet. Es konnten keine Kristalle erhalten werden. Das Pulver war schlecht bis nicht löslich in THF, Acetonitril, Dichlormethan, Chloroform, Aceton und Ethylacetat.

^{1}H-NMR (300 MHz, THF-d$_8$): δ = 2.36 (t, $^3J_{HH}$ = 7.30 Hz), 1.51 (p, $^3J_{HH}$ = 7.17 Hz), 1.29 (m), 0.89 (t, $^3J_{HH}$ = 7.32 Hz) ppm.
^{13}C{^{1}H}-NMR (75 MHz, THF-d$_8$): δ = 68.7, 68.4, 42.9, 40.3, 26.6, 26.3, 14.7, 14.4 ppm.

XVIIIb: Zu einer 1 M Lösung von Carbonyldiisocyanat in Diethylether (1.0 mL, 1.0 eq., 1.0 mmol) wurde 12-Krone-4 (0.3 mL, 2.0 eq., 2.0 mmol) gegeben und auf –78 °C gekühlt. Eine 0.5 M Lösung von *n*-Butyllithium in *n*-Hexan (4.0 mL, 2.0 eq., 2.0 mmol) wurde tropfenweise zugegeben. Es wurde für 20 h gerührt, in welcher Zeit ein Niederschlag präzipitierte. Der Feststoff wurde abfiltriert und im Vakuum getrocknet. Es wurde ein beiges Pulver (187 mg, 0.3 mmol, 32 %) erhalten.

^{1}H-NMR (300 MHz, THF-d$_8$): δ = 6.46 (m), 3.59 (12-Krone-6), 1.29 (*n*-Hexan), 0.89 (*n*-Hexan) ppm.
^{13}C{^{1}H}-NMR (75 MHz, THF-d$_8$): δ = 72.0 (12-Krone-4) ppm.

Umsetzung mit Lithiummethanolat

XIXa: Lithiummethoxid (76 mg, 2.0 eq., 2.0 mmol) wurde in THF (4 mL) suspendiert und eine 1 M Lösung von Carbonyldiisocyanat in THF (1.0 mL, 1.0 eq., 1.0 mmol) zugegeben. Nach 16.5 h wurde filtriert und der Filterkuchen im Vakuum getrocknet. Es wurde ein farbloses Pulver (108 mg, 0.6 mmol, 57 %) erhalten.

¹H-NMR (300 MHz, Py-d₅): δ = 3.82, 3.67 (THF), 1.63 (THF), 1.33, 1.28, 0.89 ppm.

¹³C{¹H}-NMR (75 MHz, Py-d₅): δ = 53.0 ppm.

$\mathbf{XIXb}$**:** Lithiummethoxid (76 mg, 2.0 eq., 2.0 mmol) wurde in THF (4 mL) suspendiert und 12-Krone-4 (0.3 mL, 2.0 eq., 2.0 mmol) hinzugegeben. Eine 1 M Lösung von Carbonyldi-isocyanat in THF (1.0 mL, 1.0 eq., 1.0 mmol) wurde zugegeben. Nach 16.5 h wurde fil-triert und der Filterkuchen im Vakuum getrocknet. Es wurde ein farbloses Pulver (240 mg, 0.4 mmol, 44 %) erhalten.

¹H-NMR (300 MHz, Py-d₅): δ = 3.81, 3.66 (12-Krone-6), 1.63 (THF), 1.34, 1.28, 1.14, 0.89 ppm.

¹³C{¹H}-NMR (75 MHz, Py-d₅): δ = 71.3 (12-Krone-4), 53.0 ppm.

6.4.9 Synthesen zum Koordinationsverhalten von Carbonyldiisocyanat

Umsetzung mit Eisen(II)bis(hexamethyldisilazanid)
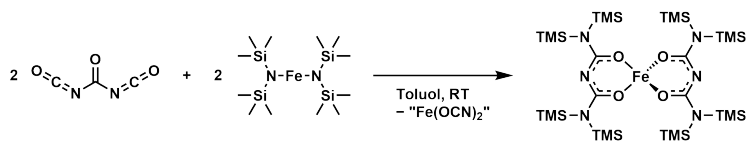
Fe(N(Si(Me₃)₂)₂) (196 mg, 0.5 eq., 521 μmol) und Carbonyldiisocyanat (117 mg, 1.0 eq., 1.0 mmol) wurden jeweils in Toluol (2 mL) gelöst. Die Lösung mit Carbonyldiisocyanat wurde auf –40 °C gekühlt und bei RT zur Fe(N(Si(Me₃)₂)₂) Lösung getropft. Es war ein sofortiger Farbumschlag von grün zu orange-braun, eine Gasentwicklung, sowie eine Er-wärmung zu beobachten. Nach 5 min war ein Niederschlag vorhanden und die Lösung wurde abdekantiert. Die Lösung wurde gedrittelt. Der erste Teil wurde bei –40 °C, der zweite Teil bei –15 °C und der dritte Teil mit *n*-Pentan überschichtet bei –40 °C gelagert. Der Feststoff wurde getrocknet.

Umsetzung mit Eisen(II)bis(diisopropyltrimethylsilylamid)
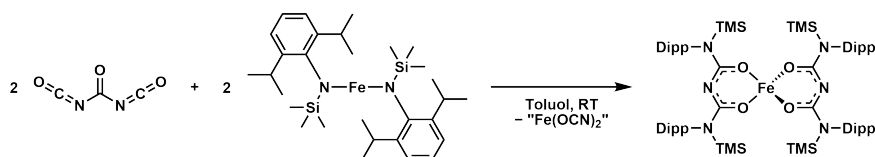
Fe(N(Dipp)(TMS))$_2$ (274 mg, 0.5 eq., 496 µmol) und Carbonyldiisocyanat (111 mg, 1.0 eq., 991 µmol) wurden jeweils in Toluol (2 mL) gelöst. Die Lösung mit Carbonyldiisocyanat wurde auf –40 °C gekühlt und bei RT zur Fe(N(Dipp)(TMS))$_2$ Lösung getropft. Ein Farbumschlag von orange-rot zu dunkelbraun und eine Gasentwicklung waren zu beobachten. Nach 5 min wurde die Reaktionslösung gedrittelt. Der erste Teil wurde bei –40 °C, der zweite Teil bei –15 °C und der dritte Teil mit *n*-Pentan überschichtet bei –40 °C gelagert. Aus dem dritten Teil konnten nach 6 Monaten grün-türkise Kristalle (114 mg, 96 µmol, 39 %) erhalten werden, welche isoliert und mit *n*-Hexan gewaschen wurden.

^{1}H-NMR (300 MHz, THF-d$_8$): δ = 26.66 (br), 20.36 (br), 19.20, 16.13, 14.30 (br), 4.84, –0.60, –2.56, –3.26, –24.81 (br), –29.91 (br) ppm.
HR MS (LIFDI, THF, C$_{64}$H$_{104}$FeN$_6$O$_4$Si$_4$): gef. (theo.) *m/z* 1188.65536 (1188.65455).
CHN gef. (theo.): C 64.73 (64.61), H 8.74 (8.81), N 8.15 (7.06).

Umsetzungen mit Übergangsmetall(II)bis(diisopropyltrimethylsilylamiden)
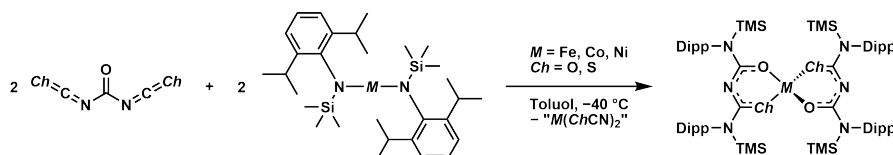
Zu *M*(N(Dipp)(TMS))$_2$ (0.5 eq., 0.25 mmol) gelöst in Toluol (2 mL) und auf –40 °C gekühlt wurde eine 1 M Lösung von CD*PsH* in Toluol (0.5 mL, 1.0 eq., 0.5 mmol) auf –40 °C gekühlt getropft. Ein Farbumschlag war zu beobachten. Die Reaktionslösung wurde zur Kristallisation bei –40 °C gelagert. Nach 4 Wochen war keine Kristallisation festzustellen. Die Reaktionslösung wurde halbiert. Die erste Hälfte wurde erneut bei –40 °C und die zweite Hälfte mit *n*-Pentan überschichtet bei –40 °C gelagert.

M: Fe (138 mg), Co (139 mg), Ni (139 mg)
HR MS (LIFDI, THF, C$_{64}$H$_{104}$NiN$_6$O$_2$S$_2$Si$_4$): gef. (theo.) *m/z* 1222.61211 (1222.60927).

Komplex	CD*PsH*	Farbe	Beobachtung
Fe(N(Si(Me$_3$)$_2$)$_2$)	CO(NCO)$_2$	braun	Gasentwicklung, Kristallisation
Co(N(Si(Me$_3$)$_2$)$_2$)	CO(NCO)$_2$	blau	Gasentwicklung
Ni(N(Si(Me$_3$)$_2$)$_2$)	CO(NCO)$_2$	lila	Gasentwicklung
Fe(N(Si(Me$_3$)$_2$)$_2$)	CO(NCS)$_2$	braun	Gasentwicklung, Polymerisation
Co(N(Si(Me$_3$)$_2$)$_2$)	CO(NCS)$_2$	grün	Gasentwicklung
Ni(N(Si(Me$_3$)$_2$)$_2$)	CO(NCS)$_2$	violett	Gasentwicklung, Polymerisation

6.4.10 Synthese von 2,4,6-Trioxo-1,3,5-oxadiazin
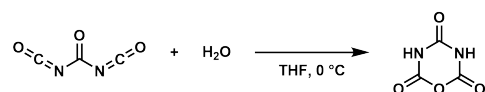
Carbonyldiisocyanat (200 mg, 1.0 eq., 1.8 mmol) wurde in THF (6 mL) gelöst und auf 0 °C gekühlt. Wasser (32 µL, 1.0 eq., 1.8 mmol) wurde hinzugegeben und für 30 min gerührt. Das Lösungsmittel wurde im Vakuum entfernt. 2,4,6-Trioxo-1,3,5-oxadiazin wurde als farbloses Pulver (193 mg, 1.5 mmol, 83 %) erhalten. Ein Kristall wurde durch Lösen von Carbonyldiisocyanat in nassem Schwefeldioxid und langsames Verdampfen des Lösungsmittels erhalten.

^{1}H-NMR (300 MHz, THF-d$_8$): δ = 10.98 (s, 2H, N*H*) ppm.
^{13}C{^{1}H}-NMR (75 MHz, THF-d$_8$): δ = 149.3 (*C*O), 146.1 (N*C*O) ppm.
HR MS (ESI, MeOH, C$_3$H$_1$N$_2$O$_4$): gef. (theo.) *m/z* 128.9943 (128.9931).
CHNO gef. (theo.): C 28.12 (27.71), H 1.78 (1.55), N 21.41 (21.54), O 48.18 (49.21).

6.4.11 Umsetzung von Carbonyldiisothiocyanat mit Ammoniak
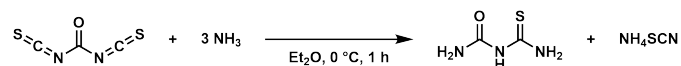
Carbonyldiisothiocyanat (0.95 g, 1.0 eq., 6.6 mmol) wurde in Diethylether (25 mL) gelöst und auf 0 °C gekühlt. Ammoniak wurde für 30 min als leichter Gasstrom in die Lösung eingeleitet. Nach 5 min war die Bildung eines gelben Feststoffes zu beobachten und nach 10 min war der Reaktionskolben vollständig mit Feststoff gefüllt. Nach 30 min war erneut eine klare Lösung im Reaktionskolben und die Gaseinleitung wurde gestoppt. Es wurde für weitere 30 min gerührt. Das Lösungsmittel wurde im Vakuum entfernt und ein gelber Feststoff erhalten. Das Rohprodukt wurde mit *n*-Hexan gewaschen und im Vakuum getrocknet. Monothiobiuret×Ammoniumthiocyanat (1.0 g, 5.3 mmol, 80 %) wurde als gelbes Pulver erhalten. Kristalle wurden durch Diffusionskristallisation aus THF und *n*-Hexan gewonnen.

^{1}H-NMR (300 MHz, THF-d$_8$): δ = 9.59 (br, 1H, N*H*), 9.37 (br, 1H, N*H*), 8.19 (br, 1H, N*H*), 7.24 (br, 4H, N*H$_4$*), 6.15 (br, 1H, N*H*), 5.67 (br, 1H, N*H*) ppm.
^{13}C{^{1}H}-NMR (75 MHz, THF-d$_8$): δ = 184.3 (*C*S), 162.5, 156.4 (*C*O), 134.9 (N*C*S) ppm.

6.4.12 Synthese von Tetramethylammoniumselenocyanat
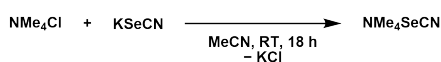
Tetramethylammoniumchlorid (10.7 g, 1.0 eq., 97.9 mmol) und Kaliumselenocyanat (14.1 g, 1.0 eq., 97.9 mmol) wurden in Acetonitril (180 mL) suspendiert. Nach 18 h wurde das farblose Nebenprodukt abfiltriert. Das Lösungsmittel wurde im Vakuum entfernt und der Rückstand getrocknet. Tetramethylammoniumselenocyanat (9.4 g, 52.6 mmol, 54 %) wurde als farbloses Pulver erhalten. Kristalle wurde durch Diffusionskristallisation aus Acetonitril und Diethylether gewonnen.

^{1}H-NMR (300 MHz, D$_2$O): δ = 3.24 (s, 12H, C*H$_3$*) ppm.
^{13}C{^{1}H}-NMR (75 MHz, D$_2$O): δ = 120.4 (Se*C*N), 55.4 (t, *C*H$_3$) ppm.
CHN gef. (theo.): C 34.17 (33.52), H 6.63 (6.75), N 16.23 (15.64).

6.4.13 Bildung von Kristallen

Isocyanursäure×Biuret×H$_2$O
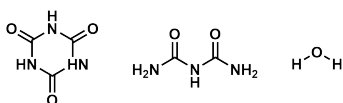
Lithiumchlorid (42 mg, 1.0 eq., 1.0 mmol) wurde in THF (1 mL) suspendiert und eine 1 M Lösung von Carbonyldiisocyanat (2.0 mL, 2.0 eq., 2.0 mmol) in THF zugegeben. Eine milchige Trübung war zu beobachten. Nach 15 min wurde filtriert und der Filterkuchen im Vakuum getrocknet. Der Feststoff wurde zur NMR spektroskopischen Analyse in DMSO-d$_6$ gelöst. Nach einigen Wochen sind durch langsames Verdampfen des Lösungsmittels farblose Kristalle von ICS-IDCDA im NMR-Rohr gewachsen.

^{1}H-NMR (300 MHz, DMSO-d$_6$): δ = 11.17 (ICS), 3.59 (THF), 1.75 (THF) ppm.
^{13}C{^{1}H}-NMR (75 MHz, DMSO-d$_6$): δ = 150.O (ICS), 147.6, 124.3, 67.1 (THF), 25.2 (THF) ppm.

N,N-Diethyl-2,4,6-trioxo-1,3,5-triazin-1-carboxamid
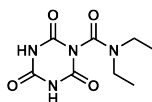
Carbonyldiisocyanat (112 mg, 1.0 eq., 1.0 mmol) gelöst in THF (1 mL) wurde auf –78 °C gekühlt und Diethylamin (146 mg, 2.0 eq., 2.0 mmol) gelöst in THF (2 mL) zugegeben. Die Lösung wurde über 5.5 h auf RT erwärmt. Das Lösungsmittel wurde im Vakuum entfernt und ein schleimiger Rückstand erhalten. Der Rückstand wurde in Dichlormethan (2.5 mL) suspendiert und filtriert. Das Filtrat wurde mit *n*-Hexan überschichtet und wenige Kristalle durch Diffusionskristallisation von ICS-CONEt$_2$ erhalten.

S-Phenyl-2,4,6-trioxo-1,3,5-triazin-1-carbothioat
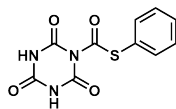
Diphenyl-*N*,*N*'-carbonylbis(*S*-thiocarbamat) (330 mg, 1.0 eq., 1.0 mmol) wurde bei 120 °C im Vakuum getrocknet. Der Feststoff wurde in Toluol (5 mL) gelöst und mit 2.5 M ätherischer Salzsäure (2.5 mL, 5.0 eq., 5.0 mmol) versetzt. Nach 18 h wurde mit *n*-Hexan (8 mL) ausgefällt. Der Niederschlag wurde abfiltriert und im Vakuum getrocknet. Mittels Diffusionskristallisation aus THF und *n*-Hexan wurden farblose Kristalle von ICS-COSPh (16 mg) erhalten.

N-(*S*-Benzyldithiocarboxy)carbonyldiamid
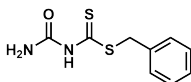
Eine Spatelspitze 6-Benzyloxy-2-thioxo-2,3-dihydro-4*H*-1,3,5-thiadiazin-4-on wurde in Dichlormethan (ca. 2 mL) gelöst. Das Lösungsmittel wurde langsam bei RT verdampfen gelassen. Wenige farblose Kristalle von CDA-CSSBz wurden erhalten.

N,*N*,*N*',*N*'-Tetraisopropylimidodicarbonsäurediamid
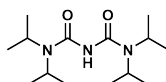
Carbonyldiisocyanat (112 mg, 1.0 eq., 1.0 mmol) wurde in Acetonitril (4 mL) gelöst und auf –41 °C gekühlt. Diisopropylamin (202 mg, 2.0 eq., 2.0 mmol) gelöst in Acetonitril (2 mL) wurde tropfenweise zugegeben. Es wurde über 3 h auf –10 °C erwärmt, die Kühlung entfernt und 3 h weitere Stunde bei RT gerührt. Das Lösungsmittel wurde im Vakuum entfernt und im Rückstand wenige Kristalle von IDCDA-*i*Pr erhalten.

7 Literaturverzeichnis

[1] S. Benz, D. Chen, A. Möller, M. Hofmann, D. Schnieders, R. Dronskowski, *Inorganics* **2022**, *10*, 132.

[2] J. H. Meessen, H. Petersen, *Urea in Ullmann's Encyclopedia of Industrial Chemistry*, John Wiley & Sons, Ltd, Weinheim, Germany, **2010**, S. 1–36.

[3] International Fertilizer Industry Association, Production of urea worldwide from 2009 to 2021 (in million metric tons), **2023**.

[4] L. Cotarca, C. Lange, K. Meurer, J. Pauluhn, *Phosgene in Ullmann's Encyclopedia of Industrial Chemistry*, John Wiley & Sons, Ltd, Weinheim, Germany, **2019**, S. 1–30.

[5] H. Boerhaave, *Elementa chemiae, quae anniversario labore docuit in publices privatiaque scholis*, Leiden, **1732**.

[6] F. Kurzer, P. M. Sanderson, *J. Chem. Educ.* **1956**, *33*, 452.

[7] H. Rouelle, *Journal de Médecine de Chirurgie et de Pharmacie* **1773**, *40*, 48–71.

[8] W. Cruickshank in *An accountant of two cases of the diabetes mellitus*, John Rollo, London, **1797**.

[9] L.-N. Vauquelin, A. F. de Fourcroy, *Ann. Chim.* **1799**, *31*, 48–71.

[10] J. Davy, *Philos. Trans. R. Soc. London* **1812**, *102*, 144–151.

[11] F. Wöhler, *Ann. Phys. Chem.* **1828**, *88*, 253–256.

[12] F. Wöhler, *Kungliga Vetenskapsakademiens Handlingar* **1824**, 328–333.

[13] C. Bosch, W. Meiser, *Process of Manufacturing Urea*, US1231226A, **1922**.

[14] A. Basaroff, *J. Chem. Soc.* **1868**, *21*, 194–195.

[15] J. Meessen, *Chem. Ing. Tech.* **2014**, *86*, 2180–2189.

[16] G. Wiedemann, *J. Prakt. Chem.* **1847**, *42*, 255–256.

[17] G. Wiedemann, *J. Prakt. Chem.* **1848**, *43*, 271–280.

[18] G. Wiedemann, *Angew. Chem. Int. Ed.* **1848**, *68*, 323–326.

[19] G. Wiedemann, *Ann. Phys. Chem.* **1848**, *150*, 67–84.

[20] E. Schmidt, *Chem. Zentralblatt* **1872**, *43*, 195–197.

[21] P. Gross, H. A. Höppe, *Chem.–Eur. J.* **2020**, *26*, 14366–14376.

[22] N. L. G. Whitehouse, *Method of Manufacturing Phosgene*, US1231226A, **1917**.

[23] C. J. Mitchell, W. Van Der Borden, K. Van Der Velde, M. Smit, R. Scheringa, K. Ahrika, D. H. Jones, *Catal. Sci. Technol.* **2012**, *2*, 2109–2115.

[24] R. Hughes, G. E. Rossi, D. Lennon, *React. Chem. Eng.* **2023**, *8*, 3150–3161.

[25] W. Hentschel, *J. Prakt. Chem.* **1887**, *36*, 99–113.

[26] W. Hentschel, *J. Prakt. Chem.* **1887**, *36*, 209–215.

[27] C. Councler, *Ber. Dtsch. Chem. Ges.* **1880**, *13*, 1697–1699.

[28] L. Cotarca, T. Geller, J. Répási, *Org. Process Res. Dev.* **2017**, *21*, 1439–1446.

[29] H. Eckert, J. Auerweck, *Org. Process Res. Dev.* **2010**, *14*, 1501–1505.

[30] P. Voßnacker, A. Wüst, T. Keilhack, C. Müller, S. Steinhauer, H. Beckers, S. Yogendra, Y. Schiesser, R. Weber, M. Reimann, R. Müller, M. Kaupp, S. Riedel, *Sci. Adv.* **2021**, *7*, 5186–5215.

[31] W. Gottardi, D. Henn, *Monatsh. Chem.* **1969**, *100*, 1860–1867.

[32] W. Gottardi, D. Henn, *Monatsh. Chem.* **1970**, *101*, 11–18.

[33] C. Jäckh, W. Sundermeyer, *Chem. Ber.* **1973**, *106*, 1752–1757.

[34] H. Hagemann, *Angew. Chem.* **1977**, *89*, 789–796.

[35] V. I. Gorbatenko, L. F. Lur'e, *Synthesis* **1980**, 112.

[36] V. I. Gorbatenko, *Tetrahedron* **1993**, *49*, 3227–3257.

[37] D. Klapstein, W. M. Nau, *Spectrochim. Acta Mol. Spectrosc.* **1994**, *50*, 307–316.

[38] O. Glemser, U. Biermann, M. Fild, *Chem. Ber.* **1967**, *100*, 1082–1086.

[39] W. Verbeek, W. Sundermeyer, *Angew. Chem. Int. Ed.* **1967**, *6*, 871–872.

[40] C. O. Della Védova, *Z. Anorg. Allg. Chem.* **1992**, *609*, 150–152.

[41] C. O. Della Védova, *Spectrochim. Acta Mol. Spectrosc.* **1992**, *48*, 1179–1185.

[42] R. J. H. Clark, L. J. Foley, S. D. Price, *J. Phys. Chem. A* **2000**, *104*, 10675–10682.

[43] L. A. Ramos, S. E. Ulic, R. M. Romano, M. F. Erben, C. W. Lehmann, E. Bernhardt, H. Beckers, H. Willner, C. O. Della Védova, *Inorg. Chem.* **2010**, *49*, 11142–11157.

[44] R. Bunnenberg, J. C. Jochims, *Chem. Ber.* **1981**, *114*, 1746–1751.

[45] L. A. Ramos, S. E. Ulic, R. M. Romano, M. F. Erben, Y. V. Vishnevskiy, C. G. Reuter, N. W. Mitzel, H. Beckers, H. Willner, X. Zeng, E. Bernhardt, M. Ge, S. Tong, C. O. D. Védova., *J. Phys. Chem. A* **2013**, *117*, 2383–2399.

[46] A. Haas, H. Reinke, *Angew. Chem.* **1967**, *79*, 687–688.

[47] A. Haas, H. Reinke, *Chem. Ber.* **1969**, *102*, 2718–2727.

[48] R. Koch, C. Wentrup, *J. Chem. Soc. Perk. Trans. 2* **2000**, 1846–1850.

[49]   S. N. Mousavi, D. Nori-Shargh, H. Yahyaei, K. M. Frahani, *Can. J. Chem.* **2012**, *90*, 333–343.

[50]   R. Appel, M. Siray, *Angew. Chem.* **1983**, *95*, 807–807.

[51]   T. Pasinszki, G. Vass, D. Klapstein, N. P. Westwood, *J. Phys. Chem. A* **2012**, *116*, 3396–3403.

[52]   T. Pasinszki, N. P. Westwood, *J. Phys. Chem. A* **1998**, *102*, 4939–4947.

[53]   T. Pasinszki, N. P. Westwood, *J. Am. Chem. Soc.* **1995**, *117*, 8425–8430.

[54]   C. W. Tullock, D. D. Copfman, *J. Org. Chem.* **1960**, *25*, 2016–2019.

[55]   D. Bielefeldt, A. Haas, *Z. Naturforsch. B* **1984**, *39*, 1211–1215.

[56]   H. G. Mack, C. O. Della Védova, H. Willner, *J. Mol. Struct.* **1993**, *291*, 197–209.

[57]   H. M. Badawi, W. Förner, K. S. Al-Ghamdi, *J. Mol. Model.* **2003**, *9*, 124–133.

[58]   T. Curtius, K. Heidenreich, *Ber. Dtsch. Chem. Ges.* **1894**, *27*, 2684–2685.

[59]   X. Zeng, M. Gerken, H. Beckers, H. Willner, *Inorg. Chem.* **2010**, *49*, 9694–9699.

[60]   A. M. Nolan, B. K. Amberger, B. J. Esselman, V. S. Thimmakondu, J. F. Stanton, R. C. Woods, R. J. McMahon, *Inorg. Chem.* **2012**, *51*, 9846–9851.

[61]   R. Malachowski, L. Jurkiewicz, J. Wojtowicz, *Ber. Dtsch. Chem. Ges.* **1937**, *70*, 1012–1016.

[62]   O. Glemser, V. Hausser, *Z. Naturforsch. B* **1948**, *3*, 159–163.

[63]   W. J. Linn, O. W. Webster, R. E. Benson, *J. Am. Chem. Soc.* **1965**, *87*, 3651–3656.

[64]   E. L. Martin, *Org. Synth.* **1971**, *51*, 70.

[65]   A. E. Dixon, *Proc. Chem. Soc.* **1902**, *18*, 240.

[66]   B. Anders, H. Malz, *Verfahren zur Herstellung von Acylsenfölen*, DE1215144B, **1966**.

[67]   R. Bunnenberg, J. C. Jochims, *Chem. Ber.* **1981**, *114*, 2075–2086.

[68]   R. Bunnenberg, J. C. Jochims, H. Härle, *Chem. Ber.* **1982**, *115*, 3587–3596.

[69]   E. Nachbaur, *Monatsh. Chem.* **1966**, *97*, 361–367.

[70]   H. Hagemann, *Verfahren zur Herstellung von Carbonyldiisocyanat*, DE2408069A1, **1975**.

[71]   H. Hagemann, *Verfahren zur Herstellung von Carbonyldiisocyanat*, DE2411674A1, **1975**.

[72]   B. Akteries, J. C. Jochims, *Chem. Ber.* **1986**, *119*, 83–95.

[73]   V. I. Gorbatenko, L. F. Lur'e, *Zh. Org. Khim.* **1980**, *16*, 464.

[74] T. M. Klapötke, B. Krumm, S. Rest, R. Scharf, J. Schwabedissen, H.-G. Stammler, N. W. Mitzel, *J. Phys. Chem. A* **2016**, *120*, 4534–4541.

[75] H. Roesky, O. Glemser, *Chem. Ber.* **1964**, *97*, 1710–1712.

[76] G. Maier, M. Naumann, H. P. Reisenauer, J. Eckwert, *Angew. Chem.* **1996**, *108*, 1800–1801.

[77] R. Bunnenberg, J. C. Jochims, *Chem. Ber.* **1981**, *114*, 2064–2074.

[78] R. Bunnenberg, C. Jochims, *Chem. Ber.* **1981**, *114*, 1132–1136.

[79] T. Curtius, A. Burkhardt, *J. Prakt. Chem.* **1898**, *58*, 205–233.

[80] A. G. Harter, T. M. Klapötke, J. Stierstorfer, M. Voggenreiter, X. Zeng, *ChemPlusChem* **2021**, *86*, 870–874.

[81] L. Fengyi, Z. Xiaoqing, S. Qiao, M. Lingpeng, Z. Shijun, A. Xicheng, Z. Jianping, G. Maofa, W. Dianxun, *Bull. Chem. Soc. Jpn.* **2005**, *78*, 1246–1250.

[82] D. R. Hartter, *Organische Cyanide und Verfahren zur Herstellung derselben*, DE21 34946A, **1971**.

[83] R. W. Begland, D. R. Hartter, *J. Org. Chem.* **1972**, *37*, 4136–4145.

[84] N. Singh, H. P. Latscha, *Z. Naturforsch. B* **1971**, *26*, 1072.

[85] K. Banert, Y. H. Joo, T. Rüffer, B. Walfort, H. Lang, *Angew. Chem. Int. Ed.* **2007**, *46*, 1168–1171.

[86] W. Gombler, *Spectrochim. Acta Mol. Spectrosc.* **1981**, *37*, 57–61.

[87] J. B. Bates, W. H. Smith, *Spectrochim. Acta Mol. Spectrosc.* **1970**, *26*, 455–464.

[88] F. A. Miller, B. M. Harney, J. Tyrrell, *Spectrochim. Acta Mol. Spectrosc.* **1971**, *27*, 1003–1018.

[89] W. J. Balfour, S. G. Fougere, D. Klapstein, W. M. Nau, *Spectrochim. Acta Mol. Spectrosc.* **1994**, *50*, 1039–1046.

[90] V. Typke, M. Dakkouri, F. Schlumberger, *J. Mol. Struct.* **1980**, *62*, 111–120.

[91] B. K. Amberger, B. J. Esselman, R. C. Woods, R. J. McMahon, *J. Mol. Spectrosc.* **2014**, *295*, 15–20.

[92] Q. Liu, H. Li, Z. Wu, D. Li, H. Beckers, G. Rauhut, X. Zeng, *Chem.-Asian J.* **2016**, *11*, 2953–2959.

[93] T. Curtius, A. Bertho, *Ber. Dtsch. Chem. Ges.* **1926**, *59*, 565–589.

[94] H. Jiang, K. Lang, H. Lu, L. Wojtas, X. P. Zhang, *J. Am. Chem. Soc.* **2017**, *139*, 9164–9167.

[95] X. Zeng, H. Beckers, H. Willner, *Angew. Chem. Int. Ed.* **2011**, *50*, 482–485.

[96] H. Li, D. Li, X. Zeng, K. Liu, H. Beckers, H. F. Schaefer, B. J. Esselman, R. J. McMahon, *J. Phys. Chem. A* **2015**, *119*, 8903–8911.

[97] X. Zeng, H. Beckers, H. Willner, J. F. Stanton, *Eur. J. Inorg. Chem.* **2012**, *2012*, 3403–3409.

[98] X. Zeng, H. Beckers, H. Willner, J. F. Stanton, *Angew. Chem. Int. Ed.* **2011**, *50*, 1720–1723.

[99] A. Perrin, X. Zeng, H. Beckers, H. Willner, *J. Mol. Spectrosc.* **2011**, *269*, 30–35.

[100] N. R. Rondla, S. M. Levi, J. M. Ryss, R. A. Vanden Berg, C. J. Douglas, *Org. Lett.* **2011**, *13*, 1940–1943.

[101] R. E. Ford, P. Knowles, E. Lunt, S. M. Marshall, A. J. Penrose, C. A. Ramsden, A. J. Summers, J. L. Walker, D. E. Wright, *J. Med. Chem.* **1986**, *29*, 538–549.

[102] R. C. Schoenfeld, B. Ganem, *Tetrahedron Lett.* **1998**, *39*, 4147–4150.

[103] Y. Yasui, T. Kinugawa, Y. Takemoto, *Chem. Commun.* **2009**, 4275–4277.

[104] Y. Yasui, H. Kamisaki, T. Ishida, Y. Takemoto, *Tetrahedron* **2010**, *66*, 1980–1989.

[105] M. T. Leplawy, A. Redliński, *Synthesis* **1975**, *1975*, 504–506.

[106] E. G. Banucci, *J. Polym. Sci. Poly. Chem.* **1973**, *11*, 2947–2960.

[107] E. G. Banucci, *Synthesis* **1973**, *1973*, 671–672.

[108] K. Kocioɫek, M. T. Leplawy, *Synthesis* **1977**, *1977*, 778–780.

[109] O. Achmatowicz, A. Zamojski, *Croat. Chem. Acta* **1957**, *29*, 269–275.

[110] F. Snatzke, H. P. Wolff, *Liebigs Ann. Chem.* **1985**, *1985*, 468–476.

[111] H. M. R. Hoffmann, *Angew. Chem.* **1969**, *81*, 597–618.

[112] T. S. Cameron, A. Decken, M. Gabriel, C. Knapp, J. Passmore, *Can. J. Chem.* **2007**, *85*, 96–104.

[113] A. Furlan, H. A. Scheld, J. R. Huber, *Chem. Phys. Lett.* **1998**, *282*, 1–6.

[114] H. A. Scheld, A. Furlan, J. R. Huber, *J. Chem. Phys.* **1999**, *111*, 923–930.

[115] H. U. Suter, J. R. Huber, T. K. Ha, *Chem. Phys. Lett.* **1999**, *311*, 474–478.

[116] Q. Li, R. T. Carter, J. R. Huber, *Chem. Phys. Lett.* **2000**, *323*, 105–110.

[117] H. Y. Lee, A. M. Mebel, S. H. Lin, *Int. J. Quantum Chem.* **2002**, *90*, 566–574.

[118] H. U. Suter, R. Pfister, A. Furlan, J. R. Huber, *J. Phys. Chem. A* **2007**, *111*, 764–769.

[119] B. Akteries, J. C. Jochims, *Chem. Ber.* **1986**, *119*, 669–682.

[120] T. M. Klapötke, B. Krumm, S. F. Rest, M. Sućeska, *Z. Anorg. Allg. Chem.* **2014**, *640*, 84–92.

[121] H. Hagemann, H. Heitzer, D. Wendisch, *Liebigs Ann. Chem.* **1976**, *1976*, 1634–1636.

[122] B. Akteries, J. C. Jochims, *Chem. Ber.* **1986**, *119*, 1133–1143.

[123] T. Curtius, *J. Prakt. Chem.* **1915**, *91*, 415–441.

[124] R. W. Begland, D. R. Hartter, D. S. Donald, A. Cairncross, W. A. Sheppard, *J. Org. Chem.* **1974**, *39*, 1235–1239.

[125] J. G. Knight, *Product Class 1: Cyanogen Halides, Cyanates and Their Sulfur, Selenium, and Tellurium Analogues, Sulfinyl and Sulfonyl Cyanides, Cyanamides, and Phosphaalkynes in Sci. Synth.* Georg Thieme Verlag, Stuttgart, **2005**.

[126] D. Klamann, *Tellurocyanates (R–Te–OCN) in Methoden der Organischen Chemie*, Stuttgart, **1990**.

[127] A. Haas, B. Koch, N. Welcman, *Z. Anorg. Allg. Chem.* **1976**, *427*, 114–122.

[128] A. Darmadi, A. Haas, B. Koch, *Z. Naturforsch.* **1980**, *35*, 526–529.

[129] A. Haas, *J. Fluor. Chem.* **1986**, *32*, 415–439.

[130] C. Trost, *Carbonyldiisothiocyanat - Darstellung, Kristallstruktur und Reaktivität gegenüber Nukleophilen*, Masterarbeit, Philipps-Universität Marburg, **2020**.

[131] A. Pachkovska, *Synthese, Struktur und Reaktivität von Oxalyldiisothiocyanat*, Bachelorarbeit, Philipps-Universität Marburg, **2020**.

[132] H. Günther, *Umsetzung von Carbonyldiisocyanat und Carbonyldiisothiocyanat mit Halogenwasserstoffen*, Bachelorarbeit, Philipps-Universität Marburg, **2021**.

[133] W. Lu, Z. Li, M. Feng, L. Zheng, S. Liu, B. Yan, J.-S. Hu, D.-J. Xue, *J. Am. Chem. Soc.* **2024**, *146*, 6345–6351.

[134] C. J. Burchell, P. Kilian, A. M. Slawin, J. D. Woollins, K. Tersago, C. Van Alsenoy, F. Blockhuys, *Inorg. Chem.* **2006**, *45*, 710–716.

[135] L. Cotarca, P. Delogu, A. Nardelli, V. Šunjić, *Synthesis* **1996**, *1996*, 553–576.

[136] F. W. Bergstrom, *J. Phys. Chem.* **1922**, *26*, 876–894.

[137] M. Koketsu, Y. Yamamura, H. Aoki, H. Ishihara, *Phosphorus Sulfur Silicon Relat. Elem.* **2006**, *181*, 2699–2708.

[138] B. S. Haddad, *Der Pharma Chem.* **2017**, *9*, 25–28.

[139] R. A. Hussain, A. Badshah, F. Yasmin, M. D. Khan, M. N. Tahir, R. A. Hussain, A. Badshah, F. Yasmin, M. D. Khan, M. N. Tahir, *Aust. J. Chem.* **2014**, *68*, 298–306.

[140] A. Molter, J. Rust, C. W. Lehmann, F. Mohra, *Arkivoc* **2011**, *2011*, 10–17.

[141] L. Henriksen, U. Ehrbar, *Synthesis* **1976**, *1976*, 519–521.

[142] G. R. Waitkins, C. R. McCrosky, *J. Am. Chem. Soc.* **1946**, *68*, 1385–1386.

[143] H. Günther, *Untersuchung zur Synthese und Charakterisierung von neuartigen Imidodi(thiokohlensäure-O-ester) basierten Übergangsmetallkomplexen und Thiocarbonyldi(iso)cyanat*, Masterarbeit, **2023**.

[144] A. Shlyaykher, F. Tambornino, *Inorg. Chem.* **2023**, *62*, 11943–11953.

[145] W. Gombler, *Z. Naturforsch. B* **1981**, *36*, 1561–1565.

[146] J. Seravalli, S. W. Ragsdale, *Biochemistry* **2008**, *47*, 6770–6781.

[147] S. Ringelband, *Synthese und Charakterisierung von Oxalyl- und Carbonyl(pseudo)-halogeniden*, Masterarbeit, Philipps-Universität Marburg, **2024**.

[148] C. Jakobi, *Doppelte [2+4] Cycloadditionen an Carbonyldiisocyanat*, Bachelorarbeit, Philipps-Universität Marburg, **2023**.

[149] J. Jirman, A. Lyčka, *Collect. Czechoslov. Chem. Commun.* **1987**, *52*, 2474–2481.

[150] B. Guo, J. G. de Vries, E. Otten, *Chem. Sci.* **2019**, *10*, 10647–10652.

[151] C. L. Orjiekwe, S. A. Adeniyi, I. U. Orjiekwe, *African J. Biotechnol.* **2013**, *12*, 4368–4373.

[152] National Institute of Advanced Industrial Science and Technology (AIST), Spectral Database for Organic Compounds (SDBS), `https://sdbs.db.aist.go.jp`.

[153] M. Hesse, H. Meier, B. Zeeh, *Spektroskopische Methoden in der organischen Chemie*, 7. Auflage, Thieme Verlag, Stuttgart, **2005**.

[154] M. Nardelli, G. Fava, G. Giraldi, *Acta Crystallogr.* **1963**, *16*, 343–352.

[155] H. C. Freeman, J. E. W. L. Smith, *Acta Crystallogr.* **1966**, *20*, 153–159.

[156] J. Lawson, W. T. Harrison, *Acta Crystallogr. Sect. E* **2005**, *61*, m525–m527.

[157] L. Zhang, T.-w. Wang, W.-s. Dong, C. Zhang, Z.-j. Lu, Z.-n. Zhou, J.-g. Zhang, *Cryst. Growth Des.* **2023**, *23*, 1959–1971.

[158] P. Pyykkö, M. Atsumi, *Chem.–Eur. J.* **2009**, *15*, 12770–12779.

[159] J. Geith, T. M. Klapötke, P. Mayer, A. Schulz, J. J. Weigand, *Acta Crystallogr. Sect. C* **2005**, *61*, o545–o547.

[160] G. C. Verschoor, E. Keulen, *Acta Crystallogr. Sect. B* **1971**, *27*, 134–145.

[161] S. Alvarez, *Dalt. Trans.* **2013**, *42*, 8617–8636.

[162] F. Odame, E. Hosten, Z. R. Tshentu, *Open Chem.* **2018**, *16*, 535–543.

[163] J. W. Bats, P. Coppens, *Acta Crystallogr. Sect. B* **1977**, *33*, 1542–1548.

[164] J. Songstad, L. J. Stangeland, J. Bjerrum, P. H. Nielsen, S. E. Rasmussen, E. Sunde, N. A. Sørensen, *Acta Chem. Scand.* **1970**, *24*, 804–808.

[165] J. Pfeiffer, C. Trost, A. Pachkovska, F. Tambornino, *Inorg. Chem.* **2021**, *60*, 10722–10728.

[166] E. Gougoula, J. Pfeiffer, M. Schnell, F. Tambornino, *submitted*.

[167] J. Pfeiffer, J. P. Wagner, F. Tambornino, *Eur. J. Inorg. Chem.* **2023**, e202300290.

[168] J. Pfeiffer, H. Günther, P. Fuzon, F. Weigend, F. Tambornino, *submitted*.

[169] J. Pfeiffer, H. Günther, L. Völlinger, D. Botros, B. Scheibe, M. Möbs, F. Kraus, F. Weigend, F. Tambornino, *Chem.–Eur. J.* **2023**, *29*, e202203983.

[170] J. Pfeiffer, M. Möbs, S. Reith, M. Tallu, F. Tambornino, *J. Mol. Struct.* **2024**, *1309*, 138198.

[171] J. Pfeiffer, C. Trost, F. Tambornino, *J. Mol. Struct.* **2024**, *1308*, 138079.

[172] W. L. Armarego, C. L. L. Chai, *Purification of Organic Chemicals*, 6. Aufl., Butterworth-Heinemann, **2009**.

[173] Stoe, Cie, X-Area, Darmstadt, Germany, **2002**.

[174] G. M. Sheldrick, *Acta Crystallogr. Sect. A* **2015**, *71*, 3–8.

[175] G. M. Sheldrick, *Acta Crystallogr. Sect. C* **2015**, *71*, 3–8.

[176] O. V. Dolomanov, L. J. Bourhis, R. J. Gildea, J. A. K. Howard, H. Puschmann, *J. Appl. Crystallogr.* **2009**, *42*, 339–341.

[177] K. Brandenburg, H. Putz, *DIAMOND, Program for X-Ray Structure Analysis*, Crystal Impact GbR, Bonn, **2005**.

[178] OriginPro, Northhampton, MA, USA, **2017**.

[179] R. Dovesi, A. Erba, R. Orlando, C. M. Zicovich-Wilson, B. Civalleri, L. Maschio, M. Rérat, S. Casassa, J. Baima, S. Salustro, B. Kirtman, *Wiley Interdiscip. Rev. Comput. Mol. Sci.* **2018**, *8*, e1360.

[180] J. P. Perdew, K. Burke, M. Ernzerhof, *Phys. Rev. Lett.* **1996**, *77*, 3865–3868.

[181] C. Adamo, V. Barone, *J. Chem. Phys.* **1999**, *110*, 6158.

[182] F. Weigend, R. Ahlrichs, *Phys. Chem. Chem. Phys.* **2005**, *7*, 3297–3305.

[183] A. J. Karttunen, T. Tynell, M. Karppinen, *J. Phys. Chem. C* **2015**, *119*, 13105–13114.

[184] S. Grimme, J. Antony, S. Ehrlich, H. Krieg, *J. Chem. Phys.* **2010**, *132*, 154104.

[185] H. J. Monkhorst, J. D. Pack, *Phys. Rev. B* **1976**, *13*, 5188–5192.

[186] C. M. Zicovich-Wilson, F. Pascale, C. Roetti, V. R. Saunders, R. Orlando, R. Dovesi, *J. Comput. Chem.* **2004**, *25*, 1873–1881.

[187] F. Pascale, C. M. Zicovich-Wilson, F. L. Gejo, B. Civalleri, R. Orlando, R. Dovesi, *J. Comput. Chem.* **2004**, *25*, 888–897.

[188] L. Maschio, B. Kirtman, R. Orlando, M. Rèrat, *J. Chem. Phys.* **2012**, *137*, 204113.

[189] L. Maschio, B. Kirtman, M. Rérat, R. Orlando, R. Dovesi, *J. Chem. Phys.* **2013**, *139*, 164102.

[190] G. Beata, G. Perego, B. Civalleri, *J. Comput. Chem.* **2019**, *40*, 2329–2338.

[191] Jmol: Ein Open-Source Java Viewer für chemisches Strukturen in 3D. `http://www.jmol.org/`.

8 Anhang

8.1 Supporting Information

8.1.1 A Crystallographic, Spectroscopic, and Computational Investigation of Carbonyl and Oxalyl Diisothiocyanate

A Crystallographic, Spectroscopic and Computational Investigation of Carbonyl and Oxalyl Diisothiocyanate

Jonathan Pfeiffer,[a] Clemens Trost,[a] Anna Pachkovska,[a] and Frank Tambornino*[a]

[a] Fachbereich Chemie, Wissenschaftlichen Zentrum für Materialwissenschaften (WZMW)
Philipps-Universität Marburg
Hans-Meerwein-Straße 4, D-35043 Marburg, Germany
E-mail: frank.tambornino@chemie.uni-marburg.de

Contents

1. NMR Spectroscopy
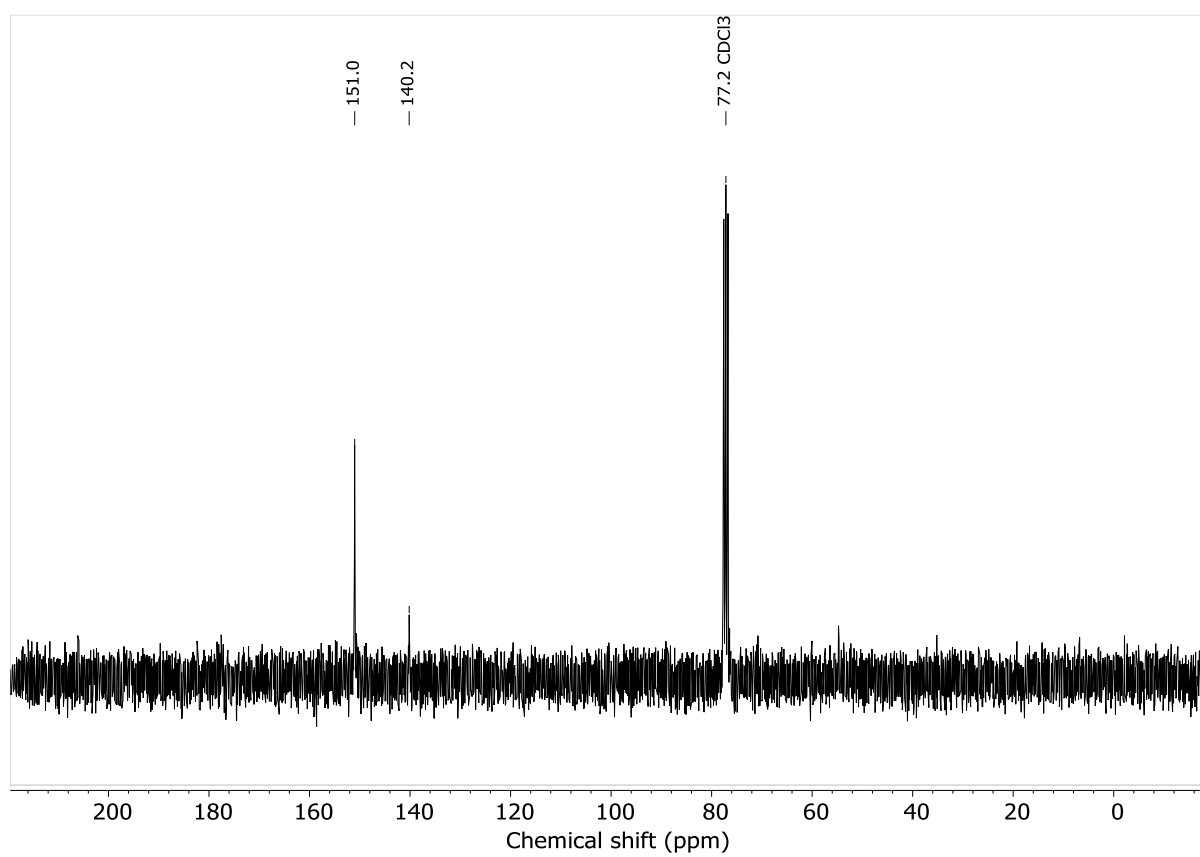
Figure S1: ^{13}C NMR spectrum of carbonyl diisothiocyanate in CDCl$_3$.
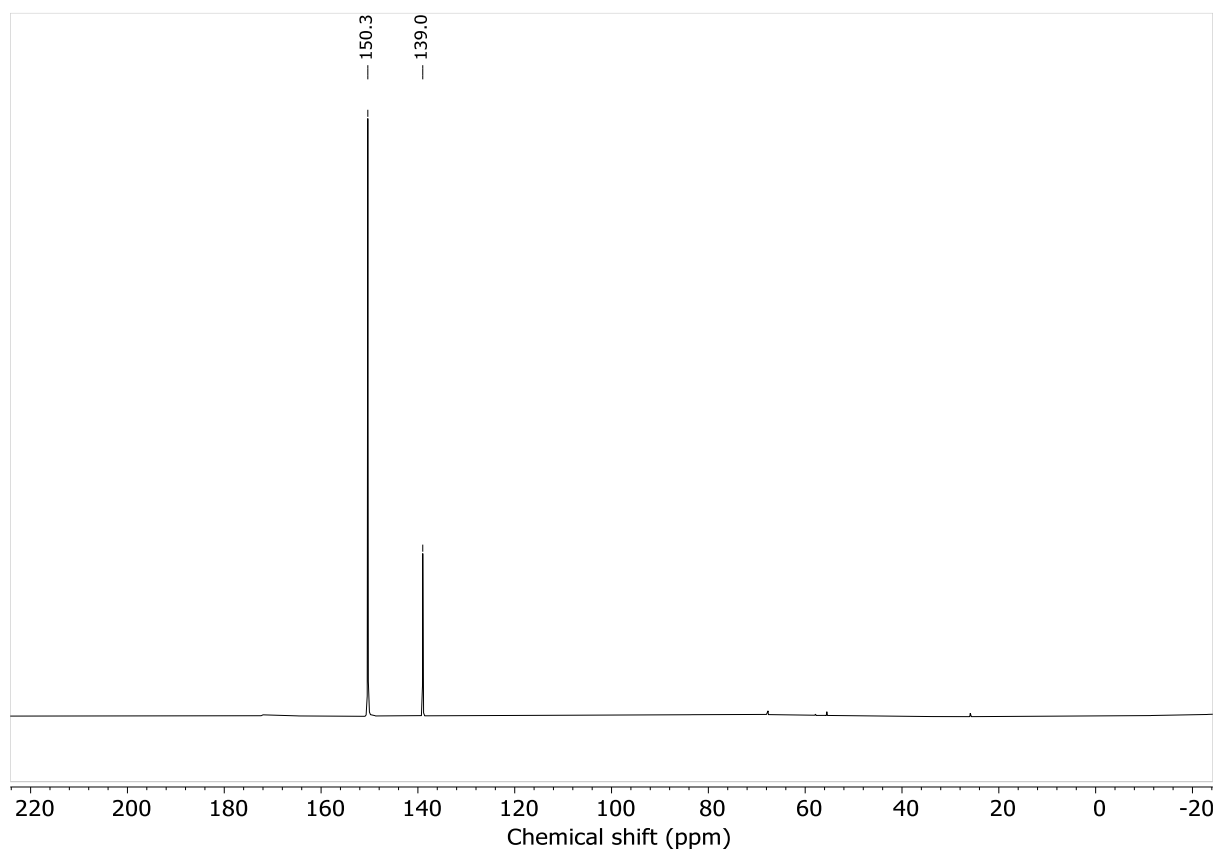
Figure S2: ^{13}C NMR spectrum of pure carbonyl diisothiocyanate without solvent.
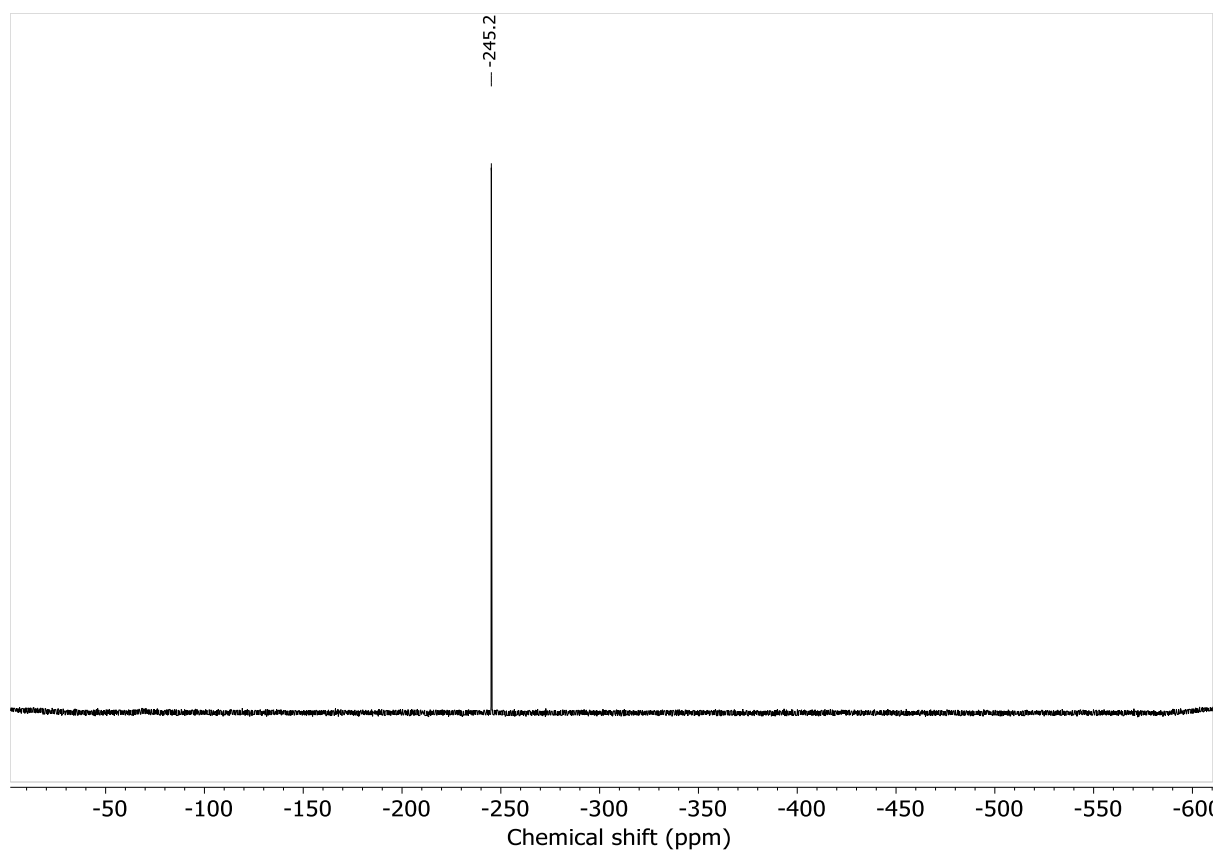
Figure S3: ^{15}N NMR spectrum of pure carbonyl diisothiocyanate without solvent.
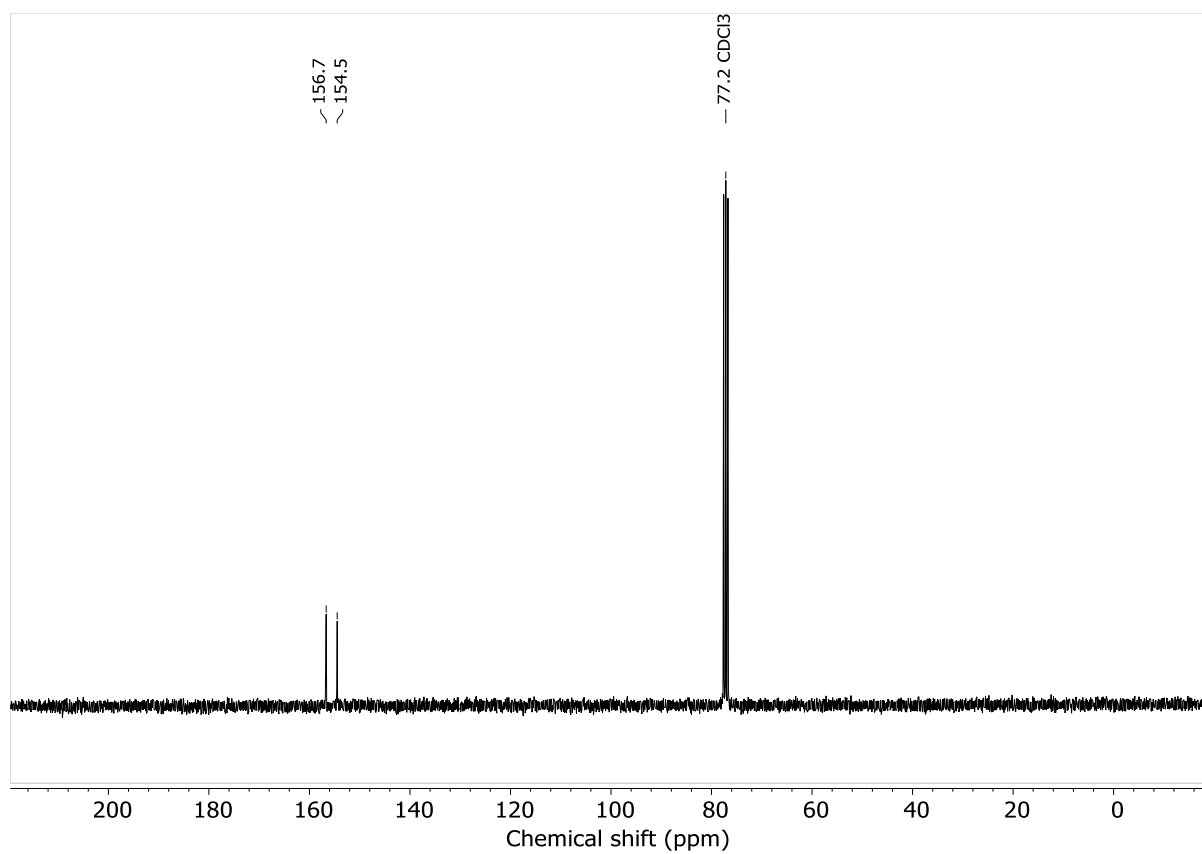
Figure S4: ^{13}C NMR spectrum of oxalyl diisothiocyanate in CDCl$_3$.
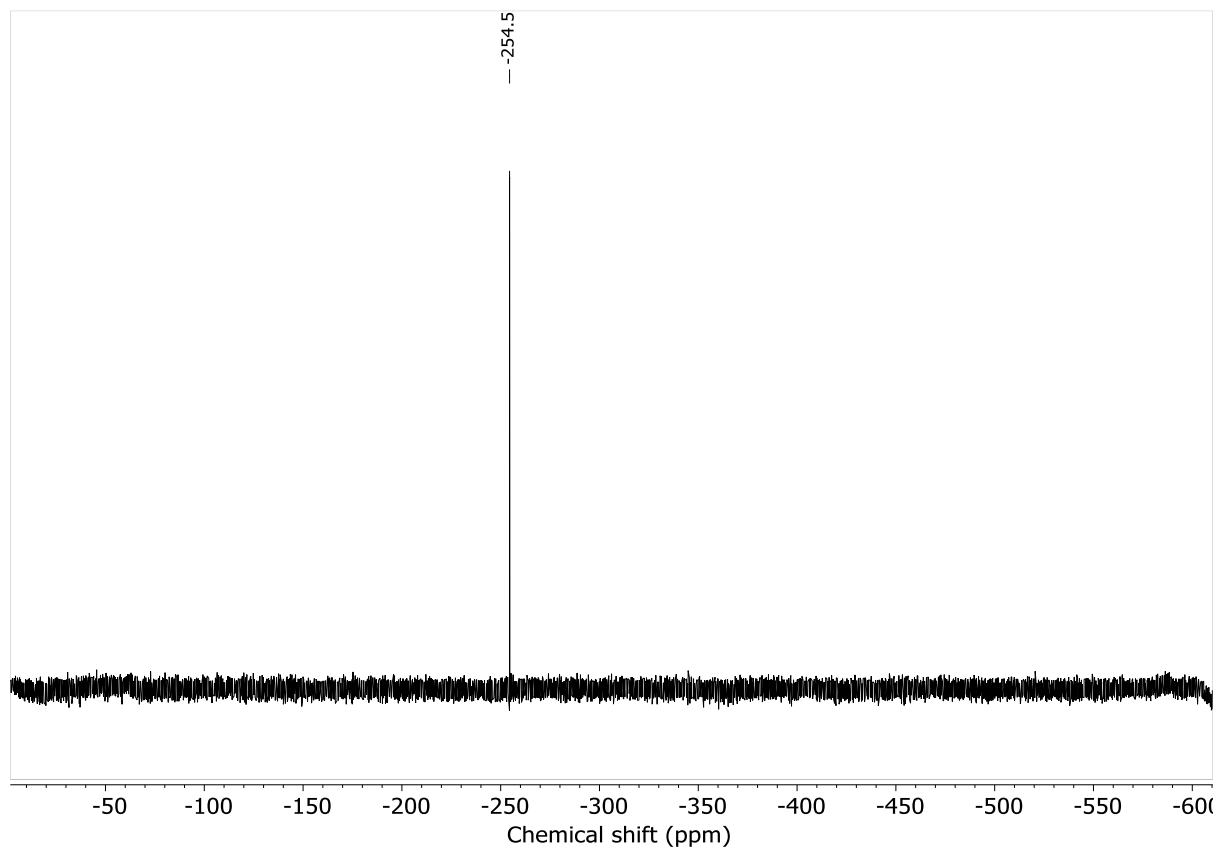
Figure S5: ^{15}N NMR spectrum of oxalyl diisothiocyanate in THF-d8.

2. IR Spectroscopy
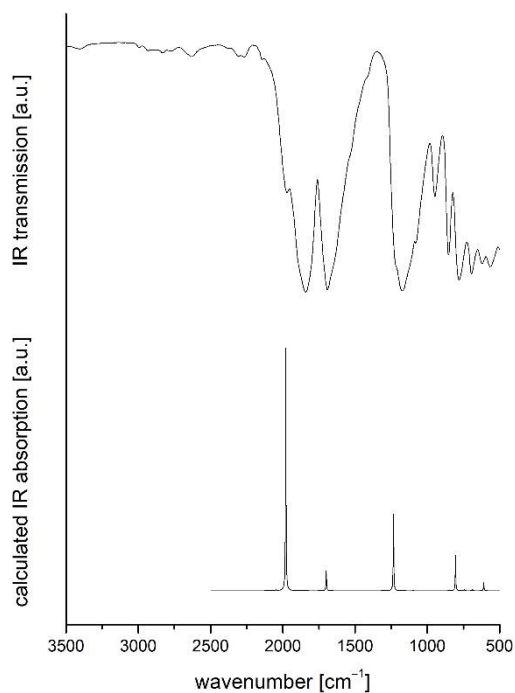
Figure S6: Top: Measured room-temperature ATR-IR spectrum of carbonyl diisothiocyanate. Bottom: Calculated solid-state IR spectrum of carbonyl diisothiocyanate.
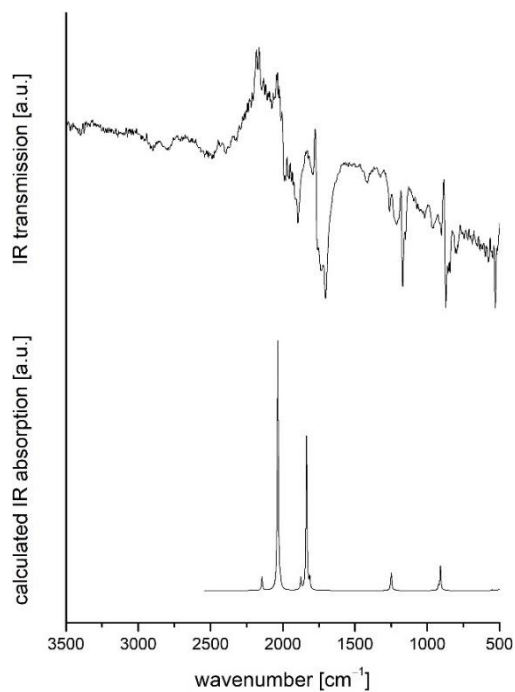
Figure S7: Top: Measured room-temperature ATR-IR spectrum of oxalyl diisothiocyanate. Bottom: Calculated solid-state IR spectrum of oxalyl diisothiocyanate.

3. Raman Spectroscopy
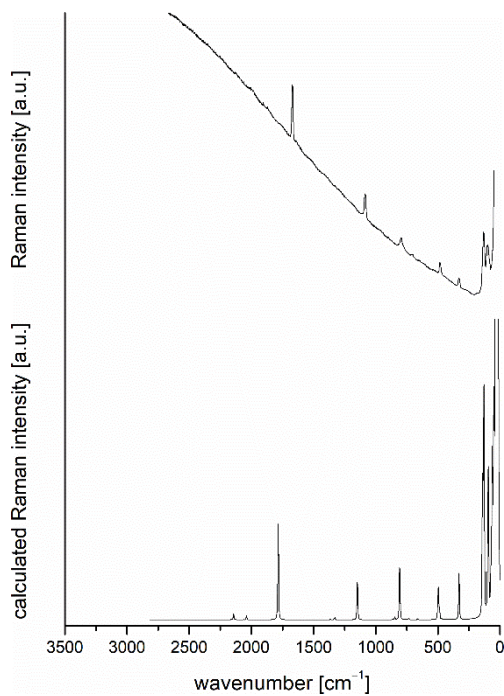
Figure S8: Measured Raman spectrum of carbonyl diisothiocyanate at −80 °C. Bottom: Calculated solid-state Raman spectrum of carbonyl diisothiocyanate.
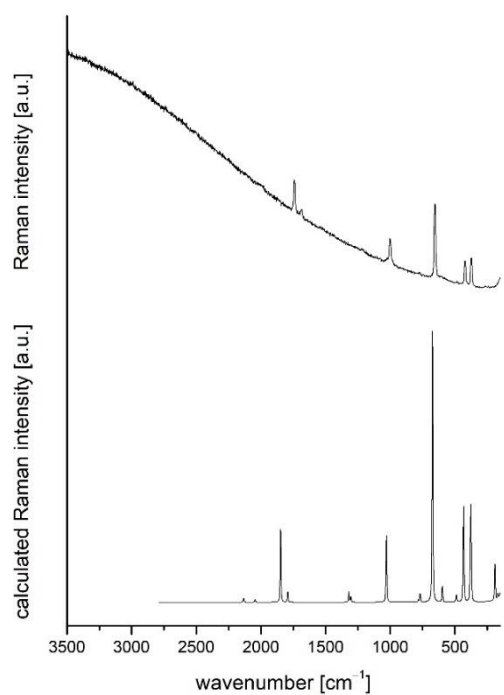
Figure S9: Top: Measured room-temperature Raman spectrum of oxalyl diisothiocyanate. Bottom: Calculated solid-state Raman spectrum of oxalyl diisothiocyanate.

4. Crystallographic data

Table S1: Selected X-ray data collection and refinement parameters for carbonyl diisothiocyanate and oxalyl diisothiocyanate.

	Carbonyl diisothiocyanate	Oxalyl diisothiocyanate
Formula	$C_3N_2O_1S_2$	$C_4N_2O_2S_2$
CCDC	2080495	2080496
Fw / g mol^{-1}	144.17	688.72
Crystal system	monoclinic	orthorhombic
Space group	$P2_1/c$ (no. 14)	$Pbca$ (no. 61)
a / Å	20.5118(13)	5.4245(2)
b / Å	3.84410(10)	20.2875(12)
c / Å	15.9661(11)	6.1642(4)
α / °	90	90
β / °	112.464(5)	90
γ / °	90	90
V / Å^3	1163.39(12)	678.37(6)
Z	8	4
Radiation, λ / Å	1.54186	1.54186
Temp / K	200	100
ρ_{calc} / g cm^{-3}	1.646	1.686
μ / mm^{-1}	7.468	6.636
θ range / °	2.995 – 65.479	4.359 – 69.919
Index range	$-24 \leq h \leq 23, -4 \leq k \leq 3, -15 \leq l \leq 18$	$-4 \leq h \leq 6, -24 \leq k \leq 24, -7 \leq l \leq 7$
Reflections collected	17346	15245
Independent reflections	2010 / 1454	643 / 504
Parameters	147	46
R_{int} / $R_{(\sigma)}$	5.47 / 3.28	6.16 / 2.45
$R1/wR2$,[a] $I \geq 2\sigma I$ (%)	3.75 / 9.58	3.22 / 7.21
$R1/wR2$,[a] all data (%)	5.34 / 10.47	4.57 / 7.44
GOF	0.903	0.961
Twin law	−1 0 −1 0 −1 0 0 0 1	—
BASF	0.251(3)	—

[a] $R1 = [\Sigma||F_o| - |F_c||]/\Sigma|F_o|$; $wR2 = \{[\Sigma w[(F_o)^2 - (F_c)^2]^2]/[\Sigma w(F_o^2)^2]\}^{1/2}$; $w = [\sigma^2(F_o)^2 + (AP)^2 + BP]^{-1}$, where $P = [(F_o)^2 + 2(F_c)^2]/3$

and the A and B values are 0.07180 and 0 for carbonyl diisothiocyanate, 0.04840 and 0 for oxalyl diisothiocyanate.

Table S2: Selected powder X-ray data collection and Rietveld refinement parameters for oxalyl diisothiocyanate.

	Oxalyl diisothiocyanate
Formula	$C_4N_2O_2S_2$
CCDC	2080497
Fw / g mol^{-1}	688.72
Crystal system	orthorhombic
Space group	$Pbca$ (no. 61)
a / Å	5.4757(2)
b / Å	20.523(7)
c / Å	6.3625(2)
α / °	90
β / °	90
γ / °	90
V / Å^3	715.004(4)
Z	4
Radiation, λ / Å	1.54186
Temp / K	298
R_{wp} / %	5.902
R_p / %	4.469
R_{Bragg} / %	3.061
GoF	2.284
Starting angle measured / ° 2θ	5
Final angle measured / ° 2θ	90
Starting angle refined/° 2θ	20
Final angle refined/ ° 2θ	70
Step width/ ° 2θ	0.015
Refined Parameters[a]	25
Background Parameters	6
Profile Parameters	9

5. Hirschfeld surface and packing analysis

Carbonyl diisothiocyanate (1)
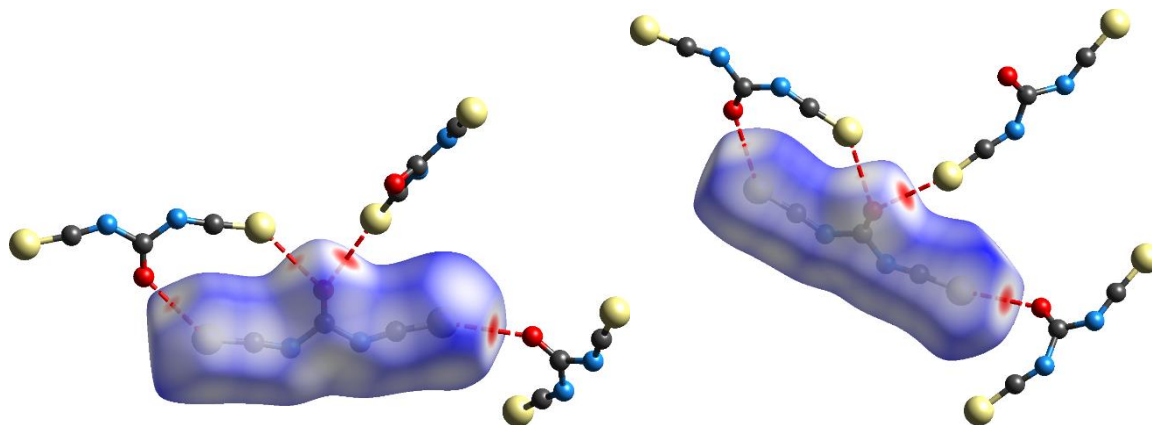
Figure S10: Hirschfeld surfaces for carbonyl diisothiocyanate crystallographic individuum 1 (left) and individuum 2 (right). Red colour on the surface indicates an intermolecular contact shorter than the sum of van-der-Waals radii and short contacts are highlighted by red dashed lines.
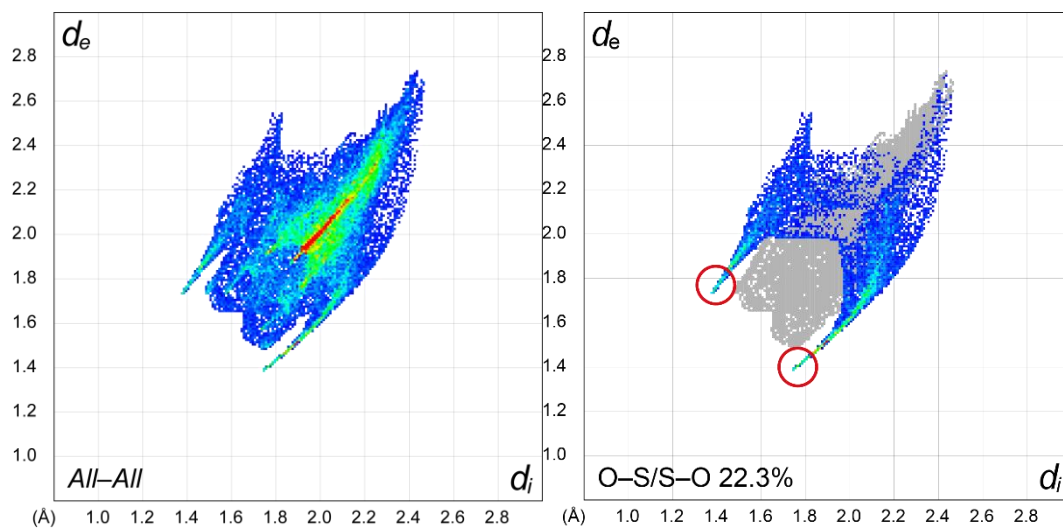
Figure S11: 2D fingerprint plots for all (left) and O–S/S–O (right) contacts. The two spikes (red circles) are the short O–S contacts.
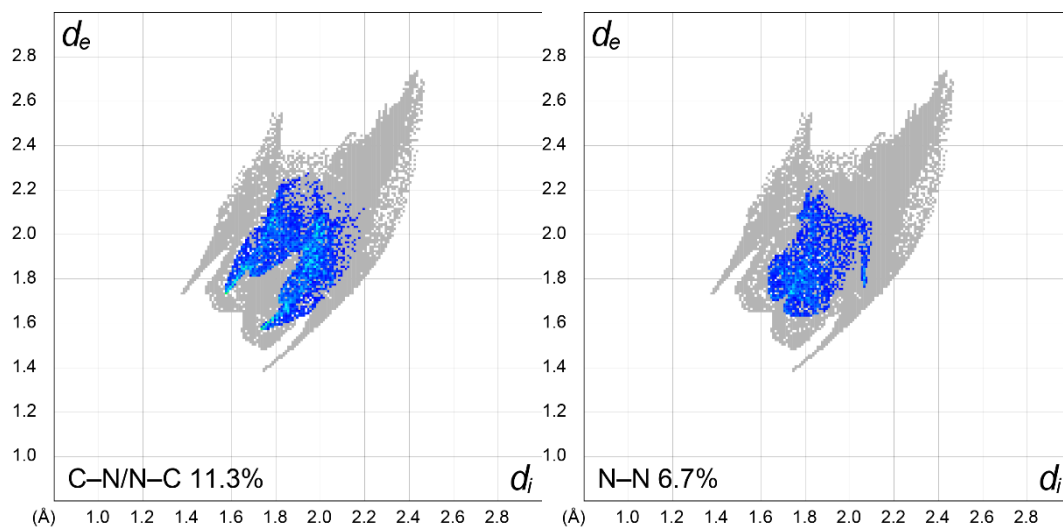
Figure S12: 2D fingerprint plots for C–N/N–C (left) and N–N (right) contacts.
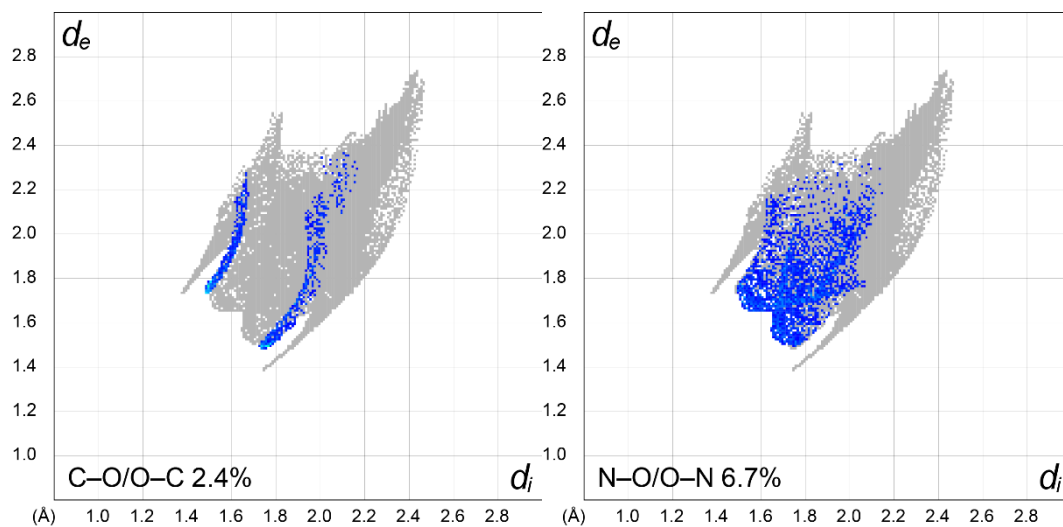
Figure S13: 2D fingerprint plots for C–O/O–C (left) and N–O/O–N (right) contacts.
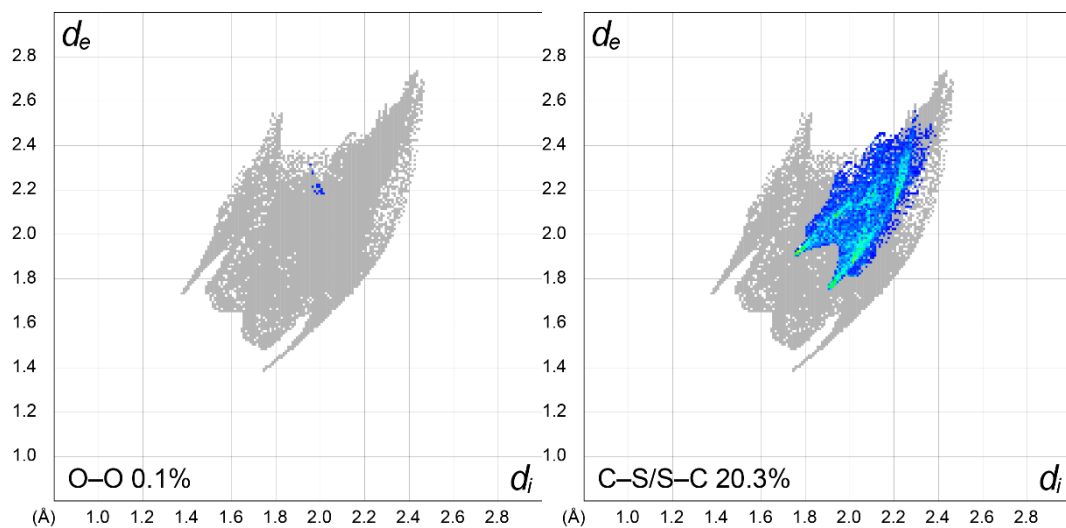
Figure S14: 2D fingerprint plots for O–O (left) and C–S/S–C (right) contacts.
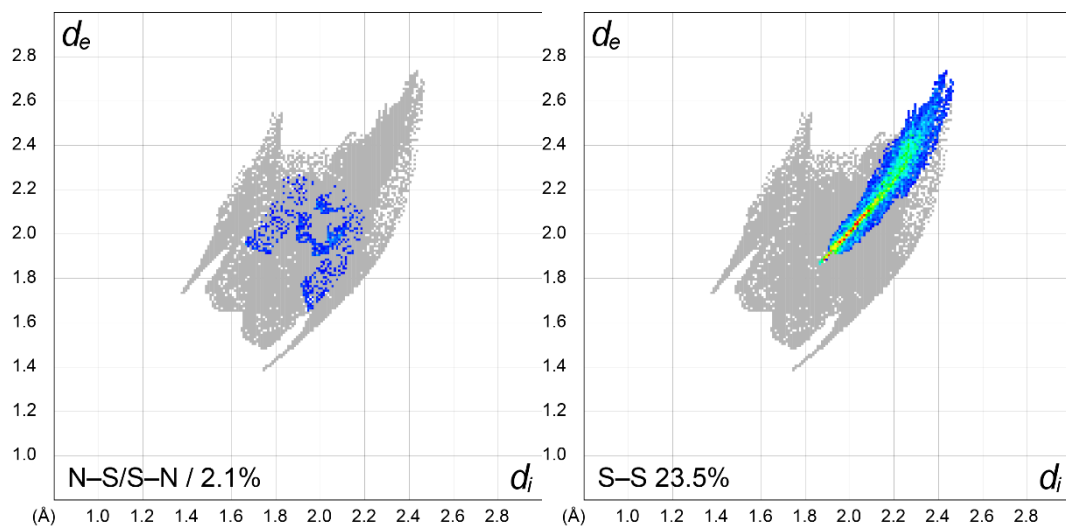
Figure S15: 2D fingerprint plots for N–S/S–N (left) and S–S (right) contacts. The latter are the main contact area on the Hirschfeld surface and lie in the range of the sum of their van-der-Waals radii.
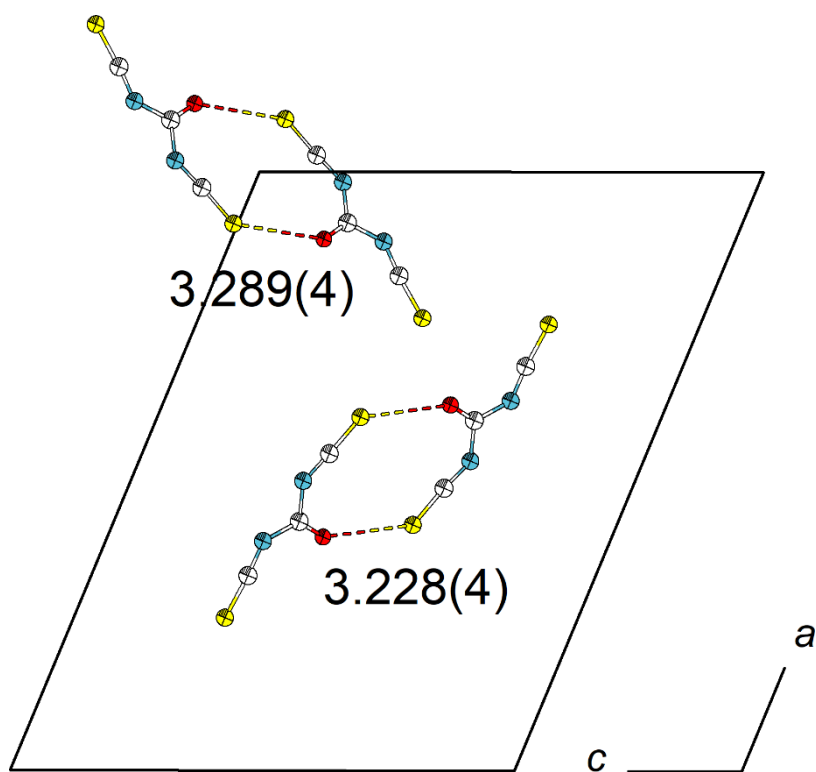
Figure S16: Bonding between the crystallographically independent carbonyl diisothiocyanate molecules to their respective symmetry generated pair. Short contacts are drawn as dashed lines.
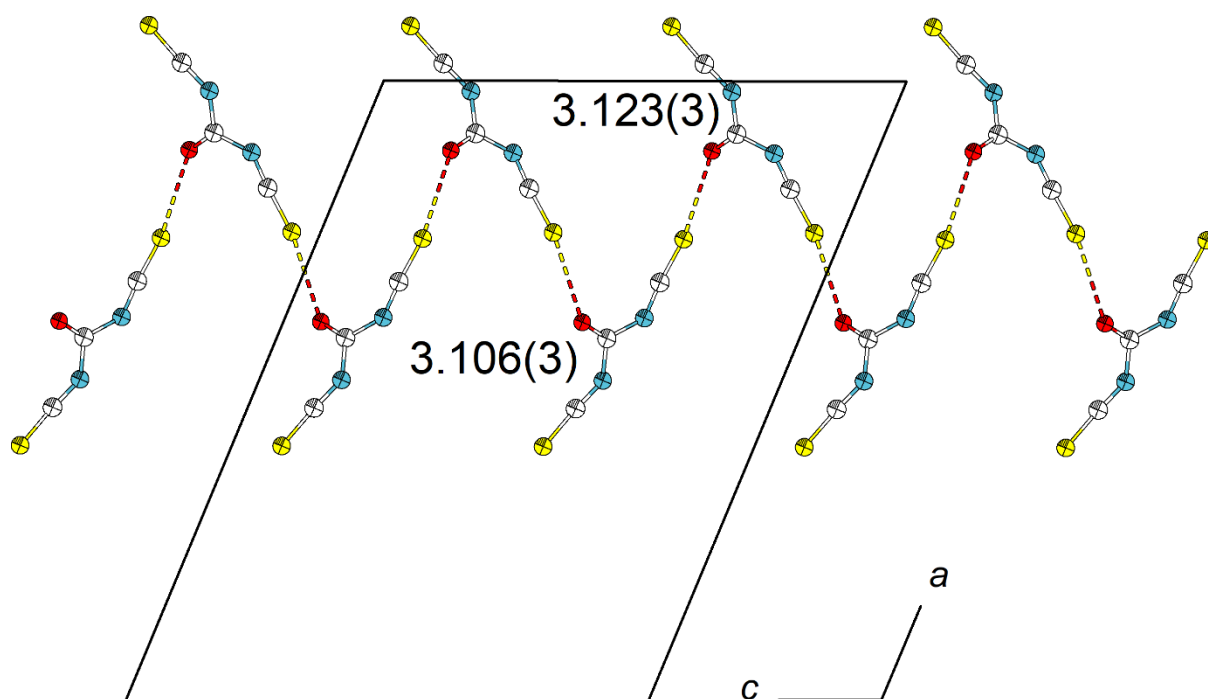
Figure S17: Bonding between the crystallographically independent molecules of carbonyl diisothiocyanate forming a puckered zig-zag-chain along [001].

Oxalyl diisothiocyanate (2)
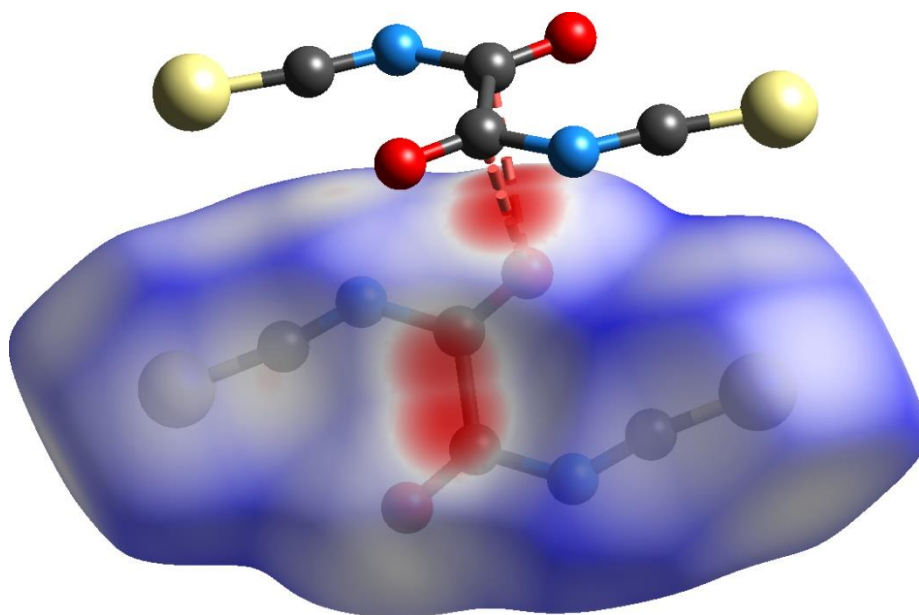
Figure S18: Hirschfeld surface for oxalyl diisothiocyanate. Red indicates an intermolecular contact shorter than the sum of van-der-Waals radii and short contacts are highlighted as red dashed lines.
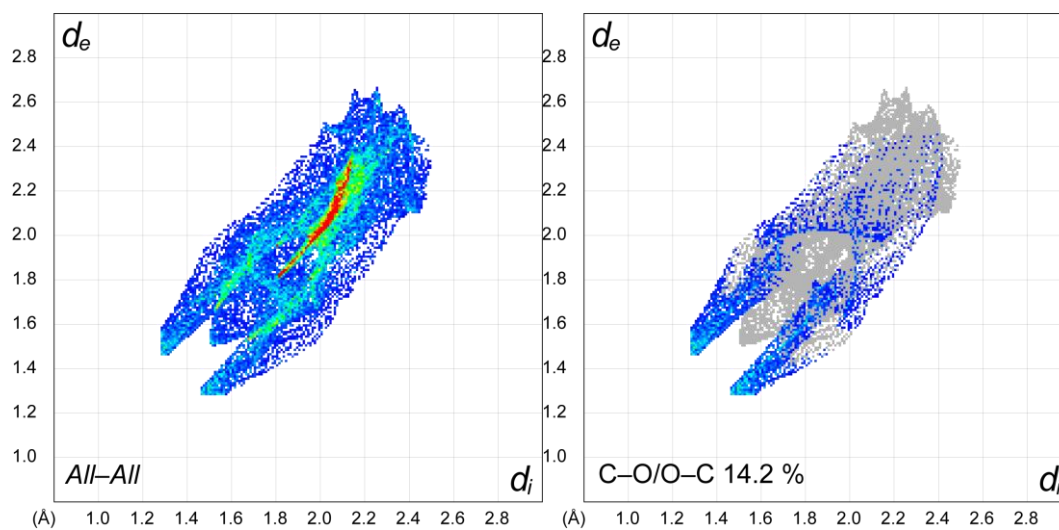
Figure S19: 2D fingerprint plots for all (left) and C–O/O–C (right) contacts in oxalyl diisothiocyanate. The two spikes (red circles) are the short C–O contacts which are closer than the sum of the van-der-Waals radii.
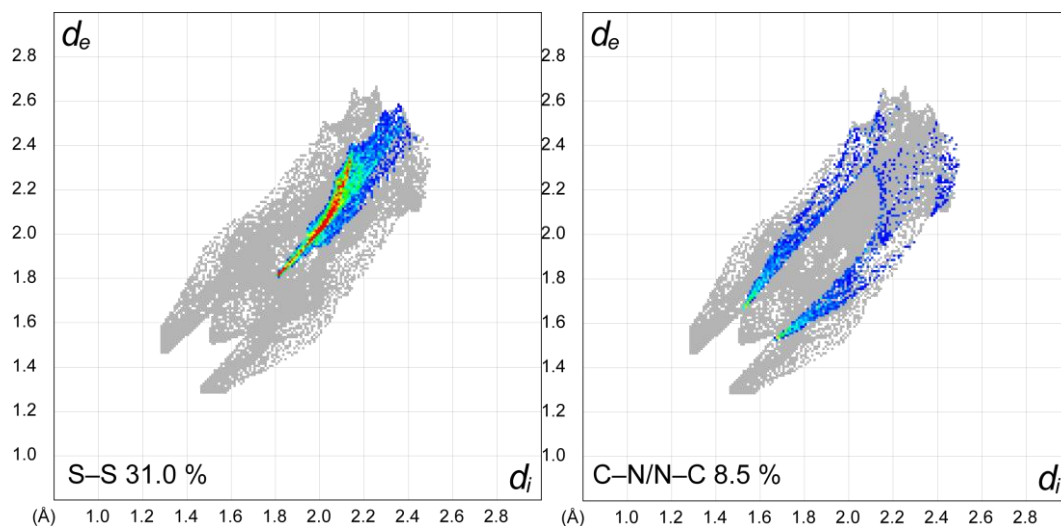
Figure S20: 2D fingerprint plots for S–S (left) and C–N/N–C (right) contacts in oxalyl diisothiocyanate. S–S contacts are responsible for interplane packing.
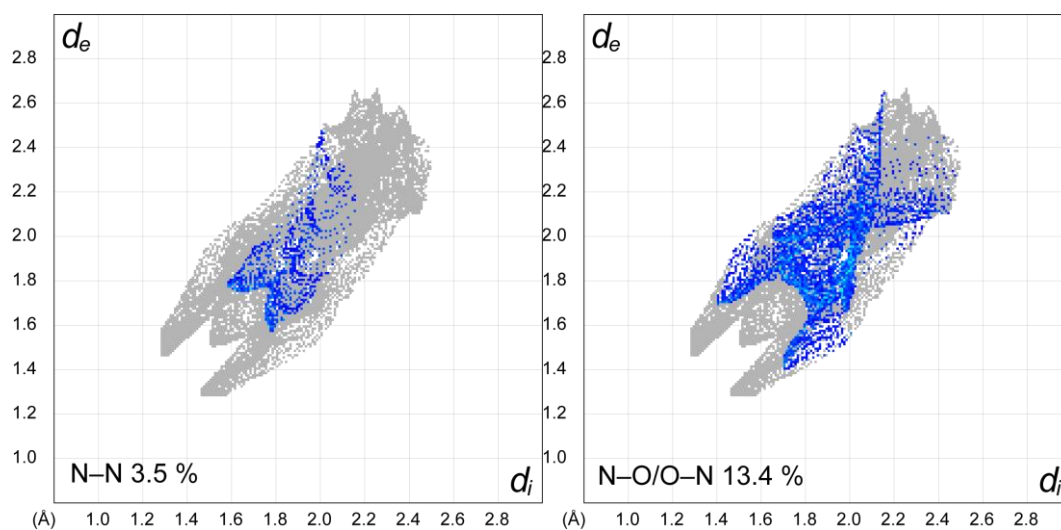
Figure S21: 2D fingerprint plots for N–N (left) and N–O/O–N (right) contacts in oxalyl diisothiocyanate.
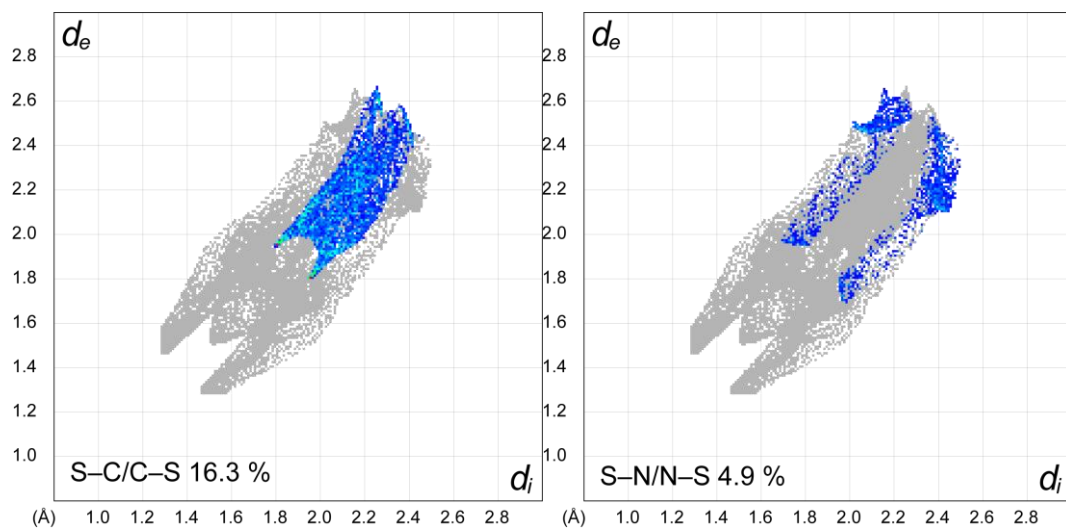
Figure S22: 2D fingerprint plots for S–C/C–S (left) and S–N/N–S (right) contacts in oxalyl diisothiocyanate.
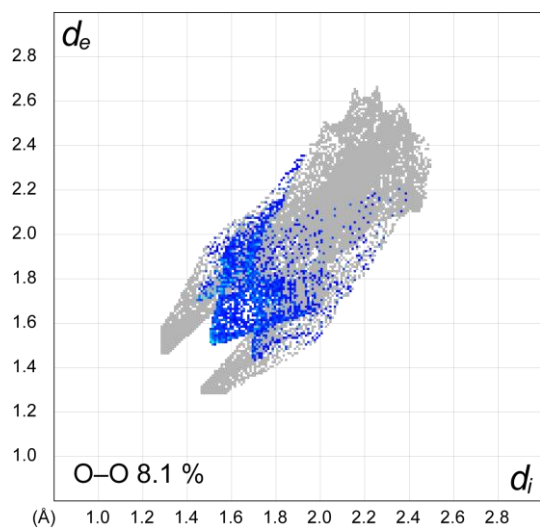
Figure S23: 2D fingerprint plots for O–O contacts in oxalyl diisothiocyanate.
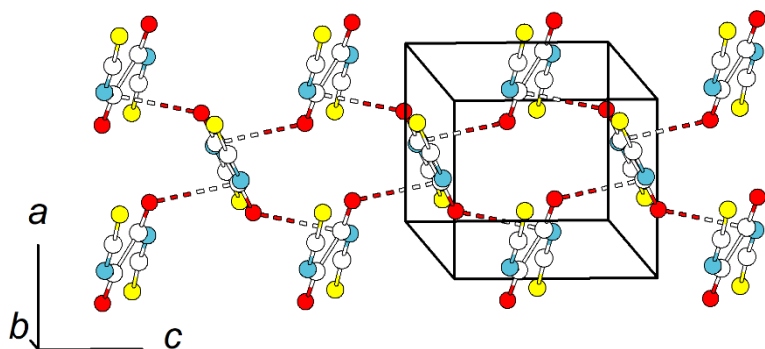
Figure S24: Section of the crystal structure of oxalyl diisothiocyanate viewed approximately along [010] emphasizing the interconnection of individual molecules. C–O short contacts are shown as dashed lines. The C–O distance is 2.769(2) Å.
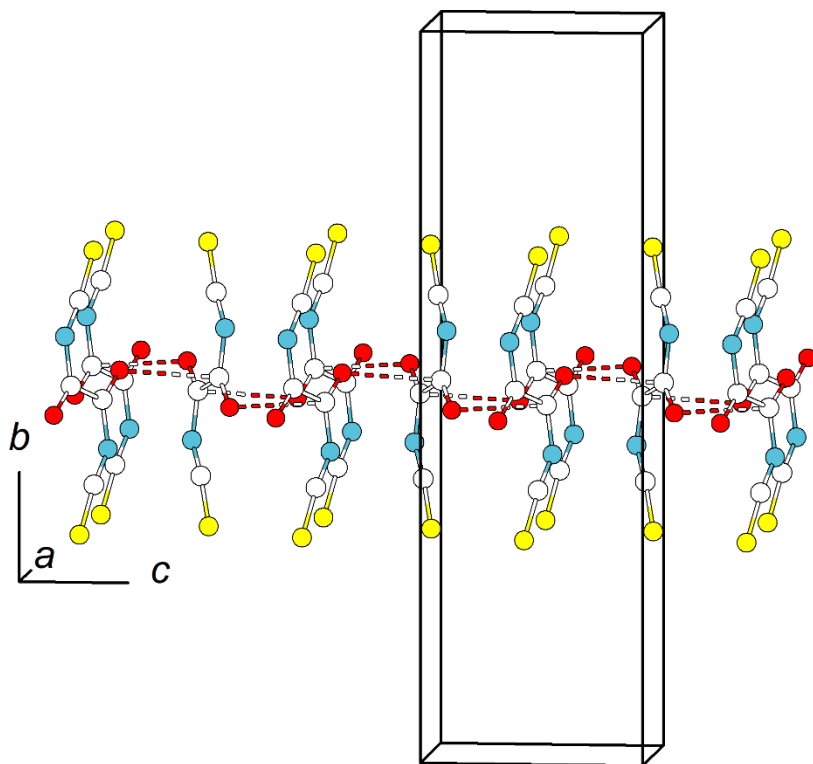
Figure S25: Section of the crystal structure of oxalyl diisothiocyanate viewed approximately along [100] emphasizing the interconnection of individual molecules and layer formation. C–O short contacts are shown as dashed lines.

6. Computational details

Table S3: Lattice parameters and atomic coordinates of the optimized solid-state structure of carbonyl diisothiocyanate.

Lattice parameter	a	b	c	β
	21.33227251	4.09862195	16.62696050	112.951696

Atom	x	y	z
S1	8.198325514532E−02	2.533371788483E−01	−1.405571729646E−02
S2	−2.399202937798E−01	2.965857406361E−01	−4.441578271379E−01
S3	−2.600560497510E−01	−2.827504872809E−01	2.930805429916E−01
S4	4.186724675546E−01	−2.553305098232E−01	4.030463365229E−01
O1	−1.114524930995E−01	−5.850335632794E−02	−1.937466673700E−01
O2	−3.884457862172E−01	4.245957350246E−01	4.185051595161E−01
N1	−2.167829284962E−02	2.763443555973E−01	−1.777081514048E−01
N2	−1.158456530094E−01	2.831946567433E−01	−3.043589494910E−01
N3	−3.828001112086E−01	−2.398621921020E−01	3.117730924371E−01
N4	−4.772788070014E−01	−2.370295453277E−01	3.437583188708E−01
C1	−8.569092417940E−02	1.470696819341E−01	−2.221727952012E−01
C2	2.229357916710E−02	2.568434731523E−01	−1.052968381037E−01
C3	−1.710067346274E−01	2.785778492811E−01	−3.638352298513E−01
C4	−4.135834538827E−01	−3.707120564249E−01	3.638099645360E−01
C5	−3.283287821908E−01	−2.669550145181E−01	3.060725936258E−01
C6	4.785244697367E−01	−2.544502460286E−01	3.718500851061E−01

Table S4: Band assignments for the calculated Raman spectra (>150cm^{-1}) of carbonyl diisothiocyanate. The notation for band assignments is the following: v–stretching, δ–deformation, s–symmetric, as–antisymmetric. The irreducible representations are given for the point groups of the respective space group types of the crystal structures. The observed bands are from measurement with a 532 nm laser if not mentioned otherwise.

v (calculated) [cm^{-1}]	v (observed) [cm^{-1}]	irrep.	assignment
			Carbonyl diisothiocyanate
2159		Ag	
2144		Ag	
2124	not observed	Bg	v_{as} – antisymmetric NCS stretching
2120		Bg	
2091		Bg	
2087		Bg	
2061	not observed	Ag	v_{as} – antisymmetric NCS stretching
2038		Ag	
1792		Ag	
1787		Bg	
1786	1670	Bg	v(C=O) stretching
1784		Ag	
1364	not observed	Bg	δ – in plane rocking δ (O=CN$_2$) deformation

1363		Bg	
1335		Ag	
1328		Ag	
1148		Ag	
1146	1084	Ag	ν(C=O) stretching coupled with ν(C–N) stretching and minor
1145		Bg	amount of ν_s(NCS) stretching
1144		Bg	
864		Bg	
863	not observed	Bg	δ – in plane rocking δ (O=CN$_2$) deformation
849		Ag	
846		Ag	
809		Ag	
805	808	Ag	δ – scissoring δ (N–C–N) deformation
803		Bg	
799		Bg	
735		Ag	
734	not observed	Bg	δ – out of plane rocking δ (O=CN$_2$) deformation
733		Ag	
733		Bg	
663		Bg	
6662	not observed	Ag	δ – in plane rocking δ (O=CN$_2$) deformation coupled with in
659		Bg	plane δ (NCS) deformation
658		Ag	
503		Bg	
502		Bg	
502		Ag	
501		Ag	
497		Ag	
495		Ag	
492	484	Bg	δ – out of plane rocking δ (NCS) deformation
492		Bg	
489		Bg	
488		Ag	
488		Bg	
486		Ag	
469		Bg	
468	not observed	Ag	δ – in plane rocking δ (NCS) deformation
468		Bg	
467		Ag	
331		Bg	
331	331	Ag	δ – scissoring δ (N–C–N) deformation coupled with minor
330		Bg	amounts of ν(NCS) stretching
329		Ag	
143		Bg	
142	not observed	Ag	δ – out of plane rocking δ (O=CN$_2$) deformation
139		Ag	

138		Bg	
131		Ag	
129	131	Bg	δ – in plane wagging (O=CN$_2$) deformation
129		Bg	
128		Ag	
101		Ag	
98	96	Bg	δ – out of plane wagging deformation
97		Ag	
94		Ag	
74		Bg	
72	not observed	Ag	lattice vibration
72		Bg	
63		Ag	
62		Ag	
56	50	Bg	lattice vibration
55		Bg	
51		Ag	

Table S5: Lattice parameters and atomic coordinates of the optimized solid-state structure of oxalyl diisothiocyanate.

Lattice parameter	a	b	c
	5.35080025	20.55573998	5.91228121

Atom	x	y	z
C1	1.202023776714E−01	1.160303126324E−02	6.052973712065E−02
C2	6.427148216656E−03	1.241252206276E−01	3.926091172470E−02
N1	1.319480718109E−01	7.744467913842E−02	8.985353724423E−02
O1	2.770877770646E−01	−2.592874331598E−02	1.217147856285E−01
S1	−1.303001156292E−01	1.892714745838E−01	−1.113016128157E−02

Table S6: Band assignments for the calculated Raman spectra ($>150\text{cm}^{-1}$) of carbonyl diisothiocyanate and oxalyl diisothiocyanate. The notation for band assignments is the following: ν–stretching, δ– deformation, s–symmetric, as–antisymmetric. The irreducible representations are given for the point groups of the respective space group types of the crystal. The observed bands are from measurement with a 532 nm laser if not mentioned otherwise.

ν (calculated) [cm^{-1}]	ν (observed) [cm^{-1}]	irrep.	assignment
			Oxalyl diisothiocyanate
2135	not observed	B1g	ν_{as} – antisymmetric NCS stretching
2134		Ag	
2045	not observed	B3g	ν_{as} – antisymmetric NCS stretching coupled with ν(C=O) stretching
2045		B2g	
1848	1742	B1g	ν(C=O) stretching coupled with ν(C–C) stretching
1848		Ag	
1793	1688 (weak)	B2g	ν(C=O) stretching coupled with ν(C–C) stretching and minor amount of ν_{as}(NCS) stretching
1792		B3g	
1321	not observed	Ag	ν(C–N) stretching coupled with symmetric NCS stretching
1319		B1g	
1305		B3g	
1304		B2g	
1030	999	Ag	ν(C–C) coupled with ν_s(NCS) and δ(N–C–O) scissoring
1030		B1g	
1026		B3g	
1025		B2g	
783	not observed	B3g	δ – out of plane δ (C–C) deformation
783		B2g	
769		B1g	
769		Ag	
677	655	B3g	δ – (O=C–C=O) symmetric stretching coupled with NCS scissoring
677		B2g	
674		B1g	
674		Ag	
599	not observed	B3g	

599		Ag	δ – (O=C–C=O) antisymmetric stretching coupled with NCS scissoring
598		B2g	
598		B1g	
495		B1g	δ – out of plane (NCS) deformation
489	not observed	Ag	
488		B2g	
487		B3g	
438		B3g	δ – (O=C–N) scissoring (major) coupled with (NCS) scissoring (minor)
437	422	B2g	
434		B1g	
433		Ag	
382		B2g	δ – (O=C–N) scissoring (minor) coupled with NCS scissoring (major)
380	373	B3g	
380		B1g	
376		Ag	
191	not observed	B2g	δ – (O=C–C=O) wagging
191		B3g	
169	not observed	B1g	δ – out of plane deformation with three nodes over the whole molecule
168		Ag	
129 (shoulder)	121[a]	B3g	lattice vibration
129 (shoulder)		B2g	
121		Ag	lattice vibration
118	121[a]	B2g	
113		B3g	
112		B1g	
94		B1g	lattice vibration
93	92[a]	Ag	
88		B1g	
87		B3g	

[a] Those bands have only been observed by excitation with a 633nm laser.

8.1.2 Rotational Conformers and Nuclear Spin Isomers of Carbonyl Diisothiocyanate

Supplementary Information for the manuscript:

Rotational Conformers and Nuclear Spin Isomers of Carbonyl Diisothiocyanate

Eva Gougoula[1,*], Jonathan Pfeiffer[2], Melanie Schnell[1, 3, *], and Frank Tambornino[2,*]

Affiliations:

[1] Deutsches-Elektronen Synchrotron DESY, Notkestr. 85, 22607 Hamburg, Germany

[2] Fachbereich Chemie, Philipps-Universität Marburg, Hans-Meerwein-Straße 4, 35043 Marburg, Germany

[3] Institut für Physikalische Chemie, Christian-Albrechts-Universität zu Kiel, D-24118 Kiel, Germany

* Corresponding authors: melanie.schnell@desy.de, eva.gougoula@desy.de, tamborni@chemie.uni-marburg.de

ORCIDs:

Eva Gougoula: https://orcid.org/0000-0002-2037-1314

Melanie Schnell: https://orcid.org/0000-0001-7801-7134

Frank Tambornino: https://orcid.org/0000-0003-3538-6049

1. Methods

1.1 Experimental Methods

Carbonyl diisothiocyanate (CDIT), a clear and viscous liquid at room temperature, was synthesized according to the procedure described by Pfeiffer and co-workers[1]. In brief, a reaction between phosgene and ammonium isothiocyanate at −78 ⁰C under an inert atmosphere (Schlenk technique) yields CDIT. The above conditions allow for isolating and storing CDIT for a sufficiently long time.

The rotational spectrum of CDIT was recorded in the 2-8 and 8-12 GHz frequency ranges using the COMPACT spectrometer in Hamburg[2,3]. The experiment requires that the molecules of interest are in the gas phase. Due to the air and moisture sensitivity of CDIT, the sample was handled under the atmosphere of a glove box (O_2 <1.2 ppm, H_2O <0.5 ppm). CDIT was loaded into the reservoir of a modified pulsed valve, which was then assembled and attached to the solenoid. The valve assembly was placed in an airtight container, equilibrated under glove box atmosphere, and transported to the vacuum chamber where it was connected to the neon gas line. The sample was then pressurized by neon at 3 bar stagnation pressure and heated to 75 ⁰C while pulsed into the vacuum chamber with an 8 Hz repetition rate.

The sequence of events following the incorporation of the gas pulse generating a molecular ensemble is described briefly. A chirped pulse spanning between 2-8 GHz with 4 *μs* duration is synthesized by an arbitrary waveform generator (AWG) and amplified by a 300 W traveling wave-tube amplifier. The pulse is broadcast into the vacuum chamber by a horn antenna and excites molecular rotational transitions in resonance with the transmitted frequencies in the fast passage regime. It is noted that the gas pulse and the chirped pulse propagate perpendicular to each other. After the halt of the polarizing pulse, the relaxation of the induced polarization of the molecular ensemble is detected by another horn antenna in the form of a free induction decay (FID) for 40 μs, followed by digitization and Fourier transformation to the frequency domain spectrum by a 100 GS/s oscilloscope. The spectra in the 8-12 GHz region are recorded following the same principles. However, a chirped pulse between 4-6 GHz is generated, which is then frequency doubled to the desired frequencies and amplified by a 50 W solid state amplifier. For both frequency ranges, the duration of the gas pulse, the timescale of the experiment, and the oscilloscope's fast-frame mode allow for eight sequential polarizations of the molecular ensemble, each

followed by a FID recording, which are then co-added in the time domain. With this method, spectra containing 1 and 3.2 million averages were recorded in the 2-8 and 8-12 GHz ranges, respectively.

2.1 Quantum Mechanical Calculations

Geometry optimizations of the three possible conformers of CDIT, *syn-syn*, *syn-anti*, and *anti-anti*, were performed with the ORCA 5.0 package[4]. The hybrid functional of Becke-Lee-Yang-Parr (B3LYP)[5] was employed with Grimme's dispersion correction[6–8] (D3BJ) along with the augmented triple-ζ (aug-cc-pVTZ) basis set[9]. The optimized geometries and calculated molecular parameters are summarized in Table 1. Second-order Møller-Plesset perturbation theory[10] (MP2) and the augmented double-ζ (aug-cc-pVDZ) basis set[9] was also used to test the performance of the two methods in the spectral analysis. The MP2 calculated parameters are summarized in Table S1 in the Supplementary Material.

Nudged elastic band calculations[11] (NEB) were performed to get an insight into the barriers to interconversion between the three possible conformers. The method of Perdew-Burke-Ernzerhoff[12] (PEBh-3c) was used to optimize the geometry of the CDIT conformers, followed by NEB calculations of the energy barriers to interconversion at the same level of theory. The calculated barriers to interconversion are summarized in Table 1. Visualization of all structures is achieved with the software Chimera 1.16[13].

2. Supporting Tables and Figures

Table S1. A summary of the theoretically calculated rotational constants of *syn-syn-* and *syn-anti*-CDIT at the B3LYP-D3(BJ)/aug-cc-pVTZ and MP2/aug-cc-pVDZ levels of theory. The numbers in brackets indicate the percentage deviation of the theoretical constants from the experimentally determined ones.

	syn-syn	
	B3LYP-D3(BJ)/aug-cc-pVTZ	MP2-aug-cc-pVDZ
A_e **(MHz)**	10335.6 (–6.4%)[‡]	10645.8 (–3.6%)
B_e **(MHz)**	443.7 (–1.4%)	437.8 (–2.7%)
C_e **(MHz)**	425.4 (–1.6%)	420.5 (–2.7%)
	syn-anti	
	B3LYP-D3(BJ)/aug-cc-pVTZ	MP2-aug-cc-pVDZ
A_e **(MHz)**	2901.6 (–1.4%)	2819.4 (–4.1%)
B_e **(MHz)**	612.0 (–2.6%)	615.0 (–1.8%)
C_e **(MHz)**	505.4 (–2.3%)	504.9 (–2.2%)

[‡]The percentage deviations are calculated by means of the formula: $\sigma = \frac{A_e - A_0}{A_0} \times 100$, adapted for each rotational constant.
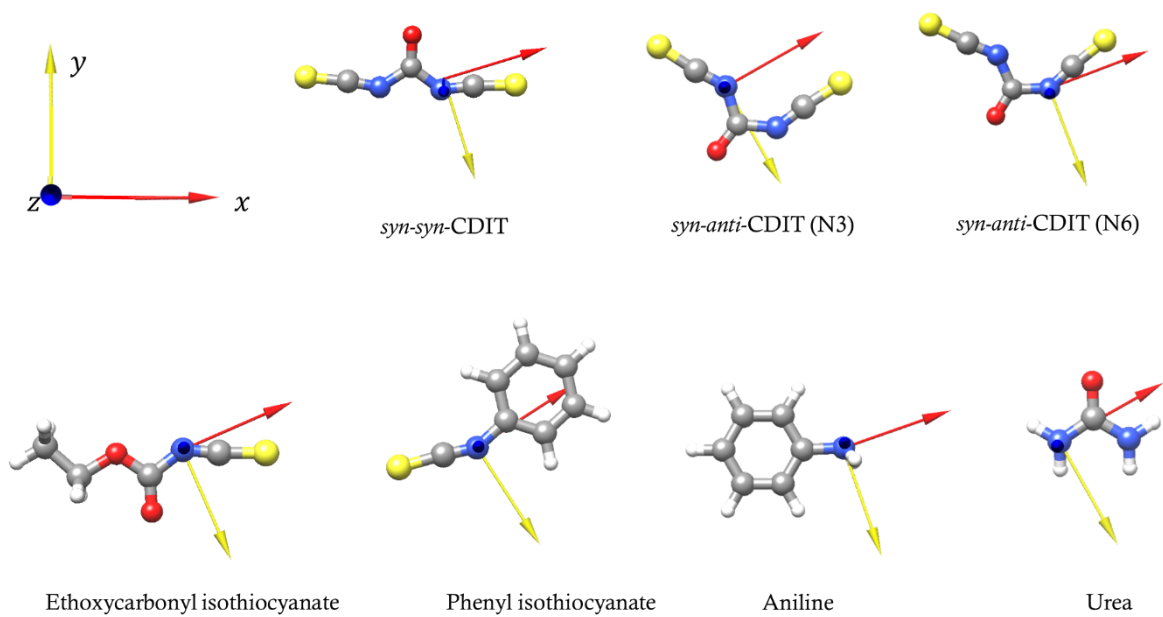
Figure S1. Positioning of the principle nuclear axes x, y, z on each N nucleus of the molecules that are included in Table 6 of the manuscript. The axes are orthogonal and follow a common orientation, regardless of the inertial axes of each molecule.

Table S2. Calculated r_e atomic coordinates of *syn-syn*-CDIT.

	a (Å)	*b* (Å)	*c* (Å)
syn-syn-CDIT @ B3LYP-D3(BJ)/aug-cc-pVTZ			
O1	0	1.553	0
C2	0	0.352	0
N3	1.143	–0.441	0
C4	2.337	–0.264	0
S5	3.892	–0.162	0
N6	–1.143	–0.441	0
C7	–2.337	–0.264	0
S8	–3.892	–0.162	0
syn-syn-CDIT @ MP2/aug-cc-pVDZ			
O1	0	1.509	0
C2	0	0.292	0
N3	2.353	–0.265	0
C4	1.146	–0.523	0
S5	3.919	–0.104	0
N6	–1.146	–0.527	0
C7	–2.353	–0.265	0
S8	–3.919	–0.104	0

Table S3. Calculated r_e atomic coordinates of *syn-anti*-CDIT.

syn-anti-CDIT @ B3LYP-D3(BJ)/aug-cc-pVTZ			
	a (Å)	*b* (Å)	*c* (Å)
O1	–0.539	–2.270	0
C2	–0.018	–1.192	0
N3	1.359	–1.010	0
C4	2.137	–0.087	0
S5	3.235	1.019	0
N6	–0.714	0.027	0
C7	–1.878	0.354	0
S8	–3.339	0.895	0
syn-anti-CDIT @ MP2/aug-cc-pVDZ			
	a (Å)	*b* (Å)	*c* (Å)
O1	–0.594	–2.276	0
C2	–0.019	–1.207	0
N3	1.379	–1.083	0
C4	2.131	–0.103	0
S5	3.216	1.037	0
N6	–0.655	0.062	0
C7	–1.854	0.364	0
S8	–3.332	0.904	0

Table S4. Calculated r_e atomic coordinates of *anti-anti*-CDIT.

	anti-anti-CDIT @ B3LYP-D3(BJ)/aug-cc-pVTZ		
	a (Å)	b (Å)	c (Å)
O1	−0.020	2.981	0
C2	−0.016	1.786	0
N3	−1.185	1.026	0
C4	−1.604	−0.101	0
S5	−2.266	−1.516	0
N6	1.158	1.036	0
C7	1.602	−0.081	0
S8	2.295	−1.481	0
	anti-anti-CDIT @ MP2/aug-cc-pVDZ		
	a (Å)	b (Å)	c (Å)
O1	−0.042	3.055	0
C2	−0.026	1.844	0
N3	−1.203	1.070	0
C4	−1.531	−0.118	0
S5	−2.127	−1.579	0
N6	1.170	1.101	0
C7	1.532	−0.076	0
S8	2.17	−1.519	0

3. List of fits with SPFIT/SPCAT

3.1 *syn-syn*-CDIT ($I_{N_3} = 1$, $I_{N_6} = 1$, $J + I_{N_3} = F_1$, and $F_1 + I_{N_2} = F$)

PARAMETERS IN FIT WITH STANDARD ERRORS ON THOSE THAT ARE FITTED:

(values rounded and degrees of freedom, Ndegf=Nlines-Nconst, statistics)

10099	A / /MHz	11046.3541(23)	1	
20099	B / /MHz	449.80106(48)	2	
30099	C / /MHz	432.26941(86)	3	
2099	D_K /kHz	[0.]	4	
1199	DJK / /kHz	1.45(10)	5	
299	D_J /kHz	[0.]	6	
110010011	3/2(Xaa) /MHz	-2.891(14)	7	
110040011	1/4(Xbb-Xc /MHz	0.1851(53)	8	
110010022	3/2(Xaa) /MHz	2.8875(94)	9	
-220010022	3 /MHz	2.8875(94)	= 1.00000 * 9	
110040022	1/4(Xbb-Xc /MHz	-0.1865(29)	10	
-220040022	1 /MHz	-0.1865(29)	= 1.00000 * 10	

Linelist L1. *syn-syn*-CDIT

J''	K_a''	K_c''	F_1''	F''	J'	K_a'	K_c'	F_1'	F'	ν (MHz)	$\nu_{obs} - \nu_{calc}$
para-(*syn-syn*-CDIT)											
8	1	8	9		9	0	9	10		2357.0905	0.0004
8	1	8	7		9	0	9	8		2357.0907	0.0110
8	1	8	8		9	0	9	9		2357.2581	0.0081
6	1	6	7		7	0	7	8		4249.0364	−0.0033
6	1	6	5		7	0	7	6		4249.0364	0.0105
6	1	6	6		7	0	7	7		4249.2238	0.0031
4	1	4	4		5	0	5	4		6107.3539	0.0083
4	1	4	3		5	0	5	4		6107.9157	0.0269
4	1	4	5		5	0	5	6		6107.9157	0.0025
4	1	4	4		5	0	5	5		6108.1534	0.0065
4	1	4	5		5	0	5	5		6108.5840	0.0051
2	1	2	2		3	0	3	2		7932.3851	0.0087
2	1	2	1		3	0	3	2		7932.6728	-0.0005
2	1	2	3		3	0	3	4		7932.8020	0.0102
2	1	2	2		3	0	3	3		7933.2515	0.0084
2	1	2	3		3	0	3	3		7933.4421	0.0084
1	1	0	1		1	0	1	0		10613.2681	0.0019
1	1	0	2		1	0	1	2		10613.9582	0.0025
1	1	0	1		1	0	1	2		10614.1320	-0.0015
1	1	0	0		1	0	1	1		10614.2601	−0.0068
1	1	0	2		1	0	1	1		10614.5359	0.0020
1	1	0	1		1	0	1	1		10614.7113	−0.0002
3	1	2	3		3	0	3	2		10657.1506	−0.0017
3	1	2	3		3	0	3	4		10657.3728	−0.0043
3	1	2	2		3	0	3	2		10657.9543	−0.0150
3	1	2	4		3	0	3	4		10657.9543	−0.0279
3	1	2	3		3	0	3	3		10657.9543	−0.0646
3	1	2	4		3	0	3	3		10658.6184	−0.0056
3	1	2	2		3	0	3	3		10658.8306	−0.0054
5	1	4	5		5	0	5	4		10736.5237	−0.0007
5	1	4	5		5	0	5	6		10736.6564	−0.0037

J''	K_a''	K_c''	F_1''	F''	J'	K_a'	K_c'	F_1'	F'	ν (MHz)	$\nu_{obs} - \nu_{calc}$
5	1	4	5		5	0	5	5		10737.3746	0.0488
5	1	4	6		5	0	5	6		10737.3746	−0.0138
5	1	4	4		5	0	5	4		10737.3746	−0.0265
5	1	4	6		5	0	5	5		10738.0698	0.0158
5	1	4	4		5	0	5	5		10738.1933	−0.0091
7	1	6	7		7	0	7	6		10852.0431	0.0804
7	1	6	7		7	0	7	8		10852.0431	−0.0172
7	1	6	7		7	0	7	7		10852.7459	0.0082
7	1	6	6		7	0	7	6		10852.8481	0.0000
7	1	6	8		7	0	7	8		10852.8481	0.0138
7	1	6	8		7	0	7	7		10853.5308	0.0193
7	1	6	6		7	0	7	7		10853.6370	0.0138
9	1	8	9		9	0	9	9		11005.0958	0.0343
9	1	8	10		9	0	9	10		11005.2084	0.0339
9	1	8	8		9	0	9	8		11005.2084	0.0213
11	1	10	11		11	0	11	11		11195.3668	−0.0215
11	1	10	12		11	0	11	12		11195.5195	0.0081
11	1	10	10		11	0	11	10		11195.5195	−0.0030
13	1	12	13		13	0	13	13		11425.0738	0.0078
13	1	12	14		13	0	13	14		11425.2159	0.0198
13	1	12	12		13	0	13	12		11425.2159	0.0098
15	1	14	15		15	0	15	15		11695.6941	0.0075
15	1	14	16		15	0	15	16		11695.8496	0.0271
15	1	14	14		15	0	15	14		11695.8496	0.0181
ortho-(*syn-syn*-CDIT)											
7	1	7	7	7	8	0	8	8	8	3306.9551	0.0031
7	1	7	7	8	8	0	8	8	9	3307.0921	−0.0171
7	1	7	7	6	8	0	8	8	7	3307.0921	−0.0286
7	1	7	6	5	8	0	8	7	6	3307.3019	−0.0123
7	1	7	6	7	8	0	8	7	8	3307.3019	−0.0003
7	1	7	8	7	8	0	8	9	8	3307.3019	−0.0001
7	1	7	8	9	8	0	8	9	10	3307.3019	0.0116
5	1	5	5	6	6	0	6	6	6	5182.0839	0.0040

J''	K_a''	K_c''	F_1''	F''	J'	K_a'	K_c'	F_1'	F'	ν (MHz)	$\nu_{obs} - \nu_{calc}$
5	1	5	6	7	6	0	6	6	7	5182.0839	−0.0056
5	1	5	6	5	6	0	6	6	5	5182.0839	−0.0057
5	1	5	5	5	6	0	6	6	6	5182.4594	0.0047
5	1	5	5	6	6	0	6	6	7	5182.6626	0.0243
5	1	5	5	4	6	0	6	6	5	5182.6626	0.0067
5	1	5	6	6	6	0	6	7	7	5182.6626	−0.0107
5	1	5	4	4	6	0	6	5	5	5182.6626	−0.0284
5	1	5	6	7	6	0	6	7	8	5182.8604	0.0033
5	1	5	6	5	6	0	6	7	6	5182.8606	−0.0140
5	1	5	4	5	6	0	6	5	6	5182.8606	−0.0140
5	1	5	4	3	6	0	6	5	4	5182.8606	−0.0317
5	1	5	5	5	6	0	6	5	5	5183.3459	−0.0072
5	1	5	6	6	6	0	6	7	6	5183.3459	0.0009
5	1	5	4	4	6	0	6	5	4	5183.3459	0.0007
3	1	3	3	4	4	0	4	4	4	7024.0519	−0.0281
3	1	3	4	3	4	0	4	4	3	7024.1167	−0.0093
3	1	3	4	5	4	0	4	4	5	7024.1167	−0.0049
3	1	3	3	3	4	0	4	4	4	7024.3184	0.0048
3	1	3	3	4	4	0	4	4	5	7024.5708	0.0029
3	1	3	3	2	4	0	4	4	3	7024.5708	−0.0372
3	1	3	2	2	4	0	4	3	3	7024.7007	0.0017
3	1	3	4	5	4	0	4	5	6	7024.8965	−0.0115
3	1	3	2	3	4	0	4	3	4	7024.8965	−0.0547
3	1	3	3	3	4	0	4	3	3	7025.3168	0.0100
3	1	3	4	4	4	0	4	5	4	7025.3168	0.0101
3	1	3	2	2	4	0	4	3	2	7025.3168	0.0001
3	1	3	3	4	4	0	4	3	4	7025.5289	0.0053
1	1	1	1	1	2	0	2	2	2	8831.1725	−0.0123
1	1	1	1	2	2	0	2	2	2	8831.1725	0.0470
1	1	1	1	2	2	0	2	2	3	8831.4185	0.0051
1	1	1	2	3	2	0	2	2	3	8832.0168	0.0023
1	1	1	1	1	2	0	2	1	1	8832.4683	−0.0354
1	1	1	1	2	2	0	2	1	1	8832.4683	0.0240

J''	K_a''	K_c''	F_1''	F''	J'	K_a'	K_c'	F_1'	F'	ν (MHz)	$\nu_{obs} - \nu_{calc}$
1	1	1	1	1	2	0	2	1	2	8832.6239	−0.0299
1	1	1	1	2	2	0	2	1	2	8832.6239	0.0294
1	1	1	2	3	2	0	2	3	4	8832.8414	0.0022
1	1	1	2	2	2	0	2	3	2	8832.8414	−0.0036
1	1	1	0	1	2	0	2	1	1	8833.7897	0.0027
1	1	1	0	1	2	0	2	1	2	8833.9383	0.0011
1	1	1	0	1	2	0	2	1	0	8834.2689	0.0016
2	1	1	1	2	2	0	2	2	2	10630.3352	−0.0184
2	1	1	1	1	2	0	2	2	2	10630.4648	0.0064
2	1	1	1	2	2	0	2	2	3	10630.6460	0.0044
2	1	1	3	4	2	0	2	2	3	10630.8932	0.0045
2	1	1	2	3	2	0	2	2	2	10631.1754	0.0022
2	1	1	3	2	2	0	2	3	3	10631.1754	0.0173
2	1	1	2	3	2	0	2	2	3	10631.4341	−0.0269
2	1	1	1	0	2	0	2	1	1	10631.4341	−0.0086
2	1	1	3	4	2	0	2	3	4	10631.7142	0.0007
2	1	1	1	2	2	0	2	1	2	10631.8185	−0.0040
2	1	1	2	3	2	0	2	3	4	10632.2876	0.0017
2	1	1	1	1	2	0	2	1	0	10632.2876	0.0301
2	1	1	1	1	2	0	2	1	0	10632.2876	0.0301
2	1	1	2	2	2	0	2	1	1	10632.6919	0.0004
2	1	1	2	3	2	0	2	1	2	10632.6919	0.0498
4	1	3	3	4	4	0	4	4	5	10692.2251	−0.0127
4	1	3	3	3	4	0	4	4	4	10692.2251	0.0044
4	1	3	5	6	4	0	4	4	5	10692.4247	0.0098
4	1	3	3	2	4	0	4	3	3	10692.5630	−0.0053
4	1	3	5	4	4	0	4	5	5	10692.5630	0.0229
4	1	3	3	4	4	0	4	3	3	10692.7469	0.0036
4	1	3	4	5	4	0	4	4	4	10692.7469	−0.0018
4	1	3	3	2	4	0	4	3	2	10693.1882	0.0021
4	1	3	3	4	4	0	4	3	4	10693.1882	−0.0054
4	1	3	5	4	4	0	4	5	4	10693.1882	−0.0071
4	1	3	5	6	4	0	4	5	6	10693.1882	−0.0130

J''	K_a''	K_c''	F_1''	F''	J'	K_a'	K_c'	F_1'	F'	ν (MHz)	$\nu_{obs} - \nu_{calc}$
4	1	3	3	3	4	0	4	3	3	10693.1882	−0.0256
4	1	3	5	5	4	0	4	5	5	10693.1882	−0.0366
4	1	3	4	3	4	0	4	4	3	10693.1882	−0.0442
4	1	3	4	5	4	0	4	4	5	10693.1882	−0.0484
4	1	3	4	4	4	0	4	4	4	10693.2965	0.0380
4	1	3	4	4	4	0	4	4	5	10693.7850	0.0387
4	1	3	3	3	4	0	4	3	2	10693.7850	−0.0465
4	1	3	4	5	4	0	4	5	6	10694.0262	0.0032
4	1	3	4	3	4	0	4	5	4	10694.0262	−0.0300
4	1	3	4	5	4	0	4	3	4	10694.2403	0.0479
4	1	3	4	4	4	0	4	3	3	10694.2403	−0.0114
6	1	5	7	8	6	0	6	6	7	10789.7149	−0.0042
6	1	5	5	4	6	0	6	5	5	10789.7149	−0.0893
6	1	5	7	6	6	0	6	6	5	10789.7149	0.0252
6	1	5	5	5	6	0	6	6	6	10789.7149	0.0731
6	1	5	6	7	6	0	6	6	6	10790.0058	−0.0186
6	1	5	7	8	6	0	6	7	8	10790.4700	−0.0168
6	1	5	7	6	6	0	6	7	6	10790.4702	−0.0045
6	1	5	5	6	6	0	6	5	6	10790.4702	−0.0023
6	1	5	5	4	6	0	6	5	4	10790.4702	0.0118
6	1	5	5	5	6	0	6	5	6	10791.0622	−0.0190
6	1	5	5	5	6	0	6	5	4	10791.2064	0.0120
6	1	5	7	7	6	0	6	7	6	10791.2064	−0.0239
6	1	5	6	6	6	0	6	6	7	10791.2064	−0.0048
6	1	5	6	5	6	0	6	7	6	10791.3185	−0.0395
6	1	5	6	7	6	0	6	7	8	10791.3185	−0.0319
6	1	5	6	6	6	0	6	5	5	10791.5302	−0.0211
8	1	7	9	10	8	0	8	9	10	10924.2310	−0.0037
8	1	7	9	8	8	0	8	9	8	10924.2310	0.0082
8	1	7	7	8	8	0	8	7	8	10924.2310	0.0098
8	1	7	7	6	8	0	8	7	6	10924.2310	0.0232
8	1	7	8	8	8	0	8	8	8	10924.4307	−0.0163
10	1	9	11	12	10	0	10	11	12	11095.3965	−0.0098

J''	K_a''	K_c''	F_1''	F''	J'	K_a'	K_c'	F_1'	F'	ν (MHz)	$\nu_{obs} - \nu_{calc}$
10	1	9	11	10	10	0	10	11	10	11095.3965	0.0010
10	1	9	9	8	10	0	10	9	8	11095.3965	0.0142
10	1	9	10	10	10	0	10	10	10	11095.6485	0.0043
12	1	11	13	14	12	0	12	13	14	11305.1827	−0.0408
12	1	11	13	12	12	0	12	13	12	11305.1827	−0.0309
12	1	11	11	10	12	0	12	11	10	11305.1827	−0.0194
12	1	11	11	11	12	0	12	11	11	11305.3300	0.0009
12	1	11	13	13	12	0	12	13	13	11305.3300	−0.0114
12	1	11	12	11	12	0	12	12	11	11305.3300	−0.0221
12	1	11	12	13	12	0	12	12	13	11305.3300	−0.0311
12	1	11	12	12	12	0	12	12	12	11305.4628	−0.0154
1	1	1	1	2	0	0	0	1	2	11478.1597	0.0065
1	1	1	2	3	0	0	0	1	2	11478.7532	−0.0010
1	1	1	0	1	0	0	0	1	2	11479.4960	0.0000
14	1	13	15	16	14	0	14	15	16	11555.1411	−0.0166
14	1	13	15	14	14	0	14	15	14	11555.1411	−0.0077
14	1	13	13	12	14	0	14	13	12	11555.1411	0.0025
14	1	13	14	14	14	0	14	14	14	11555.4344	0.0090
16	1	15	17	18	16	0	16	17	18	11846.8990	−0.0209
16	1	15	15	16	16	0	16	15	16	11846.8990	−0.0121
16	1	15	15	14	16	0	16	15	14	11846.8990	−0.0034
16	1	15	15	15	16	0	16	15	15	11847.0453	0.0039
16	1	15	16	17	16	0	16	16	17	11847.0454	−0.0222
16	1	15	16	15	16	0	16	16	15	11847.0454	−0.0145
16	1	15	17	17	16	0	16	17	17	11847.0454	−0.0058
16	1	15	16	16	16	0	16	16	16	11847.2036	0.0052

J''	K_a''	K_c''	F_1''	F''	J'	K_a'	K_c'	F_1'	F'	ν (MHz)	$\nu_{obs} - \nu_{calc}$

3.2 ^{34}S-*syn-syn*-CDIT

PARAMETERS IN FIT (values truncated and Nlines statistics):

10000	A / /MHz	11042.9488(27)	1
20000	B / /MHz	438.30798(69)	2
30000	C / /MHz	421.6377(14)	3
110010000	1.5 Chi. /MHz	2.878(12)	4
-220010000	1.5 /MHz	2.878(12)	= 1.00000 * 4
110040000	0.25 (Ch /MHz	-0.1878(42)	5
-220040000	0.25 /MHz	-0.1878(42)	= 1.00000 * 5
1100	DJK / /kHz	1.86(24)	6

MICROWAVE AVG =   -0.001051 MHz, IR AVG =   0.00000

MICROWAVE RMS =   0.014575 MHz, IR RMS =   0.00000

END OF ITERATION 1 OLD, NEW RMS ERROR=   0.97169   0.96117

distinct frequency lines in fit: 74

distinct parameters of fit: 6

	upper state	lower state	overall
limits of quantum number 1:	1 11	0 11	0 11
limits of quantum number 2:	1 1	0 0	0 1
limits of quantum number 3:	0 10	0 11	0 11
limits of quantum number 4:	0 12	0 12	0 12
limits of quantum number 5:	0 13	0 13	0 13

Linelist L2. ^{34}S-*syn-syn*-CDIT

J''	K_a''	K_c''	F_1''	F''	J'	K_a'	K_c'	F_1'	F'	ν (MHz)	$\nu_{obs} - \nu_{calc}$
6	1	6	7	8	7	0	7	8	9	4420.5455	0.0114
6	1	6	7	6	7	0	7	8	7	4420.5455	−0.0030
6	1	6	5	4	7	0	7	6	5	4420.5455	−0.0181
5	1	5	5	5	6	0	6	6	6	5329.1825	0.0112
5	1	5	6	5	6	0	6	7	6	5329.5930	−0.0055
5	1	5	6	7	6	0	6	7	8	5329.5930	0.0127
2	1	2	2	2	3	0	3	3	3	8007.5807	0.0055
2	1	2	2	3	3	0	3	3	4	8007.9188	0.0121
2	1	2	2	1	3	0	3	3	2	8007.9188	−0.0631
2	1	2	3	3	3	0	3	4	4	8008.0805	−0.0218
2	1	2	1	1	3	0	3	2	2	8008.2703	0.0004
2	1	2	3	4	3	0	3	4	5	8008.4472	−0.0101
1	1	1	1	1	2	0	2	2	2	8883.4933	−0.0307
1	1	1	1	2	2	0	2	2	2	8883.4933	0.0289
1	1	1	1	2	2	0	2	2	3	8883.7420	−0.0083
1	1	1	2	3	2	0	2	2	3	8884.3505	−0.0030
1	1	1	2	2	2	0	2	3	3	8884.5603	−0.0020
1	1	1	2	1	2	0	2	2	1	8884.5603	−0.0624
1	1	1	1	2	2	0	2	1	2	8884.9488	0.0252
1	1	1	1	1	2	0	2	1	2	8884.9488	−0.0344
1	1	1	2	3	2	0	2	3	4	8885.1715	−0.0013
1	1	1	2	1	2	0	2	1	1	8885.5758	−0.0028
1	1	1	0	1	2	0	2	1	1	8886.1085	−0.0133
1	1	1	0	1	2	0	2	1	2	8886.2710	0.0000
1	1	1	0	1	2	0	2	1	0	8886.6110	0.0119
1	1	0	2	1	1	0	1	1	0	10620.4679	−0.0273
1	1	0	1	1	1	0	1	1	2	10620.4679	0.0041
1	1	0	2	3	1	0	1	1	2	10620.7005	0.0041
1	1	0	2	2	1	0	1	2	2	10621.1640	−0.0204
1	1	0	0	1	1	0	1	1	1	10621.1640	0.0641
1	1	0	2	1	1	0	1	2	2	10621.3272	−0.0286

J''	K_a''	K_c''	F_1''	F''	J'	K_a'	K_c'	F_1'	F'	ν (MHz)	$\nu_{obs} - \nu_{calc}$
1	1	0	1	2	1	0	1	2	3	10621.3272	0.0278
1	1	0	2	3	1	0	1	2	3	10621.5611	0.0040
1	1	0	1	0	1	0	1	2	1	10621.5611	0.0603
1	1	0	2	2	1	0	1	2	1	10621.7690	0.0110
1	1	0	2	1	1	0	1	2	1	10621.9401	0.0107
1	1	0	1	1	1	0	1	0	1	10622.3788	−0.0071
1	1	0	1	2	1	0	1	0	1	10622.3788	0.0178
2	1	1	1	2	2	0	2	2	2	10636.7189	−0.0004
2	1	1	1	1	2	0	2	2	2	10636.8307	0.0063
2	1	1	1	2	2	0	2	2	3	10637.0133	0.0079
2	1	1	3	4	2	0	2	2	3	10637.2415	−0.0117
2	1	1	3	2	2	0	2	3	3	10637.5370	0.0175
2	1	1	2	3	2	0	2	2	2	10637.5370	−0.0047
2	1	1	1	0	2	0	2	1	1	10637.7922	−0.0066
2	1	1	2	3	2	0	2	2	3	10637.7922	−0.0355
2	1	1	2	1	2	0	2	2	1	10637.7922	−0.0560
2	1	1	3	3	2	0	2	3	3	10637.9732	0.0229
2	1	1	3	4	2	0	2	3	4	10638.0907	0.0181
2	1	1	3	2	2	0	2	3	2	10638.0907	−0.0430
2	1	1	1	1	2	0	2	1	0	10638.6326	0.0209
2	1	1	2	3	2	0	2	3	4	10638.6326	−0.0145
2	1	1	2	1	2	0	2	3	2	10638.8009	−0.0033
2	1	1	2	2	2	0	2	1	1	10639.0667	0.0147
3	1	2	2	3	3	0	3	3	4	10662.0114	−0.0446
3	1	2	2	2	3	0	3	3	3	10662.0114	0.0362
3	1	2	4	5	3	0	3	3	4	10662.2666	−0.0039
3	1	2	4	3	3	0	3	3	2	10662.2666	0.0520
3	1	2	3	4	3	0	3	3	3	10662.5352	−0.0761
3	1	2	3	2	3	0	3	3	3	10662.5352	0.0145
3	1	2	2	1	3	0	3	2	2	10662.5352	0.0198
3	1	2	2	3	3	0	3	2	2	10662.7468	0.0222
3	1	2	2	2	3	0	3	2	3	10663.4203	0.0065
3	1	2	3	3	3	0	3	3	4	10663.4203	−0.0044

J''	K_a''	K_c''	F_1''	F''	J'	K_a'	K_c'	F_1'	F'	ν (MHz)	$\nu_{obs} - \nu_{calc}$
3	1	2	3	3	3	0	3	2	2	10664.1168	0.0235
4	1	3	3	3	4	0	4	4	4	10695.5454	0.0018
4	1	3	3	4	4	0	4	4	5	10695.5454	−0.0120
4	1	3	5	6	4	0	4	4	5	10695.7512	0.0167
4	1	3	3	2	4	0	4	3	3	10695.9136	0.0290
4	1	3	4	5	4	0	4	4	4	10696.0775	0.0057
4	1	3	3	4	4	0	4	3	3	10696.0775	0.0179
4	1	3	5	6	4	0	4	5	6	10696.4969	−0.0188
4	1	3	5	4	4	0	4	5	4	10696.4969	−0.0120
4	1	3	3	4	4	0	4	3	4	10696.4969	−0.0100
4	1	3	3	2	4	0	4	3	2	10696.4969	−0.0013
4	1	3	4	4	4	0	4	4	5	10697.0643	−0.0018
4	1	3	3	3	4	0	4	3	2	10697.0643	−0.0795
4	1	3	4	5	4	0	4	5	6	10697.3199	−0.0177
4	1	3	4	3	4	0	4	5	4	10697.3199	−0.0501
4	1	3	4	4	4	0	4	3	3	10697.5663	−0.0019
5	1	4	4	3	5	0	5	4	4	10737.7980	0.0021
5	1	4	6	5	5	0	5	6	6	10737.7980	0.0102
5	1	4	4	3	5	0	5	4	3	10738.4797	0.0479
5	1	4	4	5	5	0	5	4	5	10738.4797	0.0341
5	1	4	6	5	5	0	5	6	5	10738.4797	0.0315
5	1	4	6	7	5	0	5	6	7	10738.4797	0.0202
5	1	4	4	4	5	0	5	4	4	10738.4797	−0.0175
5	1	4	6	6	5	0	5	6	6	10738.4797	−0.0363
5	1	4	5	4	5	0	5	5	4	10738.4797	−0.0502
5	1	4	5	6	5	0	5	5	6	10738.4797	−0.0590
5	1	4	4	4	5	0	5	4	3	10739.1187	−0.0144
5	1	4	5	5	5	0	5	5	6	10739.1187	−0.0005
5	1	4	5	4	5	0	5	6	5	10739.3144	−0.0105
5	1	4	5	6	5	0	5	6	7	10739.3144	0.0051
5	1	4	5	5	5	0	5	4	4	10739.5479	0.0251
6	1	5	7	8	6	0	6	7	8	10788.9690	0.0043
6	1	5	7	6	6	0	6	7	6	10788.9690	0.0169

J''	K_a''	K_c''	F_1''	F''	J'	K_a'	K_c'	F_1'	F'	ν (MHz)	$\nu_{obs} - \nu_{calc}$
6	1	5	5	6	6	0	6	5	6	10788.9690	0.0192
6	1	5	5	4	6	0	6	5	4	10788.9690	0.0341
7	1	6	8	9	7	0	7	8	9	10848.1277	0.0114
7	1	6	8	7	7	0	7	8	7	10848.1277	0.0241
7	1	6	6	7	7	0	7	6	7	10848.1277	0.0261
7	1	6	6	5	7	0	7	6	5	10848.1277	0.0407
8	1	7	9	10	8	0	8	9	10	10916.0058	−0.0095
8	1	7	9	8	8	0	8	9	8	10916.0058	0.0028
8	1	7	7	8	8	0	8	7	8	10916.0058	0.0044
8	1	7	7	6	8	0	8	7	6	10916.0058	0.0184
8	1	7	8	7	8	0	8	8	7	10916.1251	−0.0029
8	1	7	8	9	8	0	8	8	9	10916.1251	−0.0136
9	1	8	8	7	9	0	9	8	7	10992.7671	0.0153
9	1	8	8	9	9	0	9	8	9	10992.7671	0.0021
9	1	8	10	9	9	0	9	10	9	10992.7671	0.0008
9	1	8	8	8	9	0	9	8	8	10992.9007	0.0322
9	1	8	10	10	9	0	9	10	10	10992.9007	0.0162
9	1	8	10	10	9	0	9	10	10	10992.9007	0.0162
9	1	8	9	10	9	0	9	9	10	10992.9007	−0.0073
10	1	9	11	12	10	0	10	11	12	11078.5223	−0.0133
10	1	9	11	10	10	0	10	11	10	11078.5223	−0.0020
10	1	9	9	8	10	0	10	9	8	11078.5223	0.0115
10	1	9	10	11	10	0	10	10	11	11078.6608	−0.0096
10	1	9	9	9	10	0	10	9	9	11078.6612	0.0281
10	1	9	11	11	10	0	10	11	11	11078.6612	0.0133
10	1	9	10	9	10	0	10	10	9	11078.6612	0.0009
10	1	9	10	10	10	0	10	10	10	11078.7865	0.0050
11	1	10	12	13	11	0	11	12	13	11173.3975	−0.0355
11	1	10	12	11	11	0	11	12	11	11173.3975	−0.0248
11	1	10	10	9	11	0	11	10	9	11173.3975	−0.0121
11	1	10	10	10	11	0	11	10	10	11173.5415	0.0048
11	1	10	12	12	11	0	11	12	12	11173.5415	−0.0088
11	1	10	11	10	11	0	11	11	10	11173.5415	−0.0205

J''	K_a''	K_c''	F_1''	F''	J'	K_a'	K_c'	F_1'	F'	ν (MHz)	$\nu_{obs} - \nu_{calc}$
11	1	10	11	12	11	0	11	11	12	11173.5415	−0.0302
1	1	1	1	0	0	0	0	1	1	11463.9059	−0.0089
1	1	1	1	1	0	0	0	1	0	11464.1184	−0.0572
1	1	1	1	2	0	0	0	1	2	11464.1184	0.0027
1	1	1	2	2	0	0	0	1	1	11464.4970	−0.0207
1	1	1	2	3	0	0	0	1	2	11464.7003	−0.0184
1	1	1	2	1	0	0	0	1	1	11464.8961	−0.0236
1	1	1	0	1	0	0	0	1	2	11465.4479	−0.0152

3.3 ^{13}C-*syn-syn*-CDIT

PARAMETERS IN FIT (values truncated and Nlines statistics):

10000	A / /MHz	11029.0588(35)	1
20000	B / /MHz	447.6461(18)	2
30000	C / /MHz	430.2687(18)	3
110010000	1.5 Chi. /MHz	2.943(19)	4
-220010000	1.5 /MHz	2.943(19)	= 1.00000 * 4
110040000	0.25 (Ch /MHz	-0.1731(60)	5
-220040000	0.25 /MHz	-0.1731(60)	= 1.00000 * 5
1100	DJK / /kHz	[-1.861]	6

MICROWAVE AVG =   -0.000000 MHz, IR AVG =   0.00000

MICROWAVE RMS =   0.014865 MHz, IR RMS =   0.00000

END OF ITERATION 1 OLD, NEW RMS ERROR=   0.99100   0.99100

distinct frequency lines in fit: 32

distinct parameters of fit: 5

	upper state		lower state		overall	
limits of quantum number 1:	1	9	0	9	0	9
limits of quantum number 2:	1	1	0	0	0	1
limits of quantum number 3:	0	8	0	9	0	9
limits of quantum number 4:	0	9	0	9	0	9
limits of quantum number 5:	0	9	0	9	0	9

frequency range: 8824   11460

Linelist L3. ^{13}C-*syn-syn*-CDIT

J''	K_a''	K_c''	F_1''	F''	J'	K_a'	K_c'	F_1'	F'	ν (MHz)	$\nu_{obs} - \nu_{calc}$
1	1	1	1	2	2	0	2	2	3	8824.5748	−0.0076
1	1	1	2	2	2	0	2	3	3	8825.3893	−0.0120
1	1	1	2	3	2	0	2	3	4	8826.0094	−0.0114
1	1	1	2	2	2	0	2	3	2	8826.0094	−0.0225
1	1	0	1	1	1	0	1	1	1	10597.9722	−0.0277
1	1	0	2	1	1	0	1	1	0	10597.9722	0.0012
1	1	0	1	2	1	0	1	1	1	10597.9722	0.0001
1	1	0	2	3	1	0	1	1	2	10598.1834	0.0132
1	1	0	2	2	1	0	1	2	2	10598.6469	−0.0169
1	1	0	0	1	1	0	1	1	1	10598.6469	0.0360
1	1	0	1	2	1	0	1	2	3	10598.8155	0.0481
1	1	0	2	1	1	0	1	2	2	10598.8155	−0.0386
1	1	0	2	3	1	0	1	2	3	10599.0432	−0.0101
1	1	0	2	2	1	0	1	2	1	10599.2611	0.0086
1	1	0	2	1	1	0	1	2	1	10599.4365	−0.0062
1	1	0	1	1	1	0	1	0	1	10599.8587	−0.0260
1	1	0	1	2	1	0	1	0	1	10599.8587	0.0018
2	1	1	3	4	2	0	2	2	3	10615.4451	−0.0047
2	1	1	3	2	2	0	2	2	1	10615.4451	0.0675
2	1	1	3	2	2	0	2	3	3	10615.7403	0.0121
2	1	1	2	3	2	0	2	2	2	10615.7403	0.0150
2	1	1	2	1	2	0	2	2	1	10615.9785	−0.0630
2	1	1	1	0	2	0	2	1	1	10615.9785	−0.0483
2	1	1	2	3	2	0	2	2	3	10615.9785	−0.0403
2	1	1	2	2	2	0	2	2	2	10615.9785	0.0548
2	1	1	3	3	2	0	2	3	3	10616.1806	0.0258
2	1	1	3	4	2	0	2	3	4	10616.3016	0.0108
2	1	1	2	3	2	0	2	3	4	10616.8485	−0.0112
2	1	1	1	1	2	0	2	1	0	10616.8485	−0.0005
2	1	1	2	2	2	0	2	1	1	10617.2794	0.0113
3	1	2	2	1	3	0	3	2	1	10642.4125	0.0057

J''	K_a''	K_c''	F_1''	F''	J'	K_a'	K_c'	F_1'	F'	ν (MHz)	$\nu_{obs} - \nu_{calc}$

J''	K_a''	K_c''	F_1''	F''	J'	K_a'	K_c'	F_1'	F'	ν (MHz)	$\nu_{obs} - \nu_{calc}$
3	1	2	2	3	3	0	3	2	3	10642.4125	0.0221
3	1	2	4	3	3	0	3	4	3	10642.4125	0.0271
3	1	2	4	5	3	0	3	4	5	10642.4125	0.0390
3	1	2	2	2	3	0	3	2	2	10642.4125	0.0485
3	1	2	2	2	3	0	3	2	3	10642.7185	−0.0079
3	1	2	3	3	3	0	3	3	4	10642.7185	0.0080
5	1	4	5	5	5	0	5	5	5	10721.1279	−0.0336
5	1	4	5	6	5	0	5	5	6	10721.1279	0.0085
5	1	4	5	4	5	0	5	5	4	10721.1279	0.0154
5	1	4	6	6	5	0	5	6	6	10721.1279	0.0262
5	1	4	4	4	5	0	5	4	4	10721.1279	0.0410
6	1	5	5	4	6	0	6	5	4	10773.7903	0.0387
6	1	5	5	6	6	0	6	5	6	10773.7903	0.0263
6	1	5	7	6	6	0	6	7	6	10773.7903	0.0244
6	1	5	7	8	6	0	6	7	8	10773.7903	0.0138
7	1	6	7	8	7	0	7	7	8	10835.5808	−0.0481
7	1	6	7	6	7	0	7	7	6	10835.5808	−0.0388
7	1	6	8	8	7	0	7	8	8	10835.5808	−0.0263
7	1	6	6	6	7	0	7	6	6	10835.5808	−0.0103
7	1	6	8	9	7	0	7	8	9	10835.5808	0.0500
7	1	6	8	7	7	0	7	8	7	10835.5808	0.0609
7	1	6	6	5	7	0	7	6	5	10835.5808	0.0751
7	1	6	7	7	7	0	7	7	7	10835.7093	0.0058
8	1	7	7	7	8	0	8	7	7	10906.4933	−0.0079
8	1	7	9	9	8	0	8	9	9	10906.4933	−0.0230
8	1	7	8	7	8	0	8	8	7	10906.4933	−0.0352
8	1	7	8	9	8	0	8	8	9	10906.4933	−0.0445
9	1	8	9	9	9	0	9	9	9	10986.7980	−0.0101
1	1	1	1	0	0	0	0	1	1	11458.6422	−0.0254
1	1	1	1	1	0	0	0	1	0	11458.8639	−0.0621
1	1	1	1	2	0	0	0	1	2	11458.8639	−0.0027
1	1	1	2	2	0	0	0	1	1	11459.2558	−0.0090
1	1	1	2	3	0	0	0	1	2	11459.4591	−0.0049

J''	K_a''	K_c''	F_1''	F''	J'	K_a'	K_c'	F_1'	F'	ν (MHz)	$\nu_{obs} - \nu_{calc}$
1	1	1	2	1	0	0	0	1	1	11459.6598	−0.0031
1	1	1	0	1	0	0	0	1	2	11460.1987	−0.0025

J''	K_a''	K_c''	F_1''	F''	J'	K_a'	K_c'	F_1'	F'	ν (MHz)	$\nu_{obs} - \nu_{calc}$

3.4 ^{15}N-*syn-syn*-CDIT

PARAMETERS IN FIT (values truncated and Nlines statistics):

10000	A / /MHz	11002.9064(90)	1
20000	B / /MHz	449.3188(98)	2
30000	C / /MHz	431.7588(90)	3
110010000	1.5 Chi. /MHz	[2.9805]	4
110040000	0.25 (Ch /MHz	[-0.18775]	5
1100	DJK / /kHz	[-1.861]	6

MICROWAVE AVG =   -0.000000 MHz, IR AVG =   0.00000

MICROWAVE RMS =   0.010786 MHz, IR RMS =   0.00000

END OF ITERATION 2 OLD, NEW RMS ERROR=   0.71908   0.71908

distinct frequency lines in fit: 6

   distinct parameters of fit: 3

	upper state		lower state		overall	
limits of quantum number 1:	1	6	0	6	0	6
limits of quantum number 2:	1	1	0	0	0	1
limits of quantum number 3:	0	5	0	6	0	6
limits of quantum number 4:	1	6	1	6	1	6

frequency range: 10571   11434

Linelist L4. ^{15}N-*syn-syn*-CDIT

J''	K_a''	K_c''	F''	J'	K_a'	K_c'	F'	ν (MHz)	$\nu_{obs} - \nu_{calc}$
1	1	0	2	1	0	1	2	10571.2864	0.0048
2	1	1	1	2	0	2	1	10588.8764	–0.0185
3	1	2	4	3	0	3	4	10615.1932	0.0175
5	1	4	4	5	0	5	4	10694.7015	–0.0044
6	1	5	6	6	0	6	6	10748.0891	0.0006
1	1	1	2	0	0	0	1	11434.7375	0.0000

3.5   *syn-anti*-CDIT

PARAMETERS IN FIT (values truncated and Nlines statistics):

10000	A / /MHz	2938.6797(15)	1
20000	B / /MHz	626.51962(71)	2
30000	C / /MHz	516.14194(50)	3
110010000	1.5 Chi. /MHz	2.618(16)	4
110040000	0.25 (Ch /MHz	-0.1596(45)	5
220010000	1.5 Chi. /MHz	[0.]	6
220040000	0.25 (Ch /MHz	0.2203(57)	7
1100	DJK / /kHz	-3.099(39)	8
200	DJ / /kHz	0.2008(52)	9
2000	DK /MHz	-0.02074(16)	10
40100	d1 /kHz	-0.0779(19)	11
50000	d2 /kHz	[0.]	12
2100	HKJ /Hz	[0.]	13
3000	HK /Hz	[0.]	14

MICROWAVE AVG =   -0.000349 MHz, IR AVG =   0.00000

MICROWAVE RMS =   0.016327 MHz, IR RMS =   0.00000

END OF ITERATION 7 OLD, NEW RMS ERROR=   1.08849   1.08849

distinct frequency lines in fit: 98

   distinct parameters of fit: 10

	upper state	lower state	overall
limits of quantum number 1:	1 10	0 9	0 10
limits of quantum number 2:	0 3	0 2	0 3
limits of quantum number 3:	0 10	0 9	0 10
limits of quantum number 4:	0 10	0 9	0 10
limits of quantum number 5:	1 11	0 10	0 11

frequency range: 2422   11963

Linelist L5. *syn-anti*-CDIT

J''	K_a''	K_c''	F_1''	F''	J'	K_a'	K_c'	F_1'	F'	ν (MHz)	$\nu_{obs} - \nu_{calc}$
1	1	0	2	1	1	0	1	1	0	2422.1900	−0.0184
1	1	0	1	1	1	0	1	2	1	2422.4504	−0.0067
1	1	0	1	2	1	0	1	2	3	2422.4504	0.0157
1	1	0	2	2	1	0	1	2	2	2422.5764	−0.0103
1	1	0	0	1	1	0	1	2	1	2422.9420	0.0024
1	1	0	1	2	1	0	1	0	1	2423.2048	−0.0152
1	1	0	2	2	1	0	1	0	1	2423.3865	0.0144
4	0	4	3	4	3	1	3	4	3	2479.0136	−0.0077
4	0	4	3	3	3	1	3	2	2	2479.0136	0.0037
4	0	4	4	4	3	1	3	3	3	2479.2595	−0.0074
2	1	1	3	3	2	0	2	3	2	2536.7151	0.0028
2	1	1	2	1	2	0	2	2	1	2536.7151	0.0104
2	1	1	1	2	2	0	2	1	2	2536.8960	−0.0107
2	1	1	1	2	2	0	2	1	1	2536.8960	−0.0077
2	1	1	3	2	2	0	2	3	2	2536.8960	0.0244
3	1	2	4	4	3	0	3	4	4	2715.1840	−0.0008
3	1	2	3	3	3	0	3	3	3	2715.1840	−0.0040
3	1	2	2	2	3	0	3	2	2	2715.1840	−0.0221
3	1	2	4	5	3	0	3	4	5	2715.3646	0.0263
3	1	2	3	2	3	0	3	3	2	2715.3646	0.0171
3	1	2	4	3	3	0	3	4	3	2715.3646	−0.0075
4	1	3	4	4	4	0	4	4	4	2966.2496	−0.0466
4	1	3	5	5	4	0	4	5	5	2966.2496	0.0107
4	1	3	3	3	4	0	4	3	3	2966.2496	0.0150
4	1	3	4	5	4	0	4	4	5	2966.4576	0.0154
4	1	3	5	4	4	0	4	5	4	2966.4576	0.0172
4	1	3	4	3	4	0	4	4	4	2966.4576	0.0094
4	1	3	3	2	4	0	4	3	2	2966.4576	0.0141
5	1	4	4	4	5	0	5	4	4	3300.1086	−0.0109
5	1	4	6	6	5	0	5	6	6	3300.1086	−0.0237
5	1	4	5	5	5	0	5	5	5	3300.2085	−0.0154

5	1	4	5	6	5	0	5	5	6	3300.3899	−0.0034
1	1	1	1	2	0	0	0	1	2	3454.5288	0.0167
1	1	1	0	1	0	0	0	1	2	3455.4383	0.0197
6	1	5	5	5	6	0	6	5	5	3728.0243	0.0158
6	1	5	7	7	6	0	6	7	7	3728.0243	−0.0001
6	1	5	5	6	6	0	6	5	5	3728.1419	0.0038
6	1	5	6	7	6	0	6	6	6	3728.2667	−0.0008
6	1	5	6	7	6	0	6	6	7	3728.3590	0.0278
5	0	5	4	5	4	1	4	5	6	3774.0417	−0.0207
5	0	5	6	6	4	1	4	5	5	3774.0417	−0.0358
5	0	5	5	5	4	1	4	4	4	3774.2252	−0.0259
7	1	6	8	8	7	0	7	8	8	4260.2846	0.0169
7	1	6	6	7	7	0	7	6	7	4260.4433	−0.0187
7	1	6	7	8	7	0	7	7	8	4260.6200	0.0071
2	1	2	1	2	1	0	1	1	2	4486.5126	0.0148
2	1	2	3	3	1	0	1	1	2	4486.6855	−0.0107
2	1	2	2	2	1	0	1	1	1	4486.8704	−0.0099
2	1	2	3	4	1	0	1	2	3	4487.1317	0.0156
2	1	2	1	2	1	0	1	0	1	4487.8222	0.0153
2	1	2	1	1	1	0	1	0	1	4487.8222	−0.0238
6	0	6	5	5	5	1	5	4	4	5078.4935	−0.0020
6	0	6	6	6	5	1	5	5	5	5078.6394	0.0099
3	1	3	3	4	2	0	2	2	3	5465.5089	0.0216
3	1	3	2	2	2	0	2	3	2	5465.7091	0.0086
3	1	3	4	4	2	0	2	3	3	5465.8525	0.0253
3	1	3	2	1	2	0	2	1	1	5465.8525	0.0149
3	1	3	4	4	2	0	2	3	4	5465.8525	0.0194
3	1	3	2	1	2	0	2	1	0	5465.8525	0.0073
3	1	3	3	4	2	0	2	3	4	5466.0391	−0.0047
9	1	8	9	9	9	0	9	9	9	5662.9499	−0.0069
9	1	8	9	10	9	0	9	9	10	5663.1756	−0.0179
8	2	6	7	8	8	1	7	7	8	5970.9827	−0.0182
8	2	6	7	6	8	1	7	7	6	5970.9827	−0.0142
8	2	6	9	10	8	1	7	9	10	5970.9827	−0.0064

6	2	4	6	6	6	1	5	6	6	6239.0766	−0.0190
6	2	4	7	7	6	1	5	7	7	6239.2488	−0.0320
7	0	7	7	7	6	1	6	6	6	6378.6980	−0.0352
7	0	7	8	7	6	1	6	7	6	6378.6980	−0.0233
7	0	7	8	9	6	1	6	7	8	6378.6980	−0.0097
7	0	7	6	7	6	1	6	5	6	6378.6980	−0.0047
4	1	4	4	5	3	0	3	3	4	6395.3961	0.0156
4	1	4	3	2	3	0	3	2	1	6395.5927	−0.0183
4	1	4	4	5	3	0	3	4	5	6395.9362	−0.0136
5	2	3	5	5	5	1	4	5	5	6424.0787	0.0092
5	2	3	6	6	5	1	4	6	6	6424.3310	0.0061
5	2	3	6	7	5	1	4	6	6	6424.3310	−0.0369
4	2	2	4	4	4	1	3	4	4	6614.8737	0.0168
4	2	2	5	5	4	1	3	5	5	6615.2343	0.0156
3	2	1	4	4	3	1	2	4	4	6792.6605	0.0004
3	2	1	2	2	3	1	2	2	2	6792.8327	−0.0024
2	2	0	3	3	2	1	1	3	3	6940.4017	0.0131
2	2	1	2	3	2	1	2	2	3	7266.7666	−0.0074
2	2	1	2	1	2	1	2	2	1	7266.7666	−0.0254
2	2	1	2	3	2	1	2	3	4	7266.9813	−0.0085
2	2	1	2	1	2	1	2	1	0	7267.1307	−0.0363
2	2	1	3	4	2	1	2	2	3	7267.3212	−0.0138
2	2	1	1	1	2	1	2	1	0	7268.0233	−0.0164
5	1	5	5	6	4	0	4	4	5	7284.4296	0.0036
5	1	5	6	7	4	0	4	5	6	7284.5772	0.0125
5	1	5	4	3	4	0	4	3	2	7284.5772	−0.0223
3	2	2	2	3	3	1	3	2	3	7435.5717	0.0051
4	2	3	4	5	4	1	4	4	5	7660.5124	−0.0209
4	2	3	4	3	4	1	4	4	3	7660.5276	−0.0362
4	2	3	5	5	4	1	4	5	5	7660.5276	−0.0276
4	2	3	3	3	4	1	4	3	3	7660.5755	−0.0289
8	0	8	7	8	7	1	7	6	7	7662.3325	0.0149
8	0	8	9	10	7	1	7	8	9	7662.3325	0.0126
8	0	8	8	8	7	1	7	7	7	7662.3325	−0.0031

5	2	4	6	6	5	1	5	6	6	7943.9903	0.0226
5	2	4	6	5	5	1	5	6	5	7944.1373	−0.0084
6	1	6	7	8	5	0	5	6	7	8143.3137	0.0015
6	1	6	6	6	5	0	5	5	5	8143.3137	0.0061
6	1	6	5	4	5	0	5	4	3	8143.3137	−0.0201
6	2	5	5	5	6	1	6	5	5	8286.3926	0.0331
6	2	5	7	7	6	1	6	7	7	8286.3926	0.0386
7	2	6	7	7	7	1	7	7	7	8688.3111	0.0119
7	2	6	7	6	7	1	7	7	6	8688.4923	0.0172
9	0	9	9	10	8	1	8	8	9	8920.2199	−0.0121
9	0	9	9	9	8	1	8	8	8	8920.2199	0.0333
7	1	7	7	6	6	0	6	6	5	8984.1318	−0.0037
7	1	7	7	7	6	0	6	6	6	8984.2510	0.0011
7	1	7	6	5	6	0	6	5	6	8984.2510	0.0025
7	1	7	8	9	6	0	6	7	8	8984.2510	0.0042
7	1	7	8	7	6	0	6	7	6	8984.2510	0.0170
7	1	7	6	6	6	0	6	5	5	8984.3432	−0.0343
7	1	7	8	8	6	0	6	7	7	8984.3432	−0.0071
2	2	1	2	1	1	1	0	1	0	9331.7511	0.0066
2	2	1	3	2	1	1	0	0	1	9331.7511	0.0237
2	2	1	3	3	1	1	0	2	2	9332.0921	0.0118
2	2	1	1	1	1	1	0	1	0	9332.5976	−0.0196
8	1	8	9	8	7	0	7	8	7	9820.4055	−0.0115
8	1	8	8	9	7	0	7	7	8	9820.4055	0.0609
3	2	2	3	3	2	1	1	2	2	10364.0055	0.0055
3	2	2	4	4	2	1	1	3	3	10364.4464	−0.0023
3	2	2	2	1	2	1	1	1	0	10364.4464	−0.0066
9	1	9	9	10	8	0	8	8	9	10663.8180	0.0335
9	1	9	10	9	8	0	8	9	8	10663.8180	−0.0259
3	2	1	3	4	2	1	2	2	3	10714.4929	−0.0276
3	2	1	4	3	2	1	2	2	3	10714.4929	−0.0229
3	2	1	2	2	2	1	2	2	1	10714.4929	−0.0120
3	2	1	2	3	2	1	2	2	3	10714.4929	−0.0047
3	2	1	4	4	2	1	2	2	3	10714.4929	0.0020

3	2	1	2	1	2	1	2	1	0	10714.9140	0.0121
4	2	3	4	3	3	1	2	3	3	11340.7267	0.0140
4	2	3	3	4	3	1	2	4	4	11340.9858	0.0008
7	3	4	6	7	7	2	5	6	7	11515.6729	−0.0119
7	3	4	8	8	7	2	5	8	8	11515.6729	−0.0390
7	3	4	6	6	7	2	5	6	6	11515.6729	−0.0692
10	1	10	10	11	9	0	9	9	10	11523.8332	−0.0148
10	1	10	10	9	9	0	9	9	8	11523.8332	−0.0104
6	3	3	6	6	6	2	4	6	6	11649.6927	−0.0077
6	3	3	5	6	6	2	4	5	6	11649.9335	−0.0223
6	3	3	7	7	6	2	4	7	7	11649.9335	−0.0244
3	3	0	4	4	3	2	1	4	3	11818.9758	0.0265
3	3	0	4	3	3	2	1	4	3	11818.9758	0.0239
3	3	0	4	4	3	2	1	4	5	11818.9758	0.0180
3	3	0	4	4	3	2	1	3	3	11818.9758	0.0173
3	3	0	4	5	3	2	1	4	5	11818.9758	0.0160
3	3	0	4	3	3	2	1	3	3	11818.9758	0.0147
3	3	1	4	4	3	2	2	2	3	11838.1285	−0.0044
3	3	1	4	4	3	2	2	4	4	11838.1285	−0.0046
4	3	2	3	2	4	2	3	3	2	11848.7796	−0.0027
4	3	2	3	4	4	2	3	3	4	11848.7796	−0.0006
5	3	3	4	3	5	2	4	4	3	11869.8208	0.0048
5	3	3	4	5	5	2	4	4	5	11869.8208	0.0077
5	3	3	4	4	5	2	4	4	4	11869.8208	0.0190
6	3	4	5	6	6	2	5	5	6	11906.2567	0.0407
6	3	4	5	4	6	2	5	5	4	11906.2567	0.0372
7	3	5	6	7	7	2	6	6	7	11963.3164	0.0232
7	3	5	6	5	7	2	6	6	5	11963.3164	0.0192

4. References

1 J. Pfeiffer, C. Trost, A. Pachkovska and F. Tambornino, A Crystallographic, Spectroscopic, and Computational Investigation of Carbonyl and Oxalyl Diisothiocyanate, *Inorg. Chem.*, 2021, **60**, 10722–10728.

2 D. Schmitz, V. Alvin Shubert, T. Betz and M. Schnell, Multi-resonance effects within a single chirp in broadband rotational spectroscopy: The rapid adiabatic passage regime for benzonitrile, *J. Mol. Spectrosc.*, 2012, **280**, 77–84.

3 C. Pérez, A. Krin, A. L. Steber, J. C. López, Z. Kisiel and M. Schnell, Wetting Camphor: Multi-Isotopic Substitution Identifies the Complementary Roles of Hydrogen Bonding and Dispersive Forces, *J. Phys. Chem. Lett.*, 2016, **7**, 154–160.

4 F. Neese, Software update: The ORCA program system—Version 5.0, *WIREs Comput. Mol. Sci.*, 2022, **12**, e1606.

5 A. D. Becke, Density-functional thermochemistry. III. The role of exact exchange, *J. Chem. Phys.*, 1993, **98**, 5648–5652.

6 S. Grimme and M. Steinmetz, Effects of London dispersion correction in density functional theory on the structures of organic molecules in the gas phase, *Phys. Chem. Chem. Phys.*, 2013, **15**, 16031–16042.

7 S. Grimme, J. Antony, S. Ehrlich and H. Krieg, A consistent and accurate ab initio parametrization of density functional dispersion correction (DFT-D) for the 94 elements H-Pu, *J. Chem. Phys.*, 2010, **132**, 154104.

8 S. Grimme, S. Ehrlich and L. Goerigk, Effect of the damping function in dispersion corrected density functional theory, *J. Comput. Chem.*, 2011, **32**, 1456–1465.

9 R. A. Kendall, T. H. Dunning Jr. and R. J. Harrison, Electron affinities of the first-row atoms revisited. Systematic basis sets and wave functions, *J. Chem. Phys.*, 1992, **96**, 6796–6806.

10 C. Møller and M. S. Plesset, Note on an Approximation Treatment for Many-Electron Systems, *Phys. Rev.*, 1934, **46**, 618–622.

11 V. Ásgeirsson, B. O. Birgisson, R. Bjornsson, U. Becker, F. Neese, C. Riplinger and H. Jónsson, Nudged Elastic Band Method for Molecular Reactions Using Energy-Weighted Springs Combined with Eigenvector Following, *J. Chem. Theory Comput.*,

2021, **17**, 4929–4945.

12   S. Grimme, J. G. Brandenburg, C. Bannwarth and A. Hansen, Consistent structures and interactions by density functional theory with small atomic orbital basis sets, *J. Chem. Phys.*, 2015, **143**, 54107.

13   E. F. Pettersen, T. D. Goddard, C. C. Huang, G. S. Couch, D. M. Greenblatt, E. C. Meng and T. E. Ferrin, UCSF Chimera--a visualization system for exploratory research and analysis., *J. Comput. Chem.*, 2004, **25**, 1605–1612.

8.1.3 Photolytic Decarbonylation of Oxalyl Diisothiocyanate in Solid Argon Matrices to *syn-anti* Carbonyl Diisothiocyanate and Its Isomerization

Photolytic Decarbonylation of Oxalyl Diisothiocyanate in Solid Argon Matrices to *syn-anti* Carbonyl Diisothiocyanate and Its Isomerization

Jonathan Pfeiffer, J. Philipp Wagner,* and Frank Tambornino*

Contents

1. Additional Figures
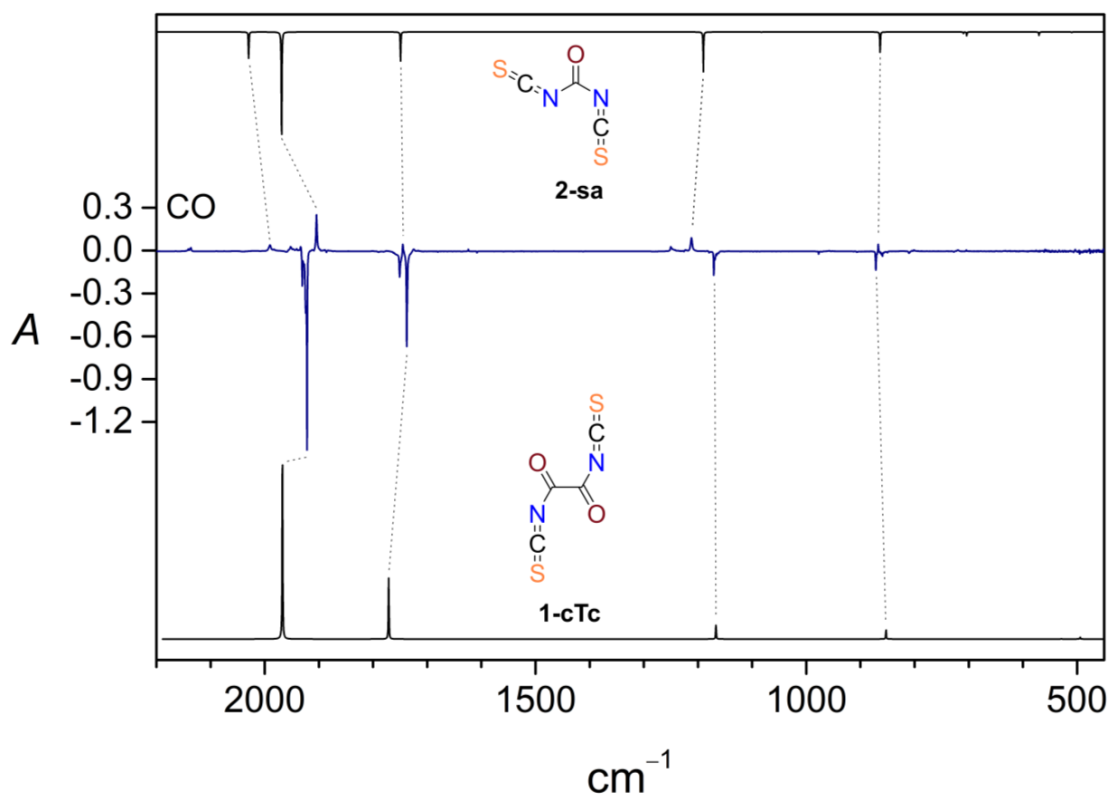
Figure S1. The blue trace in the middle corresponds to the difference IR spectrum of oxalyl diisothiocyanate in solid argon after 8 minutes of irradiation with 254 nm UV light. The experiment is compared to the B3LYP-D3/def2-TZVPP computed anharmonic VPT2 fundamentals of oxalyl and carbonyl diisothiocyanate in the bottom and top traces, respectively. The relative intensities in the computed spectra are not to scale.
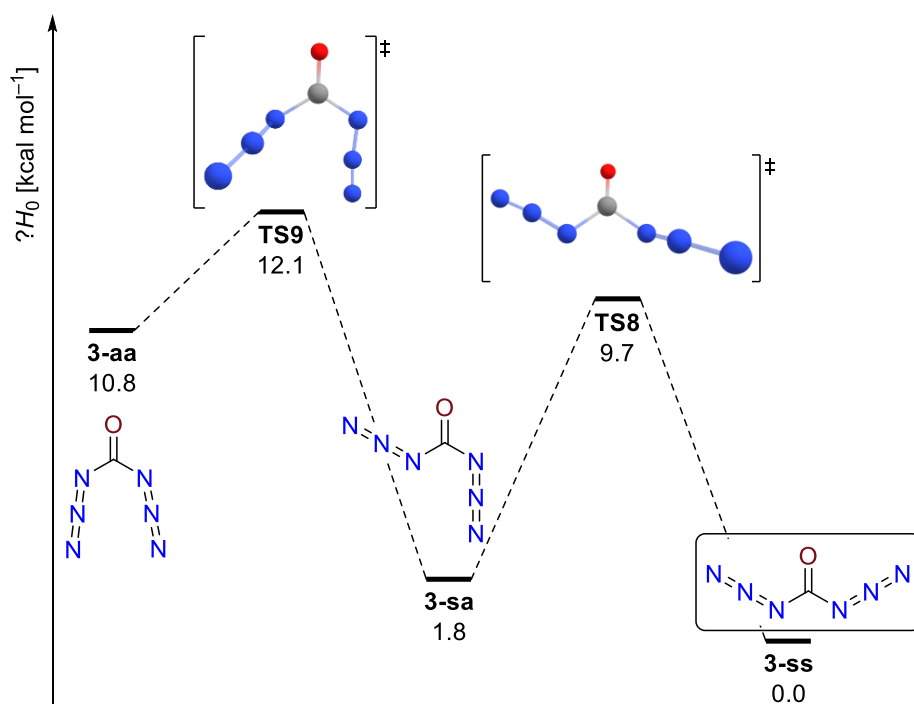
Figure S2. Conformer landscape of carbonyl diazide at the DLPNO-CCSD(T)/def2-QZVPP//B3LYP-D3/def2-TZVPP level of theory.

Scheme S1. Energetics of potential decomposition reactions of oxalyl diisothiocyanate computed at the DLPNO-CCSD(T)/def2-QZVPP//B3LYP-D3/def2-TZVPP level of theory. The enthalpies are given in units of kcal mol^{-1}.
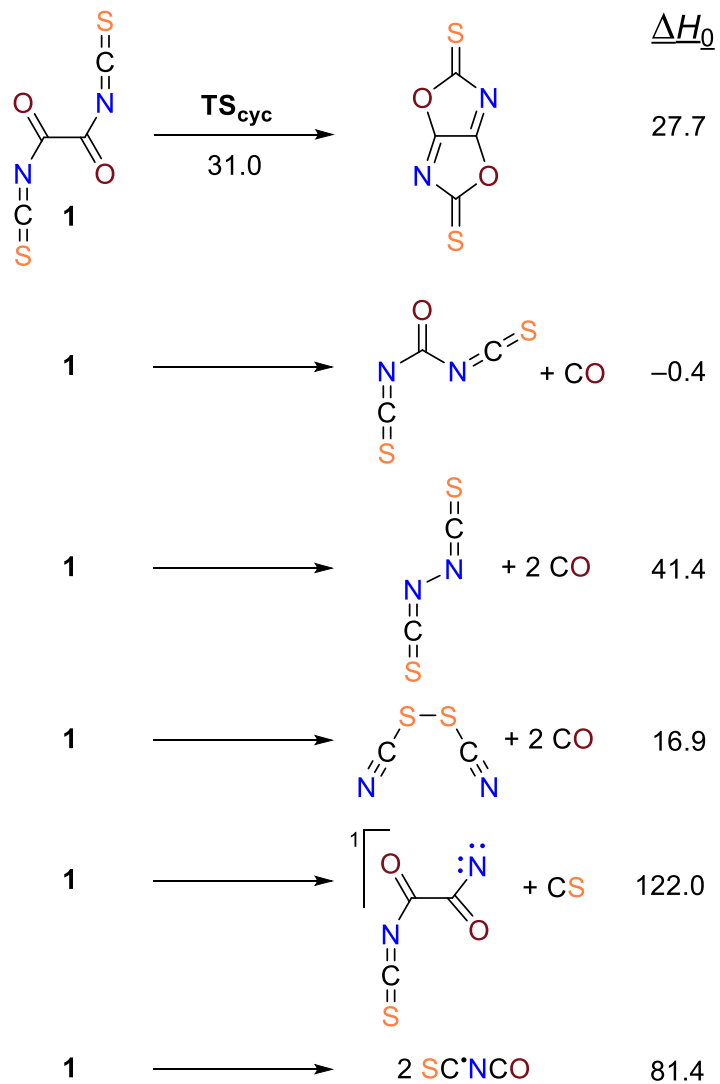
Scheme S2. Energetics of potential decomposition reactions of carbonyl diisothiocyanate computed at the DLPNO-CCSD(T)/def2-QZVPP//B3LYP-D3/def2-TZVPP level of theory. The enthalpies are given in units of kcal mol^{-1}.
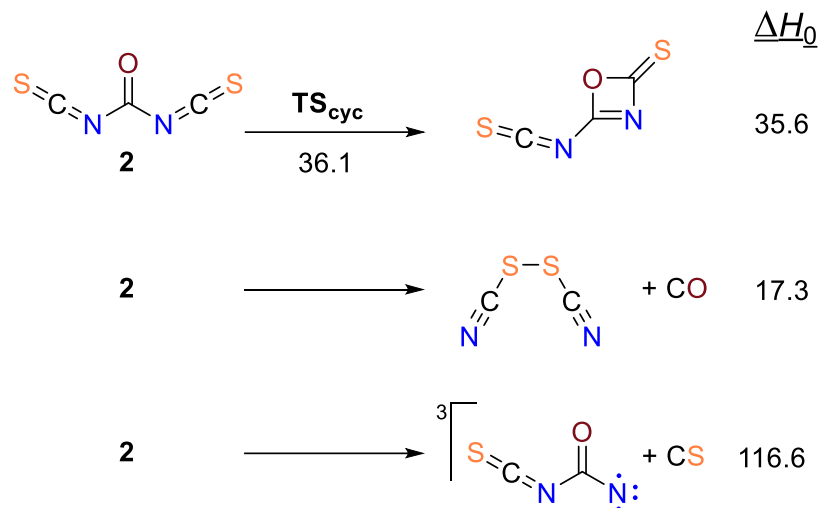
2. IR Assignments

Table S1. Comparison of the experimentally observed infrared transitions of oxalyl diisothiocyanate with the computed harmonic and anharmonic vibrational energies of conformer **aTa** at the B3LYP-D3/def2-TZVPP level of theory.

Ar, 4.2 K[a]	ω [cm^{-1}]	I [km mol^{-1}]	ν_{anh} [cm^{-1}]	symmetry	approx. description
1931, **1922**, 1924	2007	3422	1967	b_u	out of phase ν_{as}(NCS)
1751, **1738**	1793	1333	1771	b_u	ν_{as}(C=O)
1171	1196	243	1167	b_u	ν_{as}(C−N)
872	879	415	853	b_u	δ_{as}(N−C=O)
495	498	26	495	b_u	δ_{as}(N=C=O)

[a]The main absorption feature of the corresponding band is bold faced.

Table S2. Comparison of the experimentally observed infrared transitions of the oxalyl diisothiocyanate photodecomposition product with the computed harmonic and anharmonic vibrational energies of the **2-ss** conformer of carbonyl diisothiocyanate at the B3LYP-D3/def2-TZVPP level of theory.

Ar, 4.2 K[a]	ω [cm^{-1}]	I [km mol^{-1}]	ν_{anh} [cm^{-1}]	symmetry	approx. description
1990	2068	614	2030	a'	in phase ν_{as}(NCS)
1905	1995	2990	1969	a'	out of phase ν_{as}(NCS)
1724, **1745**	1775	718	1749	a'	ν(C=O)
1213	1225	906	1190	a'	ν_{as}(C−N)
867	885	370	864	a'	δ(N–C=O) (*anti*-subst.)
720	722	25	710	a''	o.o.p. γ(C=O)
705	722	69	704	a'	δ(CNC) (*syn*-subst.)
559	575	75	571	a'	δ(N=C=S) (*anti*-subst.)

[a]The main absorption feature of the corresponding band is bold faced.

Table S3. Comparison of the experimentally observed infrared transitions after annealing of the photo-decomposed oxalyl diisothiocyanate with the computed harmonic and anharmonic vibrational energies of the **2-sa** conformer of carbonyl diisothiocyanate at the B3LYP-D3/def2-TZVPP level of theory.

Ar, 4.2 K[a]	ω [cm^{-1}]	I [km mol^{-1}]	ν_{anh} [cm^{-1}]	symmetry	approx. description
1928, 1922	2000	4394	1963	b_2	out of phase ν_{as}(NCS)
1738	1749	335	1720	a_1	ν(C=O)
1250	1271	1332	1240	b_2	ν_{as}(C−N)
801	822	566	804	b_2	δ(N–C=O)
639, 630	642	144	635	b_2	δ_{as}(C–N–C)

[a]The main absorption feature of the corresponding band is bold faced.

3. Optimized Geometries and Energies
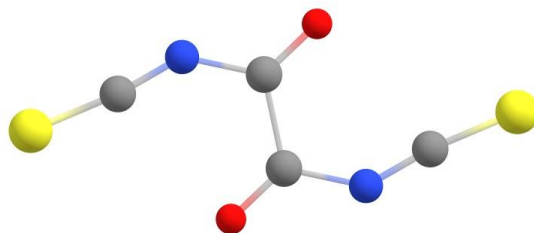
Figure S3. Optimized geometry of **aTa** (in Å) at the B3LYP-D3/def2-TZVPP level of theory. The DLPNO-CCSD(T) energy is given in units of E_h, the ZPVE in kcal mol^{-1}.

7	1.137714000	1.445425000	0.000000000
8	-1.137714000	1.320611000	0.000000000
6	-0.066858000	0.781634000	0.000000000
6	0.066858000	-0.781634000	0.000000000
8	1.137714000	-1.320611000	0.000000000
7	-1.137714000	-1.445425000	0.000000000
6	2.320405000	1.173807000	0.000000000
6	-2.320405000	-1.173807000	0.000000000
16	3.863061000	1.011088000	0.000000000
16	-3.863061000	-1.011088000	0.000000000

DLPNO-CCSD(T):   -1207.33126569113
ZPVE: 25.55405
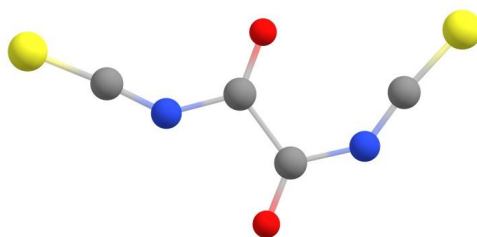
Figure S4. Optimized geometry of **aTs** (in Å) at the B3LYP-D3/def2-TZVPP level of theory. The DLPNO-CCSD(T) energy is given in units of E_h, the ZPVE in kcal mol^{-1}.

7	0.040949000	1.687909000	0.000000000
8	-1.001458000	-0.356191000	0.000000000
6	0.000000000	0.306299000	0.000000000
6	1.423085000	-0.313338000	0.000000000
8	2.408025000	0.367341000	0.000000000
7	1.431661000	-1.694000000	0.000000000
6	-0.725946000	2.621302000	0.000000000
6	0.641078000	-2.611800000	0.000000000
16	-1.617668000	3.892574000	0.000000000
16	-0.231714000	-3.896408000	0.000000000

DLPNO-CCSD(T):   -1207.32801001026
ZPVE: 25.5157
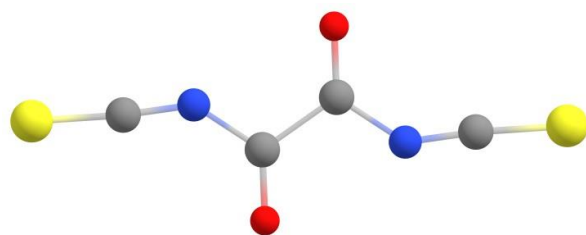
Figure S5. Optimized geometry of **sTs** (in Å) at the B3LYP-D3/def2-TZVPP level of theory. The DLPNO-CCSD(T) energy is given in units of E_h, the ZPVE in kcal mol^{-1}.

7	-0.270263000	1.798425000	0.000000000
8	1.655185000	0.545990000	0.000000000
6	0.458230000	0.617988000	0.000000000
6	-0.458230000	-0.617988000	0.000000000
8	-1.655185000	-0.545990000	0.000000000
7	0.270263000	-1.798425000	0.000000000
6	-0.070754000	2.989182000	0.000000000
6	0.070754000	-2.989182000	0.000000000
16	0.070754000	4.536565000	0.000000000
16	-0.070754000	-4.536565000	0.000000000

DLPNO-CCSD(T): -1207.32571896565
ZPVE: 25.49599
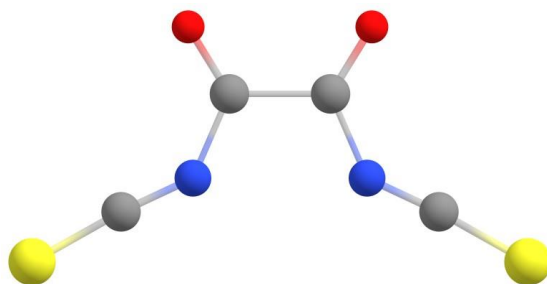
Figure S6. Optimized geometry of **sCs** (in Å) at the B3LYP-D3/def2-TZVPP level of theory. The DLPNO-CCSD(T) energy is given in units of E_h, the ZPVE in kcal mol^{-1}.

7	0.000000000	1.325794000	-0.061387000
8	0.000000000	1.399175000	2.234677000
6	0.000000000	0.770332000	1.217433000
6	0.000000000	-0.770332000	1.217433000
8	0.000000000	-1.399175000	2.234677000
7	0.000000000	-1.325794000	-0.061387000
6	0.000000000	2.420489000	-0.572308000
6	0.000000000	-2.420489000	-0.572308000
16	0.000000000	3.775600000	-1.332404000
16	0.000000000	-3.775600000	-1.332404000

DLPNO-CCSD(T):   -1207.32370562848
ZPVE: 25.4318
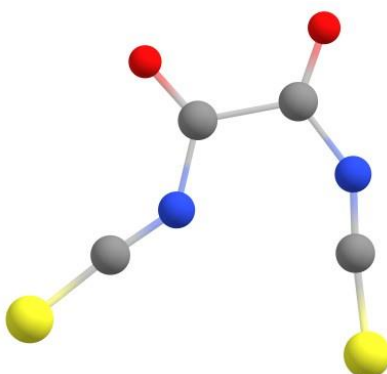
Figure S7. Optimized geometry of **sCa** (in Å) at the B3LYP-D3/def2-TZVPP level of theory. The DLPNO-CCSD(T) energy is given in units of E_h, the ZPVE in kcal mol^{-1}.

```
7     0.000000000     0.788232000     0.000000000
8     2.178390000     1.517664000     0.000000000
6     1.385992000     0.624441000     0.000000000
6     1.849566000    -0.861992000     0.000000000
8     3.013661000    -1.127285000     0.000000000
7     0.846563000    -1.819479000     0.000000000
6    -0.792017000     1.703481000     0.000000000
6    -0.345881000    -1.990150000     0.000000000
16   -1.890828000     2.798201000     0.000000000
16   -1.862191000    -2.345637000     0.000000000
```

DLPNO-CCSD(T):   -1207.32399520421
ZPVE: 25.32142
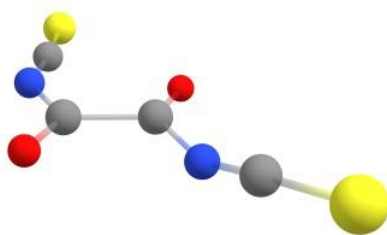
Figure S8. Optimized geometry of **TS1** (in Å) at the B3LYP-D3/def2-TZVPP level of theory. The DLPNO-CCSD(T) energy is given in units of E_h, the ZPVE in kcal mol^{-1}.

```
7     1.574535000    -0.188028000     0.409368000
8    -0.393997000    -1.312351000     0.203941000
6     0.222433000    -0.282936000     0.217471000
6    -0.454923000     1.111112000     0.055153000
8     0.186925000     2.121961000     0.031011000
7    -1.826633000     1.053834000    -0.066380000
6     2.726204000    -0.276452000     0.102352000
6    -2.708172000     0.222260000    -0.087080000
16    4.244809000    -0.366783000    -0.241964000
16   -3.950557000    -0.707056000    -0.133530000
```

DLPNO-CCSD(T):   -1207.32552483616
ZPVE: 25.32973
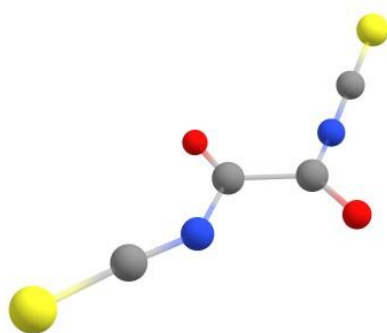
Figure S9. Optimized geometry of **TS2** (in Å) at the B3LYP-D3/def2-TZVPP level of theory. The DLPNO-CCSD(T) energy is given in units of E_h, the ZPVE in kcal mol^{-1}.

7	1.778158000	0.358906000	-0.007885000
8	0.280094000	-1.352371000	0.318104000
6	0.517537000	-0.186306000	0.166126000
6	-0.584162000	0.895170000	0.126008000
8	-0.354466000	2.055200000	-0.066594000
7	-1.834836000	0.379404000	0.368494000
6	2.927544000	-0.008540000	-0.064182000
6	-2.920600000	-0.023173000	0.075777000
16	4.435511000	-0.369215000	-0.151915000
16	-4.351148000	-0.559142000	-0.245504000

DLPNO-CCSD(T): -1207.32314451097
ZPVE: 25.30514
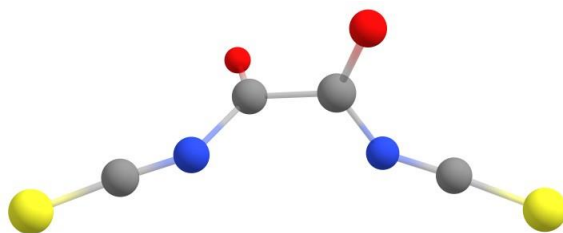
Figure S10. Optimized geometry of **TS3** (in Å) at the B3LYP-D3/def2-TZVPP level of theory. The DLPNO-CCSD(T) energy is given in units of E_h, the ZPVE in kcal mol^{-1}.

```
7     0.078741000    1.558379000   -0.061844000
8     1.372032000    0.725275000    1.653706000
6     0.456308000    0.611528000    0.888734000
6    -0.456308000   -0.611528000    0.888734000
8    -1.372032000   -0.725275000    1.653706000
7    -0.078741000   -1.558379000   -0.061844000
6     0.456308000    2.649990000   -0.426525000
6    -0.456308000   -2.649990000   -0.426525000
16    0.853705000    4.046461000   -0.973124000
16   -0.853705000   -4.046461000   -0.973124000
```

DLPNO-CCSD(T):   -1207.3211021485
ZPVE: 25.27946
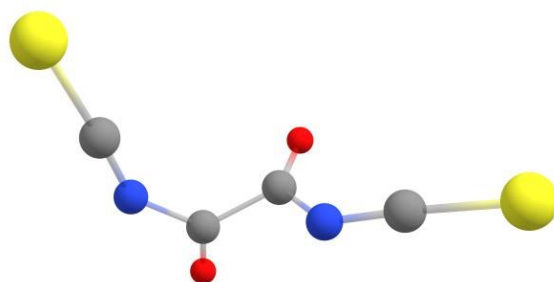
Figure S11. Optimized geometry of **TS4** (in Å) at the B3LYP-D3/def2-TZVPP level of theory. The DLPNO-CCSD(T) energy is given in units of E_h, the ZPVE in kcal mol^{-1}.

7	1.160446000	0.304630000	-0.345969000
8	0.405254000	1.105576000	1.679911000
6	0.275299000	0.974494000	0.495745000
6	-0.924814000	1.549815000	-0.264244000
8	-0.946505000	2.681729000	-0.646913000
7	-1.973790000	0.649459000	-0.432948000
6	2.225941000	-0.262734000	-0.230058000
6	-2.251502000	-0.499336000	-0.182750000
16	3.583582000	-1.009941000	-0.197399000
16	-2.703965000	-1.961966000	0.089666000

DLPNO-CCSD(T):   -1207.32121516903
ZPVE: 25.2515
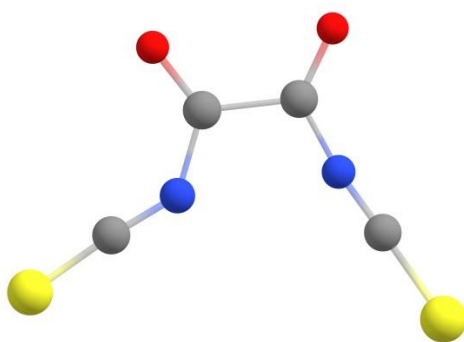
Figure S12. Optimized geometry of **TS5** (in Å) at the B3LYP-D3/def2-TZVPP level of theory. The DLPNO-CCSD(T) energy is given in units of E_h, the ZPVE in kcal mol^{-1}.

7	1.061465000	0.033732000	0.061017000
8	1.399934000	2.290616000	-0.229939000
6	0.664394000	1.367321000	-0.045209000
6	-0.865916000	1.564027000	0.082693000
8	-1.369619000	2.639786000	-0.043181000
7	-1.564785000	0.412431000	0.392940000
6	2.099335000	-0.588390000	0.032081000
6	-2.209262000	-0.559282000	0.130734000
16	3.368087000	-1.481628000	0.011755000
16	-3.046249000	-1.847647000	-0.148913000

DLPNO-CCSD(T): -1207.32110567047
ZPVE: 25.22895
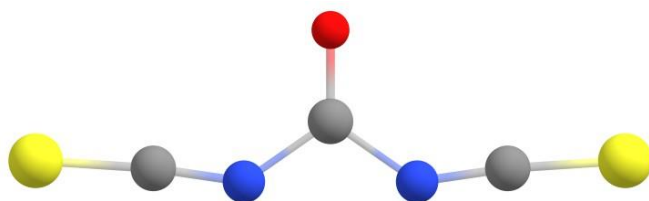
Figure S13. Optimized geometry of **2-ss** (in Å) at the B3LYP-D3/def2-TZVPP level of theory. The DLPNO-CCSD(T) energy is given in units of E_h, the ZPVE in kcal mol^{-1}.

7	0.000000000	1.142362000	-0.439771000
8	0.000000000	0.000000000	1.554278000
6	0.000000000	0.000000000	0.354003000
7	0.000000000	-1.142362000	-0.439771000
6	0.000000000	2.337265000	-0.264143000
6	0.000000000	-2.337265000	-0.264143000
16	0.000000000	3.888244000	-0.163492000
16	0.000000000	-3.888244000	-0.163492000

DLPNO-CCSD(T):   -1094.14048066973

ZPVE: 19.67876
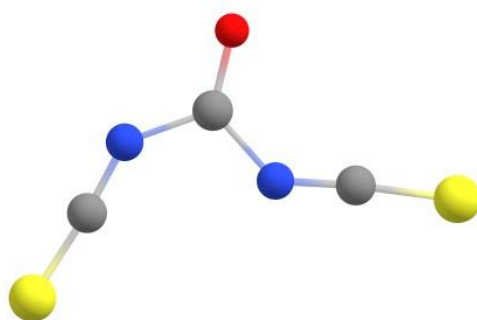
Figure S14. Optimized geometry of **2-sa** (in Å) at the B3LYP-D3/def2-TZVPP level of theory. The DLPNO-CCSD(T) energy is given in units of E_h, the ZPVE in kcal mol^{-1}.

7	0.000000000	-0.719930000	0.000000000
8	-2.283808000	-0.423980000	0.000000000
6	-1.180822000	0.039993000	0.000000000
7	-0.928071000	1.405633000	0.000000000
6	0.258842000	-1.901541000	0.000000000
6	0.025687000	2.145677000	0.000000000
16	0.709865000	-3.388043000	0.000000000
16	1.174179000	3.193490000	0.000000000

DLPNO-CCSD(T):   -1094.13924423291
ZPVE: 19.58785
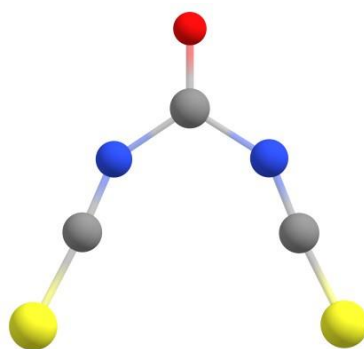
Figure S15. Optimized geometry of **2-aa** (in Å) at the B3LYP-D3/def2-TZVPP level of theory. The DLPNO-CCSD(T) energy is given in units of E_h, the ZPVE in kcal mol^{-1}.

7	0.109918000	1.166584000	1.012478000
8	0.000000000	0.000000000	2.961081000
6	0.000000000	0.000000000	1.766704000
7	-0.109918000	-1.166584000	1.012478000
6	0.000000000	1.625340000	-0.094048000
6	0.000000000	-1.625340000	-0.094048000
16	-0.120719000	2.328620000	-1.479218000
16	0.120719000	-2.328620000	-1.479218000

DLPNO-CCSD(T):   -1094.13720263617
ZPVE: 19.40655
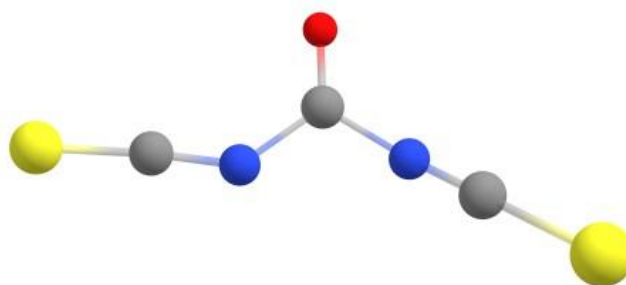
Figure S16. Optimized geometry of **TS6** (in Å) at the B3LYP-D3/def2-TZVPP level of theory. The DLPNO-CCSD(T) energy is given in units of E_h, the ZPVE in kcal mol^{-1}.

```
7     -1.246341000    0.539189000     0.437066000
8      0.332522000    2.009503000    -0.292094000
6      0.039829000    0.909475000     0.078835000
7      0.937811000   -0.141894000     0.256248000
6     -2.259715000   -0.024848000     0.142065000
6      2.121600000   -0.318353000     0.081769000
16    -3.618952000   -0.728682000    -0.168061000
16     3.624530000   -0.662238000    -0.102718000
```

DLPNO-CCSD(T):   -1094.13709779966
ZPVE: 19.48893
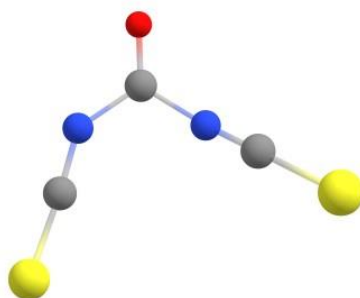
Figure S17. Optimized geometry of **TS7** (in Å) at the B3LYP-D3/def2-TZVPP level of theory. The DLPNO-CCSD(T) energy is given in units of E_h, the ZPVE in kcal mol^{-1}.

7	-0.919155000	0.680249000	0.522285000
8	-0.219586000	2.745951000	-0.154645000
6	0.018901000	1.590651000	0.022720000
7	1.269432000	1.022262000	-0.199655000
6	-1.702117000	-0.167978000	0.192653000
6	1.830683000	-0.039691000	-0.080973000
16	-2.745645000	-1.278513000	-0.145512000
16	2.646891000	-1.357930000	0.031283000

DLPNO-CCSD(T): -1094.13665378651
ZPVE: 19.44294
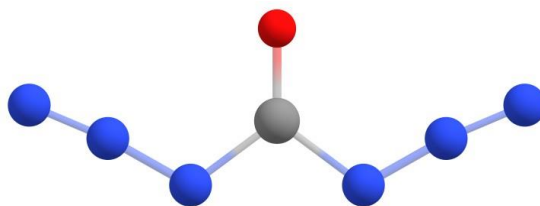
Figure S18. Optimized geometry of **3-ss** (in Å) at the B3LYP-D3/def2-TZVPP level of theory. The DLPNO-CCSD(T) energy is given in units of E_h, the ZPVE in kcal mol^{-1}.

7	0.000000000	1.132166000	-0.794946000
8	0.000000000	0.000000000	1.248243000
6	0.000000000	0.000000000	0.043997000
7	0.000000000	-1.132166000	-0.794946000
7	0.000000000	2.215675000	-0.185993000
7	0.000000000	-2.215675000	-0.185993000
7	0.000000000	3.245529000	0.248801000
7	0.000000000	-3.245529000	0.248801000

DLPNO-CCSD(T):   -441.181974657206
ZPVE: 22.56693
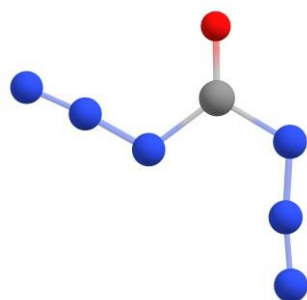
Figure S19. Optimized geometry of **3-sa** (in Å) at the B3LYP-D3/def2-TZVPP level of theory. The DLPNO-CCSD(T) energy is given in units of E$_h$, the ZPVE in kcal mol^{-1}.

```
7     -0.556833000     0.546340000     0.000000000
8     -0.620903000    -1.791026000     0.000000000
6      0.000000000    -0.767677000     0.000000000
7      1.403835000    -0.746869000     0.000000000
7     -1.798026000     0.571341000     0.000000000
7      1.966218000     0.360952000     0.000000000
7     -2.909209000     0.692189000     0.000000000
7      2.603618000     1.280943000     0.000000000
```

DLPNO-CCSD(T):   -441.179034671386
ZPVE: 22.49552
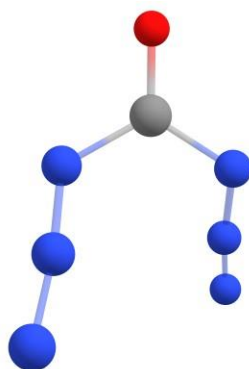
Figure S20. Optimized geometry of **3-aa** (in Å) at the B3LYP-D3/def2-TZVPP level of theory. The DLPNO-CCSD(T) energy is given in units of E_h, the ZPVE in kcal mol^{-1}.

```
7      0.000000000     1.228027000     0.463597000
8      0.000000000     0.000000000     2.379138000
6      0.000000000     0.000000000     1.189587000
7      0.000000000    -1.228027000     0.463597000
7     -0.513614000     1.269208000    -0.661516000
7      0.513614000    -1.269208000    -0.661516000
7     -0.970866000     1.447104000    -1.671412000
7      0.970866000    -1.447104000    -1.671412000
```

DLPNO-CCSD(T):   -441.164082862299
ZPVE: 22.16814
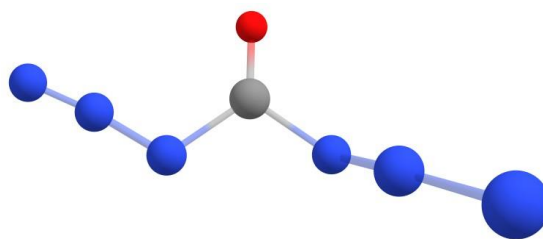
Figure S21. Optimized geometry of **TS8** (in Å) at the B3LYP-D3/def2-TZVPP level of theory. The DLPNO-CCSD(T) energy is given in units of E_h, the ZPVE in kcal mol^{-1}.

7	0.000000000	1.228027000	0.463597000
8	0.000000000	0.000000000	2.379138000
6	0.000000000	0.000000000	1.189587000
7	0.000000000	-1.228027000	0.463597000
7	-0.513614000	1.269208000	-0.661516000
7	0.513614000	-1.269208000	-0.661516000
7	-0.970866000	1.447104000	-1.671412000
7	0.970866000	-1.447104000	-1.671412000

DLPNO-CCSD(T):   -441.166133087094
ZPVE: 22.2815
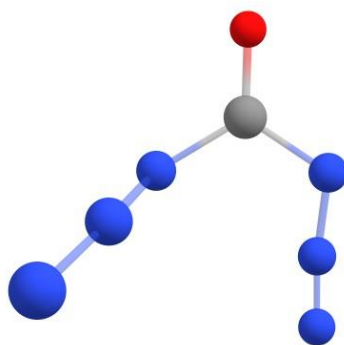
Figure S22. Optimized geometry of **TS9** (in Å) at the B3LYP-D3/def2-TZVPP level of theory. The DLPNO-CCSD(T) energy is given in units of E_h, the ZPVE in kcal mol^{-1}.

7	0.849958000	0.114693000	0.748726000
8	0.403346000	2.215865000	-0.121749000
6	0.046928000	1.094153000	0.040727000
7	-1.231124000	0.659660000	-0.366409000
7	1.442075000	-0.725464000	0.071774000
7	-1.580405000	-0.492188000	-0.058408000
7	2.036482000	-1.526995000	-0.448127000
7	-2.018176000	-1.499969000	0.156677000

DLPNO-CCSD(T):   -441.16197435702
ZPVE: 22.12853

8.1.4 Double Addition *vs.* Ring Closure: Systematic Reactivity Study of CO(NCO)$_2$ and CO(NCS)$_2$ towards Hydrogen Halides

Chemistry–A European Journal

Supporting Information

Double Addition *vs.* Ring Closure: Systematic Reactivity Study of CO(NCO)$_2$ and CO(NCS)$_2$ towards Hydrogen Halides

Jonathan Pfeiffer, Hennes Günther, Lena Völlinger, Demian Botros, Benjamin Scheibe, Martin Möbs, Florian Kraus, Florian Weigend, and Frank Tambornino*

Contents

1. Experimental section

1.1. General remarks

General synthetic methods. All reactions and manipulations were performed under an inert atmosphere of argon using standard Schlenk-line or glovebox techniques (MBraun UNIlab glovebox, maintained at < 0.1 ppm H_2O and < 0.1 ppm O_2).

Triphosgene (abcr, 98 %), 2-chloronitrobenzene (abcr, 99 %), phosgene (Synthesia, 98.5 %), hydrogen chloride (GHC, 99.9 %), hydrobromic acid 48 wt.% (Fisher Scientific), hydriodic acid 57 wt.% (Acros Organics), silver fluoride (BLDpharm, 99 %), ammonium iodide (Acros Organics, 99 %) were used as received. Trichloroisocyanuric acid (Acros Organics, 99 %) was recrystallized from 1,2-dichloroethane and ammonium thiocyanate (Merck, 99 %) from methanol. Both were dried until no further ^{1}H-NMR signals of the solvents were detected. Solvents were dried according to literature.[1] CD_3CN (Eurisotop, 99.8 %) and THF-d$_8$ (Eurisotop, 99.5 %) were recondensed, degassed and stored over molecular sieve (4 Å) prior to use. Hydrogen fluoride (Fluka Analytical, >99.9 %) was stored over K_2NiF_6 and was distilled twice before use. All operations involving anhydrous hydrogen fluoride were performed in a stainless steel (316 L) vacuum line. Reaction vessels were made out of perfluoroalkoxy alkanes (PFA), equipped with PFA needle valves (Swagelok) and baked out at 150 °C in vacuum (~$1 \cdot 10^{-2}$ mbar) before use.

Additional characterization techniques:

^{1}H, ^{13}C, and ^{19}F NMR spectra were acquired on a Bruker Avance II (300 MHz) spectrometer at 298 K if not stated otherwise.

Elemental analyses were performed by the in-house service personnel. CHN(S) analyses were performed on a *CHNS(S)-Analysator vario MICRO CUBE* (Elementar). Samples were prepared and sealed under inert conditions in a tin crucible.

Raman spectra were recorded on a Monovista CRS+ confocal Raman microscope (Spectroscopy & Imaging GmbH) using a 785 nm solid-state laser and a 300 grooves/mm grating. Samples were sealed in borosilicate ampoules and measured at room temperature.

IR spectra were recorded on a Bruker Alpha FT-IR spectrometer equipped with a diamond ATR unit mounted in a nitrogen-filled glovebox (MBraun UNIlab glovebox, maintained at < 0.1 ppm H_2O and < 0.1 ppm O_2).

1.1. Synthesis of carbonyl diisocyanate

Triphosgene (8.30 g, 28.0 mmol, 1 eq.), trichloroisocyanuric acid (11.7 g, 50.4 mmol, 1.8 eq.) and 32 g 1-chloro-2-nitrobenzene were added in a flask connected to a distillation apparatus. The solid mixture was heated to 80 °C to become a clear yellow solution. The receiving flask was cooled to 0 °C and the oil bath temperature raised to 120 °C until no further chlorine gas formation was visible. The temperature then was raised up to 175 °C and the receiving flask was cooled to −78 °C. Carbonyl diisocyanate was distilled for 5 h in a consecutive, slow argon gas stream. Afterwards it was recondensed two times to afford a colorless, clear liquid (3.75 g, 33.5 mmol, 40 %).

1.2. Synthesis of carbonyl diisothiocyanate

CDIT was synthesized according to the literature.[2]

1.3. Synthesis of carbonyl bis(carbamoylfluoride) (1)

Carbonyl diisocyanate (150 mg, 1.34 mmol, 1 eq.) was distilled into a PFA reaction vessel, and anhydrous HF (0.30 mL, 290 mg, 14.5 mmol, 10.8 eq.) was condensed at –196 °C onto the frozen starting material. The reaction mixture was warmed up to room temperature and the precipitation of a colorless solid was observed. After storing the reaction mixture at –37 °C for 18 d colorless, millimeter-sized needle shaped crystals were obtained. Multiple specimens were transferred from the anhydrous HF solution into perfluorinated oil (Fomblin YR 1800) and a suitable single crystal for X-ray crystal structure determination was selected under the microscope, a yield was not determined.

The synthesis was repeated with carbonyl diisocyanate (1.20 g, 10.7 mmol, 1 eq.) and an excess of anhydrous HF (2.0 mL, 1.9 g, 95 mmol, 8.9 eq.). After removal of anhydrous HF

carbonyl bis(carbamoylfluoride) (1.47 g, 9.70 mmol, 90 %) remained as colorless powder and was washed with *n*-hexane and cold diethyl ether. Recrystallization from dichloromethane/*n*-hexane, THF/*n*-hexane, acetonitrile/diethyl ether or diethyl ether at −75 °C was not possible.

¹H NMR (300 MHz, CD₃CN, r.t.) δ / ppm = 9.40 (N*H*).

¹³C NMR (75 MHz, CD₃CN, r.t.) δ / ppm = 146.7 (t, $^3J_{CF}$ = 10.69 Hz, *C*=O), 143.0 (d, $^1J_{CF}$ = 297.45 Hz, *C*−F).

¹⁹F NMR (282 MHz, CD₃CN, r.t.) δ / ppm = −0.70 (C*F*).

CHNS (calc./found.) C: 23.70 / 23.65, H: 1.33 / 1.51, N: 18.42 / 18.70.
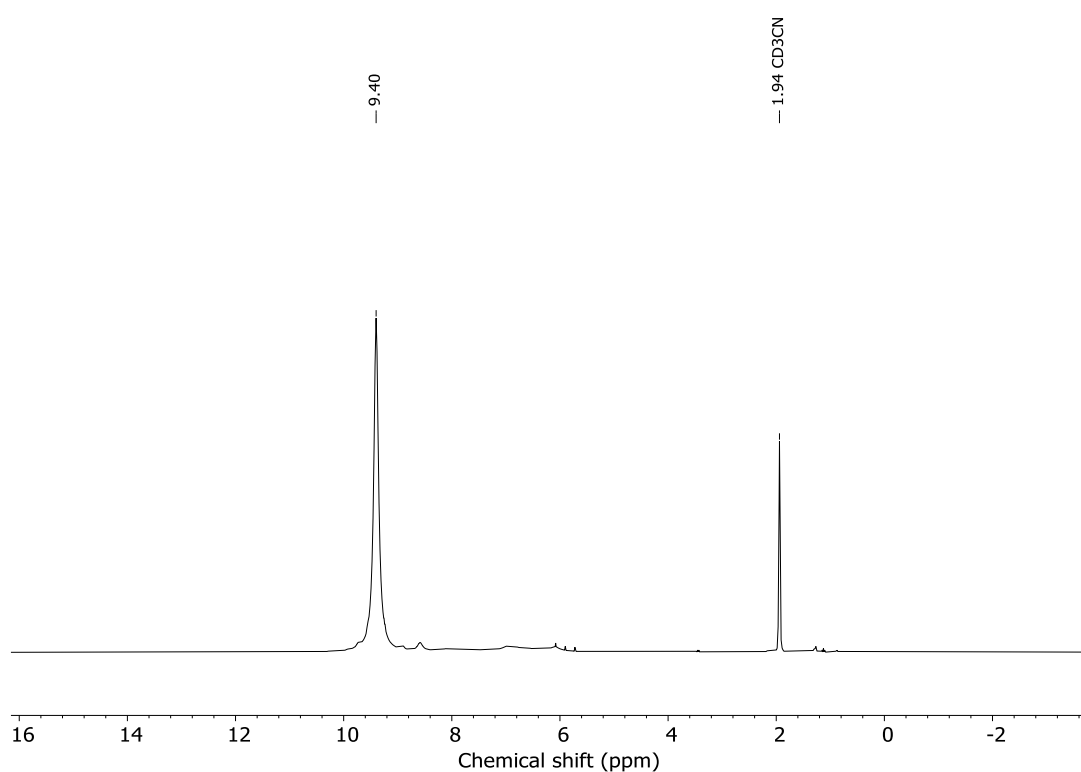
Figure S 1: ¹H NMR spectrum of carbonyl bis(carbamoylfluoride) in acetonitrile-d3 at room temperature.
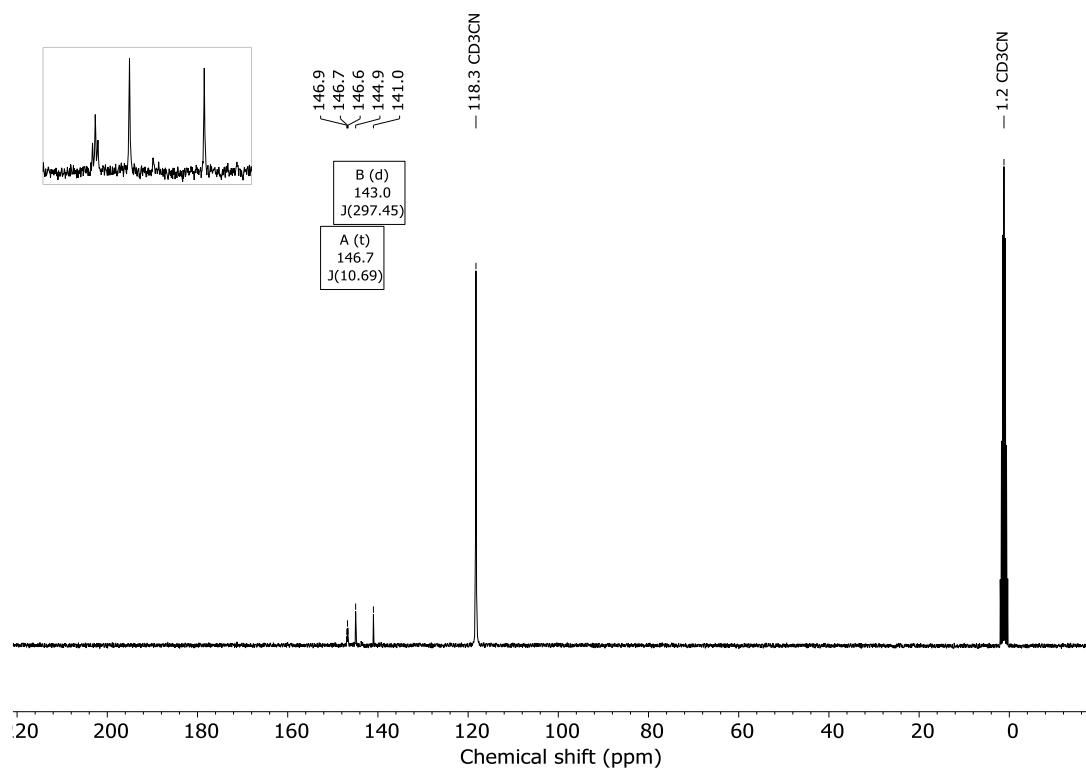
Figure S 2: ^{13}C NMR spectrum of carbonyl bis(carbamoylfluoride) in acetonitrile-d3 at room temperature. The inset shows a magnification of the region 140 – 155 ppm.
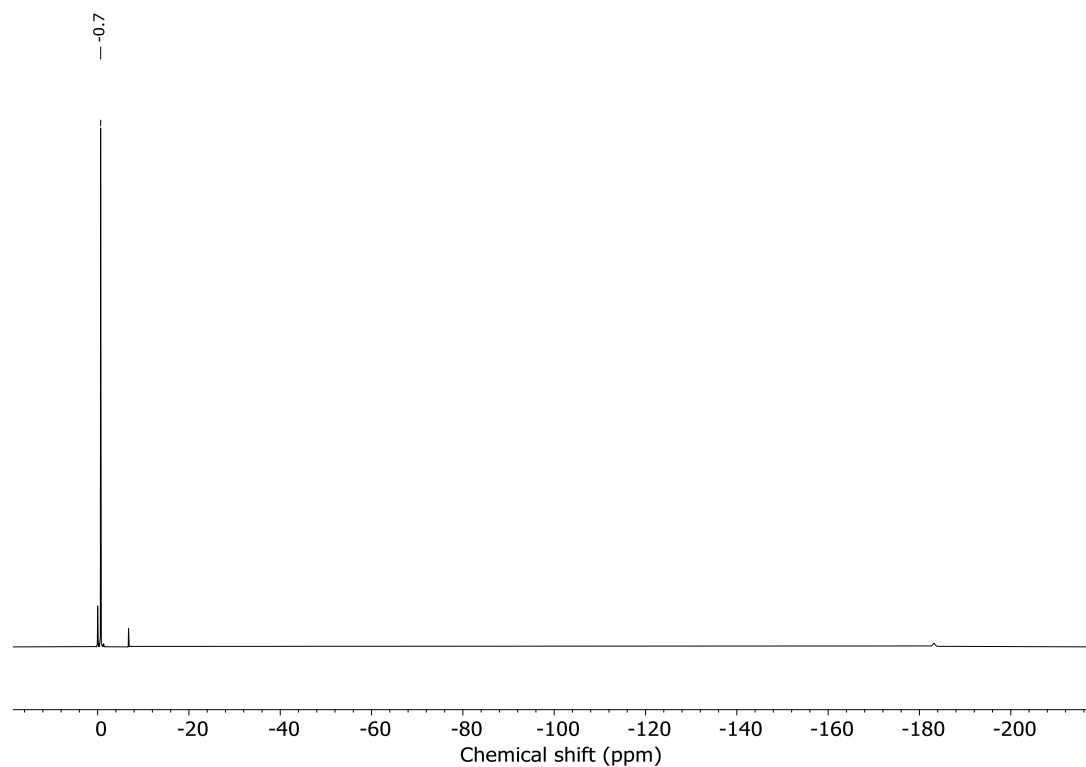
Figure S 3: ^{19}F NMR spectrum of carbonyl bis(carbamoylfluoride) in acetonitrile-d3 at room temperature.
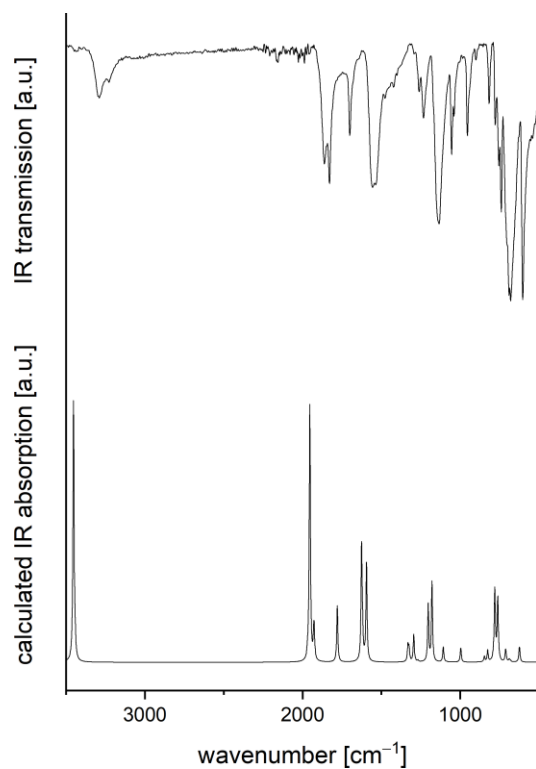
Figure S 4: Measured (top) room-temperature ATR-IR spectrum of carbonyl bis(carbamoylfluoride) and its simulated spectrum (bottom).
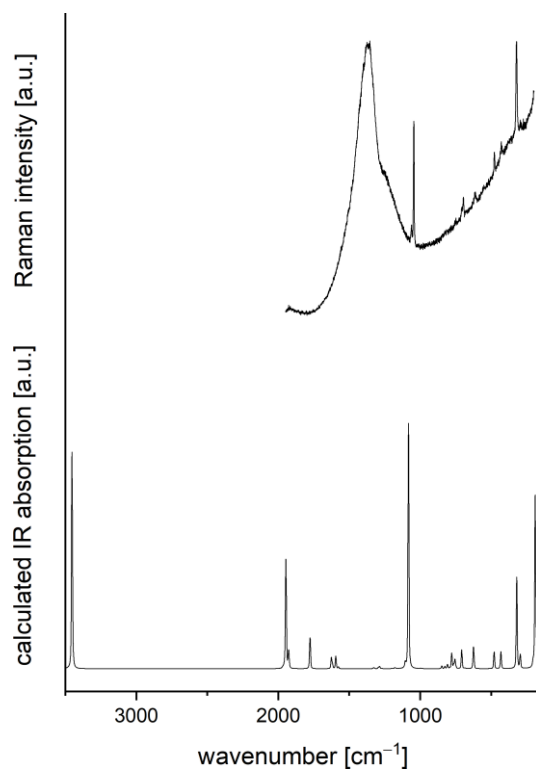
Figure S 5: Measured (top) room-temperature Raman spectrum of carbonyl bis(carbamoylfluoride) and its simulated spectrum (bottom).

1.4. Synthesis of carbonyl bis(carbamoylchloride) (2)

Hydrogen chloride gas was passed through a solution of carbonyl diisocyanate (1.08 g, 9.64 mmol, 1 eq.) in 20 mL dichloromethane cooled to −78 °C for 30 min. Hydrogen chloride gas was dried by passing it through a column packed with P_4O_{10}. Excess hydrogen chloride gas was removed from the apparatus with an argon gas stream over 10 min. The solvent was removed under reduced pressure at −20 °C precipitating a colorless powder. The powder was washed with cold *n*-hexane and dried *in vacuo* at −20 °C. Carbonyl bis(carbamoylchloride) (1.27 g, 6.87 mmol, 71 %) was received as colorless powder. Crystals suitable for X-ray diffraction measurements were obtained by slowly removing solvent from a saturated solution in diethyl ether at −78 °C. We found that carbonyl bis(carbamoylchloride) loses gaseous HCl even at room temperature leading to unprecise values for the elemental analysis. During Raman measurements carbonyl bis(carbamoylchloride) showed fluorescence at all tested wavelengths (488 nm, 532 nm, 633 nm, 785 nm).

¹H NMR (300 MHz, CD_3CN, r.t.) δ / ppm = 9.72 (N*H*).

¹³C NMR (75 MHz, CD_3CN, r.t.) δ / ppm = 146.1 (*C*−Cl), 145.1 (*C*=O).

CHNS (calc./found) C: 19.48 / 19.86, H: 1.09 / 0.69, N: 15.15 / 15.63.
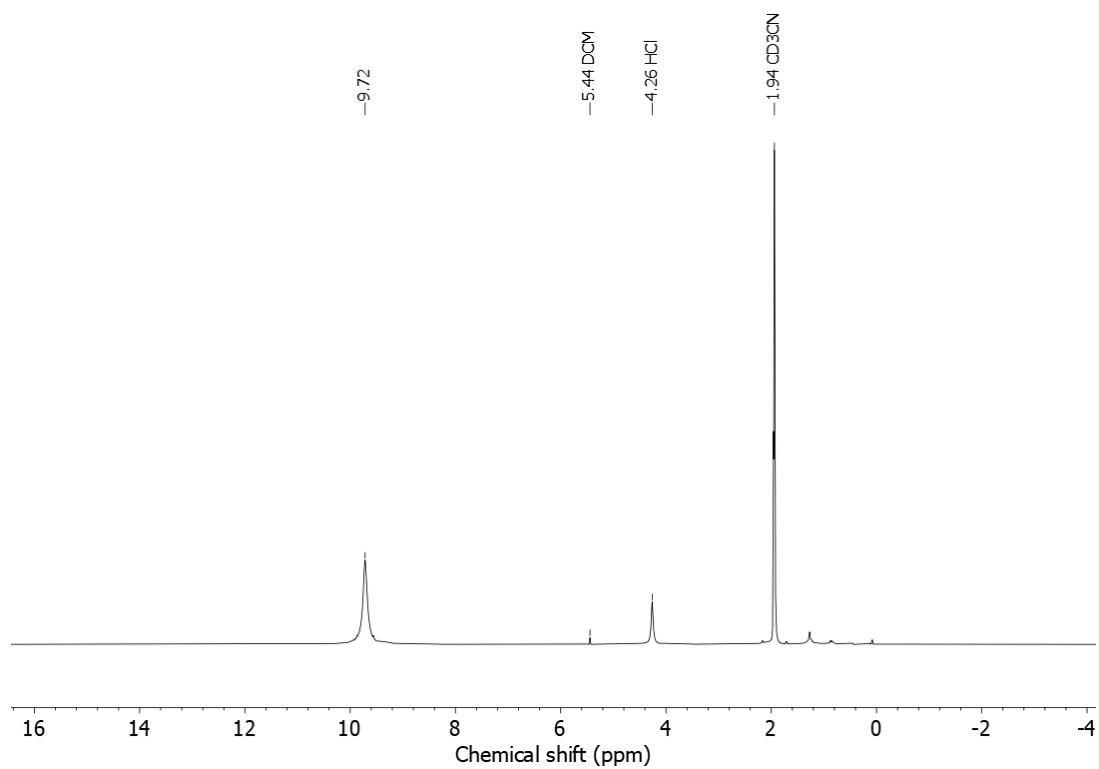
Figure S 6: ^{1}H NMR spectrum of carbonyl bis(carbamoylchloride) in acetonitrile-d3 at room temperature.
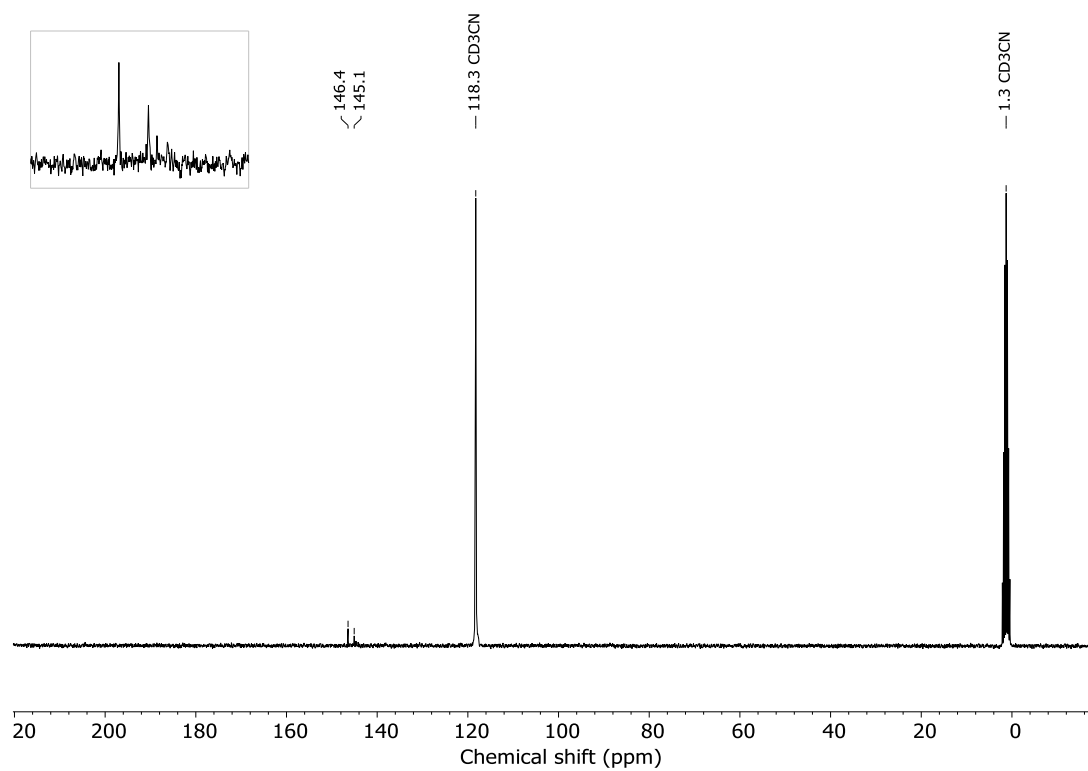
Figure S 7: ^{13}C NMR spectrum of carbonyl bis(carbamoylchloride) in acetonitrile-d3 at room temperature. The inset shows a magnification of the region between 140 and 155 ppm.
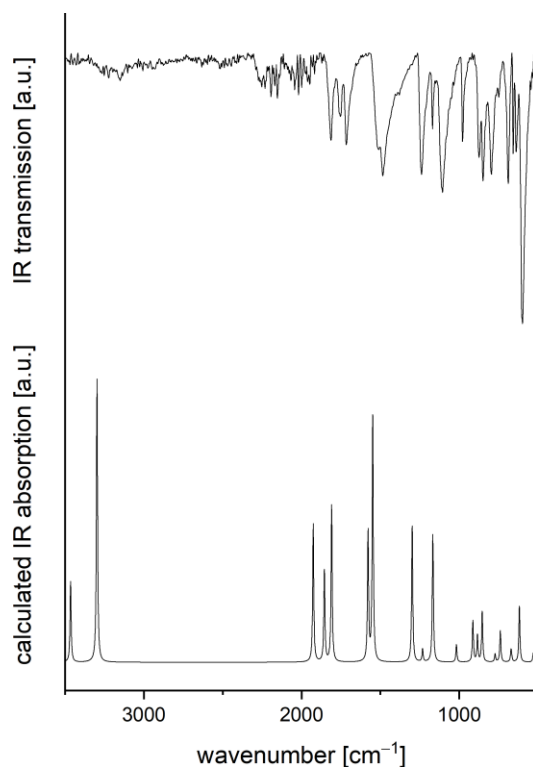
Figure S 8: Measured (top) room-temperature ATR-IR spectrum of carbonyl bis(carbamoylchloride) and its simulated spectrum (bottom).

1.5. Synthesis of carbonyl bis(carbamoylbromide) (3)

Hydrogen bromide gas was developed by dropping hydrobromic acid 48 % (12.61 mL, 111.5 mmol, 10 eq.) on P_4O_{10} and dried by passing it through a column filled with P_4O_{10} in a slow argon stream. The diluted gas stream was passed through a solution of carbonyl diisocyanate (1.24 g, 11.1 mmol, 1 eq.) in 20 mL dichloromethane cooled to −78 °C. The argon stream was maintained for 100 min. The colorless solution turned yellow. The solvent was removed under reduced pressure at −20 °C and the crude residue washed with *n*-hexane. The colorless powder was dried *in vacuo* and carbonyl bis(carbamoylbromide) (1.79, 6.54 mmol, 59 %) was isolated. Crystals suitable for X-ray diffraction measurements were obtained by slowly removing solvent from a saturated solution in diethyl ether at −78 °C. We found that carbonyl bis(carbamoylbromide) loses gaseous HBr even at room temperature leading to unprecise values for the elemental analysis. During Raman measurements carbonyl

bis(carbamoylbromide) showed fluorescence at all tested wavelengths (488 nm, 532 nm, 633 nm, 785 nm).

¹H NMR (300 MHz, CD₃CN, r.t.) δ / ppm = 9.70 (N*H*).

¹³C NMR (75 MHz, CD₃CN, r.t.) δ / ppm = 143.9 (*C*=O), 136.4 (*C*−Br).

CHNS (calc./found) C: 13.16 / 13.67, H: 0.74 / 0.044, N: 10.23 / 10.88.
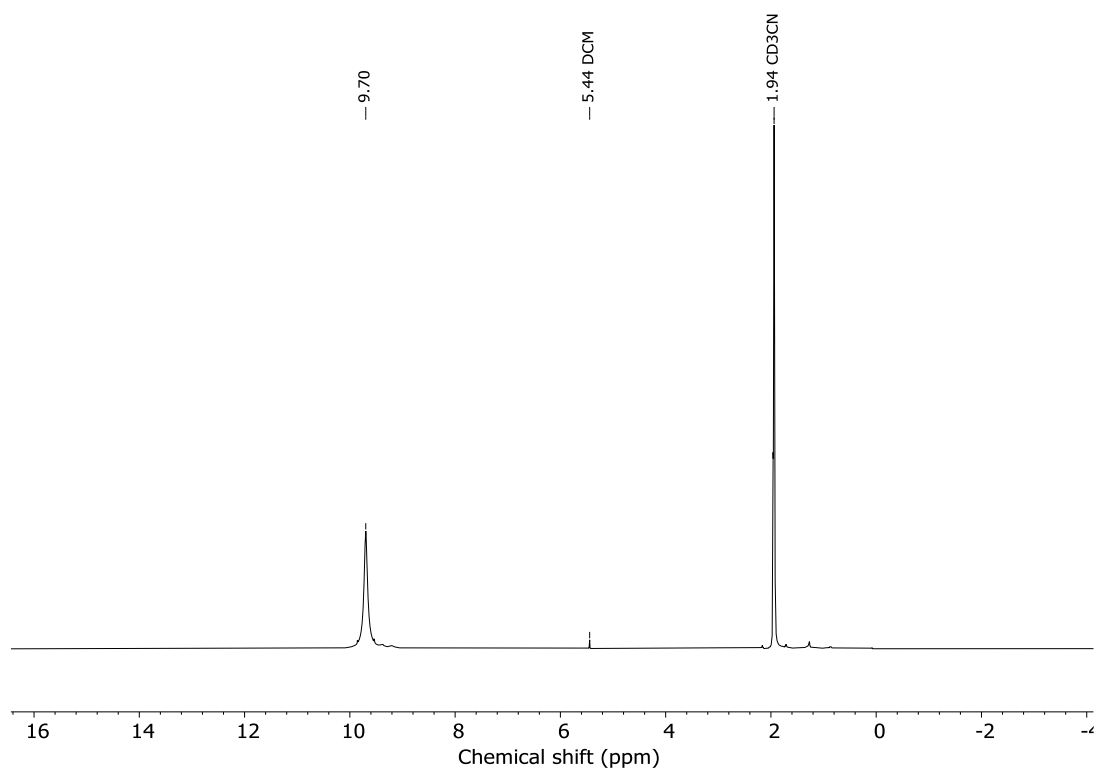
Figure S 9: ¹H NMR spectrum of carbonyl bis(carbamoylbromide) in acetonitrile-d3 at room temperature.
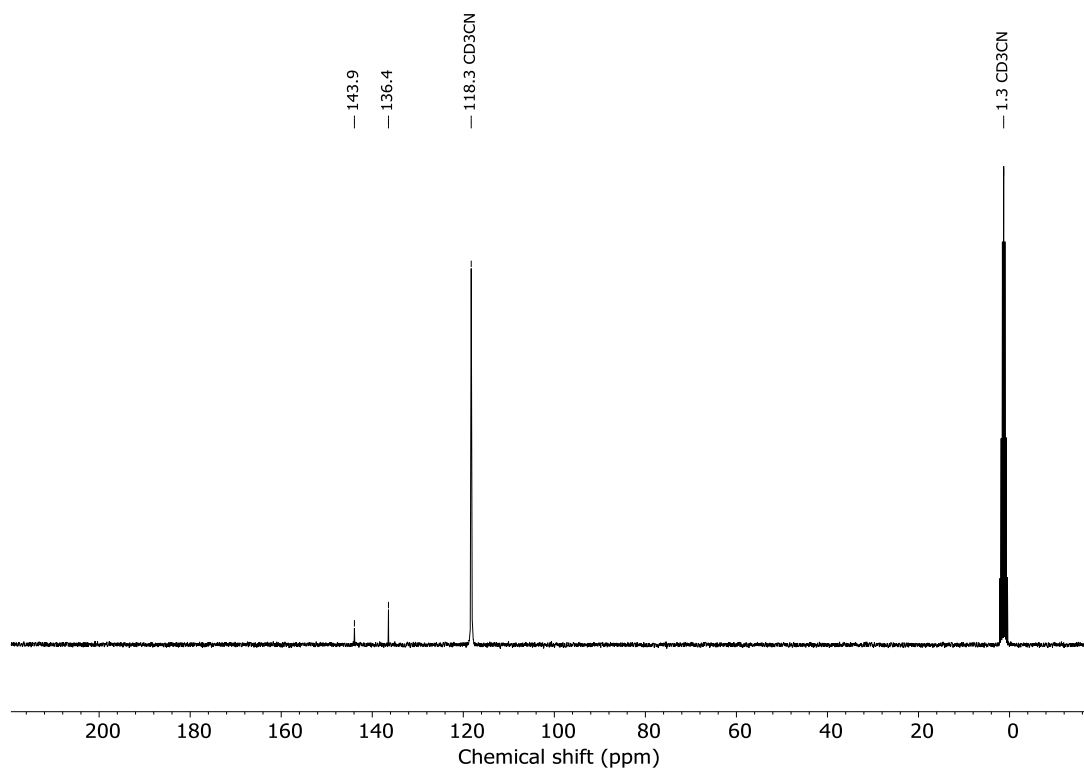
Figure S 10: ^{13}C NMR spectrum of carbonyl bis(carbamoylbromide) in acetonitrile-d3 at room temperature.
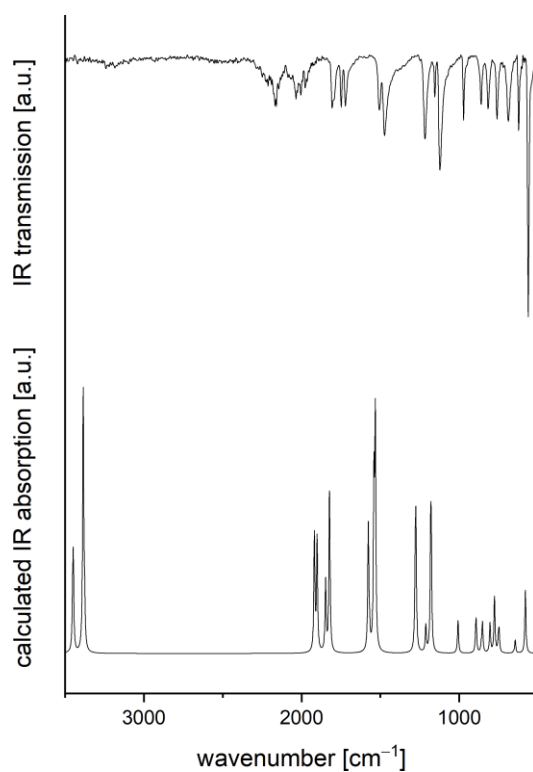
Figure S 11: Measured (top) room-temperature ATR-IR spectrum of carbonyl bis(carbamoylbromide) and its simulated spectrum (bottom).

1.6. Synthesis of carbonyl bis(carbamoyliodide) (4)

Hydrogen iodide gas was developed by dropping hydroiodic acid 57 % (30.0 mL, 227 mmol, 40 eq.) on P_4O_{10}. The hydrogen iodide gas was passed with a slow argon stream through P_4O_{10} to dry and into a solution of carbonyl diisocyanate (0.64 g, 5.68 mmol, 1 eq.) in 100 mL dichloromethane cooled to $-78\,°C$ for 2 h. The solution was warmed to $0\,°C$ and excess hydrogen iodide gas evaporated. Then the solvent was removed under reduced pressure, the precipitated, colorless powder dried *in vacuo* and carbonyl bis(carbamoyliodide) (1.35 g, 3.67 mmol, 65 %) collected. Carbonyl bis(carbamoyliodide) is very sensitive and we were not able to grow crystals suitable for X-ray diffraction. Due to the low carbon content by weight%, the calibration value for C for the elemental analysis was undershot. As such the value is of limited reliability.

^{1}H NMR (300 MHz, CD_3CN, r.t.) δ / ppm = 9.52 (N*H*).

^{13}C NMR (75 MHz, CD_3CN, r.t.) δ / ppm = 142.4 (*C*=O), 115.4 (*C*−I).

CHNS (calc./found) C: 9.80 / 10.75, H: 0.55 / 0.072, N: 7.62 / 7.93.
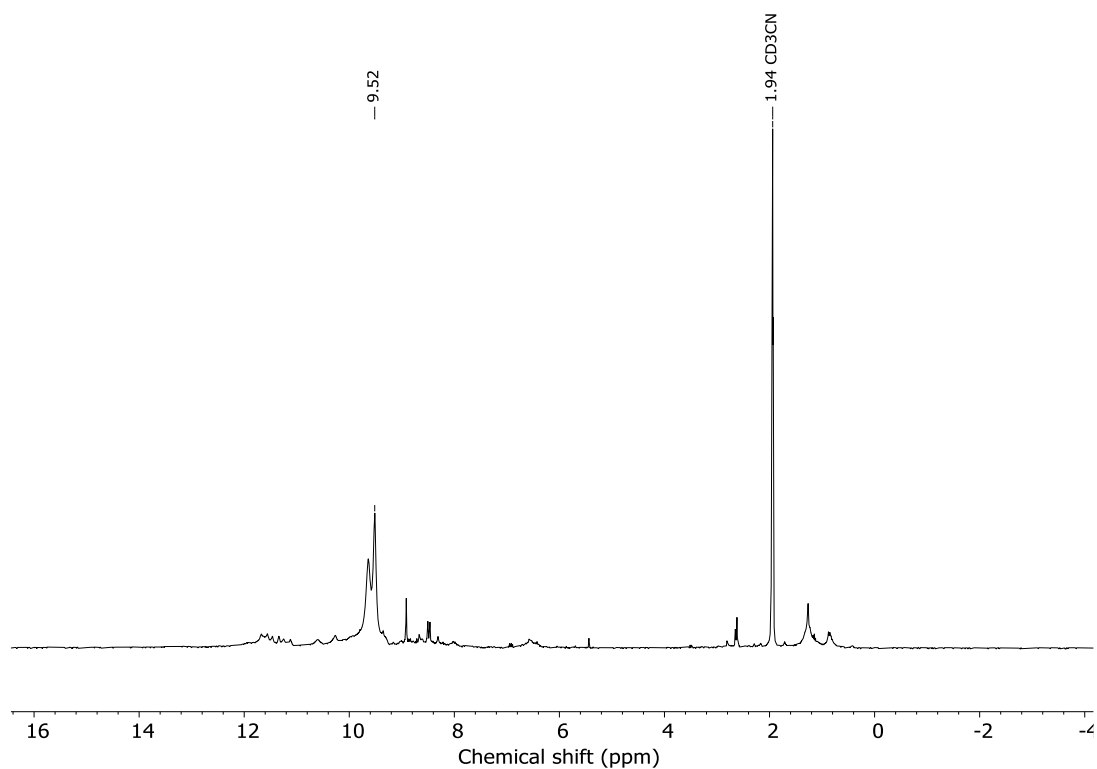
Figure S 12: ^{1}H NMR spectrum of carbonyl bis(carbamoyliodide) in acetonitrile-d3 at room temperature. The substance is highly sensitive and decomposes quickly in solution, leading to additional signals which cannot be attributed.
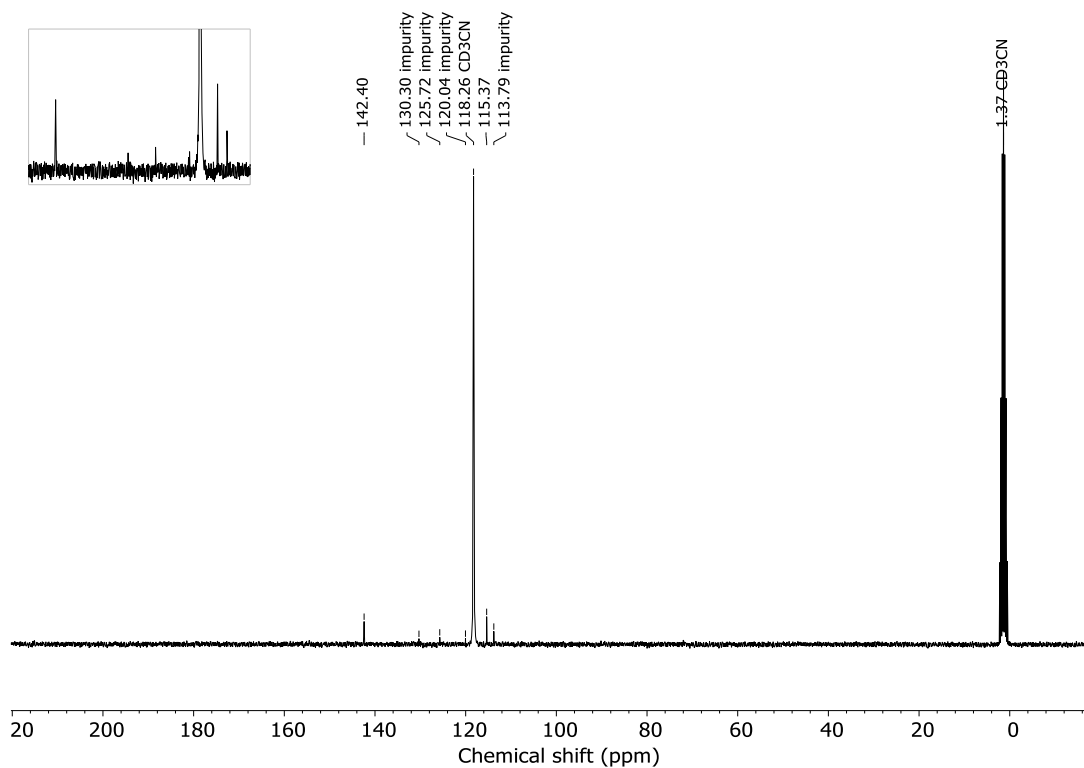
Figure S 13: ^{13}C NMR spectrum of carbonyl bis(carbamoyliodide) in acetonitrile-d3 at room temperature. The substance is highly sensitive and decomposes quickly in solution, leading to additional signals which cannot be attributed. The inset shows a magnification of the region 110 to 150 ppm.
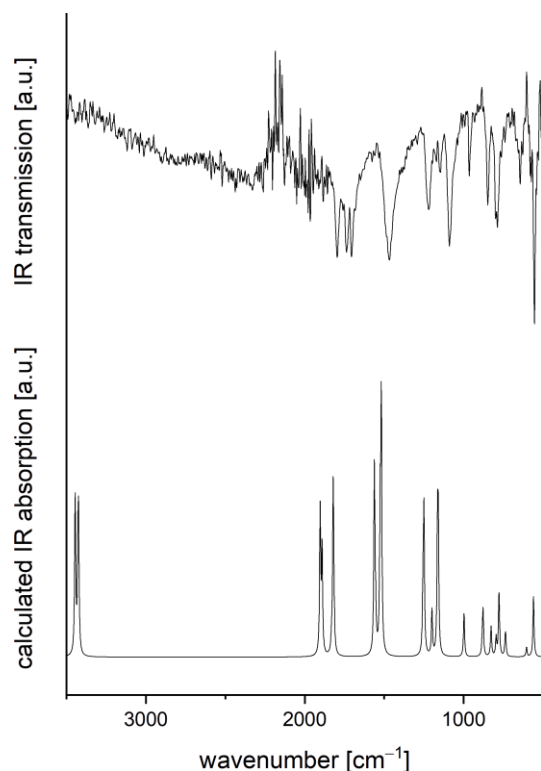
Figure S 14: Measured (top) room-temperature ATR-IR spectrum of carbonyl bis(carbamoyliodide) and its simulated spectrum (bottom) based on the crystal structure of carbonyl bis(carbamoylbromide).

1.7. Reaction between carbonyl diisothiocyanate and hydrogen fluoride gas

Carbonyl diisothiocyanate (1.4 g, 9.7 mmol, 1 eq.) was distilled into a PFA reaction vessel, and an excess of anhydrous HF (2.0 mL, 1.9 g, 95 mmol, 9.8 eq.) was condensed at –196 °C onto the solid. When the reaction mixture was warmed up to room temperature a vigorous reaction at the phase boundary between the liquid carbonyl diisothiocyanate covered by liquid anhydrous HF was observed and yellow crystalline solid was formed. When anhydrous HF was removed under reduced pressure, the yellow solid apparently decomposed and a red solid (1.18 g) remained. It was analyzed as 2,3,5,6-tetrahydro-2,6-dithioxo-4*H*-1,3,5-thiadiazine-4-one *via* ^{13}C-NMR spectroscopy. The red color is most likely from the decomposition product pararhodane $(SCN)_x$. The procedure was repeated a second time, and the observed yellow crystals were transferred directly from anhydrous HF solution into perfluorinated oil (Fomblin YR 1800). A suitable single crystal for X-ray crystal structure determination was selected under

the microscope. Crystal structure determination showed the isolated compound to be 2,3,5,6-tetrahydro-2,6-dithioxo-4H-1,3,5-thiadiazine-4-one.
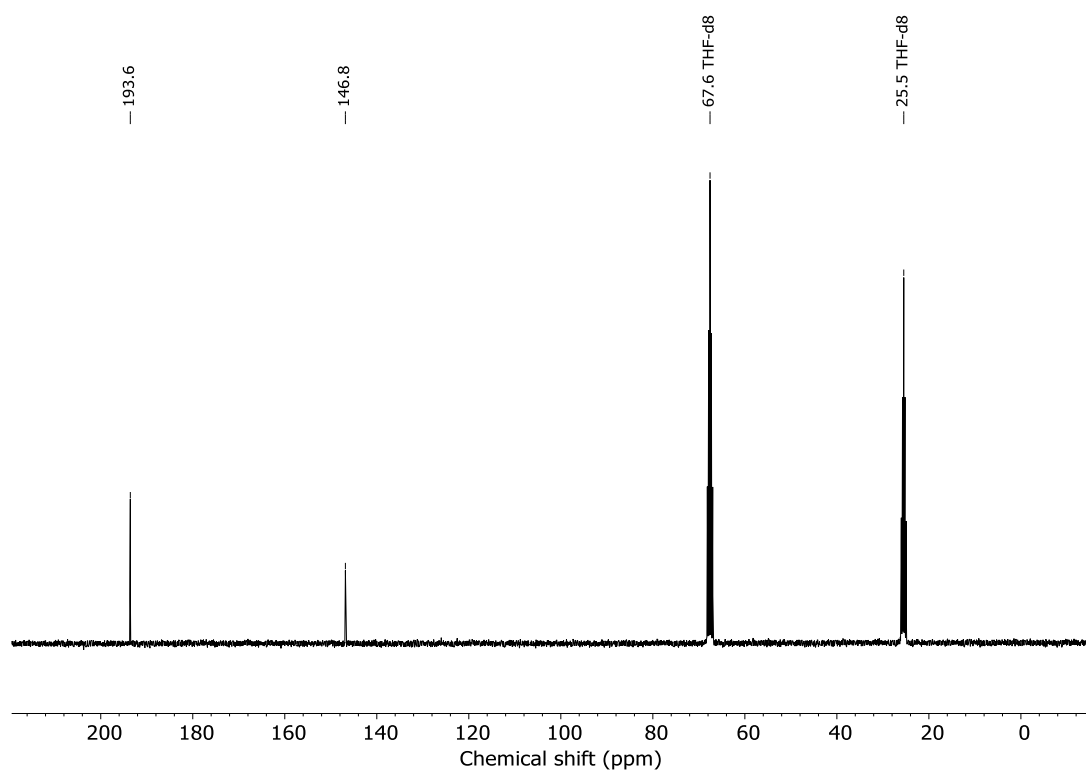
Figure S 15: ^{13}C NMR spectrum of 2,3,5,6-tetrahydro-2,6-dithioxo-4H-1,3,5-thiadiazine-4-one in THF-d8 at room temperature.

1.8. Synthesis of 6-chloro-2,3-dihydro-2-thioxo-4H-1,3,5-thiadiazin-4-one (5)

Carbonyl diisothiocyanate (2.92 g, 20.3 mmol, 1 eq.) dissolved in 100 mL diethyl ether was cooled to 0 °C. Hydrogen chloride gas was first passed through P_4O_{10} to dry and subsequently bubbled through the solution for 3 h. The solution was allowed to warm to room temperature and stirred for 20 h. The solvent was removed under reduced pressure and the precipitate dried *in vacuo*. 6-Chloro-2,3-dihydro-2-thioxo-4H-1,3,5-thiadiazin-4-one (3.53 g, 19.5 mmol, 96 %) was received as light-yellow powder. Crystals suitable for single crystal X-ray measurements could be obtained by recrystallizing from dichloromethane.

¹H NMR (300 MHz, THF-d8, r.t.) δ / ppm = 12.98 (N*H*).

¹³C NMR (75 MHz, THF-d8, r.t.) δ / ppm = 190.4 (*C*=S), 167.5 (*C*−Cl), 150.8 (*C*=O).

CHNS (calc./found) C: 19.95 / 19.86, H: 0.56 / 0.87, N: 15.51 / 15.67, S: 35.50 / 35.42.
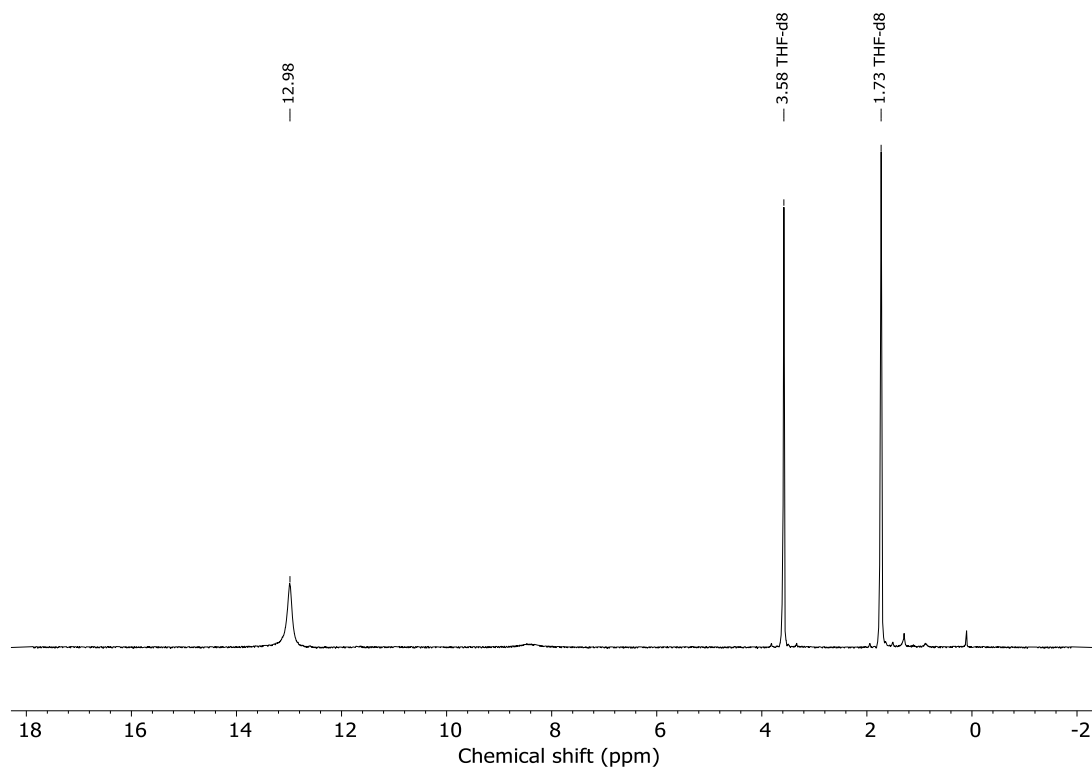
Figure S 16: ¹H NMR spectrum of 6-chloro-2,3-dihydro-2-thioxo-4*H*-1,3,5-thiadiazin-4-one in THF-d8 at room temperature.
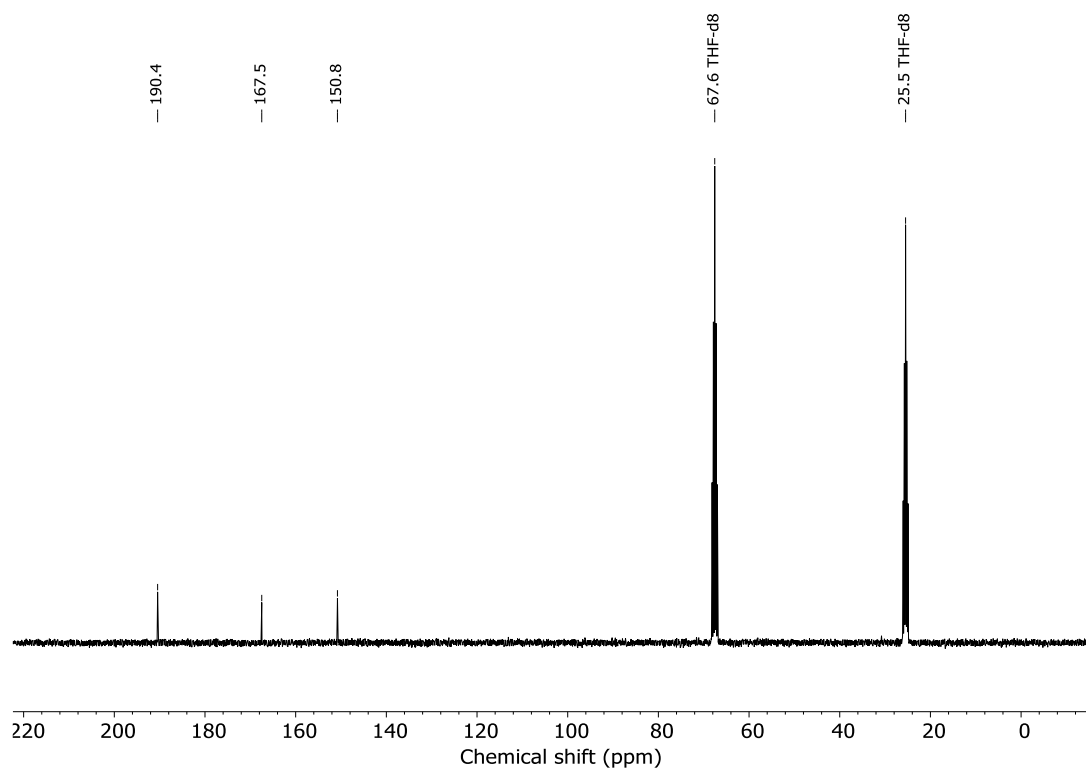
Figure S 17: ^{13}C NMR spectrum of 6-chloro-2,3-dihydro-2-thioxo-4*H*-1,3,5-thiadiazin-4-one in THF-d8 at room temperature.
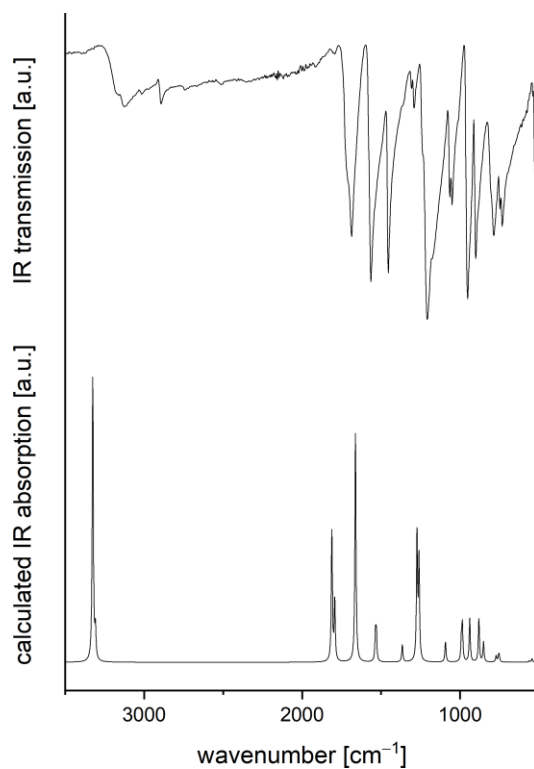
Figure S 18: Measured (top) room-temperature ATR-IR spectrum of 6-chloro-2,3-dihydro-2-thioxo-4*H*-1,3,5-thiadiazin-4-one and its simulated spectrum (bottom).

1.9. Synthesis of 6-bromo-2,3-dihydro-2-thioxo-4*H*-1,3,5-thiadiazin-4-one (6)

Hydrogen bromide gas was developed by dropping hydrobromic acid 48 % (8.90 mL, 78.7 mmol, 10 eq.) on P_4O_{10}. The gas was passed through P_4O_{10} with a slow argon stream to dry and bubbled into a solution of carbonyl diisothiocyanate (1.13 g, 7.84 mmol, 1 eq.) in 20 mL diethyl ether at 0 °C. The argon stream was maintained for 90 min. Then the solvent was removed under reduced pressure. The precipitate was washed with *n*-hexane and dried *in vacuo*. 6-Bromo-2,3-dihydro-2-thioxo-4*H*-1,3,5-thiadiazin-4-one (1.20 g, 5.33 mmol, 68 %) was received as yellow powder. Single crystals suitable for X-ray data collection were obtained by layering a THF solution with *n*-hexane.

¹H NMR (300 MHz, THF-d8, r.t.) δ / ppm = 12.97 (N*H*).

¹³C NMR (75 MHz, THF-d8, r.t.) δ / ppm = 191.6 (*C*=S), 157.7 (*C*−Br), 149.4 (*C*=O).

CHNS (calc./found) C: 16.01 / 16.68, H: 0.45 / 0.97, N: 12.45 / 13.44. S: 28.49 / 28.51.
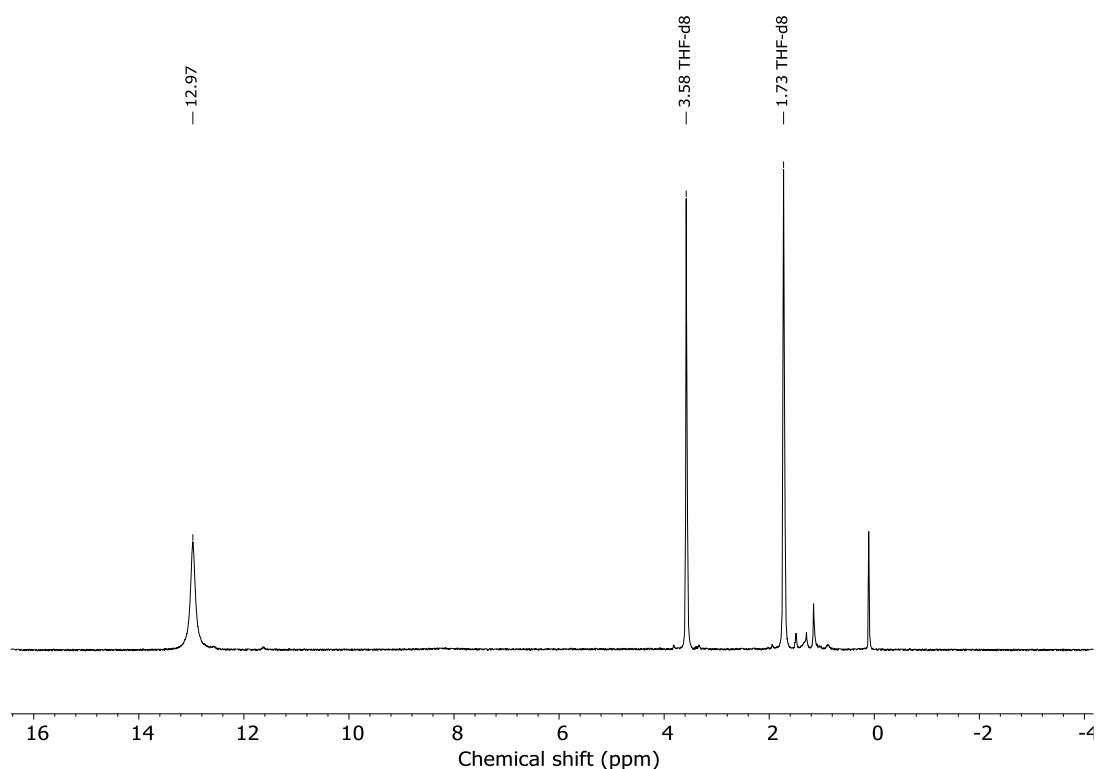
Figure S 19: ¹H NMR spectrum of 6-bromo-2,3-dihydro-2-thioxo-4*H*-1,3,5-thiadiazin-4-one in THF-d8 at room temperature.
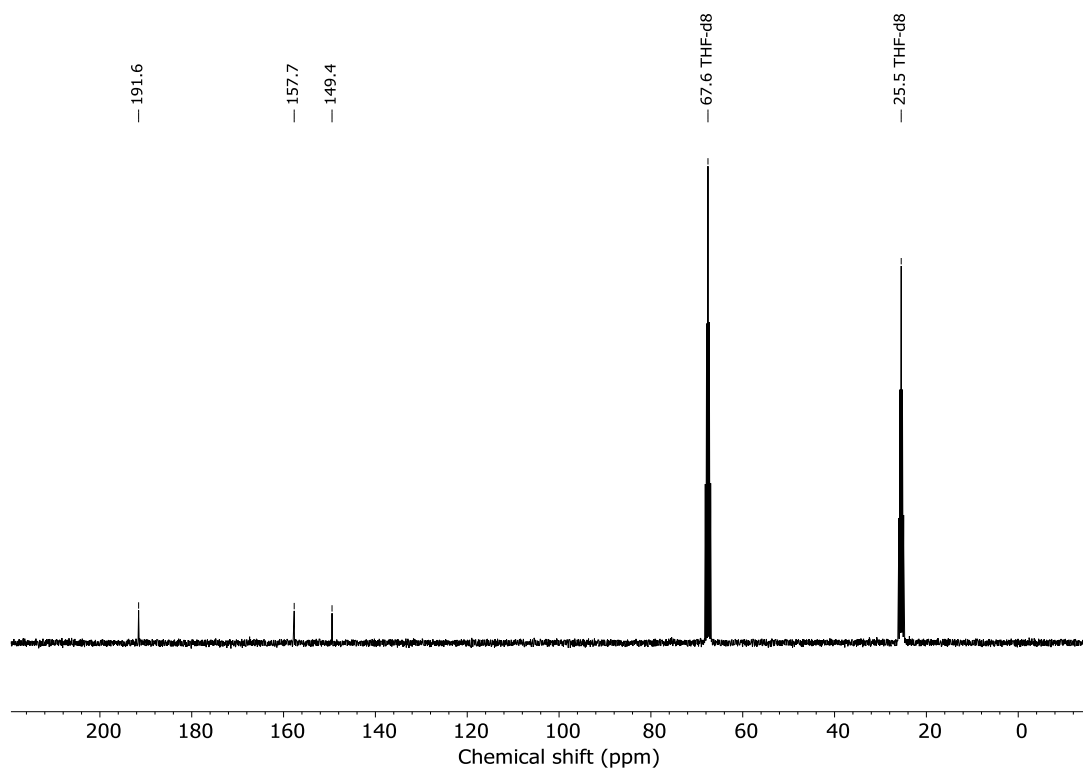
Figure S 20: ^{13}C NMR spectrum of 6-bromo-2,3-dihydro-2-thioxo-4*H*-1,3,5-thiadiazin-4-one in THF-d8 at room temperature.
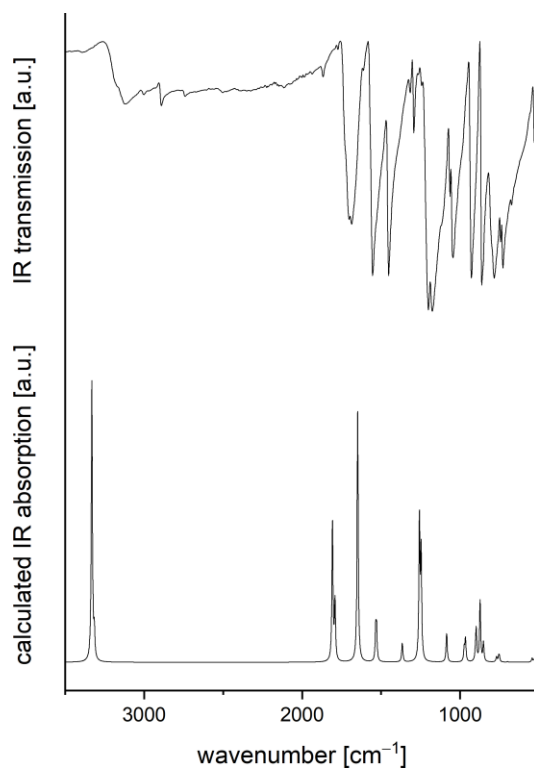
Figure S 21: Measured (top) room-temperature ATR-IR spectrum of 6-bromo-2,3-dihydro-2-thioxo-4*H*-1,3,5-thiadiazin-4-one and its simulated spectrum (bottom).

1.10. Reactions between carbonyl diisothiocyanate and hydrogen iodide towards 6-iodo-2,3-dihydro-2-thioxo-4*H*-1,3,5-thiadiazin-4-one

a) Into a solution of carbonyl diisothiocyanate (0.72 g, 5.0 mmol, 1 eq.) in 20 mL dichloromethane cooled to 0 °C hydrogen iodide gas was bubbled. The gas was developed by dropping hydroiodic acid 57 % (6.6 mL, 50 mmol, 10 eq.) onto P_4O_{10} and dried by passing it through P_4O_{10} in a slow argon stream. The solution immediately turned dark yellow and got turbid. After stirring for 1 h the solvent was removed. A brown powder was obtained, which decomposed fast into a solid with metallic luster (see Figure S22 a). 6-Iodo-2, 3-dihydro-2-thioxo-4*H*-1,3,5-thiadiazin-4-one could not be detected with NMR analysis. Reducing the equivalents of hydrogen iodide (2 eq.) or reducing the reaction temperature (−78 °C or −94 °C) led to the same result.

b) Hydrogen iodide gas (8 eq.) was developed as described in a) and condensed onto frozen (−196 °C) carbonyl diisothiocyanate (0.58 g, 4.0 mmol, 1 eq.). It was then warmed up to −94 °C and slowly warmed to room temperature. During this the reaction mixture turned red brown. A light brown to dark red residue was obtained (see Figure S22 b). NMR analysis only showed starting material. The residue was treated with *n*-hexane, showing a pink color that indicates elemental iodine.

c) To carbonyl diisothiocyanate (0.36 g, 2.5 mmol, 1 eq.) dissolved in 5 mL dichloromethane and cooled to −78 °C, a cooled (−78 °C) solution of hydrogen halide 1 molar in dichloromethane (10 mL, 10 mmol, 4 eq.) was added. The solution turned yellow immediately and was stirred for 5 minutes. The now orange, turbid solution was either filtered of or treated with *n*-hexane. Filtration afforded a yellow filtrate, which rapidly turned orange and turbid again. Removal of the solvent at −78 °C gave a dark red oil, which was characterized (^{1}H- and ^{13}C NMR) as starting material, presumably with pararhodane and iodine as side products.

Adding *n*-hexane to precipitate the product led to decomposition and formation of elemental iodine as evident by the pink hue of the *n*-hexane (see Figure S22 c).
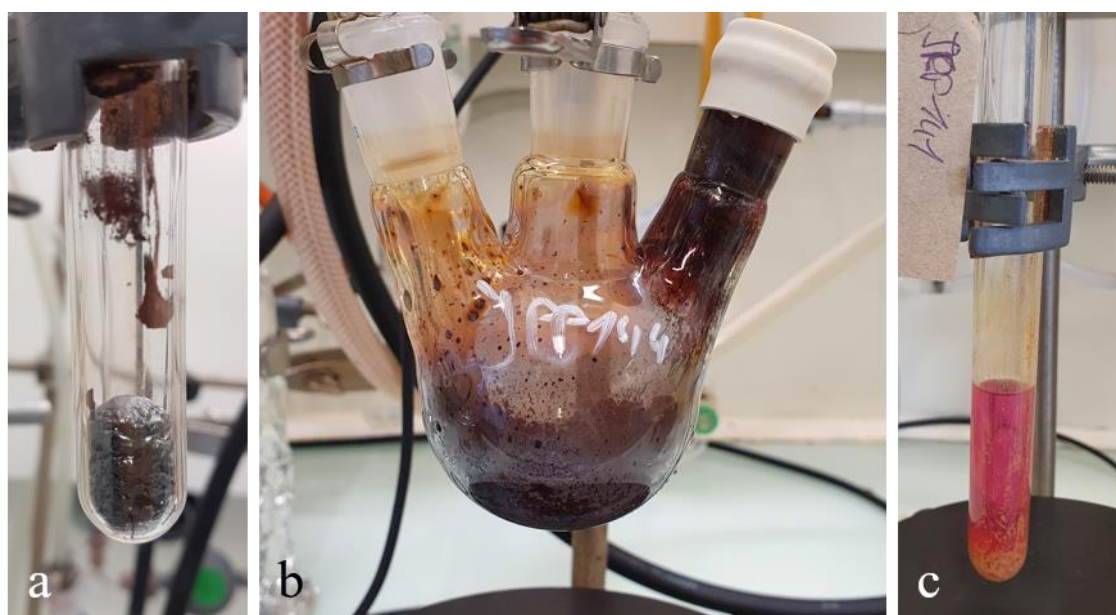
Figure S 22: Residues of reactions between carbonyl diisothiocyanate and hydrogen iodide. a) Decomposition product with metallic luster. b) Solvent free reaction product. c) Pink hue of *n*-hexane solution indicates elemental iodine.

1.11. Reactions of 6-chloro-2,3-dihydro-2-thioxo-4*H*-1,3,5-thiadiazin-4-one with fluoride and iodide salts towards 6-fluoro-2,3-dihydro-2-thioxo-4*H*-1,3,5-thiadiazin-4-one and 6-iodo-2,3-dihydro-2-thioxo-4*H*-1,3,5-thiadiazin-4-one

We tried to carry out Finkelstein reactions to substitute the chlorine atom in 6-chloro-2,3-dihydro-2-thioxo-4*H*-1,3,5-thiadiazin-4-one with fluorine or iodine atoms in acetone solution. Unfortunately, 6-chloro-2,3-dihydro-2-thioxo-4*H*-1,3,5-thiadiazin-4-one reacts with acetone giving untraceable decomposition products. We then tried to use SO_2 as solvent, but found that 6-chloro-2,3-dihydro-2-thioxo-4*H*-1,3,5-thiadiazin-4-one is insoluble.

a) NH_4I (290 mg, 2.00 mmol, 1 eq.) was suspended in 5 mL THF. A solution of 6-chloro-2,3-dihydro-2-thioxo-4*H*-1,3,5-thiadiazin-4-one (361 mg, 2.00 mmol, 1 eq.) in 5 mL THF was added. The reaction mixture turned from yellow to red-brown within 5 minutes. It was stirred

for 2.5 h and filtered. In the residue NH$_4$Cl could be detected via powder X-ray diffraction analysis. The red filtrate was concentrated to 2 mL and treated with 6 mL *n*-hexane. We did not observe any precipitation. The reaction only generated untraceable decomposition products.

b) 6-Chloro-2,3-dihydro-2-thioxo-4*H*-1,3,5-thiadiazin-4-one (181 mg, 1.00 mmol, 1 eq.) and AgF (127 mg, 1.00 mmol, 1 eq.) were suspended in 12 mL acetonitrile and stirred for two hours. The solvent was removed, the residue suspended in THF and filtered. AgCl was detected as a side product in the filter cake by powder X-ray diffraction analysis. The solvent was removed from the filtrate, affording a yellow solid. ^{13}C-NMR spectroscopy showed signals of the starting material and 2,3,5,6-tetrahydro-2,6-dithioxo-4*H*-1,3,5-thiadiazine-4-one (see below). The solid was extracted with 1.5 mL 1,4-dioxane. 2,3,5,6-tetrahydro-2,6-dithioxo-4*H*-1,3,5-thiadiazine-4-one was precipitated from the solution at 2 °C with 10 mL *n*-hexane.

2. Crystallographic data

Single crystal X-ray structure determination: Single-crystal X-ray diffraction data were collected using either an IPDS 2 or an IPDS 2T (Stoe, Darmstadt) diffraction system equipped with graphite monochromated Mo K_α radiation ($\lambda = 0.71073$ Å). Further measurements were performed on a Bruker d8-Quest (Bruker, Karlsruhe) diffraction system equipped with mirror monochromated Mo K_α radiation ($\lambda = 0.71073$ Å, Incoatec Microfocus Source) and a Photon 100 detector (CMOS).

Crystals were selected under Paratone-N oil, mounted on micromount loops and quench-cooled using an Oxford Cryosystems open flow N_2 cooling device. Data were collected at 100 K (if not stated otherwise) and processed using the X-Area program package (for datasets acquired with Stoe devices), including lattice parameter refinement and inter-frame scaling (which was carried out using LANA within X-Area). For datasets acquired with a Bruker d8-Quest, the APEX3 software suite was used for data processing. Structures were subsequently solved using Direct Methods (SHELXT)[3] and refined on F^2 with SHELXL[4] using the Olex2[5] user interface. The crystal structure drawings were generated with DIAMOND.[6]

Table S 1: Selected single crystal X-ray data collection and refinement parameters for carbonyl bis(carbamoylfluoride) (**1**, CDI-HF), carbonyl bis(carbamoylchloride) (**2**, CDI-HCl), carbonyl bis(carbamoylbromide) (**3**, CDI-HBr) and 6-chloro-2,3-dihydro-2-thioxo-4*H*-1,3,5-thiadiazin-4-one (**5**, CDIT-HCl).

	CDI-HF (**1**)	CDI-HCl (**2**)	CDI-HBr (**3**)	CDIT-HCl (**5**)
Formula	$C_3H_2F_2N_2O_3$	$C_3H_2Cl_2N_2O_3$	$C_3H_2Br_2N_2O_3$	C_3HClN_2OS2
CCDC	2228316	2228314	2228313	2228315
F. w. / g mol^{-1}	152.07	184.97	273.89	180.63
Crystal system	orthorhombic	triclinic	tetragonal	monoclinic
Space group	$P2_12_12_1$	$P\bar{1}$	$P4_1$	$P12_1/n1$
a / Å	4.6413(3)	4.8915(7)	7.9659(4)	7.0256(11)
b / Å	8.6734(6)	8.3623(11)	$= a$	5.2230(6)
c / Å	12.3970(9)	8.4998(11)	11.1269(6)	16.956(3)
α / °	90	66.843(10)	90	90
β / °	90	89.035(11)	90	98.966(13)
γ / °	90	83.972(11)	90	90
V / Å^3	499.05(6)	317.78(8)	706.06(8)	614.59(16)
Z	4	2	4	4
Radiation, λ / Å	0.71073	0.71073	0.71073	0.71073
Temp / K	100	100	100	100
ρ_{calc} / g cm^{-3}	2.024	1.933	2.577	1.952
μ / mm^{-1}	0.221	0.962	11.428	1.203
Reflections collected	50060	7614	5675	4219
Ind. Reflns. / Ind. Reflns gt	2665 / 2604	7614 / 5042	1905 / 1765	1624 / 1122
Parameters	100	91	92	86
R_{int} / $R_{(\sigma)}$ / %	2.63 / 1.02	3.96 / 8.14	2.25 / 1.93	5.88 / 3.12
$R1/wR2$,[a] $I \geq 2\sigma I$ / %	2.14 / 5.83	3.99 / 8.56	2.23 / 4.62	3.13 / 5.66
$R1/wR2$,[a] all data / %	2.21 / 5.87	7.47 / 10.13	2.68 / 4.74	6.35 / 6.25
GOF	1.113	0.916	1.049	0.921
Twin law	—	−1 0 0 0 1 0 0 0 −1	—	—
BASF	—	—[b]	—	—
Flack parameter	0.03(6)	—	0.003(15)	—

[a] $R1 = [\Sigma||F_o| - |F_c||]/\Sigma|F_o|$; $wR2 = \{[\Sigma w[(F_o)^2 - (F_c)^2]^2]/[\Sigma w(F_o^2)^2]\}^{1/2}$; $w = [\sigma^2(F_o)^2 + (AP)^2 + BP]^{-1}$, where $P = [(F_o)^2 + 2(F_c)^2]/3$ and the A and B values are 0.032600 and 0.046900 for CDI-HF, 0.051000 and 0 for CDI-HCl, 0.019900 and 1.08000 for CDI-HBr, and 0.030800 and 0 for CDIT-HCl. [b] Refined as a two component perfect twin with a HKLF 5 filetype.

Table S 2: Selected single crystal X-ray data collection and refinement parameters for 6-bromo-2,3-dihydro-2-thioxo-4*H*-1,3,5-thiadiazin-4-one (**6**, CDIT-HBr), 2,3,5,6-tetrahydro-2,6-dithioxo-4*H*-1,3,5-thiadiazine-4-one (CDIT-H2S lactame and lactime tautomer).

	CDIT-HBr (**6**)	CDIT-H2S lactame (**8a**)	CDIT-H2S lactime (**8b**)
Formula	$C_3HClN_2OS_2$	$C_3H_2N_2OS_3$	$C_3H_2N_2OS_3$
CCDC	2228319	2228317	2228318
F. w. / g mol^{-1}	225.09	178.25	178.25
Crystal system	monoclinic	monoclinic	monoclinic
Space group	$P12_1/n1$	$P2_1/c$	$P12_1/n1$
a / Å	7.1900(9)	9.4846(18)	7.0223(7)
b / Å	5.2336(4)	14.506(3)	5.2186(4)
c / Å	17.004(2)	14.687(4)	16.9913(18)
α / °	90	90	90
β / °	99.871(10)	96.035(18)	98.988(8)
γ / °	90	90	90
V / Å^3	630.38(12)	2009.5(8)	615.03(10)
Z	4	12	4
Radiation, λ / Å	0.71073	0.71073	0.71073
Temp / K	100	100	100
ρ_{calc} / g cm^{-3}	2.372	1.768	1.925
μ / mm^{-1}	7.088	1.017	1.108
Reflections collected	4133	10615	5215
Ind. Reflns. / Ind. Reflns gt	1687 / 1308	3502 / 1684	1648 / 1292
Parameters	83	244	83
R_{int}/ $R_{(\sigma)}$	4.10 / 3.71	14.96 / 14.10	3.66 / 3.33
$R1/wR2$,[a] $I \geq 2\sigma I$ / %	4.72 / 11.73	10.92 / 26.90	3.19 / 8.62
$R1/wR2$,[a] all data / %	6.40 / 12.71	21.96 / 31.92	4.56 / 9.11
GOF	1.016	1.075	1.051
Twin law	—	—	—
BASF	—	—	—
Flack parameter	—	—	—

[a] $R1 = [\Sigma||F_o| - |F_c||]/\Sigma|F_o|$; $wR2 = \{[\Sigma w[(F_o)^2 - (F_c)^2]^2]/[\Sigma w(F_o^2)^2]\}^{1/2}$; $w = [\sigma^2(F_o)^2 + (AP)^2 + BP]^{-1}$, where $P = [(F_o)^2 + 2(F_c)^2]/3$ and the A and B values are 0.086800 and 0 for CDIT-HBr, 0.16770 and 0 for CDIT-H2S lactame, 0.56800 and 0 for CDIT-H2S lactime.

2.1. Additional Pictures for carbonyl bis(carbamoylfluoride)
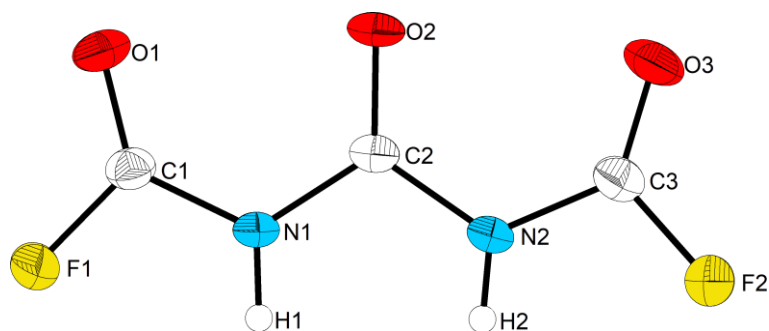
Figure S 23: Molecular structure of carbonyl bis(carbamoylfluoride) in the single crystal drawn with 70% displacement ellipsoids at 100 K. H-Atoms drawn with arbitrary radii
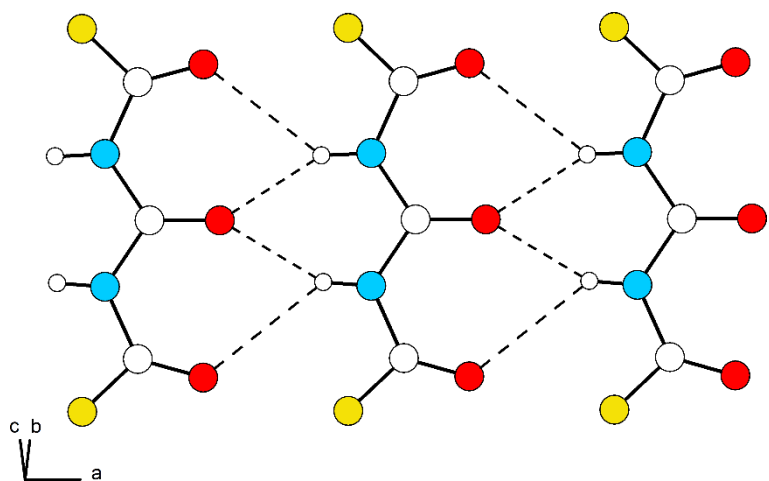
Figure S 24: Intermolecular H-bonding in carbonyl bis(carbamoylfluoride) along [100], viewed approximately along [011]. Atoms are drawn with arbitrary radii. Color code: C white, N blue, O red, F gold, H white (small).
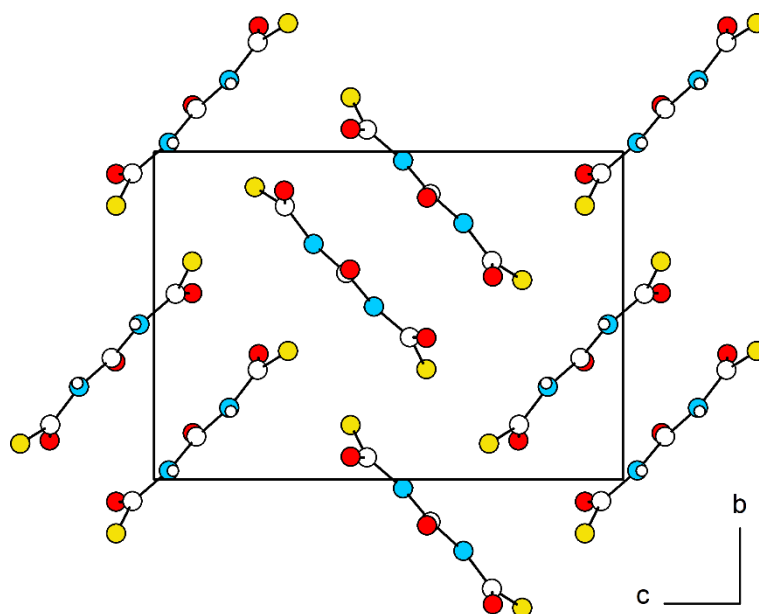
Figure S 25: Packing of carbonyl bis(carbamoylfluoride) viewed along [100]. Color code: C white, N blue, O red, F gold, H white (small). Atoms are drawn with arbitrary radii.
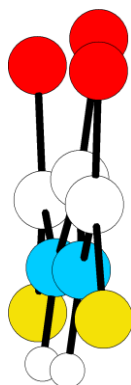
Figure S 26: Side view of a single molecule of carbonyl bis(carbamoylfluoride). All Atoms but the central C=O moiety and the H atoms lie in one plane with the C=O moiety tilted by 3.05(11)° with respect to the plane. Color code: C white, N blue, O red, F gold, H white (small). Atoms are drawn with arbitrary radii.

2.2. Additional Pictures for carbonyl bis(carbamoylchloride)
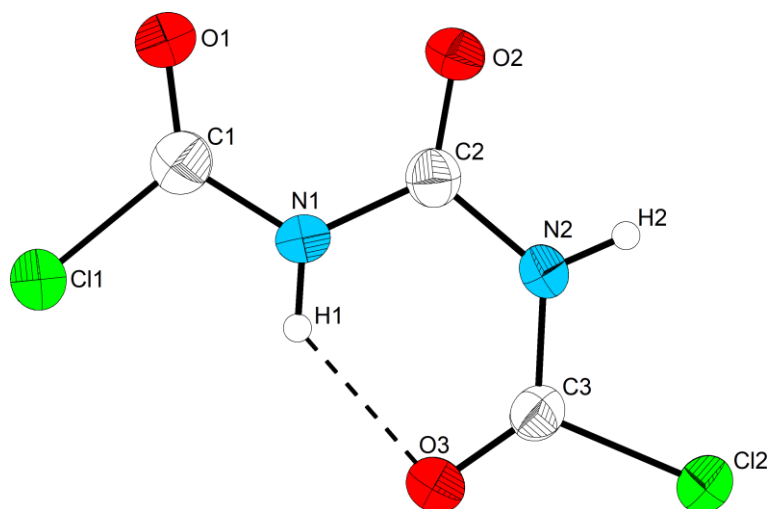
Figure S 27: Molecular structure of carbonyl bis(carbamoylchloride) in the single crystal drawn with 75% displacement ellipsoids at 100 K. Intramolecular H-bond drawn in dashed.
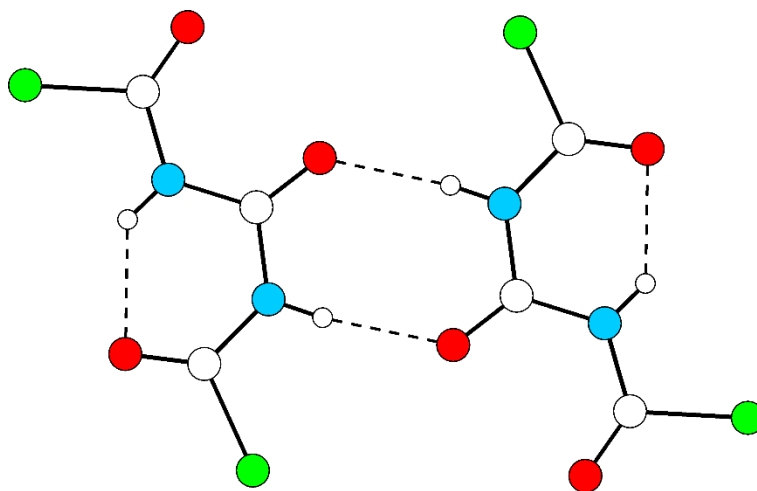
Figure S 28: Dimer of carbonyl bis(carbamoylchloride) connected through intermolecular H-bonds (shown as dashes). Color code: C white, N blue, O red, Cl green, H white (small). Atoms are drawn with arbitrary radii.
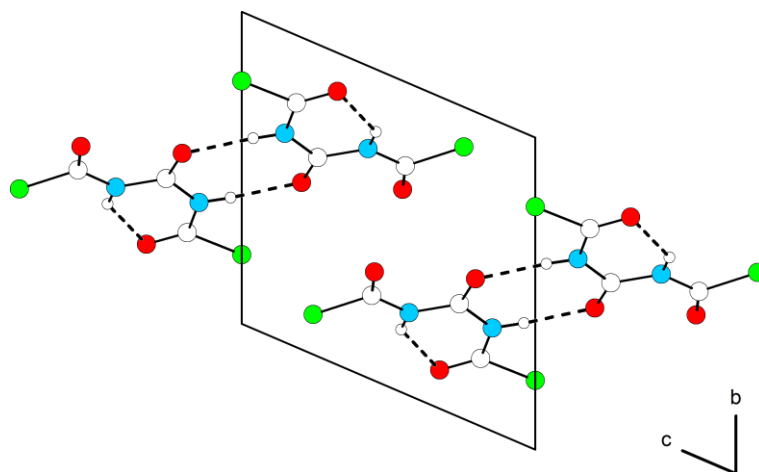
Figure S 29: Packing of carbonyl bis(carbamoylchloride) viewed along [100]. The carbonyl bis(carbamoylchloride) dimers are stacked along [100]. H-bonds are shown dashed. Color code: C white, N blue, O red, Cl green, H white (small). Atoms are drawn with arbitrary radii.
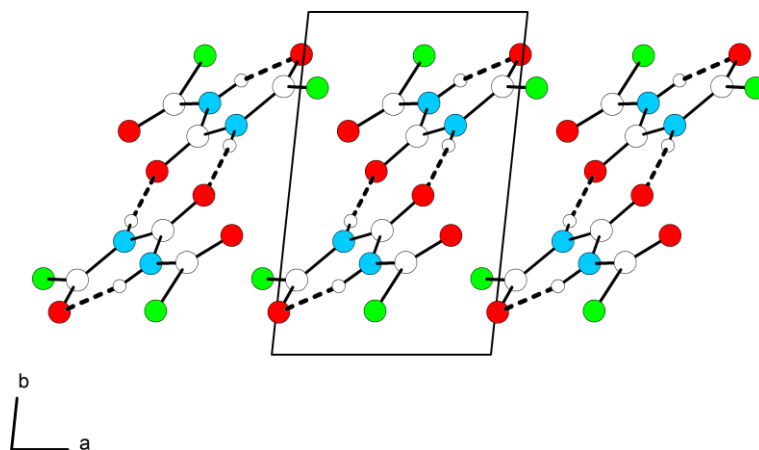
Figure S 30: Packing of carbonyl bis(carbamoylchloride) viewed along [001]. Colour code: C white, N blue, O red, Cl green, H white (small). Atoms are drawn with arbitrary radii.

2.3. Additional Pictures for carbonyl bis(carbamoylbromide)
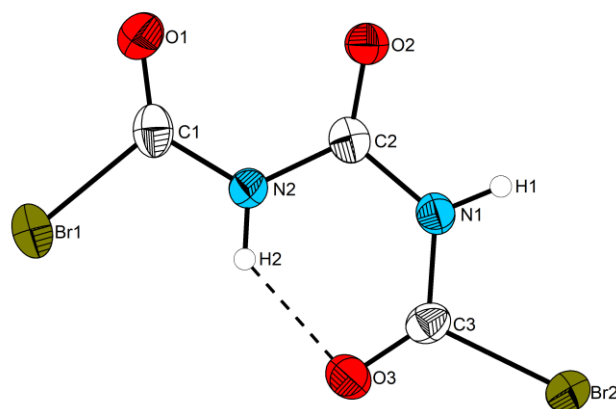
Figure S 31: Molecular structure of carbonyl bis(carbamoylbromide) in the single crystal drawn with 75% displacement ellipsoids at 100 K. Intramolecular H-bond drawn in dashed.
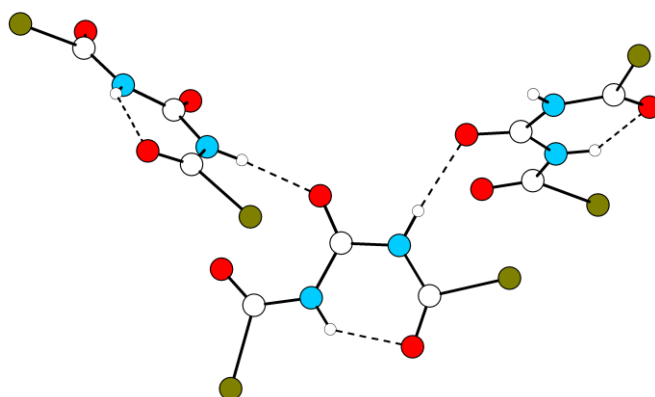
Figure S 32: Section of the H-bonding network in carbonyl bis(carbamoylbromide). Each molecule is connected to two other molecules via N–H···O hydrogen bonds. The molecules form a 4_1 screw along the [001] axis. Color code: C white, N blue, O red, Br brown, H white (small). Atoms are drawn with arbitrary radii.
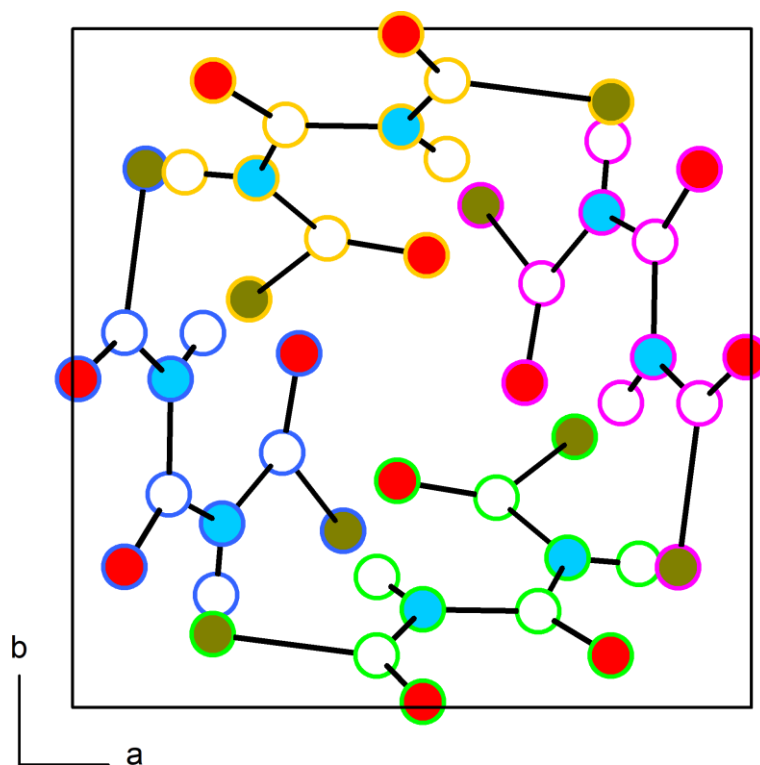
Figure S 33: Crystal structure of carbonyl bis(carbamoylbromide) viewed along [001], emphasizing the 4_1 screw axis. Barycenter of the molecules lie approximately on $z = 0$ (blue outline), $z = 0.25$ (green outline), $z = 0.5$ (purple outline) and $z = 0.75$ (orange outline). Colour code: C white, N blue, O red, Br brown, H white (small). Atoms are drawn with arbitrary radii.

2.4. Additional Pictures for 6-chloro-2,3-dihydro-2-thioxo-4*H*-1,3,5-thiadiazin-4-one and 6-bromo-2,3-dihydro-2-thioxo-4*H*-1,3,5-thiadiazin-4-one
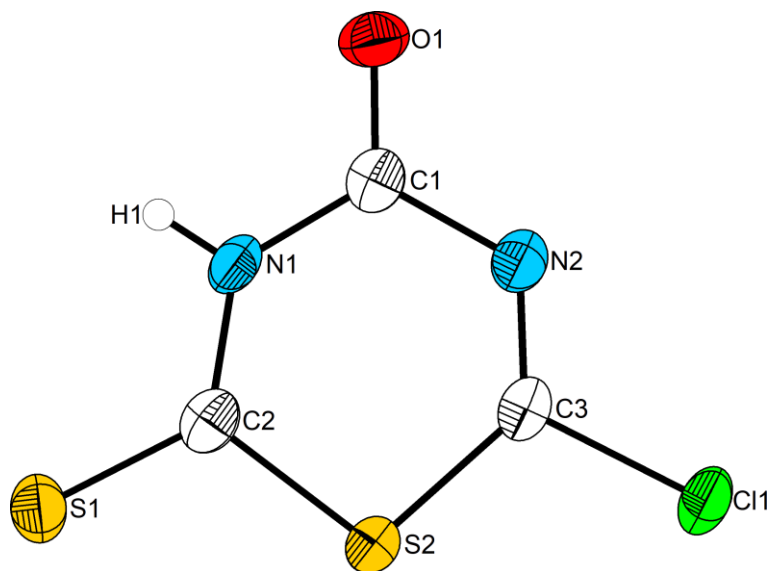
Figure S 34: Molecular structure of 6-chloro-2,3-dihydro-2-thioxo-4*H*-1,3,5-thiadiazin-4-one in the single crystal drawn with 75% displacement ellipsoids.
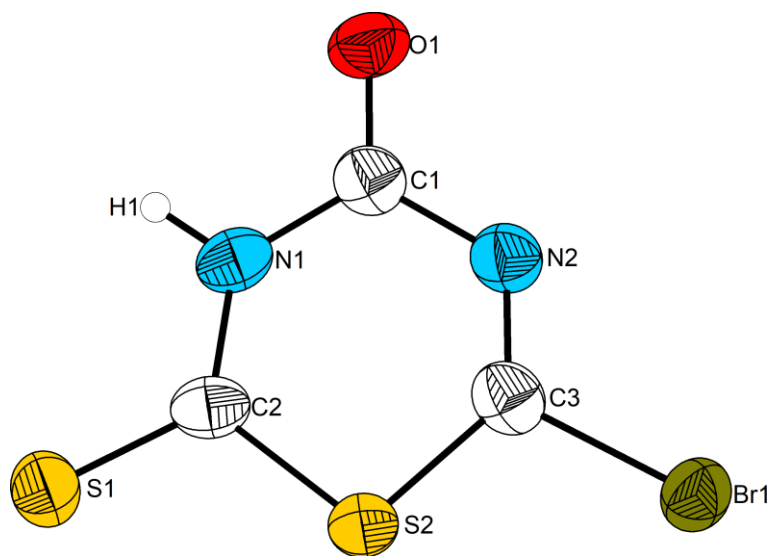
Figure S 35: Molecular structure of 6-bromo-2,3-dihydro-2-thioxo-4*H*-1,3,5-thiadiazin-4-one in the single crystal drawn with 75% displacement ellipsoids. Colour code: C white, N blue, O red, Br brown, S gold, H white (small).
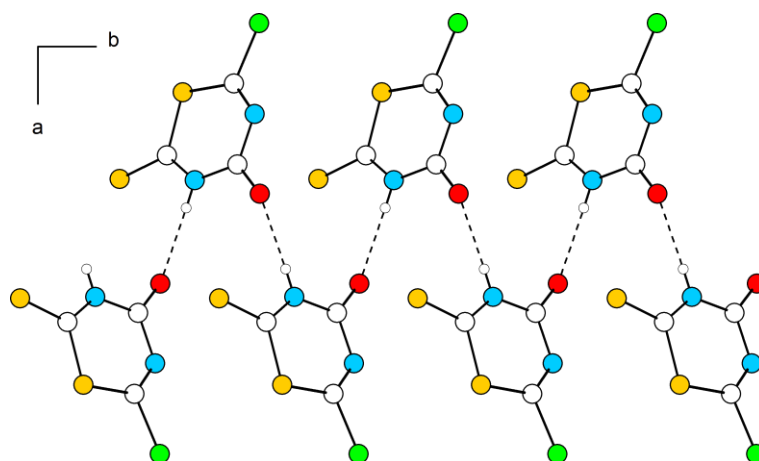
Figure S 36: Section of the H-bonding ribbon in 6-chloro-2,3-dihydro-2-thioxo-4*H*-1,3,5-thiadiazin-4-one (6-bromo-2,3-dihydro-2-thioxo-4*H*-1,3,5-thiadiazin-4-one crystallizes isotypic) forming columns extending along [010], viewed along [001]. Each molecule is connected to two other molecules via N−H···O hydrogen bond. Colour code: C white, N blue, O red, Cl green, S gold, H white (small). Atoms are drawn with arbitrary radii.
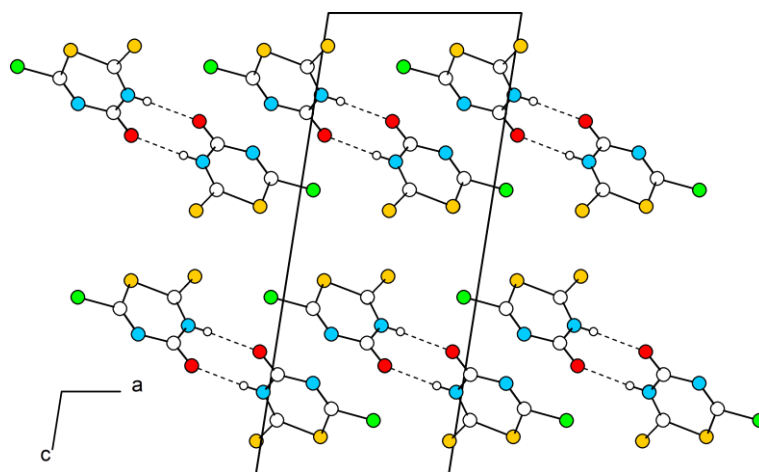
Figure S 37: Crystal structure of 6-chloro-2,3-dihydro-2-thioxo-4*H*-1,3,5-thiadiazin-4-one (6-bromo-2,3-dihydro-2-thioxo-4*H*-1,3,5-thiadiazin-4-one crystallizes isotypic) viewed along [010]. The columns form the motif of a rectangular rod packing. Atoms are drawn with arbitrary radii.

2.5. Crystal structure description of 2,3,5,6-tetrahydro-2,6-dithioxo-4*H*-1,3,5-thiadiazine-4-one

2.5.1. Thiolactime tautomer

The thiolactime tautomer of 2,3,5,6-tetrahydro-2,6-dithioxo-4*H*-1,3,5-thiadiazine-4-one crystallizes in the monoclinic crystal system with space group $P12_1/n1$ and one crystallographically independent molecule in the unit cell. The molecule is almost planar with solely the H3 position being significantly deflected from the plane. Including H3, the molecule approximates $C1$ as point group, excluding H3 it approximates point group C_s. Interatomic distances within the thiadiazines ring are similar to compounds 6-chloro-2,3-dihydro-2-thioxo-4*H*-1,3,5-thiadiazin-4-one and 6-bromo-2,3-dihydro-2-thioxo-4*H*-1,3,5-thiadiazin-4-one. d(C2=S1) = 1.641(2) Å indicates a double bond and d(C3–S3) = 1.723(2) Å a single bond.

2,3,5,6-tetrahydro-2,6-dithioxo-4H-1,3,5-thiadiazine-4-one forms an intricate H-bonding motif with both H atoms participating. Each individual molecule is connected to four other molecules: The NH group connects to one adjacent molecule *via* its O atom, the SH group to one other molecule again *via* its O atom. In turn the O atom connects to two adjacent molecules *via* one NH and SH group, respectively. Thus, sheets are formed that lie parallel to the crystallographic *ab*-plane at $z = 1/4$. The individual sheets adopt $p2_111$ layer group symmetry.
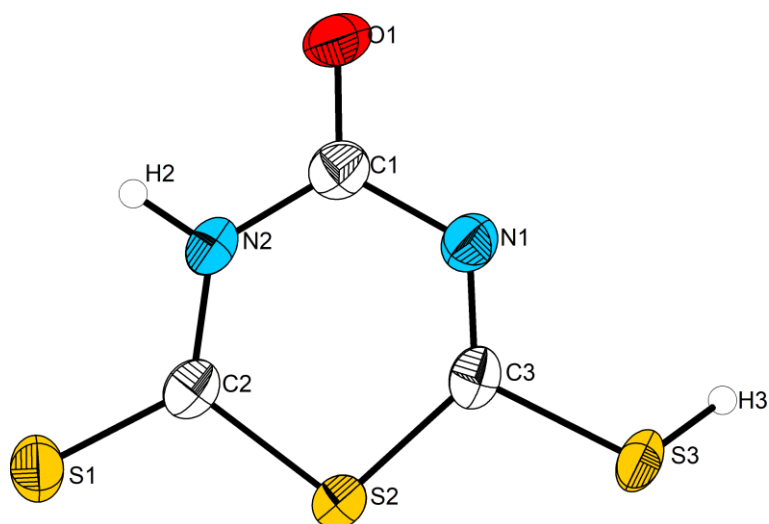
Figure S 38: Molecular structure of 2,3,5,6-tetrahydro-2,6-dithioxo-4H-1,3,5-thiadiazine-4-one in the single crystal drawn with 75% displacement ellipsoids.
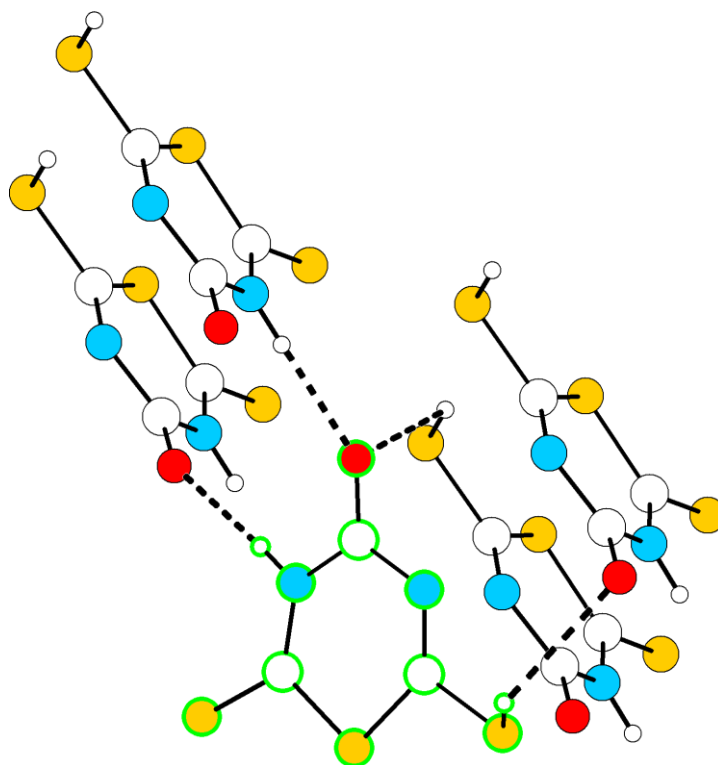
Figure S 39: Section of the H-bonding in 2,3,5,6-tetrahydro-2,6-dithioxo-4H-1,3,5-thiadiazine-4-one. Each molecule (one highlighted with green outlines) is connected to four other molecules *via* an extended S−H···O and an N–H···O bonding network. Colour code: C white, N blue, O red, S gold, H white (small). Atoms are drawn with arbitrary radii.
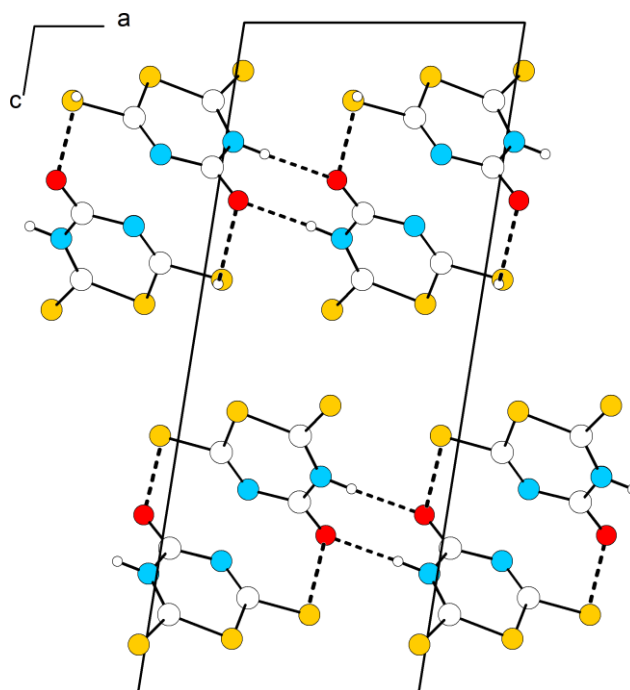
Figure S 40: Crystal structure of 2,3,5,6-tetrahydro-2,6-dithioxo-4*H*-1,3,5-thiadiazine-4-one viewed along [010]. The molecules form sheets parallel to the *ab*-plane that are held together *via* dispersion interactions. Atoms are drawn with arbitrary radii.

2.5.2. Thiolactame tautomer

The thiolactame tautomer of 2,3,5,6-tetrahydro-2,6-dithioxo-4*H*-1,3,5-thiadiazine-4-one crystallizes in the monoclinic crystal system with space group $P2_1/c$ with three crystallographically independent molecules in the unit cell. The molecules are almost planar and the molecules approximate point group C_{2v}. Interatomic distances within the thiadiazines ring are similar to the thiolactime dimer with the difference that no in-ring double bond is present (d(C–N) = 1.35(2) – 1.37(2) Å). Terminal C=S bonds are double bonds with d(C=S) = 1.61(2) – 1.64(2) Å.

The thiolactame tautomer of 2,3,5,6-tetrahydro-2,6-dithioxo-4*H*-1,3,5-thiadiazine-4-one also forms an intricate H-bonding motif with both H atoms of all crystallographically independent molecules (A, B, and C) participating. The structure is best described starting from molecule A which forms "dimers" that are connected via H-bonds (see Figure S42). Molecule B also

forms dimers and these dimes are then terminated on each side by molecule C (see Figure S42).

The resulting virtual "tetramer" is almost planar and lies approximately in the [101] plane. The

virtual tetramers are connected to each other *via* the "dimers" of molecule A in such a way that

columns are formed that extend along [010] (see Figure S45).
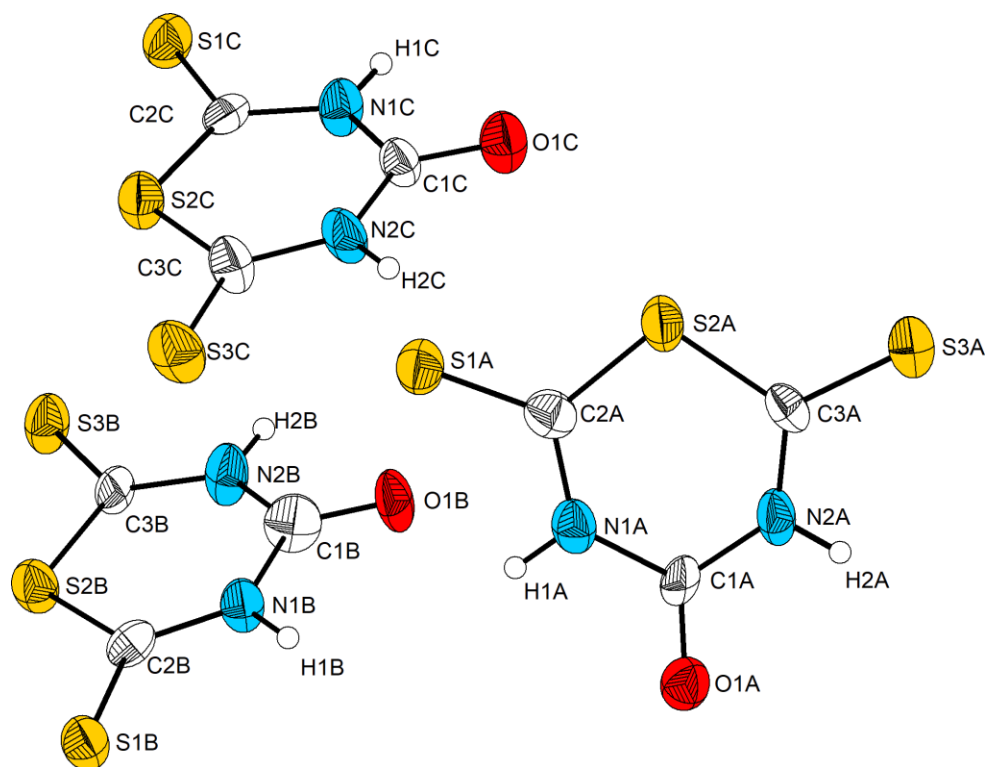
Figure S 41: Molecular structure of the three crystallographically independent 2,3,5,6-tetrahydro-2,6-dithioxo-4*H*-1,3,5-thiadiazine-4-one molecules (A, B, and C) in the single crystal drawn with 50% displacement ellipsoids.
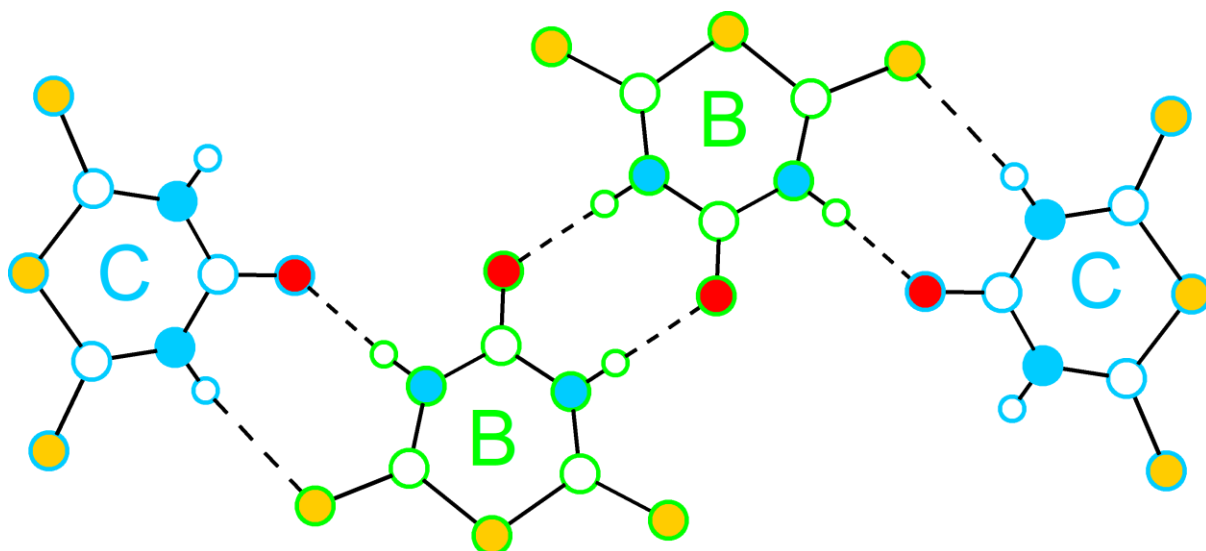
Figure S 42: Top view of an individual H-bonded virtual "tetramer" of 2,3,5,6-tetrahydro-2,6-dithioxo-4*H*-1,3,5-thiadiazine-4-one comprising molecules B (green borders) and C (blue borders). H-bonds are drawn as dashes. This motif lies approximately in the [101] plane. Atoms are drawn with arbitrary radii. Colour code: C white, N blue, O red, S gold, H white (small).
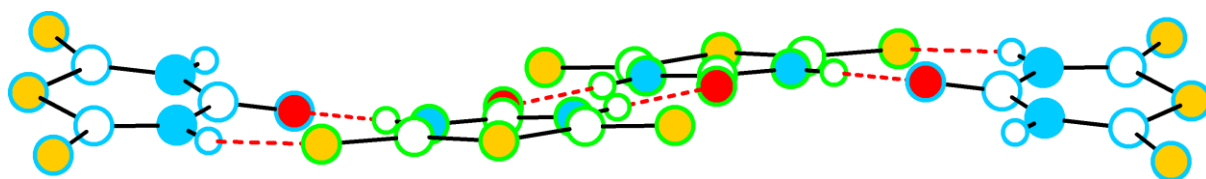
Figure S 43: Side view of an individual H-bonded virtual "tetramer" of 2,3,5,6-tetrahydro-2,6-dithioxo-4*H*-1,3,5-thiadiazine-4-one comprising molecules B (green borders) and C (blue borders). H-bonds are highlighted as red dashes. Atoms are drawn with arbitrary radii. Colour code: C white, N blue, O red, S gold, H white (small).
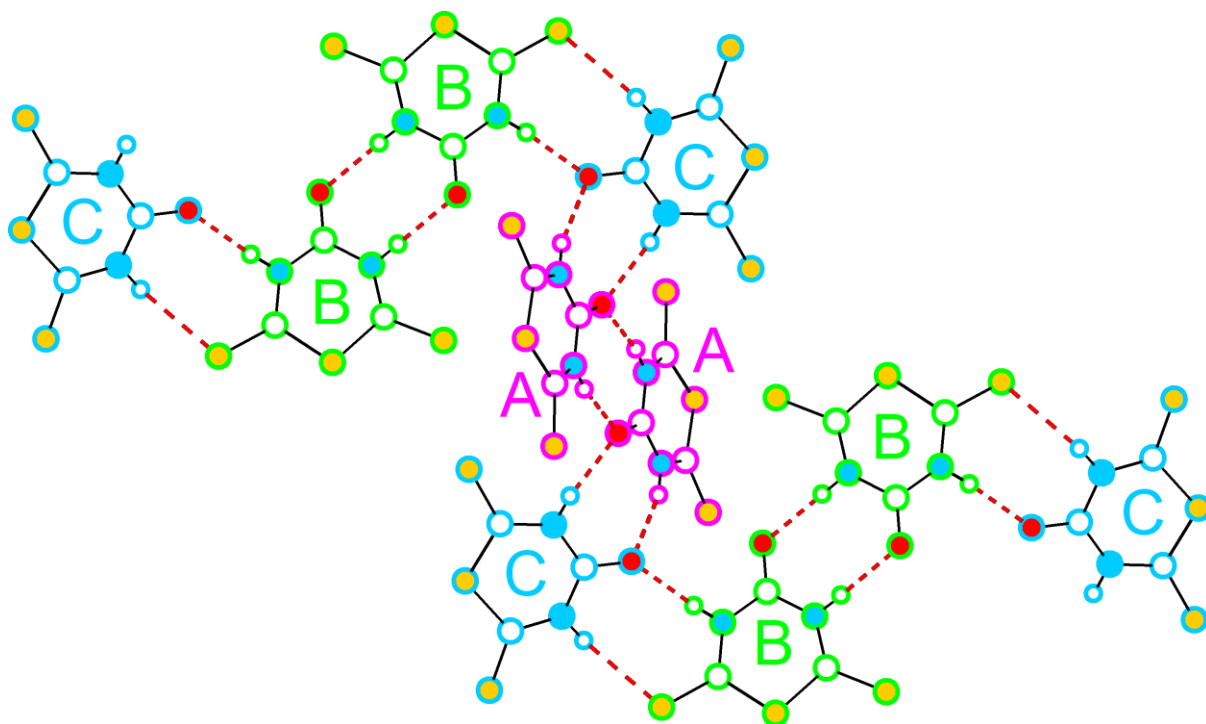
Figure S 44: One virtual dimer of molecule A (pink) connects two virtual tetramers of molecules B/C (green & blue, resp.). H-bonds are shown as dashed connections. Atoms are drawn with arbitrary radii. Colour code: C white, N blue, O red, S gold, H white (small).
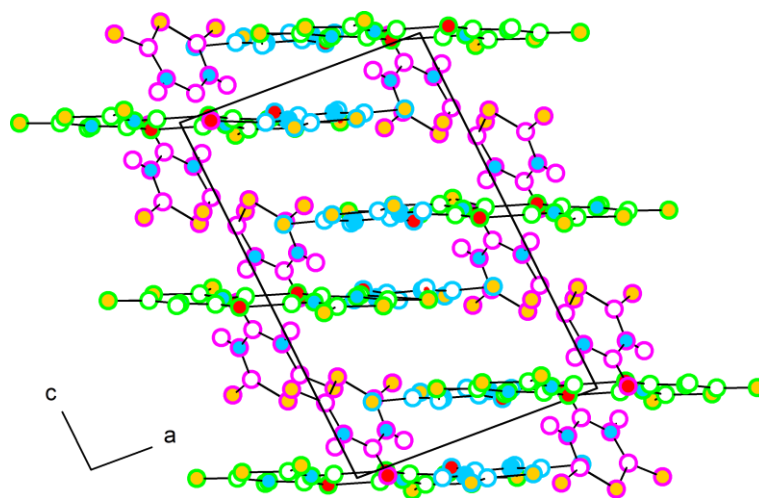
Figure S 45: Crystal structure of 2,3,5,6-tetrahydro-2,6-dithioxo-4*H*-1,3,5-thiadiazine-4-one in its lactam form viewed along [010]. Outline color code: Purple molecule A, green molecule B, blue molecule C. Atoms are drawn with arbitrary radii. Colour code: C white, N blue, O red, S gold, H white (small).

3. Details on quantum chemical calculations

3.1. Calculations with periodic boundary conditions

Periodic quantum-chemical calculations were carried out for carbonyl bis(carbamoylhalides) (Hal = F, Cl, Br) and 6-halo-2,3-dihydro-2-thioxo-4H-1,3,5-thiadiazin-4-one (Hal = Cl, Br) with the PBE0 hybrid density functional theory method (DFT-PBE0).[7,8] All calculations were performed with the CRYSTAL17 program package.[9] Triple-ζ-valence + polarization (TZVP) level basis sets were applied for H, C, N, O, S, F, Cl, Br. The basis sets have been previously derived from the Karlsruhe def2 basis sets.[10,11] Intermolecular van der Waals dispersion interactions were taken into account using Grimme's empirical D3 dispersion correction with zero damping.[12] Reciprocal space was sampled by Monkhorst−Pack type k-meshes (carbonyl bis(carbamoylfluoride): $8 \times 6 \times 4$, carbonyl bis(carbamoylchloride): $8 \times 4 \times 4$, carbonyl bis(carbamoylbromide): $8 \times 8 \times 3$, 6-chloro-2,3-dihydro-2-thioxo-4H-1,3,5-thiadiazin-4-one: $7 \times 18 \times 7$, 6-bromo-2,3-dihydro-2-thioxo-4H-1,3,5-thiadiazin-4-one: $7 \times 18 \times 7$).[13] For the evaluation of the Coulomb and exchange integrals (TOLINTEG), tolerance factors of 8, 8, 8, 8, and 16 were used for all calculations. Atomic positions and lattice parameters were fully optimized considering the space group symmetry. Default DFT integration grids and optimization convergence thresholds were applied in all calculations. The harmonic vibrational frequencies and Raman and IR intensities were obtained using CRYSTAL.[14–17] Raman and IR intensities were calculated for a polycrystalline powder sample (total isotropic intensity in arbitrary units). The Raman spectra were obtained by using a pseudo-Voigt band profile (50:50 Lorentzian:Gaussian) and a full width at half-maximum (fwhm) of 8 cm^{-1} and simulated taking into account the experimental setup (293.15 K; λ = 785 nm). Bands for the Raman spectrum were assigned by visual inspection of the normal modes with the Jmol program package at http://crysplot.crystalsolutions.eu/.[18,19]

Table S 3: Lattice parameters and atomic coordinates of the optimized solid-state structure of carbonyl bis(carbamoylfluoride) in space group $P2_12_12_1$.

Lattice parameter / Å	a	b	c
	4.63922093	8.96353243	12.38808282

Atom	x	y	z
F1	0.10857	−0.11920	−0.21290
H2	−0.02436	−0.29755	−0.33699
N3	0.19372	−0.28367	−0.34001
O4	−0.45265	−0.12360	−0.27916
C5	0.31036	−0.17202	−0.27886
F6	0.11540	0.34391	0.42180
H7	−0.02309	−0.47136	−0.45919
N8	0.19516	−0.46794	−0.46867
O9	−0.38161	−0.36249	−0.41367
C10	0.35863	−0.37054	−0.40804
C11	0.31469	0.43995	0.45567
O12	−0.44748	0.43787	0.42150

Table S 4: Lattice parameters and atomic coordinates of the optimized solid-state structure of carbonyl bis(carbamoylchloride) in space group $P\bar{1}$.

Lattice parameter / Å and °	a	b	c
	4.92010385	8.12645100	8.26069649
	α	β	γ
	69.365415	87.406478	83.854522

Atom	x	y	z
Cl1	0.08707	−0.22765	0.00726
H2	−0.24006	−0.19189	−0.45992
N3	−0.39912	−0.26820	−0.42879
O4	0.24907	−0.35020	0.45055
C5	0.43723	−0.26875	0.44183
Cl6	−0.45310	−0.11478	0.24255
H7	−0.30943	−0.40308	−0.01539
N8	−0.26857	−0.33412	−0.14317
O9	0.39343	−0.46941	−0.20309
C10	−0.06802	−0.22352	−0.18197
C11	−0.43716	−0.36530	−0.25756
O12	0.00309	−0.13269	−0.32215

Table S 5: Lattice parameters and atomic coordinates of the optimized solid-state structure of carbonyl bis(carbamoylbromide) in space group $P4_1$.

Lattice parameter / Å	a	b	c
	8.26126026	$= a$	11.10437865

Atom	x	y	z
Br1	−0.40902	−0.26069	0.24506
H2	−0.20921	0.45434	−0.47534
N3	−0.14352	−0.47431	−0.41878
O4	−0.33349	0.48809	0.39320
C5	−0.31165	−0.37000	0.37909
Br6	−0.10878	0.22478	−0.32264
H7	−0.21837	−0.14885	0.429035
N8	−0.22157	−0.26979	0.44900
O9	−0.06428	−0.20992	−0.39101
C10	−0.13701	−0.31159	−0.44666
C11	−0.07408	0.456795	−0.31991
O12	−0.00125	−0.47897	−0.24130

Table S 6: Lattice parameters and atomic coordinates of the optimized solid-state structure of 6-chloro-2,3-dihydro-2-thioxo-4H-1,3,5-thiadiazin-4-one. CRYSTAL 17 uses the standard setting so the structures were transformed from $P12_1/n1$ to P121/c1 with $a = 16.9560$, $b = 5.2230$, $c = 17.3128$ Å, $\alpha = 90.00$, $\beta = 156.37$, and $\gamma = 90.00°$.

Lattice parameter / Å / °	a	b	c
	16.40277939	5.26674155	16.87999278
	α	β 155.792515	γ

Atom	x	y	z
Cl1	−0.31586	−0.06662	0.06584
S2	0.39137	−0.46153	−0.19259
S3	0.04796	0.22733	0.47487
O4	0.18527	−0.06065	0.41785
N5	0.15021	−0.39179	0.46971
N6	0.41896	−0.09305	−0.28004
C7	0.18504	0.46596	−0.43447
C8	0.24902	−0.17593	−0.46924
C9	0.48362	−0.19702	−0.16050
H10	0.03007	−0.44642	0.32968

Table S 7: Lattice parameters and atomic coordinates of the optimized solid-state structure of 6-bromo-2,3-dihydro-2-thioxo-4H-1,3,5-thiadiazin-4-one. CRYSTAL 17 uses the standard setting so the structures were transformed from $P12_1/n1$ to P12$_1$/c1 with a = 17.0040, b = 5.2336, c = 17.2891 Å, α = 90.00, β = 155.81, and γ = 90.00°.

Lattice parameter / Å / °	a	b	c
	16.22510001	5.34267442	16.69792137
	α	β	γ
		155.118324	

Atom	x	y	z
Br1	0.30960	−0.05821	−0.07657
S2	−0.38732	−0.46198	0.19543
S3	−0.05237	0.22677	−0.48093
O4	−0.17894	−0.06354	0.41339
N5	−0.14896	−0.39418	−0.46951
H6	−0.03152	−0.44893	−0.33169
N7	−0.41140	−0.09575	0.28635
C8	−0.24396	−0.17802	0.47287
C9	−0.47626	−0.19898	0.16645
C10	−0.18483	0.46483	0.43360

Table S8: Band assignments for the calculated IR spectra (450cm^{-1}) of carbonyl bis(carbamoylfluoride). The notation for band assignments is the following: v–stretching, δ–deformation. The irreducible representations are given for the point groups of the respective space group types of the crystal structures.

v (calculated) [cm^{-1}]	v (observed) [cm^{-1}]	irrep.	assignment
			Carbonyl bis(carbamoylfluoride)
623		B_1	
625	603	B_2	δ(O1=C1–F1) and δ(O2=C3–F2) bending, anti-phase
626		B_3	
680		B_2	
687	690	B_3	δ(N–H) twist
691		B_1	
707		B_3	
709	691	B_1	δ(O=C–F) bending
712		B_2	
748		B_3	combination of δ(N1–C1–F1) and δ(N2–C3–F2) wagging, in phase and δ(N1–C2–N2) wagging anti phase
749	691	B_1	
754		B_2	
761		B_1	combination of δ(N1–C1–F1) and δ(N2–C3–F2) wagging, anti-phase
765	740	B_3	
768		B_2	
777		B_1	
781	754	B_3	δ(N–H) wagging
791		B_2	
808		B_1	
809	778	B_3	δ(N–H) wagging
826		B_2	
846		B_1	
847	817	B_3	δ(N–C–N) rocking
852		B_2	
995		B_1	
998	954	B_3	δ(N–C–N) rocking
1002		B_2	
1083		B_2	
1084	1056	B_3	δ(N–C–N) bending
1086		B_1	
1099		B_3	
1107	1056	B_1	v_s(N–C–N) stretching
1107		B_2	
1179		B_1	
1199	1133	B_2	δ(HN–C–NH) in plane rocking
1203		B_3	
1268		B_3	δ(C1–N1–C2–N2–C3) in plane bending combined with v(C–F) stretching
1284	1233	B_1	
1294		B_2	

1319		B_2	
1324	1260	B_1	combination of δ(C1–N1–C2–N2–C3) bending and rocking combined with v(C–F) stretching
1331		B_3	
1594		B_1	
1595		B_3	
1607		B_2	
1619	1555 & 1535	B_1	δ(N–H) in plane rocking and bending
1625		B_3	
1626		B_2	
1777		B_3	
1779	1698	B_1	v(C=O) stretching C2=O2
1779		B_2	
1920		B_2	
1926	1828	B_3	v(C=O) stretching C1=O1, C3=O3, anti-phase
1929		B_1	
1953		B_2	
1960	1861	B_1	v(C=O) stretching of C1=O1, C2=O2, C3=O3, in phase
1968		B_3	
3442		B_3	
3442	3288 & 3225	B_2	v(N–H) stretching of N1–H1 and N2–H2 anti phase
3442		B_1	
3452		B_2	
3453	3288 & 3225	B_3	v(N–H) stretching of N1–H1 and N2–H2 in phase
3453		B_1	

Table S9: Band assignments for the calculated IR spectra (>450cm^{-1}) of carbonyl bis(carbamoylchloride). The notation for band assignments is the following: v–stretching, δ–deformation. The irreducible representations are given for the point groups of the respective space group types of the crystal structures.

v (calculated) [cm^{-1}]	v (observed) [cm^{-1}]	irrep.	assignment
			Carbonyl bis(carbamoylchloride)
530	514	A_u	whole molecule bending
618	599	A_u	v(C–Cl) stretching
667	638	A_u	combination of δ(Cl1–C1(=O1)–N1) and δ(N2–C3–Cl2) wagging, anti-phase with δ(N1–H1) wagging
671	656	A_u	combination of δ(Cl1–C1(=O1)–N1) and δ(N2–C3–Cl2) wagging, in phase
739	689	A_u	δ(N1–H1) wagging
772	749	A_u	δ(N2–C2(=O2)–N3) wagging
854	796	A_u	δ(N2–H2) wagging
884	850	A_u	combination of δ(N2–H2) rocking and v(C–Cl) stretching
913	875	A_u	δ(C2–N2–C3) bending combined with v_s(C2–N2–C3) stretching
1017	980	A_u	δ(C1–N1–C2) bending combined with v_s(C1–N1–C2) stretching
1167	1105	A_u	v(C1–N1) stretching
1232	1169	A_u	δ(N1–H1) and δ(N2–H2) in plane rocking combined with v(N2–C3) stretching
1298	1239	A_u	v_{as} (C2–N2) in plane stretching
1548	1511 & 1482	A_u	δ(N1–H1) and δ(N2–H2) in plane rocking
1578		A_u	
1809	1715	A_u	v(C2=O2) stretching
1855	1752	A_u	v(C3=O3) stretching
1925	1812	A_u	v(C1=O1) stretching
3297	not observed	A_u	v(N2–H2) stretching
3464	not observed	A_u	v(N1–H1) stretching

Table S10: Band assignments for the calculated IR spectra (450cm^{-1}) of carbonyl bis(carbamoylbromide). The notation for band assignments is the following: ν–stretching, δ–deformation. The irreducible representations are given for the point groups of the respective space group types of the crystal structures.

ν (calculated) [cm^{-1}]	ν (observed) [cm^{-1}]	irrep.	assignment
			Carbonyl bis(carbamoylbromide)
580	562	E	ν(C–Br) stretching combined with whole molecule bending
581		A	
644	623	A	combination of δ(Br1–C1(=O1)–N1) and δ(Br2–C3(=O3)–N2) wagging, in phase
645		E	
654	623	A	combination of δ(Br1–C1(=O1)–N1) and δ(Br2–C3(=O3)–N2) wagging, anti-phase
656		E	
747	689	E	δ(N1–H1) and δ(N2–H2) wagging
752		A	
775	689	A	δ(N1–H1) twist and δ(N1–C2(=O2)–N2) wagging
776		E	
801	759	A	δ(N1–H1) and δ(N2–H2) twist and δ(N1–C2(=O2)–N2) wagging
804		E	
852	817	E	δ(Br1–C1(=O1)–N1) and δ(Br2–C3(=O3)–N2) bending anti-phase
860		A	
892	860	A	δ(Br1–C1(=O1)–N1) and δ(Br2–C3(=O3)–N2) bending in phase
897		E	
1007	971	A	ν_s(C1–N1–C2) stretching
1007		E	
1177	1122	A	ν(N1–C1) and ν(N2–C3) stretching
1181		E	
1212	1155	E	ν(N1–C2) stretching
1213		A	
1274	1217	A	ν(N2–C2) stretching
1279		E	
1532	1472	A	δ(N1–H1) and δ(N2–H2) in plane bending
1540		E	
1568	1507	A	δ(N1–H1) and δ(N2–H2) in plane rocking
1576		E	
1820	1721	A	ν(C2=O2) stretching
1823		E	
1847	1748	E	ν(C3=O3) stretching
1849		A	
1901	1805	A	ν(C1=O1) stretching
1918		E	
3376	not observed	A	ν(N1–H1) stretching
3384		E	
3447	not observed	A	ν(N1–H1) stretching
3451		E	

Table S11: Band assignments for the calculated IR spectra (450cm^{-1}) of 6-chloro-2,3-dihydro-2-thioxo-4H-1,3,5-thiadiazin-4-one. The notation for band assignments is the following: v–stretching, δ–deformation. The irreducible representations are given for the point groups of the respective space group types of the crystal structures.

v (calculated) [cm^{-1}]	v (observed) [cm^{-1}]	irrep.	assignment
			6-Chloro-2,3-dihydro-2-thioxo-4H-1,3,5-thiadiazin-4-one
539	not observed	A_u	whole molecule bending
544		A_u	
544	526	B_u	δ(N1–C2(=S1)–S2) wagging
545		B_u	
558	not observed	A_u	δ(N2–C3(–Cl1)–S2) wagging
562		B_u	
704	734	A_u	whole molecule bending and rocking
706		B_u	
753	748	A_u	δ(N1–C1(=O1)–N2) wagging
757		B_u	
771	785	B_u	δ(N1–C1(=O1)–N2) wagging
772		A_u	
851	901	A_u	δ(H1–N1) twist
881		B_u	
938	952	B_u	v(C3–Cl1) stretching
939		A_u	
985	1050	B_u	combination of v(C3–S2) and v_s(N1–C1–N2) stretching, anti-phase
991		A_u	
1091	1064	B_u	v(S1=C2) stretching
1094		A_u	
1260	1209	B_u	v(N1–C1) stretching
1272		A_u	
1360	1290	A_u	v(N1–C2) stretching
1366		B_u	
1529	1453	A_u	δ(H1–N1) bending
1535		B_u	
1662	1566	B_u	v(N2–C3) stretching
1663		A_u	
1793	1688	A_u	v(C1=O1) stretching
1811		B_u	
3308	3123	A_u	v(H1–N1) stretching
3325		B_u	

Table S12: Band assignments for the calculated IR spectra (450cm^{-1}) of 6-bromo-2,3-dihydro-2-thioxo-4H-1,3,5-thiadiazin-4-one. The notation for band assignments is the following: ν–stretching, δ–deformation. The irreducible representations are given for the point groups of the respective space group types of the crystal structures.

ν (calculated) [cm^{-1}]	ν (observed) [cm^{-1}]	irrep.	assignment
			6-Bromo-2,3-dihydro-2-thioxo-4H-1,3,5-thiadiazin-4-one
525		A_u	
530	not observed	B_u	δ(N2–C3(–Br1)–S2) wagging
535		A_u	
543		B_u	
546	511	B_u	δ(N1–C2(=S1)–S2) wagging
546		A_u	
698	727	A_u	whole molecule bending and rocking
698		B_u	
751	744	A_u	δ(N1–C1(=O1)–N2) wagging
756		B_u	
768	785	B_u	δ(N1–C1(=O1)–N2) wagging
770		A_u	
852	826	A_u	δ(H1–N1) twist
873		B_u	
898	927	A_u	ν(C3–Br1) stretching
903	927	B_u	δ(H1–N1) twist and ν(C3–Br1) stretching
966	1044	B_u	ν(S1=C2) stretching
974		A_u	
1084	1064	B_u	ν(N1–C1) stretching
1086		A_u	
1246	1176	B_u	ν(N1–C2) stretching
1257	1198	A_u	
1361	1292	A_u	δ(H1–N1) bending
1366		B_u	
1528	1450	A_u	ν(N2–C3) stretching
1534		B_u	
1648	1553	B_u	ν(C1=O1) stretching
1649		A_u	
1791	1686	A_u	ν(H1–N1) stretching
1807	1700	B_u	
3315	3119	A_u	ν(S1=C2) stretching
3330		B_u	

3.2. Further calculations with Turbomole

Calculations were performed with the TURBOMOLE code on the PBE0/def2-TZVP level of theory unless explicitly noted otherwise. For the carbonyl bis(carbamoyl halides), compound **1** is stable at r.t. while compounds **2** and **3** slowly decompose and compound **4** is even more sensitive and prone to decomposition. Stepwise exchange of the halogen atoms *in silico* starting from **1** corroborates this trend. The replacement of F with Cl (see Scheme S 1 a) is endergonic by 299.3 kJ/mol. Consecutive replacement of Cl with Br, and Br with I is also endergonic albeit with only 1/3rd of the energy: 106.6 kJ/mol (Cl➔Br) and 112.3 kJ/mol (Br➔I). For the thiadiazine framework this trend is also observable but less pronounced: F➔Cl 137.7 kJ/mol, Cl➔Br 54.7 kJ/mol, Br➔I 53.3 kJ/mol (Scheme S 1, right). While for molecules **1–4** the calculations are consistent with the experimental findings, for molecules **5** & **6** the calculations cannot explain our unsuccessful attempts to isolate the respective fluorinated and iodinated compounds. As the decomposition of compound **2** yields HCl we repeated the calculations with the assumption that hydrogen halides were reaction partners (see Scheme S 1 b). Here, for carbonyl bis(carbamoylhalides) the exchange of F with Cl, Br, or I atoms is endergonic which is probably testament of the high H–F bonding energy. Subsequent exchanges Cl➔Br (−2.8 kJ/mol) and Br➔I (−1.7 kJ/mol) are slightly exergonic and no clear trend is obvious. Again, for the thiadiazines, exchange F➔Cl is endergonic but only by 9.9 kJ/mol. The energies for the subsequent exchanges Cl➔Br (0 kJ/mol) and Br➔I (−3.7 kJ/mol) are small and no clear trend is obvious. In the laboratory it was observed that washing the reaction product of CDIT and HI with *n*-hexane led to the formation of elemental iodine as was evident by the pink hue of the washing solvent. Consequently, we performed calculations with the dihalogen molecules Y_2 ($Y2 = F_2 – I_2$) as reaction partners (see Scheme S 1 c). All hypothetical exchange reactions are endergonic for both carbonyl bis(carbamoylhalides) and thiadiazine based compounds: For the former exchanging F➔Cl (400.1 kJ/mol) is least favorable with Cl➔Br (76.1 kJ/mol) and

Br→I (89.6 kJ/mol) at almost one quarter of the energy. The trend is similar for the latter class but again less pronounced with roughly ½ of the energies calculated for carbonyl bis(carbamoylhalides): F→Cl (188.0 kJ/mol), Cl→Br (39.5 kJ/mol), Br→I (41.9 kJ/mol).
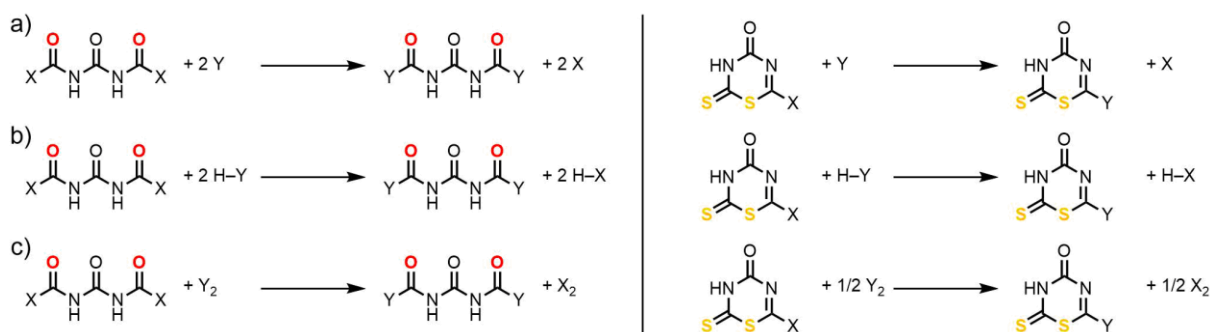
Scheme S 1: In silico replacement of the halogen atoms in **1-4** (left) and **5–6** (right) either by single atoms (a), the respective hydrogen halide molecule (b), or dihalogen molecules (c). For details see text.

Moreover, the energies for the reaction in Scheme 3 of the main document at several other levels of theory, namely PBE0 plus D4 dispersion correction [E. Caldeweyher, J. Mewes, S. Ehlert, S. Grimme, Phys. Chem. Chem. Phys., 2020,22, 8499-8512], PBE0 plus COSMO, SCS-MP2 [S. Grimme, J. Chem. Phys. 2003, 118, 9095-9192] and PBE [J. P. Perdew, K. Burke, M. Ernzerhof, Phys. Rev. Lett. 1996, 77, 3865-3868], are sampled in Table S13. They all show the same trend.

Table S13. Energies in kJ/mol without thermic contributions for the reactions E-Chain→ E-Ring+HX, E=O,S, X=F,Cl,Br (see also Scheme 3 in the main document) at level PBE0 and additionally PBE0 plus D4 dispersion correction, SCS-MP2, and PBE. Def2-TZVP bases were used throughout.

	PBE		PBE0		PBE0 +D4		PBE0 +COSMO		SCS-MP2 @PBE0	
	O	S	O	S	O	S	O	S	O	S
F	72.1	-17.4	67.4	-18.9	68.3	-19.6	78.4	-10.0	67.7	-23.3
Cl	52.3	-27.7	45.1	-32.9	49.0	-29.4	57.7	-21.7	45.9	-27.3
Br	67.0	-19.0	51.6	-27.2	56.4	-22.6	63.1	-17.6	54.8	-16.9
I	70.6	-11.1	51.6	-22.3	57.7	-15.9	63.4	-12.4	56.9	-8.6

Finally, we recalculated the energy profile for the rotation (Figure 4 in the main document) without employing COSMO with functionals PBE and PBE0; for the latter also including the D4 dispersion correction. The results are sampled in Table S14. Differences between PBE, PBE0 and PBE0+D4 are small (less than 5 kJ/mol), but COSMO has a significant influence, in particular on the relative energy of the chain-type conformer (~+10 kJ/mol with COSMO, but ~+40 kJ/mol without), and to lesser extend on the barrier height (~40 kJ/mol with COSMO, but ~55 kJ/mol without).

Table S14. Energies in kJ/mol relative to the ring-type conformer at 35 equidistant points along the pathway to the chain-type conformer(see also Figure 4 in the main document) at levels PBE, PBE0, PBE0+D4 and PBE=+COSMO. Def2-TZVP bases were used throughout. The first line refers to the ring-type, the last to the chain-type conformer

F				Cl				Br				I			
PBE	PBE0	PBE0 +D4	PBE0 +COS	PBE	PBE0	PBE0 +D4	PBE0 +COS	PBE	PBE0	PBE0 +D4	PBE0 +COS	PBE	PBE0	PBE0 +D4	PBE0 +COS
0.0	0.0	0.0	0.0	0.0	0.0	0.0	0.0	0.0	0.0	0.0	0.0	0.0	0.0	0.0	0.0
0.1	0.2	0.2	0.3	0.1	0.2	0.2	-0.5	0.2	0.2	0.2	-0.1	0.2	0.2	0.2	0.4
0.6	0.7	0.6	0.8	0.6	0.6	0.6	-0.0	0.7	0.7	0.7	0.1	0.6	0.6	0.6	0.7
1.4	1.5	1.5	1.6	1.3	1.4	1.4	0.7	1.5	1.6	1.6	1.0	1.3	1.4	1.4	1.4
2.4	2.6	2.6	2.8	2.4	2.6	2.6	2.0	2.7	2.9	2.9	2.3	2.3	2.5	2.5	2.6
3.9	4.2	4.2	4.6	3.7	4.0	4.1	3.5	4.2	4.6	4.5	4.0	3.7	4.0	4.0	4.0
5.7	6.1	6.1	6.5	5.5	5.9	5.9	5.3	6.2	6.6	6.6	6.1	5.3	5.8	5.8	5.9
7.9	8.4	8.4	8.7	7.6	8.1	8.1	7.5	8.5	9.1	9.0	8.3	7.4	7.9	8.0	8.0
10.4	11.1	11.1	11.3	10.0	10.7	10.7	9.7	11.2	11.9	11.9	10.8	9.7	10.4	10.5	10.3
13.4	14.2	14.2	14.1	12.9	13.7	13.7	12.6	14.2	15.1	15.1	13.8	12.5	13.3	13.4	12.8
16.7	17.6	17.6	17.2	16.1	17.0	17.1	15.4	17.6	18.6	18.6	16.6	15.5	16.6	16.7	15.8
20.3	21.4	21.4	20.1	19.6	20.6	20.7	18.1	21.2	22.3	22.3	19.4	18.9	20.0	20.2	18.5
24.2	25.3	25.4	23.0	23.3	24.4	24.6	21.1	24.9	26.1	26.2	22.2	22.4	23.7	24.0	21.1
28.2	29.3	29.4	26.0	27.1	28.3	28.5	24.0	28.6	29.9	30.0	24.8	26.1	27.4	27.7	24.0
32.1	33.3	33.4	28.8	30.9	32.1	32.4	26.7	32.1	33.5	33.7	27.2	29.7	31.1	31.5	26.6
35.9	37.1	37.3	31.6	34.5	35.8	36.1	29.2	35.5	37.0	37.2	29.7	33.2	34.6	35.1	29.1
39.5	40.8	41.0	34.2	38.1	39.4	39.7	31.5	38.8	40.2	40.5	31.6	36.6	38.1	38.6	31.4
43.0	44.3	44.5	36.6	41.4	42.8	43.2	34.0	41.9	43.3	43.7	33.9	39.8	41.3	42.0	33.8
46.3	47.6	47.9	38.5	44.6	45.9	46.4	35.6	44.7	46.1	46.6	35.1	42.9	44.4	45.1	35.6
49.3	50.7	51.0	40.1	47.5	48.8	49.3	36.7	47.3	48.7	49.3	35.9	45.7	47.2	48.0	36.3
52.0	53.4	53.7	39.5	50.0	51.3	52.0	36.3	49.5	50.9	51.7	35.3	48.1	49.6	50.5	35.8
54.3	55.7	56.1	36.9	52.1	53.5	54.2	34.1	51.2	52.7	53.5	33.2	50.0	51.5	52.6	33.9
57.7	59.5	60.1	34.2	54.3	56.1	57.1	31.8	51.4	53.5	54.7	30.6	50.5	52.8	54.0	31.4
55.6	57.4	58.1	31.2	52.2	54.2	55.2	29.0	49.3	51.5	52.7	28.0	48.4	50.8	52.1	28.8
53.4	55.2	56.0	28.3	50.1	52.1	53.1	26.2	47.1	49.3	50.6	25.1	46.2	48.6	50.0	26.1
51.2	53.0	53.8	25.6	47.9	50.0	51.0	23.5	44.9	47.2	48.5	22.1	44.0	46.5	47.9	23.2
49.1	50.9	51.7	22.8	45.9	47.9	49.0	21.0	42.8	45.1	46.4	19.6	42.0	44.4	45.9	20.7
47.1	49.0	49.8	20.1	44.0	46.0	47.2	18.4	40.9	43.2	44.6	17.0	40.0	42.5	44.0	18.1
45.4	47.2	48.1	17.7	42.3	44.3	45.5	16.2	39.2	41.5	42.9	14.9	38.3	40.7	42.3	15.9
43.9	45.7	46.5	15.8	40.8	42.8	44.0	14.3	37.7	40.0	41.4	13.0	36.7	39.2	40.8	14.0
42.6	44.4	45.3	14.0	39.5	41.5	42.8	12.7	36.5	38.8	40.2	11.5	35.4	37.9	39.5	12.5
41.7	43.4	44.3	13.0	38.6	40.6	41.8	11.7	41.9	37.8	39.2	10.6	34.4	36.9	38.5	11.5
40.9	42.7	43.6	11.9	37.8	39.9	41.1	10.7	34.8	37.1	38.5	9.6	33.6	36.1	37.8	10.5
40.5	42.2	43.2	11.1	37.4	39.5	40.7	9.9	34.3	36.6	38.1	8.7	33.0	35.6	37.3	9.7
40.3	42.1	43.0	10.3	37.2	39.3	40.6	9.3	34.0	36.4	37.9	8.1	32.7	35.4	37.1	9.0
40.4	42.2	43.2	10.1	37.2	39.4	40.7	9.1	33.9	36.4	37.9	7.9	32.6	35.4	37.1	8.9
40.6	42.4	43.4	9.8	37.3	39.6	40.9	8.9	33.9	36.5	38.0	7.7	32.7	35.5	37.1	8.7

4. References

[1] W. L. F. Armarego, C. L. L. Chai, *Purification of Laboratory Chemicals*, Elsevier Inc., Oxford, **2009**.

[2] J. Pfeiffer, C. Trost, A. Pachkovska, F. Tambornino, *Inorg. Chem.* **2021**, *60*, 10722–10728.

[3] G. M. Sheldrick, *Acta Crystallogr. Sect. A* **2015**, *71*, 3–8.

[4] G. M. Sheldrick, *Acta Crystallogr. Sect. A* **2008**, *64*, 112–122.

[5] O. V Dolomanov, L. J. Bourhis, R. J. Gildea, J. A. K. Howard, H. Puschmann, *J. Appl. Crystallogr.* **2009**, *42*, 339–341.

[6] K. Brandenburg, H. Putz, *DIAMOND, Program for X-Ray Structure Analysis*, Crystal Impact GbR, Bonn, Gemany, **2005**.

[7] C. Adamo, V. Barone, *J. Chem. Phys.* **1999**, *110*, 6158–6170.

[8] J. P. Perdew, K. Burke, M. Ernzerhof, *Phys. Rev. Lett.* **1996**, *77*, 3865–3868.

[9] R. Dovesi, A. Erba, R. Orlando, C. M. Zicovich-Wilson, B. Civalleri, L. Maschio, M. Rérat, S. Casassa, J. Baima, S. Salustro, et al., *Wiley Interdiscip. Rev. Comput. Mol. Sci.* **2018**, *8*, 1–36.

[10] F. Weigend, R. Ahlrichs, *Phys. Chem. Chem. Phys.* **2005**, *7*, 3297–3305.

[11] A. J. Karttunen, T. Tynell, M. Karppinen, *J. Phys. Chem. C* **2015**, *119*, 13105–13114.

[12] S. Grimme, J. Antony, S. Ehrlich, H. Krieg, *J. Chem. Phys.* **2010**, *132*, 1–19.

[13] H. J. Monkhorst, J. D. Pack, *Phys. Rev. B* **1976**, *13*, 5188–5192.

[14] C. M. Zicovich-Wilson, F. Pascale, C. Roetti, V. R. Saunders, R. Orlando, R. Dovesi, *J. Comput. Chem.* **2004**, *25*, 1873–1881.

[15] F. Pascale, C. M. Zicovich-Wilson, F. López Gejo, B. Civalleri, R. Orlando, R. Dovesi, *J. Comput. Chem.* **2004**, *25*, 888–897.

[16] L. Maschio, B. Kirtman, M. Rérat, R. Orlando, R. Dovesi, *J. Chem. Phys.* **2013**, *139*, 1–13.

[17] L. Maschio, B. Kirtman, R. Orlando, M. Rèrat, *J. Chem. Phys.* **2012**, *137*, 204113.

[18] D. L. Smith, V. I. Saunders, *Acta Crystallogr. Sect. B* **1982**, *38*, 907–909.

[19] "Jmol: an open-source Java viewer for chemical structures in 3D. http://www.jmol.org," can be found under http://www.jmol.org, **2021**.

8.1.5 Intra- and Intermolecular Hydrogen Bonding in *N,N'*-Carbonyl bis(carbamates), -(*S*-thiocarbamates) and *N,N'*-biscarbamoyl ureas

Intra- and Intermolecular Hydrogen Bonding in *N,N'*-Carbonyl bis(carbamates), -(*S*-thiocarbamates) and *N,N'*-biscarbamoyl ureas

Jonathan Pfeiffer[a], Martin Möbs[a], Sascha Reith[a], Mirko Tallu[a], Frank Tambornino[a]*

[a]Fachbereich Chemie, Philipps-Universität Marburg, Hans-Meerwein-Straße 4, 35043 Marburg, Germany

Contents

1. Experimental section

1.1. General remarks

General synthetic methods. All reactions and manipulations were performed under an inert atmosphere of argon using standard Schlenk-line or glovebox techniques (MBraun UNIlab glovebox, maintained at < 0.1 ppm H_2O and < 0.1 ppm O_2).

All chemicals were purchased commercially, purified, and dried according to literature.[1] $CDCl_3$ (Eurisotop, 99.8 %) and THF-d8 (Eurisotop, 99.5 %) were recondensed, degassed and stored over molecular sieve (3 Å or 4 Å) prior to use. Carbonyl diisocyanate was synthesised after literature procedure.[2]

Additional characterization techniques:

^1H and ^{13}C NMR spectra were acquired on a Bruker *Avance II* (300 MHz) or a Bruker *Avance III HD* (300 MHz) spectrometer at 298 K if not stated otherwise.

Elemental analyses and mass spectrometry were performed by the in-house service personnel. CHN(S) analyses were performed on a *CHNS(S)-Analysator vario MICRO CUBE* (Elementar). Electro spray ionisation was performed on a *LTQ-FT Ultra* (Thermo Fischer Scientific).

IR spectra were recorded on a Bruker *Alpha FT-IR* spectrometer equipped with a diamond ATR unit mounted in a nitrogen-filled glovebox (MBraun UNIlab glovebox, maintained at < 0.1 ppm H_2O and < 0.1 ppm O_2).

Hirschfeld surface analyses were conducted with the Crystal Explorer (V 21.5)[3] software suite.

1.2. General synthesis of CO(NH(CO)NR₂)₂

To a 1 M solution of carbonyl diisocyanate in diethyl ether (5.0 mL, 5.0 mmol, 1.0 eq.) cooled to −78 °C a 1 M solution of amine (10.0 mL, 10.0 mmol, 2.0 eq.) was added dropwise. The solution was allowed to warm to room temperature and stirred for 16 h to 18 h. The solvent was removed *in vacuo* and the residue suspended in dichloromethane (15 mL). To the suspension 0.5 M aqueous HCl (10 mL) was added. The organic phase was separated, and the aqueous phase extracted four times with dichloromethane (15 mL). The combined organic phases were dried with MgSO₄. The solvent was removed. To the residue diethyl ether (2 mL) was added and the product precipitated with *n*-hexane (8 mL). The solvent mixture was decanted off and the obtained solid dried *in vacuo*.

It is to mention that during synthesis a few problems appeared, which lead to impure reaction products. First, the reactions are hard to control, because even at −78 °C amines are rapidly reacting with carbonyl diisocyanate (which is volatile) in the gas phase, which is visible through smoke development. Secondly, the starting material precipitates with the product as agglomerate out of solution, leading to bad yields. Both can be detected in the crude product by ^{1}H-NMR spectroscopy and mass spectrometry. Thirdly, the solubility of the products is highly depending on the aryl group: *N,N'*-bis(methylcarbamoyl) urea is not soluble in diethyl ether, *N,N'*-bis(isopropylcarbamoyl) urea is easily soluble in diethyl ether. This leads to difficult purification from side products, as is visible in NMR spectroscopy.

1.2.1. Synthesis of CO(NH(CO)NMe₂)₂ − 1Me

For the reaction a 2 M solution of dimethyl amine in THF was diluted with diethyl ether. CO(NH(CO)NMe$_2$)$_2$ was obtained as colourless powder (37%, 1.84 mmol, 372 mg). Crystals could be obtained by layering a solution in dichloromethane with *n*-hexane.

CHNS for C$_7$H$_{14}$N$_4$O$_3$ Found % (calc. %): C 39.90 (41.58), H 7.06 (6.98), N 27.45 (27.71).

^{1}H NMR (THF-d8): δ = 9.99 (s, 2H, N*H*), 2.94 (s, 12H, C*H₃*) ppm.

^{13}C{^{1}H} NMR (THF-d8): δ = 154.9 ((*CO*)N(CH$_3$)$_2$), 151.6 (N(*CO*)N), 36.6 (*CH₃*) ppm.

Mass (ESI+, MeOH) for [M+H$^+$] = C$_7$H$_{14}$N$_4$O$_3$H$^+$ m/z found (calc.): 205.1135 (205.1139).
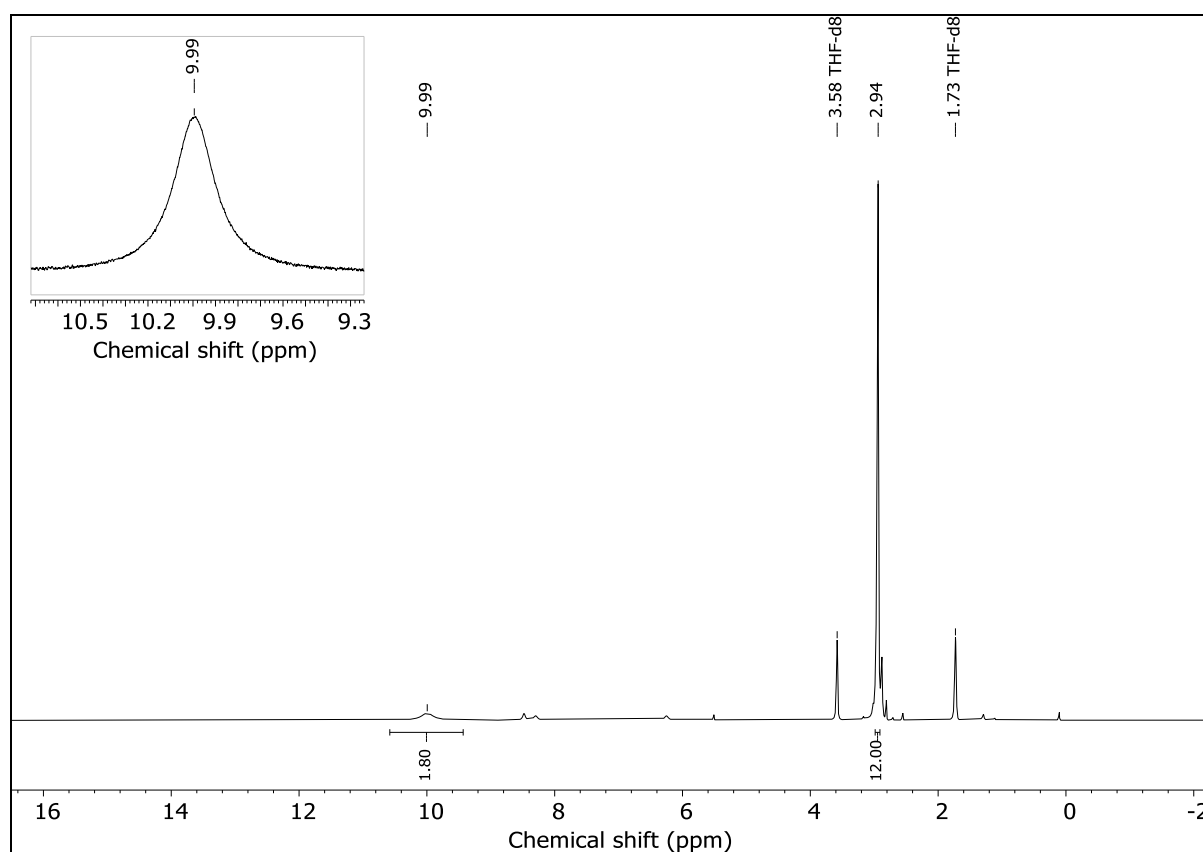
Figure S 1: ^{1}H NMR spectrum of CO(NH(CO)NMe₂)₂ in THF-d8.
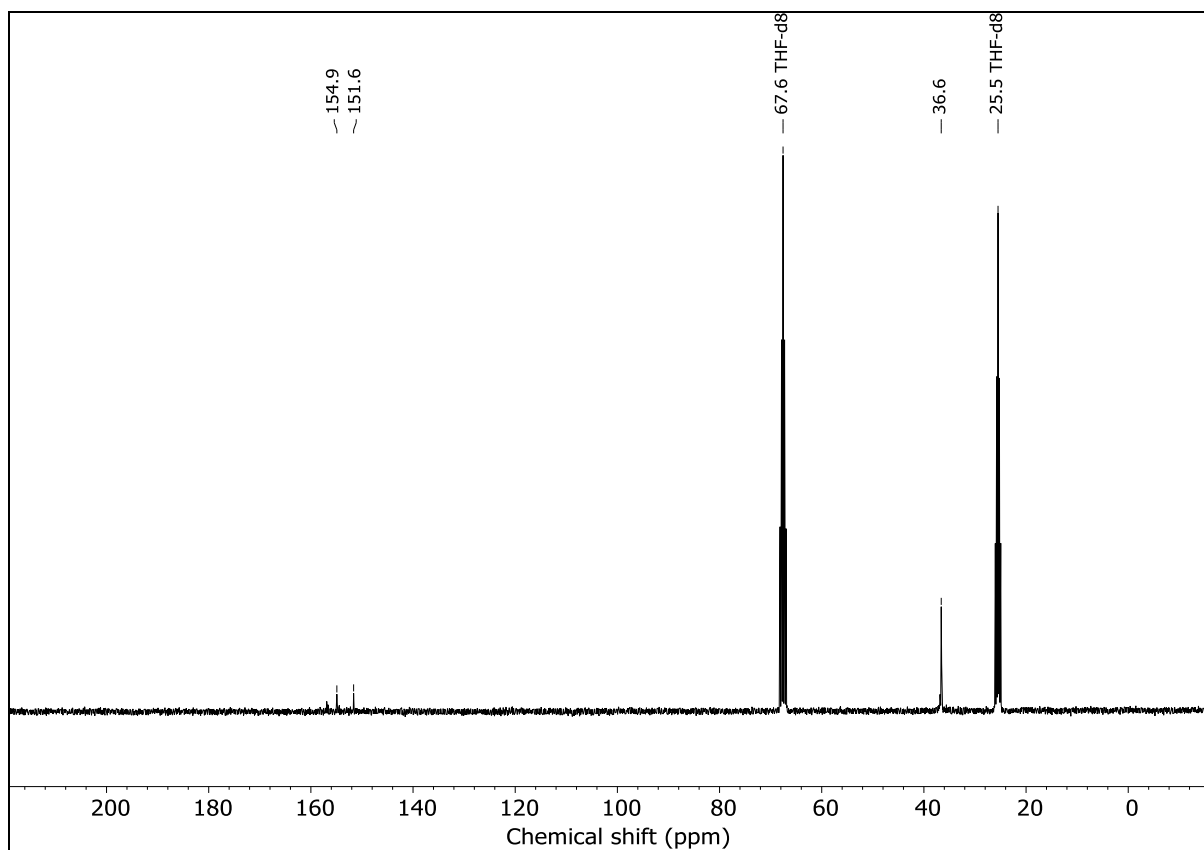
Figure S 2: ^{13}C NMR spectrum of $CO(NH(CO)NMe_2)_2$ in THF-d8.
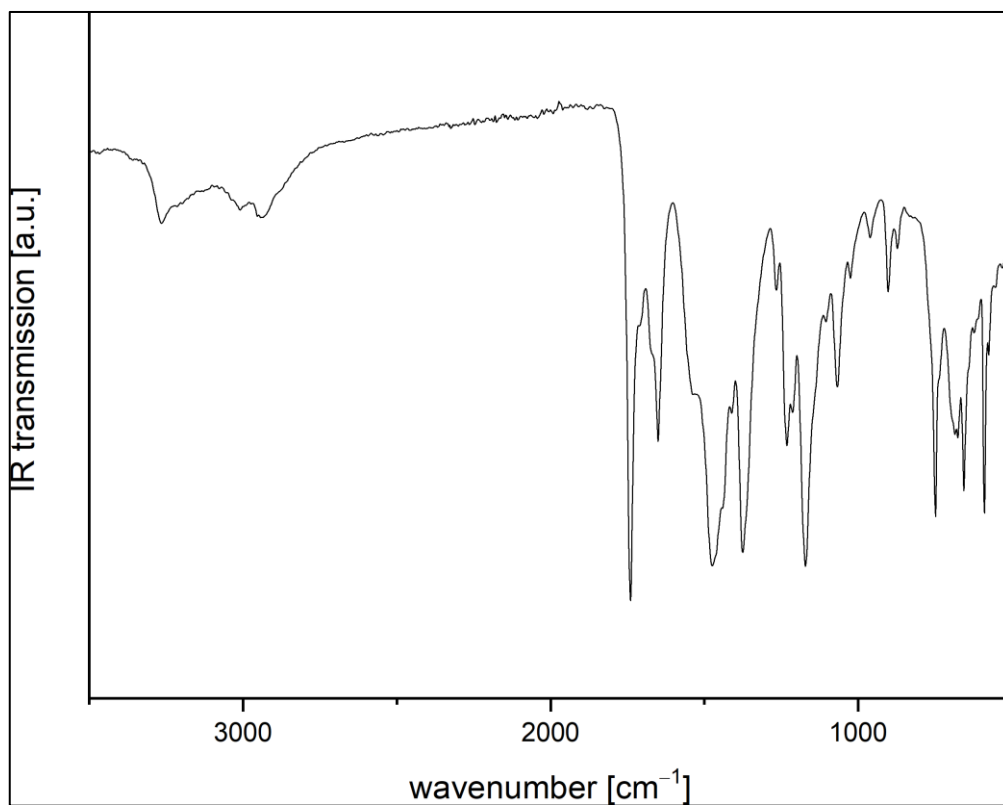
Figure S 3: Measured room-temperature ATR-IR spectrum $CO(NH(CO)NMe_2)_2$.

1.2.2. Synthesis of CO(NH(CO)NEt₂)₂ – 1Et

CO(NH(CO)NEt$_2$)$_2$ was obtained as colourless powder (22%, 1.07 mmol, 276 mg). Crystals could be obtained by slow evaporating the solvent of a diethyl ether solution.

CHNS for C$_{11}$H$_{22}$N$_4$O$_3$ Found % (calc. %): C 50.42 (51.15), H 8.78 (8.58), N 21.03 (21.69).

¹H NMR (THF-d8): δ = 10.28 (s, 2H, N*H*), 3.36 (q, 8H, $^3J_{HH}$ = 7.11 Hz, C*H₂*CH₃), 1.15 (t, 12H, $^3J_{HH}$ = 6.98 Hz, CH₂C*H₃*) ppm.

¹³C{¹H} NMR (THF-d8): δ = 153.8 ((*C*O)N(C$_2$H$_5$)$_2$), 152.3 (N(*C*O)N), 42.4 (*C*H₂CH₃), 14.2 (CH₂*C*H₃) ppm.

Mass (ESI+, MeOH) for [M+H$^+$] = C$_{11}$H$_{22}$N$_4$O$_3$H$^+$ m/z found (calc.): 259.1759 (259.1765).
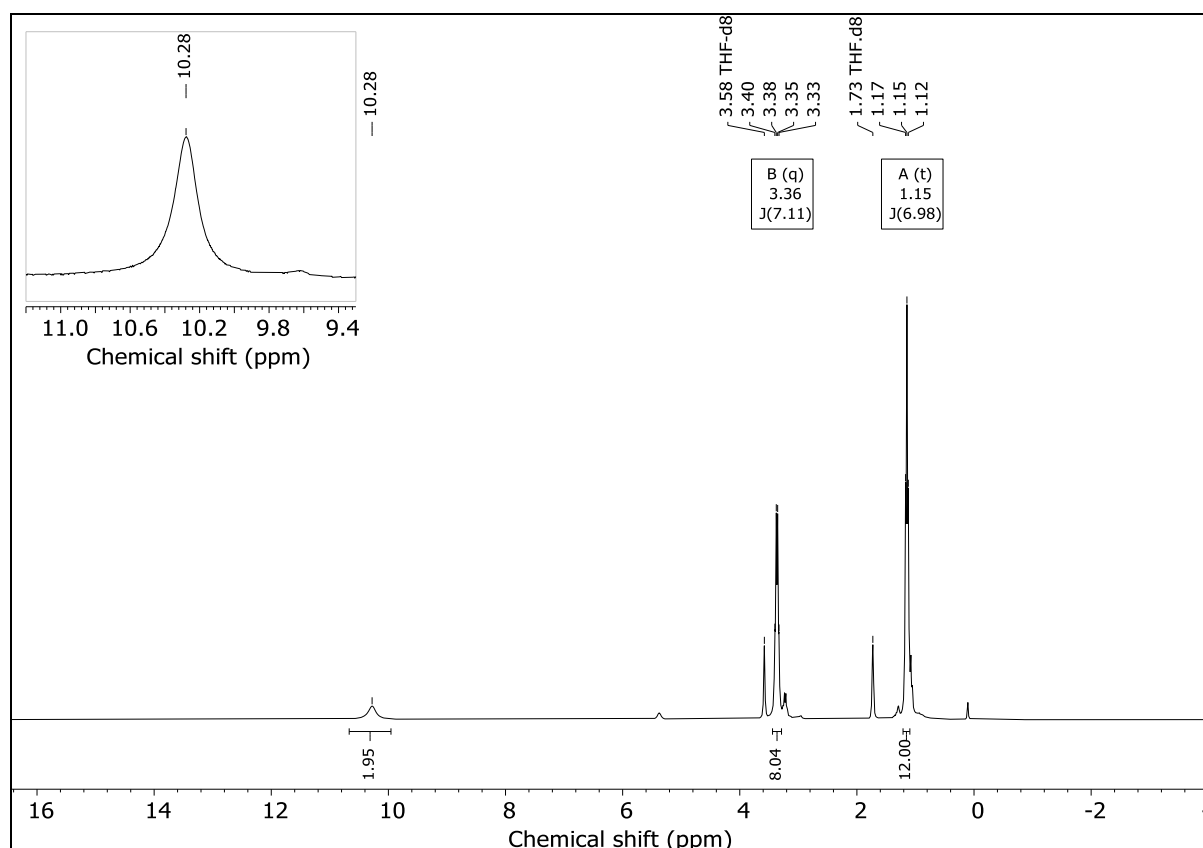
Figure S 4: ¹H NMR spectrum of CO(NH(CO)NEt₂)₂ in THF-d8.
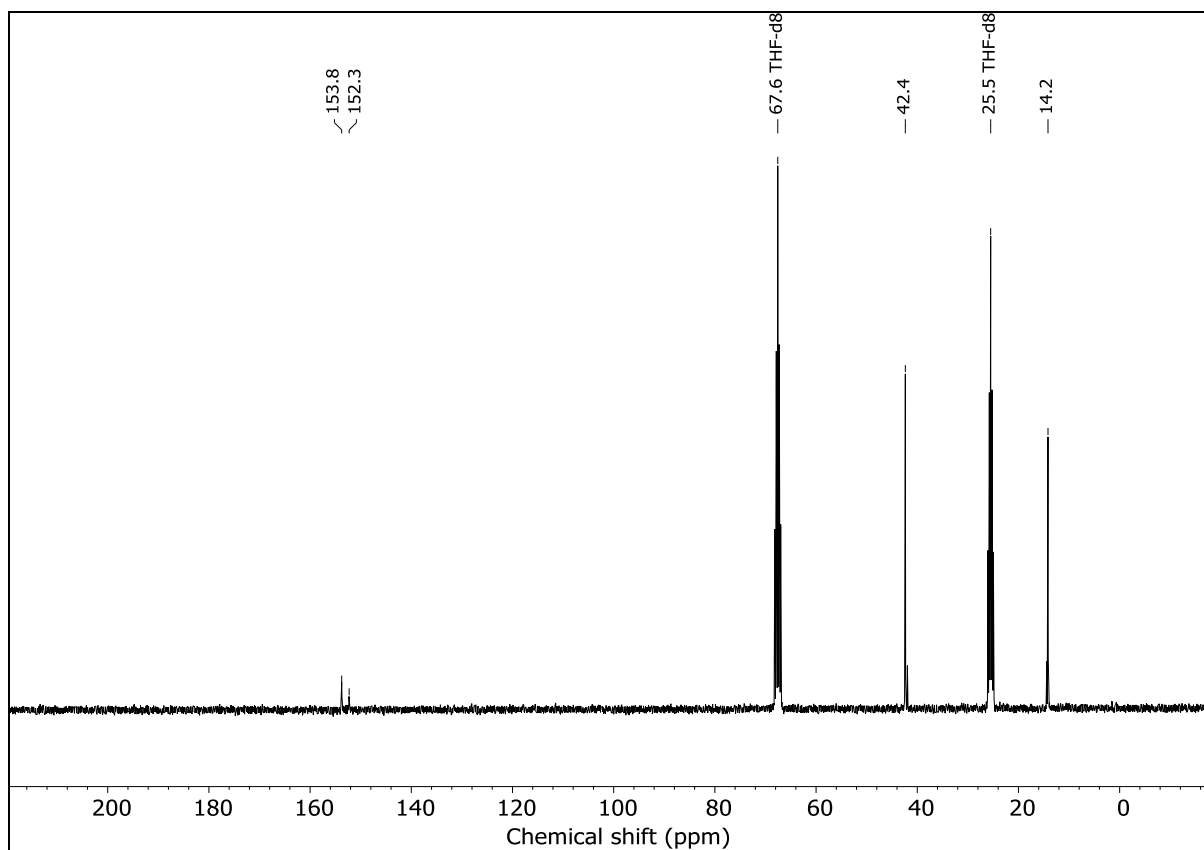
Figure S 5: ^{13}C NMR spectrum of CO(NH(CO)NEt$_2$)$_2$ in THF-d8.
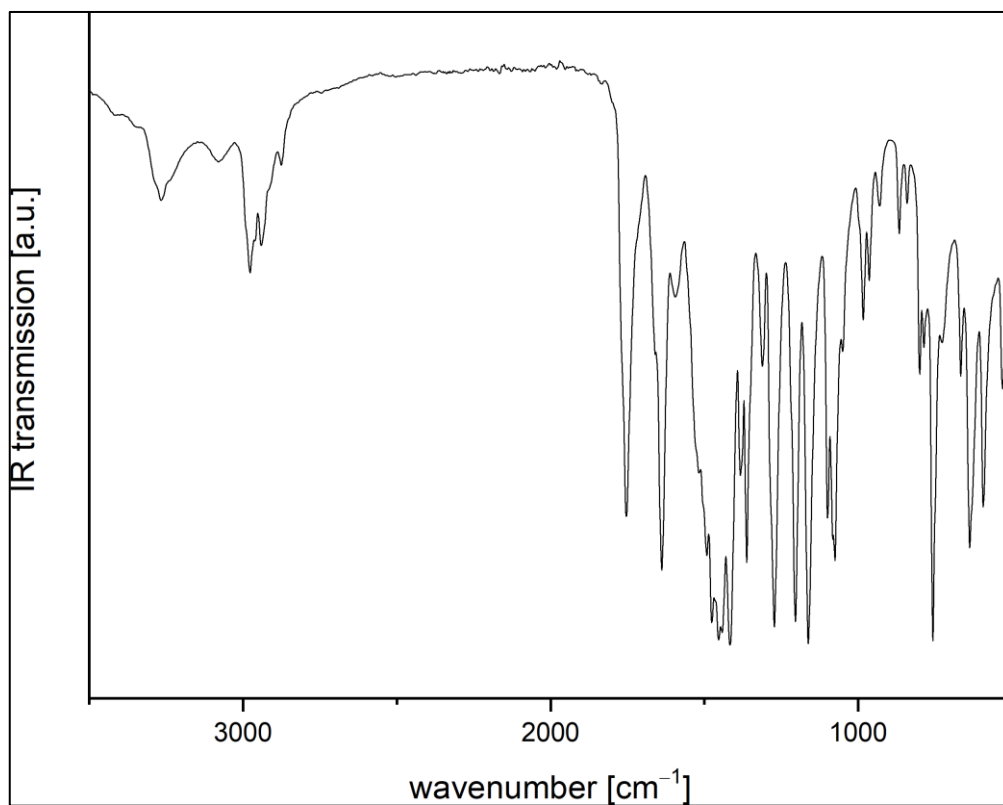
Figure S 6: Measured room-temperature ATR-IR spectrum CO(NH(CO)NEt$_2$)$_2$.

1.2.3. Synthesis of CO(NH(CO)N*i*Pr₂)₂ − 1*i*Pr

CO(NH(CO)N*i*Pr₂)₂ was obtained as colourless powder (19%, 0.95 mmol, 300 mg).

CHNS for $C_{15}H_{30}N_4O_3$ Found % (calc. %): C 56.56 (57.30), H 10.11 (9.62), N 17.25 (17.82)

¹H NMR (CDCl₃): δ =

¹³C{¹H} NMR (CDCl₃): δ =

Mass (ESI+, MeOH) for [M+H⁺] = $C_{15}H_{30}N_4O_3H^+$ m/z found (calc.): 315.2386 (315.2391).
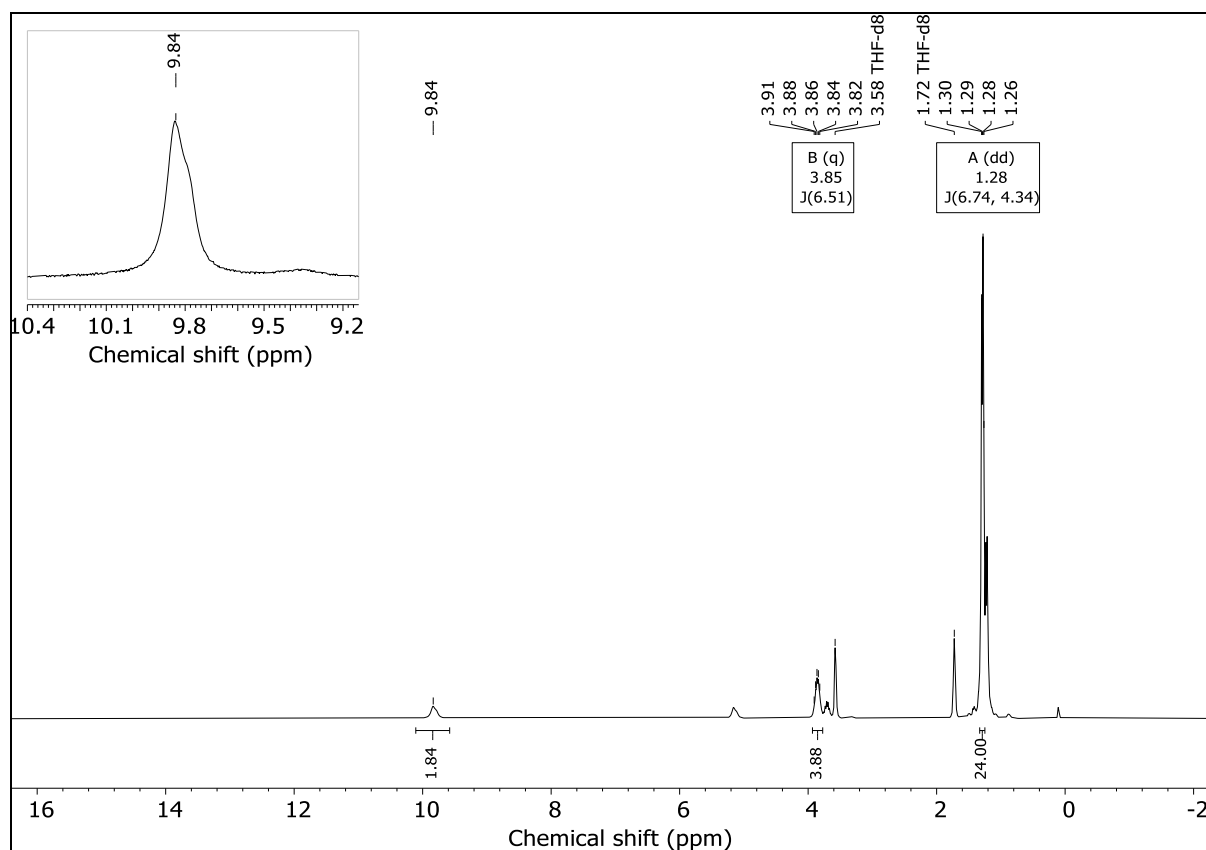
Figure S 7: ¹H NMR spectrum of CO(NH(CO)N*i*Pr₂)₂ in THF-d8.
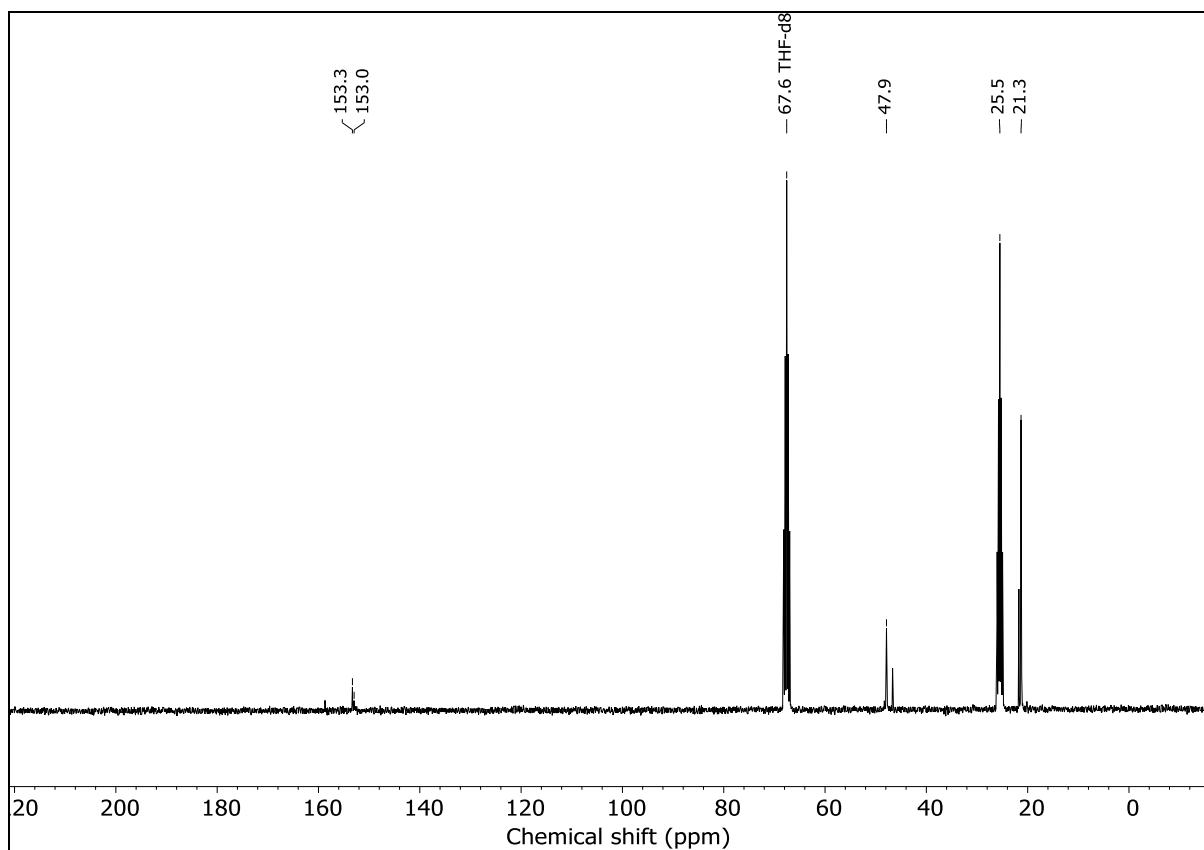
Figure S 8: ^{13}C NMR spectrum of CO(NH(CO)N*i*Pr$_2$)$_2$ in THF-d8.
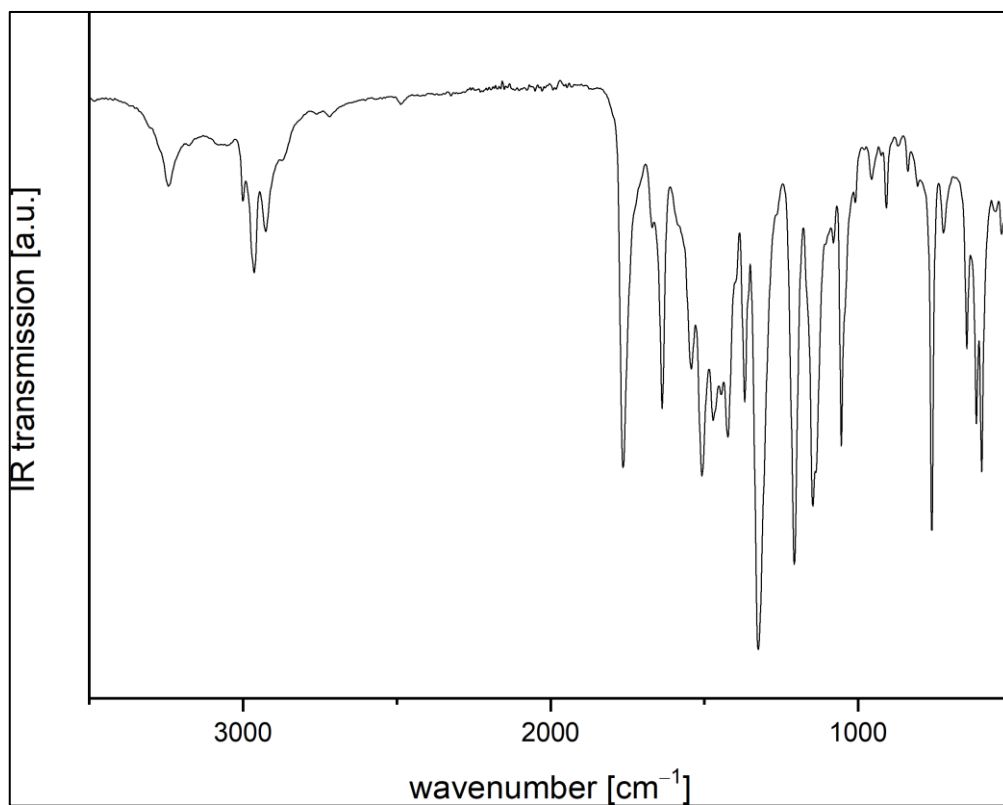
Figure S 9: Measured room-temperature ATR-IR spectrum CO(NH(CO)N*i*Pr$_2$)$_2$.

1.3. General synthesis of CO(NH(CO)OR)₂

As not other mentioned the following procedure applies to all syntheses. To a 1 M solution of carbonyl diisocyanate in THF (1.0 mL, 1.0 mmol, 1.0 eq.) cooled to 0 °C a 1 M solution of alcoholic nucleophile (2.0 mL, 2.0 mmol, 2.0 eq.) was added dropwise. The solution was allowed to warm to room temperature and stirred for 16 h to 18 h. *n*-Hexane (6.0 mL) was added, and the solution stirred for few minutes. The solvent was evaporated under reduced pressure and the reaction product obtained as powder. Further purification was done by washing with diethyl ether and *n*-hexane.

1.3.1. Synthesis of CO(NH(CO)OMe)₂ – 2Me

The reaction was carried out in a 5.0 mmol approach according to carbonyl diisocyanate. The crude product was sublimed at 120 °C in a dynamic vacuum ($1 \cdot 10^{-2}$ mbar). CO(NH(CO)OMe)₂ was obtained as colourless powder (78%, 3.93 mmol, 692 mg). Slow evaporating the solvent of a THF solution afforded single crystals.

CHN for $C_5H_8N_2O_5$ Found % (calc. %): C 33.97 (34.10), H 4.523 (4.58), N 16.22 (15.91).

¹H NMR (CDCl₃): δ = 9.10 (s, 2H, N*H*), 3.81 (s, 6H, C*H₃*) ppm.

¹³C{¹H} NMR (CDCl₃): δ = 152.7 (N(*CO*)N), 148.7 (N(CO)O), 53.6 (*CH₃*) ppm.

Mass (ESI+, MeOH) for $[M+H^+] = C_5H_8N_2O_5H^+$ m/z found (calc.): 177.0506 (177.0511).
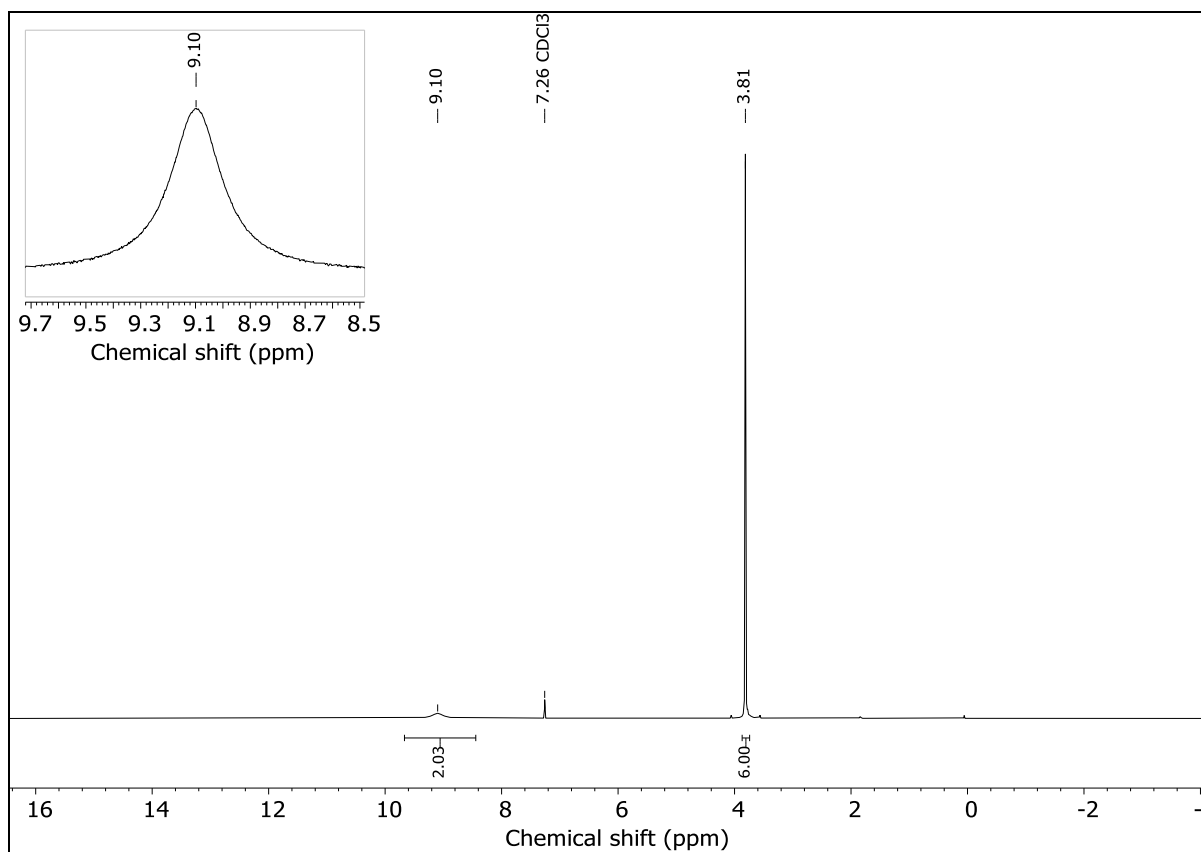
Figure S 10: ^{1}H NMR spectrum of CO(NH(CO)OMe)$_2$ in CDCl$_3$.
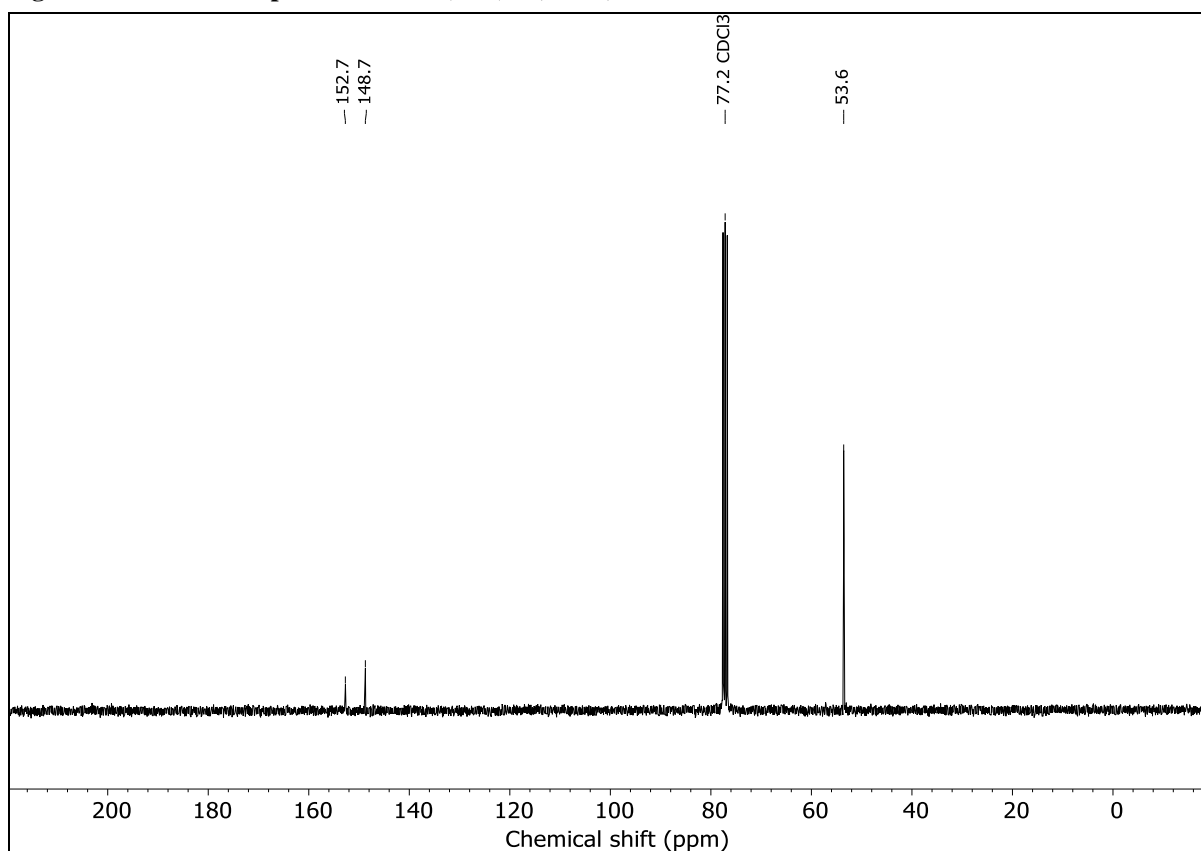
Figure S 11: ^{13}C NMR spectrum of CO(NH(CO)OMe)$_2$ in CDCl$_3$.
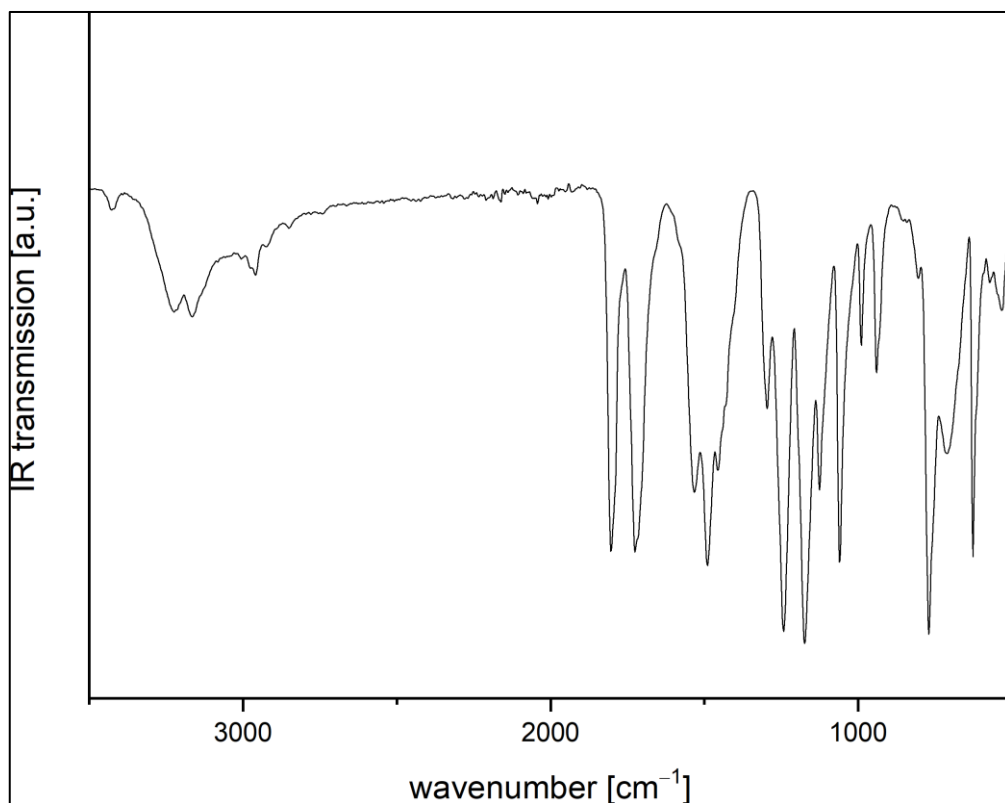
Figure S 12: Measured room-temperature ATR-IR spectrum of CO(NH(CO)OMe)₂.

1.3.2. Synthesis of CO(NH(CO)OEt)₂ – 2Et

CO(NH(CO)OEt)$_2$ was obtained as colourless, fluffy powder (62%, 0.62 mmol, 126 mg). Crystals could be obtained by slow evaporating the solvent of a THF solution.

CHN for C$_7$H$_{12}$N$_2$O$_5$ Found % (calc. %): C 41.11 (41.18), H 6.144 (5.92), N 13.79 (13.72).

^{1}H NMR (CDCl$_3$): δ = 9.05 (s, 2H, N*H*), 4.24 (q, 4H, $^3J_{HH}$ = 7.10 Hz, C*H*$_2$CH$_3$), 1.30 (t, 6H, $^3J_{HH}$ = 7.12 Hz, CH$_2$C*H*$_3$) ppm.

^{13}C{^{1}H} NMR (CDCl$_3$): δ = 152.2 (N(*CO*)N), 148.9 (N(*CO*)O), 62.9 (*C*H$_2$CH$_3$), 14.2 (CH$_2$*C*H$_3$) ppm.

Mass (ESI+, MeOH) for [M+Na$^+$] = C$_7$H$_{12}$N$_2$O$_5$Na$^+$ m/z found (calc.): 227.0644 (227.0644).
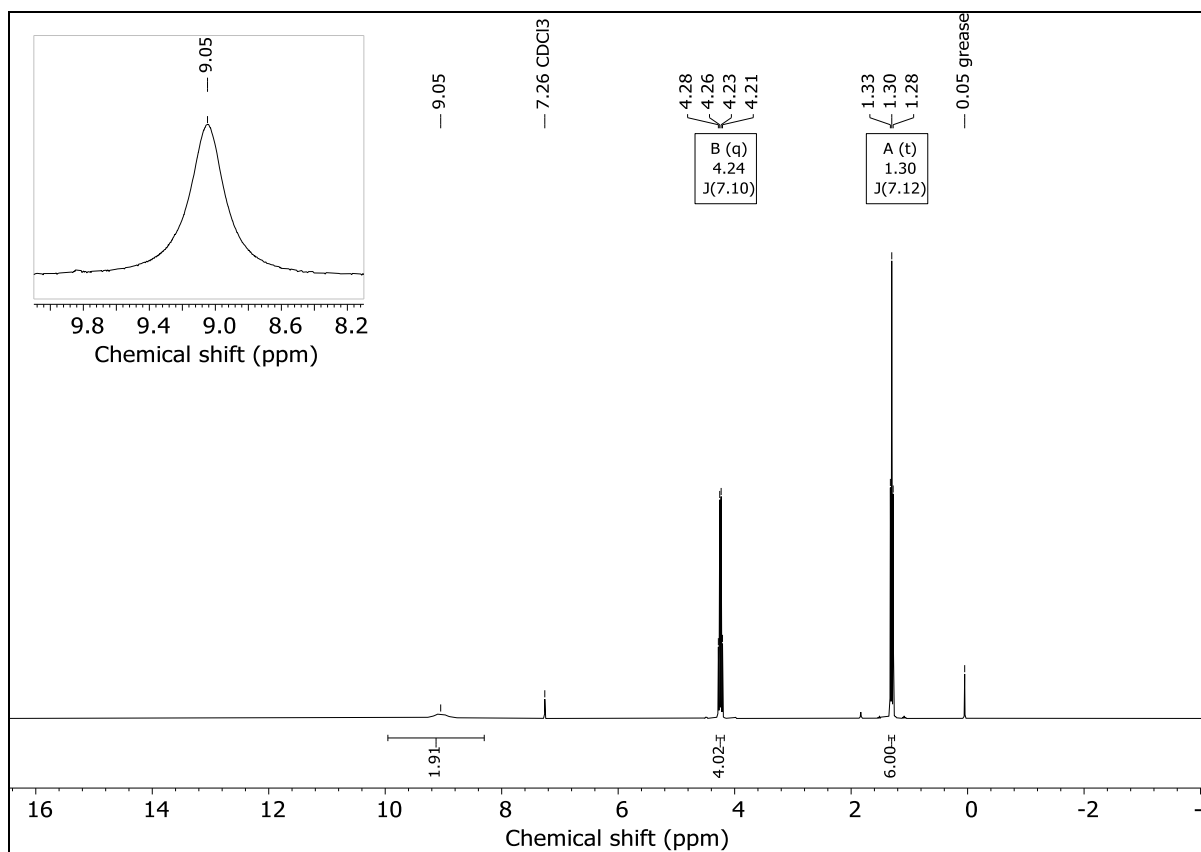
Figure S 13: ^{1}H NMR spectrum of CO(NH(CO)OEt)$_2$ in CDCl$_3$.
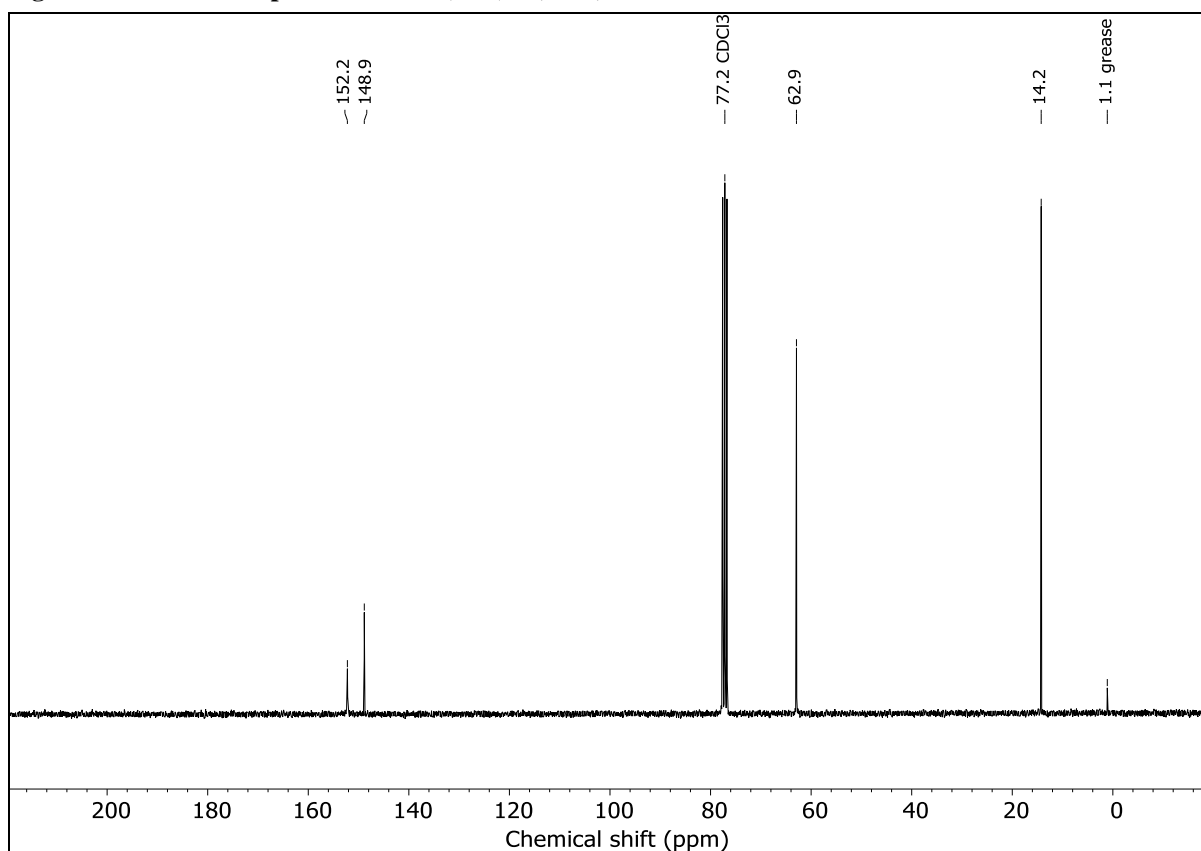
Figure S 14: ^{13}C NMR spectrum of CO(NH(CO)OEt)$_2$ in CDCl$_3$.
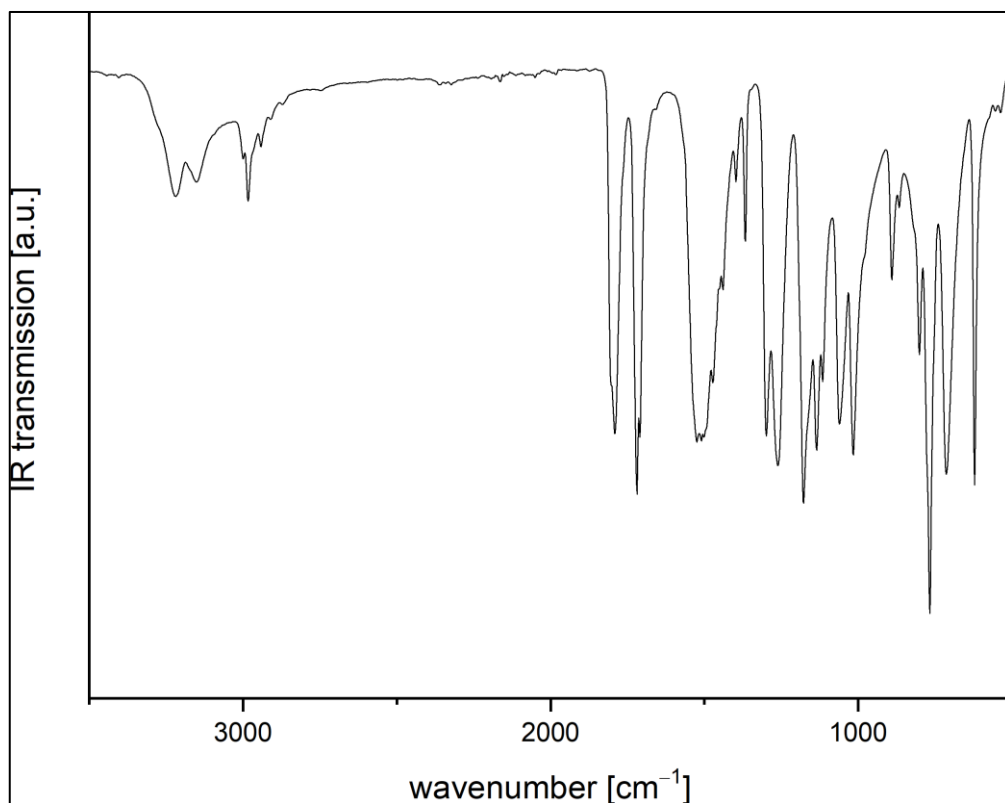
Figure S 15: **Measured room-temperature ATR-IR spectrum of CO(NH(CO)OEt)₂.**

1.3.3. Synthesis of CO(NH(CO)O*i*Pr)₂ − 2*i*Pr

CO(NH(CO)O*i*Pr)₂ was obtained as colourless powder (58%, 0.57 mmol, 134 mg) and it was crystallized by slow evaporating a THF solution.

CHN for $C_9H_{16}N_2O_5$ Found % (calc. %): C 45.80 (46.55), H 7.039 (6.94), N 12.49 (12.06).

¹H NMR (CDCl₃): δ = 8.93 (s, 2H, N*H*), 5.00 (hept, 2H, $^3J_{HH}$ = 6.21 Hz, C*H*), 1.28 (d, 6H,

$^3J_{HH}$ = 6.32 Hz, C*H₃*) ppm.

¹³C{¹H} NMR (CDCl₃): δ = 151.8 (N(*C*O)N), 148.9 (N(*C*O)O), 71.0 (*C*H), 21.8 (*C*H₃) ppm.

Mass (ESI+, MeOH) for [M+Na⁺] = $C_9H_{16}N_2O_5Na^+$ m/z found (calc.): 255.0958 (255.0957).
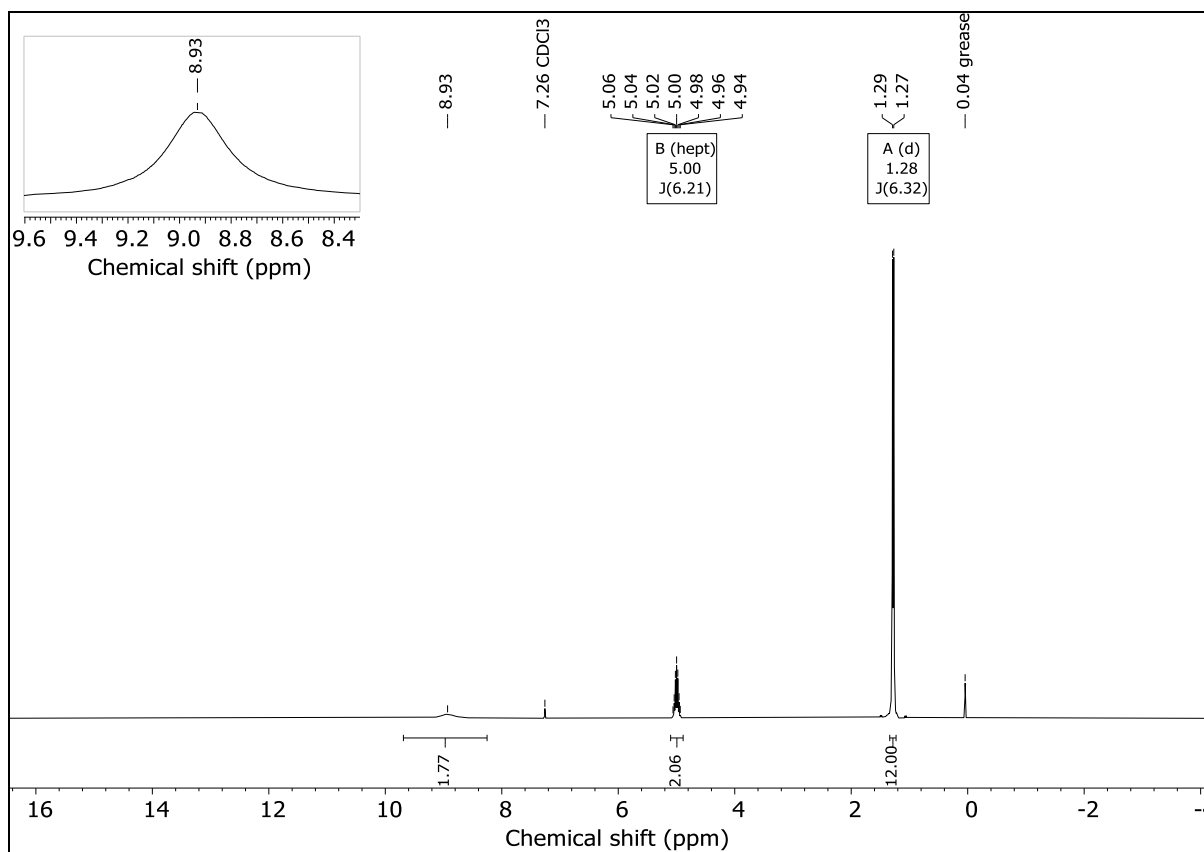
Figure S 16: ^{1}H NMR spectrum of CO(NH(CO)O*i*Pr)$_2$ in CDCl$_3$.
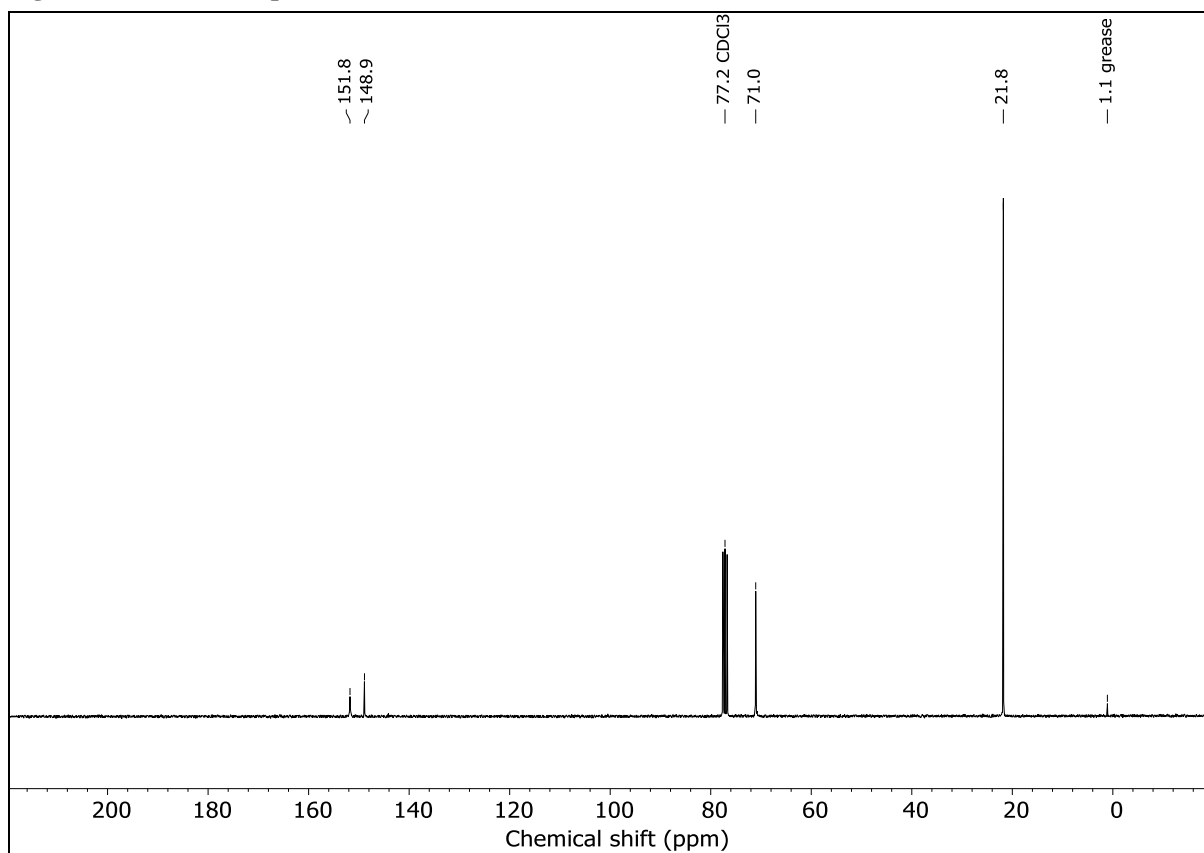
Figure S 17: ^{13}C NMR spectrum of CO(NH(CO)O*i*Pr)$_2$ in CDCl$_3$.
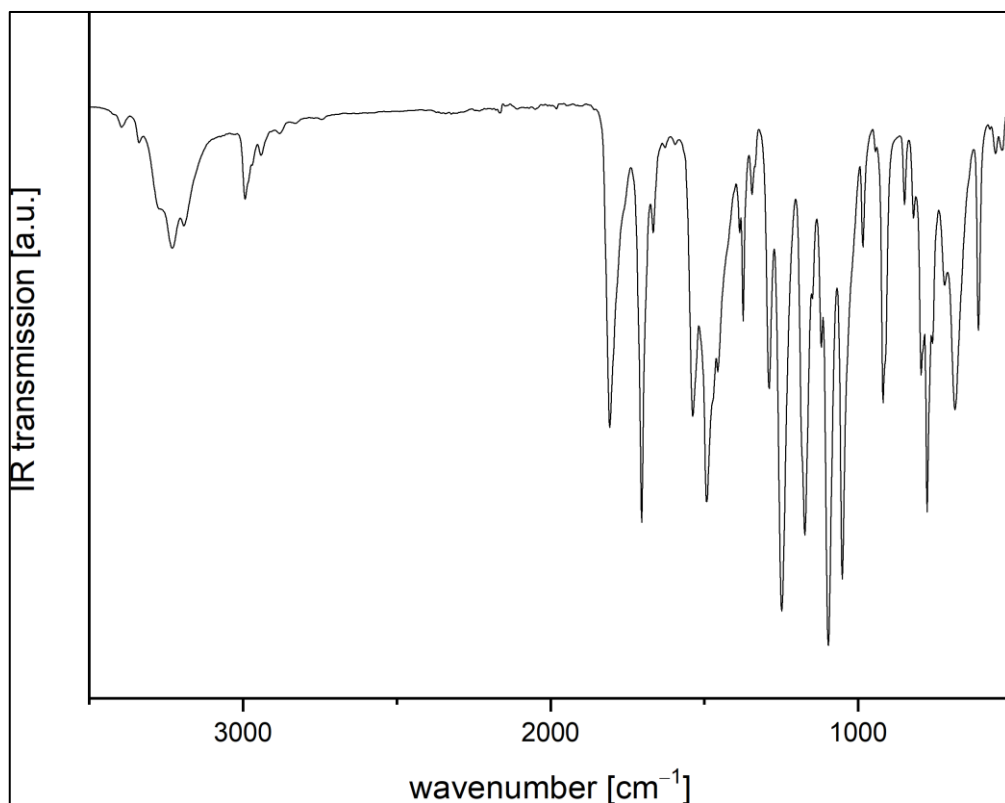
Figure S 18: Measured room-temperature ATR-IR spectrum of CO(NH(CO)O*i*Pr)₂.

1.3.4. Synthesis of CO(NH(CO)O*n*Bu)₂ – 2*n*Bu

CO(NH(CO)O*n*Bu)₂ was obtained as colourless powder (66%, 0.66 mmol, 172 mg).

CHN for $C_{11}H_{20}N_2O_5$ Found % (calc. %): C 49.89 (50.76), H 7.886 (7.75), N 10.84 (10.76).

¹H NMR (CDCl₃): δ = 9.03 (s, 2H, N*H*), 4.18 (t, 4H, $^3J_{HH}$ = 6.65 Hz, OC*H*₂), 1.64 (p, 4H,

$^3J_{HH}$ = 6.69 Hz, OCH₂C*H*₂), 1.37 (dq, 4H, $^3J_{HH}$ = 14.42 Hz, $^3J_{HH}$ = 7.31 Hz, C*H*₂CH₃),

0.92 (t, 4H, $^3J_{HH}$ = 7.36 Hz, CH₂C*H*₃) ppm.

¹³C{¹H} NMR (CDCl₃): δ = 152.3 (N(*C*O)N), 148.8 (N(*C*O)O), 66.7 (O*C*H₂), 30.6

(OCH₂*C*H₂), 19.0 (*C*H₂CH₃), 13.7 (CH₂*C*H₃) ppm.

Mass (ESI+, MeOH) for [M+H⁺] = $C_{11}H_{20}N_2O_5H^+$ m/z found (calc.): 261.1452 (261.1450).
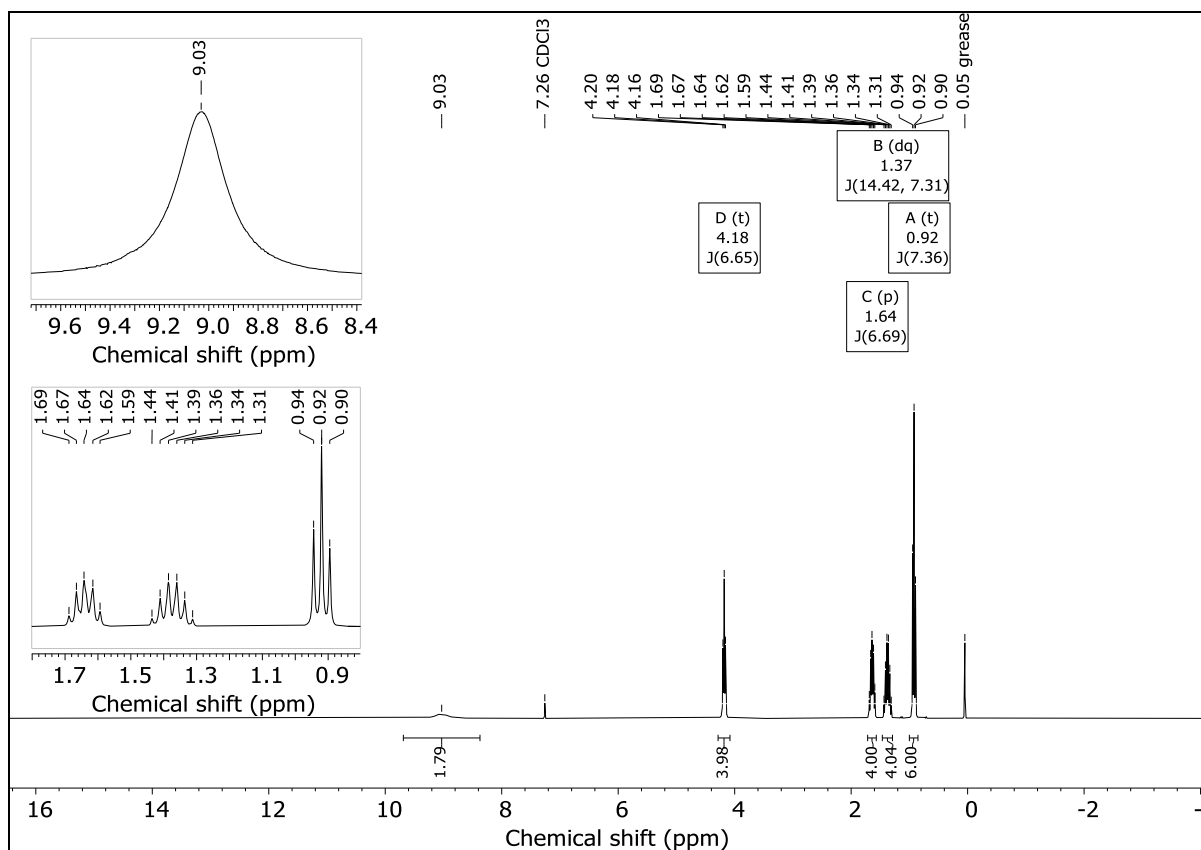
Figure S 19: ¹H NMR spectrum of CO(NH(CO)O*n*Bu)₂ in CDCl₃.
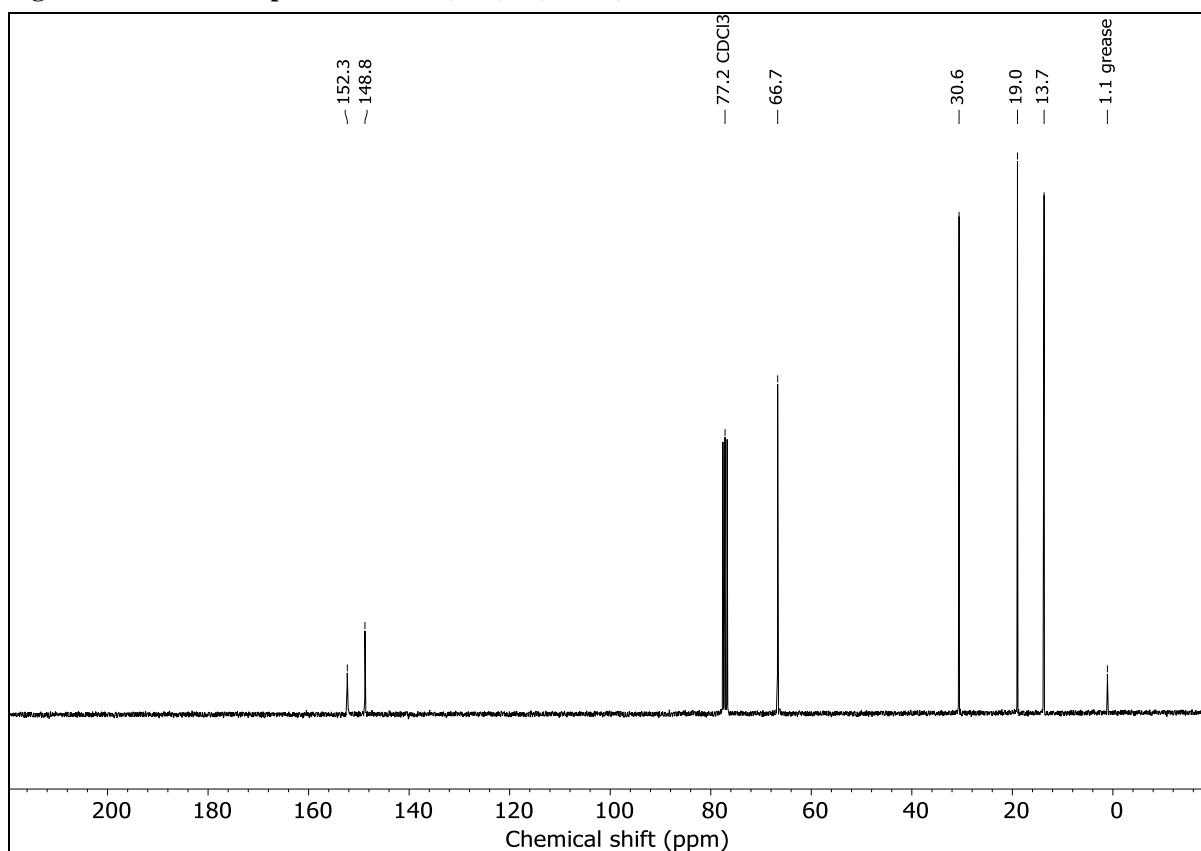
Figure S 20: ¹³C NMR spectrum of CO(NH(CO)O*n*Bu)₂ in CDCl₃.
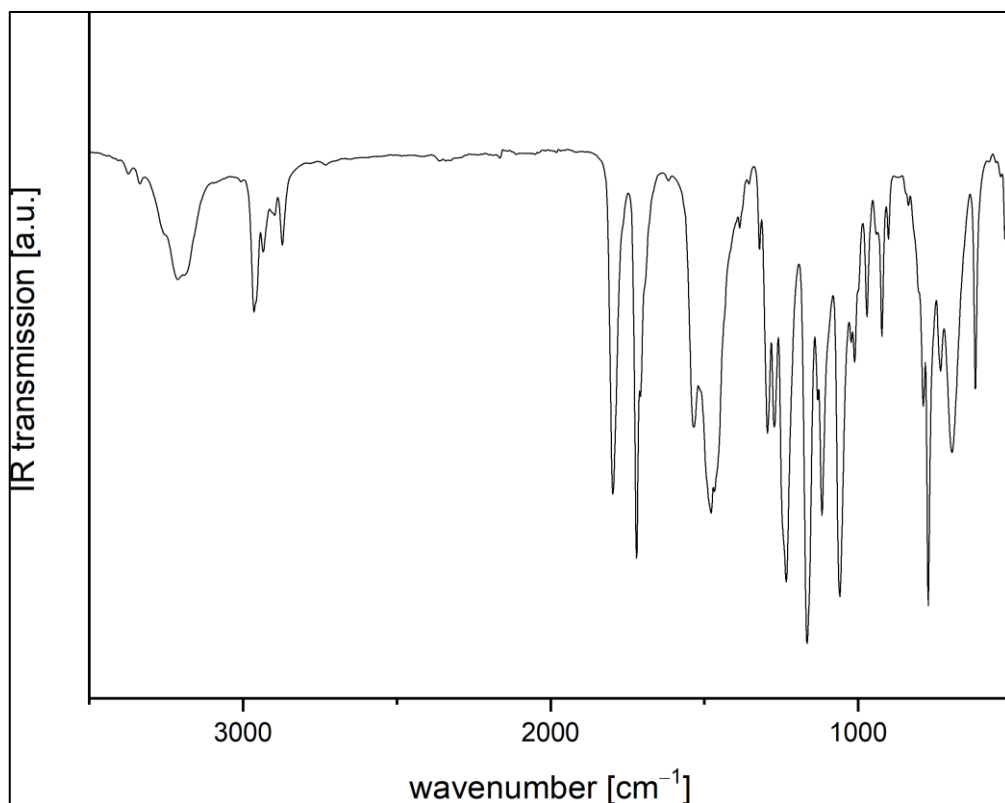
Figure S 21: Measured room-temperature ATR-IR spectrum of CO(NH(CO)O*n*Bu)₂.

1.3.5. Synthesis of CO(NH(CO)O*s*Bu)₂ − 2*s*Bu

CO(NH(CO)O*s*Bu)₂ was obtained as colourless powder (52%, 0,52 mmol, 135 mg). Crystals could be obtained by slow evaporating a saturated *n*-hexane solution, but were not suitable for single crystal X-ray diffraction.

CHN for $C_{11}H_{20}N_2O_5$ Found % (calc. %): C 48.32 (50.76), H 7.330 (7.75), N 12.15 (10.76).

¹H NMR (CDCl₃): δ = 8.85 (s, 2H, N*H*), 4.84 (h, 2H, $^3J_{HH}$ = 6.27 Hz, OC*H*), 1.61 (m, 4H, OCHC*H₂*), 1.26 (d, 6H, $^3J_{HH}$ = 6.26 Hz, OCHC*H₃*), 0.91 (t, 6H, $^3J_{HH}$ = 7.46 Hz, CH₂C*H₃*) ppm.

¹³C{¹H} NMR (CDCl₃): δ = 152.0 (N(*C*O)N), 148.7 (N(*C*O)O), 75.6 (O*C*H), 28.8 (OCH*C*H₂), 19.5 (OCH*C*H₃), 9.6 (CH₂*C*H₃) ppm.

Mass (ESI+, MeOH) for [M+NH₄⁺] = $C_{11}H_{20}N_2O_5NH_4^+$ m/z found (calc.): 278.1718 (278.1716).
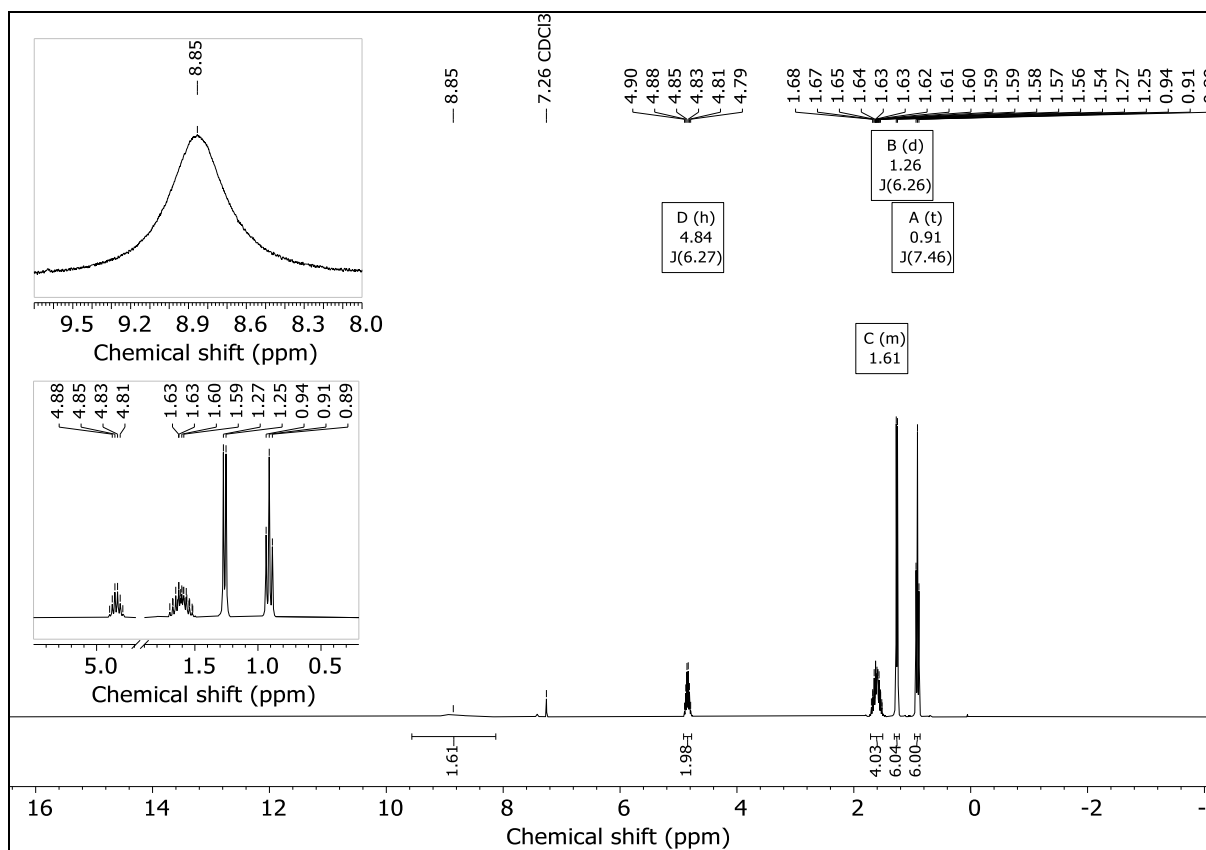
Figure S 22: ^{1}H NMR spectrum of CO(NH(CO)O*s*Bu)$_2$ in CDCl$_3$.
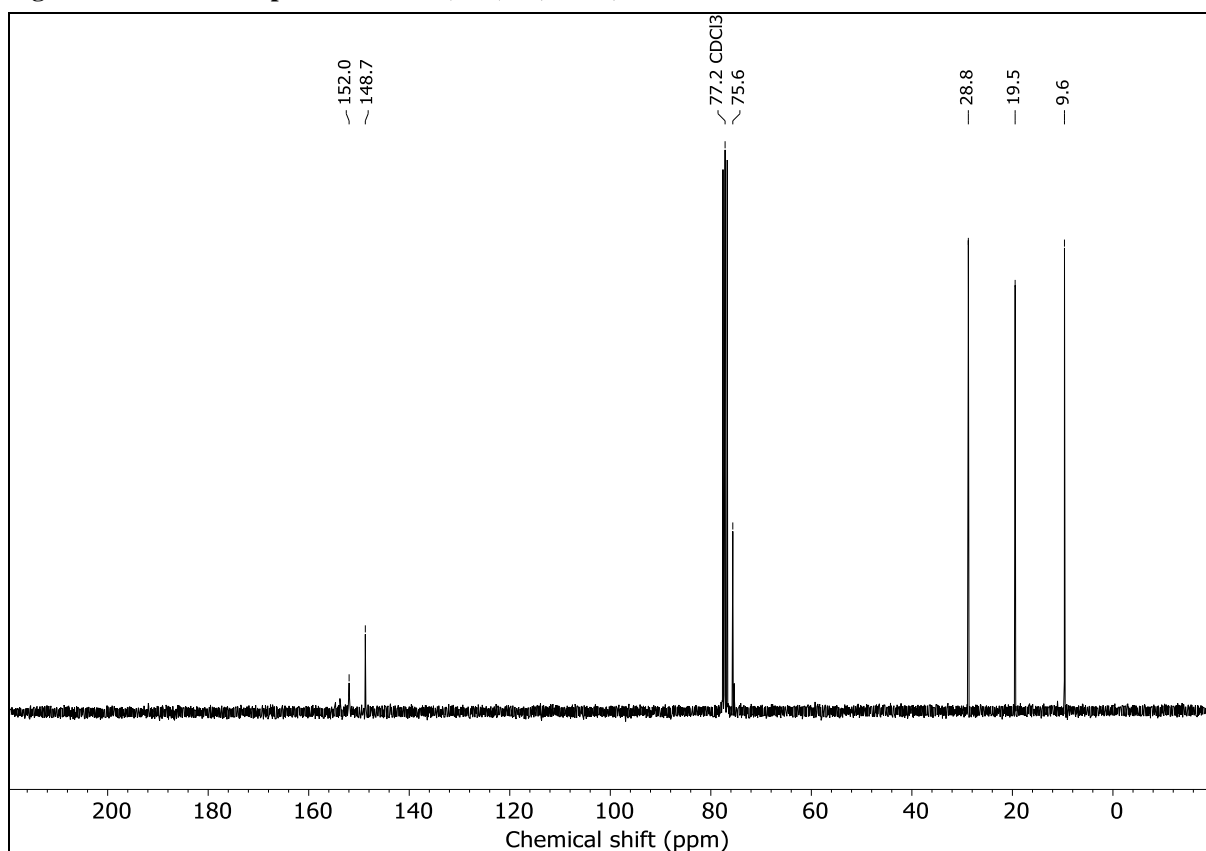
Figure S 23: ^{13}C NMR spectrum of CO(NH(CO)O*s*Bu)$_2$ in CDCl$_3$.
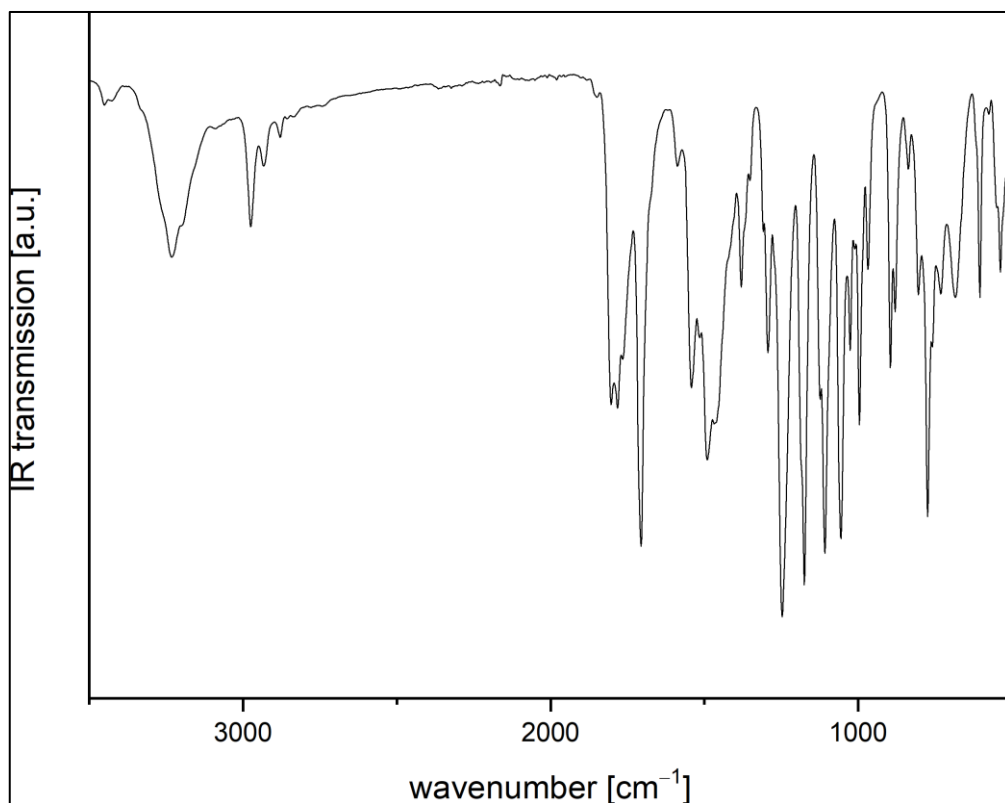
Figure S 24: Measured room-temperature ATR-IR spectrum of CO(NH(CO)O*s*Bu)₂.

1.3.6. Synthesis of CO(NH(CO)O*t*Bu)₂ – 2*t*Bu

CO(NH(CO)O*t*Bu)₂ was obtained as colourless powder (77%, 0.77 mmol, 200 mg). It was crystallized by slow evaporating from a THF solution.

CHN for $C_{11}H_{20}N_2O_5$ Found % (calc. %): C 49.50 (50.76), H 7.446 (7.75), N 10.66 (10.76).

¹H NMR (THF-d8): δ = 9.73 (s, 2H, N*H*), 1.47 (s, 18H, C*H₃*) ppm.

¹³C{¹H} NMR (THF-d8): δ = 152.5 (N(*C*O)N), 148.9 (N(*C*O)O), 82.5 (*C*CH₃), 28.4 (*C*H₃) ppm.

Mass (ESI+, MeOH) for [M+H⁺] = $C_{11}H_{20}N_2O_5H^+$ m/z found (calc.): 261.1442 (261.1445).
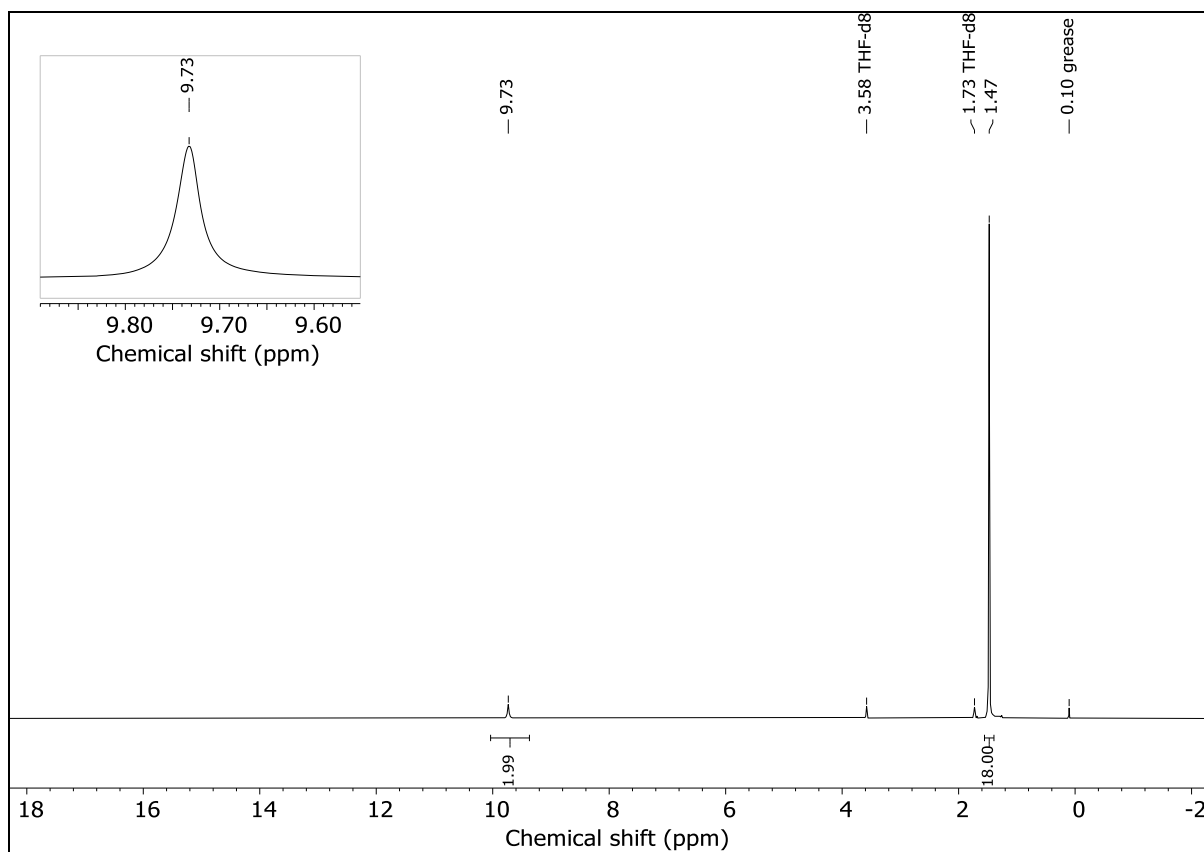
Figure S 25: ^{1}H NMR spectrum of CO(NH(CO)O*t*Bu)$_2$ in THF-d8.
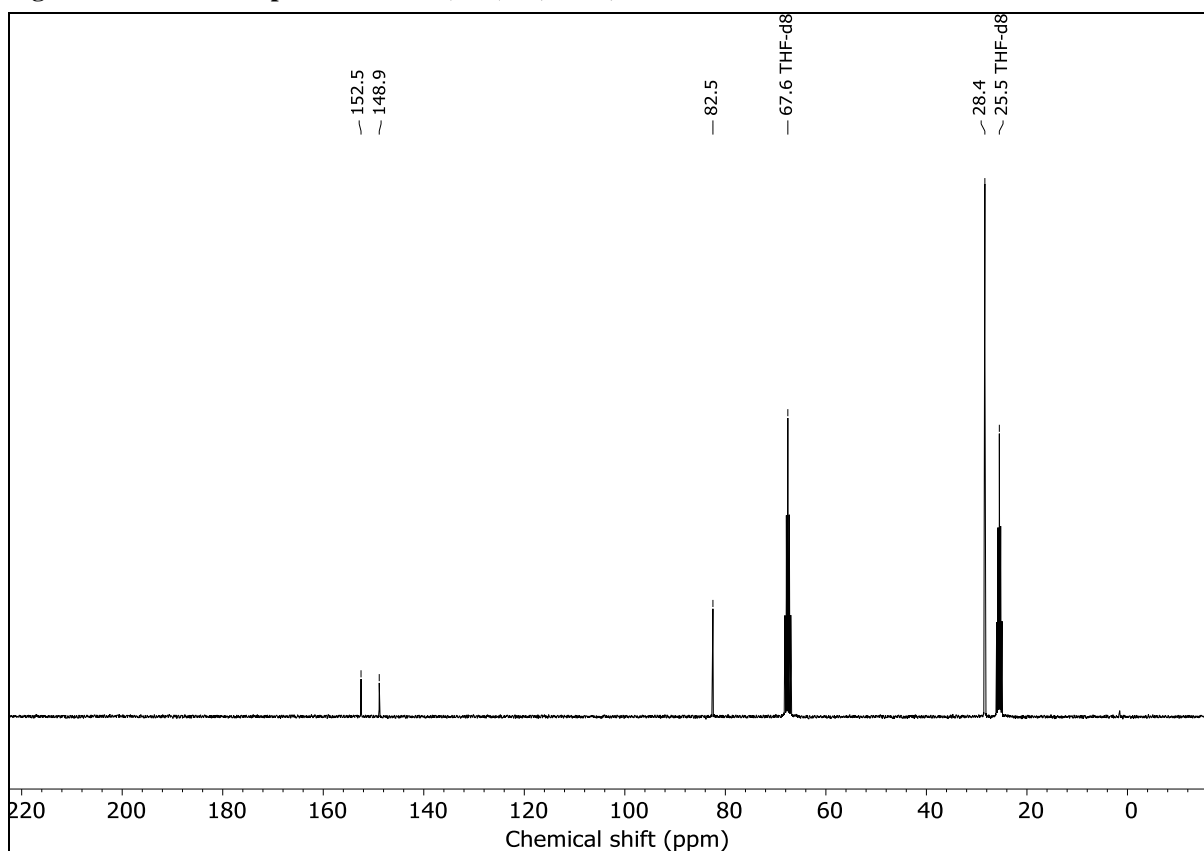
Figure S 26: ^{13}C NMR spectrum of CO(NH(CO)O*t*Bu)$_2$ in THF-d8.
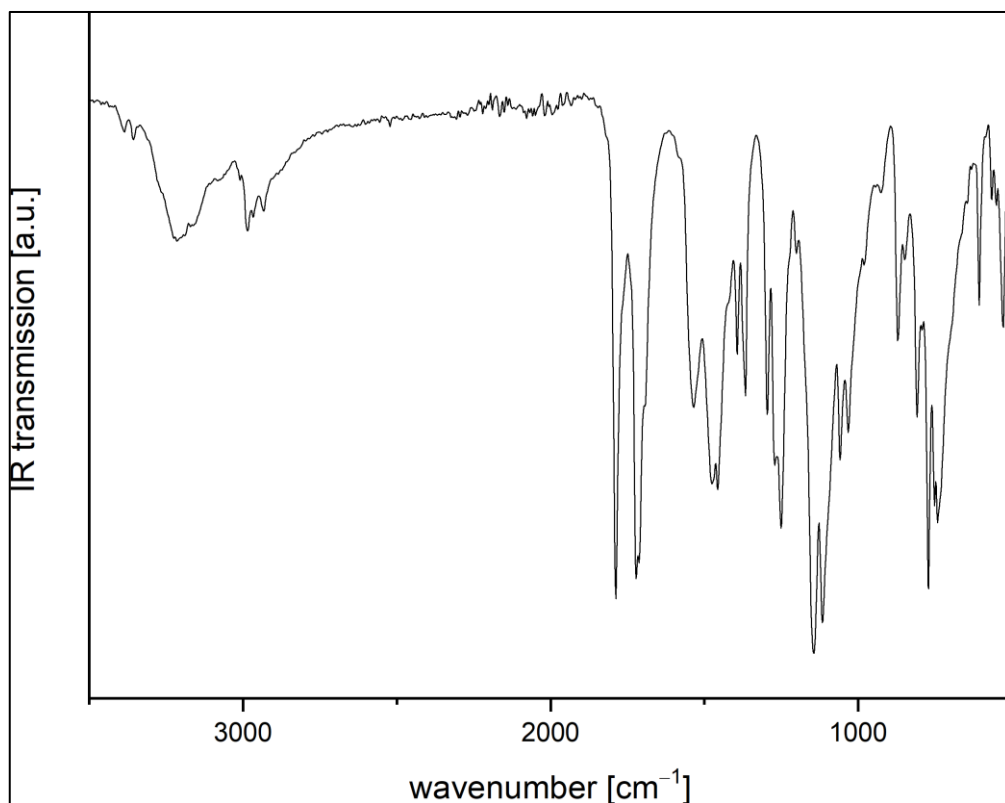
Figure S 27: Measured room-temperature ATR-IR spectrum of CO(NH(CO)O*t*Bu)₂.

1.3.7. Synthesis of CO(NH(CO)O*n*Pen)₂ – 2*n*Pen

CO(NH(CO)O*n*Pen)₂ was obtained as colourless powder (74%, 0.74 mmol, 214 mg).

CHN for $C_{11}H_{20}N_2O_5$ Found % (calc. %): C 53.32 (54.15), H 8.371 (8.39), N 9.76 (9.72).

¹H NMR (CDCl₃): δ = 9.04 (s, 2H, N*H*), 4.17 (7, 4H, $^3J_{HH}$ = 6.75 Hz, OC*H₂*), 1.66 (m, 4H, OCH₂C*H₂*) 1.32 (m, 8H, C*H₂*C*H₂*CH₃), 0.89 (m, 6H, C*H₃*) ppm.

¹³C{¹H} NMR (CDCl₃): δ = 152.3 (N(*C*O)N), 148.8 (N(*C*O)O), 67.0 (O*C*H₂), 28.3 (OCH₂*C*H₂), 27.9 (*C*H₂CH₂CH₃), 22.3 (CH₂*C*H₂CH₃), 14.0 (*C*H₃) ppm.

Mass (ESI+, MeOH) for [M+Na⁺] = $C_{13}H_{24}N_2O_5Na^+$ m/z found (calc.): 311.1584 (311.1583).

Figure S 28: ¹H NMR spectrum of CO(NH(CO)O*n*Pen)₂ in CDCl₃.

Figure S 29: ¹³C NMR spectrum of CO(NH(CO)O*n*Pen)₂ in CDCl₃.
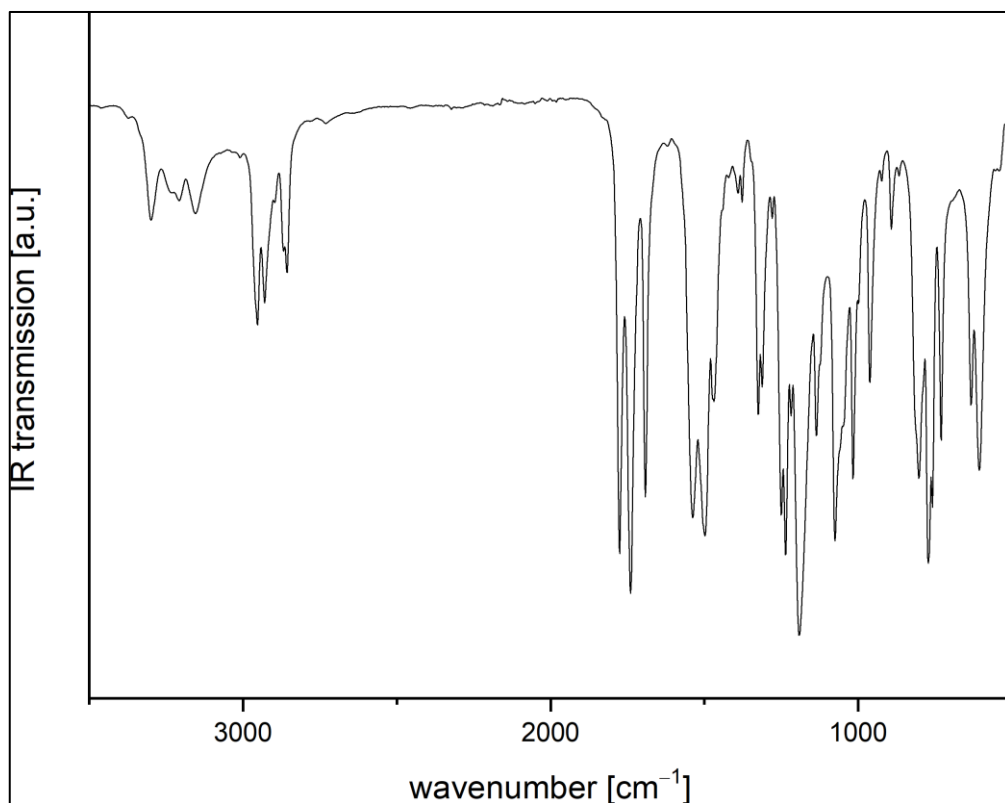
Figure S 30: Measured room-temperature ATR-IR spectrum of CO(NH(CO)OnPen)$_2$.

1.3.8. Synthesis of CO(NH(CO)OnOct)$_2$ – 2nOct

CO(NH(CO)OnOct)$_2$ was washed with cold diethyl ether and cold n-hexane. It was obtained es colourless powder (80%, 0.80 mmol, 299 mg). Crystals were obtained by slow evaporating a THF solution.

CHN for C$_{19}$H$_{36}$N$_2$O$_5$ Found % (calc. %): C 60.68 (61.26), H 9.841 (9.74), N 7.65 (7.52).

^{1}H NMR (CDCl$_3$): δ = 8.81 (s, 2H, NH), 4.18 (t, 4H, $^1J_{HH}$ = 6.72 Hz, OCH_2), 1.66 (m, 4H, OCH$_2$CH_2) 1.28 (m, 20H, OCH$_2$(CH_2)$_5$CH$_3$), 0.87 (m, 6H, CH_3) ppm.

^{13}C{^{1}H} NMR (CDCl$_3$): δ = 152.3 (N(CO)N), 148.4 (N(CO)O), 67.1 (OCH$_2$), 31.9 (OCH$_2$(CH$_2$)$_5$CH$_3$), 29.2 (OCH$_2$(CH$_2$)$_5$CH$_3$) 28.6 (OCH$_2$$CH_2$), 25.8 (OCH$_2$($CH_2$)$_5CH_3$), 22.7 (OCH$_2$($CH_2$)$_5CH_3$), 14.2 ($CH_3$) ppm.

Mass (ESI+, MeOH) for [M+Na$^+$] = C$_{19}$H$_{36}$N$_2$O$_5$Na$^+$ m/z found (calc.): 395.2526 (395.2522).
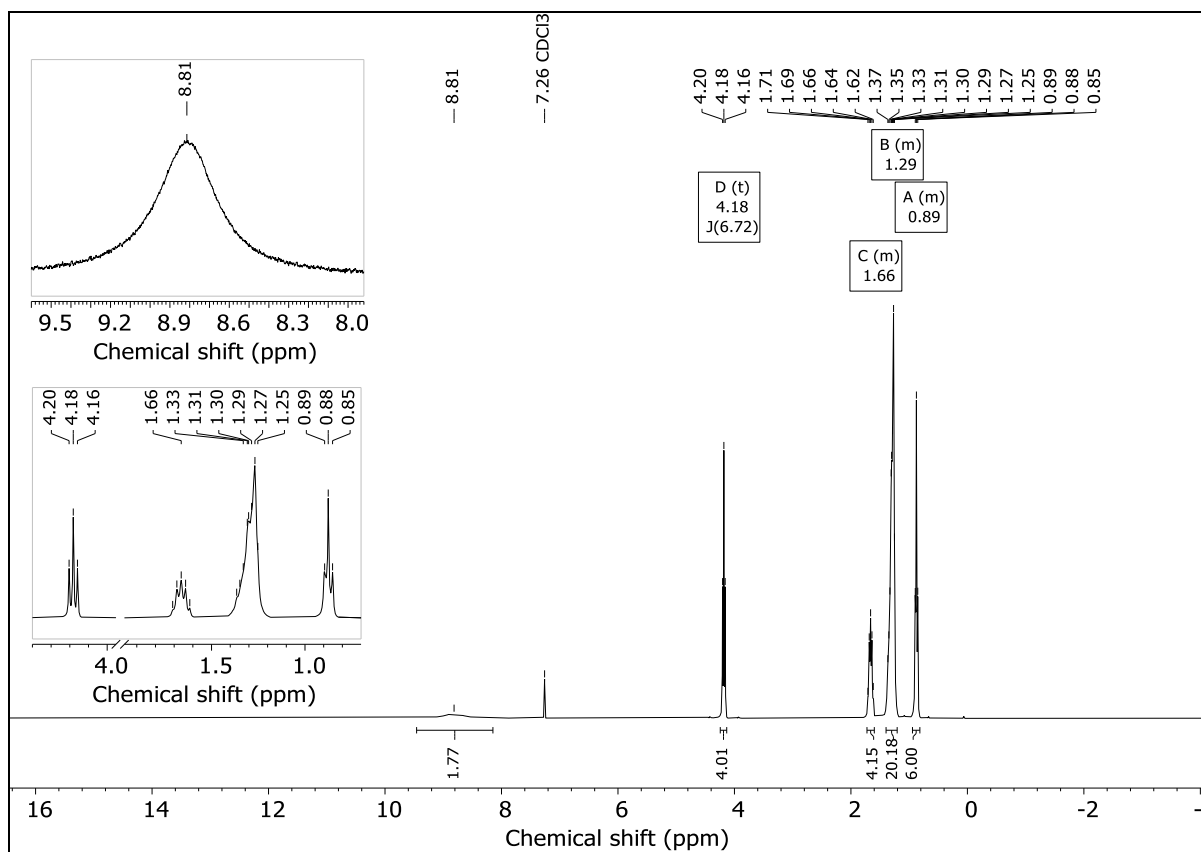
Figure S 31: ^{1}H NMR spectrum of CO(NH(CO)O*n*Oct)$_2$ in CDCl$_3$.
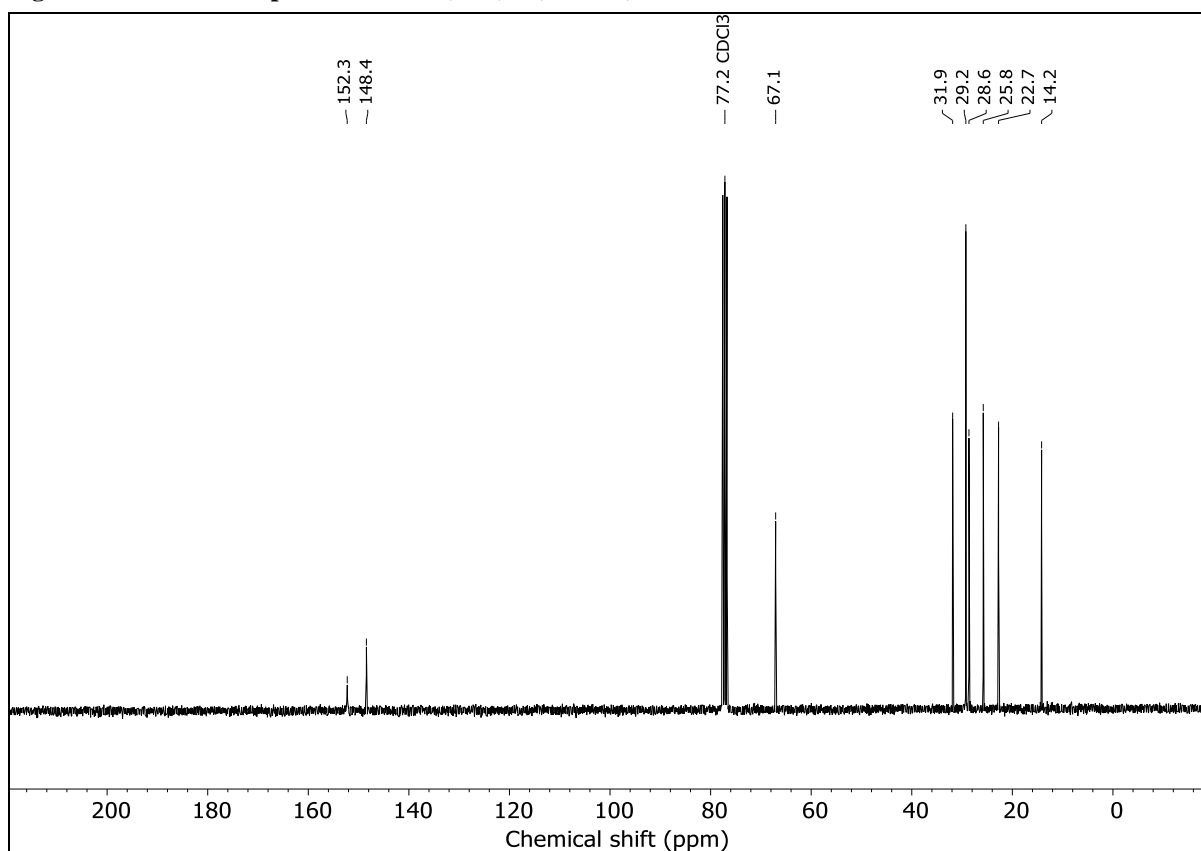
Figure S 32: ^{13}C NMR spectrum of CO(NH(CO)O*n*Oct)$_2$ in CDCl$_3$.
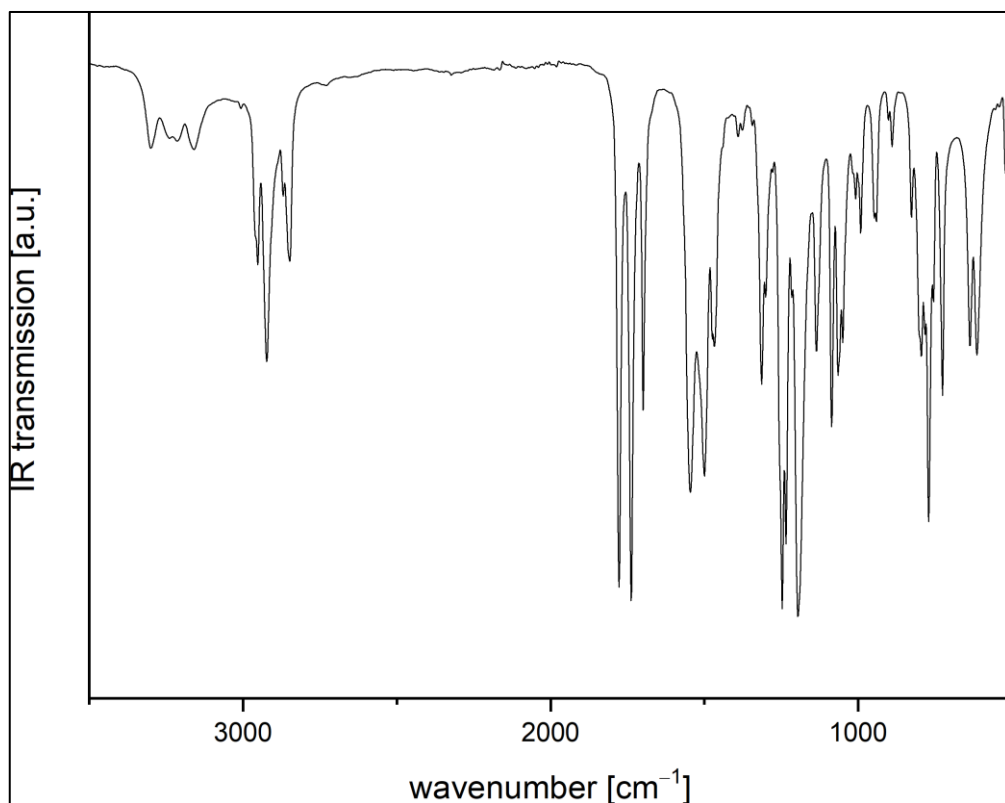
Figure S 33: Measured room-temperature ATR-IR spectrum of CO(NH(CO)O*n*Oct)₂.

1.3.9. Synthesis of CO(NH(CO)OAd)₂ – 2Ad

CO(NH(CO)OAd)₂ was dried in vacuo at 70 °C and obtained as colourless powder (80%, 0.80 mmol, 299 mg). Crystals were obtained by layering a solution in toluene with *n*-pentane.

CHN for $C_{23}H_{32}N_2O_5$ Found % (calc. %): C 62.90 (64.54), H 7.078 (7.54), N 6.63 (6.55).

¹H NMR (CDCl₃): δ = 8.45 (s, 2H, N*H*), 2.19 (m, 6H, C*H*(CH₂)₃), 2.13 (m, 12H, OC(C*H*₂)₃)

      1.66 (m, 12H, C*H*₂(CH)₂) ppm.

¹³C{¹H} NMR (CDCl₃): δ = 150.5 (N(*C*O)N), 148.8 (N(*C*O)O), 83.4 (O*C*(CH₂)₃), 41.4

      (OC(*C*H₂)₃), 36.1 (*C*H₂(CH)₂) 31.1 (*C*H(CH₂)₃) ppm.

Mass (ESI+, MeOH) for [M+Na⁺] = $C_{23}H_{32}N_2O_5Na^+$ m/z found (calc.): 439.2209 (439.2209).
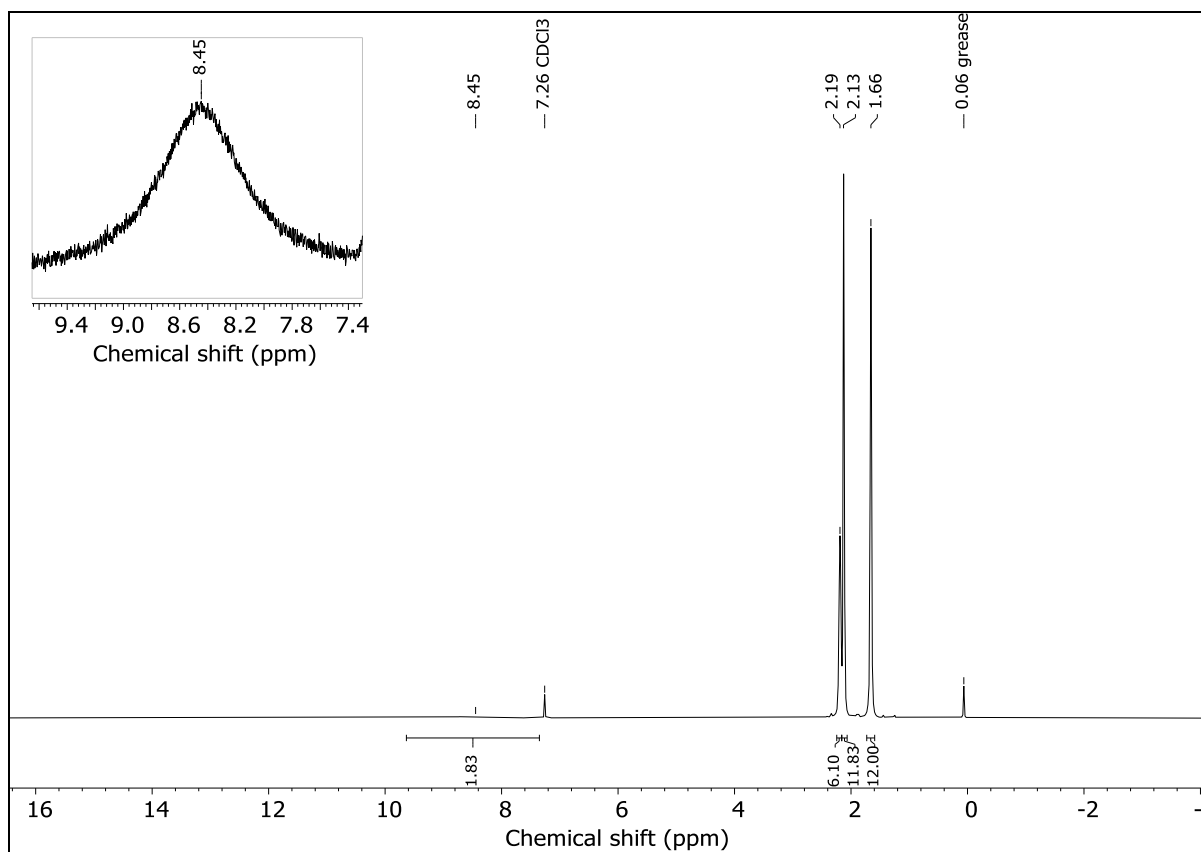
Figure S 34: ^{1}H NMR spectrum of CO(NH(CO)OAd)$_2$ in CDCl$_3$.
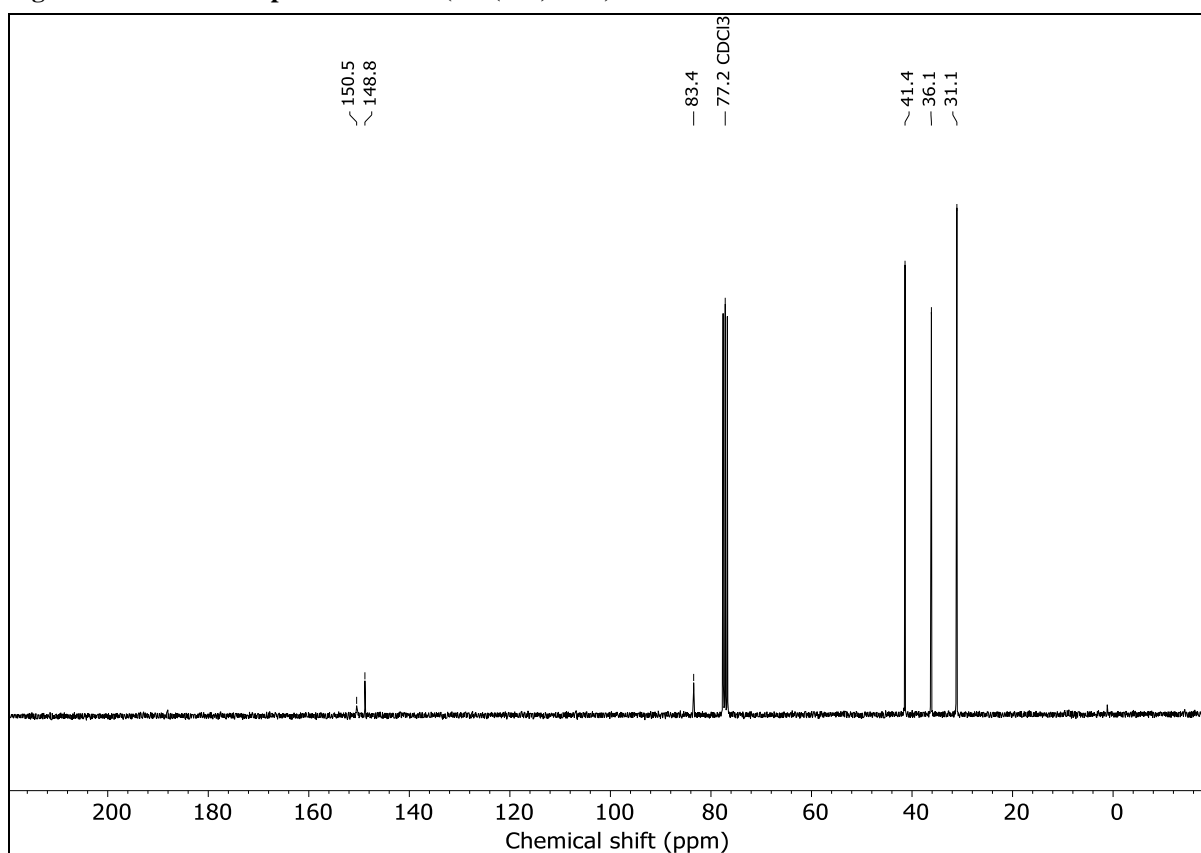
Figure S 35: ^{13}C NMR spectrum of CO(NH(CO)OAd)$_2$ in CDCl$_3$.
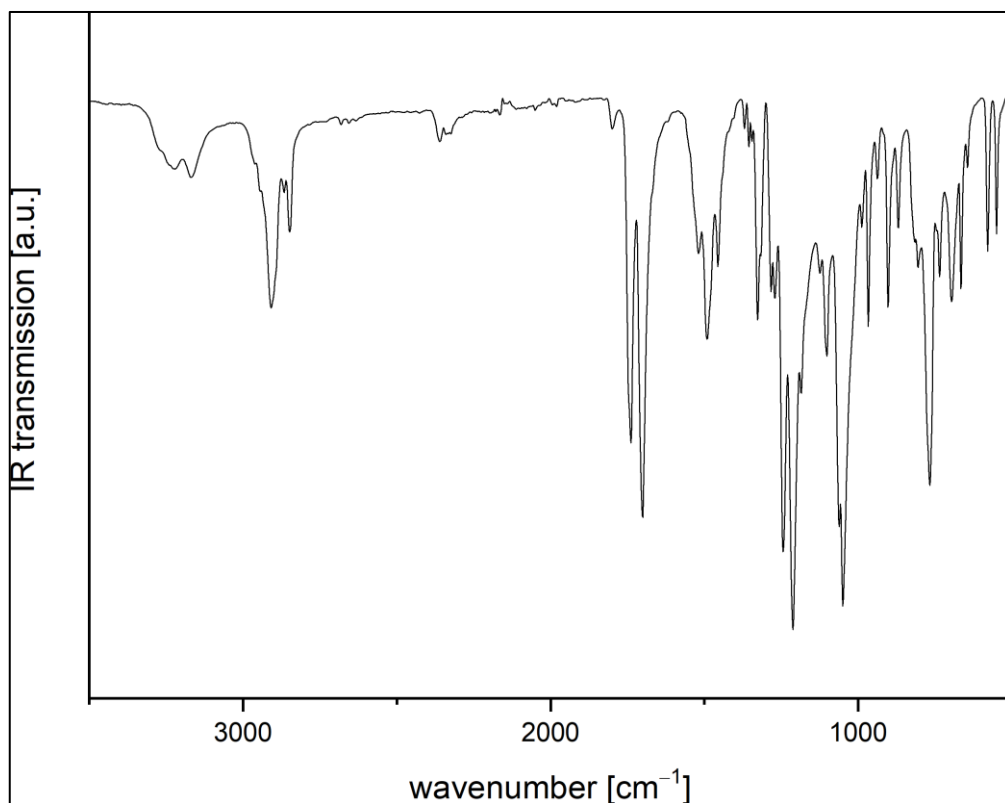
Figure S 36: Measured room-temperature ATR-IR spectrum of CO(NH(CO)OAd)₂.

1.3.10. Synthesis of CO(NH(CO)OBz)₂ – 2Bz

CO(NH(CO)OBz)2 was obtained as colourless powder (62%, 0.62 mmol, 202 mg). Crystals could be obtained by layering a THF solution with *n*-hexane.

CHN for $C_{17}H_{16}N_2O_5$ Found % (calc. %): C 62.33 (62.19), H 5.041 (4.91), N 8.64 (8.53).

¹H NMR (THF-d8): δ = 10.02 (s, 2H, N*H*), 7.34 (m, 10H, OCH₂C₆*H₅*), 5.17 (s, 4H,

OC*H₂*C₆H₅) ppm.

¹³C{¹H} NMR (THF-d8): δ = 153.5 (N(*C*O)N), 148.5 (N(*C*O)O), 137.0 ($C_{ipso\text{-Ph}}$), 129.4

($C_{ortho\text{-Ph}}$), 129.3 ($C_{meta\text{-Ph}}$), 129.2 ($C_{para\text{-Ph}}$), 68.3 (O*C*H₂C₆H₅) ppm.

Mass (ESI+, MeOH) for $[M+Na^+] = C_{17}H_{16}N_2O_5Na^+$ m/z found (calc.): 323.0942 (351.0951).
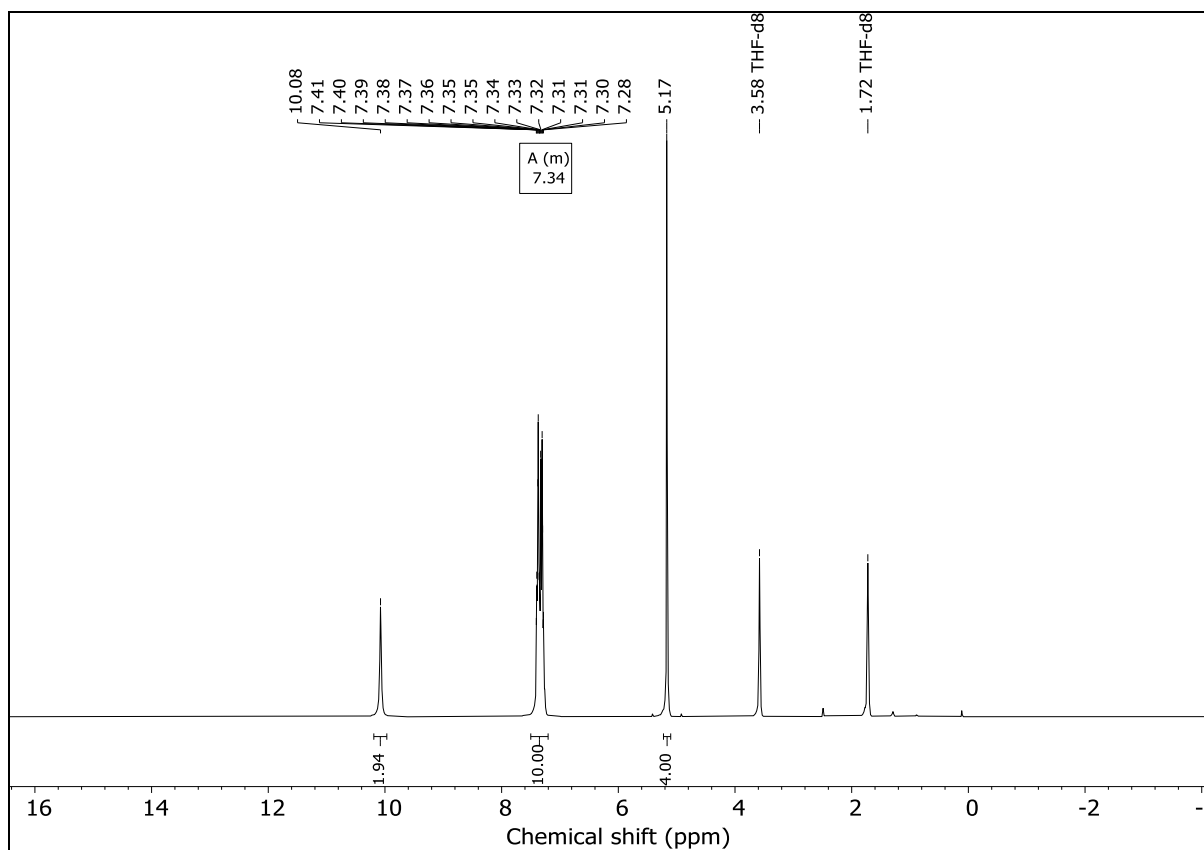
Figure S 37: ^1H NMR spectrum of CO(NH(CO)OBz)$_2$ in THF-d8.
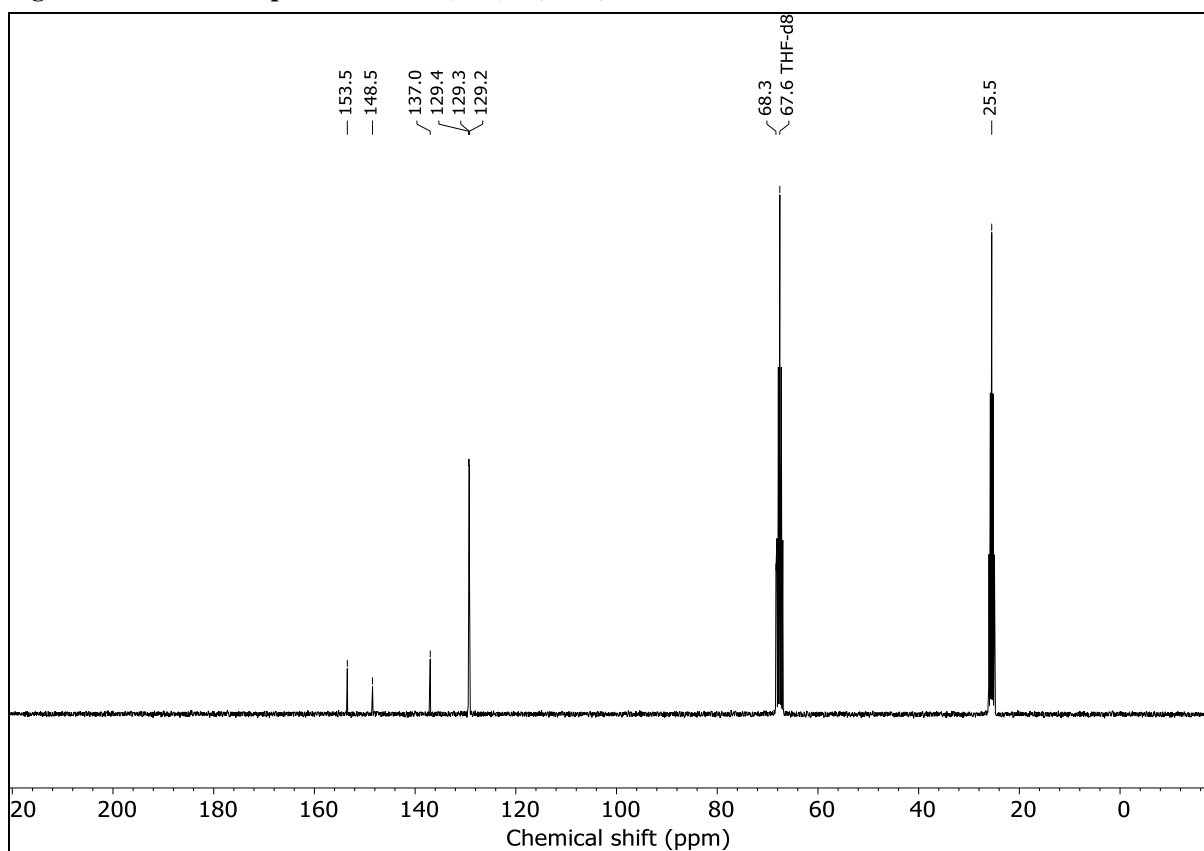
Figure S 38: ^{13}C NMR spectrum of CO(NH(CO)OBz)$_2$ in THF-d8.
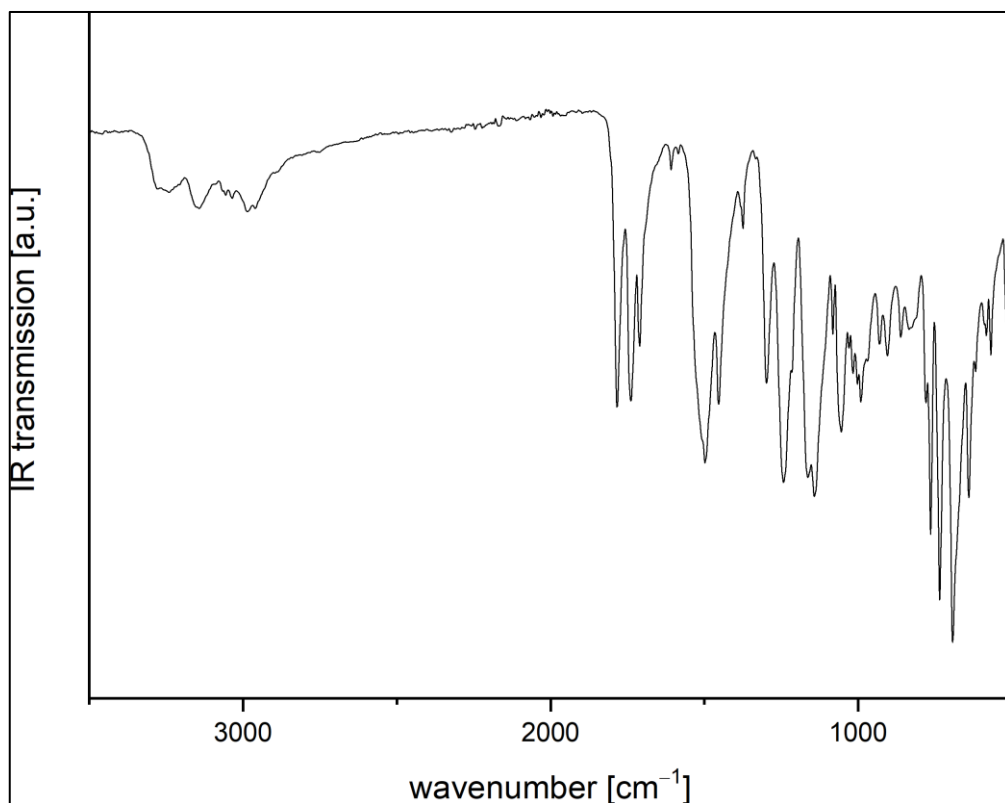
Figure S 39: Measured room-temperature ATR-IR spectrum of CO(NH(CO)OBz)₂.

1.3.11. Synthesis of CO(NH(CO)OPh)₂ – 2Ph

The reaction was carried out in a 3.0 mmol approach according to carbonyl diisocyanate. CO(NH(CO)OPh)₂ was obtained as colourless powder (71%, 2.1 mmol, 641 mg). It was crystalized by slow evaporating a THF solution.

CHN for $C_{15}H_{12}N_2O_5$ Found % (calc. %): C 58.78 (60.00), H 4.175 (4.03), N 9.16 (9.33).

^{1}H NMR (CDCl$_3$): δ = 9.22 (2H, NH), 7.45 (m, 4H, $H_{ortho\text{-Ph}}$), 7.33 (m, 2H, $H_{para\text{-Ph}}$), 7.22 (m, 4H, ($H_{meta\text{-Ph}}$) ppm.

^{13}C{^{1}H} NMR (CDCl$_3$): δ = 150.5 (N(CO)N), 149.8 ($C_{ipso\text{-Ph}}$), 147.9 (N(CO)O), 129.8 ($C_{ortho\text{-Ph}}$), 126.8 ($C_{para\text{-Ph}}$), 121.3 ($C_{meta\text{-Ph}}$) ppm.

Mass (ESI+, MeOH) for [M+Na$^+$] = $C_{15}H_{12}N_2O_5Na^+$ m/z found (calc.): 323.0638 (323.0636).
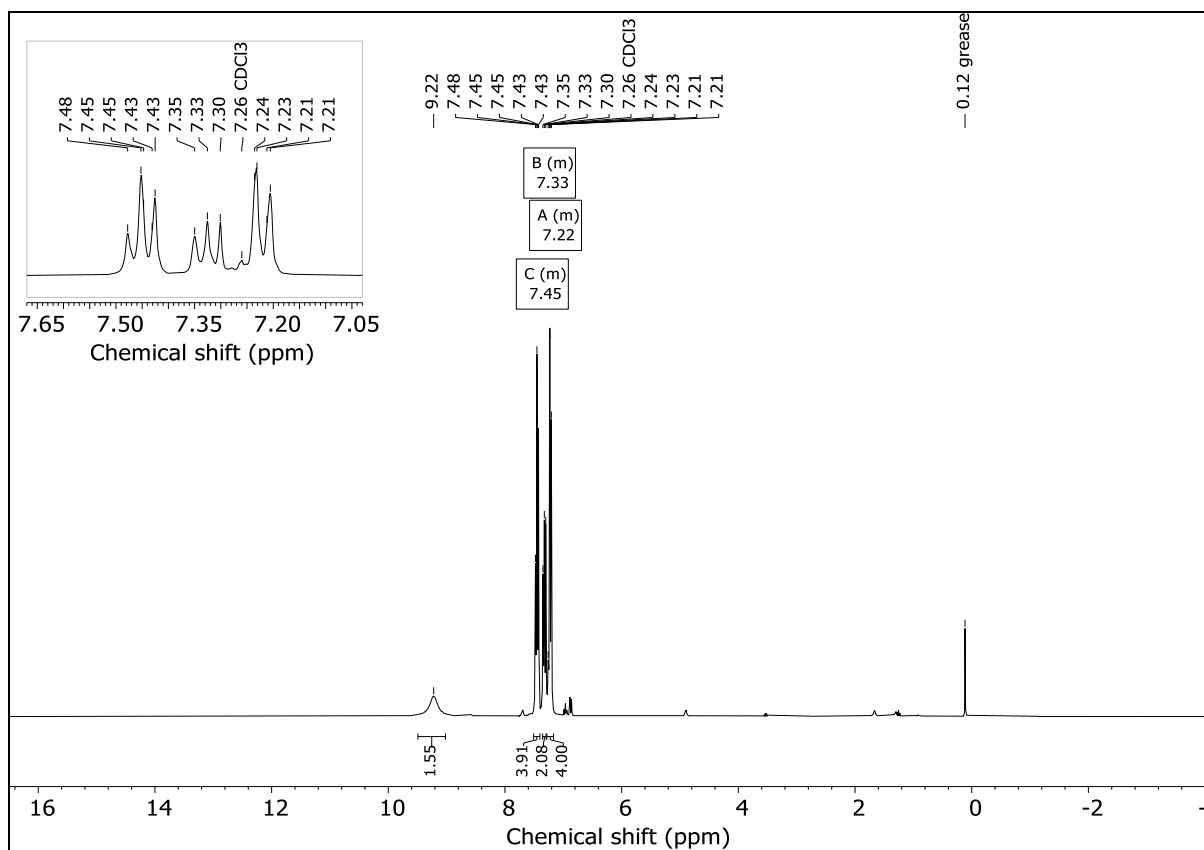
Figure S 40: ¹H NMR spectrum of CO(NH(CO)OPh)₂ in CDCl₃.
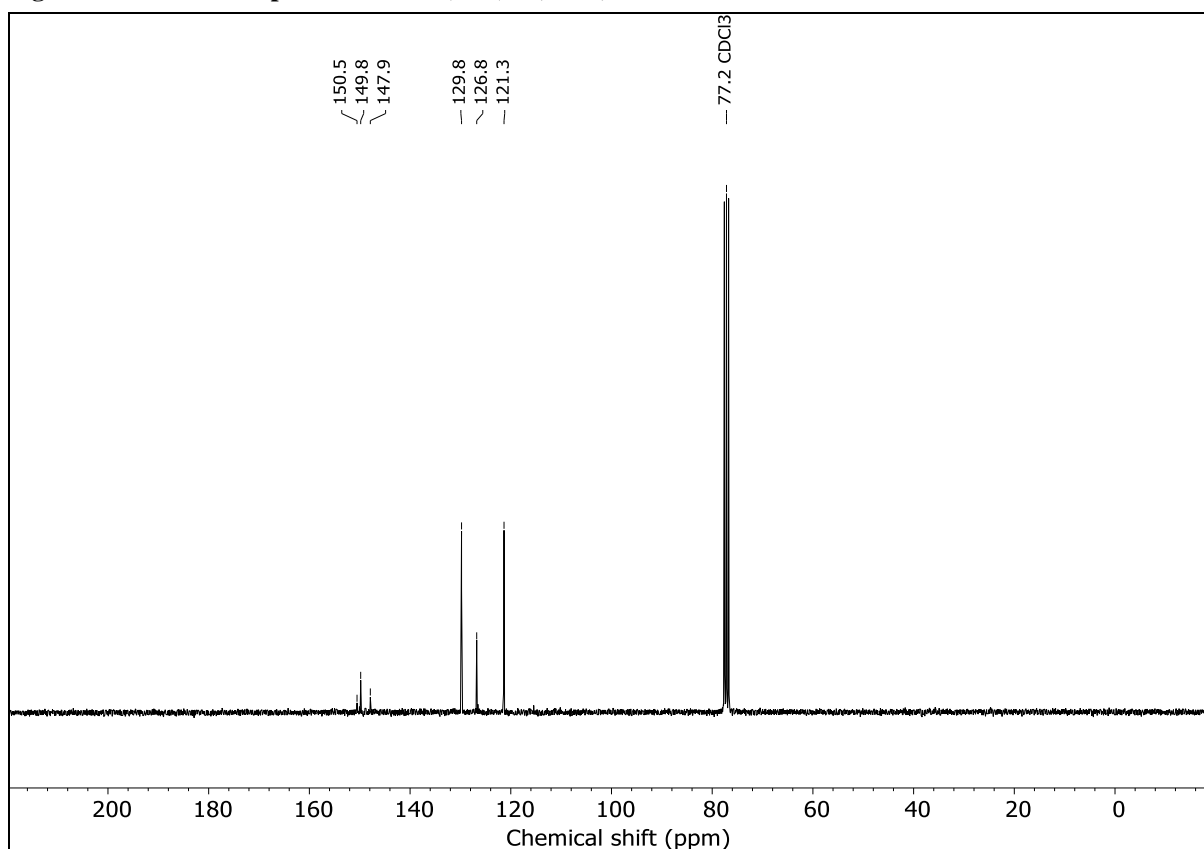
Figure S 41: ¹³C NMR spectrum of CO(NH(CO)OPh)₂ in CDCl₃.
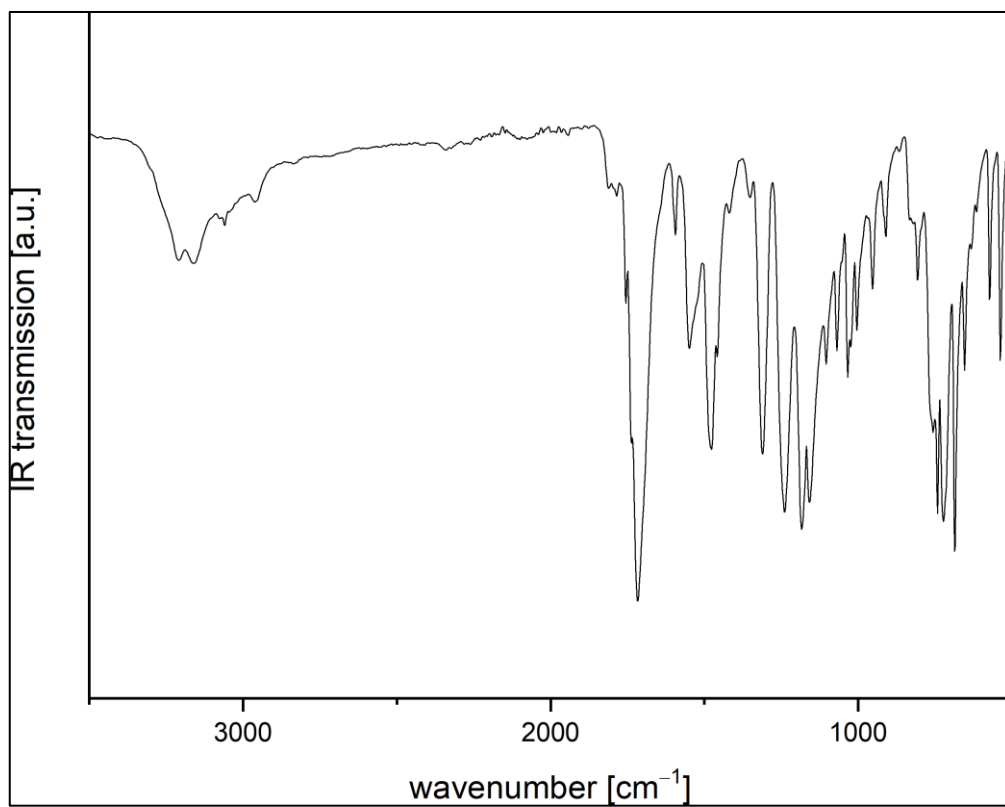
Figure S 42: Measured room-temperature ATR-IR spectrum of CO(NH(CO)OPh)$_2$.

1.4. General synthesis of CO(NH(CO)SR)₂

As no other mentioned the following procedure applies to all syntheses. To a 1 M solution of carbonyl diisocyanate in THF (1.0 mL, 1.0 mmol, 1.0 eq.) cooled to 0 °C a 1 M solution of thiol in THF (2.0 mL, 2.0 mmol, 2.0 eq.) was added dropwise. The reaction was stirred for 16 h to 18 h and allowed to warm to room temperature. The solvent was removed, and the residue suspended in dichloromethane (3 mL). The solvent was evaporated under reduced pressure and the remaining solid dried *in vacuo* at 70 °C.

1.4.1. Synthesis of CO(NH(CO)SEt)₂ – 3Et

CO(NH(CO)SEt)₂ was obtained as colourless powder (97%, 0.97 mmol, 230 mg).

CHNS for $C_7H_{12}N_2O_3S_2$ Found % (calc. %): C 35.64 (35.58), H 4.969 (5.12), N 12.40 (11.86), S 26.80 (27.13).

¹H NMR (CDCl₃): δ = 9.32 (s, 2H, N*H*), 2.97 (q, 4H, , $^1J_{HH}$ = 7.39 Hz, SC*H₂*), 1.33 (t, 6H, $^1J_{HH}$ = 7.39 Hz, CH₂C*H₃*) ppm.

¹³C{¹H} NMR (CDCl₃): δ = 170.0 (N(*C*O)S), 148.6 (N(*C*O)N), 24.9 (*C*H₂CH₃), 14.7 (CH₂*C*H₃) ppm.

Mass (ESI+, MeOH) for [M+H⁺] = $C_7H_{12}N_2O_3S_2H^+$ m/z found (calc.): 237.0368 (237.0368).
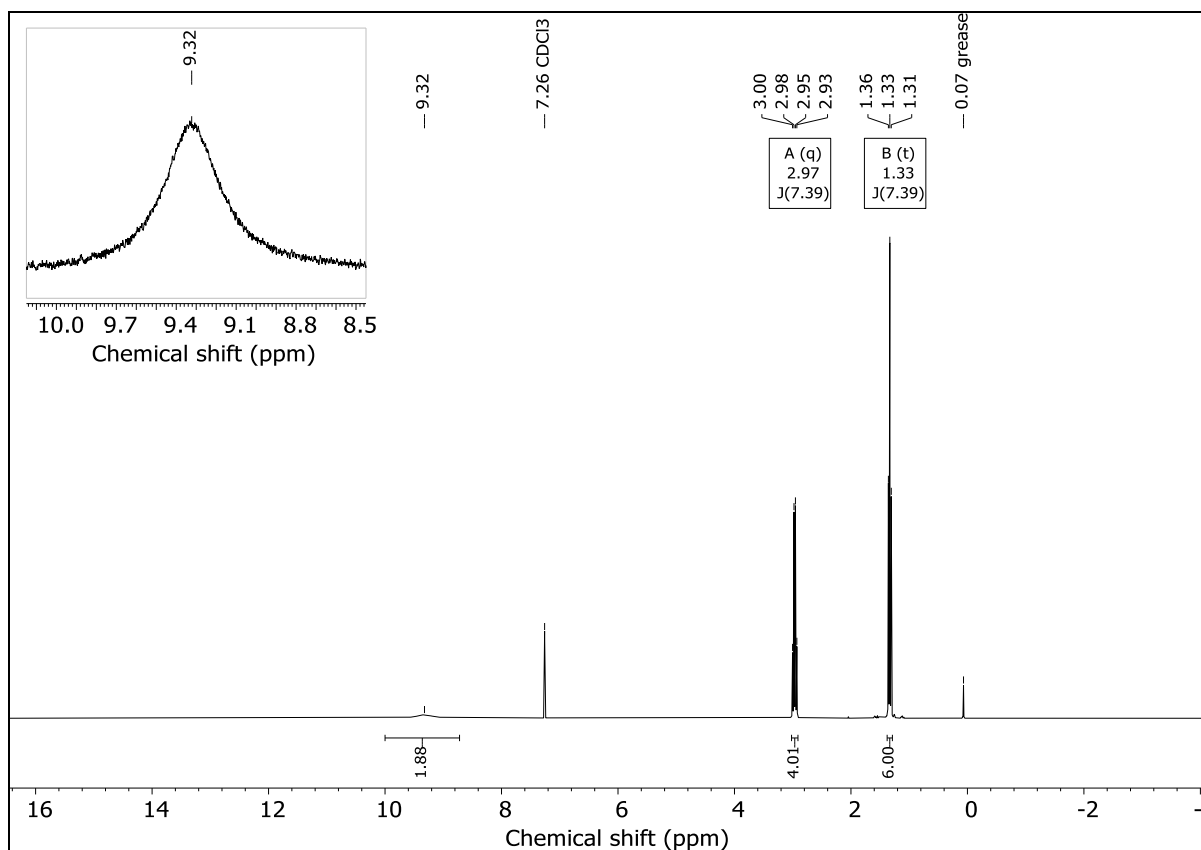
Figure S 43: ^{1}H NMR spectrum of CO(NH(CO)SEt)$_2$ in CDCl$_3$.
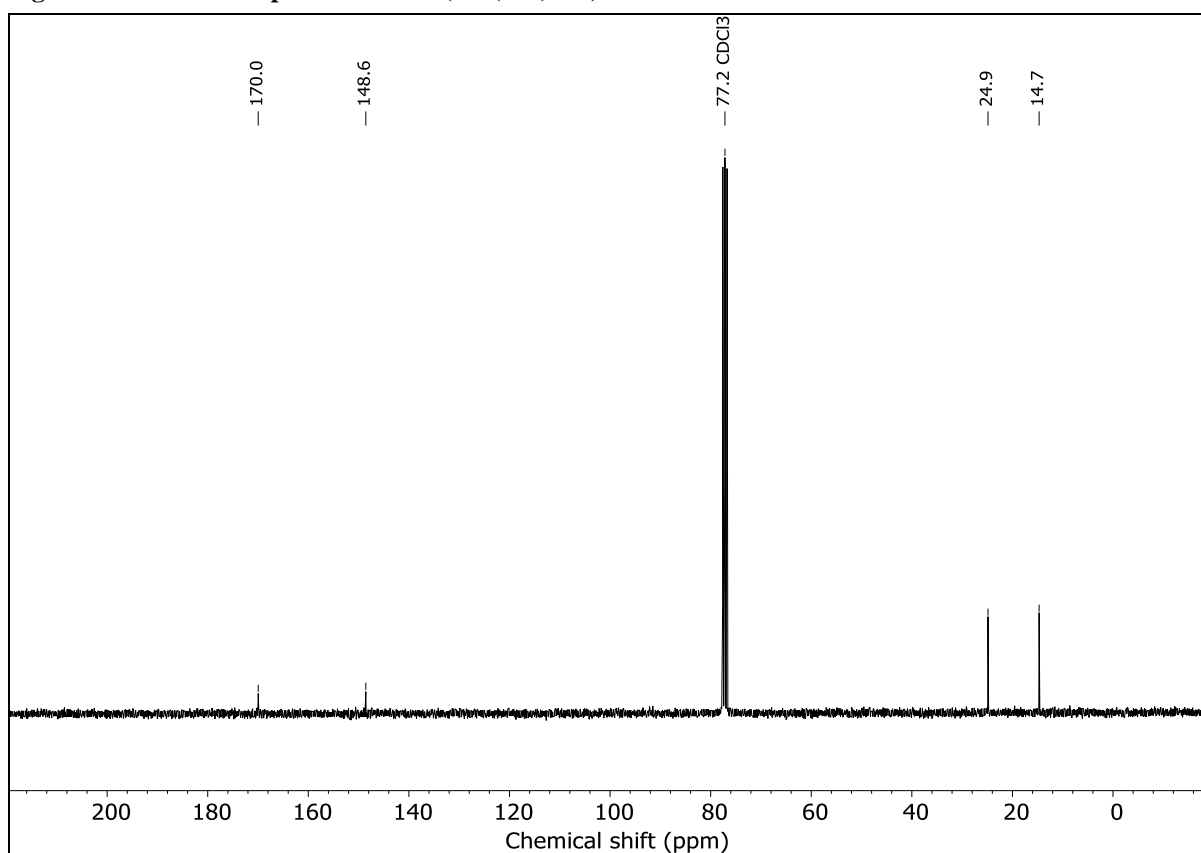
Figure S 44: ^{13}C NMR spectrum of CO(NH(CO)SEt)$_2$ in CDCl$_3$.
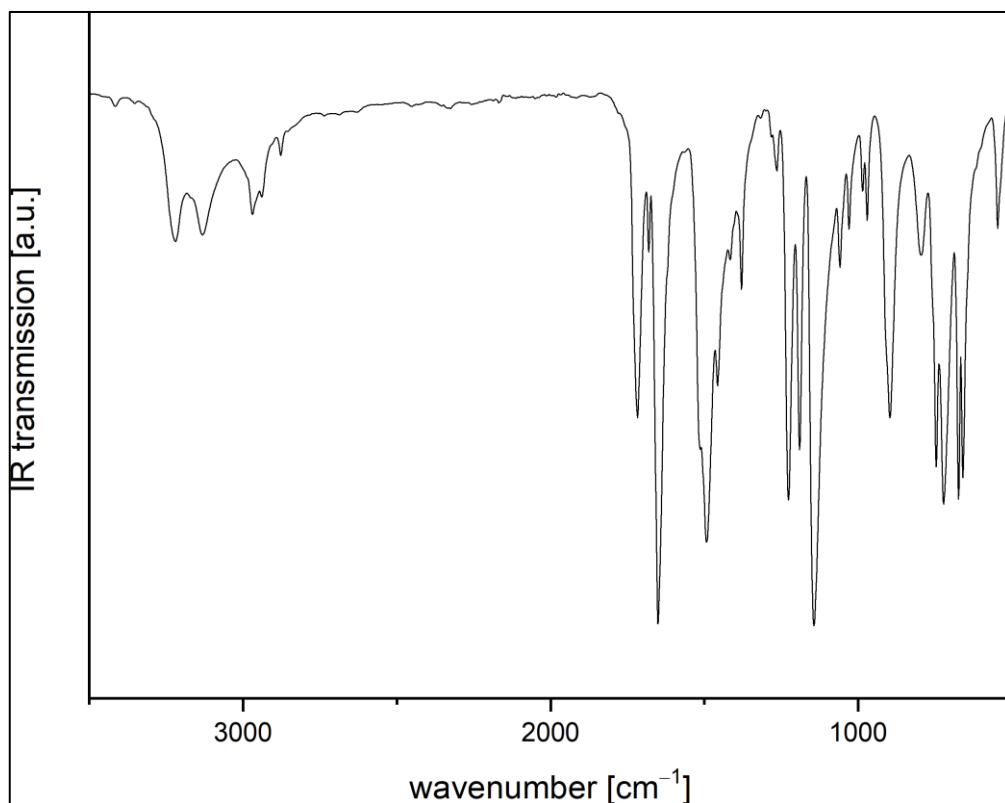
Figure S 45: Measured room-temperature ATR-IR spectrum of CO(NH(CO)SEt)₂.

1.4.2. Synthesis of CO(NH(CO)SPh)₂ – 3Ph

CO(NH(CO)SPh)₂ was obtained as colourless powder (96%, 0.96 mmol, 320 mg). Crystals were obtained by layering a toluene solution with *n*-hexane.

CHNS for $C_{23}H_{28}N_2O_3S_2$ Found % (calc. %): C 53.37 (54.20), H 3.722 (3.64), N 8.31 (8.43), S 18.94 (19.29).

^{1}H NMR (CDCl₃): δ = 9.57 (s, 2H, N*H*), 7.53 (m, 4H, *H*$_{Ph}$), 7.46 (m, 6H, *H*$_{Ph}$) ppm.

^{13}C{^{1}H} NMR (CDCl₃): δ = 168.9 (N(*C*O)S), 149.0 (N(*C*O)N), 135.6 (*C*$_{ortho}$-Ph), 130.6 (*C*$_{para}$-Ph), 129.7 (*C*$_{meta}$-Ph), 126,1 (*C*$_{ipso}$-Ph) ppm.

Mass (ESI+, MeOH) for [M+Na$^+$] = $C_{23}H_{28}N_2O_3S_2Na^+$ m/z found (calc.): 355.0183 (355.0187).
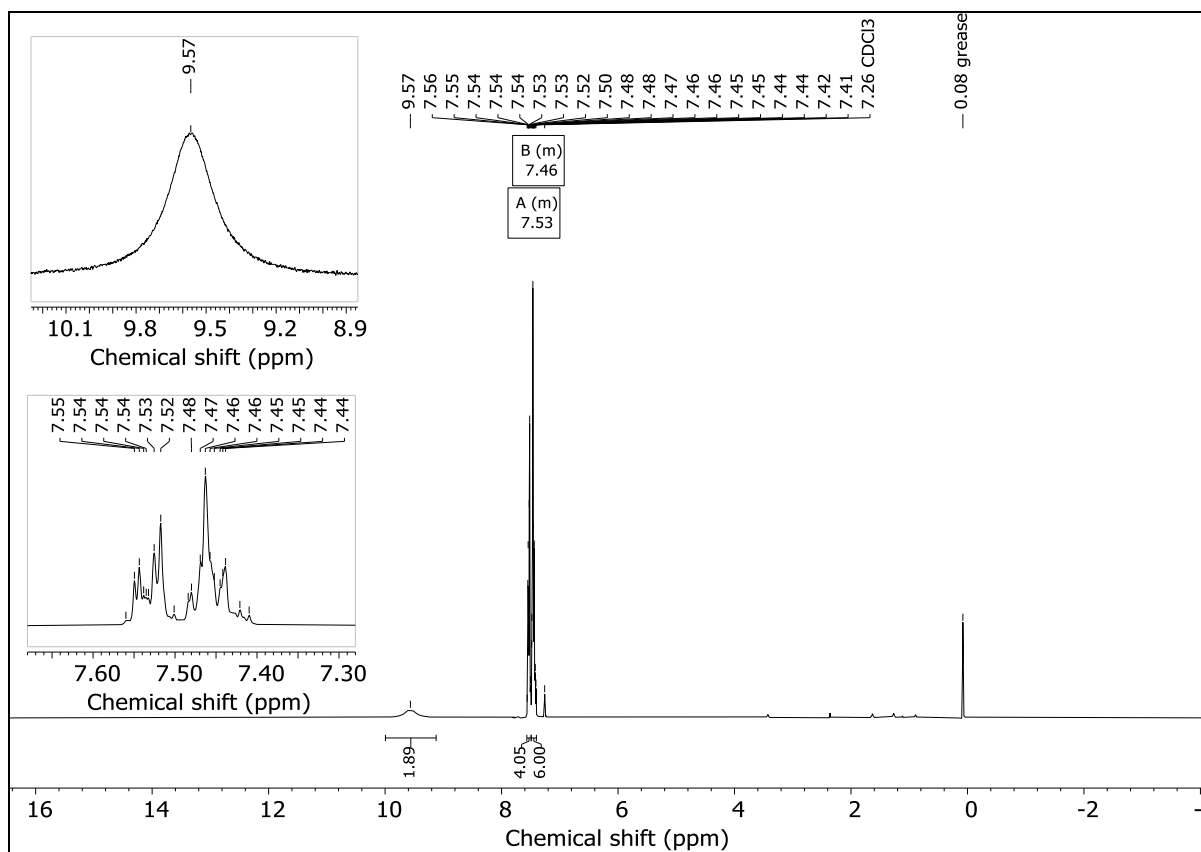
Figure S 46: ^1H NMR spectrum of $CO(NH(CO)SPh)_2$ in $CDCl_3$.
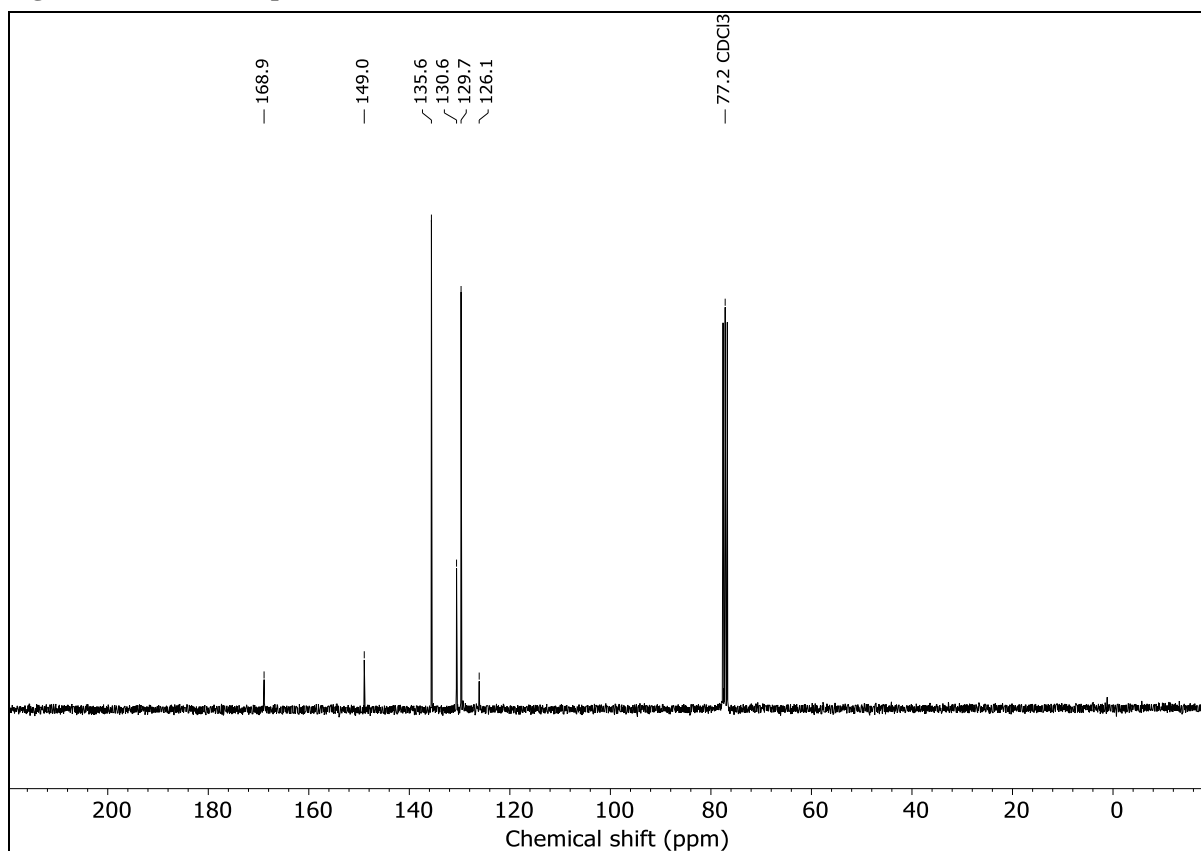
Figure S 47: ^{13}C NMR spectrum of $CO(NH(CO)SPh)_2$ in $CDCl_3$.
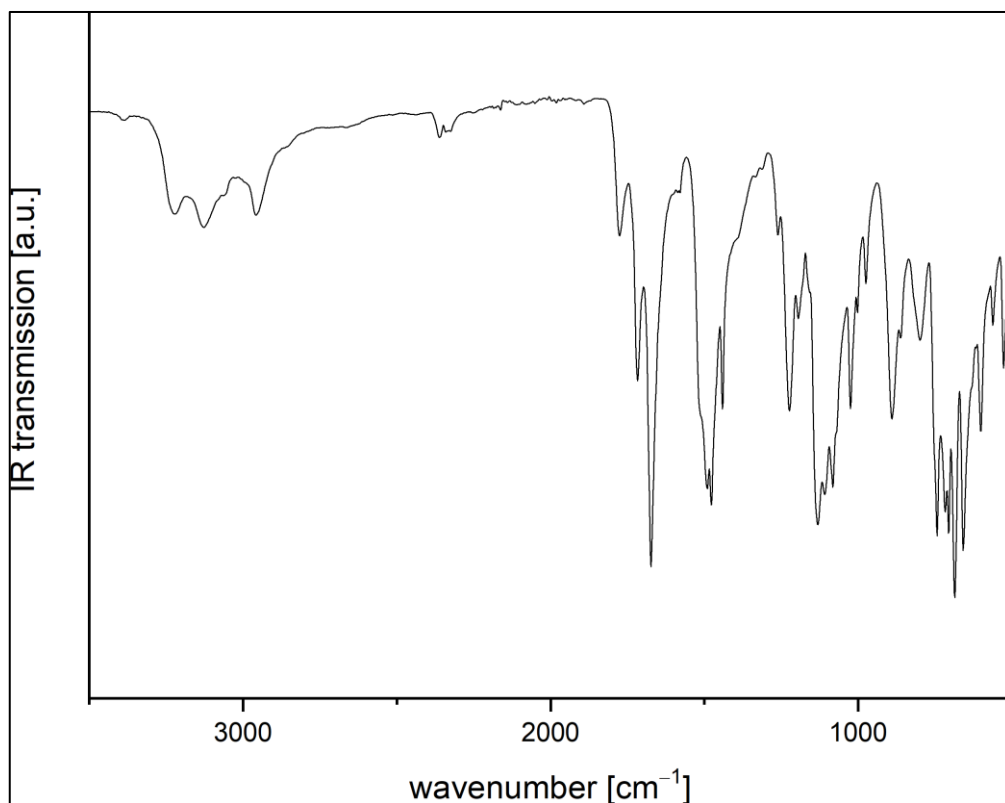
Figure S 48: Measured room-temperature ATR-IR spectrum of CO(NH(CO)SPh)₂.

1.4.3. Synthesis of CO(NH(CO)SPh-*para-t*Bu)₂ – 3Ph-*p-t*Bu

CO(NH(CO)SPh-*para-t*Bu)₂ was obtained as colourless powder (69%, 0.68 mmol, 304 mg).

Crystals were obtained by layering a THF solution with *n*-hexane.

CHNS for $C_{23}H_{28}N_2O_3S_2$ Found % (calc. %): C 61.92 (62.13), H 6.415 (6.35), N 6.35 (6.30), S 14.03 (14.42).

^{1}H NMR (CDCl₃): δ = 9.37 (s, 2H, N*H*), 7.45(s, 8H, *H*$_{Ph}$), 1.33 (s, 18H, C*H*₃)

^{13}C{^{1}H} NMR (CDCl₃): δ = 169.2 (N(*C*O)S), 154.1 (*C*$_{ipso\text{-Ph}}$), 148.7 (N(*C*O)N), 135.3 (*C*$_{ortho\text{-Ph}}$), 126.9 (*C*$_{meta\text{-Ph}}$), 122.6 (*C*$_{para\text{-Ph}}$), 35.0 (*C*(CH₃)₃), 31.3 (C(*C*H₃)₃) ppm.

Mass (ESI+, MeOH) for [M+H⁺] = $C_{23}H_{28}N_2O_3S_2H^+$ m/z found (calc.): 445.1613 (445.1620).
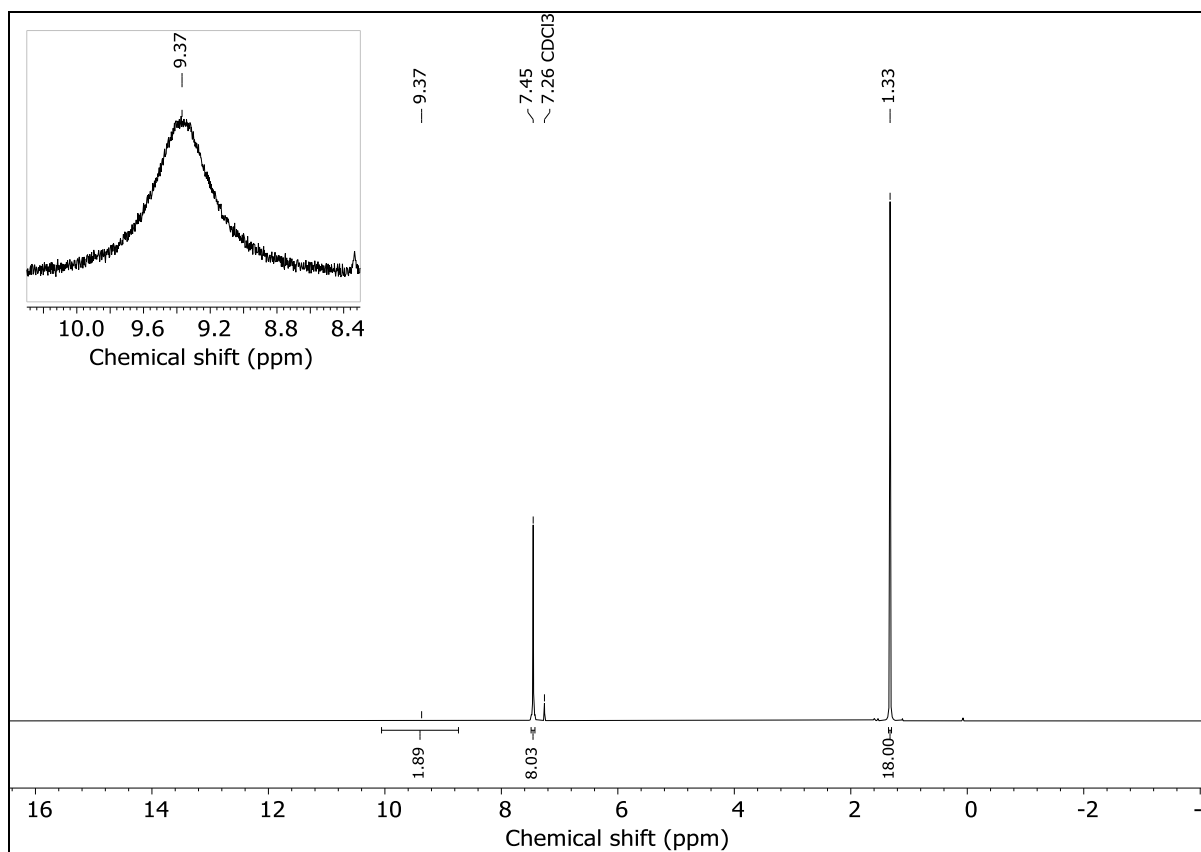
Figure S 49: ^{1}H NMR of CO(NH(CO)SPh-*para-t*Bu)$_2$ in CDCl$_3$.
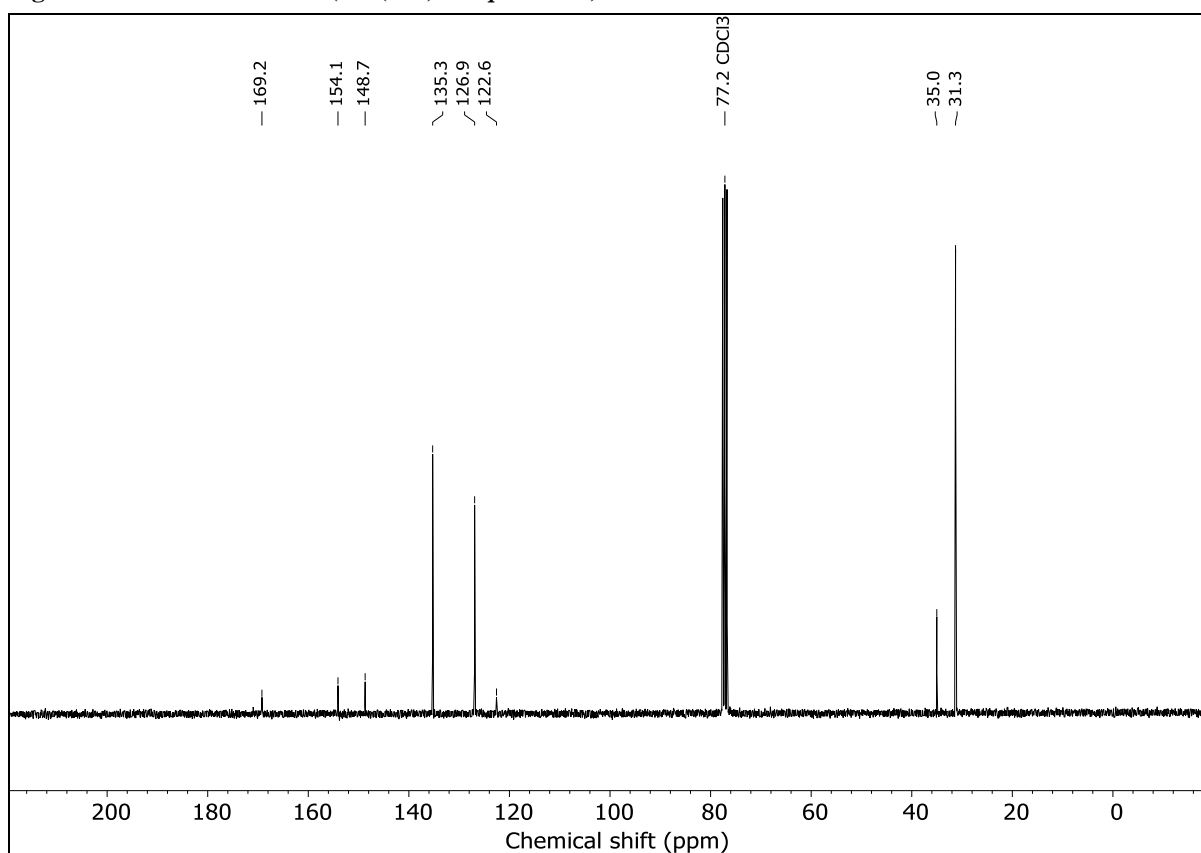
Figure S 50: ^{13}C NMR of CO(NH(CO)SPh-*para-t*Bu)$_2$ in CDCl$_3$.
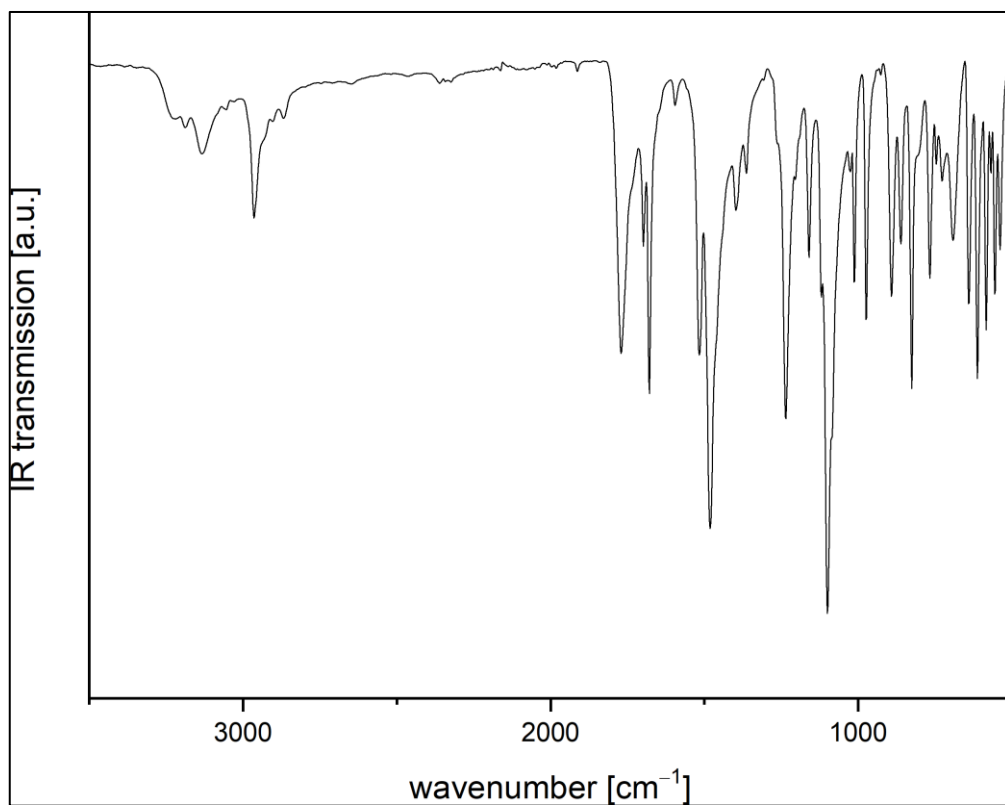
Figure S 51: Measured room-temperature ATR-IR spectrum CO(NH(CO)SPh-*para-t*Bu)₂.

2. Crystallographic data

Single crystal X-ray structure determination: Single-crystal X-ray diffraction data were collected using a StadiVari (Stoe, Darmstadt) diffraction system equipped with mirror monochromated Cu K$_\alpha$ radiation (λ = 1.54186 Å, Xenocs Microfocus Source) and a Pilatus 300K detector.

Crystals were selected under Paratone-N oil, mounted on micromount loops and quench-cooled using an Oxford Cryosystems open flow N$_2$ cooling device. Data were collected at 100 K (if not stated otherwise) and processed using the X-Area program package (for datasets acquired with Stoe devices), including unit cell parameter refinement and inter-frame scaling (which was carried out using LANA within X-Area. Structures were subsequently solved using direct methods (SHELXT)[4] and refined on F^2 with SHELXL[5] using the Olex2[6] user interface. The crystal structure drawings were generated with DIAMOND.[7]

Table S 1: Selected single crystal X-ray data collection and refinement parameters for 2Me, 2Et, 2*i*Pr, 2*t*Bu.

	2Me	2Et	2*i*Pr	2*t*Bu
Formula	$C_{10}H_{16}N_4O_{10}$	$C_7H_{12}N_2O_5$	$C_9H_{16}N_2O_5$	$C_{11}H_{20}N_2O_5$
CCDC				
Fw / g mol^{-1}	352.27	204.19	232.24	260.29
Crystal system	monoclinic	monoclinic	monoclinic	monoclinic
Space group	P2$_1$/c	P2$_1$/c	P2$_1$/c	C2/c
a / Å	23.8304(8)	12.7228(5)	11.8511(5)	18.5543(3)
b / Å	9.2887(3)	4.6891(2)	6.1900(2)	5.71640(10)
c / Å	6.9924(2)	16.3559(7)	16.4193(7)	26.4720(3)
α / °	90	90	90	90
β / °	97.117(2)	95.998(3)	95.866(3)	98.9820(10)
γ / °	90	90	90	90
V / Å^3	1535.87(8)	970.43(7)	1198.18(8)	2773.29(7)
Z	4	4	4	8
Radiation, λ / Å	CuKα (λ = 1.54186)	CuKα (λ = 1.54186)	CuKα (λ = 1.54186)	CuKα (λ = 1.54186)
Temp / K	100.00	100.0	100.0	100.0
ρ_{calc} / g cm^{-3}	1.523	1.398	1.287	1.247
μ / mm^{-1}	1.209	1.032	0.897	0.827
θ range / °	10.232 to 151.006	6.986 to 135	7.498 to 140.826	6.762 to 151.8
Index range	-29 ≤ h ≤ 23, -10 ≤ k ≤ 11, -8 ≤ l ≤ 8	-15 ≤ h ≤ 15, -5 ≤ k ≤ 5, -19 ≤ l ≤ 13	-13 ≤ h ≤ 14, -7 ≤ k ≤ 6, -19 ≤ l ≤ 12	-19 ≤ h ≤ 23, -7 ≤ k ≤ 6, -32 ≤ l ≤ 33
Reflections collected	27209	18211	12124	57346
Ind. Reflns. / Ind. Reflns gt	3162	1751	2244	2875
Parameters	238	137	157	178
R$_{int}$ / R$_{(\sigma)}$	0.0350 / 0.0275	0.0424 / 0.0259	0.0789 / 0.0757	0.0283 / 0.0190
$R1/wR2$,[a] $I \geq 2\sigma I$ (%)	0.0312 / 0.0817	0.0293 / 0.0710	0.0328 / 0.0587	0.0253 / 0.0649
$R1/wR2$,[a] all data (%)	0.0481 / 0.0845	0.0413 7 0.0737	0.0764 / 0.0653	0.0328 / 0.0662
GOF	0.935	0.917	0.807	0.982

[a] R1 = [Σ||F$_o$| − |F$_c$||]/Σ|F$_o$|; wR2 = {[Σw[(F$_o$)^2 − (F$_c$)^2]^2]/[Σw(F$_o$^{2})^2]}$^{1/2}$; w = [σ^2(F$_o$)^2 + (AP)^2 + BP]$^{-1}$, where P = [(F$_o$)^2 + 2(F$_c$)^2]/3 and the A and B values are 0.0501 and 0.00 for **2Me**, 0.0506 and 0.00 for **2Et**, 0.0281 and 0.00 for **2*i*Pr**, 0.042 and 0.00 for **2*t*Bu**.

Table S 2: Selected single crystal X-ray data collection and refinement parameters for 2nOct, 2Ad, 2Bz, 2Ph.

	2*n*Oct	2Ad	2Bz	2Ph
Formula	$C_{19}H_{36}N_2O_5$	$C_{46}H_{64}N_4O_{10}$	$C_{17}H_{16}N_2O_5$	$C_{15}H_{12}N_2O_5$
CCDC				
Fw / g mol^{-1}	372.50	833.01	328.32	300.27
Crystal system	triclinic	monoclinic	triclinic	monoclinic
Space group	P-1	P2$_1$/n	P-1	P2$_1$/n
a / Å	4.6757(2)	17.1974(9)	5.9225(2)	16.5902(15)
b / Å	9.0595(4)	6.7082(3)	9.2646(3)	4.3312(2)
c / Å	25.0211(12)	19.7940(11)	14.8960(5)	20.4487(17)
α / °	95.538(4)	90	76.966(3)	90
β / °	90.907(4)	114.086(4)	79.795(3)	110.885(6)
γ / °	100.361(4)	90	79.738(3)	90
V / Å^3	1037.14(8)	2084.69(19)	775.50(5)	1372.81(19)
Z	2	2	2	4
Radiation, λ / Å	CuKα (λ = 1.54186)	CuKα (λ = 1.54186)	CuKα (λ = 1.54186)	CuKα (λ = 1.54186)
Temp / K	100.0	100.0	175.0	100.0
ρ_{calc} / g cm^{-3}	1.193	1.327	1.406	1.453
μ / mm^{-1}	0.694	0.759	0.878	0.939
θ range / °	7.104 to 134.934	8.842 to 151.242	6.154 to 134.99	5.926 to 152.098
Index range	-5 ≤ h ≤ 5, -10 ≤ k ≤ 5, -29 ≤ l ≤ 29	-21 ≤ h ≤ 21, -8 ≤ k ≤ 8, -24 ≤ l ≤ 24	-5 ≤ h ≤ 7, -11 ≤ k ≤ 11, -17 ≤ l ≤ 17	-19 ≤ h ≤ 20, -5 ≤ k ≤ 5, -22 ≤ l ≤ 25
Reflections collected	19950	49603	33679	21516
Ind. Reflns. / Ind. Reflns gt	3688	49603	2769	2842
Parameters	245	273	226	201
R$_{int}$/ R$_{(\sigma)}$	0.1196 / 0.0955	0.1205 / 0.1017	0.0452 / 0.0394	0.2954 / 0.1627
$R1/wR2$,[a] $I \geq 2\sigma I$ (%)	0.0437 / 0.0820	0.0611 / 0.1409	0.0285 / 0.0852	0.1678 / 0.4295
$R1/wR2$,[a] all data (%)	0.1071 / 0.0933	0.1169 / 0.1645	0.0501 / 0.0611	0.2088 / 0.4437
GOF	0.799	0.906	0.810	1.207
Twin law		0.202 -0.019 -0.788 0 -1 0 1.202 0.019 -0.212		0.317 0 -0.683 0 -1 0 -1.317 0 -0.317
BASF		0.5109(16)		0.99883

[a] R1 = [Σ||F$_o$| − |F$_c$||]/Σ|F$_o$|; wR2 = {[Σw[(F$_o$)^2 − (F$_c$)^2]^2]/[Σw(F$_o$^{2})^2]}$^{1/2}$; w = [σ^2(F$_o$) + (AP)^2 + BP]$^{-1}$, where P = [(F$_o$)^2 + 2(F$_c$)^2]/3 and the A and B values are 0.0401 and 0.00 for **2nOct**, 0.0829 and 0.00 for **2Ad**, 0.0326 and 0.00 for **2Bz**, 0.2 and 0.00 for **2Ph**.

Table S 3: Selected single crystal X-ray data collection and refinement parameters for 1Me, 2Et, 3Ph, 3Ph-*p*-*t*Bu.

	1Me	2Et	3Ph	3Ph-*p*-*t*Bu
Formula	$C_7H_{14}N_4O_3$	$C_{11}H_{22}N_4O_3$	$C_{15.01}H_{12.01}N_2O_{2.99}S_{2.01}$	$C_{23}H_{28}N_2O_3S_2$
CCDC				
Fw / g mol^{-1}	202.22	258.32	332.68	444.59
Crystal system	orthorhombic	orthorhombic	triclinic	orthorhombic
Space group	$P2_12_12$	$P2_12_12_1$	P-1	$P2_12_12_1$
a / Å	13.170(5)	6.6263(10)	11.7269(15)	6.0106(8)
b / Å	13.365(5)	9.6525(15)	14.3665(18)	14.0174(18)
c / Å	10.828(6)	21.047(5)	16.101(2)	26.825(5)
α / °	90	90	111.529(10)	90
β / °	90	90	102.063(10)	90
γ / °	90	90	102.953(10)	90
V / Å^3	1905.9(14)	1346.2(4)	2328.8(6)	2260.1(6)
Z	6	4	6	4
Radiation, λ / Å	CuKα (λ = 1.54186)	CuKα (λ = 1.54186)	CuKα (λ = 1.54186)	CuKα (λ = 1.54186)
Temp / K	100.0	100.0	100.0	100.0
ρ_{calc} / g cm^{-3}	1.410	1.275	1.423	1.307
μ / mm^{-1}	0.941	0.775	3.247	2.351
θ range / °	8.166 to 143.946	8.402 to 150.384	6.232 to 139.818	6.59 to 109.992
Index range	$-16 \leq h \leq 14$, $-11 \leq k \leq 16$, $-12 \leq l \leq 13$	$-8 \leq h \leq 8$, $-5 \leq k \leq 11$, $-26 \leq l \leq 26$	$-6 \leq h \leq 13$, $-17 \leq k \leq 17$, $-19 \leq l \leq 19$	$-6 \leq h \leq 6$, $-12 \leq k \leq 14$, $-26 \leq l \leq 28$
Reflections collected	33076	21085	48334	21514
Ind. Reflns. / Ind. Reflns gt	3689	2732	8593	2845
Parameters / Restraints	263 / 0	171	789 / 733	278 / 218
R_{int}/ $R_{(\sigma)}$	0.0536 / 0.0325	0.0225 / 0.0151	0.0516 / 0.0530	0.4030 / 0.2792
$R1/wR2$,[a] $I \geq 2\sigma I$ (%)	0.0374 / 0.0925	0.0329 / 0.0784	0.0424 / 0.1003	0.1211 / 0.3008
$R1/wR2$,[a] all data (%)	0.0435 / 0.0950	0.0365 / 0.0803	0.0736 / 0.1093	0.2540 / 0.3500
GOF	1.009	1.041	0.898	0.916
Twin law	-1 0 0 0 -1 0 0 0 -1 2			-1 0 0 0 -1 0 0 0 -1
BASF	0.45637			0.64565
Flack parameter	0.5(3)	0.10(10)		

[a] $R1 = [\Sigma||F_o| - |F_c||]/\Sigma|F_o|$; $wR2 = \{[\Sigma w[(F_o)^2 - (F_c)^2]^2]/[\Sigma w(F_o^2)^2]\}^{1/2}$; $w = [\sigma^2(F_o)^2 + (AP)^2 + BP]^{-1}$, where $P = [(F_o)^2 + 2(F_c)^2]/3$ and the A and B values are 0.0692 and 0.00 for **1Me**, 0.0407 and 0.417 for **1Et**, 0.0609 and 0.00 for **3Ph**, 0.151 and 0.00 for **3Ph-*p*-*t*Bu**.

3. Hirshfeld surface analysis

Table S 4: Contribution of every atomic interaction to the Hirshfeld surface created by fingerprint plots. Values are given in [%].

compound	H–H	H–C	H–O	H–N	C–O	C–C	C–N	N–N	N–O	O–O	H–S	C–S	S–S	N–S	O–S
1Me	51.0	3.6	32.6	3.8	1.9	0.7	4.2	0.2	2.1	0.0	–	–	–	–	–
1Me	52.2	3.4	31.6	3.6	1.9	0.7	4.2	0.2	2.1	0.0	–	–	–	–	–
1Et	64.3	5.8	22.1	5.1	1.3	0.0	0.0	0.0	0.8	0.6	–	–	–	–	–
2Me	28.6	4.6	51.6	2.6	4.9	0.8	1.0	0.0	3.5	2.4	–	–	–	–	–
2Me	27.9	5.7	51.5	3.7	3.7	0.4	1.9	0.3	1.9	2.9	–	–	–	–	–
2Et	44.5	5.3	36.7	3.6	3.1	0.4	0.4	0.4	1.2	4.3	–	–	–	–	–
2iPr	53.5	4.6	32.7	3.7	2.2	0.0	0.0	0.0	1.7	1.6	–	–	–	–	–
2tBu	62.3	3.7	26.1	3.0	1.1	0.7	0.6	0.5	0.3	1.8	–	–	–	–	–
2nOct	72.0	3.3	19.1	2.2	1.4	0.1	0.0	0.0	0.8	1.1	–	–	–	–	–
2Ad	70.9	4.0	19.3	2.7	1.1	0.0	0.0	0.0	1.0	1.0	–	–	–	–	–
2Bz	44.1	20.0	23.2	1.8	2.8	3.0	1.6	0.5	0.0	2.9	–	–	–	–	–
2Ph	36.5	20.6	27.5	2.0	3.9	3.6	0.4	0.2	1.8	3.6	–	–	–	–	–
3Ph-*p-t*Bu	49.3	17.3	17.3	2.0	1.3	0.2	0.0	0.0	0.8	0.7	8.7	1.1	0.3	0.6	0.4

References

[1]   W.L.F. Armarego, C.L.L. Chai, Purification of Organic Chemicals, 6th ed., 2009.

[2]   J. Pfeiffer, H. Günther, L. Völlinger, D. Botros, B. Scheibe, M. Möbs, F. Kraus, F. Weigend, F. Tambornino, Double Addition vs . Ring Closure: Systematic Reactivity Study of $CO(NCO)_2$ and $CO(NCS)_2$ towards Hydrogen Halides, Chem. – A Eur. J. 29 (2023) e202203983.

[3]   P.R. Spackman, M.J. Turner, J.J. McKinnon, S.K. Wolff, D.J. Grimwood, D. Jayatilaka, M.A. Spackman, CrystalExplorer : a program for Hirshfeld surface analysis, visualization and quantitative analysis of molecular crystals, J. Appl. Crystallogr. 54 (2021) 1006–1011.

[4]   G.M. Sheldrick, SHELXT – Integrated space-group and crystal-structure determination, Acta Crystallogr. Sect. A Found. Adv. 71 (2015) 3–8.

[5]   G.M. Sheldrick, A short history of SHELX, Acta Crystallogr. Sect. A Found. Crystallogr. 64 (2008) 112–122.

[6]   O. V. Dolomanov, L.J. Bourhis, R.J. Gildea, J.A.K. Howard, H. Puschmann, OLEX2 : a complete structure solution, refinement and analysis program, J. Appl. Crystallogr. 42 (2009) 339–341.

[7]   K. Brandenburg, H. Putz, DIAMOND, Program for X-Ray Structure Analysis, Crystal Impact GbR, Bonn, Gemany, 2005.

8.1.6 Synthesis, Crystal Structure Study and Spectroscopic Analysis of Substituted 2,3-dihydro-2-thioxo-4*H*-1,3,5-thiadiazin-4-ones

Electronic Supporting Information (ESI)

Synthesis, Crystal Structure Study and Spectroscopic Analysis of Substituted 2,3-dihydro-2-thioxo-4*H*-1,3,5-thiadiazin-4-ones

Jonathan Pfeiffer[a], Clemens Trost[a], Frank Tambornino[a]*

[a]Fachbereich Chemie, Philipps-Universität Marburg, Hans-Meerwein-Straße 4, 35043 Marburg, Germany

*Corresponding author. E-mail address: Frank.Tambornino@chemie.uni-marburg.de (F. Tambornino)

Contents

1. Experimental section

1.1. General remarks

General synthetic methods. All reactions and manipulations were performed under an inert atmosphere of argon using standard Schlenk-line or glovebox techniques (MBraun UNIlab glovebox, maintained at < 0.1 ppm H_2O and < 0.1 ppm O_2).

All chemicals were purchased commercially, purified, and dried according to literature.[1] THF-d8 (Eurisotop, 99.5 %) was recondensed, degassed and stored over molecular sieve (4 Å) prior to use. Carbonyl diisothiocyanate was synthesized by literature procedure and distilled before use.[2]

Additional characterization techniques:

^{1}H and ^{13}C NMR spectra were acquired on a Bruker *Avance II* (300 MHz) or a Bruker *Avance III HD* (300 MHz) spectrometer at 298 K if not stated otherwise.

Elemental analyses and mass spectrometry were performed by the in-house service personnel. CHN(S) analyses were performed on a *CHNS(S)-Analysator vario MICRO CUBE* (Elementar). Electro spray ionisation was performed on a *LTQ-FT Ultra* (Thermo Fischer Scientific).

IR spectra were recorded on a Bruker *Alpha FT-IR* spectrometer equipped with a diamond ATR unit mounted in a nitrogen-filled glovebox (MBraun UNIlab glovebox, maintained at < 0.1 ppm H_2O and < 0.1 ppm O_2).

Hirschfeld surface analyses were carried out with the Crystal Explorer (V 21.5)[3] software suite.

1.2. Synthesis of 6-thioxo-1,3,5-thiadiazinane-2,4-dione – 1

To carbonyl diisothiocyanate (0.55 g, 3.8 mmol, 1.0 eq.) in THF (5 ml) water (0.14 g, 7.6 mmol, 2.0 eq.) was added dropwise at room temperature. The solution was cooled to 0 °C and stirred for 16 h. After evaporation of the solvent the compound was obtained as a yellow solid (0.48 g, 3.0 mmol, 78%). Single crystals suitable for X-ray diffraction were obtained by dissolution of a small amount of solid in a 1:1:1 mixture of H_2O/DCM/*n*-hexane and subsequent evaporation of the solvent on air.

CHNS for $C_3H_2N_2O_2S_2$ Found % (calc. %): C 22.68 (22.22), H 1.38 (1.24), N 17.45 (17.27), S 41.48 (39.54).

^{1}H NMR (THF-d8): δ = 12.56 (s, 1H, N*H*), 11.62 (s, 1H, N*H*) ppm.

^{13}C{^{1}H} NMR (THF-d8): δ = 193.0 (*C*=S), 163.1 (S–*C*=O), 149.4 (*C*=O) ppm.

Mass (ESI+, MeOH) for $[M^+]$ = $C_3H_2N_2O_2S_2^+$ m/z found (calc.): 161.9795 (161.9552).
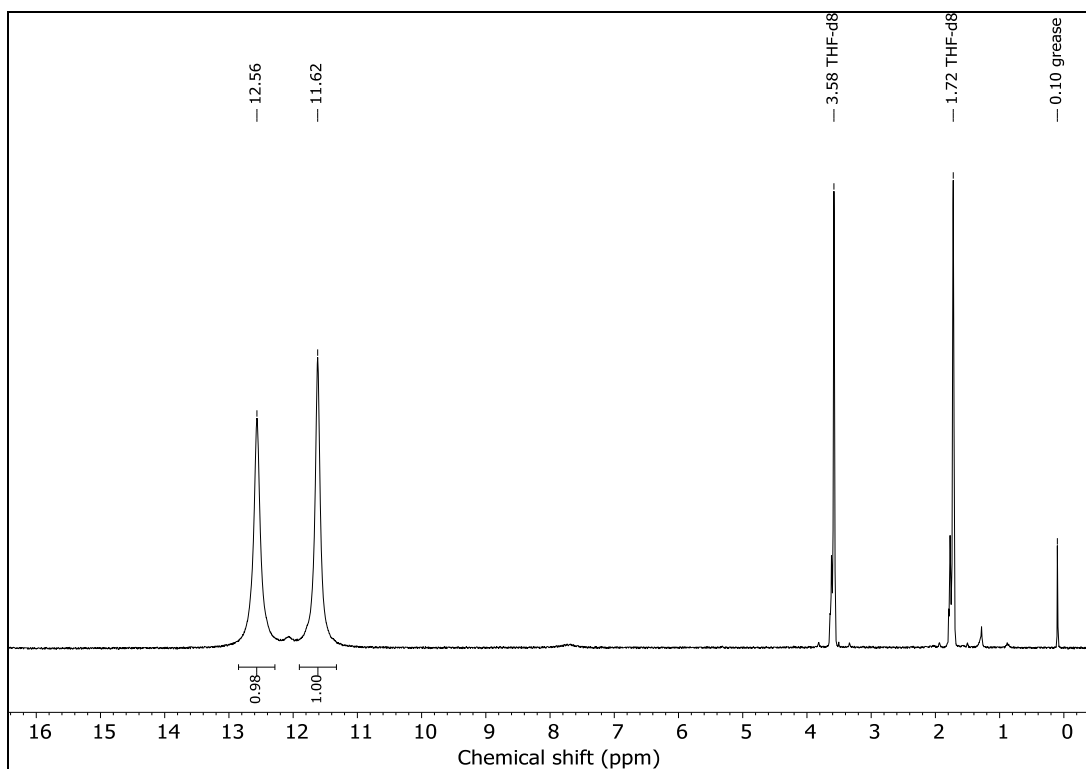
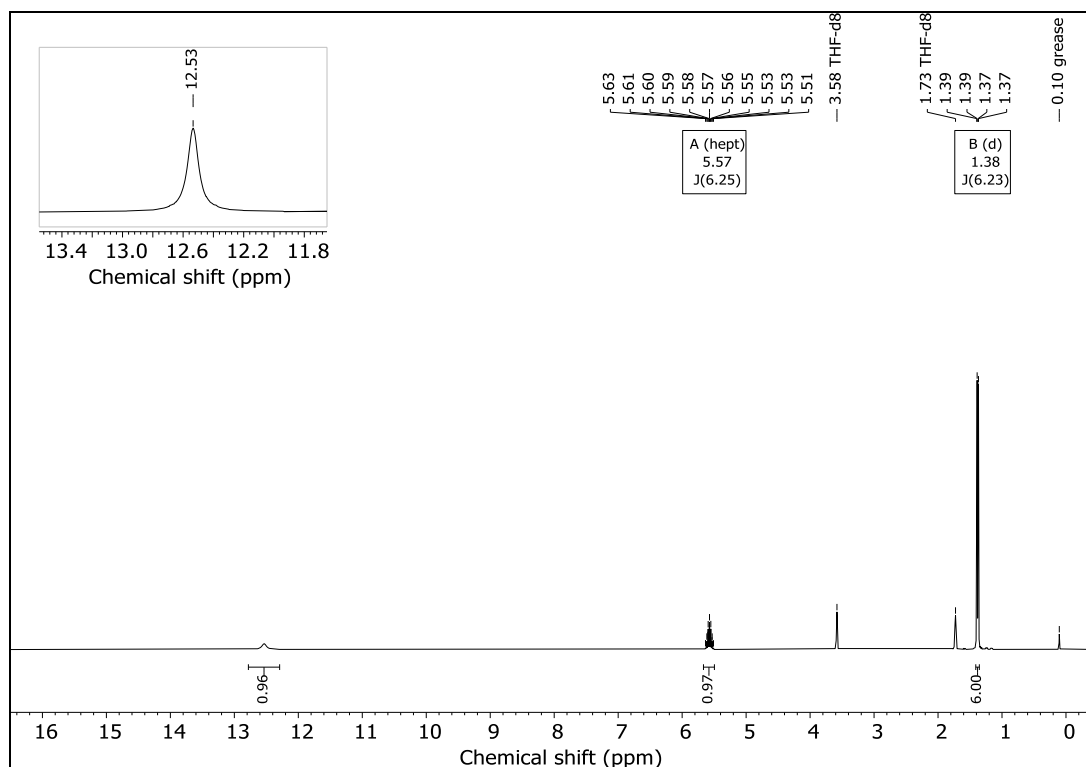**Figure S 1: ¹H NMR spectrum of 1 in THF-d8.**
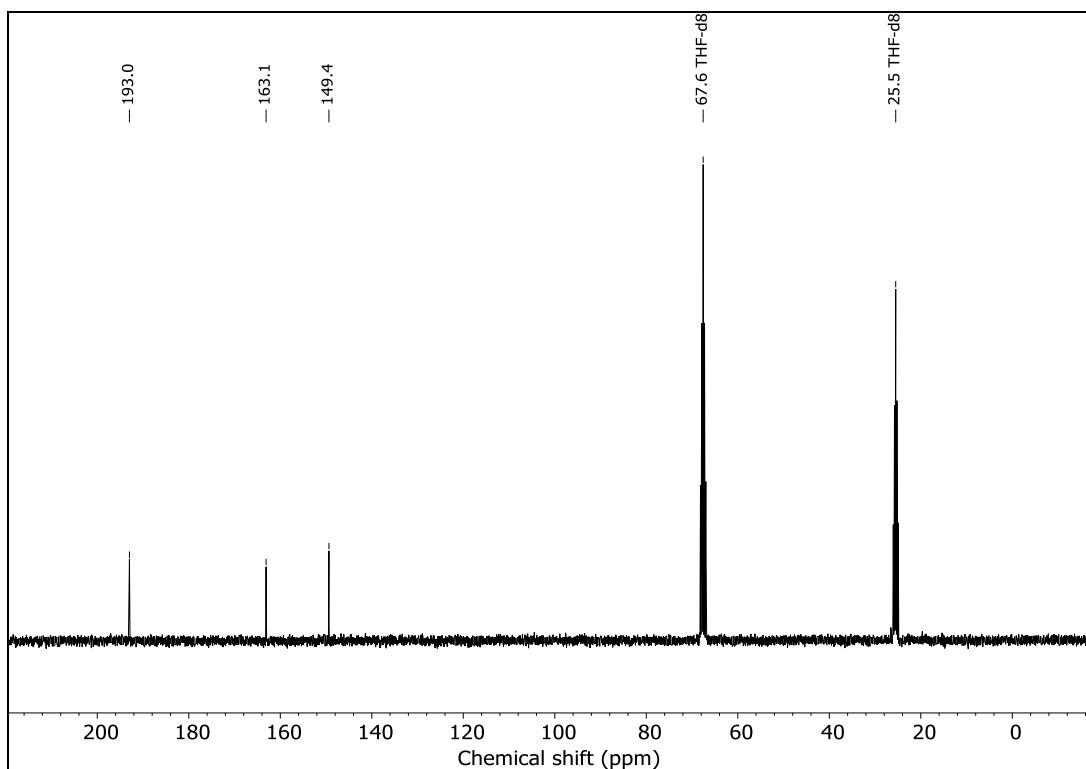
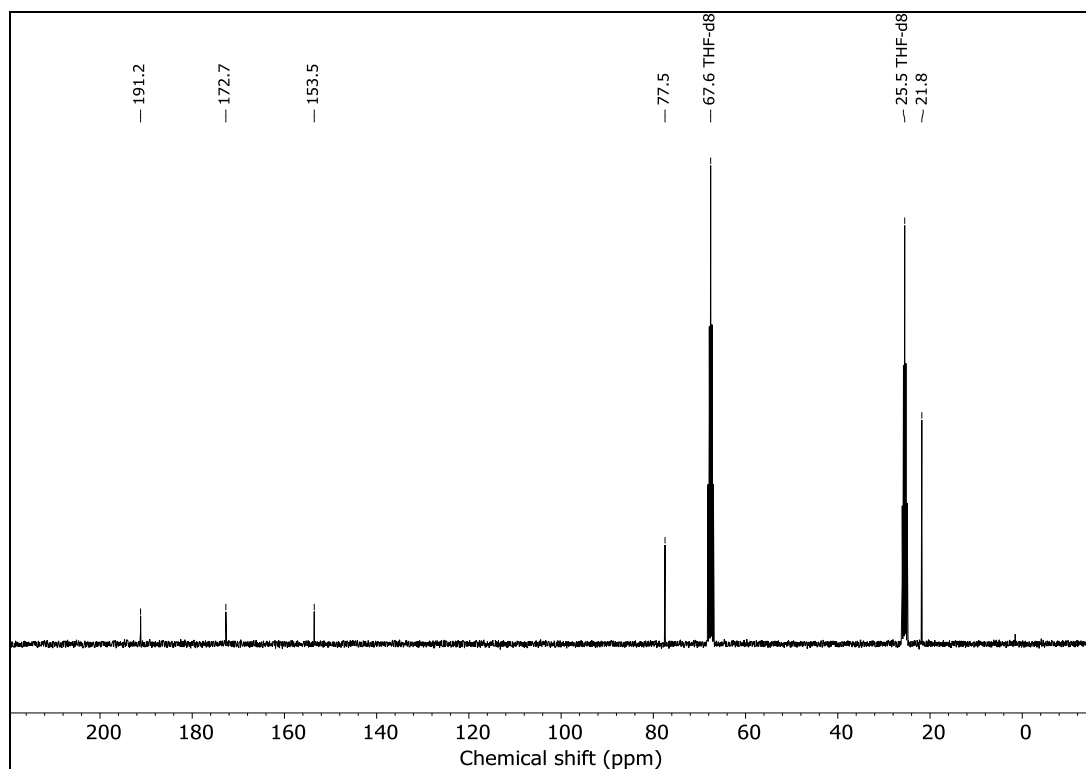**Figure S 2: ¹³C NMR spectrum of 1 in THF-d8.**
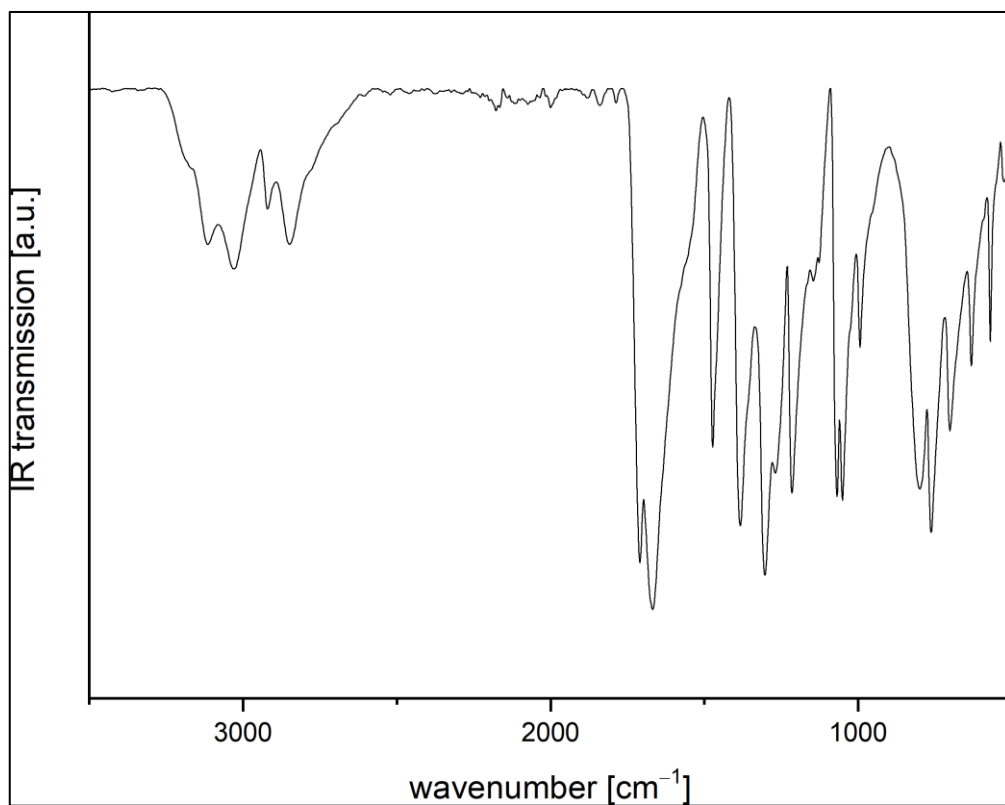
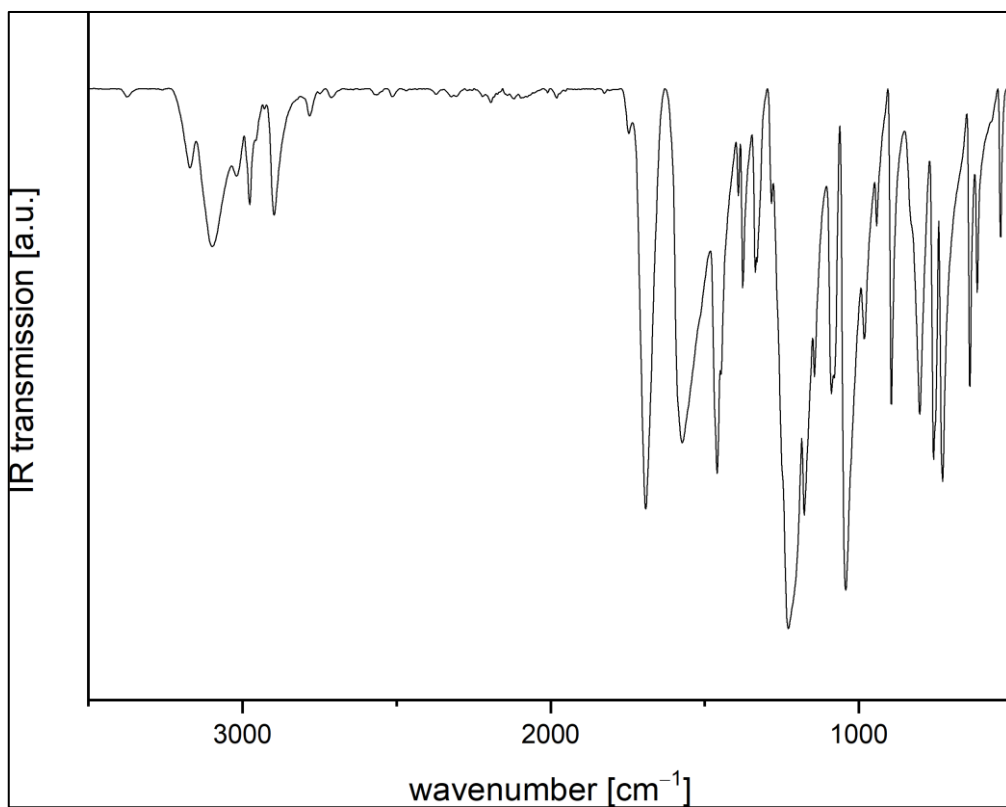**Figure S 3: Measured room-temperature ATR-IR spectrum of 1.**

1.3. Synthesis of 6-methoxy-2-thioxo-2,3-dihydro-4*H*-1,3,5-thiadiazin-4-one – 2Me

To a 1M solution of methanol (7.5 ml, 7.5 mmol, 2.0 eq.) in THF neat carbonyl diisothiocyanate (0.55 g, 3.8 mmol, 1.0 eq.) was added dropwise at room temperature. The resulting solution was stirred for 16 h. After evaporation of the solvent the compound was obtained as a yellow solid (0.63 g, 3.6 mmol, 94%). Single crystals suitable for X-ray diffraction were obtained by dissolution of a small amount of solid in THF and subsequent evaporation of the solvent on air.

CHNS for $C_4H_4N_2O_2S_2$ Found % (calc. %): C 27.54 (27.27), H 2.46 (2.29), N 15.66 (15.90), S 37.67 (36.39).

^{1}H NMR (THF-d8): δ = 12.59 (s, 1H, N*H*), 4.09 (s, 3H, C*H$_3$*) ppm.

^{13}C{^{1}H} NMR (THF-d8): δ = 190.7 (*C*=S), 173.9 (S–*C*=N), 153.4 (*C*=O), 58.1 (*C*H$_3$) ppm.
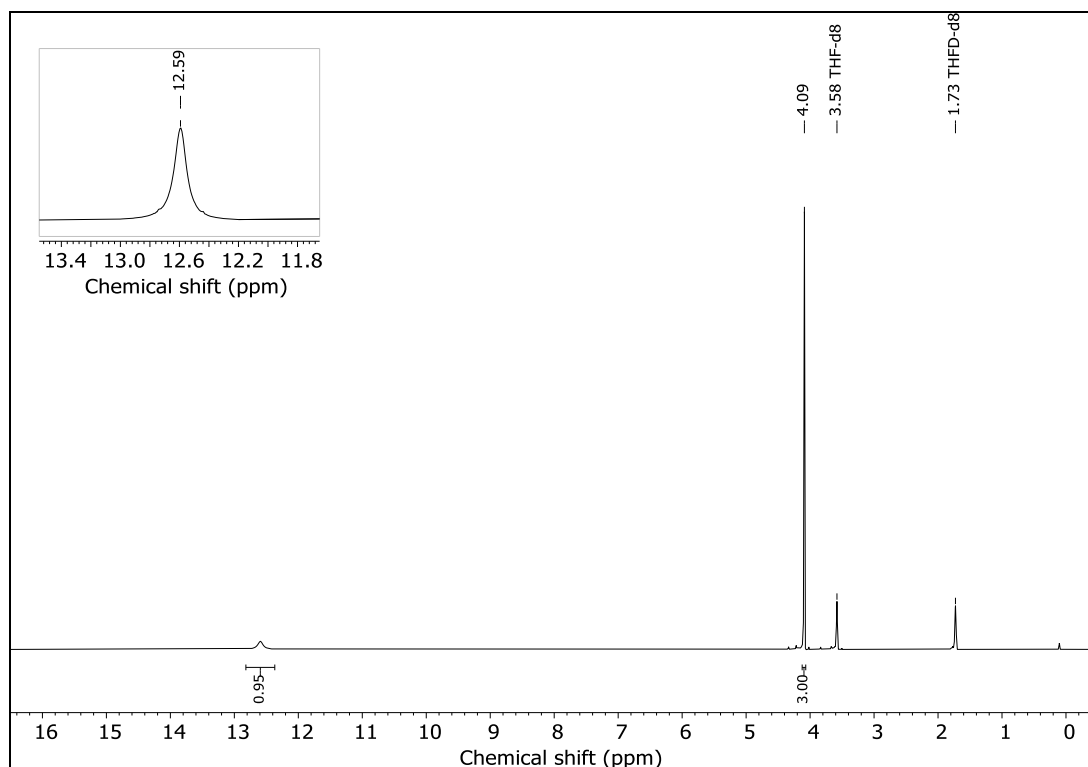
Figure S 4: ^{1}H NMR spectrum of 2Me in THF-d8.
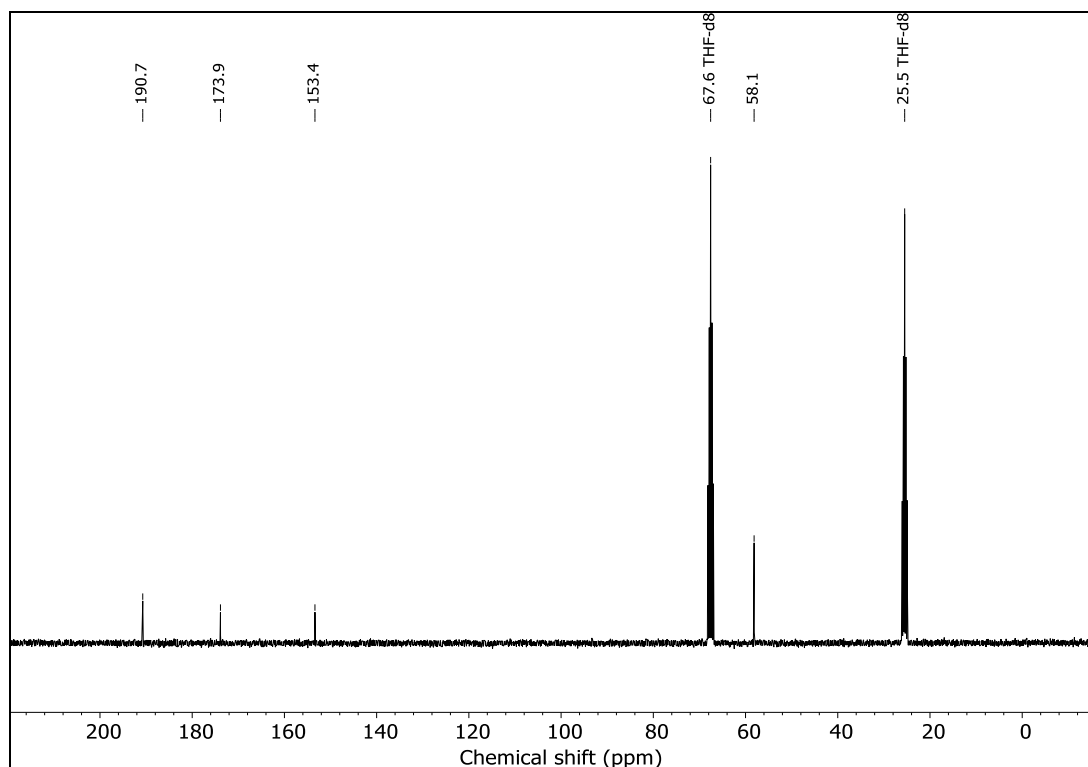
Figure S 5: ^{13}**C NMR spectrum of 2Me in THF-d8.**
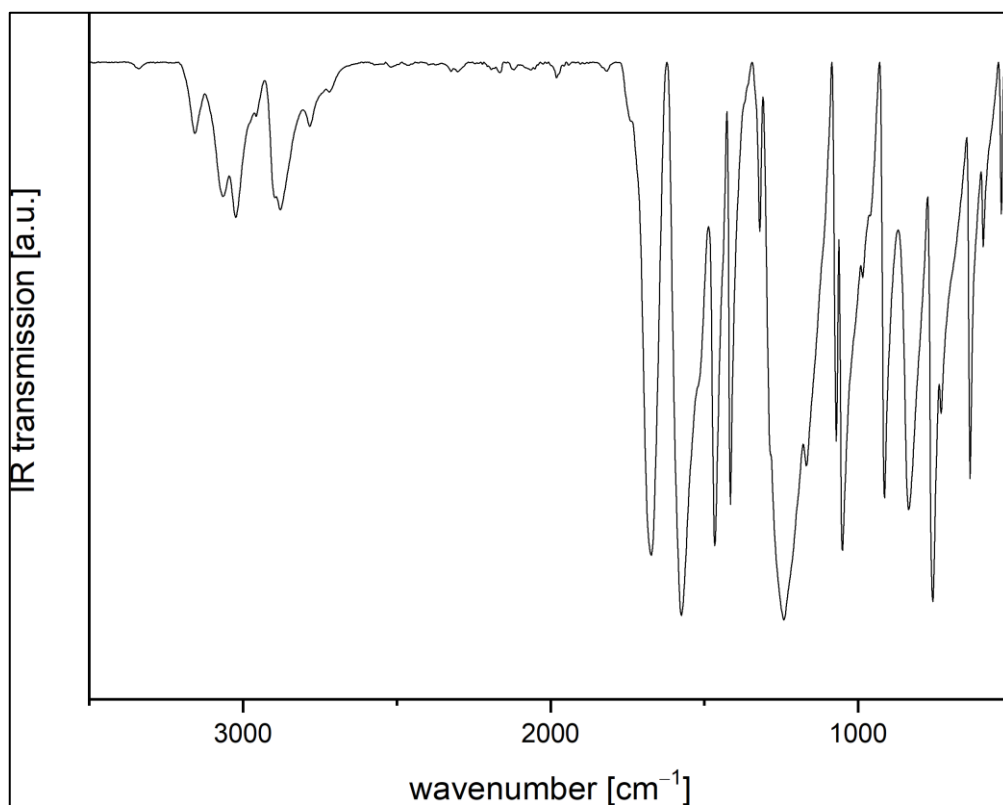
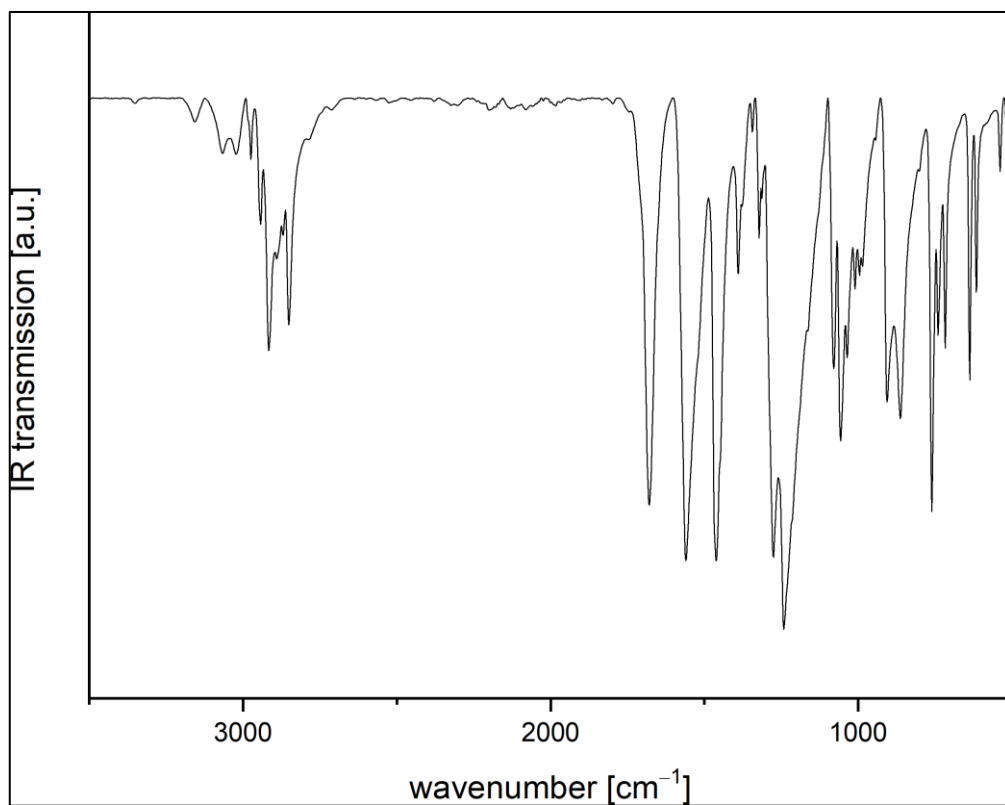**Figure S 6: Measured room-temperature ATR-IR spectrum of 2Me.**

1.4. Synthesis of 6-ethoxy-2-thioxo-2,3-dihydro-4*H*-1,3,5-thiadiazin-4-one – 2Et

To a 1M solution of ethanol (7.5 mL, 7.5 mmol, 2.0 eq.) in THF neat carbonyl diisothiocyanate (0.55 g, 3.8 mmol, 1.0 eq.) was added dropwise at room temperature. The resulting solution was stirred for 16 h. After evaporation of the solvent the compound was obtained as a yellow solid (0.69 g, 3.6 mmol, 95%). Single crystals suitable for X-ray diffraction were obtained by dissolution of a small amount solid in THF and subsequent evaporation of the solvent on air. Due to the high sulfur content by weight%, the calibration value for S for the elemental analysis was overshot.

CHN for $C_5H_6N_2O_2S_2$ Found % (calc. %): C 32.11 (31.57), H 3.06 (3.18), N 14.77 (14.73), S 35.96 (33.71).

¹H NMR (THF-d8): δ = 12.56 (s, 1H, N*H*), 4.59 (q, 2H, $^3J_{HH}$ = 7.09 Hz, C*H₂*CH₃), 1.38 (t, 3H, $^3J_{HH}$ = 7.07 Hz, CH₂C*H₃*) ppm.

¹³C{¹H} NMR (THF-d8): δ = 190.9 (*C*=S), 173.2 (S–*C*=N), 153.5 (*C*=O), 68.6 (*C*H₂CH₃), 14.3 (CH₂*C*H₃) ppm.

Mass (ESI+, MeOH) for [M+H⁺] = $C_5H_6N_2O_2S_2H^+$ m/z found (calc.): 190.9949 (190.9943).
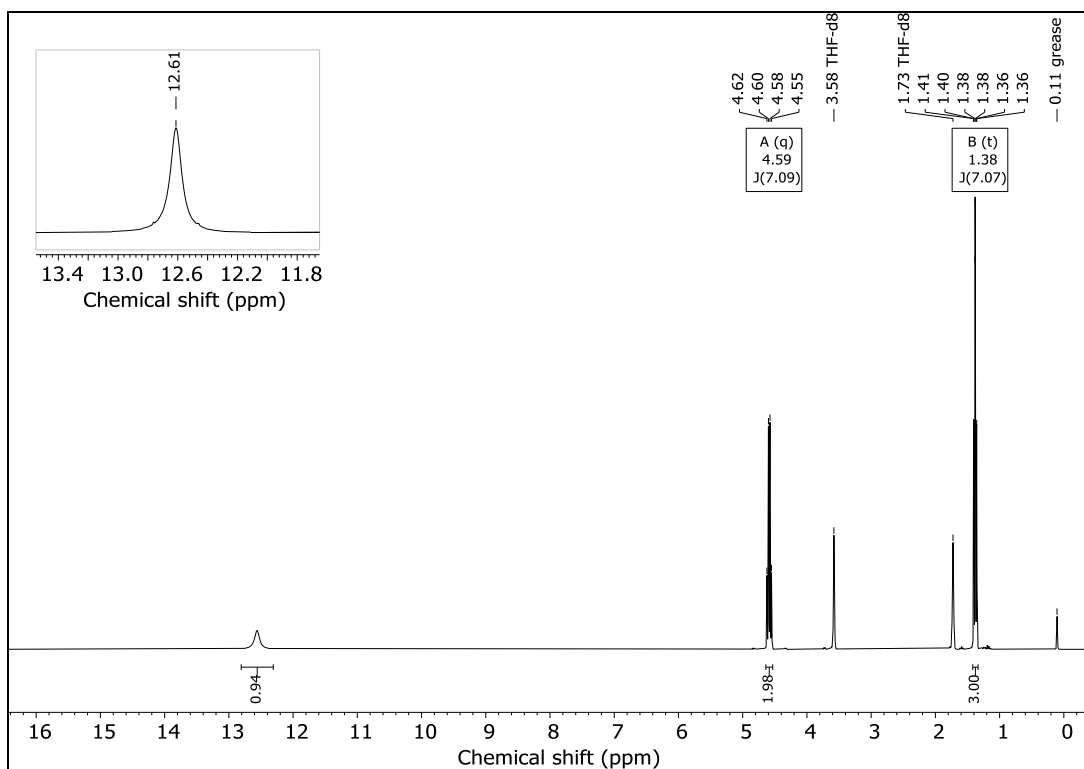
Figure S 7: ¹H NMR spectrum of 2Et in THF-d8.
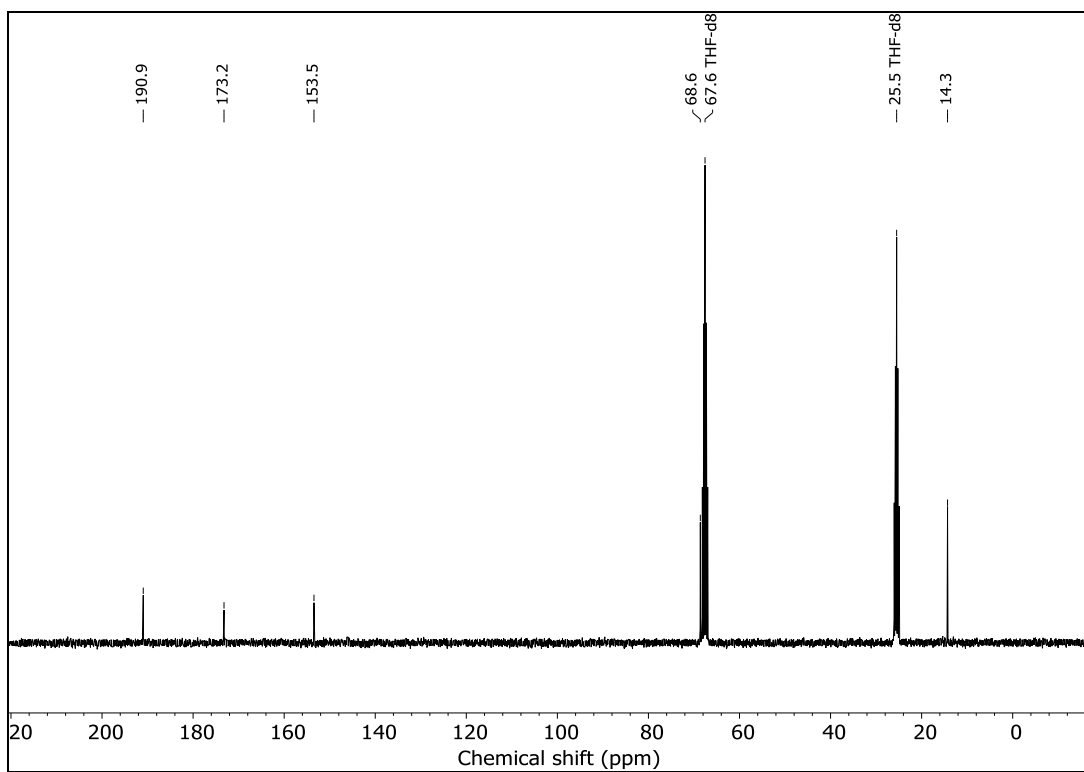
Figure S 8: ¹³C NMR spectrum of 2Et in THF-d8.

S.I.9
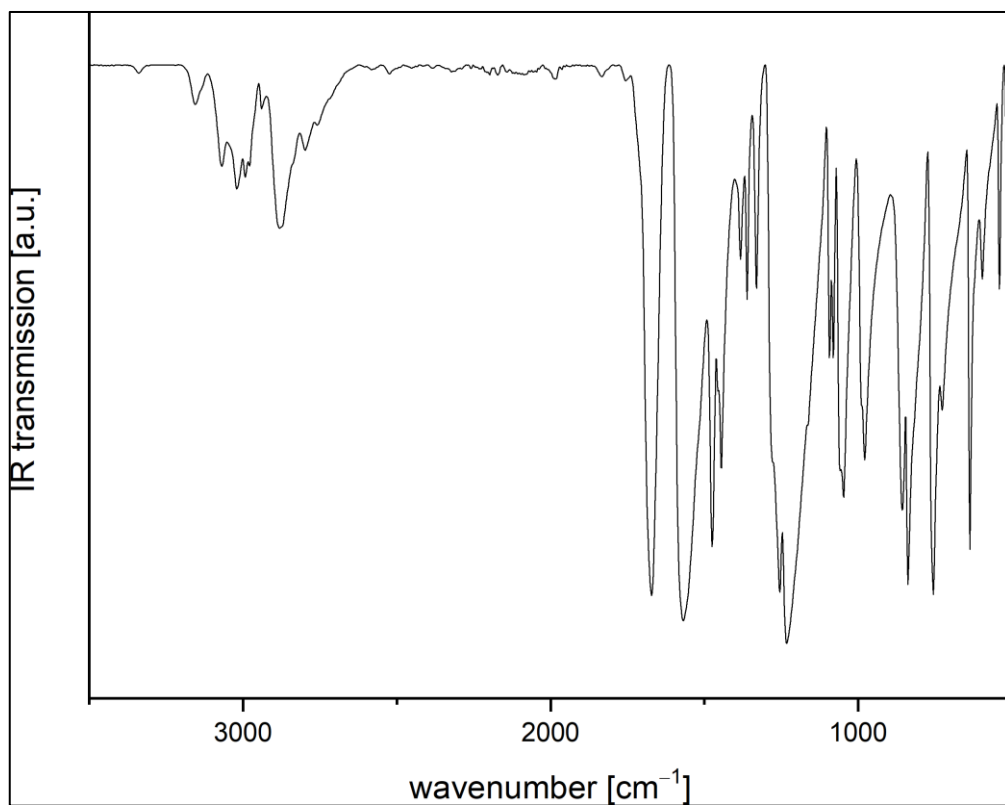
Figure S 9: Measured room-temperature ATR-IR spectrum of 2Et.

1.5. Synthesis of 6-isopropoxy-2-thioxo-2,3-dihydro-4*H*-1,3,5-thiadiazin-4-one – 2*i*Pr

To a 1M solution of 2-propanol (7.5 mL, 7.5 mmol, 2.0 eq.) in THF neat carbonyl diisothiocyanate (0.55 g, 3.8 mmol, 1.0 eq.) was added dropwise at room temperature. The resulting solution was stirred for 16 h. After evaporation of the solvent the compound was obtained as a yellow solid (0.75 g, 3.7 mmol, 96%). Single crystals suitable for X-ray diffraction were obtained by dissolution of a small amount solid in THF and subsequent evaporation of the solvent on air. Due to the high sulfur content by weight%, the calibration value for S for the elemental analysis was overshot.

CHN for $C_6H_8N_2O_2S_2$ Found % (calc. %): C 35.88 (35.28), H 3.81 (3.95), N 13.74 (13.71), S 33.41 (31.39).

¹H NMR (THF-d8): δ = 12.53 (s, 1H, N*H*), 5.57 (h, 1H, $^3J_{HH}$ = 6.25 Hz, C*H*(CH₃)₂), 1.38 (d, $^3J_{HH}$ = 6.23 Hz, CH(C*H*₃)₂) ppm.

¹³C{¹H} NMR (THF-d8): δ = 191.2 (*C*=S), 172.7 (S–*C*=N), 153.5 (*C*=O), 77.5 (*C*H(CH₃)₂), 21.8 (CH(*C*H₃)₂) ppm.

Mass (ESI+, MeOH) for [M+H⁺] = $C_6H_8N_2O_2S_2H^+$ m/z found (calc.): 205.0106 (205.0100).

Figure S 10: ¹H NMR spectrum of 2*i*Pr in THF-d8.

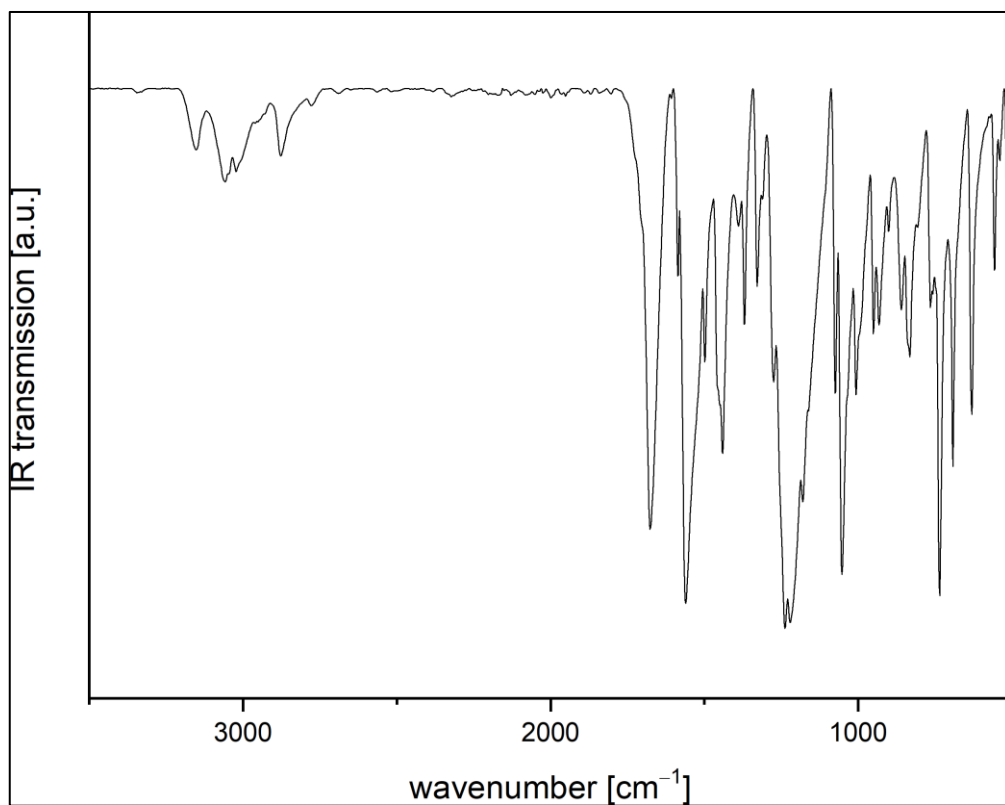**Figure S 11: ¹³C NMR spectrum of 2*i*Pr in THF-d8.**

Figure S 12: Measured room-temperature ATR-IR spectrum of 2*i*Pr.

1.6. Synthesis of 6-octyloxy-2-thioxo-2,3-dihydro-4*H*-1,3,5-thiadiazin-4-one – 2*n*Oct

To a 1M solution of octanol (7.5 ml, 7.5 mmol, 2.0 eq.) in THF neat carbonyl diisothiocyanate (0.55 g, 3.8 mmol, 1.0 eq.) was added dropwise at room temperature. The resulting solution was stirred for 16 h. Subsequently, *n*-hexane (5 ml) was added to precipitate the product. The product was filtered and washed with *n*-hexane (2 ml). After evaporation of the solvent the compound was obtained as a yellow solid (0.69 g, 2.5 mmol, 66%). Single crystals suitable for X-ray diffraction were obtained by dissolution of a small amount solid in THF and subsequent evaporation of the solvent on air.

CHN for $C_{11}H_{18}N_2O_2S_2$ Found % (calc. %): C 48.90 (48.15), H 6.22 (6.61), N 10.33 (10.21), S 24.03 (23.37).

¹H NMR (THF-d8): δ = 12.56 (s, 1H, N*H*), 4.54 (t, 2H, $^3J_{HH}$ = 6.68 Hz, OC*H₂*), 1.78 (m, 2H, $^3J_{HH}$ = 6.97 Hz, $^3J_{HH}$ = 7.06 Hz, OCH₂C*H₂*), 1.34 (m, 10H, CH₂(C*H₂*)₅CH₃), 0.88 (m, 3H, C*H₃*) ppm.

¹³C{¹H} NMR (THF-d8): δ = 191.0 (*C*=S), 173.4 (S–*C*=N), 153.5 (*C*=O), 72.5 (O*C*H₂), 32.9 (OCH₂*C*H₂), 30.3 (CH₂(*C*H₂)₅CH₃), 30.2 (CH₂(*C*H₂)₅CH₃), 29.3 (CH₂(*C*H₂)₅CH₃), 26.7 (CH₂(*C*H₂)₅CH₃), 23.7 (CH₂(*C*H₂)₅CH₃), 14.5 (*C*H₃) ppm.

Mass (ESI+, MeOH) for [M+Na⁺] = $C_{11}H_{18}N_2O_2S_2Na^+$ m/z found (calc.): 297.0711 (297.0702).
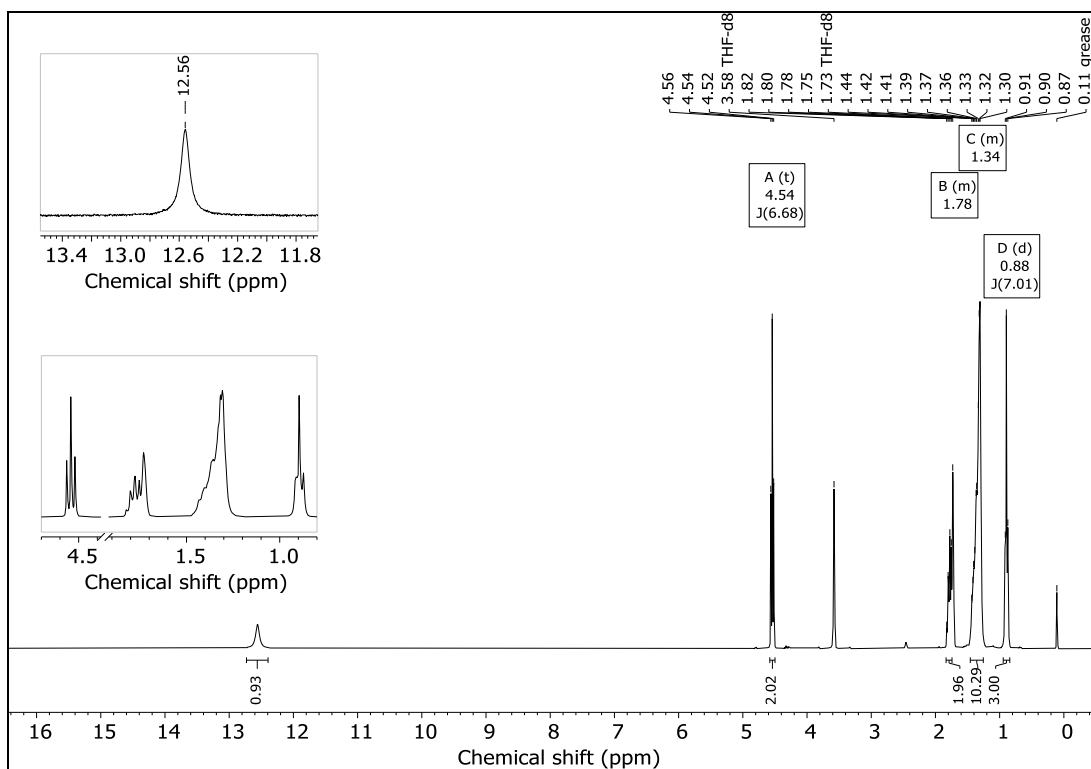
Figure S 13: ^{1}H NMR spectrum of **2*n*Oct** in THF-d8.
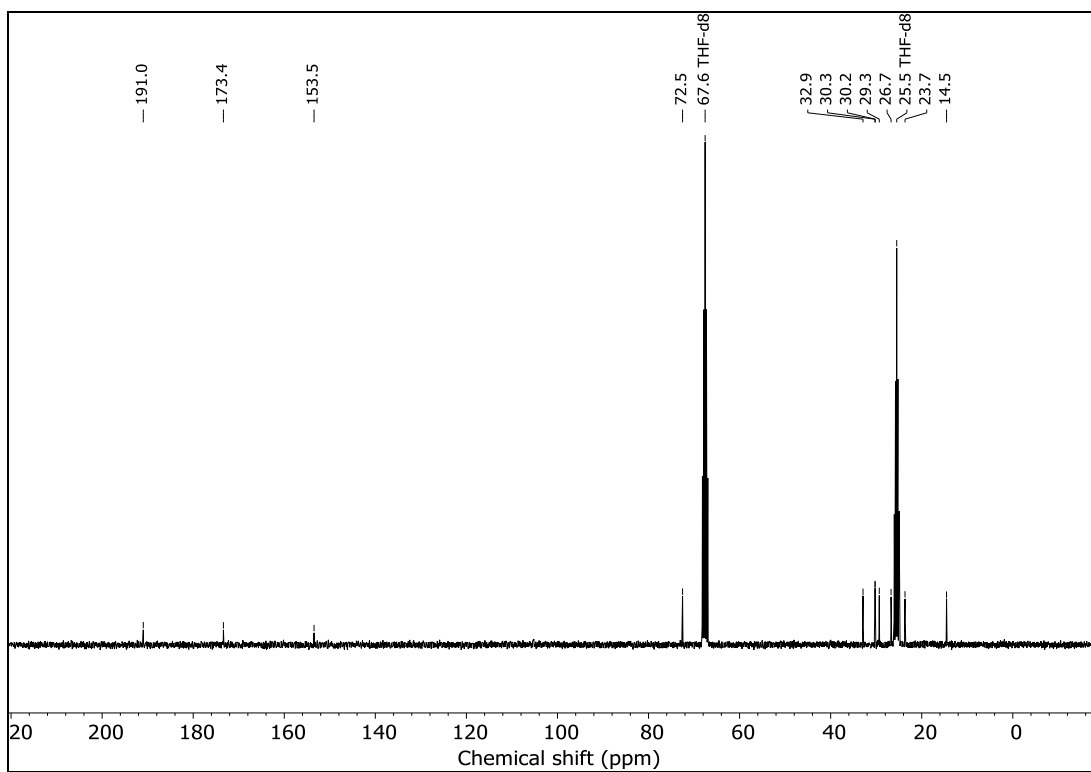
**Figure S 14:** ^{13}C NMR spectrum of **2*n*Oct** in THF-d8.

Figure S 15: Measured room-temperature ATR-IR spectrum of 2*n*Oct.

1.7. Synthesis of 6-benzyloxy-2-thioxo-2,3-dihydro-4_H_-1,3,5-thiadiazin-4-one – 2Bz

To a 1M solution of benzyl alcohol (7.5 ml, 7.5 mmol, 2.0 eq.) in THF neat carbonyl diisothiocyanate (0.55 g, 3.8 mmol, 1.0 eq.) was added dropwise at room temperature. The resulting solution was stirred for 16 h. Subsequently _n_-hexane (5 ml) was added to precipitate the product. The product was filtered and washed with _n_-hexane (2 ml). After evaporation of the solvent the compound was obtained as a yellow solid (0.86 g, 3.4 mmol, 89%). Single crystals suitable for X-ray diffraction were obtained by dissolution of a small amount solid in THF and subsequent evaporation of the solvent on air. Due to the high sulfur content by weight%, the calibration value for S for the elemental analysis was overshot.

CHN for $C_{10}H_8N_2O_2S_2$ Found % (calc. %): C 48.25 (47.60), H 3.11 (3.20), N 11.13 (11.10), S 26.83 (25.41).

¹H NMR (THF-d8): δ = 12.60 (s, 1H, N_H_), 7.40 (m, 5H, CH$_2$C$_6$_H$_5$_), 5.57 (s, 2H, C_H$_2$_C$_6$H$_5$) ppm.

¹³C{¹H} NMR (THF-d8): δ = 190.9 (C=S), 173.2 (S–C=N), 153.4 (C=O), 135.4 ($C_{ipso\text{-Ph}}$), 130.1 ($C_{meta\text{-Ph}}$), 129.9 ($C_{para\text{-Ph}}$), 129.6 ($C_{ortho\text{-Ph}}$), 73.5 (_C_H$_2$C$_6$H$_5$) ppm.

Mass (ESI+, MeOH) for [M+H⁺] = $C_{10}H_8N_2O_2S_2H^+$ m/z found (calc.): 253.0107 (253.0100).
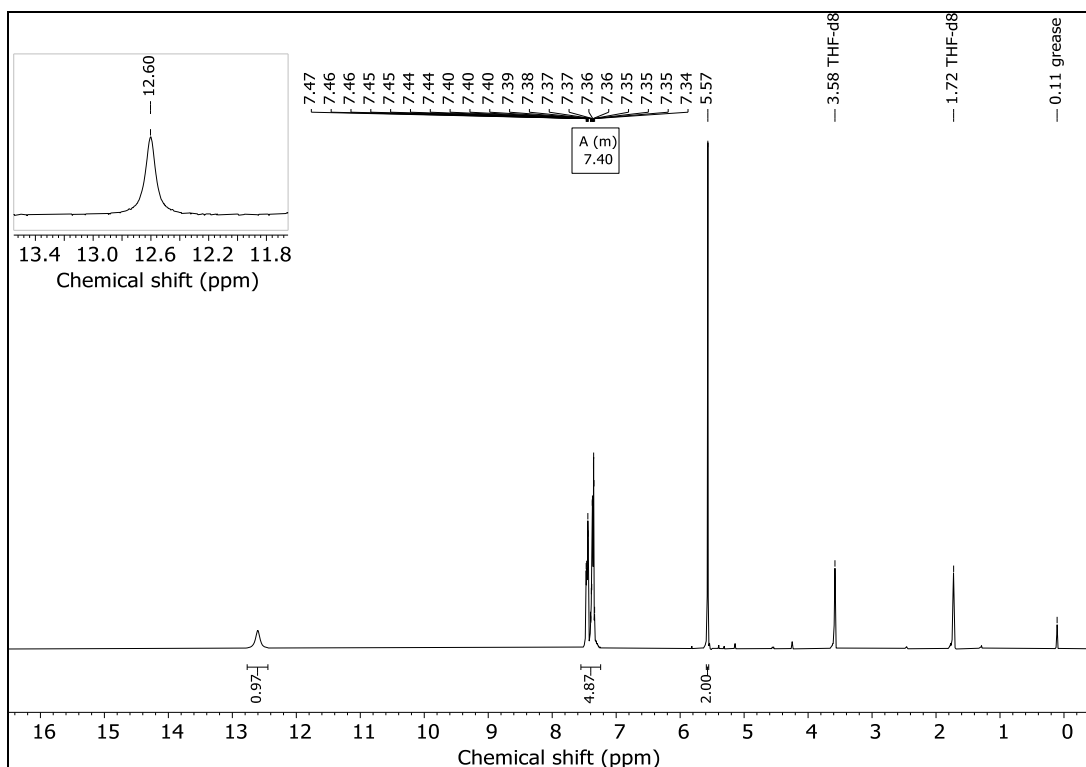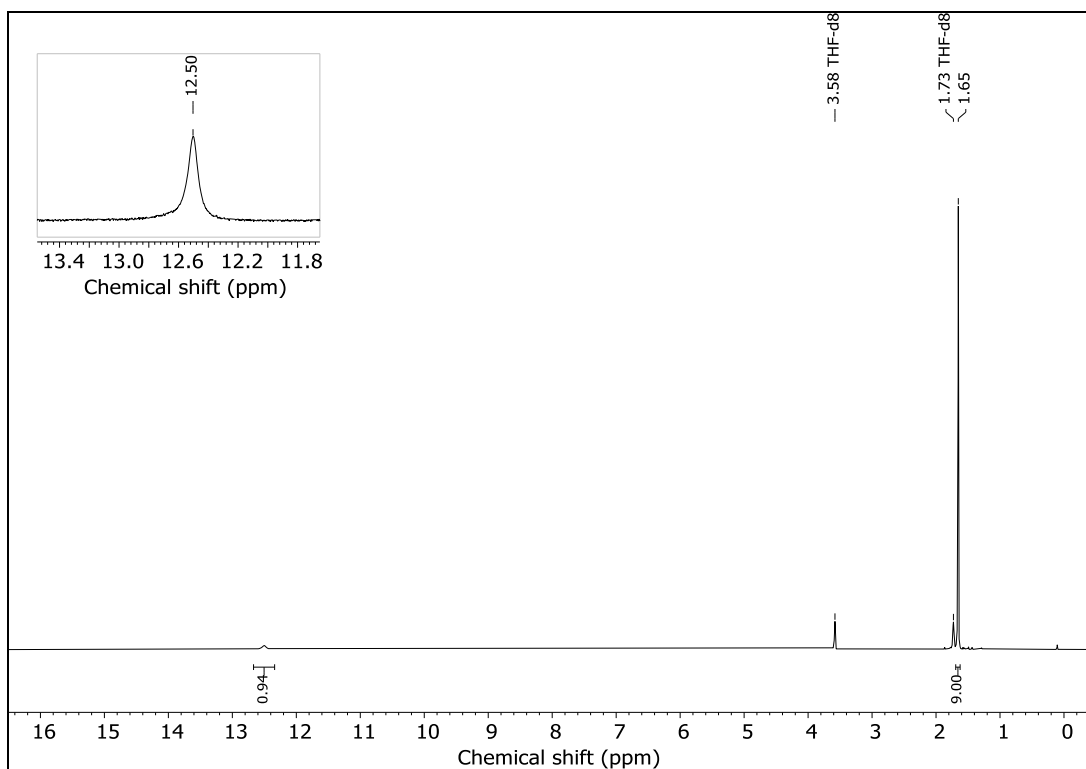
**Figure S 16: ¹H NMR spectrum of 2Bz in THF-d8.**
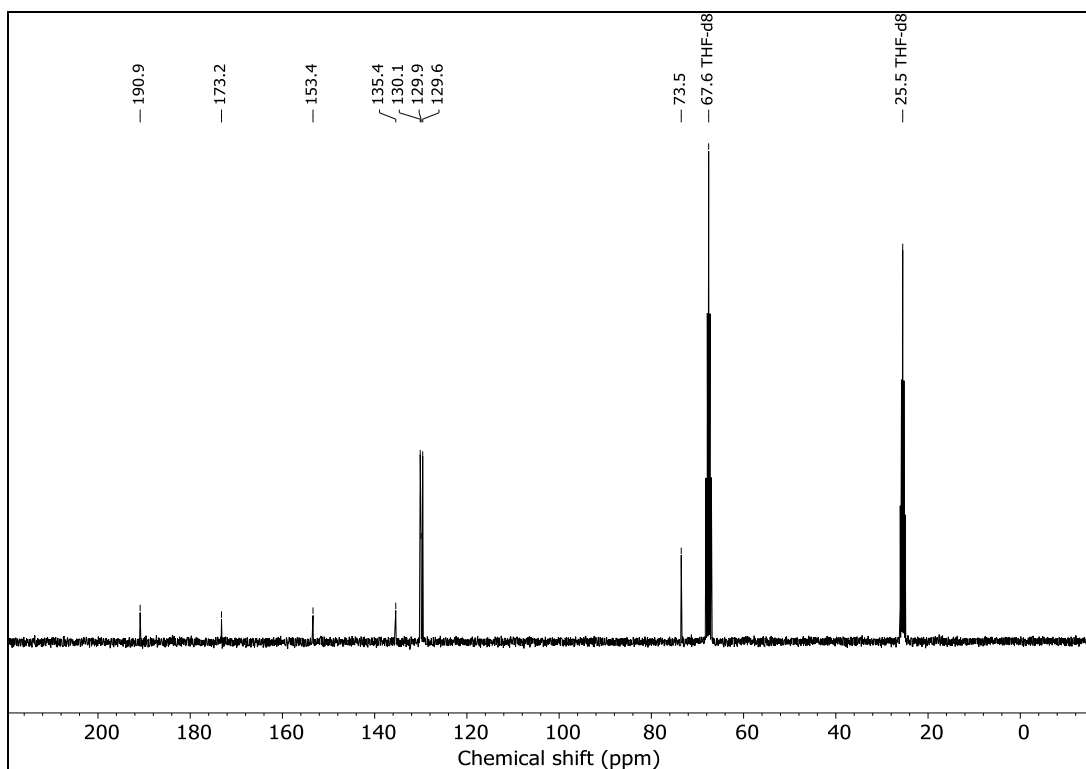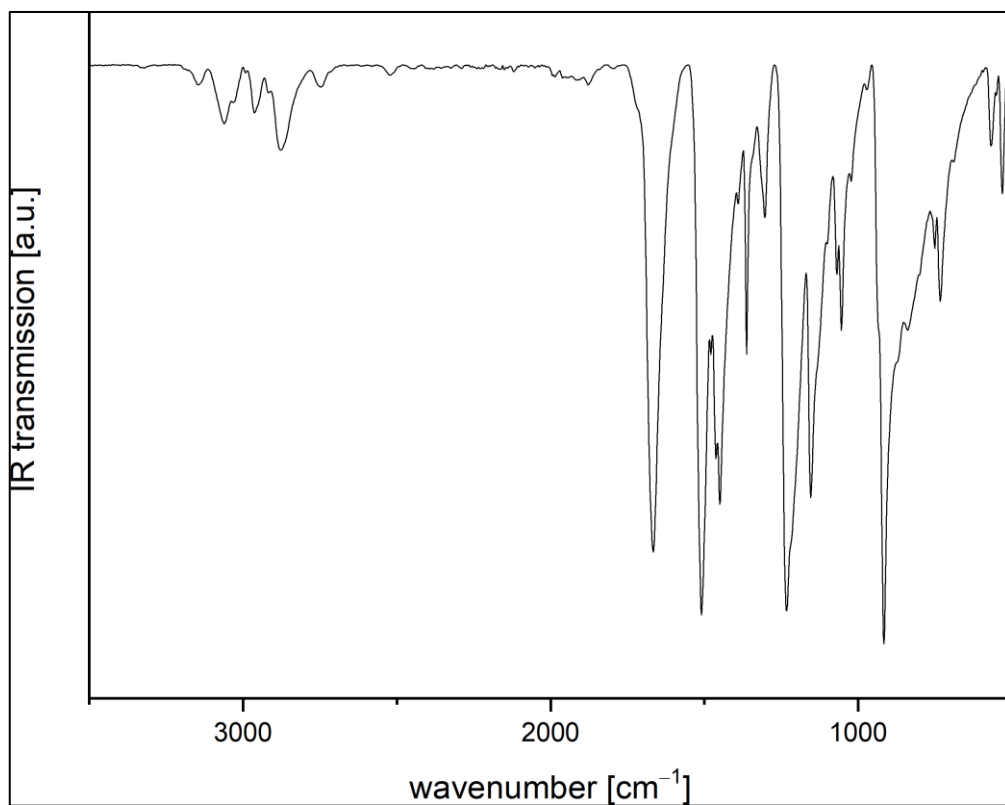

Figure S 17: ¹³C NMR spectrum of 2Bz in THF-d8.

Figure S 18: Measured room-temperature ATR-IR spectrum of 2Bz.

1.8. Synthesis of 6-ethylthio-2-thioxo-2,3-dihydro-4*H*-1,3,5-thiadiazin-4-one – 3Et

To a 1M solution of ethanethiol (3.5 ml, 3.5 mmol, 1.0 eq.) in THF neat carbonyl diisothiocyanate (0.50 g, 3.5 mmol, 1.0 eq.) was added dropwise at room temperature. The resulting solution was stirred for 16 h. After evaporation of the solvent the compound was obtained as a yellow solid (0.71 g, 3.4 mmol, 99%). Single crystals suitable for X-ray diffraction were obtained by dissolution of a small amount solid in a 1:1 mixture of DCM/Et$_2$O and subsequent evaporation of the solvent on air. Due to the high sulfur content by weight%, the calibration value for S for the elemental analysis was overshot.

CHN for C$_5$H$_6$N$_2$O$_1$S$_3$ Found % (calc. %): C 29.26 (29.11), H 2.56 (2.93), N 13.69 (13.58), S 49.67 (46.62).

^{1}H NMR (THF-d8): δ = 12.52 (s, 1H, N*H*), 3.32 (q, 2H, $^3J_{HH}$ = 7.34 Hz, C*H$_2$*CH$_3$), 1.38 (t, 3H, $^3J_{HH}$ = 7.34 Hz CH$_2$C*H$_3$*) ppm.

^{13}C{^{1}H} NMR (THF-d8): δ = 190.9 (*C*=S), 182.4 (S–*C*=N), 150.2 (*C*=O), 27.1 (*C*H$_2$CH$_3$), 14.6 (CH$_2$*C*H$_3$) ppm.

Mass (ESI+, MeOH) for [M+H$^+$] = C$_5$H$_6$N$_2$O$_1$S$_3$H$^+$ m/z found (calc.): 206.9721 (206.9715).
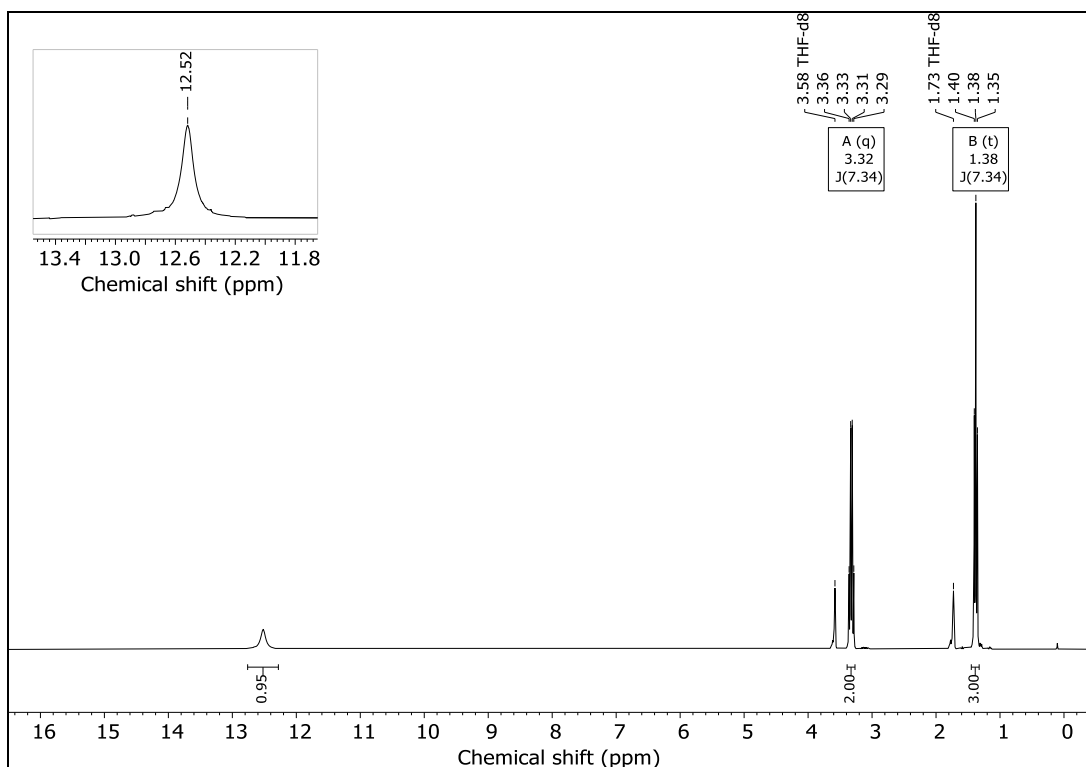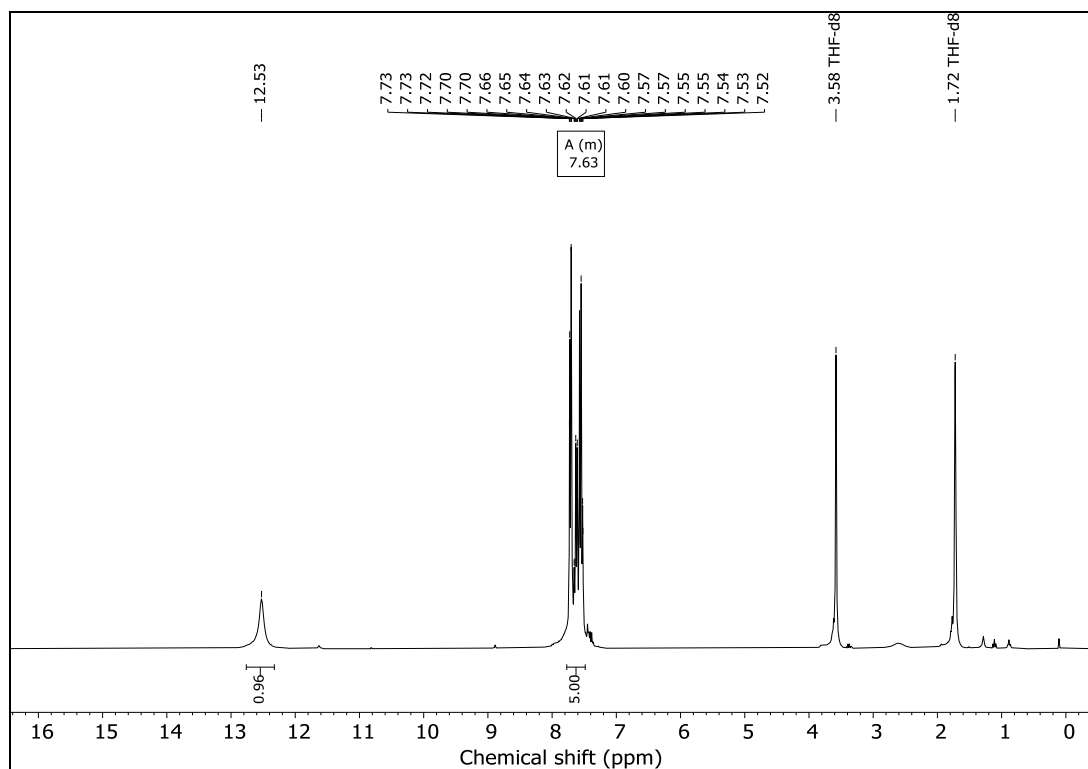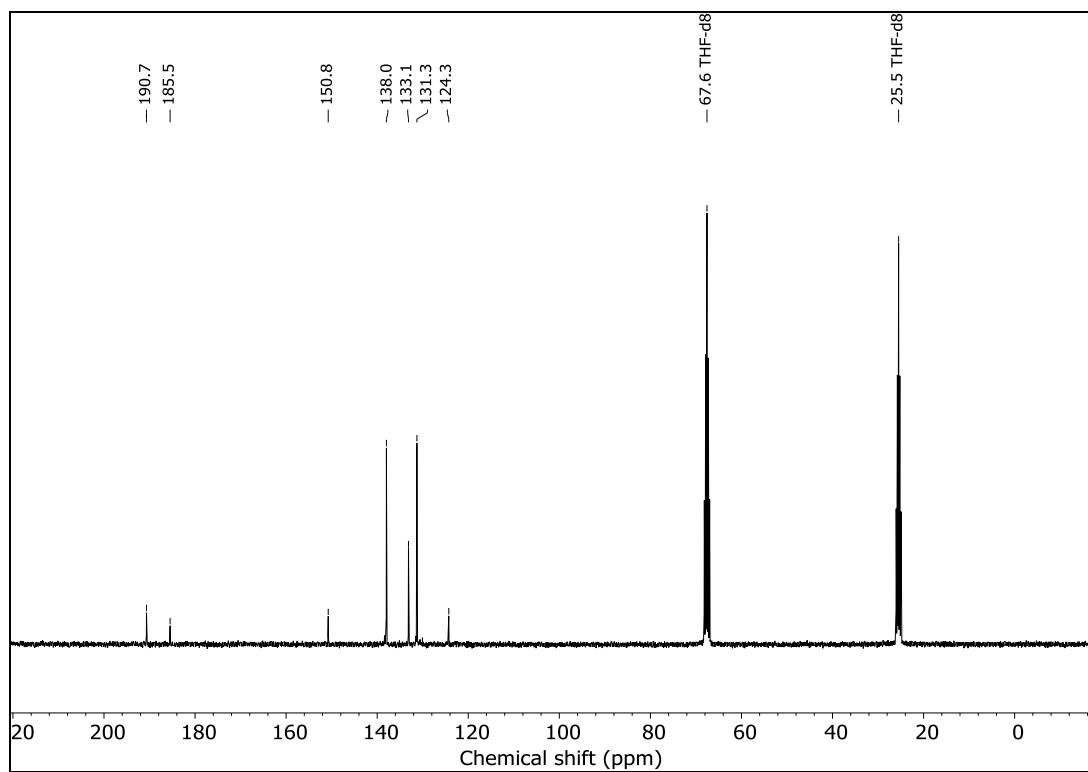
Figure S 19: ^{1}H NMR spectrum of 3Et in THF-d8.
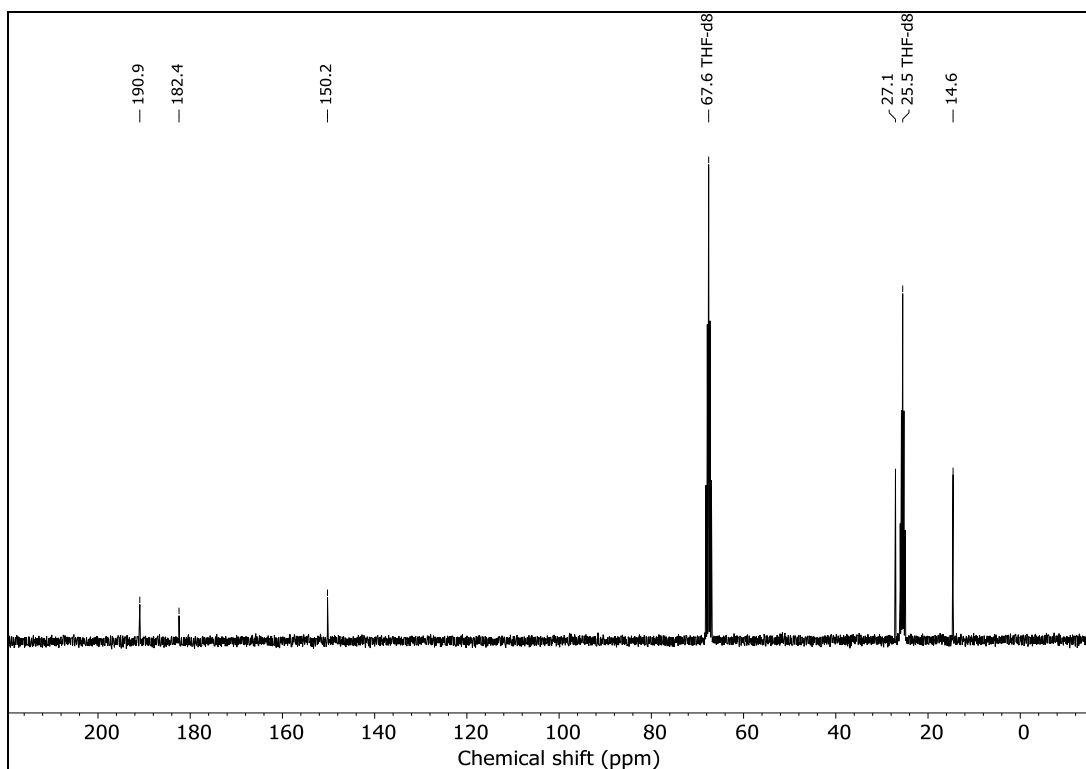
Figure S 20: ^{13}C NMR spectrum of 3Et in THF-d8.
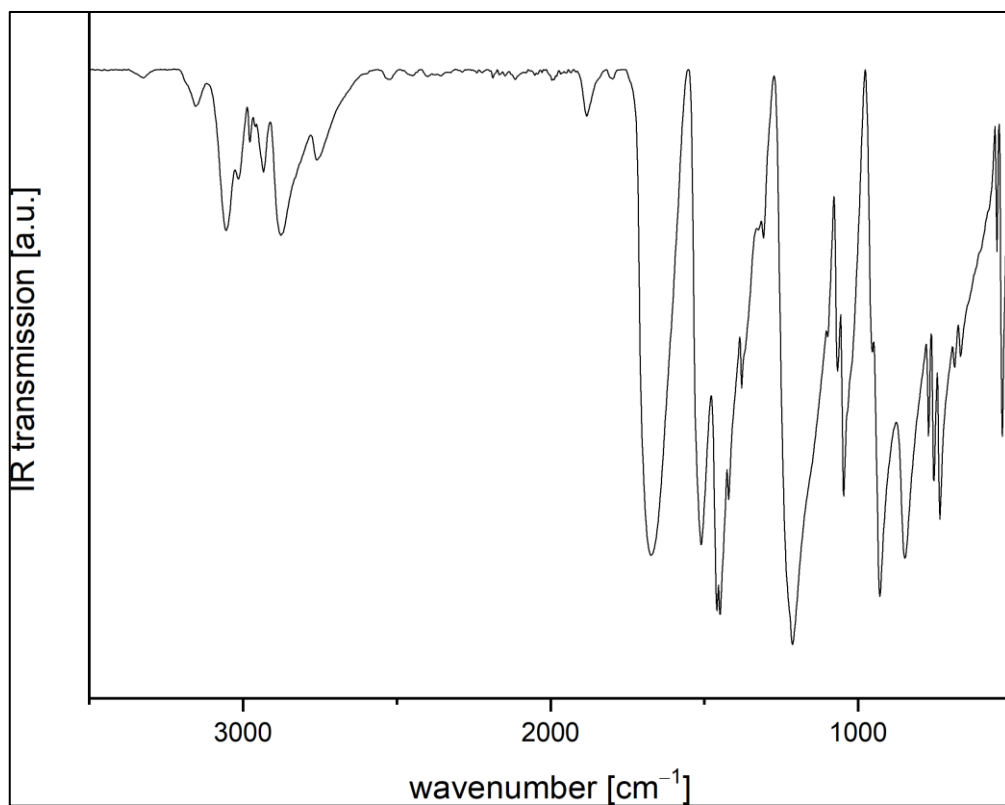
Figure S 21: Measured room-temperature ATR-IR spectrum of 3Et.

1.9. Synthesis of 6-(*tert*-butylthio)-2-thioxo-2,3-dihydro-4*H*-1,3,5-thiadiazin-4-one – 3*t*Bu

To a 1M solution of *tert*-butylthiol (2.0 ml, 2.0 mmol, 1.0 eq.) in THF neat carbonyl diisothiocyanate (0.29 g, 2.0 mmol, 1.0 eq.) was added dropwise at room temperature. The resulting solution was stirred for 16 h. After evaporation of the solvent the compound was suspended in a 1:1 mixture of *n*-hexane/Et$_2$O (4 ml), filtered and washed with *n*-hexane. After evaporation of the solvent the compound was obtained as a yellow solid (0.31 g, 1.3 mmol, 66%). We were not able to obtain crystals suitable for single crystal X-ray diffraction.

CHN for C$_7$H$_{10}$N$_2$O$_1$S$_3$ Found % (calc. %): C 36.29 (35.88), H 4.29 (4.30), N 11.76 (11.95), S 41.50 (41.04).

^{1}H NMR (THF-d8): δ = 12.50 (s, 1H, N*H*), 1.65 (s, 9H, C(C*H*$_3$)$_3$) ppm.

^{13}C{^{1}H} NMR (THF-d8): δ = 191.5 (*C*=S), 181.5 (S–*C*=N), 150.1 (*C*=O), 55.7 (*C*(CH$_3$)$_3$), 30.3 (C(*C*H$_3$)$_3$) ppm.

Figure S 22: ¹H NMR spectrum of 3*t*Bu in THF-d8.
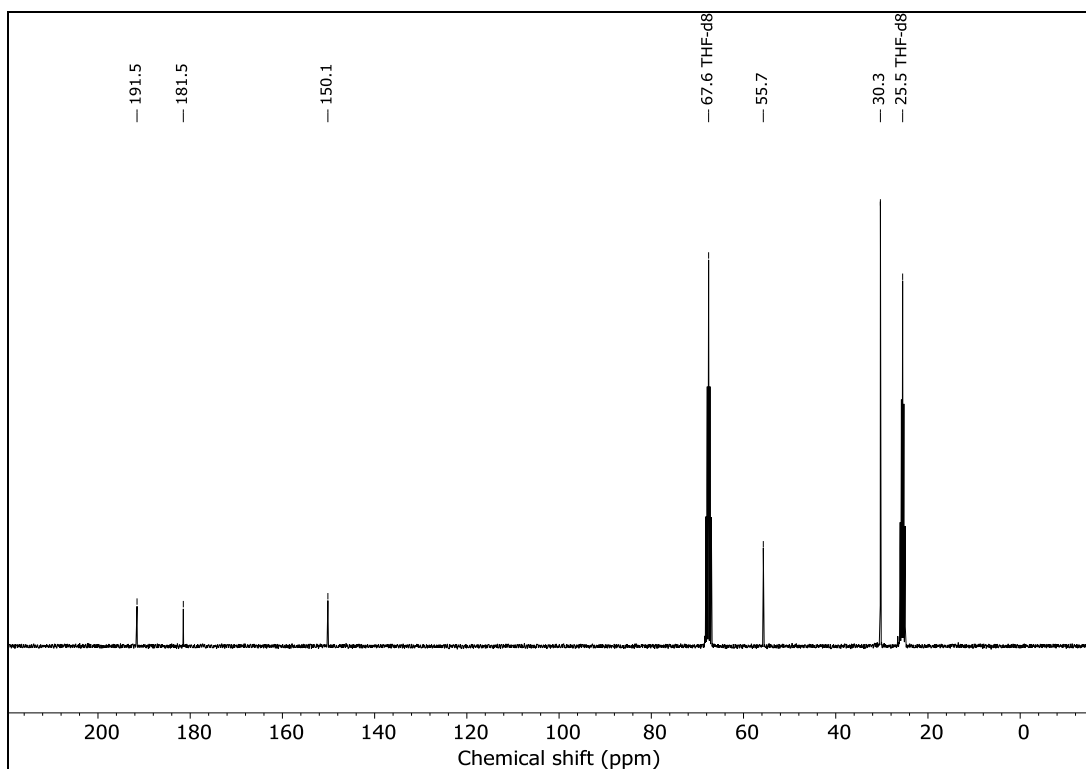
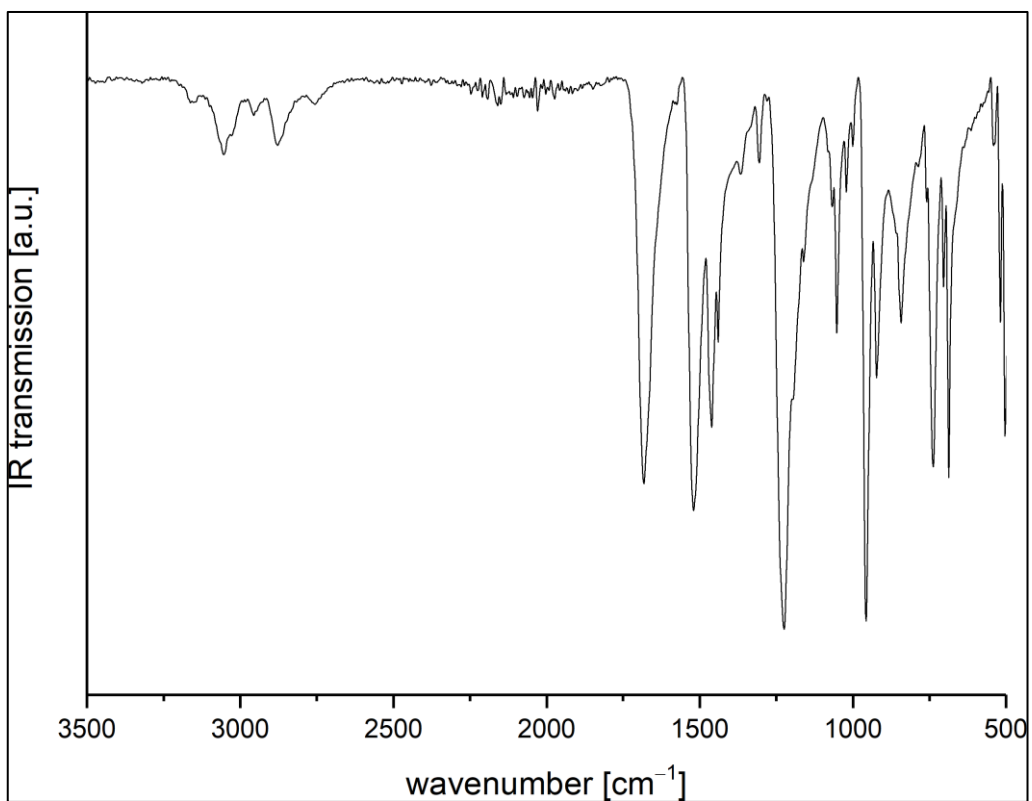**Figure S 23: ¹³C NMR spectrum of 3*t*Bu in THF-d8.**
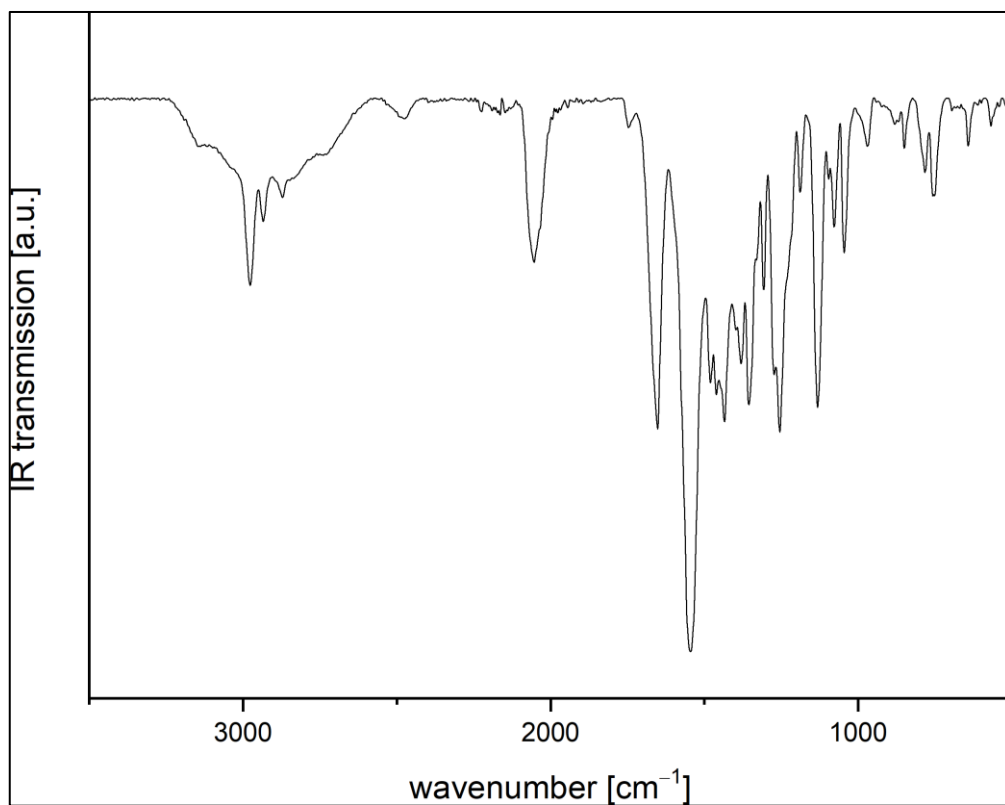
Figure S 24: Measured room-temperature ATR-IR spectrum of 3*t*Bu.

1.10. Synthesis of 6-phenylthio-2-thioxo-2,3-dihydro-4*H*-1,3,5-thiadiazin-4-one – 3Ph

To a 1M solution of thiphenol (2.0 ml, 2.0 mmol, 1.0 eq.) in THF neat carbonyl diisothiocyanate (0.29 g, 2.0 mmol, 1.0 eq.) was added dropwise at room temperature. The resulting solution was stirred for 16 h. After evaporation of the solvent the compound was suspended in a 1:1 mixture of *n*-hexane/Et$_2$O (4 ml), filtered and washed with *n*-hexane. After evaporation of the solvent the compound was obtained as a yellow solid (0.37 g, 1.5 mmol, 73%). Single crystals suitable for X-ray diffraction were obtained by dissolution of a small amount solid in THF and subsequent evaporation of the solvent on air. Due to the high sulfur content by weight%, the calibration value for S for the elemental analysis was overshot.

CHN for C$_5$H$_6$N$_2$O$_1$S$_3$ Found % (calc. %): C 42.48 (42.50), H 2.52 (2.38), N 10.95 (11.01),

S 38.63 (37.82).

^{1}H NMR (THF-d8): δ = 12.53 (s, 1H, N*H*), 7.63 (m, 5H, C$_6$*H$_5$*) ppm.

^{13}C{^{1}H} NMR (THF-d8): δ = 190.7 (*C*=S), 185.5 (S–*C*=N), 150.8 (*C*=O), 138.0 (*C$_{ortho}$*-Ph),

133.1 (*C$_{ipso}$*-Ph), 131.3 (*C$_{meta}$*-Ph), 124.3 (*C$_{para}$*-Ph) ppm.

Mass (ESI+, MeOH) for [M+Na$^+$] = C$_9$H$_6$N$_2$O$_1$S$_3$Na$^+$ m/z found (calc.): 276.9542 (276.9534).

Figure S 25: ¹H NMR spectrum of 3Ph in THF-d8.

Figure S 26: ¹³C NMR spectrum of 3Ph in THF-d8.

Figure S 27: Measured room-temperature ATR-IR spectrum of 3Ph.

1.11. Synthesis of 6-diethylamino-2-thioxo-2,3-dihydro-4*H*-1,3,5-thiadiazin-4-one –

4Et

To a 1M solution of carbonyl diisothiocyanate (0.29 g, 2.0 mmol, 1.0 eq) in Et$_2$O cooled to −78°C a 0.33M solution of diethyl amine (5.8 ml, 1.91 mmol, 0.96 eq.) in Et$_2$O was added dropwise. A precipitate formed immediately. The suspension was stirred for 10 min. The compound was filtered, dried *in vacuo* and obtained as a yellow solid (0.19 g, 0.9 mmol, 46%). Single crystals suitable for X-ray diffraction were obtained by dissolution of a small amount solid in THF and subsequent evaporation of the solvent on air.

^{1}H NMR (THF-d8): δ = 12.14 (s, 1H, N*H*), 3.72 (q, 4H, $^3J_{HH}$ = 7.25 Hz, C*H*$_2$CH$_3$), 1.32 (t, 6H, $^3J_{HH}$ = 7.27 Hz, CH$_2$C*H*$_3$) ppm.

^{13}C{^{1}H} NMR (THF-d8): δ = 190.1 (*C*=S), 163.2 (S–*C*=N), 153.2 (*C*=O), 43.1 (*C*H$_2$CH$_3$), 11.7 (CH$_2$*C*H$_3$) ppm.

Mass (ESI+, MeOH) for [M+H$^+$] = C$_7$H$_{11}$N$_3$O$_1$S$_2$H$^+$ m/z found (calc.): 218.0413 (218.0416).
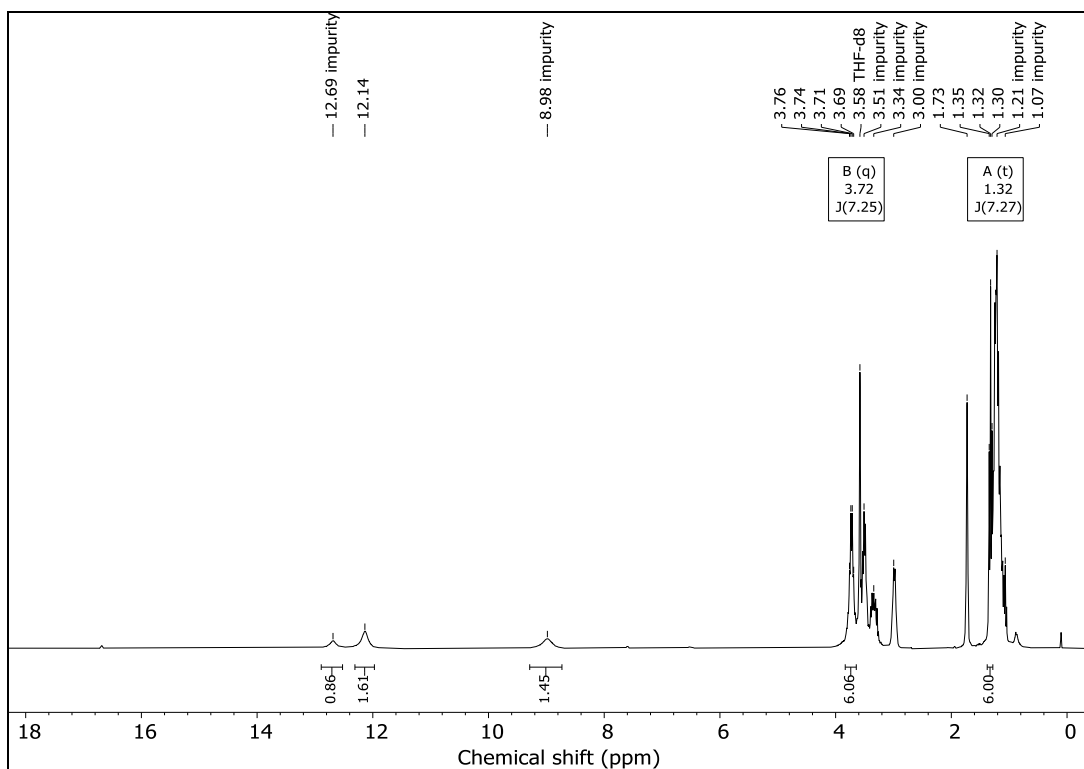
Figure S 28: ^{1}H NMR spectrum of **4Et** in THF-d8.
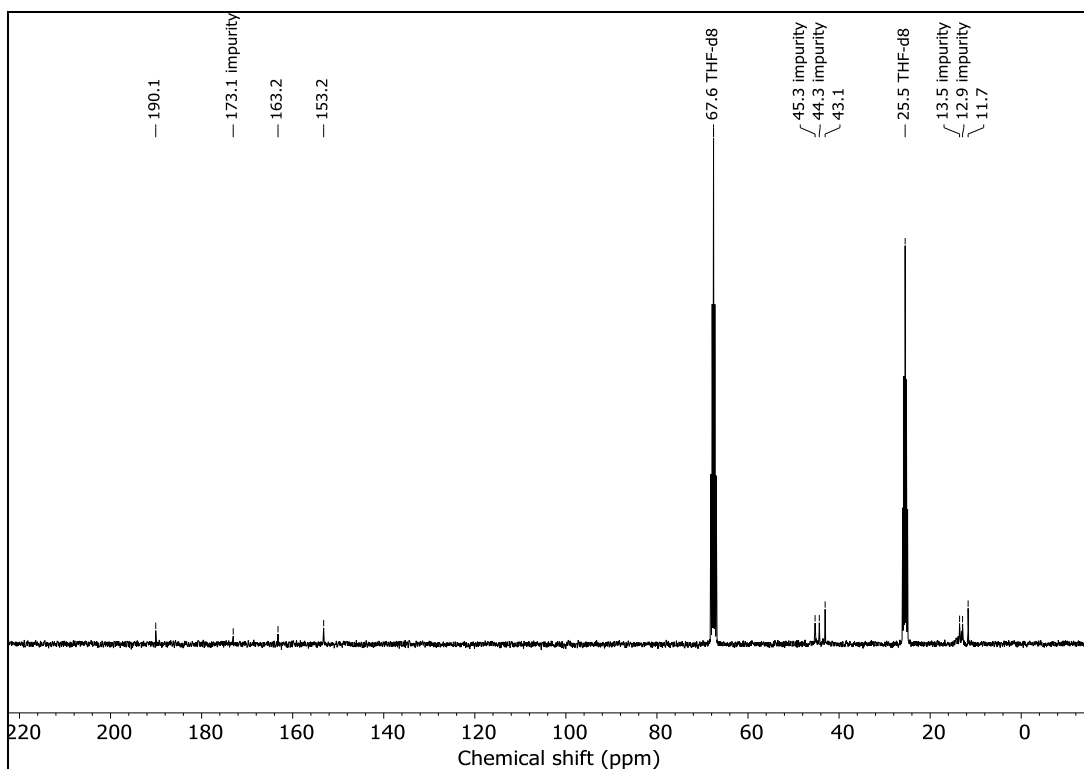
Figure S 29: ^{13}C NMR spectrum of **4Et** in THF-d8.

Figure S 30: Measured room-temperature ATR-IR spectrum of 4Et.

1.12. Synthesis of 6-diisopropylamino-2-thioxo-2,3-dihydro-4*H*-1,3,5-thiadiazin-4-one – 4*i*Pr

To a 1M solution of carbonyl diisothiocyanate (0.29 g, 2.0 mmol, 1.0 eq) in Et$_2$O cooled to −78°C a 0.33Msolution of diisopropyl amine (5.8 ml, 1.91 mmol, 0.96 eq.) in Et$_2$O was added dropwise. A precipitate formed immediately. The suspension was stirred for 10 min. The compound was filtered, dried *in vacuo* and obtained as a yellow solid (0.25 g, 1.0 mmol, 54%). Single crystals suitable for X-ray diffraction were obtained by dissolution of a small amount solid in THF and subsequent evaporation of the solvent on air.

^{1}H NMR (THF-d8): δ = 12.09 (s, 1H, N*H*), 3.38 (m, 2H, C*H*(CH$_3$)$_2$), 1.36 (d, 12H, $^3J_{HH}$ = 6.58 Hz, CH(C*H*$_3$)$_2$) ppm.

^{13}C{^{1}H} NMR (THF-d8): δ = 190.8 (*C*=S), 161.8 (S–*C*=N), 152.5 (*C*=O), 48.1 (*C*H(CH$_3$)$_2$), 19.3 (CH(*C*H$_3$)$_2$) ppm.

Mass (ESI+, MeOH) for [M+H$^+$] = C$_9$H$_{15}$N$_3$O$_1$S$_3$H$^+$ m/z found (calc.): 246.0725 (246.0729).
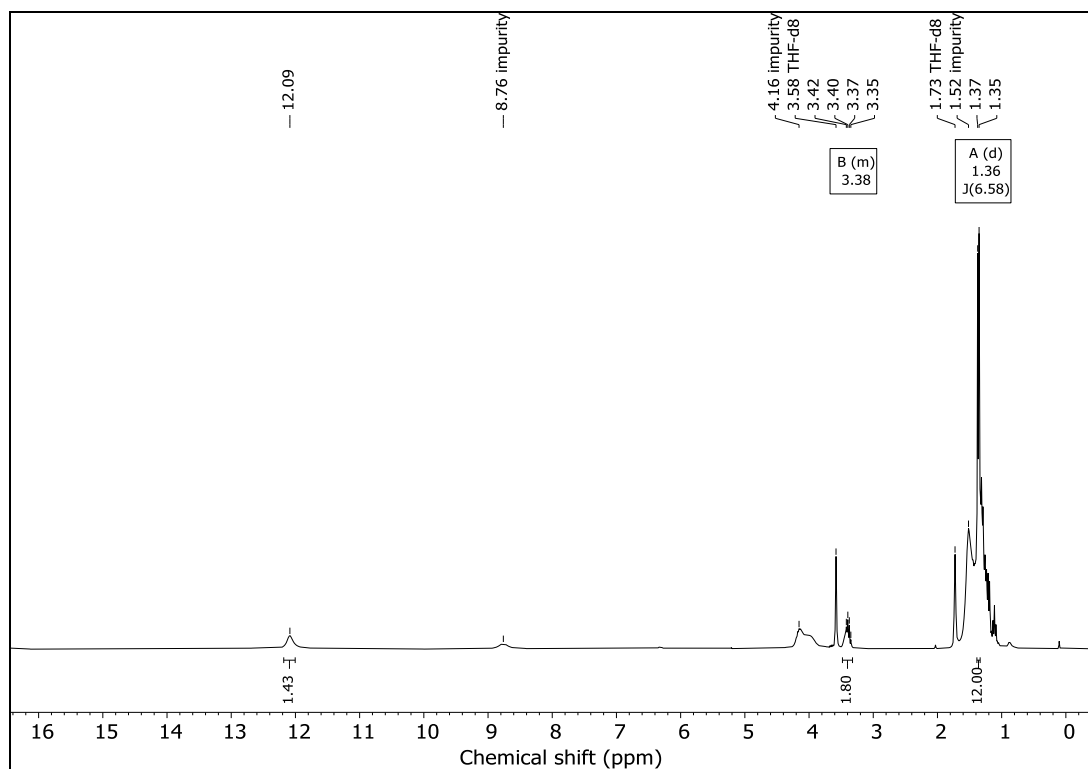
Figure S 31: ¹H NMR spectrum 4*i*Pr in THF-d8.
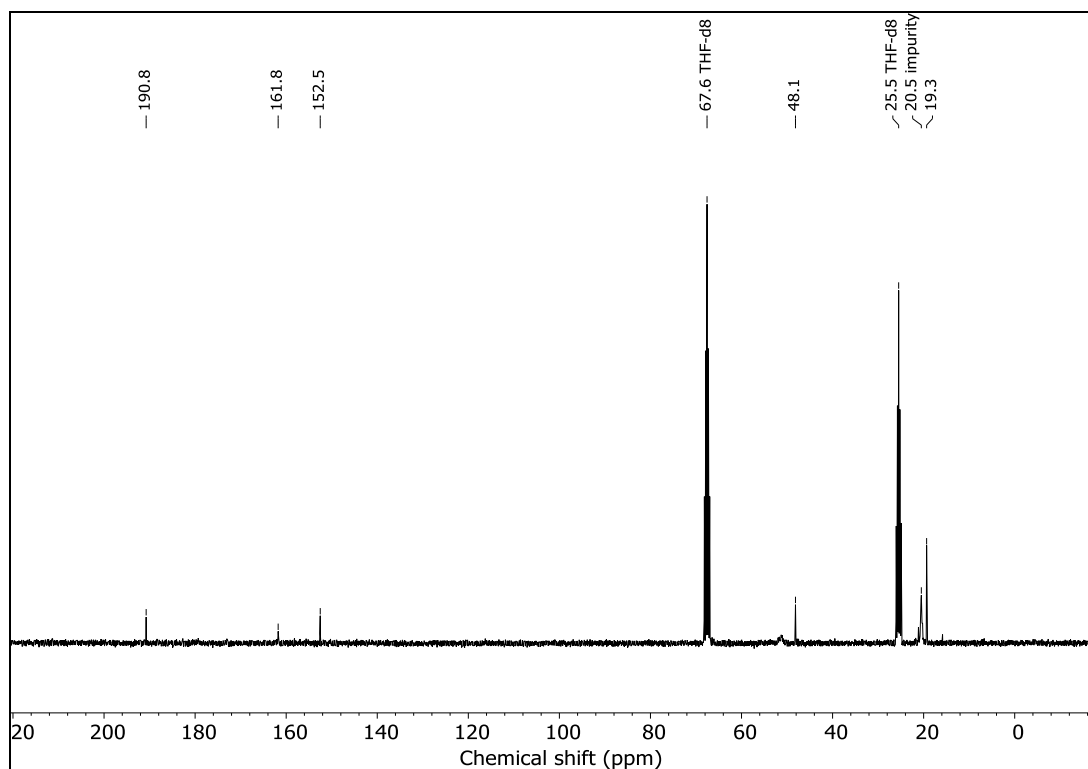
Figure S 32: ¹³C NMR spectrum of 4*i*Pr in THF-d8.
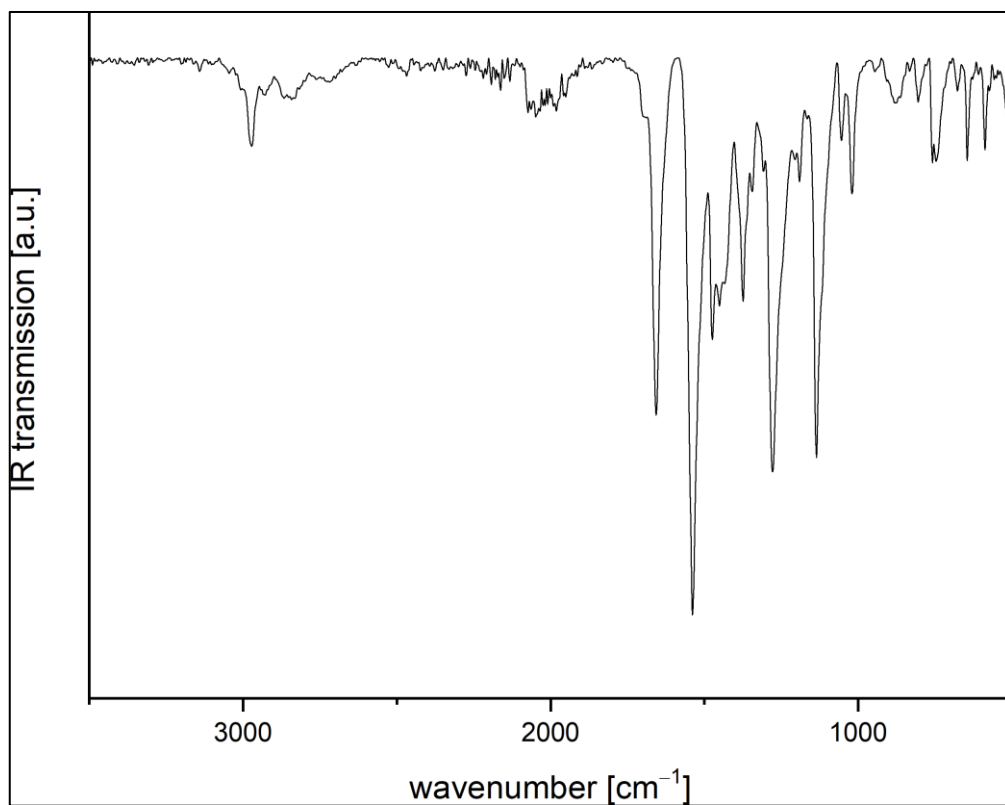
Figure S 33: Measured room-temperature ATR-IR spectrum of 4*i*Pr.

2. Crystallographic data

Single crystal X-ray structure determination: Single-crystal X-ray diffraction data were collected using a StadiVari (Stoe, Darmstadt) diffraction system equipped with mirror monochromated Cu K$_\alpha$ radiation (λ = 1.54186 Å, Xenocs Microfocus Source) and a Pilatus 300K detector, or an IPDS 2T (Stoe, Darmstadt) diffraction system equipped with graphite monochromated Mo K$_\alpha$ radiation (λ = 0.71073 Å) or an IPDS-II (Stoe, Darmstadt) diffraction system quipped with graphite monochromated Mo K$_\alpha$ radiation (λ = 0.71073 Å).

Crystals were selected under Paratone-N oil, mounted on micromount loops and quench-cooled using an Oxford Cryosystems open flow N$_2$ cooling device. Data were collected at 100 K (if not stated otherwise) and processed using the X-Area program package (for datasets acquired with Stoe devides), including unit cell parameter refinement and inter-frame scaling (which was carried out using LANA within X-Area). For datasets acquired with a Bruker d8-Quest, the APEX3 software suite was used for data processing. Structures were subsequently solved using direct methods (SHELXT[4]) and refined on F^2 with SHELXL[5] using the Olex2[6] user interface. The crystal structure drawings were generated with DIAMOND.[7]

Table S 1: Selected single crystal X-ray data collection and refinement parameters for

	1	2Me	2Et	2iPr
Formula	$C_3H_4N_2O_3S_2$	$C_4H_4N_2O_2S_2$	$C_5H_6N_2O_2S_2$	$C_6H_8N_2O_2S_2$
CCDC	2332715	2332716	2332718	2332811
Fw / g mol^{-1}	180.20	176.21	190.24	204.26
Crystal system	monoclinic	triclinic	monoclinic	monoclinic
Space group	$P2_1/n$	$P–1$	$P2_1/n$	$P2_1/n$
a / Å	9.5883(3)	3.9780(10)	9.9403(5)	4.5718(16)
b / Å	5.77650(10)	9.631(3)	4.9482(3)	10.499(2)
c / Å	12.4825(4)	9.796(2)	16.1597(8)	18.377(5)
α / °	90	67.575(18)	90	90
β / °	106.425(3)	86.40(2)	103.949(4)	96.44(2)
γ / °	90	78.56(2)	90	90
V / Å^3	663.15(3)	339.99(15)	771.40(7)	876.5(4)
Z	4	2	4	4
Radiation, λ / Å	CuKα (λ = 1.54186)	MoKα (λ = 0.71073)	CuKα (λ = 1.54186)	MoKα (λ = 0.71073)
Temp / K	100.00	100.00	100.00	100.00
ρ_{calc} / g cm^{-3}	1.805	1.721	1.638	1.548
μ / mm^{-1}	6.919	0.716	5.884	0.567
Reflections collected	10814	4959	11655	6675
Ind. Reflns. / Ind. Reflns gt	1232 / 1154	1784 / 1118	1406 / 1205	2372 / 1387
Parameters	108	92	106	115
R_{int}/ $R_{(\sigma)}$	0.0270 / 0.0121	0.0656 / 0.0761	0.0337 / 0.0186	0.0744 / 0.0904
$R1/wR2$,[a] $I \geq 2\sigma I$ (%)	0.0283 / 0.0776	0.0548 / 0.1331	0.0329 / 0.0858	0.0668 / 0.1702
$R1/wR2$,[a] all data (%)	0.0296 / 0.0783	0.0974 / 0.1534	0.0384 / 0.0886	0.1286 / 0.2016
GOF	1.062	0.971	1.000	0.938
Twin law	–	–	–	–
BASF	–	–	–	–
Flack parameter	–	–	–	–

[a] R1 = [Σ||F$_o$| − |F$_c$||]/Σ|F$_o$|; wR2 = {[Σw[(F$_o$)^2 − (F$_c$)^2]^2]/[Σw(F$_o^2$)^2]}$^{1/2}$; w = [σ^2(F$_o$)^2 + (AP)^2 + BP]$^{-1}$, where P = [(F$_o$)^2 + 2(F$_c$)^2]/3 and the A and B values are 0.0602 and 0.1848 for **1**, 0.0927 and 0.0000 for **2Me**, 0.0706 and 0.000 for **2Et**, 0.1308 and 0.000 for **2iPr**.

Table S 2: Selected single crystal X-ray data collection and refinement parameters for

	2nOct	**2Bz**	**3Et**	**3Ph**
Formula	$C_{11}H_{18}N_2O_2S_2$	$C_{10}H_8N_2O_2S_2$	$C_5H_6N_2OS_3$	$C_9H_6N_2OS_3$
CCDC	2332722	2332812	2332720	2332721
Fw / g mol^{-1}	274.39	252.30	206.30	254.34
Crystal system	triclinic	monoclinic	monoclinic	triclinic
Space group	P-1	$P2_1/c$	$P2_1/c$	P-1
a / Å	5.4100(4)	10.9207(5)	4.48610(10)	4.9909(3)
b / Å	8.0932(6)	13.6738(4)	19.1071(4)	14.5449(8)
c / Å	15.4550(11)	14.5857(6)	9.9353(3)	14.9431(9)
α / °	97.724(6)	90	90	96.951(5)
β / °	93.894(6)	101.962(3)	100.367(2)	92.195(5)
γ / °	92.674(6)	90	90	98.269(4)
V / Å^3	667.93(9)	2130.75(15)	837.72(4)	1063.87(11)
Z	2	8	4	4
Radiation, λ / Å	CuKα (λ = 1.54186)	CuKα (λ = 1.54186)	CuKα (λ = 1.54186)	CuKα (λ = 1.54186)
Temp / K	100.00	100.00	100.00	100.00
ρ_{calc} / g cm^{-3}	1.364	1.573	1.636	1.588
μ / mm^{-1}	3.562	4.430	7.646	6.156
Reflections collected	11515	49132	17748	16813
Ind. Reflns. / Ind. Reflns gt	2286 / 1712	3831 / 2851	1740 / 1524	3973 / 2697
Parameters	159	289	106	272
R_{int}/ $R_{(\sigma)}$	0.0453 / 0.0403	0.0463 / 0.0212	0.0290 / 0.0168	0.0534 / 0.0626
$R1$/$wR2$,[a] $I \geq 2\sigma I$ (%)	0.0421 / 0.1018	0.0921 / 0.2283	0.0287 / 0.0723	0.0686 / 0.1815
$R1$/$wR2$,[a] all data (%)	0.0549 / 0.1052	0.1053 / 0.2376	0.0323 / 0.0731	0.0926 / 0.1917
GOF	0.925	1.000	0.978	0.940
Twin law	–	–	–	–
BASF	–	–	–	–
Flack parameter	–	–	–	–

[a] R1 = [Σ||F$_o$| − |F$_c$||]/Σ|F$_o$|; wR2 = {[Σw[(F$_o$)^2 − (F$_c$)^2]^2]/[Σw(F$_o$^{2})^2]}$^{1/2}$; w = [σ^2(F$_o$)^2 + (AP)^2 + BP]$^{-1}$, where P = [(F$_o$)^2 + 2(F$_c$)^2]/3 and the A and B values are 0.0725 and 0.0000 for **2nOct**, 0.1938 and 0.0000 for **2Bz**, 0.0572 and 0.000 for **3Et**, 0.1374 and 0.000 for **3Ph**.

Table S 3: Selected single crystal X-ray data collection and refinement parameters for

	4Et	4iPr
Formula	$C_7H_{11}N_3OS_2$	$C_9H_{15}N_3OS_2$
CCDC	2332723	2332717
Fw / g mol^{-1}	217.31	245.36
Crystal system	orthorhombic	triclinic
Space group	*Pbca*	*P*-1
a / Å	12.6047(2)	7.9820(5)
b / Å	11.9526(2)	10.7339(7)
c / Å	26.3912(5)	14.4296(10)
α / °	90	77.565(5)
β / °	90	81.384(5)
γ / °	90	81.534(5)
V / Å^3	3976.07(12)	1185.18(14)
Z	16	4
Radiation, λ / Å	CuKα (λ = 1.54186)	CuKα (λ = 1.54186)
Temp / K	100.00	100.00
ρ_{calc} / g cm^{-3}	1.452	1.375
μ / mm^{-1}	4.587	3.909
Reflections collected	42943	20445
Ind. Reflns. / Ind. Reflns gt	4107 / 3365	4049 / 2830
Parameters	267	279
R_{int}/ $R_{(\sigma)}$	0.0410 / 0.0238	0.0516 / 0.0595
$R1$/$wR2$,[a] $I \geq 2\sigma I$ (%)	0.0297 / 0.0793	0.0312 / 0.0638
$R1$/$wR2$,[a] all data (%)	0.0374 / 0.0816	0.0541 / 0.0666
GOF	0.970	0.870
Twin law	–	–
BASF	–	–
Flack parameter	–	–

[a] R1 = [Σ||F$_o$| − |F$_c$||]/Σ|F$_o$|; wR2 = {[Σw[(F$_o$)^2 − (F$_c$)^2]^2]/[Σw(F$_o^2$)^2]}$^{1/2}$; w = [σ^2(F$_o$)^2 + (AP)^2 + BP]$^{-1}$, where P = [(F$_o$)^2 + 2(F$_c$)^2]/3 and the A and B values are 0.0585 and 0.0000 for **4Et**, 0.0348 and 0.0000 for **4iPr**.

3. Hirshfeld surface analysis

Table S 4: Relative contribution of interactions to the Hirshfeld surface in percent [%].

compound	H···O	H···S	H···N	H···H	H···C	C···C	C···N	N···N	O···C	O···N	O···O	S···C	S···N	S···O	S···S
1	23.7	23.1	1.9	6.0	3.1	0.0	0.0	0.0	8.3	4.5	5.0	7.6	2.9	6.0	7.9
2Me	22.4	17.9	6.9	12.7	2.2	1.1	2.7	0.0	3.3	2.5	0.0	7.0	2.0	9.4	9.9
2Et	24.6	19.4	6.7	18.8	3.3	0.2	0.1	0.0	2.4	0.4	0.0	8.4	4.7	3.7	7.4
2*i*Pr	22.4	16.8	4.6	26.9	5.0	0.8	2.1	0.8	0.0	0.4	0.4	5.6	1.7	2.9	9.7
2*n*Oct	9.5	20.3	3.6	49.9	0.9	1.0	0.6	0.4	4.0	0.4	1.1	2.1	2.6	3.3	0.3
2Bz	14.9	25.6	4.2	25.1	7.5	7.3	2.6	0.0	1.3	0.0	1.9	4.5	3.5	1.1	0.7
3Et	17.6	27.2	5.2	16.7	5.8	1.0	2.2	0.9	0.0	0.6	0.3	6.4	1.9	0.0	14.2
3Ph	13.3	27.1	8.0	15.3	12.1	2.4	3.8	0.1	2.3	0.1	0.1	5.8	2.4	0.7	6.6
4Et	14.6	31.9	6.7	32.5	9.5	0.1	0.8	0.3	1.0	0.3	0.0	0.7	1.5	0.4	0.1
4*i*Pr	14.9	27.1	3.3	42.4	6.2	0.8	0.3	0.0	0.0	0.0	0.0	3.1	1.8	0.2	0.1

4. References

[1] W. L. F. Armarego, C. L. L. Chai, *Purification of Organic Chemicals*, **2009**.

[2] J. Pfeiffer, C. Trost, A. Pachkovska, F. Tambornino, *Inorg. Chem.* **2021**, *60*, 10722–10728.

[3] P. R. Spackman, M. J. Turner, J. J. McKinnon, S. K. Wolff, D. J. Grimwood, D. Jayatilaka, M. A. Spackman, *J. Appl. Crystallogr.* **2021**, *54*, 1006–1011.

[4] G. M. Sheldrick, *Acta Crystallogr. Sect. A Found. Adv.* **2015**, *71*, 3–8.

[5] G. M. Sheldrick, *Acta Crystallogr. Sect. A Found. Crystallogr.* **2008**, *64*, 112–122.

[6] O. V. Dolomanov, L. J. Bourhis, R. J. Gildea, J. A. K. Howard, H. Puschmann, *J. Appl. Crystallogr.* **2009**, *42*, 339–341.

[7] K. Brandenburg, H. Putz, *DIAMOND, Program for X-Ray Structure Analysis*, Crystal Impact GbR, Bonn, Gemany, **2005**.

8.1.7 Thiocarbonyl pseudohalides – the curious case of thiocarbonyl dithiocyanate

Thiocarbonyl pseudohalides – the curious case of thiocarbonyl dithiocyanate

Jonathan Pfeiffer, Hennes Günther, Patrick Fuzon, Florian Weigend, and Frank Tambornino*

Contents

1. Experimental section

1.1. General remarks

General synthetic methods. All reactions and manipulations were performed under an inert atmosphere of argon using standard Schlenk-line or glovebox techniques (MBraun UNIlab glovebox, maintained at < 0.1 ppm H_2O and < 0.1 ppm O_2).

Thiophosgene (Sigma-Aldrich), silver nitrate (Acros Organics, 99.85%) and nickel chloride (Sigma-Aldrich, 98%) were used as received. Ammonium thiocyanate (Merck, 99 %) was recrystallized from methanol and dried until no further ^{1}H-NMR signals of the solvent was detected. Silver thiocyanate was synthesized from silver nitrate and ammonium thiocyanate. Solvents were dried according to literature.[1] CD_3CN (Eurisotop, 99.8 %) and THF-d$_8$ (Eurisotop, 99.5 %) were recondensed, degassed and stored over molecular sieve (4 Å) prior to use.

Additional characterization techniques:

^{1}H, ^{13}C, and ^{15}N NMR spectra were acquired on a Bruker Avance II (300 MHz) spectrometer at 298 K if not stated otherwise.

Elemental analyses and mass spectrometry were performed by the in-house service personnel. CHN(S) analyses were performed on a *CHNS(S)-Analysator vario MICRO CUBE* (Elementar). Samples were prepared and sealed under inert conditions in a tin crucible. Electro spray ionization (ESI) was performed on a *LTQ-FT Ultra* (Thermo Fischer Scientific) and liquid injection field desorption ionization (LIFDI) was performed on an AccuTOF GCv (Jeol).

Raman spectra were recorded on a Monovista CRS+ confocal Raman microscope (Spectroscopy & Imaging GmbH) using a 633 nm solid-state laser and a 300 grooves/mm grating. Samples were sealed in borosilicate ampoules and measured at −25 °C and −75 °C. IR spectra were recorded on a Bruker Alpha FT-IR spectrometer equipped with a diamond ATR unit mounted in a nitrogen-filled glovebox (MBraun UNIlab glovebox, maintained at < 0.1 ppm H_2O and < 0.1 ppm O_2).

1.1. Synthesis of thiocarbonyl dithiocyanate

Thiocarbonyl dithiocyanate was synthesized after a modified literature procedure.[2] All steps were carried out below −20 °C. Ammonium thiocyanate, NH_4SCN (1.55 g, 20.4 mmol, 2 eq.), was dissolved in approx. 30 mL liquid sulfur dioxide, SO_2, at −20 °C. Thiophosgene, $CS(Cl)_2$ (1.17 g, 0.782 mL, 10.2 mmol, 1 eq.), was added entirely and led to precipitation of ammonium chloride, NH_4Cl, (detected by powder X-ray diffraction). The mixture was stirred for 3.5 hours at −20 °C. SO_2 was removed *in vacuo* at −20 °C or beneath. The crude product was dissolved in 20 mL chloroform, the side product filtered off and washed with 6 mL chloroform. The solvent was removed from the filtrate and thiocarbonyl dithiocyanate, $CS(SCN)_2$ (1.42 g, 8.86 mmol, 87 %), was obtained as an orange powder. $CS(SCN)_2$ is storable for months at −75 °C. Single crystals suitable for X-ray diffraction were grown by cooling a saturated solution in dichloromethane from −20 °C to −75 °C for four weeks.

13C NMR (75 MHz, $CDCl_3$, r.t.) δ / ppm = 188.6 (*C*=S), 105.5 (S–*C*≡N).

CHNS (calc./found.) C: 22.49 / 23.34, N: 17.48 / 16.81, S: 60.03 / 57.25.
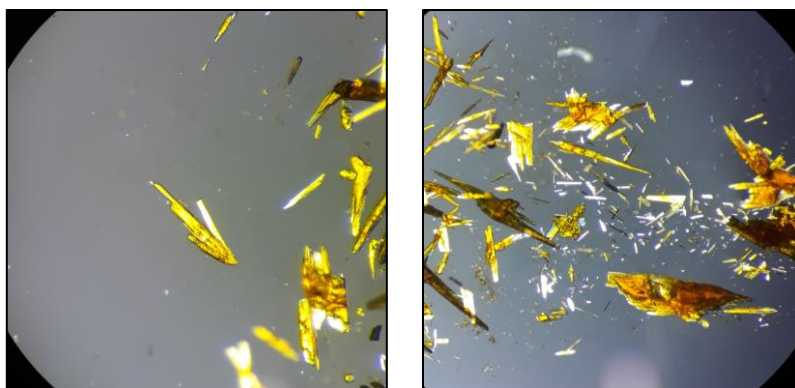
Figure S 1: Two representative images of crystalline thiocarbonyl dithiocyanate under paratone oil photographed through a stereomicroscope.

Figure S 2: Bulk sample of thiocarbonyl dithiocyanate in a Schlenk-flask
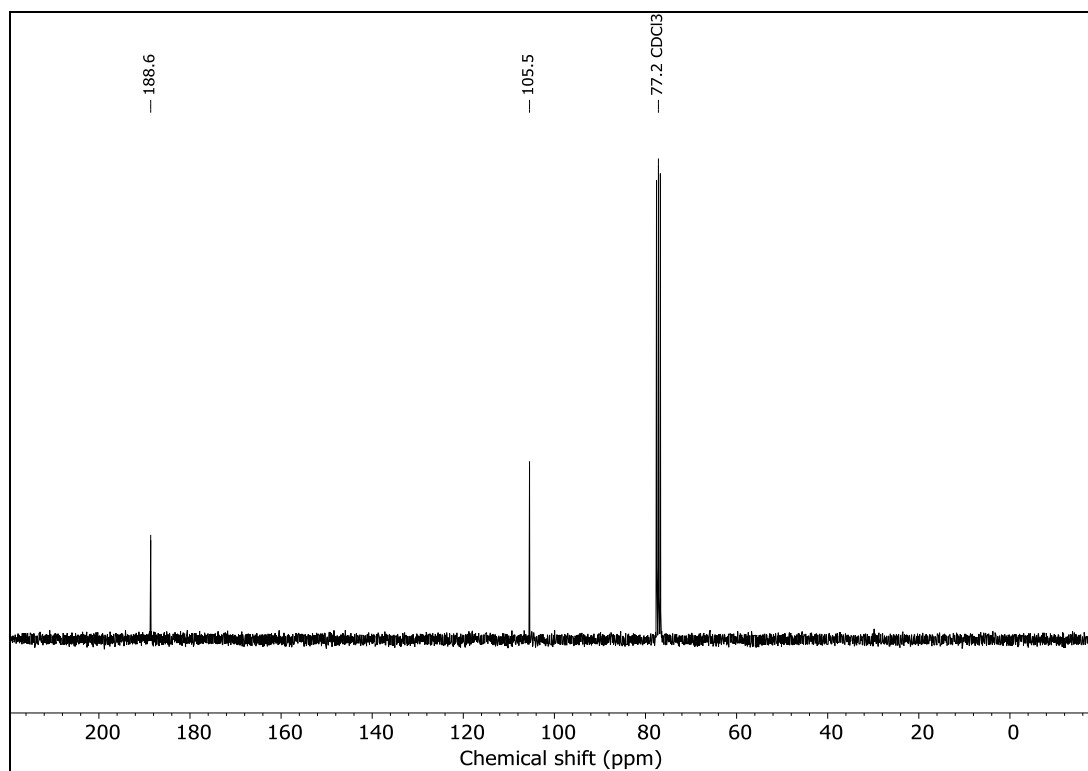
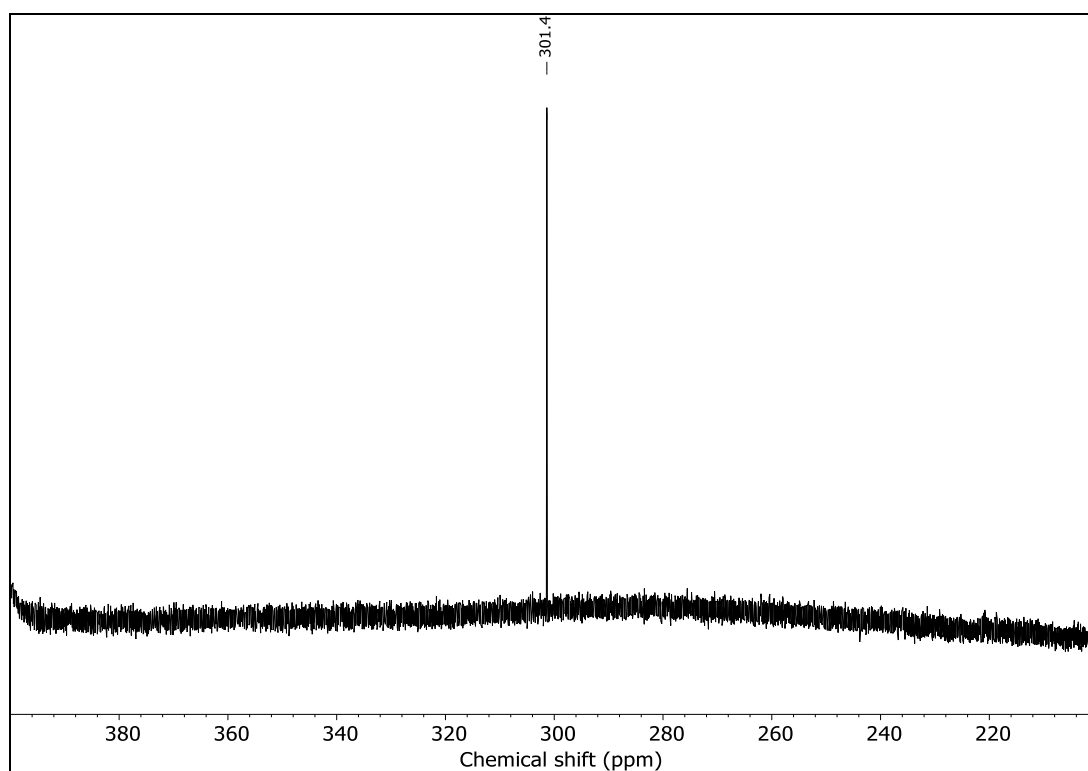Figure S 3: ^{13}C NMR spectrum of thiocarbonyl dithiocyanate in CDCl$_3$ at room temperature.
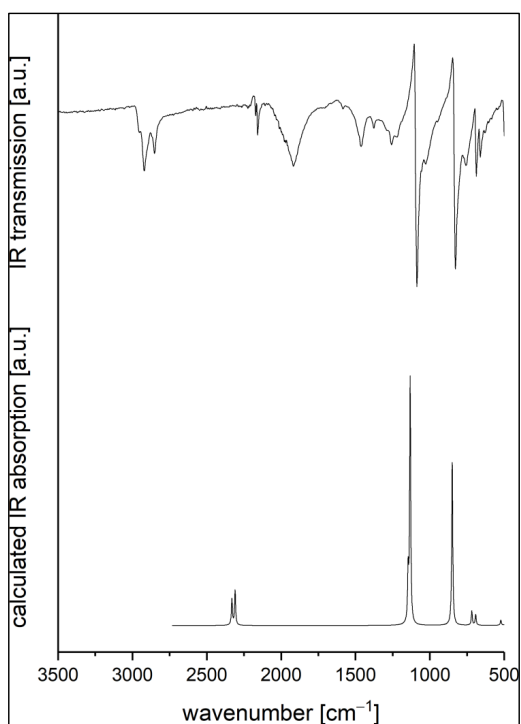
Figure S 4: Measured IR spectrum at room temperature (top) and calculated (bottom) IR intensities for thiocarbonyl dithiocyanate.
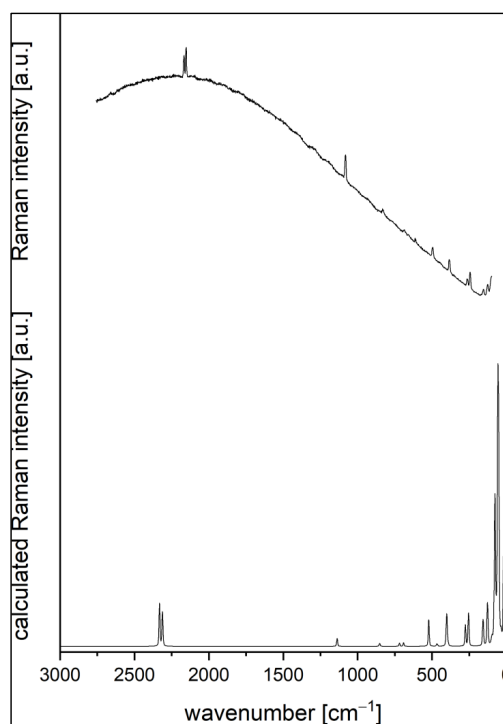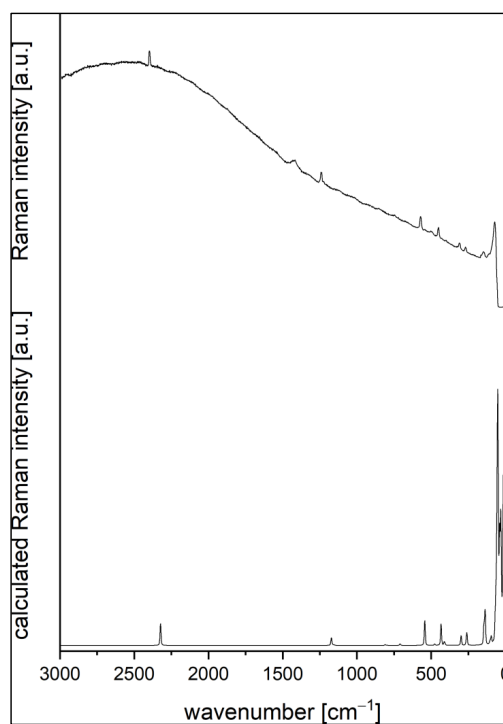

Figure S 5: Measured Raman spectrum at −25 °C (top) and calculated (bottom) Raman intensities for thiocarbonyl dithiocyanate.

1.2. Synthesis of chlorothiocarbonyl thiocyanate

Silver thiocyanate, AgSCN (830 mg, 5.00 mmol, 1 eq.), was ground in an agate mortar together with glass powder to increase the surface ratio (approx. same volume as AgSCN). Thiophosgene, $CS(Cl)_2$ (575 mg, 0.383 mL, 5.00 mmol, 1 eq.), was condensed in vacuum onto the mixture at -196 °C. The orange-red mixture was allowed to come to -20 °C and then stored under vacuum (1×10^{-3} mbar) at -20 °C for 24 hours. All volatiles were condensed into a new flask at -196 °C and allowed to warm to -20 °C. The obtained red liquid consisted of $CS(Cl)_2$ and CS(SCN)Cl (detected by ^{13}C NMR spectroscopy). Thiophosgene was removed by condensing it from -20 °C to -78 °C, leaving behind chlorothiocarbonyl thiocyanate, CS(SCN)Cl (160 mg, 1.16 mmol, 23 %), as red liquid. Single crystals were grown on the diffractometer in a glass capillary (Ø = 0.1 mm) by slow cooling. Due to the high sulfur content by weight%, the calibration value for S for the elemental analysis was overshot.

^{13}C NMR (75 MHz, CDCl$_3$, r.t.) δ / ppm = 178.7 (*C*=S), 107.1 (S–*C*≡N).

^{15}N NMR (50 MHz, neat, 253 K) δ / ppm = 301.4 (S–C≡*N*).

CHNS (calc./found.) C: 22.49 / 23.34, N: 17.48 / 16.81, S: 60.03 / 57.25.

Figure S 6: Sample of chlorothiocarbonyl thiocyanate in a Schlenk-flask
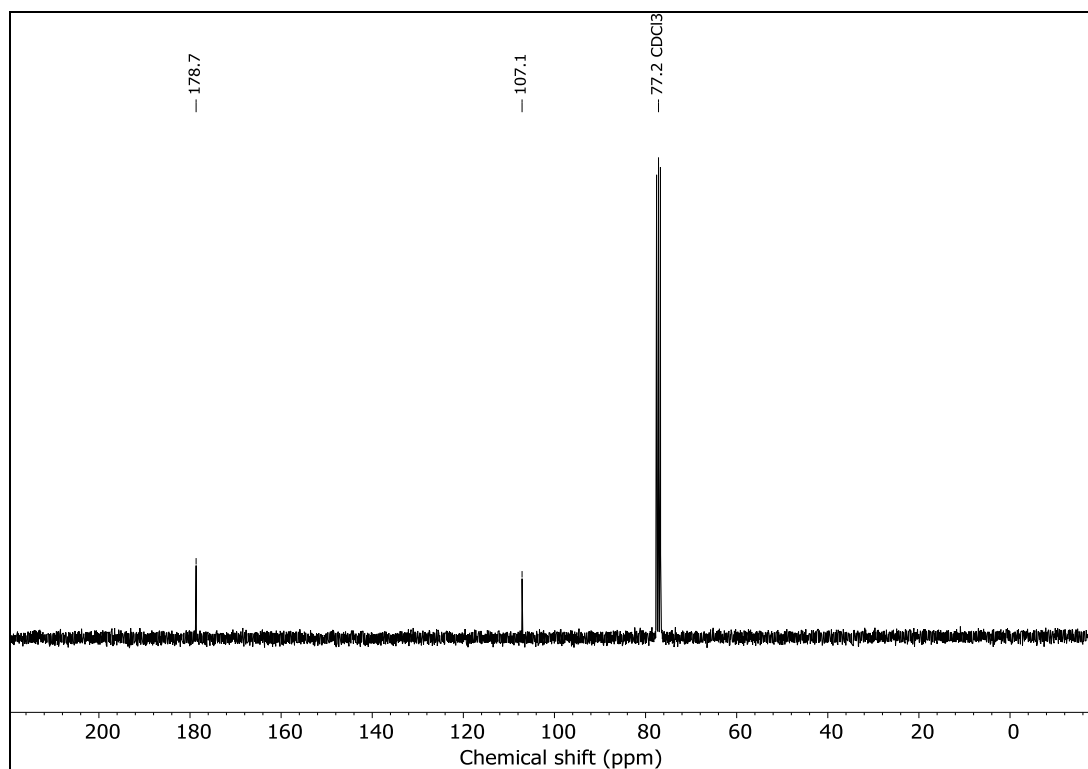
Figure S 7: ^{13}C NMR spectrum of chlorothiocarbonyl thiocyanate in CDCl$_3$ at room temperature.

Figure S 8: ^{15}N NMR spectrum of neat chlorothiocarbonyl thiocyanate at 253 K.
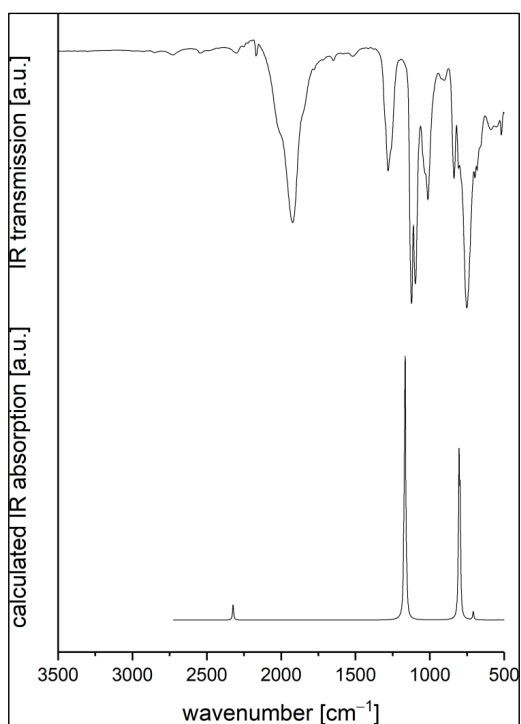
Figure S 9: Measured IR spectrum at room temperature as liquid (top) and calculated (bottom) IR intensities from the solid-state structure data for chlorothiocarbonyl thiocyanate.

Figure S 10: Measured Raman spectrum at −75 °C (top) and calculated (bottom) Raman intensities for chlorothiocarbonyl thiocyanate.

1.3. Synthesis of thioimidodicarbonic-*O,O*-diethyl ester

Thiocarbonyl dithiocyanate, $CS(SCN)_2$ (330 mg, 2.06 mmol, 1 eq.), was suspended in 5 mL dichloro methane at −50 °C. Ethanol (5.0 mL, 84.44 mmol, 41 eq.) was added dropwise, the reaction mixture was allowed to warm to room temperature and stirred for 48 hours. Dichloro methane was removed in vacuo and thioimidodicarbonic-*O,O*-diethyl ester, $NH((C=S)OC_2H_5)_2$ (218 mg, 1.13 mmol, 55 %) obtained as orange powder. Single crystals were grown by slow evaporation of the solvent of a saturated solution in *n*-hexane.

^{1}H NMR (300 MHz, CDCl$_3$, r.t.) δ / ppm = 9.22 (s, 1H, N*H*), 4.56 (q, 4H, $^3J_{HH}$ = 7.11 Hz, OC*H*$_2$CH$_3$), 1.41 (t, 6H, $^3J_{HH}$ = 7.12 Hz, OCH$_2$C*H*$_3$).

^{13}C NMR (75 MHz, CDCl$_3$, r.t.) δ / ppm = 186.1 (*C*=S), 69.6 (O*C*H$_2$CH$_3$), 13.8 (OCH$_2$*C*H$_3$).

CHNS (calc./found.) C: 37.29 / 39.03, H: 5.74 / 6.00, N: 7.25 / 7.92, S: 33.17 / 33.70.

Mass (ESI+, MeOH) for [M+H$^+$] = $C_6H_{11}N_1O_2S_2H^+$ m/z found (calc.): 193.0304 (193.0231).
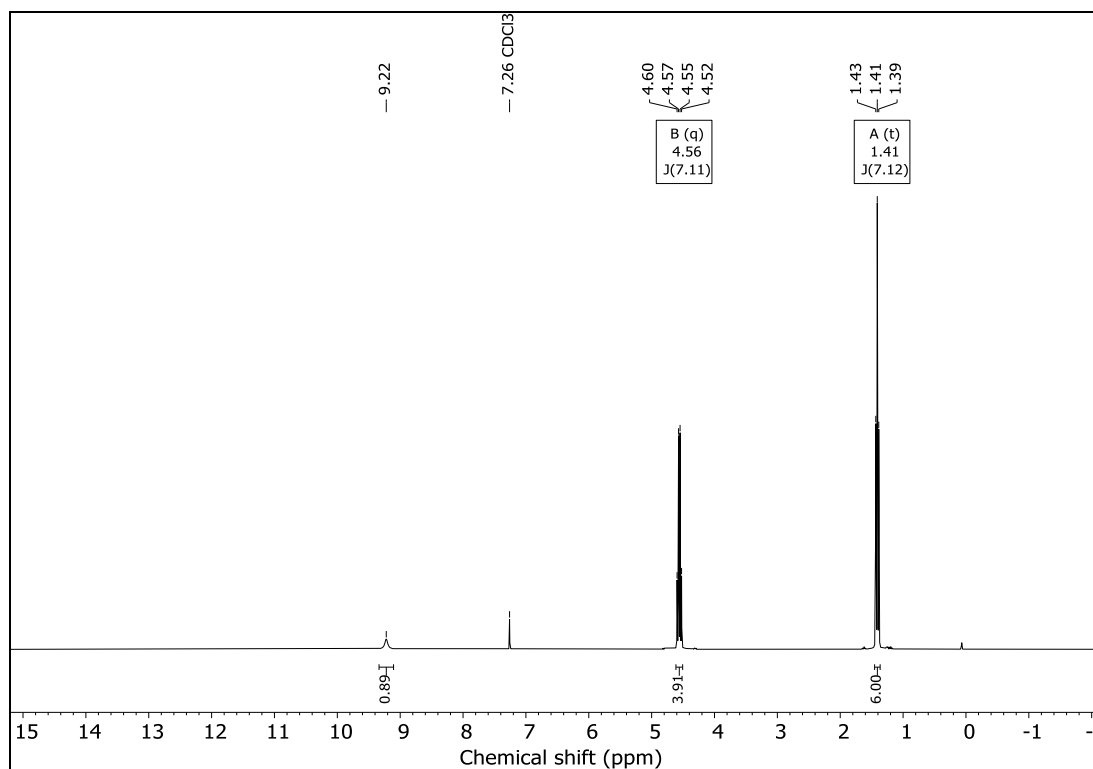
Figure S 11: ^{1}H NMR spectrum of thioimidodicarbonic-*O,O*-diethyl ester in CDCl$_3$ at room temperature.
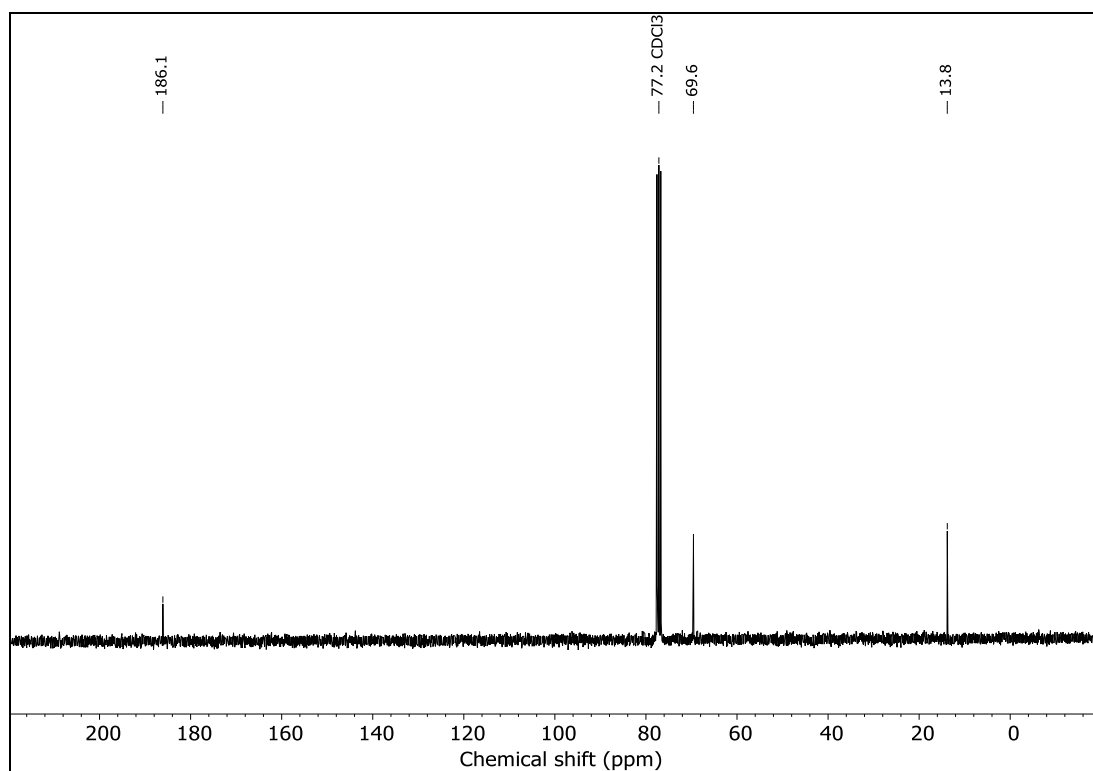
Figure S 12: ^{13}C NMR spectrum of thioimidodicarbonic-*O,O*-diethyl ester in CDCl$_3$ at room temperature.
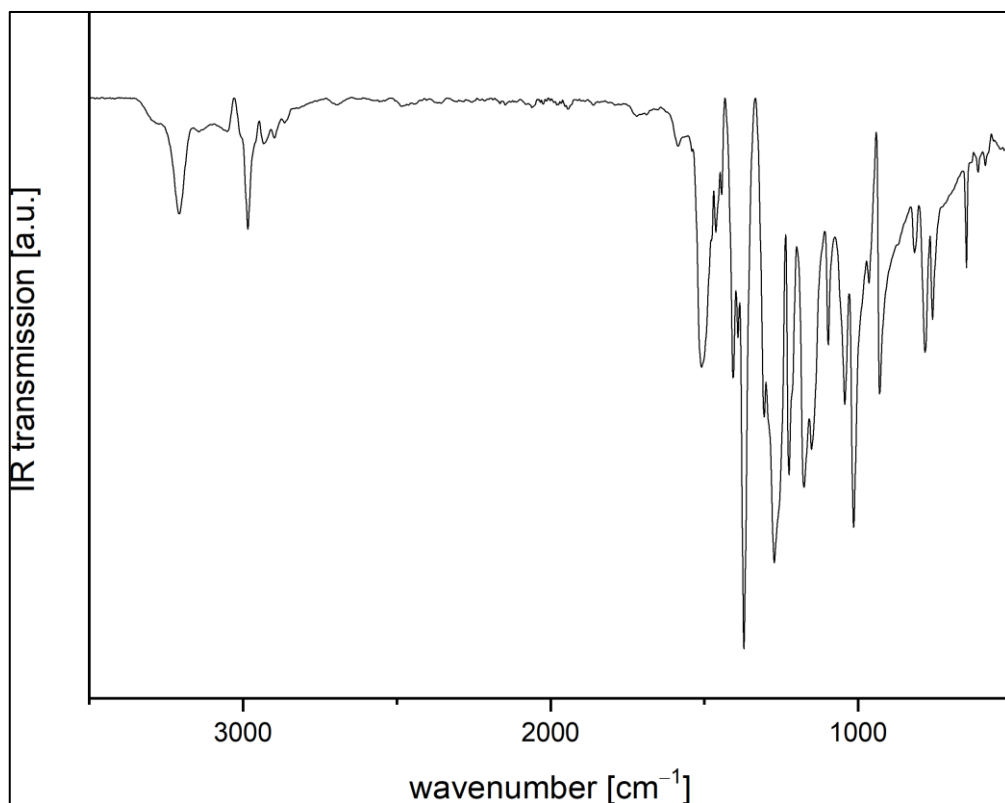
Figure S 13: Measured IR spectrum at room temperature of thioimidodicarbonic-*O,O*-diethyl ester.

1.4. Synthesis of bis(*O,O*-diethyl-1,3-dithioimidodicarbonato)nickel

Thioimidodicarbonic-*O,O*-diethyl ester (299 mg, 1.54 mmol, 2.2 eq.) and nickel chloride, NiCl$_2$ (91 mg, 0.70 mmol, 1.0 eq.), were suspended in 15 mL ethanol. Pyridine (170 µL, 2.11 mmol, 3.0 eq.) was added upon which a precipitate formed, and the mixture was stirred for 48 hours. The suspension was cooled to 0 °C and the precipitate filtered off. The solid was dried *in vacuo* and bis(*O,O*-diethyl-1,3-dithioimidodicarbonato)nickel (238 mg, 0.54 mmol, 76 %) obtained as brown powder. Single crystals were grown by slow evaporating the solvent of a saturated solution in acetonitrile.

¹H NMR (300 MHz, CD₃CN, r.t.) δ / ppm = 4.43 (q, 4H, $^3J_{HH}$ = 7.09 Hz, OCH_2CH₃), 1.32 (t, 6H, $^3J_{HH}$ = 7.08 Hz, OCH₂CH_3).

¹³C NMR (75 MHz, CD₃CN, r.t.) δ / ppm = 192.5 (*C*=S), 69.3 (O*C*H₂CH₃), 14.4 (OCH₂*C*H₃).

CHNS (calc./found.) C: 32.52 / 31.50, H: 4.55 / 4.310, N: 6.32 / 6.76, S: 28.93 / 29.76.

Mass (LIFDI+, THF) for [M⁺] = C₁₂H₂₀N₂O₄S₄Ni⁺ m/z found (calc.): 441.9676 (441.9659).
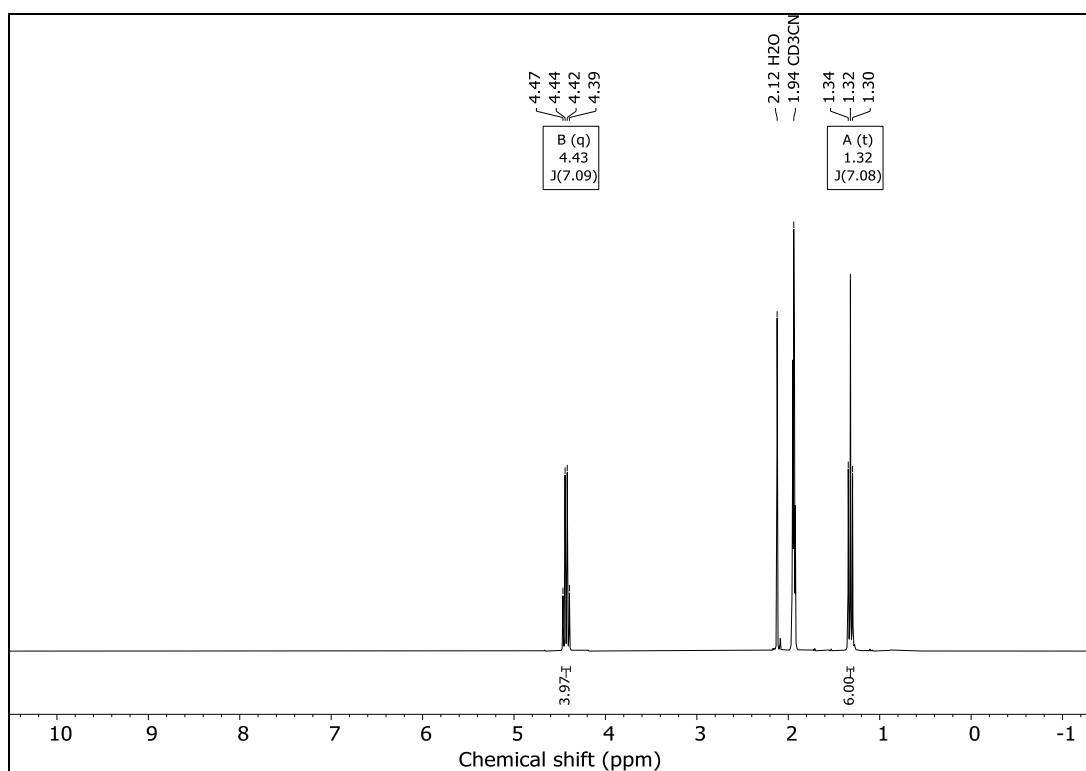
Figure S 14: ¹H NMR spectrum of bis(*O,O*-diethyl-1,3-dithioimidodicarbonato)nickel in CD₃CN at room temperature.
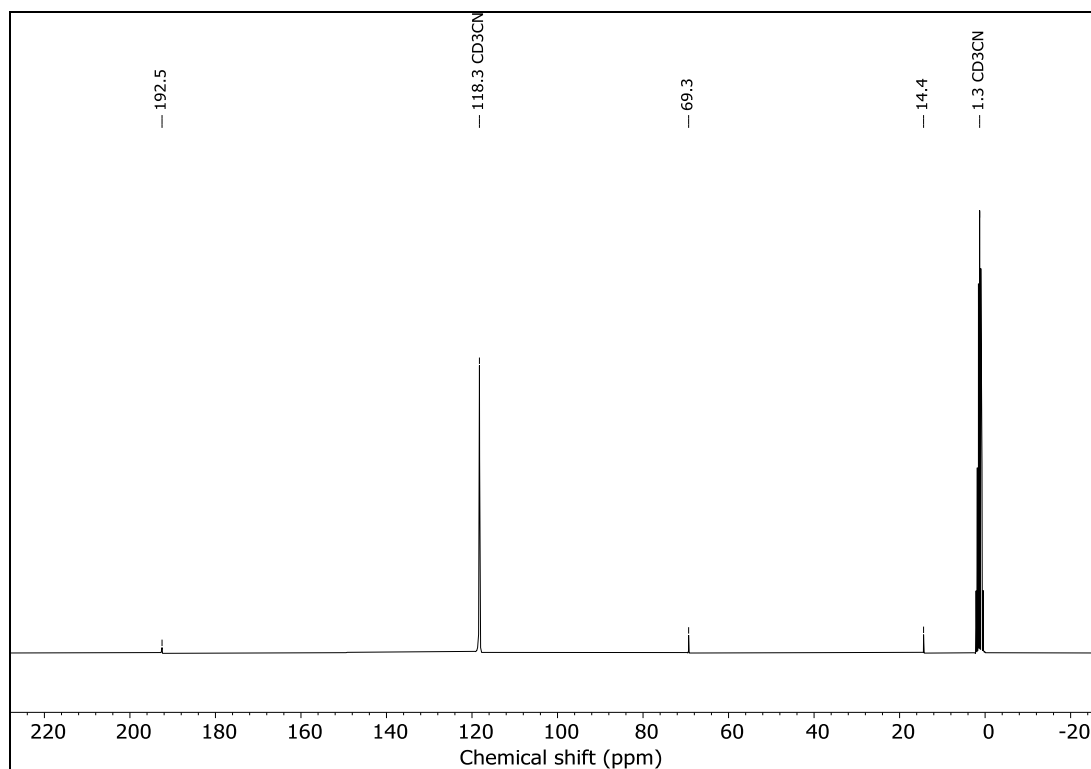
Figure S 15: ^{13}C NMR spectrum of bis(O,O-diethyl-1,3-dithioimidodicarbonato)nickel in CD$_3$CN at room temperature.
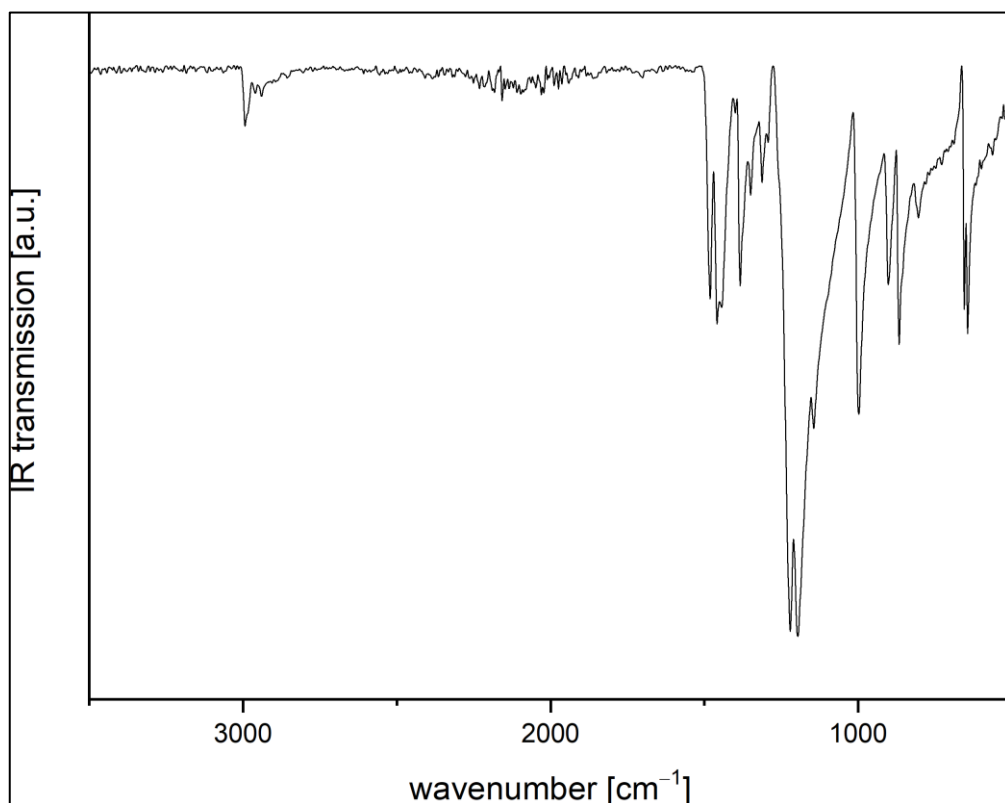
Figure S 16: Measured IR spectrum at room temperature of bis(O,O-diethyl-1,3-dithioimidodicarbonato)nickel.

1.5. Synthesis approaches towards thiocarbonyl diisothiocyanate

a) Sodium thiocyanate (856 mg, 10.5 mmol, 2.1 eq.) was suspended in 15 mL ethyl acetate and cooled to −78 °C. Thiophosgene (0.38 mL, 5.0 mmol, 1.0 eq.) was added dropwise. The suspension was stirred for two hours at −50 °C and warmed for one hour to −40 °C. The suspension was filtrated under cooling of the orange-red filtrate at −40 °C. The solvent was narrowed down *in vacuo* at −40 °C. In the residue only the starting material thiophosgene was detected by ^{13}C-NMR spectroscopy. The filtered off solid was detected as sodium chloride by powder X-ray diffraction. Reaction at room temperature led to the same results.

b) Sodium thiocyanate (317 mg, 4.0 mmol, 2.0 eq.) was suspended in 5 mL chloroform and three drops pyridine were added. Thiophosgene (0.15 mL, 2.0 mmol, 1.0 eq.) was added slowly. The reaction mixture was stirred for one and a half hours during which a color change from red to brown occurred. The suspension was filtered. The solid was detected as sodium thiocyanate by powder X-ray diffraction. No signals were found in the ^{13}C-NMR spectroscopy of the filtrate.

c) Silver thiocyanate (810 mg, 4.88 mmol, 2.5 eq.) was mixed with glass powder. Thiophosgene (0.15 mL, 1.96 mmol, 1.0 eq.) was condensed in vacuum onto the mixture at −196 °C. The mixture was stored under vacuum at −20 °C for 24 hours. All volatiles were condensed into a new flask at −196 °C and allowed to warm to −20 °C. By ^{13}C-NMR spectroscopy thiophosgene, chlorothiocarbonyl thiocyanate and carbon disulfide were detected. The solid residue was identified as a mixture of silver thiocyanate and silver chloride through powder X-ray diffraction. Storing the reaction mixture under argon atmosphere at −20 °C for 24 hours led to the same result.

d) Silver thiocyanate (332 mg, 2.0 mmol, 2.0 eq.) was suspended in 5 mL 1,2-diflurobenzene and thiophosgene (0.08 mL, 1.0 mmol, 1.0 eq.) added. It was heated to 60 °C for one hour. The suspension was filtered. The precipitate was identified as a mixture of silver thiocyanate and silver chloride through powder X-ray diffraction. In the filtrate thiophosgene and chlorothiocarbonyl thiocyanate were detected by ^{13}C-NMR spectroscopy.

e) [Cu(IPr)(NCS)] was solved in 5 mL dichloromethane and cooled to −40 °C. Thiophosgene was added and the solution allowed to warm to −20 °C over one hour, in which time the solution turned from yellow to orange. The solution was concentrated at −20 °C to −40 °C *in vacuo* while turning dark brown. The residue was identified as thiophosgene and [Cu(IPr)(Cl)] or [Cu(IPr)(NCS)] via ^{13}C-NMR spectroscopy.

f) Thiourea (154 mg, 2.0 mmol, 1.0 eq.) was suspended in THF, cooled to 0 °C and thiophosgene (0.31 mL, 4.0 mmol, 2.0 eq.) added. Ethyl di(isopropyl)amine (1.4 mL, 8.0 mmol, 4.0 eq.) was added dropwise. The reaction turned from yellow to orange red and was stirred for one and a half hours. The suspension was filtered. The colorless precipitate was detected as ethyl di(isopropyl)ammonium chloride through ^{13}C-NMR spectroscopy. From the red filtrate the solvent was removed *in vacuo* at 0 °C. The dark red, viscous residue only contained ethyl di(isopropyl)ammonium chloride in the ^{13}C-NMR spectrum.

g) Lawesson's reagent was suspended in different solvents and carbonyl diisothiocyanate was added. The reaction mixture was stirred for different reaction times at variable temperatures. The precipitates were filtered off. The filtrate was narrowed down carefully *in vacuo.* Filtered off solid and filtrate residue were analyzed with ^{13}C-NMR spectroscopy. Only in two reactions two very weak signals which could potentially be assigned to thiocarbonyl diisothiocyanate were detected. It was impossible to isolate any product.

Table S 1: Overview of the reaction conditions for carbonyl diisothiocyanate with Lawesson's reagent.

solvent	temperature	time	detected ^{13}C-NMR signals
THF	r.t.	17 h	190.0 ppm / 146.8 ppm
n-hexane	r.t.	4 h	no signals
n-hexane	reflux	1 h	starting material
toluene	60 °C	2 h	189.3 ppm / 144.9 ppm
toluene	reflux	2 h	no signals
toluene	50 °C	70 h	no signals

h) Thiocarbonyl dithiocyanate was solved in dichloromethane. The flask was darkened and irradiated with UV light at a wavelength of 390 nm (PR160L-390nm, Kessil). Different irradiation cycles were performed successively and after each one a ^{13}C-NMR spectrum recorded. Isomerization to thiocarbonyl diisothiocyanate was not observed.

Table S 2: Overview of the reaction conditions for isomerization attempts.

cycle	temperature	time	intensity
1.	−30 °C	5 min	50 %
2.	−40 °C	20 min	50%
3.	−40 °C	15 min	100 %
4.	−20 °C to 0 °C	1 h	100 %

2. Crystallographic data

Single crystal X-ray structure determination: Single-crystal X-ray diffraction data were collected using a StadiVari (Stoe, Darmstadt) diffraction system equipped with mirror monochromated Cu K_α radiation (λ = 1.54186 Å, Xenocs Microfocus Source) and a Pilatus 300K detector. Crystals were selected under Paratone-N oil, mounted on micromount loops and quench-cooled using an Oxford Cryosystems open flow N_2 cooling device. Data were collected at 100 K and processed using the X-Area program package, including unit cell parameter refinement and inter-frame scaling (which was carried out using LANA within X-Area). Structures were subsequently solved using direct methods (SHELXT)[3] and refined on F^2 with SHELXL[4] using the Olex2[5] user interface. The crystal structure drawings were generated with DIAMOND.[6]

Powder X-ray diffractometry: Powder diffraction patterns were recorded on a STADI MP (STOE, Darmstadt) powder diffraction system equipped with mirror monochromated CuKα1 radiation (λ= 1. 54175 Å) and a Silicon strip MYTHEN 1K detector. Data was collected at room temperature in transmission mode (Debye-Scherrer Geometry). The powder samples were ground in agate mortars. The samples were flame-sealed in glass capillaries (inner diameter of 0.1–0.5 mm, Hilgenberg, Malsberg, Germany). For phase identification the detected diffraction pattern was compared to patterns calculated from single crystal data.

Rietveld refinements[7] were performed with the TOPAS 6.0 program package.[8] The structural models derived from single crystal x-ray data were used as starting points for the refinements. Background functions were modelled using shifted Chebyshev polynomials, profile functions were described with the modified Thompson-Cox-Hastings pseudo-Voigt "TCHZ" function as implemented in TOPAS. For details regarding Rietveld refinements see Table S 4.

Table S 3: Selected single crystal X-ray data collection and refinement parameters for thiocarbonyl dithiocyanate, chlorothiocarbonyl thiocyanate, thioimidodicarbonic-*O,O*-diethyl ester and bis(*O,O*-diethyl-1,3-dithioimidodicarbonato)nickel.

	CS(SCN)$_2$	CS(SCN)Cl	HN((C=S)OC$_2$H$_5$)$_2$	[Ni (((S=C)OC$_2$H$_5$)$_2$N)$_2$]
Formula	C3 N2 S3	C2 Cl N S2	C6 H11 N O2 S2	C12 H20 N2 Ni O4 S4
CCDC				
F. w. / g mol^{-1}	160.23	137.60	193.28	443.25
Crystal system	monoclinic	monoclinic	monoclinic	monoclinic
Space group	*P*2$_1$/*n*	*P*2$_1$/*c*	*P*2$_1$/*c*	*P*2$_1$/*c*
a / Å	5.9384(2)	6.3005(2)	7.1491(3)	18.8725(4)
b / Å	5.7917(2)	22.0171(5)	17.1140(6)	7.0820(2)
c / Å	17.6562(6)	7.4131(2)	7.6929(4)	14.8003(3)
α / °	90	90	90	90
β / °	97.103(3)	104.256(2)	98.302(4)	112.9290(10)
γ / °	90	90	90	90
V / Å^3	602.60(4)	996.67(5)	931.36(7)	1821.84(8)
Z	4	8	4	4
Radiation, λ / Å	CuKα (λ = 1.54186)	CuKα (λ = 1.54186)	CuKα (λ = 1.54186)	CuKα (λ = 1.54186)
Temp / K	100	100	100	100
ρ$_{calc}$ / g cm^{-3}	1.766	1.834	1.378	1.616
μ / mm^{-1}	10.306	13.270	4.839	5.993
Reflections collected	5482	24024	13159	18999
Ind. Reflns. / Ind. Reflns gt	1059 / 941	1799 / 1555	1718 / 1438	3730 / 3207
Parameters	73	110	102	216
R$_{int}$ / R$_{(σ)}$ / %	1.39 / 1.35	4.55 / 1.62	5.96 / 2.82	3.50 / 2.88
*R*1/*wR*2,[a] *I* ≥ 2σ*I* / %	3.27 / 8.66	3.60 / 10.79	5.79 / 13.78	4.58 / 11.82
*R*1/*wR*2,[a] all data / %	3.66 / 8.80	4.05 / 10.97	6.75 / 15.09	5.05 / 12.03
GOF	1.068	1.161	1.087	0.986
Twin law	—	—	—	1 0 1 0 −1 0 0 0 −1
BASF	—	—	—	0.01461(4)
Flack parameter	—	—	—	—

[a] $R1 = [\Sigma||F_o| - |F_c||]/\Sigma|F_o|$; $wR2 = \{[\Sigma w[(F_o)^2 - (F_c)^2]^2]/[\Sigma w(F_o^2)^2]^{1/2}\}$; $w = [\sigma^2(F_o)^2 + (AP)^2 + BP]^{-1}$, where $P = [(F_o)^2 + 2(F_c)^2]/3$ and the A and B values are 0.051500 and 0.820900 for CS(SCN)$_2$, 0.070900 and 0.344300 for CS(SCN)Cl , 0.113300 and 0 for HN((C=S)OC$_2$H$_5$)$_2$, and 0.096900 and 0 for [Ni (((S=C)OC$_2$H$_5$)$_2$N)$_2$].

Table S 4 Selected powder X-ray data collection and refinement parameters for thiocarbonyl dithiocyanate.

	CS(SCN)$_2$
Formula	C3 S3 N2
CCDC	
Fw / g mol^{-1}	160.23
Crystal system	monoclinic
Space group	$P2_1/n$
a / Å	5.97974(8)
b / Å	5.85117(11)
c / Å	18.1365(3)
α / °	90
β / °	97.6449(9)
γ / °	90
V / Å^3	628.928(18)
Z	4
Radiation, λ / Å	1.54175
Temp / K	298
ρ_{calc} / g cm^{-3}	1.692
R_{wp} / %	8.71276
R_p / %	6.54511
R_{Bragg} / %	2.34813
GoF	1.03212
Starting angle measured / ° 2θ	5.000
Final angle measured / ° 2θ	70.000
Starting angle refined/° 2θ	8.000
Final angle refined/ ° 2θ	70.000
Step width/ ° 2θ	0.015
Refined Parameters	79
Background Parameters	12
Profile Parameters[a]	29

[a] Profile parameters include spherical harmonics function with order 8 to model preferred orientation.
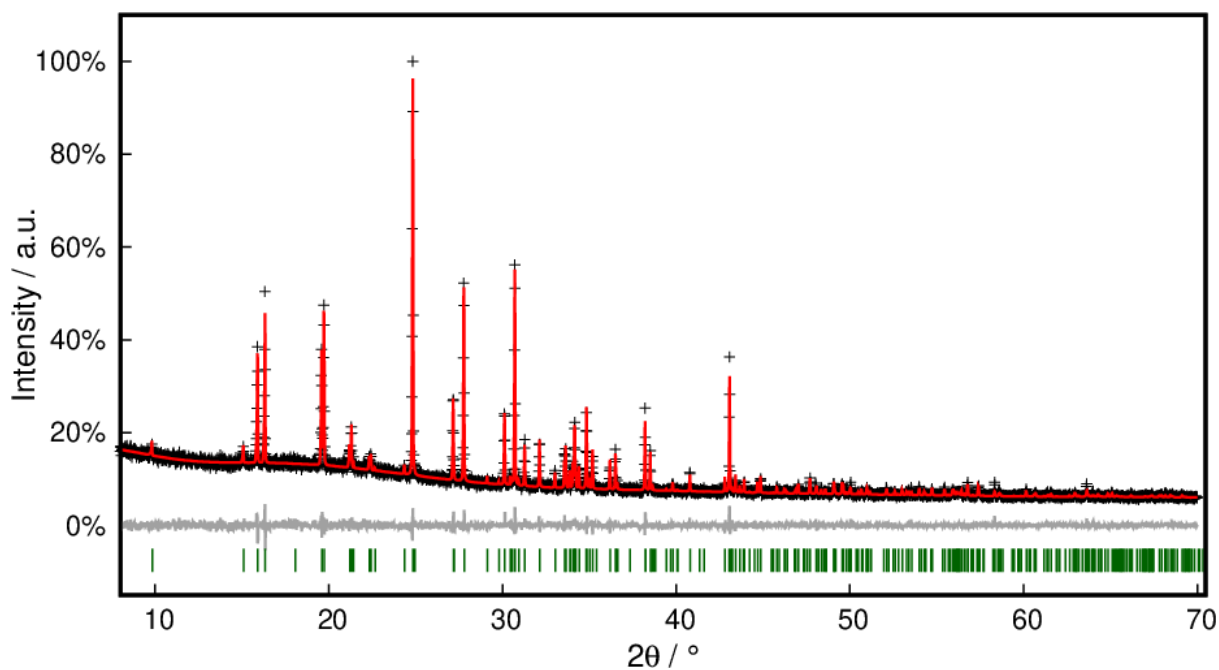
Figure S 17: Rietveld refinement of thiocarbonyl dithiocyanate. Black crosses display measured data, the red line represents the refined model, green bars indicate Bragg positions, and the grey line displays the difference plot. Further data is compiled in Table S 4.

2.1. Additional Pictures for thiocarbonyl dithiocyanate
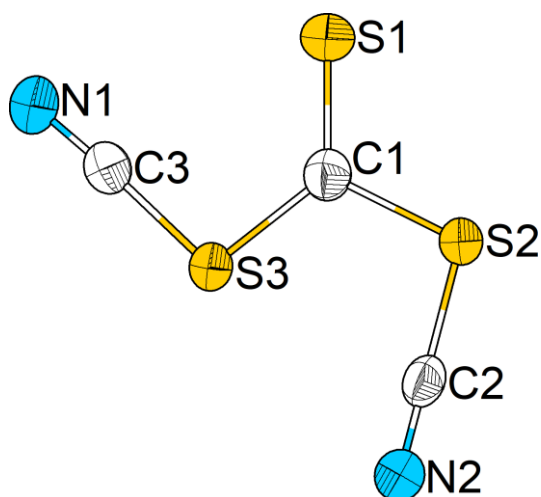
Figure S 18: Molecular structure of thiocarbonyl dithiocyanate in the single crystal drawn with 75% displacement ellipsoids at 100 K.
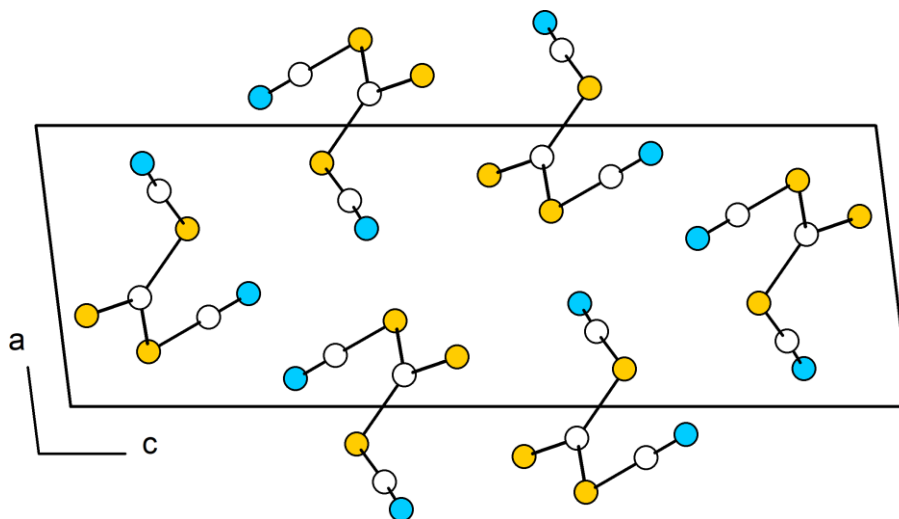
Figure S 19: Crystal structure of thiocarbonyl dithiocyanate viewed along [010]. Atoms are drawn with arbitrary radii. Colour code: S yellow, C white, N blue.
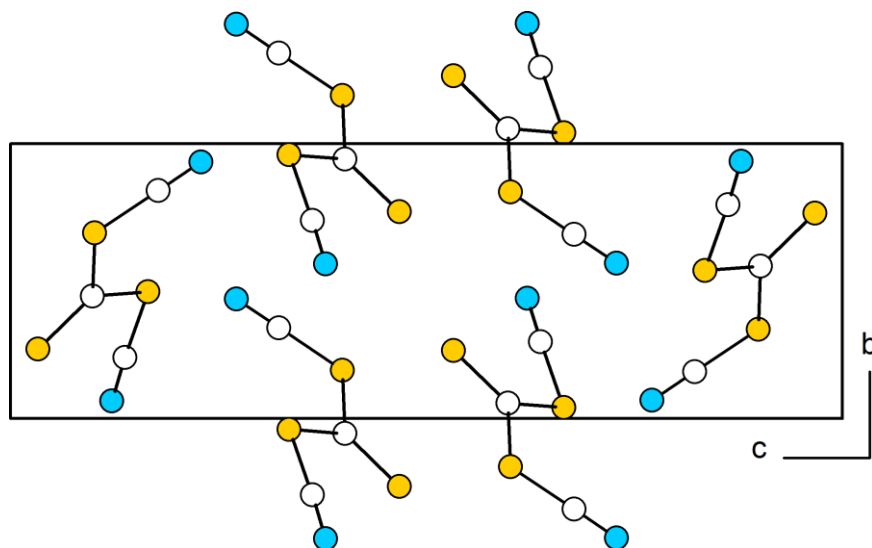
Figure S 20: Crystal structure of thiocarbonyl dithiocyanate viewed along [100]. Atoms are drawn with arbitrary radii. Colour code: S yellow, C white, N blue.

2.2. Additional Pictures for chlorothiocarbonyl thiocyanate
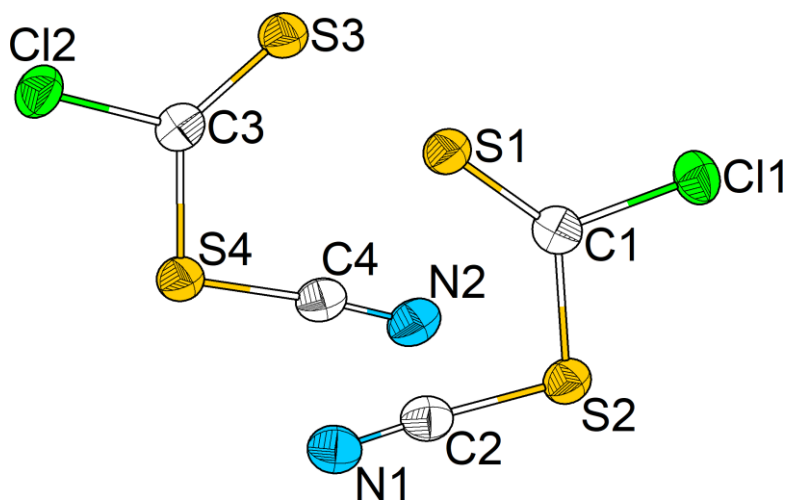
Figure S 21: Molecular structure of the two crystallographically independent chlorothiocarbonyl thiocyanate molecules in the single crystal drawn with 50% displacement ellipsoids at 100 K.
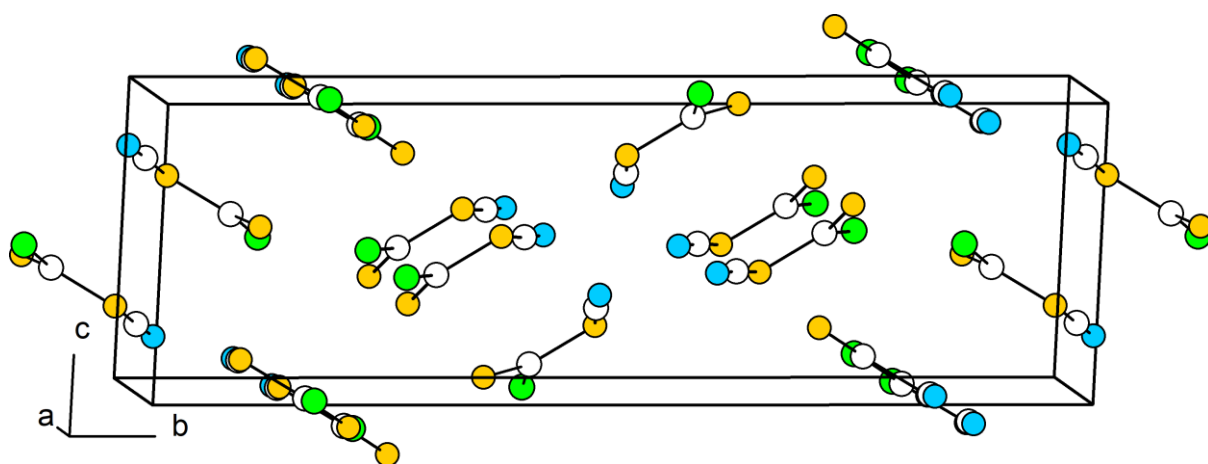
Figure S 22: Crystal structure of chlorothiocarbonyl thiocyanate viewed approximately along [100]. Atoms drawn with arbitrary radii. Colour code: S yellow, N blue, C white, Cl green.
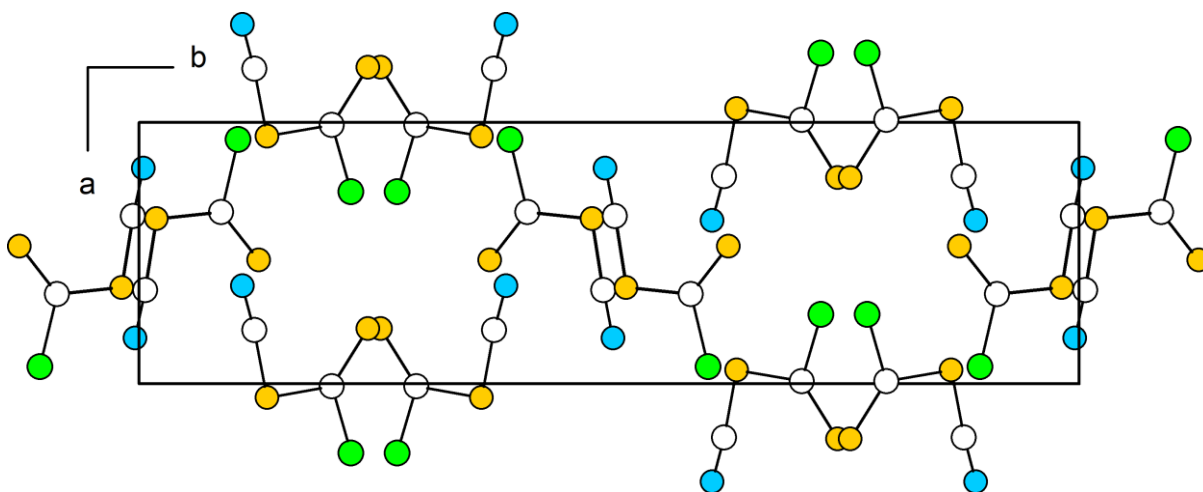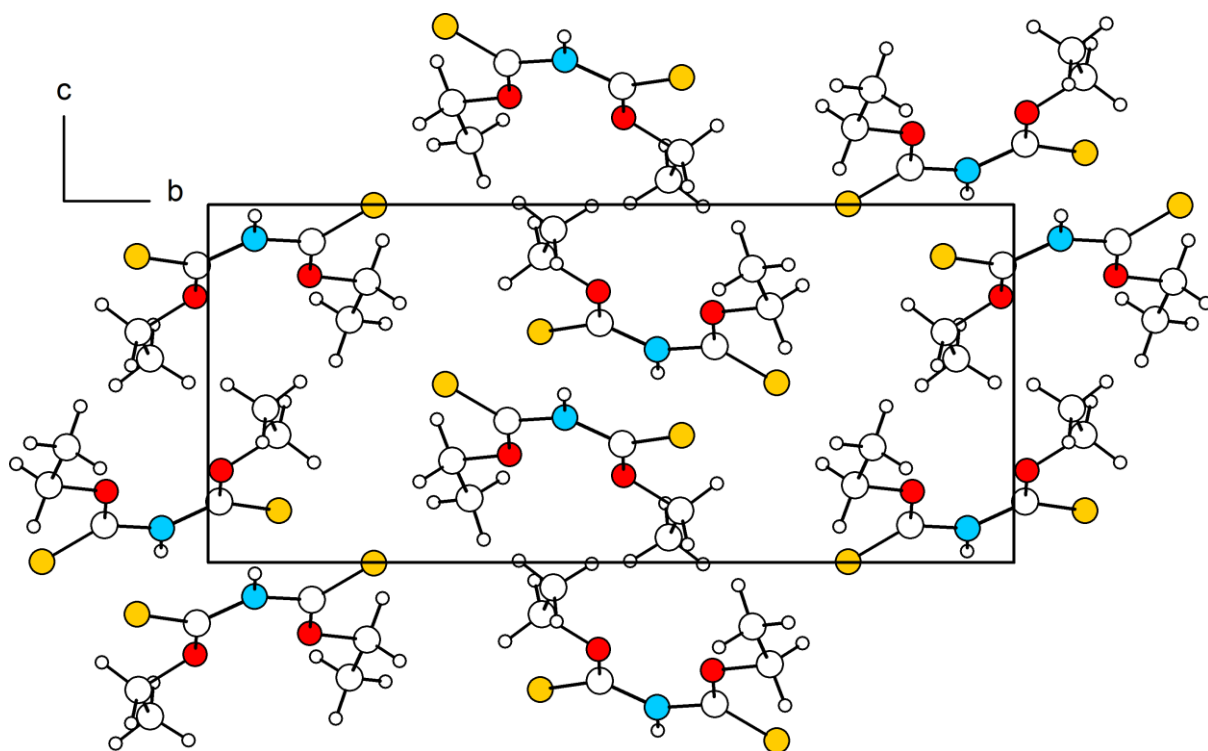
Figure S 23: Crystal structure of chlorothiocarbonyl thiocyanate viewed along [001]. Atoms drawn with arbitrary radii. Colour code: S yellow, N blue, C white, Cl green.

2.3. Additional Pictures for thioimidodicarbonic-*O,O*-diethyl ester
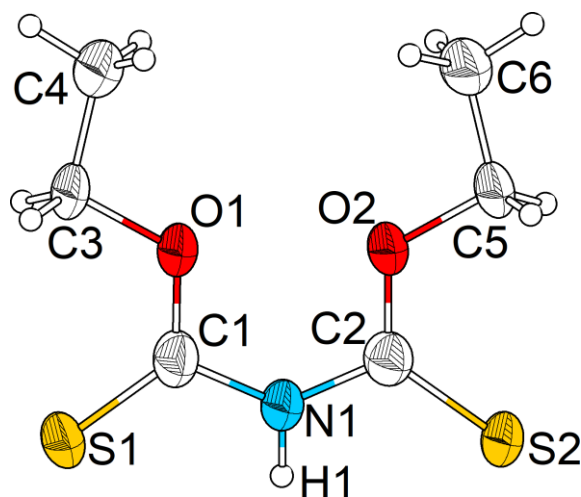
Figure S 24: Molecular structure of the thioimidodicarbonic-*O,O*-diethyl ester molecule in the single crystal drawn with 75% displacement ellipsoids at 100 K. Hydrogen atoms drawn with arbitrary radii.
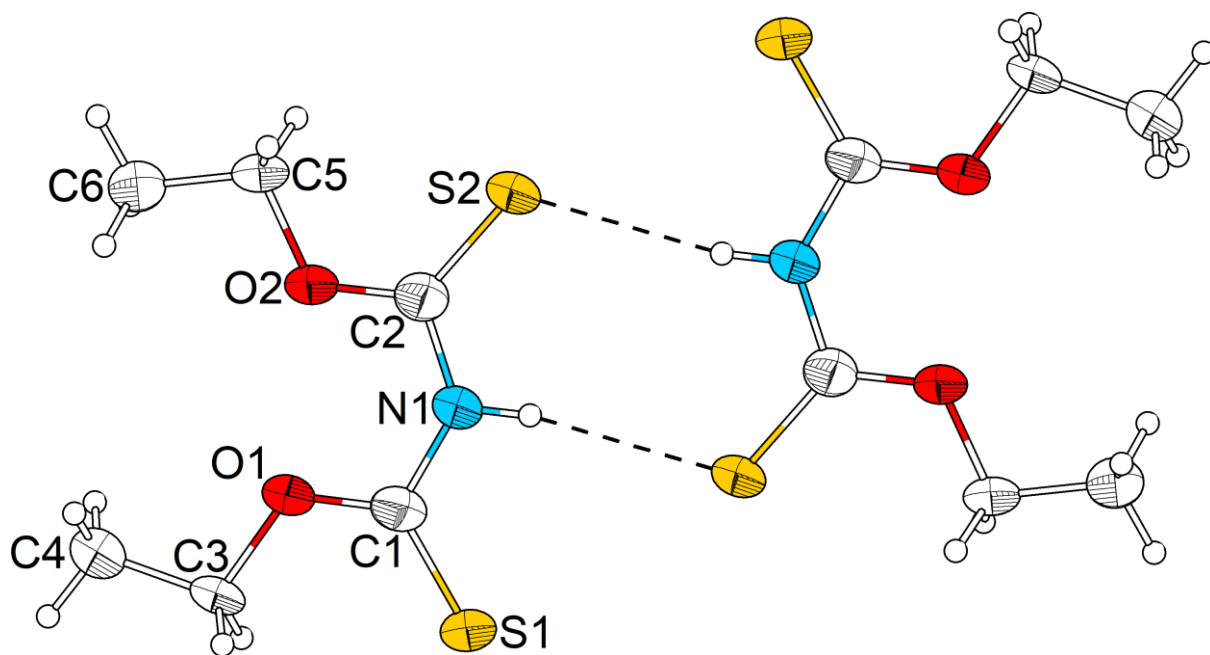
Figure S 25: Dimer formation of thioimidodicarbonic-*O*,*O*-diethyl ester in the single crystal drawn with 75% displacement ellipsoids at 100 K. Hydrogen atoms drawn with arbitrary radii. Black dashed lines represent the hydrogen sulfur bridging bond.

Figure S 26: Crystal structure of thioimidodicarbonic-*O*,*O*-diethyl ester viewed along [100]. Atoms drawn with arbitrary radii. Colour code: S yellow, N blue, C white, O red, H small white.
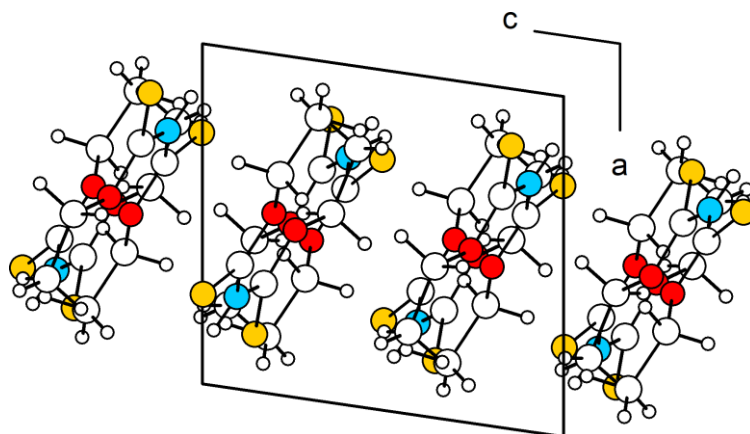
Figure S 27: Crystal structure of thioimidodicarbonic-*O,O*-diethyl ester viewed along [010]. Atoms drawn with arbitrary radii. Colour code: S yellow, N blue, C white, O red, H small white.

2.4. Additional Pictures for bis(*O,O*-diethyl-1,3-dithioimidodicarbonato)nickel
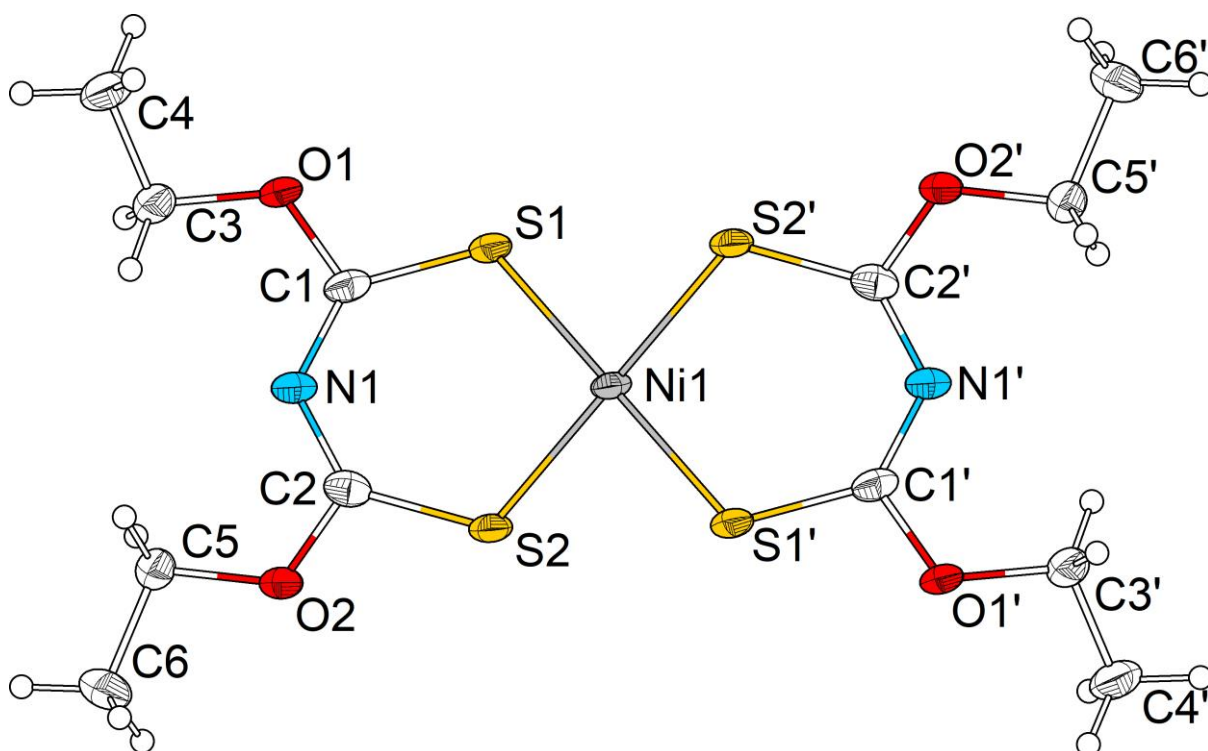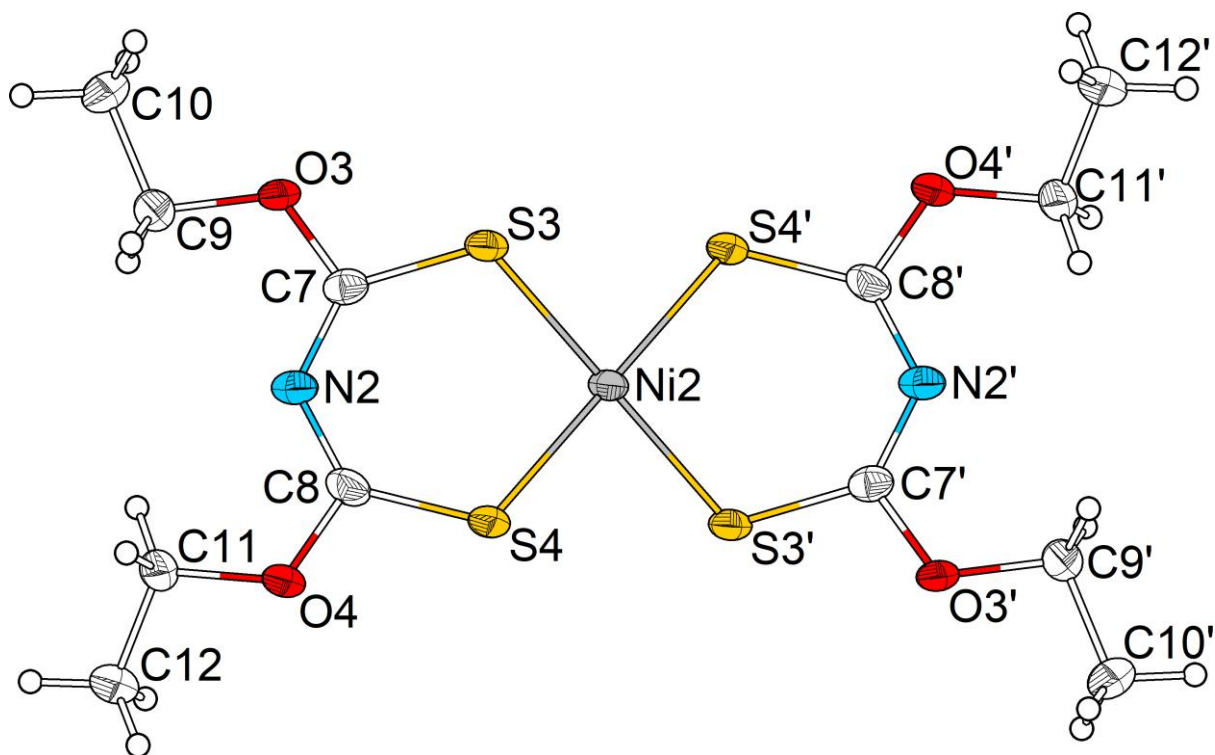

Figure S 28: Molecular structure of the first crystallographically independent bis(*O,O*-diethyl-1,3-dithioimidodicarbonato)nickel molecule in the single crystal drawn with 75% displacement ellipsoids at 100 K. Hydrogen atoms drawn with arbitrary radii.

Figure S 29: Molecular structure of the second crystallographically independent bis(*O*,*O*-diethyl-1,3-dithioimidodicarbonato)nickel molecule in the single crystal drawn with 75% displacement ellipsoids at 100 K. Hydrogen atoms drawn with arbitrary radii.
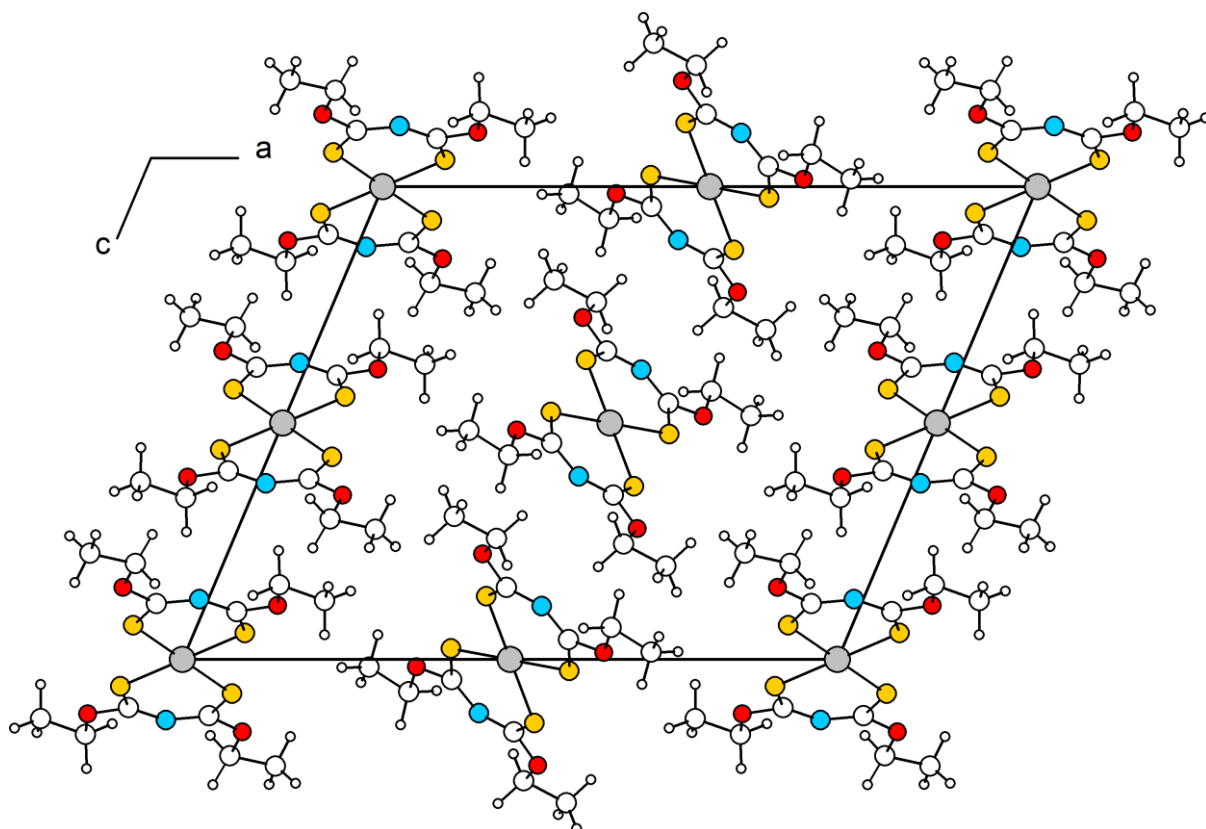
Figure S 30: Crystal structure of bis(*O,O*-diethyl-1,3-dithioimidodicarbonato)nickel viewed along [010]. Atoms drawn with arbitrary radii. Colour code: S yellow, N blue, C white, O red, H small white, Ni gray.
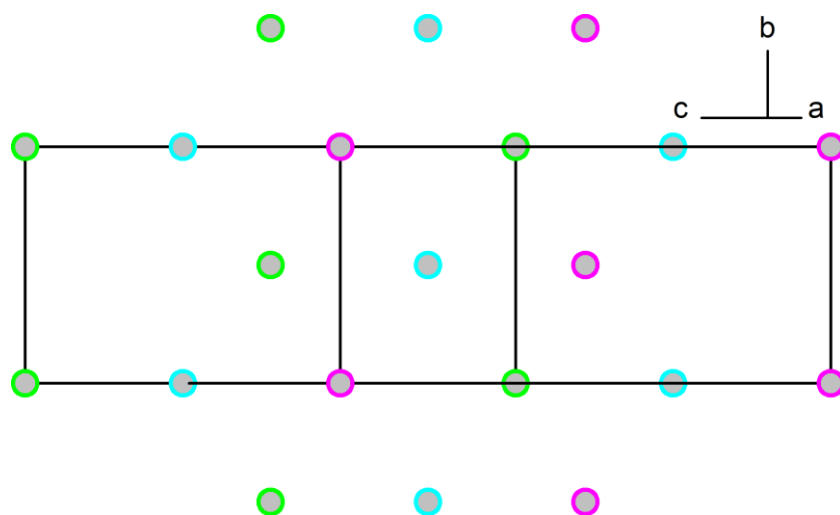

Figure S 31: Topology of the Ni-atoms of the structure of bis(*O,O*-diethyl-1,3-dithioimidodicarbonato)nickel viewed approximately along [10 0 0]. Atoms of the same colour lie in the same *cb*-plane on *a*=0 (green), *a*=1/2 (blue) and *a*=1 (purple. The motif of the cubic closest packing is visible.

3. Additional details on Hirshfeld surface analysis
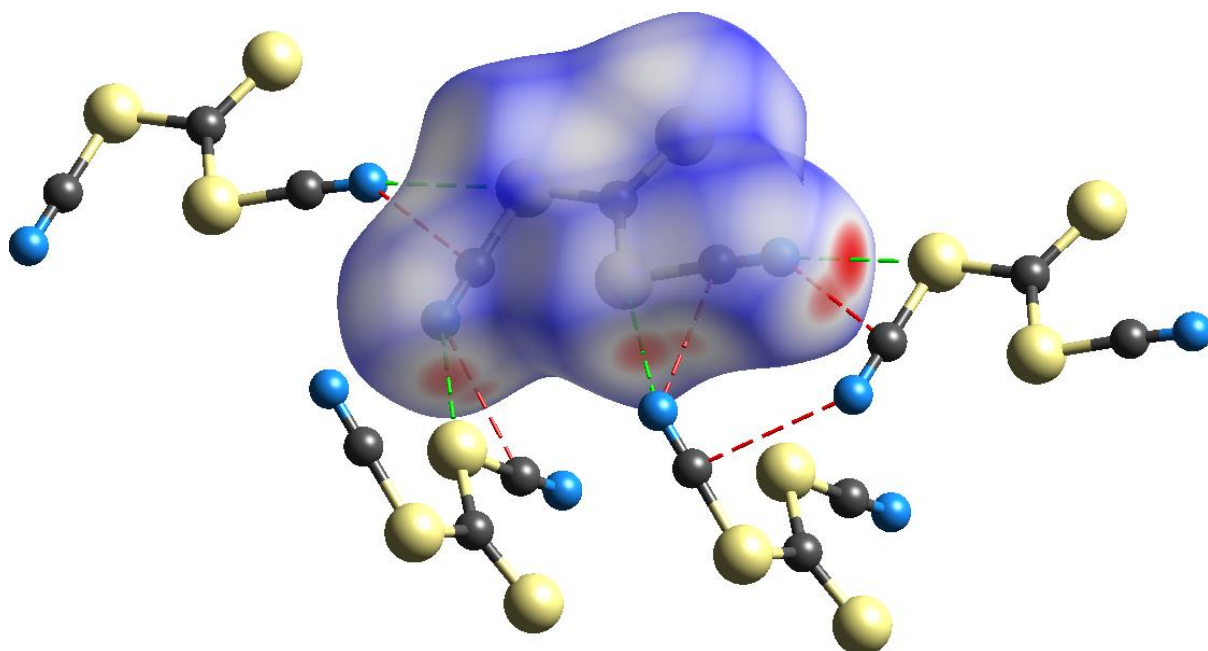
3.1. Thiocarbonyl dithiocyanate

Figure S 32: Hirshfeld surface of thiocarbonyl dithiocyanate shown with neighbouring molecules. Red areas indicate short contacts. Red dashed lines indicate C–N and green dashed lines S–N short contacts.
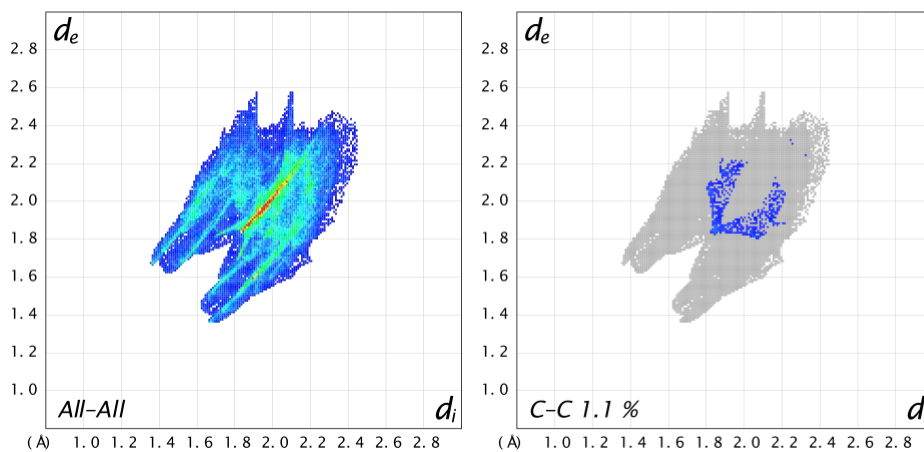

Figure S 33: Fingerprint plots for thiocarbonyl dithiocyanate mapped from the Hirshfeld surface. Left shows all surface contacts and right C–C contacts with their overall amount.
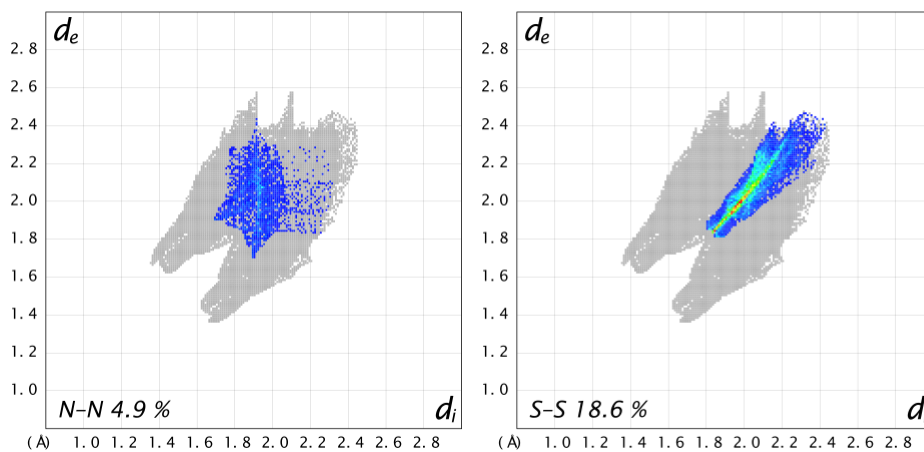
Figure S 34: Fingerprint plots for thiocarbonyl dithiocyanate mapped from the Hirshfeld surface. Left shows N–N contacts and right S–S contacts with their overall amount.
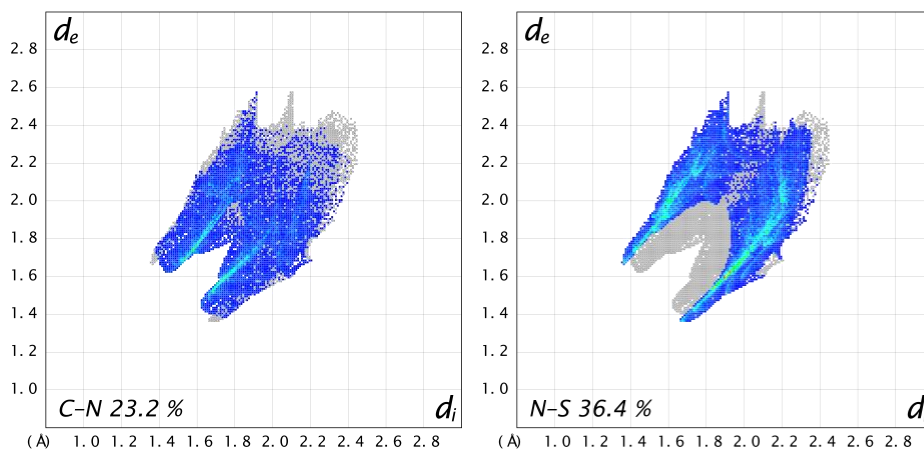

Figure S 35: Fingerprint plots for thiocarbonyl dithiocyanate mapped from the Hirshfeld surface. Left shows C–N contacts and right N–S contacts with their overall amount.
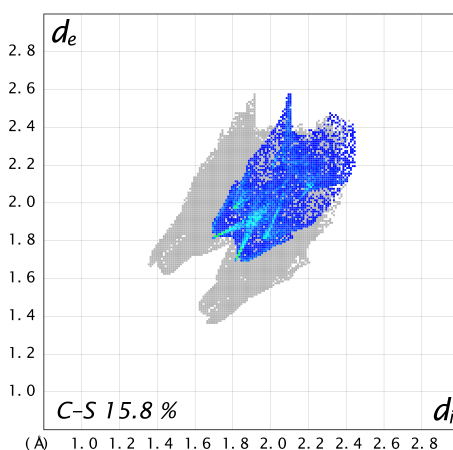

Figure S 36: Fingerprint plot for thiocarbonyl dithiocyanate mapped from the Hirshfeld surface, shows C–S contacts with their overall amount.

3.2. Chlorothiocarbonyl thiocyanate

Figure S 37: Hirshfeld surface of chlorothiocarbonyl thiocyanate of the first independent molecule shown with neighbouring molecules. Red areas indicate short contacts. Red dashed lines indicate S–Cl and green dashed lines S–N short contacts.
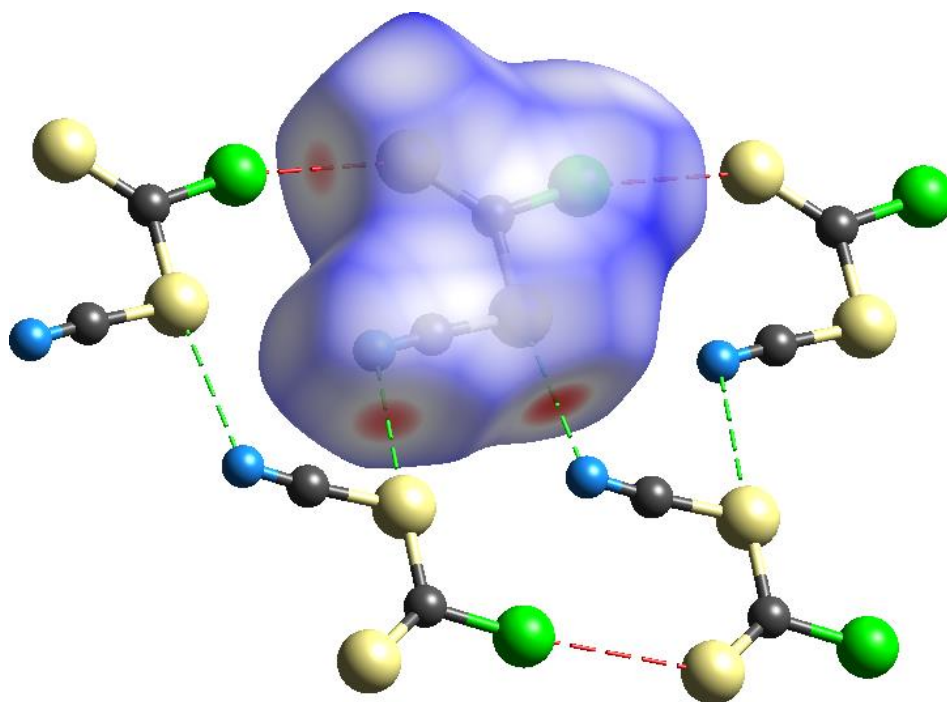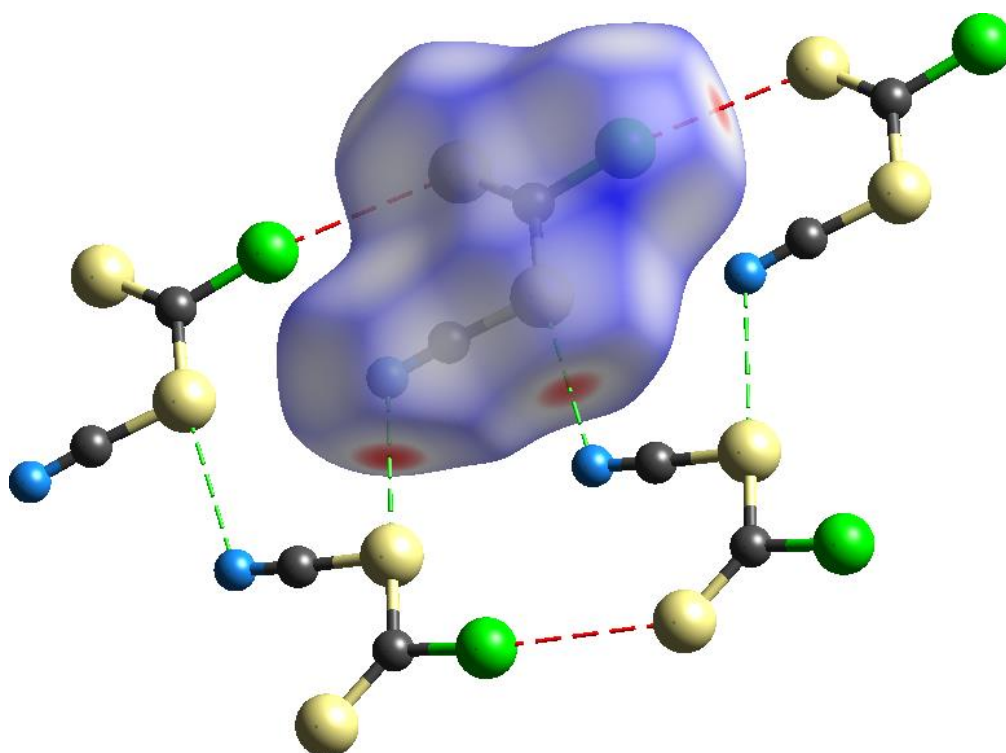

Figure S 38: Hirshfeld surface of chlorothiocarbonyl thiocyanate of the second independent molecule shown with neighbouring molecules. Red areas indicate short contacts. Red dashed lines indicate S–Cl and green dashed lines S–N short contacts.

Figure S 39: Fingerprint plots for chlorothiocarbonyl thiocyanate mapped from the Hirshfeld surface, shows all surface contacts of both independent individuals.

Figure S 40: Fingerprint plots for chlorothiocarbonyl thiocyanate mapped from the Hirshfeld surface, shows all C–C contacts and their amount of both independent individuals.

Figure S 41: Fingerprint plots for chlorothiocarbonyl thiocyanate mapped from the Hirshfeld surface, shows all N–N contacts and their amount of both independent individuals.

Figure S 42: Fingerprint plots for chlorothiocarbonyl thiocyanate mapped from the Hirshfeld surface, shows all S–S contacts and their amount of both independent individuals.
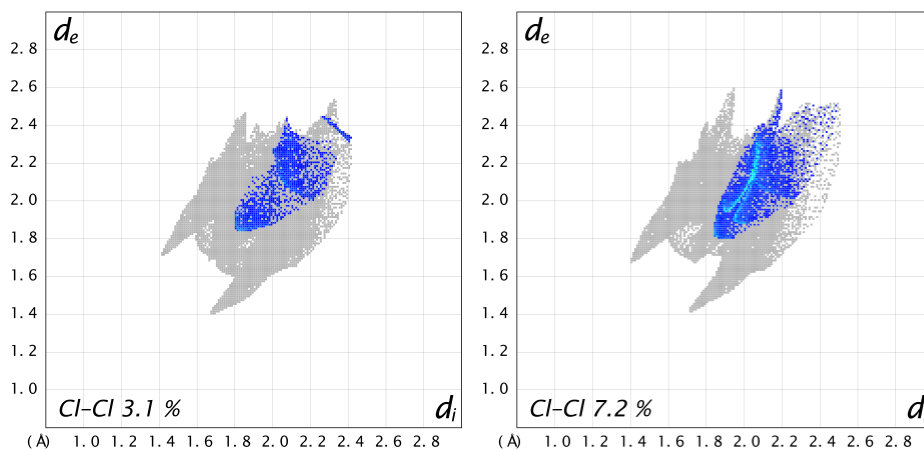
Figure S 43: Fingerprint plots for chlorothiocarbonyl thiocyanate mapped from the Hirshfeld surface, shows all Cl–Cl contacts and their amount of both independent individuals.
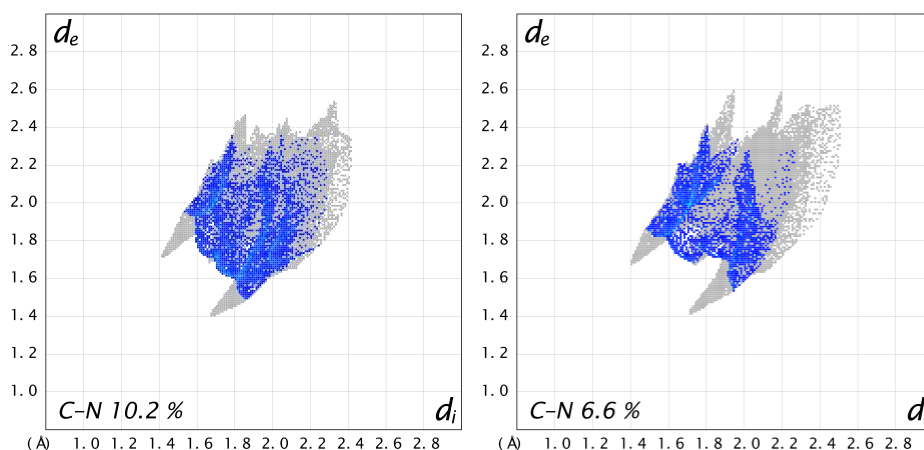
Figure S 44: Fingerprint plots for chlorothiocarbonyl thiocyanate mapped from the Hirshfeld surface, shows all C–N contacts and their amount of both independent individuals.
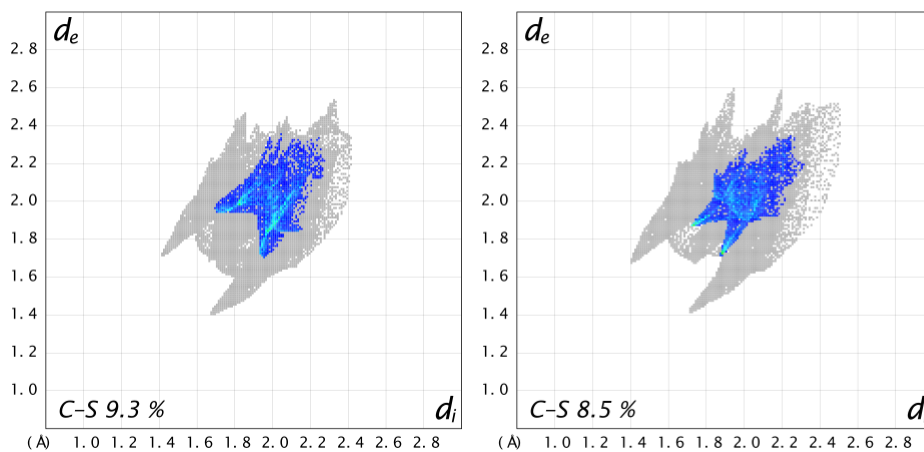
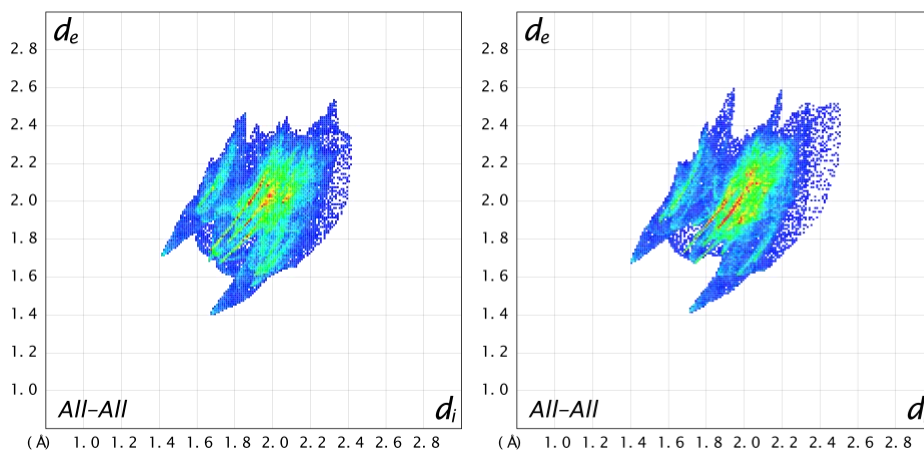Figure S 45: Fingerprint plots for chlorothiocarbonyl thiocyanate mapped from the Hirshfeld surface, shows all C–S contacts and their amount of both independent individuals.
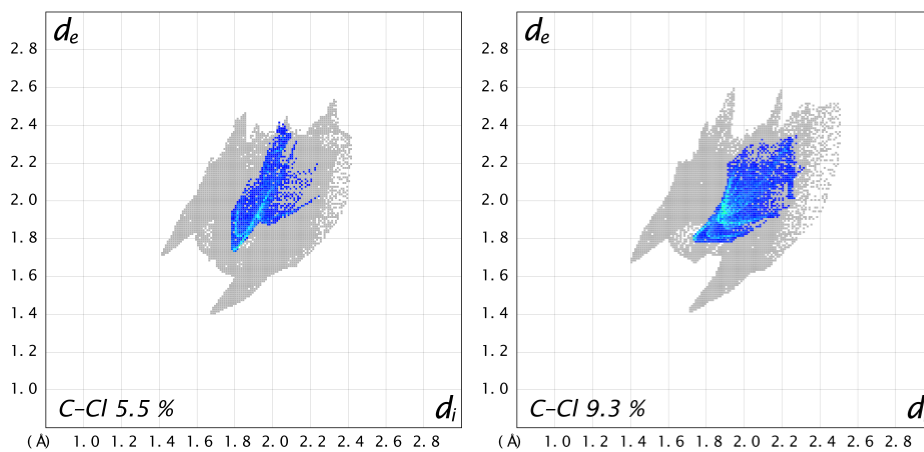
Figure S 46: Fingerprint plots for chlorothiocarbonyl thiocyanate mapped from the Hirshfeld surface, shows all C–Cl contacts and their amount of both independent individuals.
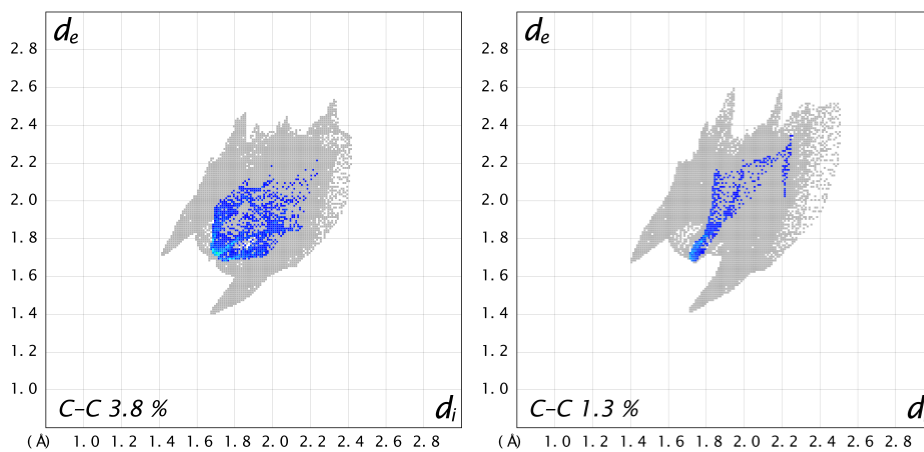

Figure S 47: Fingerprint plots for chlorothiocarbonyl thiocyanate mapped from the Hirshfeld surface, shows all N–S contacts and their amount of both independent individuals.
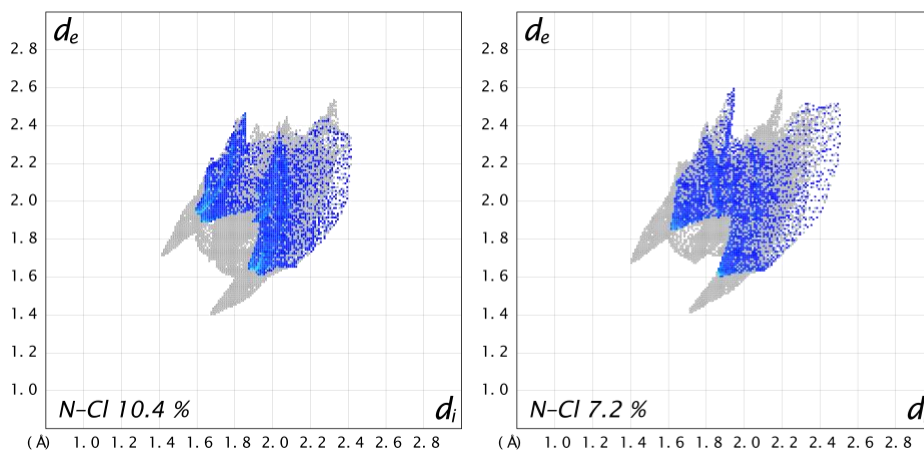
Figure S 48: Fingerprint plots for chlorothiocarbonyl thiocyanate mapped from the Hirshfeld surface, shows all N–Cl contacts and their amount of both independent individuals.
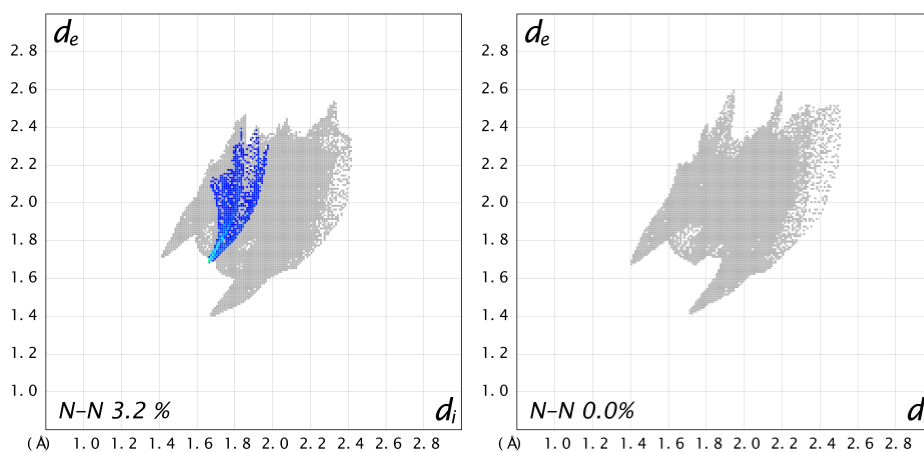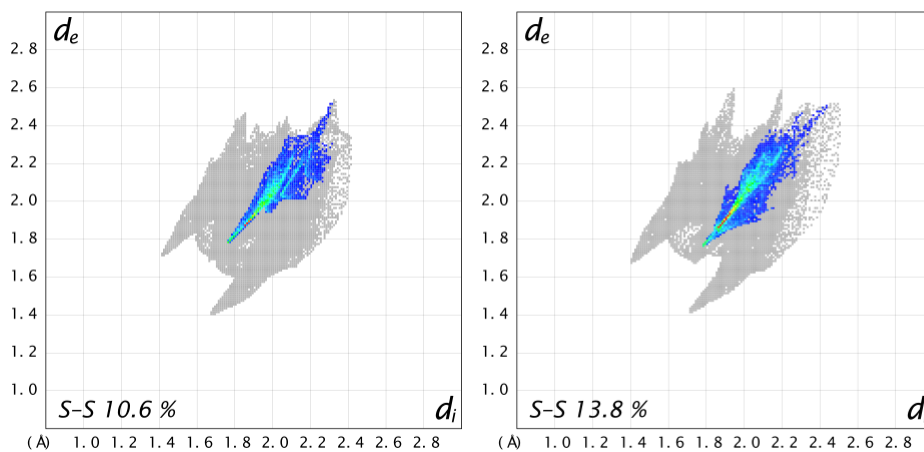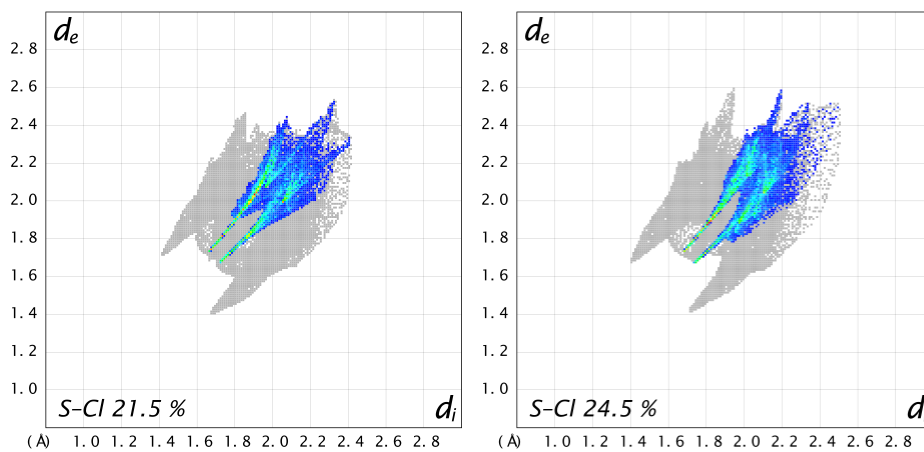

Figure S 49: Fingerprint plots for chlorothiocarbonyl thiocyanate mapped from the Hirshfeld surface, shows all S–Cl contacts and their amount of both independent individuals.
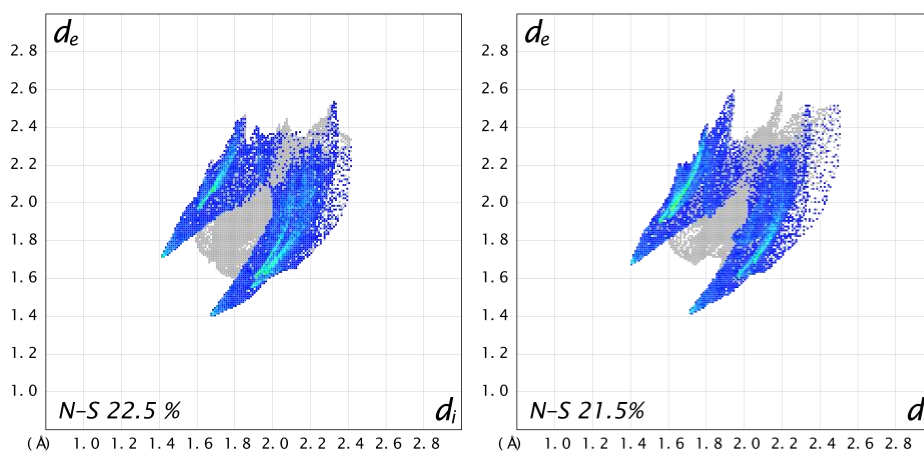
4. Details on quantum chemical calculations

4.1. Calculations with periodic boundary conditions

Periodic quantum-chemical calculations were carried out for thiocarbonyl dithiocyanate and chlorothiocarbonyl thiocyanate with the PBE0 hybrid density functional theory method (DFT-PBE0).[9,10] All calculations were performed with the CRYSTAL17 program package.[11] Triple-ζ-valence + polarization (TZVP) level basis sets were applied for C, N, O, S, Cl. The basis sets have been previously derived from the Karlsruhe def2 basis sets.[12,13] Intermolecular van der Waals dispersion interactions were taken into account using Grimme's empirical D3 dispersion correction with zero damping.[14] Reciprocal space was sampled by Monkhorst−Pack type k-meshes (CS(SCN)$_2$: $8 \times 8 \times 4$, CS(SCN)Cl: $8 \times 2 \times 7$).[15] For the evaluation of the Coulomb and exchange integrals (TOLINTEG), tolerance factors of 8, 8, 8, 8, and 16 were used for all calculations. Atomic positions and lattice parameters were fully optimized considering the space group symmetry. Default DFT integration grids and optimization convergence thresholds were applied in all calculations. The harmonic vibrational frequencies and Raman and IR intensities were obtained using CRYSTAL.[16–19] Raman and IR intensities were calculated for a polycrystalline powder sample (total isotropic intensity in arbitrary units). The Raman spectra were obtained by using a pseudo-Voigt band profile (50:50 Lorentzian:Gaussian) and a full width at half-maximum (fwhm) of 8 cm^{-1} and simulated taking into account the experimental setup (293.15 K; $\lambda = 532$ nm). Bands for the Raman spectrum were assigned by visual inspection of the normal modes with the Jmol program package at http://crysplot.crystalsolutions.eu/.[20,21]

Table S 5: Lattice parameters and atomic coordinates of the optimized solid-state structure of thiocarbonyl dithiocyanate in space group $P2_1/c$. Note that the measured structure is in $P2_1/n$ and was transformed to $P2_1/c$ to make the calculation possible within the CRYSTAL17 code.

Lattice parameter / Å	a	b	c
	19.56279647	5.95064520	19.55711592

Lattice parameter / °	β		
	162.703233		

Atom	x	y	z
S1	0.46342	0.41246	−0.36845
S2	0.08728	−0.35681	0.19456
S3	0.29011	0.24625	0.32764
N4	0.17073	−0.12765	0.39995
N5	−0.26538	0.02587	−0.13723
C6	0.13794	−0.22214	0.31803
C7	−0.37935	0.18169	−0.23740
C8	0.28674	0.41833	0.38835

Table S 6: Lattice parameters and atomic coordinates of the optimized solid-state structure of chlorothiocarbonyl thiocyanate in space group $P2_1/c$.

Lattice parameter / Å	a	b	c
	6.48955635	22.73746818	7.88164631

Lattice parameter / °	β		
	103.623198		

Atom	x	y	z
S1	−0.38366	−0.48272	−0.23171
Cl2	−0.09227	−0.39568	−0.07681
Cl3	−0.26225	−0.27584	−0.43651
S4	−0.05021	−0.36522	0.42674
S5	0.45945	−0.37442	−0.07045
S6	0.20176	−0.26151	−0.38212
N7	0.17532	0.49383	−0.28143
N8	0.36793	−0.39261	0.39812
C9	0.35252	−0.49438	−0.25930
C10	0.20221	−0.37915	0.41412
C11	−0.01290	−0.29758	−0.45768
C12	−0.35988	−0.41393	−0.12175

Table S 7: Band assignments for the calculated IR spectra of thiocarbonyl dithiocyanate. The notation for band assignments is the following: ν–stretching, δ–deformation. The irreducible representations are given for the point groups of the respective space group types of the crystal structures.

ν (calculated) [cm^{-1}]	ν (observed) [cm^{-1}]	irrep.	assignment
			Thiocarbonyl dithiocyanate
522	500	A_u	δ(S3–C3≡N1) in plane scissoring
523		B_u	
691	661	B_u	ν_s(C2–S2) stretching
692		A_u	
717	687	B_u	ν_s(C3–S3) stretching
718		A_u	
849	827	B_u	δ(S2–C1–S3) in plane bending
849		A_u	
1132	1087	B_u	ν_s(C1=S1) stretching
1146		A_u	
2309	2158	A_u	ν_s(C2≡N2) stretching
2310		B_u	
2331	2172	A_u	ν_s(C3≡N1) stretching
2332		B_u	

Table S 8: Band assignments for the calculated Raman spectra of thiocarbonyl dithiocyanate. The notation for band assignments is the following: ν–stretching, δ–deformation. The irreducible representations are given for the point groups of the respective space group types of the crystal structures.

ν (calculated) [cm^{-1}]	ν (observed) [cm^{-1}]	irrep.	assignment
			Thiocarbonyl dithiocyanate
156	155	A_g	whole molecule bending and rocking
159		B_g	
253	244	A_g	δ(S1=C1-S2–C2≡N2) bending
256		B_g	
275	264	A_g	δ(S1=C1-S3–C3≡N1) bending
276		B_g	
391	384	B_g	δ(S2–C2≡N2) twisting
392		A_g	
400	384	A_g	whole molecule in plane rocking
401		B_g	
404	384	B_g	δ(S3–C3≡N1) twisting
405		A_g	
463	not observed	A_g	δ(S2–C1–S3) wagging combined with δ(S2–C2≡N2) scissoring
464		B_g	
467		B_g	
468		A_g	
521	495	A_g	δ(S3–C3≡N1) scissoring
522		B_g	

691	not observed	A_g	v_s(C2–S2) stretching
692		B_g	
718	not observed	B_g	v_s(C3–S3) stretching
719		A_g	
851	832	B_g	δ(S2–C1–S3) bending
852		A_g	
1137	1080	B_g	v_s(C1=S1) stretching
1138		A_g	
2310	2166	B_g	v_s(C2≡N2) stretching
2312		A_g	
2331	2152	B_g	v_s(C3≡N1) stretching
2332		A_g	

Table S 9: Band assignments for the calculated IR spectra of chlorothiocarbonyl thiocyanate. The notation for band assignments is the following: v–stretching, δ–deformation. The irreducible representations are given for the point groups of the respective space group types of the crystal structures.

v (calculated) [cm^{-1}]	v (observed) [cm^{-1}]	irrep.	assignment
			Chlorothiocarbonyl thiocyanate
542		B_u	
543	not observed	A_u	δ(S–C≡N) in plane scissoring
544		A_u	
545		B_u	
707		A_u	
707	not observed	B_u	v_s(C–S) stretching
710		A_u	
710		B_u	
796		A_u	
803	748	B_u	δ(S–C–Cl) in plane rocking
803		A_u	
809		B_u	
1154		A_u	
1165	1124	B_u	v_s(C=S) stretching
1169		A_u	
1175		B_u	
2322		B_u	
2323	2168	A_u	v_s(C≡N) stretching
2324		A_u	
2325		B_u	

Table S 10: Band assignments for the calculated Raman spectra of chlorothiocarbonyl thiocyanate. The notation for band assignments is the following: ν–stretching, δ–deformation. The irreducible representations are given for the point groups of the respective space group types of the crystal structures.

ν (calculated) [cm^{-1}]	ν (observed) [cm^{-1}]	irrep.	assignment
		Chlorothiocarbonyl thiocyanate	
259		A_g	
260	240	B_g	δ(S=C–S–C≡N) rocking
263		A_g	
264		B_g	
296		A_g	
297	277	B_g	whole molecule bending
298		A_g	
299		B_g	
405		A_g	
406	not observed	B_g	δ(S–C≡N) twisting
411		A_g	
412		B_g	
433		B_g	
433	404	A_g	δ(S–C≡N) bending
434		A_g	
434		B_g	
474		A_g	
475	448	B_g	δ(S–C–Cl) wagging
476		A_g	
477		B_g	
542		B_g	
543	513	A_g	δ(S–C≡N) in plane scissoring
544		A_g	
544		B_g	
707		A_g	
708	not observed	B_g	ν_s(C–S) stretching
710		B_g	
710		A_g	
796		A_g	
797	not observed	B_g	δ(S–C–Cl) in plane rocking
807		B_g	
809		A_g	
1153		B_g	
1162	1115	A_g	ν_s(C=S) stretching
1172		A_g	
1175		B_g	
2322		A_g	
2322	2158	B_g	ν_s(C≡N) stretching
2323		A_g	
2323		B_g	

4.2. Calculations with Turbomole

Calculations were done with the program suite TURBOMOLE.[22] The PBE0 functional[23] was employed with def2-TZVP bases.[12] Further the conductor-like screening model (COSMO) in a very recent implementation[24] closely following Garcia et al.[25] with infinite dielectric constant was used. Fine DFT grids (gridsize 5) and weight derivatives were employed, the SCF energy was converged to 10^{-9} E_H. Structure optimizations were converged to a gradient norm of 10^{-3}. Transition states were identified with the reaction path optimizing tool in TURBOMOLE.[26] It was ensured that all minimum structures show no imaginary frequency, and that all transition states show exactly one imaginary frequency. Thermal corrections were evaluated from the vibrations by the harmonic-oscillator-rigid-rotor model. Cartesian coordinates of all structures are sampled in file structures.xyz. The tables S11, S12 and S13 contain the raw data for the Figures 5, 6 and 7.

Table S 11: Energies [kJ/mol] relative to the corresponding most stable isomers for the title compound and related compounds. E' denotes the E-atom directly binding to the central C atom, the other atoms are labelled from left to right; for further clarification see also Figure 5. "elec" denotes the electronic energy, "therm" the thermal contribution to the free enthalpy according to the harmonic-oscillator-rigid-rotor model for T=300K, "sum" the sum of both.

	E'=O, E=S			E'=S, E=S			E'=O, E=O		
	elec	therm	sum	elec	therm	sum	elec	therm	sum
E'-ECNCNCE-ss	0.0	0.0	0.0	0.0	0.0	0.0	0.0	0.0	0.0
E'-ECNCNCE-sa	2.9	−0.2	2.7	5.6	−0.2	5.4	1.4	−0.1	1.3
E'-ECNCNCE-aa	6.7	−0.2	6.5	9.6	−0.1	9.5	converges to sa		
E'-ECNCECN-ss	50.5	−2.7	47.8	50.9	−2.8	48.1	121.6	−1.2	120.4
E'-ECNCECN-sa	55.1	−2.7	52.4	49.7	−2.7	47.0	127.0	−1.4	125.6
E'-ECNCECN-aa	59.5	−2.8	56.7	converges to sa			139.5	−2.0	137.5
E'-NCECECN-ss	110.9	−5.2	105.7	110.2	−5.3	104.9	273.3	−2.3	271.0
E'-NCECECN-sa	112.7	−5.2	107.5	106.5	−5.3	101.2	281.4	−2.6	278.8
E'-NCECECN-aa	132.9	−5.4	127.5	123.6	−5.4	118.2	312.3	−3.6	308.7

Table S 12: Energies [kJ/mol] for the exchange of Cl⁻ with (SCN)⁻ in CSCl₂, relative to the starting point. See also Table S11. A1 and A2 are minima when (SCN)⁻ plus CSCl₂ or Cl⁻ plus CSClSCN are calculated as whole systems, the zero-point of energies is defined by (SCN)⁻ plus CSCl₂ calculated separately. Int denotes an intermediate state with both two Cl and SCN bond to C, Tr1 is the transition state from A1 to Int, Tr2 that from Int to A2. For further clarification see also Figure 6.

	(SCN)⁻ + CSCl₂ → SCNCSCl-s + Cl⁻			(SCN)⁻ + CSCl₂ → SCNCSCl-a + Cl⁻			(SCN)⁻ + CSCl₂ → NCSCSCl-s + Cl⁻			(SCN)⁻ + CSCl₂ → NCSCSCl-a + Cl⁻		
	elec	therm	sum	elec	therm	sum	elec	therm	sum	elec	therm	sum
A1	−2.9	−0.1	−3.0	−1.3	0.0	−1.3	−2.0	0.0	−2	−1.9	0.0	−1.9
Tr1	55.5	−4.2	51.3	61.3	−4.4	56.9	39.7	−4.5	35.2	41.4	−4.4	37.0
Int	−7.5	0.2	−7.3	−7.6	0.2	−7.4	23.4	−2.3	21.1	15.4	−2.2	13.2
Tr2	−3.7	−1.9	−5.6	−3.3	-2.0	−5.3	39.1	−4.3	34.8	32.0	−4.1	27.9
A2	−60.9	2.6	−58.3	−60.8	2.56	−58.2	−12.4	0.1	−12.3	−7.2	0.1	−7.1
Prod	−57.2	3.6	−53.6	−57.1	2.56	−54.5	−8.6	0.1	−8.5	−5.4	0.1	−5.3

Table S 13: Energies [kJ/mol] for the exchange of Cl- atom with (SCN)- in CSClSCN, relative to the corresponding starting points. See also Table S 12. For further clarification see also Figure 6.

	(SCN)⁻ + SCNCSCl-s → S-SCNCNCS-ss + Cl⁻			(SCN)⁻ + SCNCSCl-a → S-SCNCNCS-sa + Cl⁻			(SCN)⁻ + NCSCSCl-s → S-NCSCSCN-ss + Cl⁻			(SCN)⁻ + NCSCSCl-a → S-NCSCSCN-sa + Cl⁻		
	elec	therm	sum	elec	therm	sum	elec	therm	sum	elec	therm	sum
A1	−2.2	0	−2.2	−1.8	0	−1.8	−2.2	0	−2.2	−2.3	0	−2.3
Tr1	62.7	−4.14	58.6	64.5	−4.25	60.3	39.0	−4.47	30.1	34.0	−4.37	29.6
Int	–	–	–	-	-	-	23.2	−2.32	18.6	15.5	−2.09	13.4
Tr2	–	–	–	-	-	-	30.6	−4.46	21.7	33.5	−4.18	29.3
A2	−59.4	2.77	−56.6	−54.4	2.68	−51.7	2.2	0	2.2	−5.0	0.02	−5.0
Prod	−55.7	2.77	−52.9	−50.3	2.67	−47.7	6.1	−0.01	6.1	−1.0	0.02	−1.0

Table S 14: Orbital energies [eV] of the *syn-syn* and *syn-anti* conformers from CS(SCN)$_2$ and CO(SCN)$_2$, as well as the energy difference *sa–ss*. Negative sign means an energy decrease from *ss* to *sa* and positive sign stands for an energy increase from *ss* to *sa*. Marked in yellow are p-orbitals in the molecule plane with an energy change higher than 0.1 eV marked in red.

|	S-NCSCSCN-ss	S-NCSCSCN-sa	O-NCSCSCN-ss	O-NCSCSCN-sa	S-NCSCSCN sa–ss	O-NCSCSCN sa–ss
HOMO	-7.624	-7.662	-9.863	-9.941	–0.038	–0.078
-1	-8.239	-8.044	-10.142	-10.047	+0.195	+0.095
-2	-8.399	-8.574	-10.327	-10.161	–0.175	+0.166
-3	-10.313	-10.221	-10.579	-10.760	+0.092	–0.181
-4	-10.534	-10.648	-11.030	-11.062	–0.114	–0.032
-5	-10.598	-10.816	-11.655	-11.700	0.218	–0.045
-6	-11.369	-11.326	-11.712	-11.725	+0.043	–0.013
-7	-11.462	-11.447	-12.346	-12.417	+0.015	–0.071
-8	-11.657	-11.624	-14.305	-14.299	+0.033	+0.006
-9	-11.949	-12.107	-14.432	-14.674	–0.158	–0.242
-10	-12.470	-12.537	-15.852	-14.838	–0.067	+1.014
-11	-13.212	-12.622	-16.452	-16.465	+0.59	–0.013
-12	-14.017	-13.781	-16.523	-16.577	+0.236	–0.054
-13	-14.763	-16.033	-19.401	-20.640	–1.27	–1.239
-14	-18.340	-17.774	-23.051	-22.564	+0.566	+0.487
-15	-21.940	-21.971	-26.459	-26.501	–0.031	–0.042
-16	-23.172	-23.201	-26.616	-26.574	–0.029	+0.042
-17	-25.340	-25.410	-31.501	-31.571	–0.07	–0.07
-18	-26.521	-26.533	-33.187	-33.102	–0.012	+0.085
-19	-26.644	-26.711	-35.031	-35.040	–0.067	–0.009
sum					–0.479	–0.194
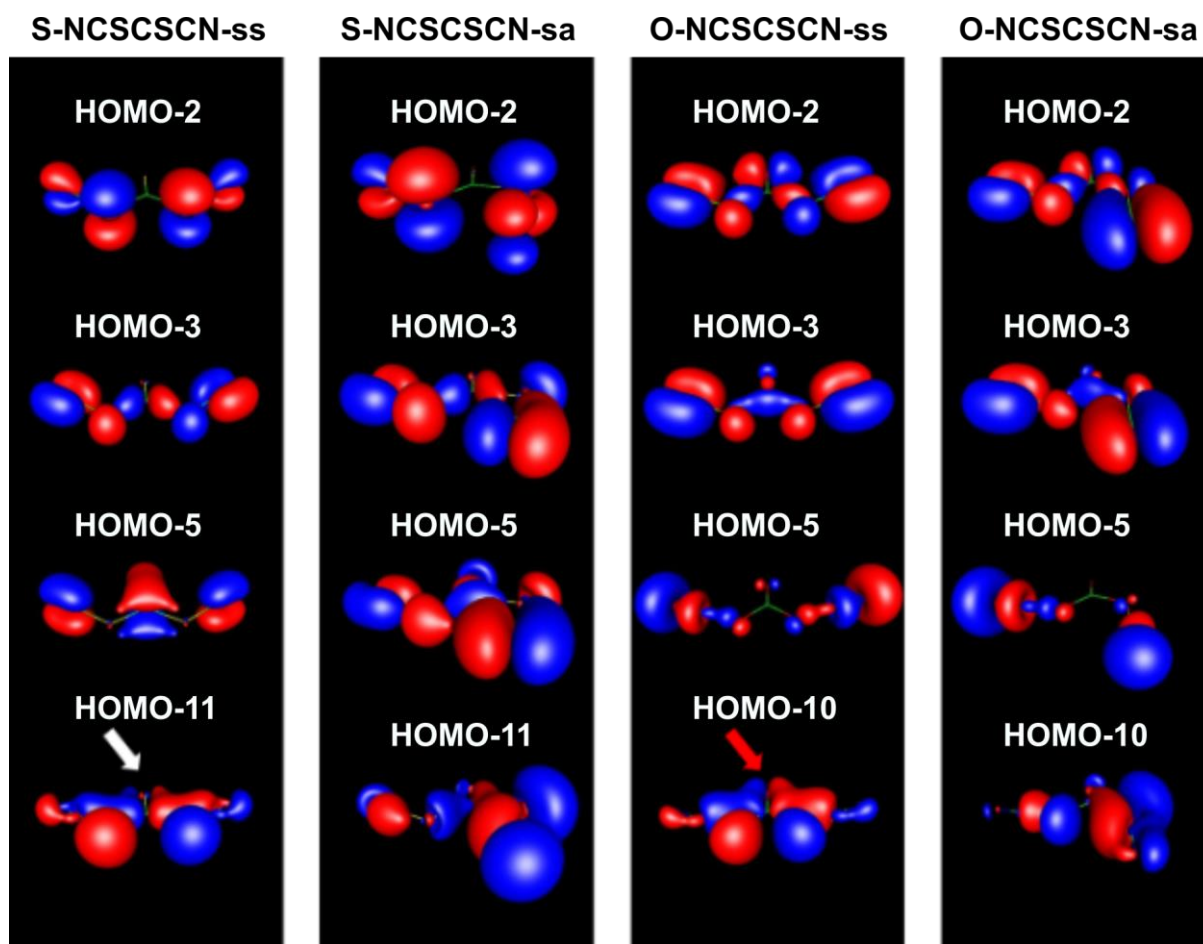
Figure S 50: Relevant orbitals of the *syn-syn* and *syn-anti* conformers from CS(SCN)$_2$ and CO(SCN)$_2$, which are responsible for the *syn-anti* conformer of CS(SCN)$_2$ being more stable than *syn-syn*. The HOMO-10 of CO(SCN)$_2$ in *ss* configuration has a slight double bond character to the C−O bond (red arrow). This double bond character is not present in the *ss*-isomer of CS(SCN)$_2$ (white arrow).

5. References

[1]   W. L. F. Armarego, C. L. L. Chai, *Purification of Organic Chemicals*, **2009**.

[2]   R. Bunnenberg, C. Jochims, *Chem. Ber* **1981**, *114*, 1132–1136.

[3]   G. M. Sheldrick, *Acta Crystallogr. Sect. A Found. Adv.* **2015**, *71*, 3–8.

[4]   G. M. Sheldrick, *Acta Crystallogr. Sect. A Found. Crystallogr.* **2008**, *64*, 112–122.

[5]   O. V. Dolomanov, L. J. Bourhis, R. J. Gildea, J. A. K. Howard, H. Puschmann, *J. Appl. Crystallogr.* **2009**, *42*, 339–341.

[6]   K. Brandenburg, H. Putz, *DIAMOND, Program for X-Ray Structure Analysis*, Crystal Impact GbR, Bonn, Gemany, **2005**.

[7]   H. M. Rietveld, *J. Appl. Crystallogr.* **1969**, *2*, 65–71.

[8]   A. A. Coelho, *J. Appl. Crystallogr.* **2018**, *51*, 210–218.

[9]   C. Adamo, V. Barone, *J. Chem. Phys.* **1999**, *110*, 6158.

[10]   J. P. Perdew, K. Burke, M. Ernzerhof, **1996**.

[11]   R. Dovesi, A. Erba, R. Orlando, C. M. Zicovich-Wilson, B. Civalleri, L. Maschio, M. Rérat, S. Casassa, J. Baima, S. Salustro, B. Kirtman, *Wiley Interdiscip. Rev. Comput. Mol. Sci.* **2018**, *8*, e1360.

[12]   F. Weigend, R. Ahlrichs, *Phys. Chem. Chem. Phys.* **2005**, *7*, 3297–3305.

[13]   A. J. Karttunen, T. Tynell, M. Karppinen, *J. Phys. Chem. C* **2015**, *119*, 13105–13114.

[14]   S. Grimme, J. Antony, S. Ehrlich, H. Krieg, *J. Chem. Phys.* **2010**, *132*, 154104.

[15]   H. J. Monkhorst, J. D. Pack, *Phys. Rev. B* **1976**, *13*, 5188–5192.

[16]   C. M. Zicovich-Wilson, F. Pascale, C. Roetti, V. R. Saunders, R. Orlando, R. Dovesi, *J. Comput. Chem.* **2004**, *25*, 1873–1881.

[17]   F. Pascale, C. M. Zicovich-Wilson, F. L. Gejo, B. Civalleri, R. Orlando, R. Dovesi, *J. Comput. Chem.* **2004**, *25*, 888–897.

[18]   L. Maschio, B. Kirtman, M. Rérat, R. Orlando, R. Dovesi, *J. Chem. Phys.* **2013**, *139*, 164102.

[19]   L. Maschio, B. Kirtman, R. Orlando, M. Rèrat, *J. Chem. Phys.* **2012**, *137*, 204113.

[20]   G. Beata, G. Perego, B. Civalleri, *J. Comput. Chem.* **2019**, *40*, 2329–2338.

[21]   "Jmol: an open-source Java viewer for chemical structures in 3D. http://www.jmol.org/," can be found under http://www.jmol.org/, **n.d.**

[22]   **N.d.**

[23]   J. P. Perdew, M. Ernzerhof, K. Burke, *J. Chem. Phys.* **1996**, *105*, 9982–9985.

[24]   A. Pausch, **2024**, *submitted*.

[25]   M. Garcia-Ratés, F. Neese, *J. Comput. Chem.* **2020**, *41*, 922–939.

[26]   P. Plessow, *J. Chem. Theory Comput.* **2013**, *9*, 1305–1310.

8.2 Analytische Daten

8.2.1 NMR Spektren
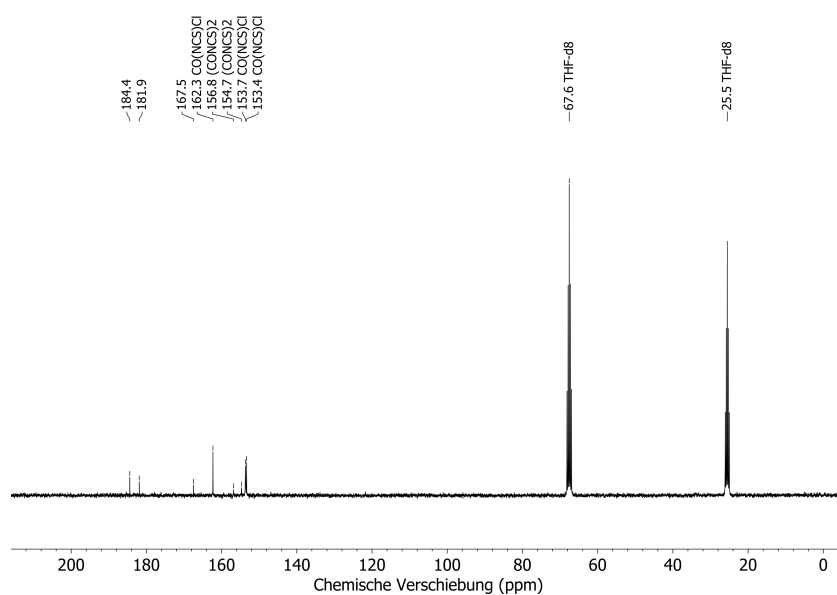
Abbildung 8.1: ^{13}C-NMR-Spektrum von Cl(CO)$_2$NCS aus **XV** in THF-d$_8$.
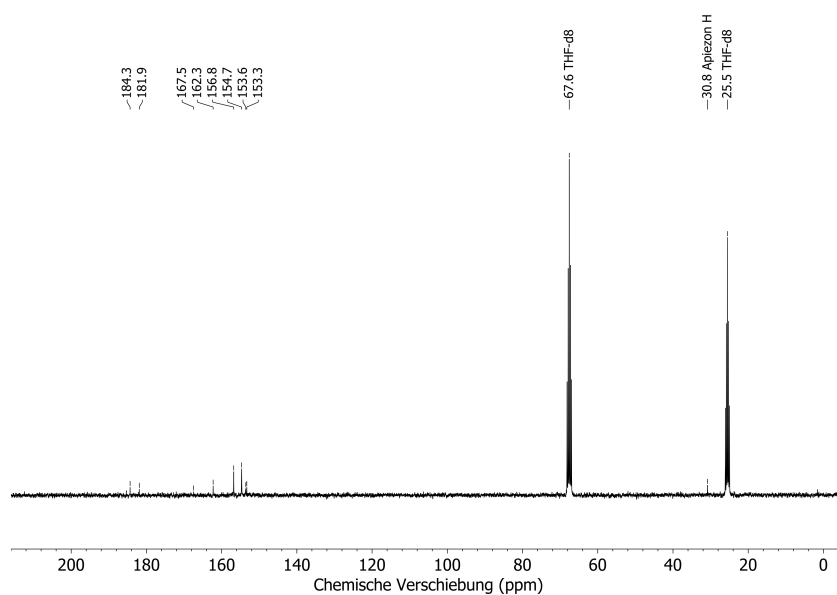
Abbildung 8.2: ^{13}C-NMR-Spektrum von Cl(CO)$_2$NCS aus der Reaktion von (COCl)$_2$ mit AgSCN in THF-d$_8$.
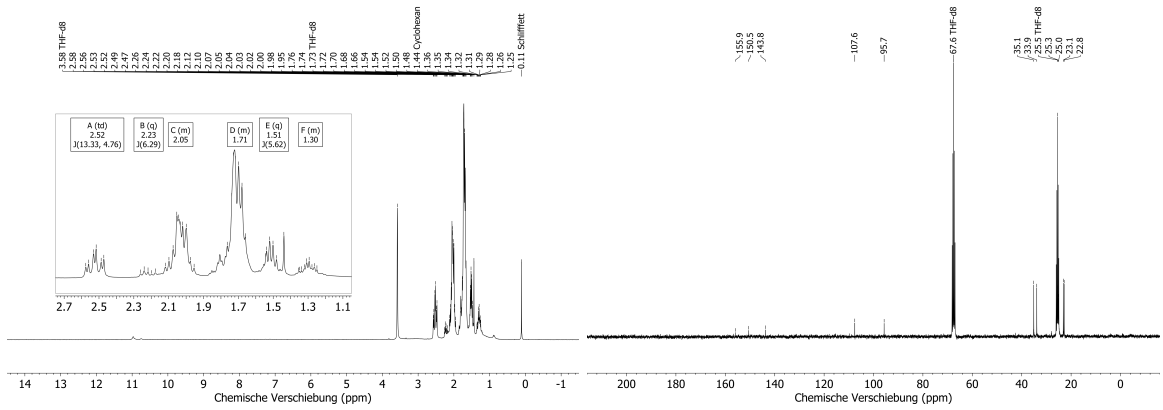
Abbildung 8.3: ^{1}H-NMR- (links) und ^{13}C{^{1}H}-NMR-Spektrum (rechts) des Produktes aus CO(NCO)$_2$ und Cyclohexanon.
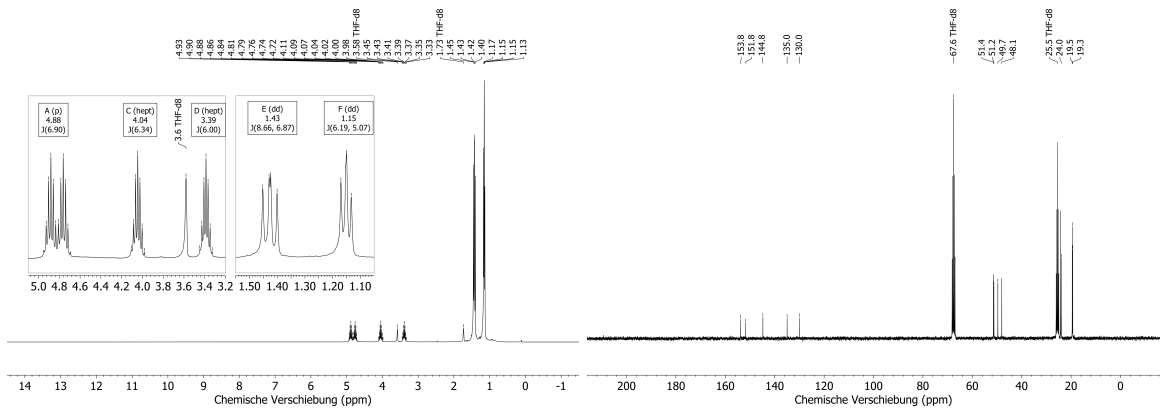
Abbildung 8.4: ^{1}H-NMR- (links) und ^{13}C{^{1}H}-NMR-Spektrum (rechts) des Produktes aus CO(NCO)$_2$ und *N,N'*-Dicyclohexylcarbodiimid.
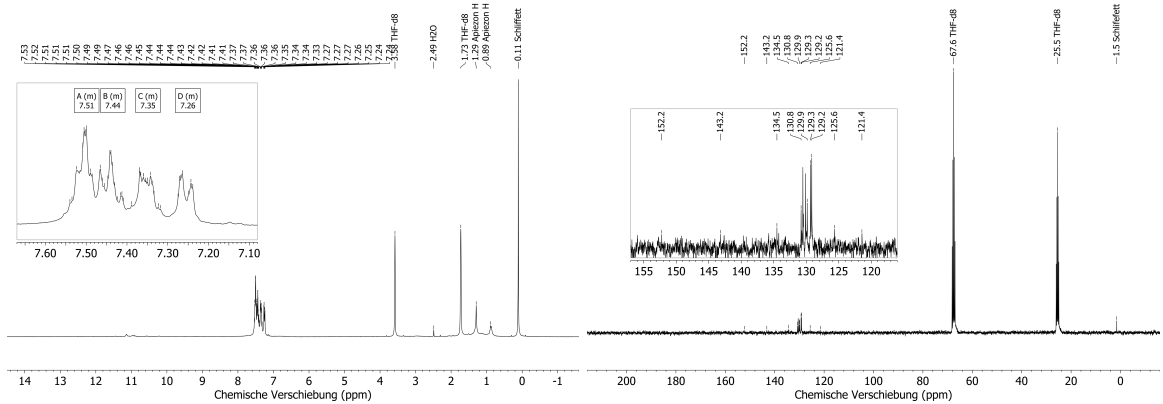

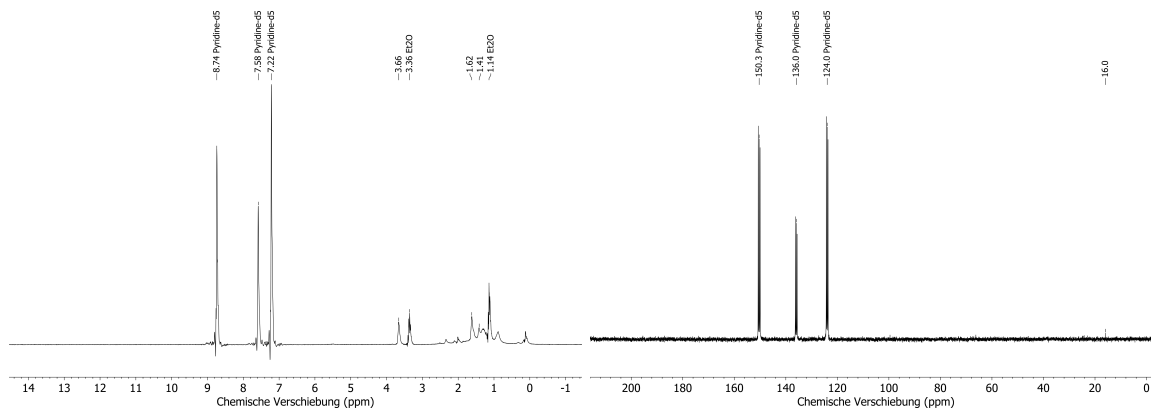**Abbildung 8.5:** ^{1}H-NMR- (links) und ^{13}C{^{1}H}-NMR-Spektrum (rechts) des Produktes aus CO(NCO)$_2$ und Phenylisocyanat.

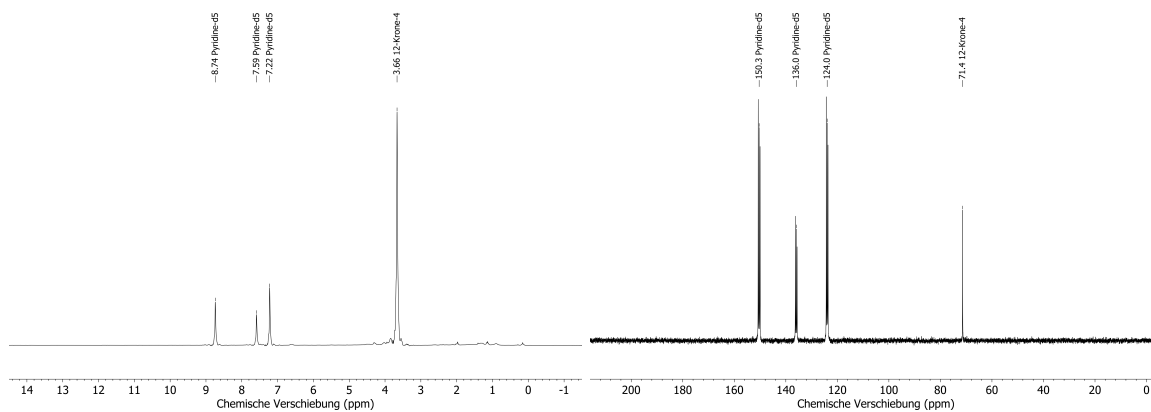**Abbildung 8.6:** ^{1}H-NMR- (links) und ^{13}C{^{1}H}-NMR-Spektrum (rechts) des Pulvers aus Reaktion **XVIIa**.

Abbildung 8.7: ^{1}H-NMR- (links) und ^{13}C{^{1}H}-NMR-Spektrum (rechts) des Pulvers aus Reaktion **XVIIb**.
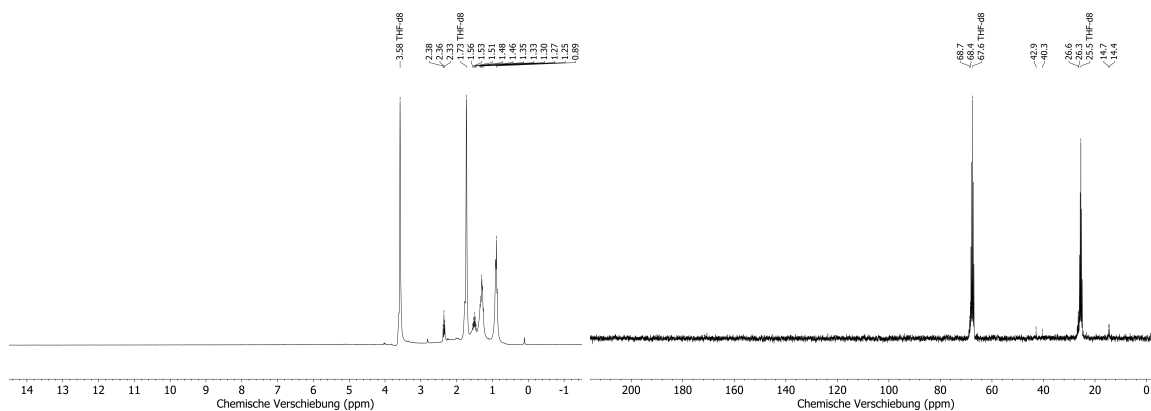
Abbildung 8.8: ^{1}H-NMR- (links) und ^{13}C{^{1}H}-NMR-Spektrum (rechts) des Pulvers aus Reaktion **XVIIIa**.
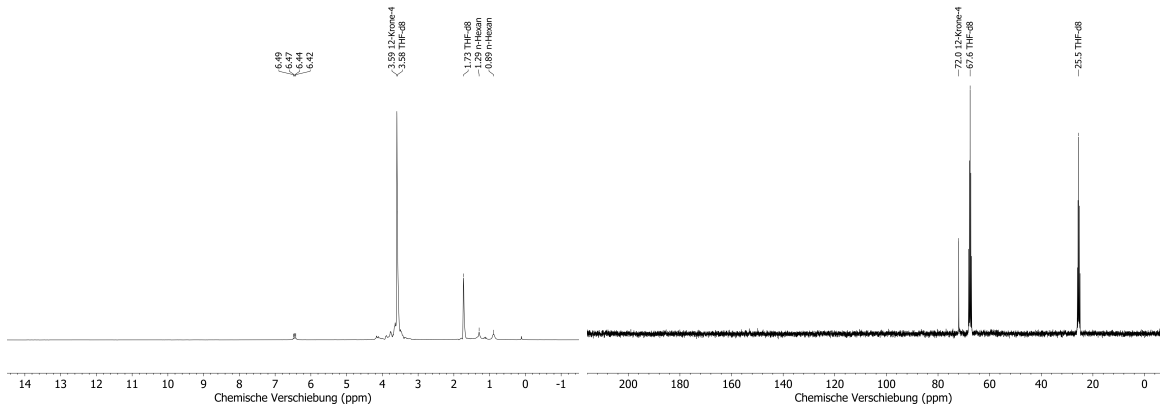
Abbildung 8.9: ^{1}H-NMR- (links) und ^{13}C{^{1}H}-NMR-Spektrum (rechts) des Pulvers aus Reaktion **XVIIIb**.
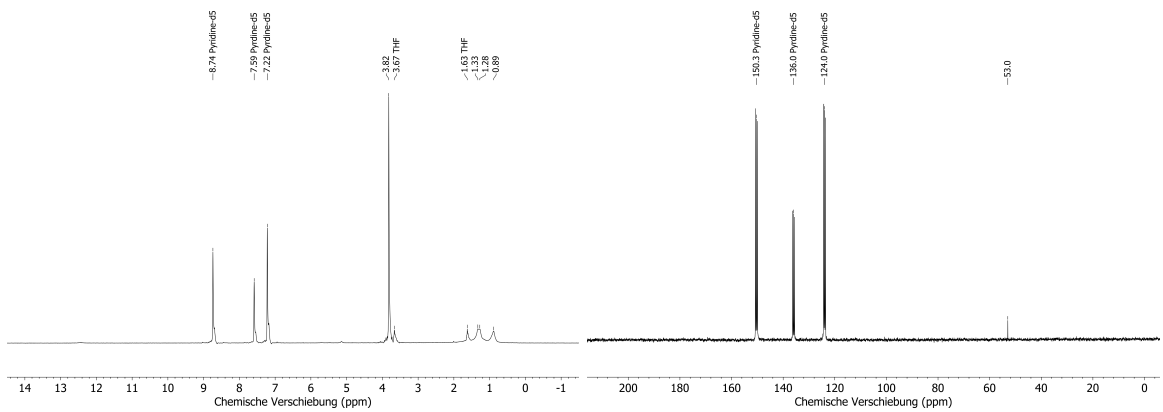
Abbildung 8.10: ^{1}H-NMR- (links) und ^{13}C{^{1}H}-NMR-Spektrum (rechts) des Pulvers aus Reaktion **XIXa**.
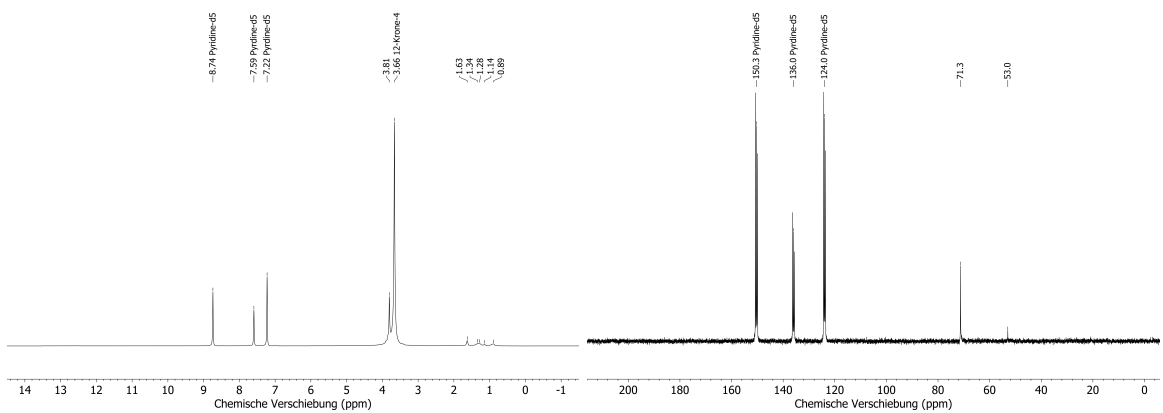
Abbildung 8.11: ^{1}H-NMR- (links) und ^{13}C{^{1}H}-NMR-Spektrum (rechts) des Pulvers aus Reaktion **XIXa**.
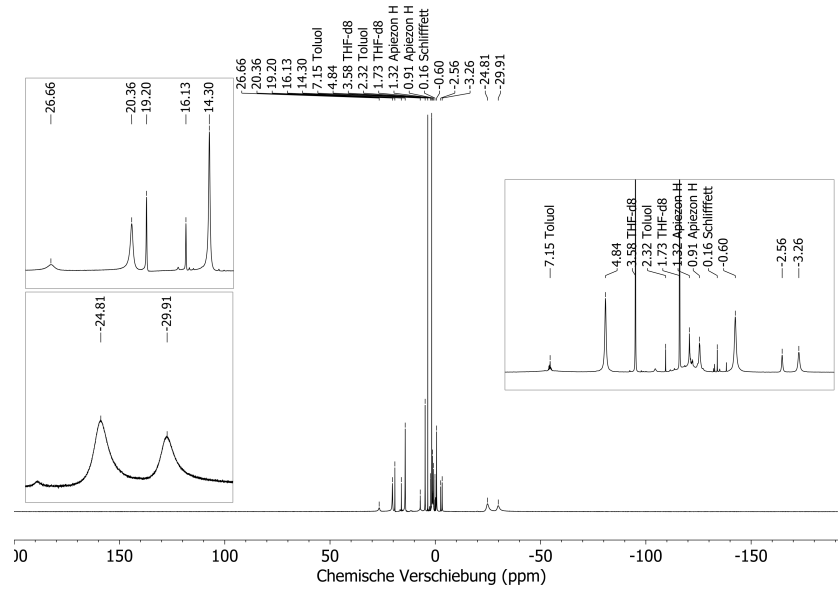
Abbildung 8.12: ^{1}H-NMR-Spektrum von Fe(DTCH)$_2$.
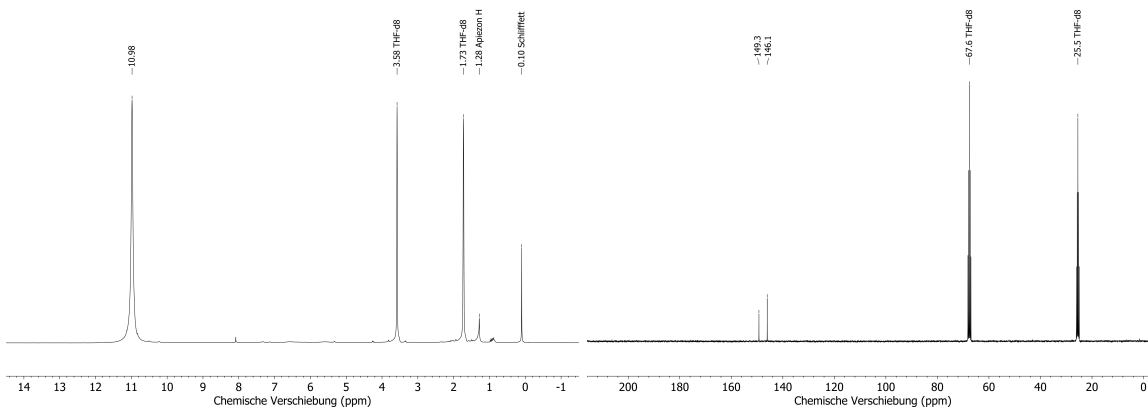
Abbildung 8.13: ^{1}H-NMR- (links) und ^{13}C{^{1}H}-NMR-Spektrum (rechts) von 2,4,6-Trioxo-1,3,5-oxadiazin.
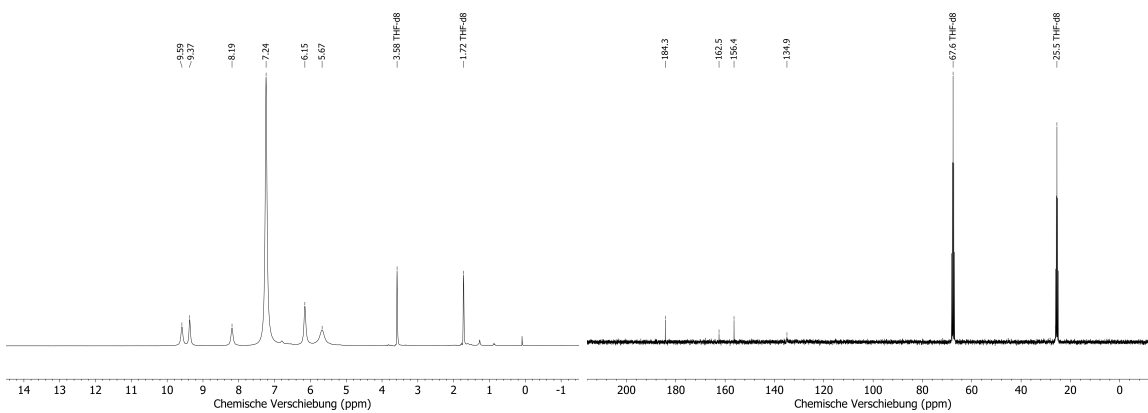
Abbildung 8.14: ^{1}H-NMR- (links) und ^{13}C{^{1}H}-NMR-Spektrum (rechts) von TIDC-DA×NH$_4$SCN.
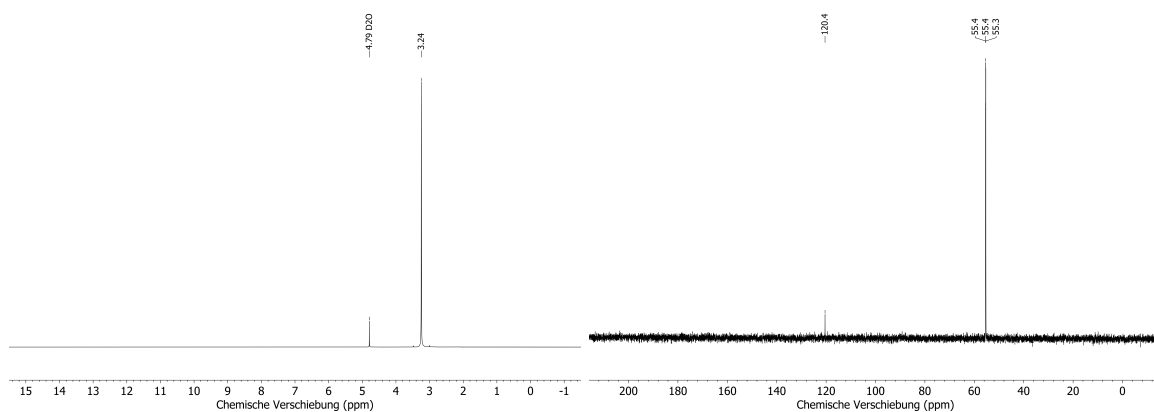
Abbildung 8.15: ^{1}H-NMR- (links) und ^{13}C{^{1}H}-NMR-Spektrum (rechts) von NMe$_4$SeCN.

8.2.2 Schwingungsspektren – IR und Raman
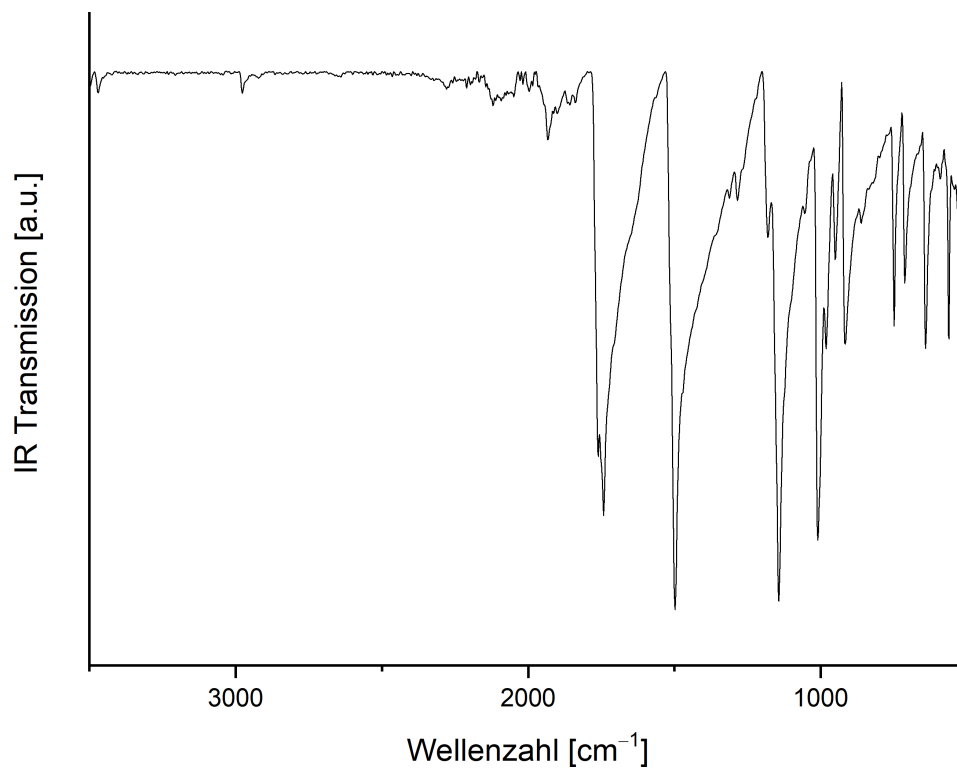
Abbildung 8.16: IR-Spektrum von 2-Chlorthiazol-4,5-dion.
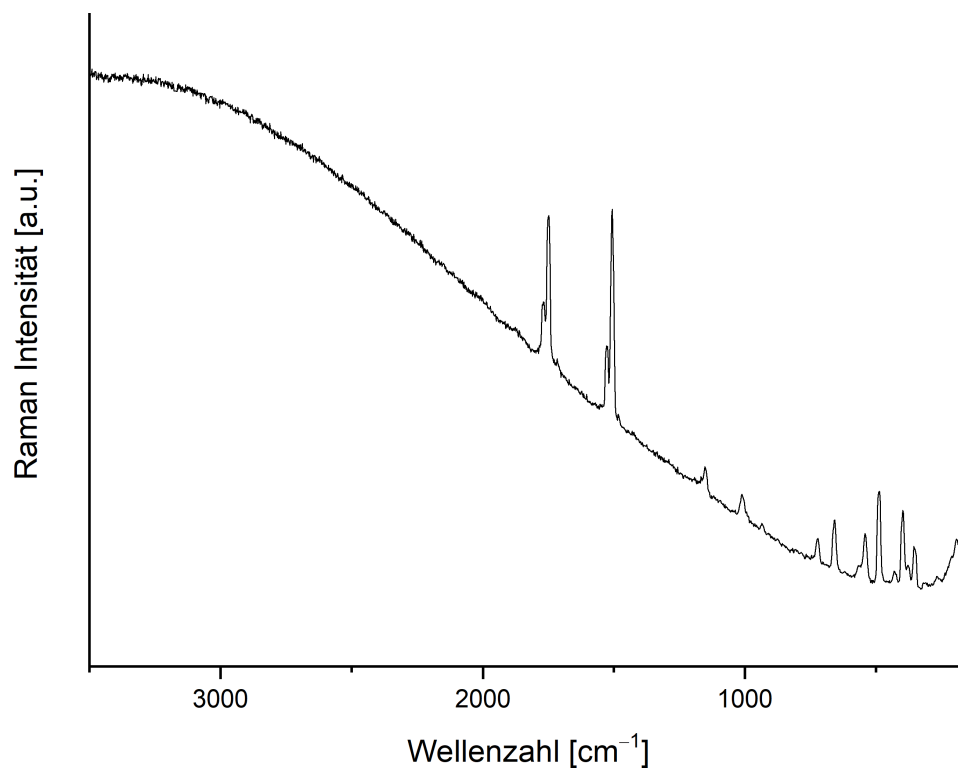
Abbildung 8.17: Raman-Spektrum von 2-Chlorthiazol-4,5-dion.

Abbildung 8.18: IR-Spektrum von Fe(DTCH)$_2$.
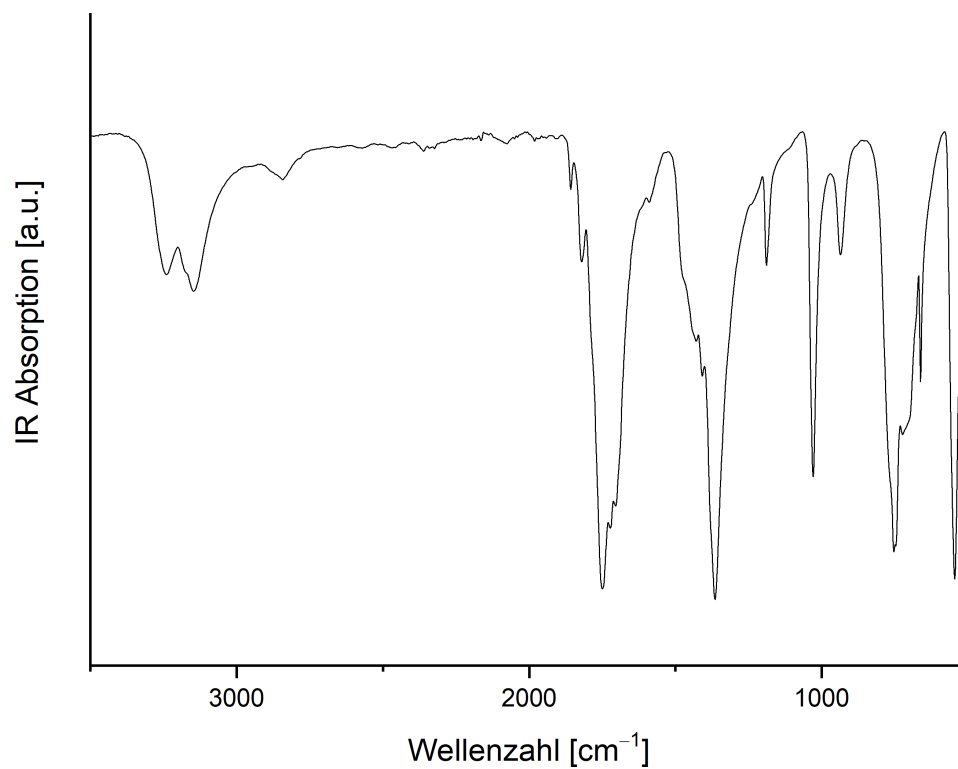
Abbildung 8.19: IR-Spektrum von 2,4,6-Trioxo-1,3,5-oxadiazin.
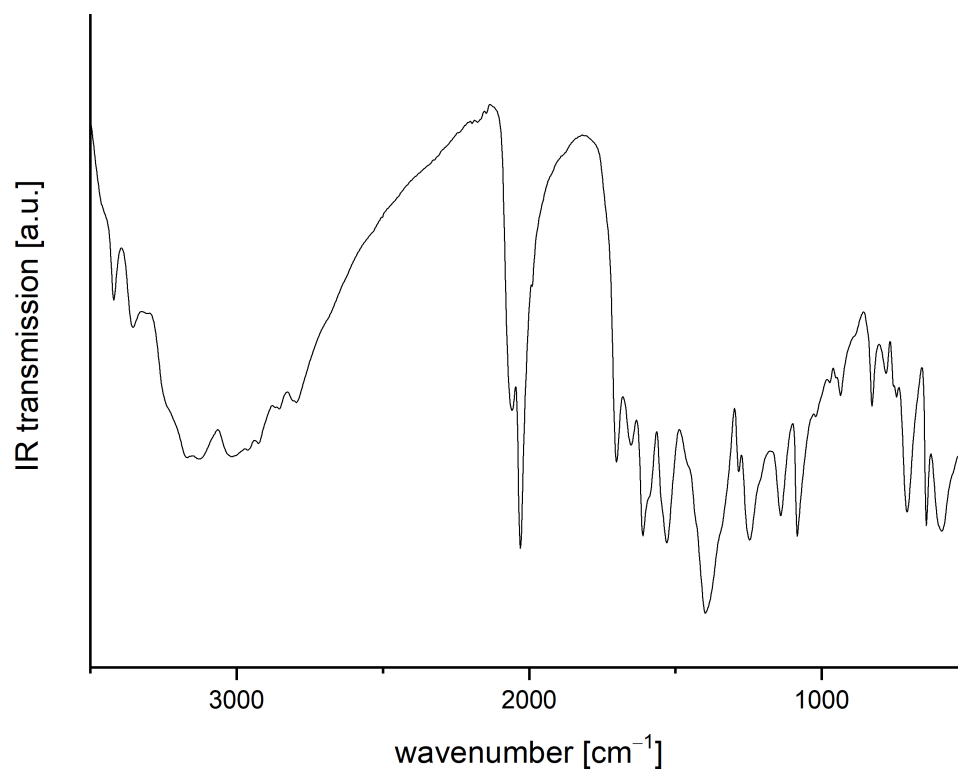
Abbildung 8.20: IR-Spektrum von TIDCDA×NH$_4$SCN.

8.2.3 Massenspektren

Data:240208_FD_138_Tm
Comment:
Description:
Ionization Mode:FD+
History:Average(MS[1] 3.01..3.05)

Acquired:13.02.2024 09:58:20
Operator:AccuTOF
m/z Calibration File:FD_Calib_082222_b
Created:00:00:00
Created by:

Charge number:1
Element:^{12}C:0 .. 10, ^{1}H:0 .. 10, ^{35}Cl:0 .. 2, ^{48}Ti:0 .. 1

Tolerance:5.00[ppm], 2.00 .. [mDa]
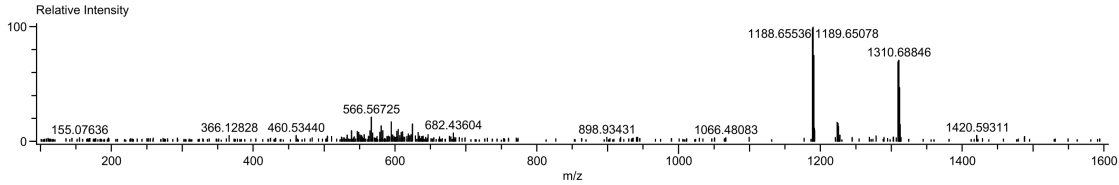
Unsaturation Number:-1.5 .. 50.0 (Fraction:Both)

Relative Intensity

155.07636 366.12828 460.53440 566.56725 682.43604 898.93431 1066.48083 1188.65536 1189.65078 1310.68846 1420.59311

m/z

Data:240208_FD_138_Tm
Comment:
Description:
Ionization Mode:FD+
History:Average(MS[1] 3.01..3.05)

Acquired:13.02.2024 09:58:20
Operator:AccuTOF
m/z Calibration File:FD_Calib_082222_b
Created:14.02.2024 09:56:51
Created by:Lorakis

Charge number:1
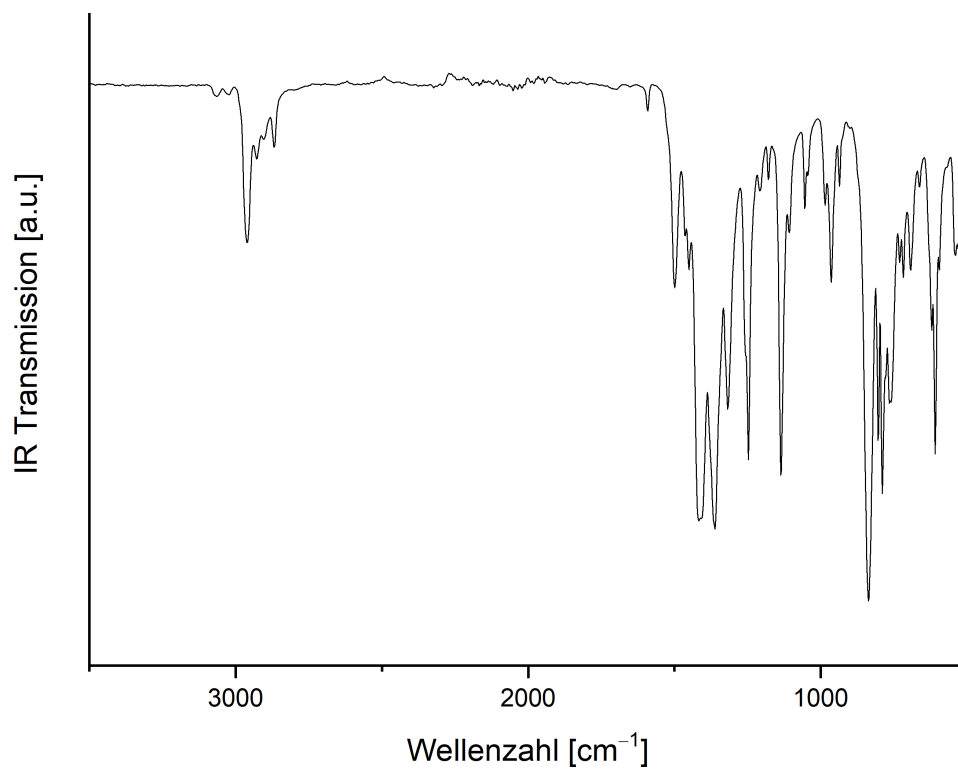Element:^{12}C:0 .. 64, ^{1}H:0 .. 104, ^{56}Fe:0 .. 1, ^{14}N:0 .. 6, ^{16}O:0 .. 4, ^{28}Si:0 .. 4

Tolerance:5.00[ppm], 2.00 .. [mDa]

Unsaturation Number:-1.5 .. 50.0 (Fraction:Both)

Relative Intensity

1186.67265 1188.65536 1189.65078 1191.64301

m/z
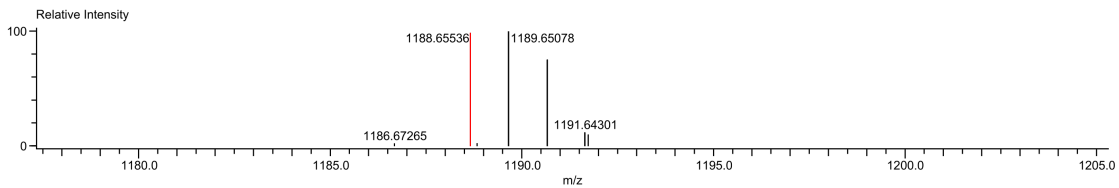
Composition:$C_{64}H_{104}FeN_6O_4Si_4$
Mono Isotopic Mass:1188.65455
Description:

Average Mass:1189.73560

Created:14.02.2024 09:56:53
Nominal Mass:1188
Created by:Lorakis
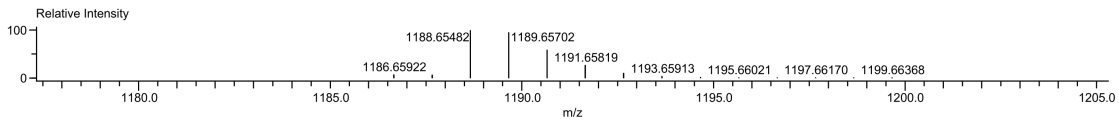
Relative Intensity

1186.65922 1188.65482 1189.65702 1191.65819 1193.65913 1195.66021 1197.66170 1199.66368

m/z

Mass	Intensity	Relative Intensity	Calc. Mass	Mass Difference [mDa]	Mass Difference [ppm]	Possible Formula	Unsaturation Number
1188.65536	3417.20	97.96	1188.65455	0.81	0.68	$^{12}C_{64}{}^{1}H_{104}{}^{56}Fe_1{}^{14}N_6{}^{16}O_4{}^{28}Si_4$	20.5

Abbildung 8.21: Vollständiges Massenspektrum inklusive des hochaufgelösten Signals von Fe(DTCH)$_2$.

Data:230203_FD_073_Tm_c
Comment:
Description:
Ionization Mode:FD+
History:Average(MS[1] 0.81..0.85)

Acquired:09.02.2023 10:21:36
Operator:AccuTOF
m/z Calibration File:FD_Calib_082222_b
Created:00:00:00
Created by:

Charge number:1
Element:^{12}C:0 .. 7, ^{1}H:0 .. 18, ^{14}N:0 .. 5, ^{31}P:0 .. 1

Tolerance:5.00[ppm], 2.00 .. [mDa]
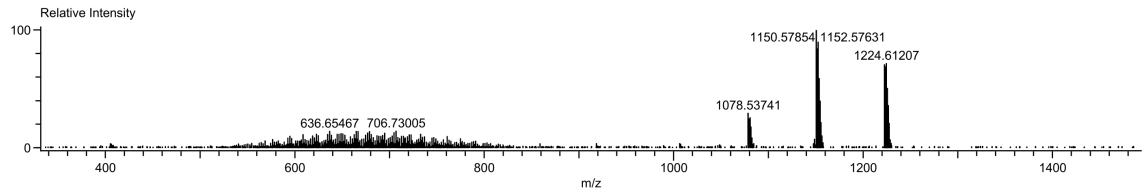
Unsaturation Number:-1.5 .. 50.0 (Fraction:Both)

Relative Intensity

100

636.65467 706.73005

1078.53741

1150.57854 1152.57631
1224.61207

0

400   600   800   1000   1200   1400

m/z

Data:230203_FD_073_Tm_c
Comment:
Description:
Ionization Mode:FD+
History:Average(MS[1] 0.81..0.85)

Acquired:09.02.2023 10:21:36
Operator:AccuTOF
m/z Calibration File:FD_Calib_082222_b
Created:09.02.2023 15:04:08
Created by:Lorakis

Charge number:1
Element:^{12}C:0 .. 64, ^{1}H:0 .. 104, ^{14}N:0 .. 6, ^{58}Ni:0 .. 1, ^{16}O:0 .. 2, ^{32}S:0 .. 2, ^{28}Si:0 .. 4

Tolerance:5.00[ppm], 2.00 .. [mDa]

Unsaturation Number:-1.5 .. 50.0 (Fraction:Both)

Relative Intensity

100

1220.61229 1221.70220

1222.61211 1223.61346 1224.61207

1224.15467

1225.61337
1226.61299

1227.60464
1228.59550 1229.60107

0

1220.0   1222.0   1224.0   1226.0   1228.0   1230.0   1232.0

m/z
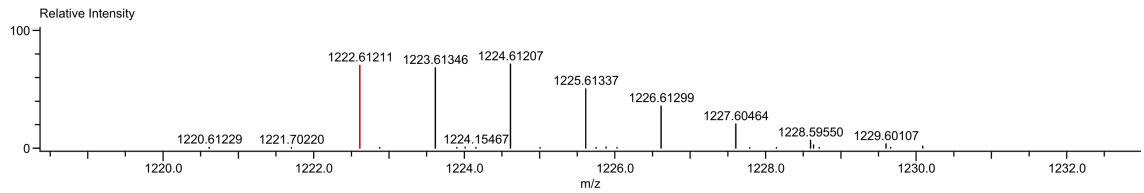
Composition:C$_{64}$H$_{104}$N$_6$NiO$_2$S$_2$Si$_4$
Mono Isotopic Mass:1222.60927
Description:

Average Mass:1224.71720

Created:09.02.2023 15:04:11
Nominal Mass:1223
Created by:Lorakis
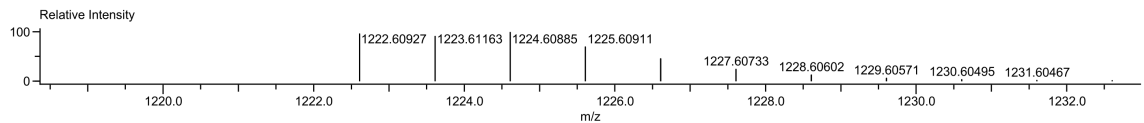
Relative Intensity

100

1222.60927 1223.61163 1224.60885 1225.60911

1227.60733
1228.60602 1229.60571 1230.60495 1231.60467

0

1220.0   1222.0   1224.0   1226.0   1228.0   1230.0   1232.0

m/z

Mass	Intensity	Relative Intensity	Calc. Mass	Mass Difference [mDa]	Mass Difference [ppm]	Possible Formula	Unsaturation Number
1222.61211	8008.10	70.30	1222.60927	2.85	2.33	^{12}C$_{64}$^{1}H$_{104}$^{14}N$_6$^{58}Ni$_1$^{16}O$_2$^{32}S$_2$^{28}Si$_4$	22.5

Abbildung 8.22: Vollständiges Massenspektrum inklusive des hochaufgelösten Signals von der Umsetzung aus CO(NCS)$_2$ mit Ni(N(Dipp)(TMS))$_2$.
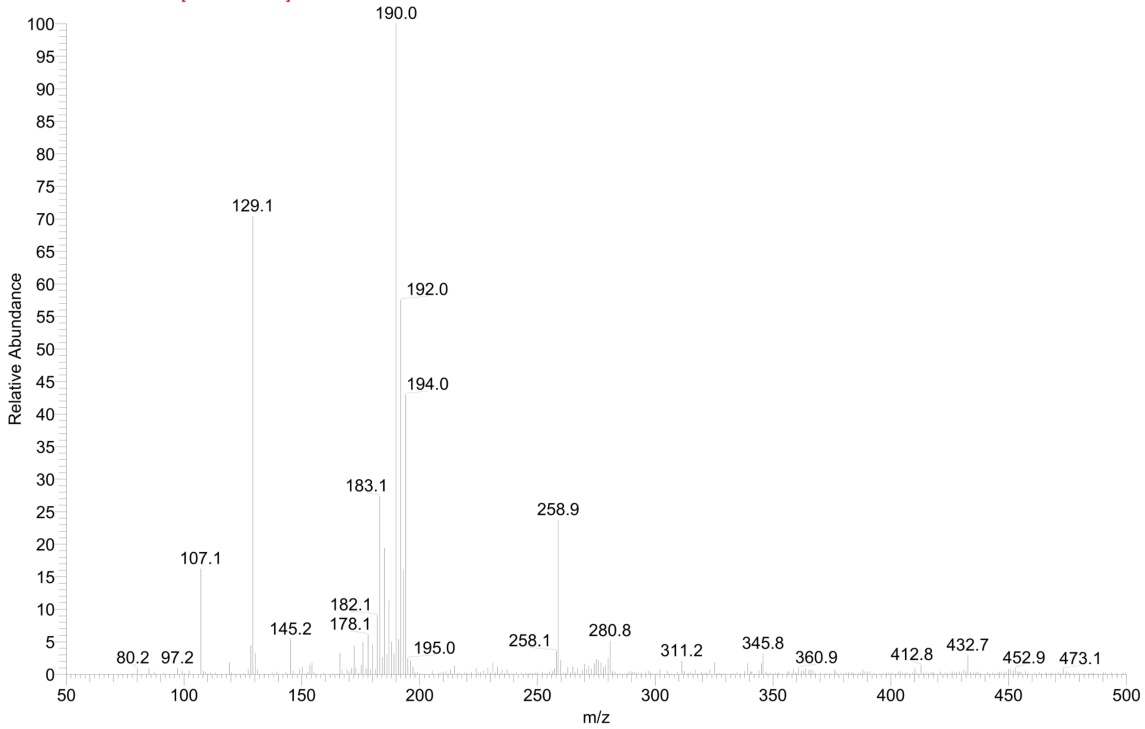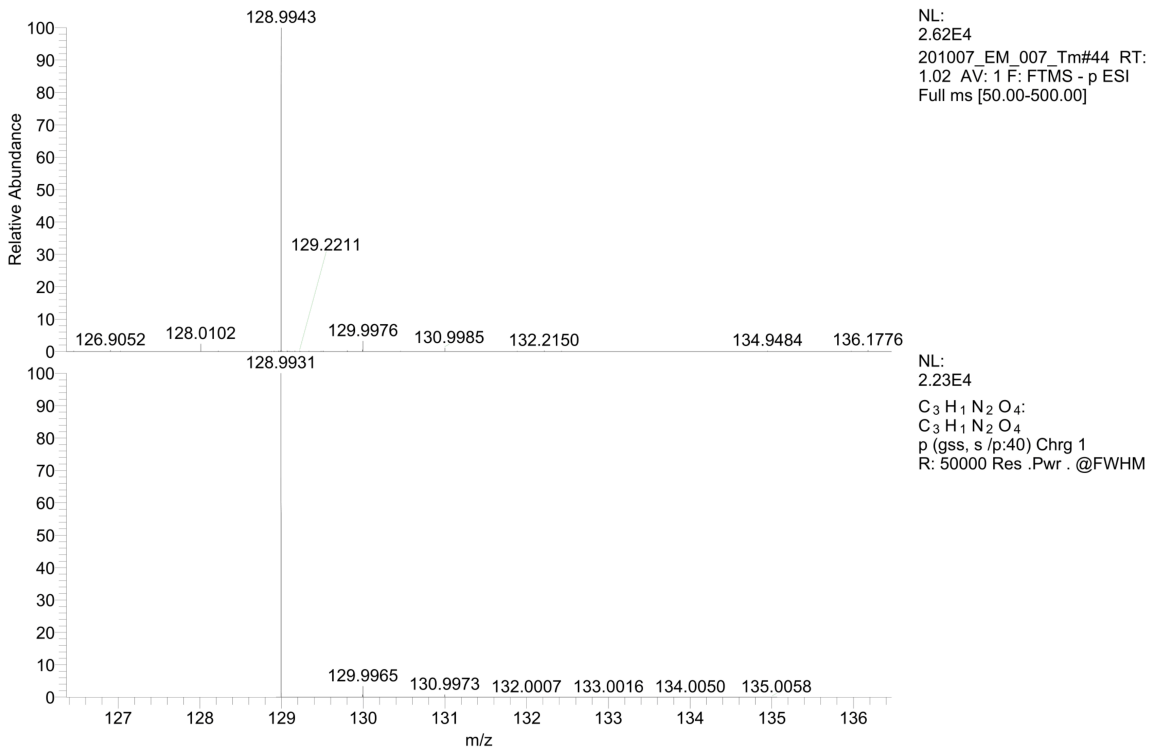
Abbildung 8.23: Vollständiges Massenspektrum inklusive des hochaufgelösten Signals von 2,4,6-Trioxo-1,3,5-oxadiazin.

8.2.4 Kristallographische Daten

Abbildung 8.24: Verknüpfung von ICS-CONEt$_2$ (links) und ICS-COSPh (rechts) über Wasserstoffbrückenbindungen zu benachbarten Molekülen im Festkörper. Ein Molekül ist zur Deutlichkeit grün hervorgehoben.

Tabelle 8.1: Parameter der Strukturverfeinerung von 2-Chlorthiazol-4,5-dion, Fe(DTCH)$_2$, 2,4,6-Trioxo-1,3,5-oxadiazin und ICS-CONEt$_2$.

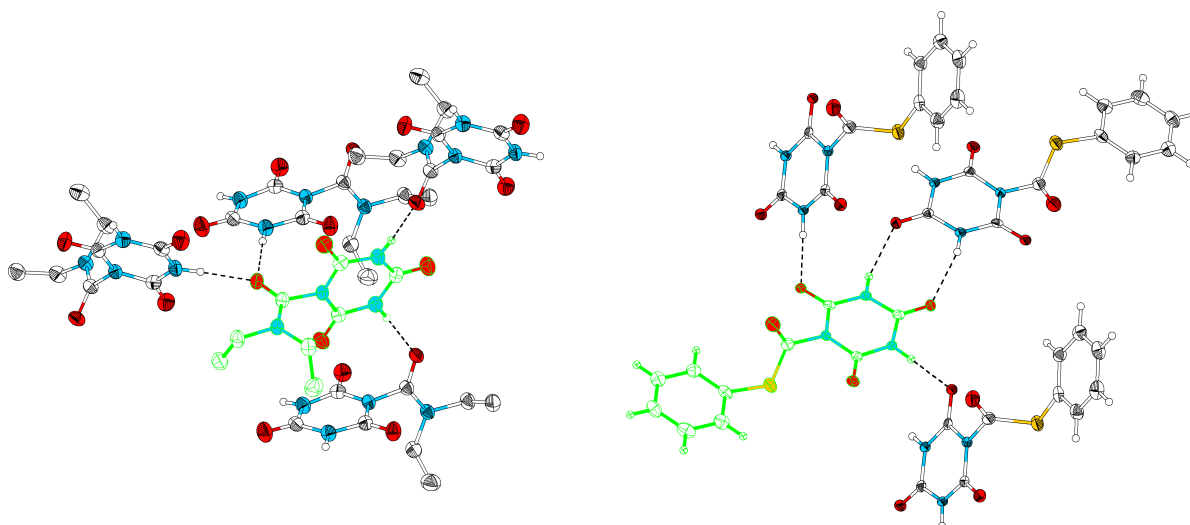| Molekül	2-Chlorthiazol-4,5-dion	Fe(DTCH)$_2$	2,4,6-Trioxo-1,3,5-oxadiazin	ICS-CONEt$_2$
Summenformel	C$_3$ClNO$_2$S	C$_{64}$H$_{104}$FeN$_6$O$_4$Si$_4$	C$_3$H$_2$N$_2$O$_4$	C$_8$H$_{12}$N$_4$O$_4$
Molekulargewicht / g mol^{-1}	149.55	1189.74	130.07	228.22
Temperatur / K	100	100	100	100
Kristallsystem	monoklin	monoklin	orthorhombisch	orthorhombisch
Raumgruppe	P2$_1$/n	C2/c	Pnma	P2$_1$2$_1$2$_1$
a / Å	5.8002(2)	31.9731(11)	8.0350(8)	7.536(3)
b / Å	6.3811(2)	9.8071(5)	11.9026(10)	9.971(3)
c / Å	13.5134(5)	23.2858(8)	4.8887(5)	13.053(5)
α / °	90	90	90	90
β / °	98.753(3)	105.638(3)	90	90
γ / °	90	90	90	90
V / Å^3	494.33(3)	7031.3(5)	467.54(8)	980.9(6)
Z	4	4	4	4
ρ / g cm^{-3}	2.009	1.124	1.848	1.545
μ / mm^{-1}	9.921	0.329	1.568	1.075
F(000)	296.0	2576.0	264.0	480.0
Strahlung, λ / Å	1.54186	0.71073	1.54186	1.54186
2Θ Reichweite / °	13.258 – 149.4	3.632 – 58.296	26.066 – 134.938	11.166 – 139.888
Index Reichweite	$-7 \leq h \leq 6$	$-43 \leq h \leq 43$	$-8 \leq h \leq 9$	$-9 \leq h \leq 9$
	$-7 \leq k \leq 3$	$-13 \leq k \leq 13$	$-14 \leq k \leq 14$	$-11 \leq k \leq 12$
	$-16 \leq l \leq 16$	$-31 \leq l \leq 28$	$-4 \leq l \leq 5$	$-15 \leq l \leq 14$
gemessene Reflexe	9193	35788	3078	11027
unabhängige Reflexe	9729	9446	368	1802
Daten / Parameter	9729 / 74	9446 / 371	368 / 47	1802 / 147
R$_{int}$ / R$_\sigma$	0.0272 / 0.0139	0.0717 / 0.1062	0.0921 / 0.0424	0.0485 / 0.0397
R$_1$ / wR$_2$ [I$\geq$2σ (I)]	0.0323 / 0.0898	0.0388 / 0.0798	0.1702 / 0.3874	0.0338 / 0.0946
R$_1$ / wR$_2$ [Alle Daten]	0.0340 / 0.0908	0.0889 / 0.0852	0.2119 / 0.4211	0.0466 / 0.0990
Goodness-of-fit	1.051	0.817	1.850	0.991
Restelektronendichte / e Å^{-3}	0.66 / −0.37	0.36 / −0.19	1.85 / −1.24	0.19 / −0.15
Zwillingsgesetz	−	−	−	−
BASF	−	−	−	−
Flack Parameter	−	−	−	0.04(16)

Tabelle 8.2: Parameter der Strukturverfeinerung von ICS-COSPh, CDA-CSSBz, IDCDA-iPr, ICS-IDCDA, TIDCDA×NH₄SCN und NMe₄SeCN.

Molekül	ICS-COSPh	CDA-CSSBz	IDCDA-iPr	ICS-IDCDA	TIDCDA×NH₄SCN	NMe₄SeCN
Summenformel	$C_{10}H_7N_3O_4S$	$C_9H_{10}N_2OS_2$	$C_{14}H_{29}N_3O_2$	$C_{10}H_{18}N_{12}O_{11}$	$C_3H_9N_5OS_2$	$C_5H_{12}N_2Se$
Molekulargewicht / g mol⁻¹	265.25	226.31	271.40	482.36	195.27	179.13
Temperatur / K	100	100	100	100	100	100
Kristallsystem	monoklin	monoklin	orthorhombisch	triklin	monoklin	monoklin
Raumgruppe	$P2_1/c$	$P2_1/n$	$Pbca$	$P\bar{1}$	$P2_1/n$	$P2_1/c$
a / Å	11.070(2)	4.6898(4)	12.3349(13)	8.260(4)	6.5186(3)	7.8656(5)
b / Å	8.3106(13)	34.396(2)	10.7196(11)	10.905(4)	14.0737(4)	8.6002(4)
c / Å	11.778(3)	6.5734(6)	24.619(4)	11.919(5)	9.4589(4)	11.9513(8)
α / °	90	90	90	67.17(3)	90	90
β / °	92.652(17)	104.748(7)	90	79.78(3)	94.167(3)	95.374(5)
γ / °	90	90	90	69.80(3)	90	90
V / Å³	1082.4(4)	1025.42(15)	3255.3(7)	927.4(7)	865.47(6)	804.90(8)
Z	4	4	8	2	4	4
ρ / g cm⁻³	1.628	1.466	1.108	1.727	1.499	1.478
μ / mm⁻¹	2.812	0.486	0.591	0.155	5.262	4.579
F(000)	544.0	472.0	1200.0	500.0	408.0	360.0
Strahlung, λ / Å	1.54186	0.71073	1.54186	0.71073	1.54186	0.71073
2Θ Reichweite / °	7.996 – 139.258	6.518 – 58.254	7.182 – 134.976	3.712 – 58.352	11.292 – 139.304	4.736 – 63.362
Index Reichweite	$-13 \leq h \leq 13$; $-9 \leq k \leq 6$; $-14 \leq l \leq 14$	$-6 \leq h \leq 6$; $-46 \leq k \leq 46$; $-8 \leq l \leq 8$	$-11 \leq h \leq 14$; $-6 \leq k \leq 12$; $-29 \leq l \leq 29$	$-11 \leq h \leq 11$; $-14 \leq k \leq 14$; $-16 \leq l \leq 14$	$-7 \leq h \leq 7$; $-8 \leq k \leq 16$; $-11 \leq l \leq 11$	$-11 \leq h \leq 11$; $-11 \leq k \leq 12$; $-17 \leq l \leq 17$
gemessene Reflexe	14585	8288	62776	11431	13367	30450
unabhängige Reflexe	15164	2762	73213	4872	1620	2757
Daten / Parameter	15164 / 163	2762 / 128	73213 / 181	4872 / 303	1620 / 132	2757 / 78
Rint / Rσ	0.0455 / 0.0390	0.0426 / 0.0611	0.0596 / 0.0250	0.2457 / 0.4413	0.0533 / 0.0332	0.0604 / 0.0314
R₁ / wR₂ [I>2σ (I)]	0.0442 / 0.1296	0.0398 / 0.0909	0.0463 / 0.1187	0.1004 / 0.2289	0.0287 / 0.0680	0.0463 / 0.1182
R₁ / wR₂ [Alle Daten]	0.0598 / 0.1340	0.0743 / 0.0997	0.0588 / 0.1228	0.4000 / 0.3595	0.0418 / 0.0721	0.0792 / 0.1431
Goodness-of-fit	1.083	0.901	0.941	0.810	0.964	1.146
Restelektronendichte / e Å⁻³	0.46 / -0.46	0.28 / -0.37	0.20 / -0.19	0.45 / -0.47	0.33 / -0.24	1.54 / -1.19
Zwillingsgesetz	–	–	–	–	–	-1 0 0 0 -1 0 0.285 0 1
BASF	–	–	–	–	–	0.05376
Flack Parameter	–	–	–	–	–	–

8.2.5 Details zu quantenchemischen Berechnungen

Tabelle 8.3: Gitterparameter und Atompositionen der optimierten Struktur von 2-Chlorthiazol-4,5-dion. Die Raumgruppe wurde zur Berechnung mit *CRYSTAL17* von $P12_1/n$ in $P12_1/c1$ mit a = 13.5408 Å, b = 6.3843 Å, c = 13.9082 Å und β = 155.62° transformiert.

Gitterparameter		
a	*b*	*c*
14.22138353	6.20324307	15.05155583
α	β	γ
90	156.081335	90

Atom	*x*	*y*	*z*
Cl1	–0.237 84	–0.152 81	0.22904
S2	0.20654	–0.375 64	–0.413 32
O3	–0.469 57	–0.422 02	–0.260 87
O4	0.26937	–0.130 54	0.40669
N5	0.00318	–0.120 89	0.29129
C6	–0.010 78	–0.203 35	0.35650
C7	0.20561	–0.186 15	0.42333
C8	0.35232	–0.343 40	–0.392 13

Tabelle 8.4: Zuordnung der berechneten IR Schwingungsbanden von 2-Chlorthiazol-4,5-dion. Die irreduziblen Darstellungen werden für die Punktgruppen der jeweiligen Raumgruppentypen der Kristallstrukturen angegeben.

ν (ber.) [cm^{-1}]	ν (gem.) [cm^{-1}]	Irrep.	Zuordnung
479		*Bu*	ν_s(C2−S1) Streckschwingung
484		*Au*	
548	528	*Au*	δ(O1=C1−C2=O2) Pendelschwingung
550		*Bu*	
580	560	*Au*	δ(N1−C3) Torsionsschwingung
580		*Bu*	
660	640	*Bu*	ν_s(C3−S1) Streckschwingung
662		*Au*	
736	712	*Au*	ν_as(N1−C1−C2) Pendelschwingung
740		*Bu*	
761	748	*Au*	δ(C1−C2) Torsionsschwingung
766		*Bu*	
950	915	*Bu*	ν_s(C1−C2) Streckschwingung
957		*Au*	
1031	1009	*Bu*	ν_s(C2−S1−C3) Streckschwingung
1037		*Au*	
1192	1142	*Au*	ν_s(N1−C1) Streckschwingung
1193		*Bu*	
1581	1496	*Bu*	ν_s(N1=C3) Streckschwingung
1589		*Au*	
1867	1740	*Au*	synchrone ν_s(C1=O1) & ν_s(C2=O2) Streckschwingung
1871		*Bu*	ν_s(C2=O2) Streckschwingung
1884	1760	*Au*	asynchrone ν_s(C1=O1) & ν_s(C2=O2) Streckschwingung
1886		*Bu*	ν_s(C1=O1) Streckschwingung

Tabelle 8.5: Zuordnung der berechneten Raman Schwingungsbanden von 2-Chlorthiazol-4,5-dion. Die irreduziblen Darstellungen werden für die Punktgruppen der jeweiligen Raumgruppentypen der Kristallstrukturen angegeben.

ν (ber.) [cm^{-1}]	ν (gem.) [cm^{-1}]	Irrep.	Zuordnung
258	194	*Ag*	Pendelschwingung des gesamten Moleküls
260		*Bg*	
351	270	*Ag*	δ(O1=C1−C2=O2) Spreizschwingung
358		*Bg*	
398	355	*Ag*	ν_s(C3−Cl1) Streckschwingung kombiniert mit
400		*Bg*	ν_{as}(C3−S1−C2) Streckschwingung
433	398	*Ag*	δ(C1−C2) Kippschwingung
439		*Bg*	
483	428	*Bg*	ν_s(C2−S1) Streckschwingung
486		*Ag*	
549	488	*Ag*	δ(O1=C1−C2=O2) Pendelschwingung
550		*Bg*	
579	540	*Ag*	δ(N1−C3) Torsionsschwingung
580		*Bg*	
660	nicht	*Bg*	ν_s(C3−S1) Streckschwingung
662	gem.	*Ag*	
735	660	*Ag*	ν_{as}(N1−C1−C2) Pendelschwingung
741		*Bg*	
761	722	*Ag*	δ(C1−C2) Torsionsschwingung
766		*Bg*	
956	935	*Ag*	ν_s(C1−C2) Streckschwingung
957		*Bg*	
1024	1009	*Bg*	ν_s(C2−S1−C3) Streckschwingung
1028		*Ag*	
1187	1151	*Ag*	ν_s(N1−C1) Streckschwingung
1206		*Bg*	
1586	1506	*Ag*	ν_s(N1=C3) Streckschwingung
1612	1527	*Bg*	
1868	1478	*Ag*	synchrone ν_s(C1=O1) & ν_s(C2=O2) Streckschwingung
1878		*Bg*	asynchrone ν_s(C1=O1) & ν_s(C2=O2) Streckschwingung
1885	1769	*Ag*	asynchrone ν_s(C1=O1) & ν_s(C2=O2) Streckschwingung
1904		*Bg*	synchrone ν_s(C1=O1) & ν_s(C2=O2) Streckschwingung

8.3 Publikationsliste

Die in dieser Arbeit enthaltenen Publikationen sind durch fett gedruckte Nummerierung gekennzeichnet.

[8] *Rotational Conformers and Nuclear Spin Isomers of Carbonyl Diisothiocyanate*

E. Gougoula, J. Pfeiffer, F. Tambornino, M. Schnell, *submitted.*

[7] *Thiocarbonyl pseudohalides – the curious case of thiocarbonyl dithiocyanate*

J. Pfeiffer, H. Günther, P. Fuzon, F. Weigend, F. Tambornino, *submitted.*

[6] *Intra- and Intermolecular Hydrogen Bonding in N,N'-Carbonyl bis(carbamates), -(S-thiocarbamates) and N,N'-biscarbamoyl ureas*

J. Pfeiffer, M. Möbs, S. Reith, M. Tallu, F. Tambornino, *J. Mol. Struct.* **2024**, *1309*, 138198.

[5] *Synthesis, Crystal Structure Study and Spectroscopic Analysis of Substituted 2,3-dihydro-2-thioxo-4H-1,3,5-thiadiazin-4-ones*

J. Pfeiffer, C. Trost, F. Tambornino, *J. Mol. Struct.* **2024**, *1308*, 138079.

[4] *Photolytic Decarbonylation of Oxalyl Diisothiocyanate in Solid Argon Matrices to syn-anti Carbonyl Diisothiocyanate and Its Isomerization*

J. Pfeiffer, J. P. Wagner, F. Tambornino, *Eur. J. Inorg. Chem.* **2023**, *26*, e202300290.

[3] *Double Addition vs. Ring Closure: Systematic Reactivity Study of CO(NCO)$_2$ and CO(NCS)$_2$ towards Hydrogen Halides*

J. Pfeiffer, H. Günther, L. Völlinger, D. Botros, B. Scheibe, M. Möbs, F. Kraus, F. Weigend, F. Tambornino, *Chem. Eur. J.* **2023**, e202203983.

[2] *A Crystallographic, Spectroscopic, and Computational Investigation of Carbonyl and Oxalyl Diisothiocyanate*

J. Pfeiffer, C. Trost, A. Pachkovska, F. Tambornino, *Inorg. Chem.* **2021**, *60*, 10722-10728.

[1] *C-Halide bond cleavage by a two-coordinate iron(I) complex*

C. G. Werncke, J. Pfeiffer, I. Müller, L. Vendier, S. Sabo-Etienne, S. Bontemps, *Dalton Trans.* **2019**, *48*, 1757-1765.

8.4 Wissenschaftlicher Lebenslauf

517

8.4 Wissenschaftlicher Lebenslauf

Danksagung

Zuerst möchte ich der Prüfungskommission bestehend aus Dr. Frank Tambornino, Prof. Dr. Crispin Lichtenberg, Prof. Dr. Paultheo von Zezschwitz und Prof. Dr. Wolf-Christian Pilgrim für die Übernahme der Prüfung danken. Dr. Tambornino und Prof. Dr. Lichtenberg gilt ein besonderer Dank für die Übernahme der schriftlichen Gutachten.

Den Serviceabteilungen des Fachbereichs Chemie (NMR-Spektroskopie, Kristallstruktur-analyse, Massenspektrometrie und Elementanalytik) möchte ich hiermit für all die wichtigen Messungen, ohne die niemals die Ergebnisse dieser Dissertation zustande gekommen wären, danken. Danke für eure Mühen und vor allem die Wartung aller Geräte. Den Werkstätten der Feinmechanik, Elektronik und Glasapparatebau gilt ein großer Dank für die Reparatur ständig defekter Geräte und die Anfertigung neuer Geräte. Zuletzt möchte ich den Mitgliedern der Wirtschaftsverwaltung für ein reibungslosen Ablauf und die Bearbeitung aller anfallenden bürokratischen Aufgaben danken.

Meine Promotion wäre ebenfalls unmöglich gewesen ohne das Kekulé-Stipendium des Fonds der Chemischen Industrie. Danke für Euer Geld!

Ein ganz besonderer Dank gilt dir Frank. Du hast mir vor 4 Jahren angeboten aus deinem Arbeitspunkt eine Arbeitslinie zu bilden, welche sich inzwischen zu einem vollen Arbeitskreis gebogen hat. Gemeinsam haben wir uns auf die Reise zu unbekannten Carbonylen begeben. Ich bin dir dankbar, dass du mir stets dein Vertrauen und die Freiheit gegeben hast dein herausforderndes und spannendes Forschungsthema zu entdecken und weiterzuentwickeln. Auf dem Weg zum Gipfel der Carbonylpseudohalogenide gab es einige (Seleno-)Schluchten, welche es zu bezwingen galt. Dank dir konnte ich diesen ersten Gipfel erreichen. Auch wenn dein Weg zum letzten Gipfel noch lang ist, bin ich stolz dich auf der ersten Etappe begleitet zu haben. Vielen Dank Frank!

Ein großer Dank gilt meinen Kolleg*innen (Mitarbeitern *hust, hust*). Ich danke vor allem dir Alena für die gemeinsame Zeit im Labor. Unsere Zusammenarbeit war immer sehr angenehm, nie langweilig und meist spaßig. Ich habe dir gerne die musikalische Welt der 90er eröffnet. Zudem möchte ich Lachs und Schinken *aka* Hennes und Sven für ein sehr lockeres und witziges Jahr 2023 danken. Ich danke euch Dreien für die stets konstruktiven Diskussionen und den Spaß an der Arbeit. Ich wünsche euch weiterhin viel Erfolg bei eurer Promotion!

Ohne studentische Hilfe wäre eine Promotion manchmal einfacher, manchmal aber auch anstrengender, dennoch ist man irgendwie darauf angewiesen. So möchte ich allen Studierenden, die sich meinem durchaus schwierigen Thema gestellt und zu all den Ergebnissen beigetragen haben, danken. Ich hatte Spaß euch zu betreuen und mein (Un-)Wissen mit euch zu teilen. Zu diesen Studierenden zählen die Bachelorand*innen Anna, Celina und Hennes, die Vertiefer*innen Mirko, Lena, Paula, Patrick, Alena, Sven und Hennes, die Masteranden Clemens, Sven und Hennes, sowie die HiWis Paula und Hennes. Dankeschön!

Ebenfalls dürfen sich all diejenigen angesprochen fühlen, die ich zwar nicht direkt betreut habe, sich aber in unserem Labor oder den Nachbarlaboren getummelt haben. Eine Liste mir euren Namen wäre einfach zu lang.

Der universitäre Alltag kann ganz schön nervenaufreibend und anstrengend sein, weswegen das ein oder andere Kaltgetränk nach getaner Arbeit sehr erlösend sein kann. Dieses schmeckt natürlich umso besser mit guten Freunden und Kollegen. Ich werde die ganzen Feiern und Feten, Barbecues im Sommer und *special* Abende im Winter vermissen. Für all die schönen Erinnerungen sind natürlich die Mitglieder der anorganischen Chemie und der erweiterte Kreis ausgewählter Personen der letzten 5 bis 6 Jahre verantwortlich, zu welchen namentlich die Arbeitskreise Dehnen, von Hänisch, Kraus, Werncke, Sundermeyer, Lichtenberg, Heine und von Zezschwitz gehören. Euch alle hier namentlich zu erwähnen ist mir einfach zu anstrengend, also fühlt euch nach belieben angesprochen. Danke für die schöne Zeit!

Meinen besten Freunden gilt ein ganz spezieller Dank. Ohne euch wären diese 4 Jahre Promotion wesentlich unerträglicher gewesen. Ihr habt mich an schlechten Tagen immer abgelenkt, wieder aufgebaut oder ein offenes Ohr gehabt. An guten Tagen haben wir zusammen gescherzt, getanzt und gesungen, um das beste aus jedem Tag zu machen. Meinem Jugendfreund Bene dir danke ich, dass du immer für mich da bist, wenn ich dich brauche. Auch wenn der Kontakt manchmal selten ist, so ist die Freundschaft zu dir immer noch so wie zur guten alten Schulzeit. Es bedeutet mir viel inzwischen ein Teil deiner Familie zu sein. Dankeschön Digga! Jörn dich durfte ich während meines Masters zu einer Zeit kennen lernen, in der ich mit dem Studium am hadern war. Du hast mir in den Arsch getreten und einen großen Teil dazu beigetragen, dass ich sowohl das Studium, als auch die Promotion abgeschlossen habe. Wir haben in dieser Zeit gemeinsam viel erlebt. Ich bin dir dankbar für die Hilfe, den Sport, das Essen (vor allem der Grünkohl) und jedes Bier. Danke für alles! Auch unsere Wege haben sich gekreuzt Paula. Über die letzten Jahre sind wir zu wirklich guten Freunden geworden, gemeinsam durch Höhen und Tiefen, Dick und Dünn gegangen. Gegenseitig haben wir uns ständig motiviert, was nicht immer

leicht und manchmal auch eine Herausforderung war, aber uns immer zum Ziel geführt hat. Ich bin dir sehr dankbar für die Bereicherung in meinem Leben und deine nie endende Unterstützung. Vielen Dank, "kleine Schwester"!

Zuletzt möchte ich meiner Familie, besonders meinen Eltern Marion und Klaus Peter für jegliche Unterstützung während meines gesamten Studiums und den immer anhaltenden Rückhalt einen ganz besonders ehrenvollen Dank aussprechen. Auch meiner Schwester Mara und ihrer Familie ist mein Dank zuteil. Danke, dass ihr immer für einen da seid und den Rücken stärkt. Ich lieb euch alle!